METAL ORGANIC COORDINATION NETWORKS COMPRISED OF DIVALENT METAL CENTERS AND MULTIATOM CARBOXYLATE LINKERS

Sadhika Khullar

A thesis submitted for the partial fulfillment of
the degree of Doctor of Philosophy

Department of Chemical Sciences
Indian Institute of Science Education and Research Mohali

July 2013

Dedicated to

My Parents, Sister and Brother

Declaration

The work presented in this thesis has been carried out by me under the guidance of Dr. Sanjay K. Mandal at the Indian Institute of Science Education and Research Mohali. This work has not been submitted in part or in full for a degree, a diploma, or a fellowship to any other university or institute. Whenever contributions of others are involved, every effort is made to indicate this clearly, with due acknowledgement of collaborative research and discussions. This thesis is a bona fide record of original work done by me and all sources listed within have been detailed in the bibliography.

Sadhika Khullar

In my capacity as the supervisor of the candidate's thesis work, I certify that the above statements by the candidate are true to the best of my knowledge.

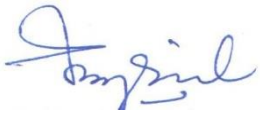

Dr. Sanjay K. Mandal

Acknowledgements

I would like to express my sincere gratitude towards my supervisor, Dr. Sanjay K. Mandal, for his continuous support, motivation, patience, enthusiasm, and immense knowledge. His guidance has helped me all the time for my work in the lab and in writing this thesis. I have learnt a lot from him. He has always encouraged us to do an analytical thinking of our work and taught us how to become a good scientist. His great problem solving abilities showed us a different approach in finding ways to conduct our research work. I also want to thank him for giving me extensive training in X-ray diffractometry which is one of most important analytical tool for my studies. I could not have imagined having a better supervisor and mentor.

I would like to thank Prof. N. Sathyamurthy, Director, IISER Mohali for providing the infrastructure and all the necessary facilities to work in this institute.

I would also like to thank my doctoral committee members, Prof. Ramesh Kapoor and Prof. K. S. Viswanathan for their valuable comments.

I thank all my labmates - Navnita Kumar, Biswajit Laha, Sandeep Kashyap, Vijay, Gaurav, Karan and Amita Agrawal for their support and help. I want to thank summer students - Selva Prakash, Babita, Uday, Manpreet and Gitanjali - for their help in my work.

I also want to thank my friends - Shelly, Nidhi, Zeba and Bhupesh - for their support, encouragement and help.

I am thankful to lab assistants - Mangat Bhaiya, Bhadur Bhaiya and Vishal - for their help whenever needed.

I want to acknowledge NMR, Raman and X-ray facilities at IISER Mohali, CIL at NIPER Mohali, CMCSRI Bhavnagar and IIT Kanpur for sample analysis.

I am grateful to CSIR, Government of India for a fellowship during my graduate studies.

Last but not the least, I would like to appreciate my parents, my sister Sandhi and my brother Richy for their continuous support, patience and encouragement.

List of Figures

Chapter I

Figure 1.1. Components of MOCNs.
Figure 1.2. Proposed Classification of MOCNs.
Figure 1.3. Schematic representation of the formation of various products including 1D CPs (linear or zig-zag type) and squares.
Figure 1.4. Schematic representation of the formation of various products including 1D CPs and squares/rectangles.
Figure 1.5. Schematic representation of the formation of 2D and 3D MOFs.
Figure 1.6. Formation of an SCN of 1D CPs.
Figure 1.7. Formation of a SCN of Squares/Rectangles.
Figure 1.8. Ancillary ligands used in this study.
Figure 1.9. Structures of the carboxylates used in this study.
Figure 1.10. Schematic drawings of the 1:2 and 1:1 complexes.

Chapter III

Figure 3.1. The dinuclear unit, $[Mn_2(bpma)_2(adc)_2(H_2O)_2]$, in **1**.
Figure 3.2. The Tetrameric synthon of **1**.
Figure 3.3. 3D Supramolecular assembly of tetrameric synthon in **1**.
Figure 3.4. A schematic drawing of **2**.
Figure 3.5. Ladder shaped supramolecular assembly in **2** through π-π interactions.
Figure 3.6. A view of the dinuclear subunit in the 2D supramolecular assembly of **4**$\cdot 5H_2O$.
Figure 3.7. A perspective view of the 2D supramolecular assembly of **4**$\cdot 5H_2O$ (top); its space-filling representation showing the water channel (bottom).
Figure 3.8. A perspective view of the 2D supramolecular assembly of **4**$\cdot 6H_2O$ (left); its space-filling representation showing the water channel (right).
Figure 3.9. For comparison, the structure of **4**$\cdot 6H_2O$ after deleting one water molecule.
Figure 3.10. Representation of water clusters in **4**$\cdot 6H_2O$ (top) and $4\cdot 5H_2O$ (bottom), respectively. Contacts between water molecules (coordinated and free) and the carboxylate oxygen atoms of adc^{2-} are considered. For clarity all hydrogen atoms are omitted.
Figure 3.11. (a) A schematic view of the 2D supramolecular assembly of **4**$\cdot 4H_2O\cdot CH_3OH$ (left); (b) its space-filling representation showing the channel filled with water and methanol between the one-dimensional layers (right).
Figure 3.12. Experimental and simulated powder patterns for **1** and **2** (top); experimental powder patterns for **3**, **5** and **6** (bottom).
Figure 3.13. Simulated and experimental powder patterns for **4**$\cdot 5H_2O$ and its various forms.
Figure 3.14. Experimental powder patterns for **7** (left) and **9** (right).
Figure 3.15. Raman spectra of **1**, **2**, **3** and **5**.
Figure 3.16. Raman spectra of **4**$\cdot 5H_2O$, **4** and **4**$\cdot H_2O\cdot CH_3OH$.
Figure 3.17. TGA scans for **1** (left) and **2** (right).
Figure 3.18. TGA scans for **3** (left) and **6** (right).
Figure 3.19. TGA scan for **4**$\cdot 5H_2O$.
Figure 3.20. TGA scan for **5**.
Figure 3.21. TGA scans for **7** (left) and **10** (right).

List of Figures (contd.)

Figure 3.22. Schematic representation of the solid-state structural transformation of **4**·$5H_2O$ to 2D and 3D supramolecular assemblies **4** and **4**·$4H_2O$, respectively, during the dehydration and rehydration processes.
Figure 3.23. FTIR spectra of **4**·$5H_2O$ at 80 ℃ under vacuum at intervals.
Figure 3.24. Water adsorption isotherms for **1**, **2** and **4** (Bluelines: **1** after pretreatment, Redlines: **1** without pretreatment, Pinklines: **2**; Greenlines: **4**; filled squares, adsorption and circles, desorption).
Figure 3.25. A ball and stick presentation of **13**.
Figure 3.26. Formation of a 2D Supramolecular assembly from the 1D Supramolecular assemblies and lattice water molecules in **13**.
Figure 3.27. Hydrogen bonded network in **13** showing three different motifs.
Figure 3.28. A perspective view of **16** (left) and its space-filling model (right).
Figure 3.29. Supramolecular assembly of squares in **16** showing a hexameric motif.
Figure 3.30. A capped stick presentation of 17.
Figure 3.31. Hydrogen bonded network showing motifs in **17** (Hanging contacts and hydrogens are deleted for clarity).
Figure 3.32. Raman spectra of **13**, **16** and **17**.
Figure 3.33. TGA scans of **13** and **17**.
Figure 3.34. TGA scan of **16**.
Figure 3.35. Structure of the cation in **19**.
Figure 3.36. Supramolecular assembly in **19**.
Figure 3.37. Structure of the cation in **20**.
Figure 3.38. Supramolecular assembly in **20**.
Figure 3.39. Structure of **21**.
Figure 3.40. Supramolecular assembly in **21**.
Figure 3.41. A perspective view of **22**.
Figure 3.42. A perspective view of **23**.
Figure 3.43. Chair-shaped supramolecular assembly in **23**.
Figure 3.44. A perspective view of **24**.
Figure 3.45. 2D supramolecular assembly in **24**.
Figure 3.46a. A perspective view of the polymeric chain 1 in **27**.
Figure 3.46b. A perspective view of the polymeric Chain 2 in **27**.
Figure 3.47. 2D Supramolecular assembly in **27** via π–π interactions.
Figure 3.48. V-shaped 1D coordination polymer of **28**.
Figure 3.49. 2D supramolecular assembly in **28**.
Figure 3.50. V-shaped 1D CP of **29**.
Figure 3.51. Experimental and simulated powder patterns for **22**, **23**, **24** and **25**.
Figure 3.52. Experimental and simulated powder patterns for **26**, **27**, **28** and **29**.
Figure 3.53. TGA scans for **22**-**25** (left) and **26**-**29** (right).
Figure 3.54. Rectangular (**30a**) and rod-shaped (**30b**) crystals from the reaction mixture.
Figure 3.55. A perspective view of **30a**.
Figure 3.56. 2D Supramolecular assembly in **30a**.
Figure 3.57. A perspective view of **30b**.
Figure 3.58. 2D Supramolecular assembly in **30b**.

List of Figures (contd.)

Figure 3.59. A perspective view of **31**.
Figure 3.60. 2D Supramolecular Assembly in **31**.
Figure 3.61. A perspective view of **32** and its space-filling model.
Figure 3.62. A part of 3D MOF showing pores filled with lattice water molecules in **32**.
Figure 3.63. A perspective view of **33**.
Figure 3.64. A space-filling model of **33**.
Figure 3.65. Supramolecular coordination network: encapsulation of hexamer of water in **33**.
Figure 3.66. Experimental (red) and simulated (black) powder patterns for **31**(left) and 32 (right).
Figure 3.67. TGA scans for **31**, **32** and **33**.
Figure 3.68. Emission spectra of **24** (left) and **28** (right).
Figure 3.69. Emission spectra of **27** (left) and **33** (right).
Figure 3.70. A ball and stick representation of the dimanganese subunit in **34**.
Figure 3.71. A perspective view of the hydrogen bonded network in **34**.
Figure 3.72. Hydrogen bonded network in **34** showing motifs.
Figure 3.73. A perspective view of **34** showing π–π interactions between two pyridine rings in two different planes.
Figure 3.74. A ball and stick representation of the dimanganese subunit in **35**.
Figure 3.75. 2D supramolecular assembly showing hexamer of encapsulated water molecules in **35**.
Figure 3.76. A view of pre-hexamer formation of water in **35a**.
Figure 3.77. A perspective view showing π–π interactions between two pyrdine rings of two dimangenese subunits in **35**.
Figure 3.78. A perspective view showing π–π interactions between two pyridine rings of two dimangenese subunits in **35a**.
Figure 3.79. A ball and stick representation of the dimanganese subunit in **36**.
Figure 3.80. A perspective view of the hydrogen bonded network in **36**.
Figure 3.81. A comparison of the motifs formed through hydrogen bonding interactions of encapsulated water molecules and uncoordinated carboxylate oxygens in **34**, **35** and **36**.
Figure 3.82. A perspective view of **36** showing π–π interactions between two pyridine rings in two different planes.
Figure 3.83. Experimental and simulated powder patterns for **34**, **35** and **36**.
Figure 3.84. Raman spectra of **34**, **35** and **36**.
Figure 3.85. TGA scan of **35**.
Figure 3.86. TGA scans of **34** (left) and **36** (right).
Figure 3.87. FTIR spectra for **37** (left) and **38** (right).
Figure 3.88. TGA scan of **37**.
Figure 3.89. V-shaped 1D CP of **40**.
Figure 3.90. Supramolecular assembly in **40**.
Figure 3.91. Simulated and experimental powder patterns for **39** and **40**.
Figure 3.92. TGA scans of **39** and **40**.
Figure 3.93. Coordination environment around Mn(II) in **41b**.
Figure 3.94. A perspective view of 2D spiral 41b (left) and its space filling representation (right).
Figure 3.95. Representation of hydrogen bonding in the 3D assembly of **41b**. Hydrogen atoms are omitted for clarity.

List of Figures (contd.)

Figure 3.96. Formation of the 3D network via π–π interactions in **41b**.
Figure 3.97. A perspective view of the $Mn_2(tppn)(H_2O)_6$ subunits in **42**.
Figure 3.98. Formation of the 3D supramolecular assembly of **42** via hydrogen bonding. Only one of the disordered oxygen of a carboxylate group of the adc group is shown. Hydrogen atoms are omitted for clarity.
Figure 3.99. Crystal structure of the cation in **43**.
Figure 3.100. Crystal structure of the cation in **44**.
Figure 3.101. 1D chain structure of **45** (top) and hydrogen bonding interactions in **45** (bottom).
Figure 3.102. Formation of the 3D network via π–π interactions in **45**. For clarity, lattice water molecules and adc anions are omitted.
Figure 3.103. A perspective view of **47**.
Figure 3.104. Hydrogen bonded network of **47**. For clarity, hydrogens are omitted.
Figure 3.105. Formation of the 3D network via π–π interactions in **47**.
Figure 3.106. Structure of $[Mn_2(tppn)_2(fumarate)]^{2+}$ in **49**.
Figure 3.107. A perspective view of **50**.
Figure 3.108. 3D Supramolecular assembly in **50**.
Figure 3.109. A perspective view of **51** (perchlorates and hydrogens are omitted for clarity).
Figure 3.110. Supramolecular assembly in **51**.
Figure 3.111. Supramolecular assembly in **51** via π–π interactions.
Figure 3.112. A perspective view of **52**.
Figure 3.113. Struture of the $[Mn_2(tpbn)(H_2O)_6]$ subunit in **53**.
Figure 3.114. Hydrogen bonded network in **53**.
Figure 3.115. A perspective view of **54**.
Figure 3.116. Space-filling Model of 2D MOF of **54** showing pores.
Figure 3.117. A topological view of **54**.
Figure 3.118. Another Topological view of **54**.
Figure 3.119a. Experimental and simulated X-ray powder patterns of **41**, **42**, **43** and **44**.
Figure 3.119b. Experimental and simulated X-ray powder patterns of **50**.
Figure 3.120. Raman spectra for **41**, **42**, **43** and **44**.
Figure 3.121. TGA scan of **41a**.
Figure 3.122. TGA scan of **42**.
Figure 3.123. TGA scan of **45**.
Figure 3.124. TGA scans of **46** and **47**.
Figure 3.125. TGA scan of **53**.
Figure 3.126. TGA scans of **50** (left) and **54** (right).
Figure 3.127. A perspective view of **55**.
Figure 3.128. A view of the discrete tetranuclear Mn(II) complex, **56**.
Figure 3.129. Supramolecular assembly of the discrete tetranuclear unit in **56**.
Figure 3.130. Coordination environment around Mn(II) in **57**.
Figure 3.131. A perspective view of **57**.
Figure 3.132. A topological view of **57**.
Figure 3.133. TGA scans of **55**, **56** and **57**.
Figure 3.134. A perspective view of **58** (perchlorates anions are omitted for clarity).
Figure 3.135. Supramolecular assembly in **58**.

List of Figures (contd.)

Figure 3.136. An arrangement of perchlorate anions in supramolecular assembly of **58**.
Figure 3.137. Structure of $[\{Cu_2(tppn)(H_2O)_2(ClO_4)\}_2(succinate)]^{4+}$ in **61**.
Figure 3.138. Supramolecular assembly in **61**.
Figure 3.139. A perspective view of **63**.
Figure 3.140. Molecule A (left) and B (right) in **64**.
Figure 3.141. Supramolecular assembly of molecule A in **64**.
Figure 3.142. Supramolecular assembly of molecule B in **64**.
Figure 3.143. A view of molecular rectangle **65**.
Figure 3.144. Association of molecular rectangles in **65** via hydrogen bonding.
Figure 3.145. Supramolecular assembly in **65**.
Figure 3.146. A view of π–π interactions in **65**.
Figure 3.147. A perspective view of 1D CP of **66**.
Figure 3.148. A view of supramolecular assembly in **66**.
Figure 3.149. A perspective view of **67**.
Figure 3.150. Supramolecular assembly in **67** (all hanging contacts are deleted for clarity).
Figure 3.151. A perspective view of **68**.
Figure 3.152. Supramolecular assembly in **68**.
Figure 3.153. Molecular rectangle **70**.
Figure 3.154. Supramolecular assembly in **70**.
Figure 3.155. A perspective view of 1D chains of **71**(left) and their association via Hydrogen bonding (right).
Figure 3.156. A perspective view of **73**.
Figure 3.157. Supramolecular assembly in **73**.
Figure 3.158. A perspective view of 1D helical CP of **74**.
Figure 3.159. Intramolecular hydrogen-bonding in 1D CP of **74**.
Figure 3.160. 2D Supramolecular assembly via π–π interactions in **74**.
Figure 3.161. Structure of molecular rectangle, **75**.
Figure 3.162. 2D Supramolecular assembly in **75**.
Figure 3.163. A perspective view of **76** (Only cationic part is shown).
Figure 3.164. An arrangement of perchlorate anions chain in **76**.
Figure 3.165. Hydrogen bonded network and perchlorate anion arrangement in **76**.
Figure 3.166. A part of the CP in **77**.
Figure 3.167. A perspective view of 2D CP of **77**.
Figure 3.168. A schematic view of **79** (top) and sodium ion inside the CP (bottom).
Figure 3.169. A view of the metallacycle in **80**.
Figure 3.170. A perspective view of **81** (perchlorates and water not included).
Figure 3.171. Supramolecular assembly in **81**.
Figure 3.172. An octanuclear discrete MOF of **82**.
Figure 3.173. Supramolecular assembly in **82**.
Figure 3.174. Structure of **83** (left) and its space-filling model (right).
Figure 3.175. 2D network of molecular rectangles in **83** through hydrogen bonding interactions.
Figure 3.176. A view of π–π interactions in two planes in **83**.
Figure 3.177. Molecular rectangles of **84** showing two conformations of tpbn.
Figure 3.178. Formation of supramolecular assembly via π–π interactions in **84**.

List of Figures (contd.)

Figure 3.179. Structure of molecular rectangle, **85**.
Figure 3.180. A perspective view of 2D CP of **87**.
Figure 3.181. A part of CP of **87**.
Figure 3.182. A perspective view of heterometallic CP of **87**.
Figure 3.183. UV-Vis spectra for **65**, **74** and **75**.
Figure 3.184. UV-Vis spectra for **83**, **84** and **85**.
Figure 3.185. Isotopic patterns for m/z = 1 for **83**, **84** and **85**.
Figure 3.186. Cyclic voltammograms of **83**-**85**.
Figure 3.187. Excitation (left) and Emission (right) spectra for **83**, **84** and **85**.
Figure 3.188. Water adsorption isotherms for **83** (green) and **84** (pink).
Figure 3.189. A perspective view of 3D CP of **88**; perchlorate anions and water molecules are omitted.
Figure 3.190. A perspective view of **89** (perchlorate anions and lattice water molecules are omitted for clarity).
Figure 3.191. A part of 3D MOF of **89** showing two kinds of pores.
Figure 3.192. Distribution of pores in 3D MOF of **89**.
Figure 3.193. A topological view of **89**.
Figure 3.194. Water adsorption isotherm for **89**.
Figure 3.195. A perspective view of **90**.
Figure 3.196. The supramolecular network in **90**.
Figure 3.197. A perspective view of **91**.
Figure 3.198. An arrangement of disulphonate anions in the supramolecular assembly of **91**.
Figure 3.199. A perspective of **92**.
Figure 3.200. A part of the supramolecular assembly in **92**.
Figure 3.201. UV-Vis spectra for **90**, **91** and **92**.
Figure 3.202. A perspective view of **94**.
Figure 3.203. A perspective view of **95**.
Figure 3.204. A space-filling model of **95**.
Figure 3.205. A part of the supramolecular assembly in **95** (different color is chosen for clarity)
Figure 3.206. FTIR spectrum of **95**.
Figure 3.207. TGA scan for **95**.
Figure 3.208. A ball and stick representation of **96**.
Figure 3.209. Hydrogen bonded network in **96**.
Figure 3.210. A perspective view of **97** (water molecules are omitted for clarity).
Figure 3.211. A topological view of **97**.
Figure 3.212. Another topological view of **97**.
Figure 3.213. A perspective view of **99**.
Figure 3.214. 2D Supramolecular assembly in **99**.
Figure 3.215. Raman spectrum of **97**.
Figure 3.216. Water adsorption isotherm for **97**.
Figure 3.217. Experimental powder X-ray diffraction patterns for **97** and its host-guest analogs.
Figure 3.218. Excitation (left) and Emission (right) spectra of **97**.
Figure 3.219. TGA scans of **96** (left) and **98** (right).
Figure 3.220. TGA Scan of **97**.

List of Figures (contd.)

Figure 3.221. A ball and stick representation of **101**.
Figure 3.222. A perspective view of the supramolecular assembly in **101**.
Figure 3.223. A space-filling model to show supramolecular cavity in **101**.
Figure 3.224. A view showing π–π interactions in **101**.
Figure 3.225. A perspective view of **102** (left) and its topological view (right).
Figure 3.226. An arrangement of Zn(II) and $HBTC^{2-}$ in **102**.
Figure 3.227. A perspective view of 3D CP of **103** and its space-filling model.
Figure 3.228. A persepective view of the supramolecular assembly in **103**.
Figure 3.229. FTIR spectrum of **101**.
Figure 3.230. FTIR spectrum of **103**.
Figure 3.231. TGA scans of **102** and **103**.

List of Schemes

Scheme 1. General synthesis of tridentate ligands.
Scheme 2. Synthesis of tpa.
Scheme 3. General synthesis of polypyridyl hexadentate ligands.
Scheme 4. Synthesis of the bpbg ligand.
Scheme 5. General methods for the synthesis of MOCNs.
Scheme 6. Synthesis of **1**-**5**.
Scheme 7. Synthesis of **10**.
Scheme 8. Synthesis of **11**-**18**.
Scheme 9. General synthesis of **19**-**21**.
Scheme 10. Synthesis of **22**-**25**.
Scheme 11. Synthesis of **26**-**29**.
Scheme 12. Synthesis of **30**-**33** under hydrothermal conditions.
Scheme 13. Synthesis of **34**-**36**.
Scheme 14. Synthesis of **37** and **38**.
Scheme 15. Synthesis of **39** and **40**.
Scheme 16. Synthesis of **41**-**47**.
Scheme 17. Synthesis of **48**.
Scheme 18. Synthesis of **49**-**50**.
Scheme 19. Synthesis of **54**.
Scheme 20. Synthesis of **55**-**57**.
Scheme 21. Synthesis of **58**-**60**.
Scheme 22. Synthesis of **61**-**63**.
Scheme 23. Synthesis of **64**-**66**.
Scheme 24. Synthesis of **67**-**68**.
Scheme 25. Synthesis of **69**-**70**.
Scheme 26. Synthesis of **71**-**72**.
Scheme 27. Synthesis of **74**-**75**.
Scheme 28. Synthesis of **76**-**78**.
Scheme 29. Synthesis of **82**-**87**.
Scheme 30. Synthesis of **88**-**89**.
Scheme 31. Synthesis of **90**-**92**.
Scheme 32. Synthesis of **93**-**94**.
Scheme 33. Synthesis of **95**.
Scheme 34. Synthesis of **96** and **97**.
Scheme 35. Synthesis of **99** and **100**.
Scheme 36. Synthesis of **101**-**103**.

List of Tables

Table 3.1. Hydrogen bonding parameters for **1**.
Table 3.2. Hydrogen bonding parameters for **4**·**6**H_2O, **4**·**5**H_2O, **4**, **4**·**4**H_2O·CH_3OH and **4**·**4**H_2O.
Table 3.3. Pore Sizes within the dimetal subunits in **1**, **2** and **4**·**6**H_2O and its various forms.
Table 3.4. Hydrogen bonding parameters for **13**.
Table 3.5. Hydrogen bonding parameters for **16**.
Table 3.6. Hydrogen bonding parameters for **17**.
Table 3.7. Hydrogen bonding parameters for **19**.
Table 3.8. Hydrogen bonding parameters for **20**.
Table 3.9. Hydrogen bonding parameters for **21**.
Table 3.10. Hydrogen bonding parameters for **24**.
Table 3.11. Hydrogen bonding parameters for **28**.
Table 3.12. Hydrogen bonding parameters for **30a**.
Table 3.13. Hydrogen bonding parameters for **30b**.
Table 3.14. Hydrogen bonding parameters for **31**.
Table 3.15. Hydrogen bonding parameters for **32**.
Table 3.16. Hydrogen bonding parameters for **33**.
Table 3.17. Hydrogen bonding parameters for **34**, **35**, **35a** and **36**.
Table 3.18. Hydrogen bonding parameters for **41b**, **42**, **45** and **47**.
Table 3.19. Hydrogen bonding parameters for **50**.
Table 3.20. Hydrogen bonding parameters for **51**.
Table 3.21. Hydrogen bonding parameters for **53**.
Table 3.22. Hydrogen bonding parameters for **58**.
Table 3.23. Hydrogen bonding parameters for **61**.
Table 3.24. Hydrogen bonding parameters for **64**.
Table 3.25. Hydrogen bonding parameters for **65**.
Table 3.26. Hydrogen bonding parameters for **66**.
Table 3.27. Hydrogen bonding parameters for **67**.
Table 3.28. Hydrogen bonding parameters for **68**.
Table 3.29. Hydrogen bonding parameters for **70**.
Table 3.30. Hydrogen bonding parameters for **71**.
Table 3.31. Hydrogen bonding parameters for **73**.
Table 3.32. Hydrogen bonding parameters for **74**.
Table 3.33. Hydrogen bonding parameters for **76**.
Table 3.34. Hydrogen bonding parameters for **83**, **84** and **85**.
Table 3.35. Mass spectral data for **64**, **65**, **74**, **75**, **83**, **84** and **85**.
Table 3.36. Hydrogen bonding parameters for **90**.
Table 3.37. Hydrogen bonding parameters for **91**.
Table 3.38. Hydrogen bonding parameters for **92**.
Table 3.39. Hydrogen bonding parameters for **95**.
Table 3.40. Hydrogen bonding parameters for **96**.
Table 3.41. Hydrogen bonding paramters for **99**.
Table 3.42. Hydrogen bonding parameters for **101**.
Table 3.43. Hydrogen bonding parameters for **103**.

List of Tables (contd.)

Appendix

Table A1. Crystal Structure data and Refinement parameters for **1** and **2**.
Table A2. Crystal Structure data and Refinement parameters for **4**·**5**H_2O and its various forms.
Table A3. Crystal Structure data and Refinement parameters for **13**, **16** and **17**.
Table A4. Crystal Structure data and Refinement parameters for **19**, **20** and **21**.
Table A5. Crystal Structure data and Refinement parameters for **22**, **23** and **24**.
Table A6. Crystal Structure data and Refinement parameters for **27**, **28** and **29**.
Table A7. Crystal Structure data and Refinement parameters for **30a** and **30b**.
Table A8. Crystal Structure data and Refinement parameters for **31**, **32** and **33**.
Table A9. Crystal Structure data and Refinement parameters for **34** and **36**.
Table A10. Crystal Structure data and Refinement parameters for **35** and **35a**.
Table A11. Crystal Structure data and Refinement parameters for **40**.
Table A12. Crystal Structure data and Refinement parameters for **41**, **43** and **44**.
Table A13. Crystal Structure data and Refinement parameters for **44**, **45** and **4**7.
Table A14. Crystal Structure data and Refinement parameters for **49** and **50**.
Table A15. Crystal Structure data and Refinement parameters for **51**.
Table A16. Crystal Structure data and Refinement parameters for **52** and **53**.
Table A17. Crystal Structure data and Refinement parameters for **54**.
Table A18. Crystal Structure data and Refinement parameters for **55**, **56** and **57**.
Table A19. Crystal Structure data and Refinement parameters for **58**.
Table A20. Crystal Structure data and Refinement parameters for **61** and **63**.
Table A21. Crystal Structure data and Refinement parameters for **64**, **65** and **66**.
Table A22. Crystal Structure data and Refinement parameters for **67** and **68**.
Table A23. Crystal Structure data and Refinement parameters for **70** and **71**.
Table A24. Crystal Structure data and Refinement parameters for **73**.
Table A25. Crystal Structure data and Refinement parameters for **74** and **75**.
Table A26. Crystal Structure data and Refinement parameters for **76** and **77**.
Table A27. Crystal Structure data and Refinement parameters for **79** and **80**.
Table A28. Crystal Structure data and Refinement parameters for **83**, **84** and **8**5.
Table A29. Crystal Structure data and Refinement parameters for **87**.
Table A30. Crystal Structure data and Refinement parameters for **88** and **89**.
Table A31. Crystal Structure data and Refinement parameters for **90**, **91** and **92**.
Table A32. Crystal Structure data and Refinement parameters for **94**.
Table A33. Crystal Structure data and Refinement parameters for **95**.
Table A34. Crystal Structure data and Refinement parameters for **96** and **97**.
Table A35. Crystal Structure data and Refinement parameters for **99**.
Table A36. Crystal Structure data and Refinement parameters for **101** and **102**.
Table A37. Crystal Structure data and Refinement parameters for **103**.
Table A38. Selected bond distances and angles for **1**.
Table A39. Selected bond distances and angles for **2**.
Table A40. Selected bond distances and angles for **4**.
Table A41. Selected bond distances and angles for **13** and **17**.
Table A42. Selected bond distances and angles for **16**.

List of Tables (contd.)

Table A43. Selected bond distances and angles for **19**.
Table A44. Selected bond distances and angles for **20**.
Table A45. Selected bond distances and angles for **21**.
Table A46. Selected bond distances and angles for **22**, **23** and **24**.
Table A47. Selected bond distances and angles for **27**.
Table A48. Selected bond distances and angles for **28**.
Table A49. Selected bond distances and angles for **29**.
Table A50. Selected bond distances and angles for **30a**.
Table A51. Selected bond distances and angles for **30b**.
Table A52. Selected bond distances and angles for **31**.
Table A53. Selected bond distances and angles for **32**.
Table A54. Selected bond distances and angles for **33**.
Table A55. Selected bond distances and angles for **34**, **35** and **36**.
Table A56. Selected bond distances and angles for **40**.
Table A57. Selected bond distances and angles for **41b**.
Table A58. Selected bond distances and angles for **42**.
Table A59. Selected bond distances and angles for **43b** and **44b**.
Table A60. Selected bond distances and angles for **45.**
Table A61. Selected bond distances and angles for **47**.
Table A62. Selected bond distances and angles for **49**.
Table A63. Selected bond distances and angles for **50**.
Table A64. Selected bond distances and angles for **51**.
Table A65. Selected bond distances and angles for **52**.
Table A66. Selected bond distances and angles for **53**.
Table A67. Selected bond distances and angles for **54**.
Table A68. Selected bond distances and angles for **55**.
Table A69. Selected bond distances and angles for **56**.
Table A70. Selected bond distances and angles for **57**.
Table A71. Selected bond distances and angles for **58**.
Table A72. Selected bond distances and angles for **61**.
Table A73. Selected bond distances and angles for **63**.
Table A74. Selected bond distances and angles for **64**.
Table A75. Selected bond distances and angles for **65**.
Table A76. Selected bond distances and angles for **66**.
Table A77. Selected bond distances and angles for **67**.
Table A78. Selected bond distances and angles for **68**.
Table A79. Selected bond distances and angles for **70**.
Table A80. Selected bond distances and angles for **71**.
Table A81. Selected bond distances and angles for **73**.
Table A82. Selected bond distances and angles for **74**.
Table A83. Selected bond distances and angles for **75**.
Table A84. Selected bond distances and angles for **76**.
Table A85. Selected bond distances and angles for **77**.
Table A86. Selected bond distances and angles for **79**.

List of Tables (contd.)

Table A87. Selected bond distances and angles for **80**.
Table A88. Selected bond distances and angles for **83**, **84** and **85**.
Table A89. Selected bond distances and angles for **87**.
Table A90. Selected bond distances and angles for **88**.
Table A91. Selected bond distances and angles for **89**.
Table A92. Selected bond distances and angles for **90**.
Table A93. Selected bond distances and angles for **91**.
Table A94. Selected bond distances and angles for **92**.
Table A95. Selected bond distances and angles for **94**.
Table A96. Selected bond distances and angles for **95**.
Table A97. Selected bond distances and angles for **96**.
Table A98. Selected bond distances and angles for **97**.
Table A99. Selected bond distances and angles for **99**.
Table A100. Selected bond distances and angles for **101**.
Table A101. Selected bond distances and angles for **102**.
Table A102. Selected bond distances and angles for **103**.

Acronyms and Abbreviations

AcOH	acetic acid
adc	acetylene dicarboxylate
H_2adc	acetylene dicarboxylic acid
bipy	2,2′-bipyridine
4,4′-bipy	4,4′-bipyridine
H_3BTC	benzene-1,3,5-tricarboxylic acid
BTC	benzene-1,3,5-tricarboxylate
bpa	N,N′-bis-(2-pyridylmethyl)-amine
bpma	N,N′-bis-(2-pyridylmethyl)-methylamine
bpea	N,N′-bis-(2-pyridylmethyl)-ethylamine
bpipa	N,N′-bis-(2-pyridylmethyl)-isopropylamine
bpta	N,N′-bis-(2-pyridylmethyl)-t-butylamine
bpba	N,N′-bis-(2-pyridylmethyl)-benzylamine
bpbn	N,N′-bis-(2-pyridylmethyl)-1,4-diaminobutane
B.p.	Boiling point
tpa	N,N,N-tris-(2-pyridylmethyl)-amine
tpen	N,N,N′,N′-tetrakis-(2-pyridylmethyl)-1,2-diaminoethane
1,2-tppn	N,N,N′,N′-tetrakis-(2-pyridylmethyl)-1,2-diaminopropane
tppn	N,N,N′,N′-tetrakis-(2-pyridylmethyl)-1,3-diaminopropane
tpbn	N,N,N′,N′-tetrakis-(2-pyridylmethyl)-1,4-diaminobutane
tppen	N,N,N′,N′-tetrakis-(2-pyridylmethyl)-1,5-diaminopentane
tphxn	N,N,N′,N′-tetrakis-(2-pyridylmethyl)-1,6-diaminohexane
tphn	N,N,N′,N′-tetrakis-(2-pyridylmethyl)-1,7-diaminoheptane
bpbg	N,N'-bis(2-pyridylmethyl)-N,N'-bis-(acetamide)-1,4-diaminobutane
CP	Coordination Polymer
CDC	cyclohexanedicarboxylate
CTC	cyclohexanetricarboxylate
DMF	N,N'-dimethylformamide
DMSO	dimethylsulfoxide
dicarb	dicarboxylate
FTIR	Fourier Transform Infrared
H_2fum	fumaric acid
fum	fumarate
MOF	Metal Organic Frameworks
MOCN	Metal Organic Coordination Networks
M.p.	melting point
H_2mal	maleic acid
mal	maleate
NDS	naphthalene-2,6-disulphonate
1D	one dimensional
H_2ox	oxalic acid
py	pyridine
HT	hydrothermal
H_2PDC	2,6-pyridinedicarboxylic acid

Acronyms and Abbreviations (contd.)

PDC	2,6-pyridinedicarboxylate
RT	room temperature
Na_2adc	disodium acetylene dicarboxylate
SC	Single Crystal
SCNs	Supramolecular Coordination Networks
succ	succinate
H_2succ	succinic acid
tere	terephthalate
H_2tere	terephthalic acid
F_4tere	tetrafluoroterephthalate
H_2tdc	2,5-thiophenedicarboxylic acid
2D	two dimensional
3D	three dimensional
tdc	2,5-thiophenedicarboxylate
UV-Vis	Ultraviolet-Visible

Contents

	Page
Declaration	iii
Acknowledgement	iv
List of Figures	v
List of Schemes	xii
List of Tables	xiii
Acronyms and Abbreviations	xvii
Synopsis	xx
Introduction	1
Experimental Section	15
Materials and Methods	15
Physical Measurements	15
Synthesis of Ancillary Ligands	18
Synthesis of Metal Organic Coordination Networks	24
Results and Discussion	51
Ancillary Ligands	51
Metal Organic Coordination Networks (MOCNs)	55
MOCNs with Tridentate Ligands	56
MOCNs with Tetradentate Ligands	114
MOCNs with Hexadentate Ligands	135
Conclusions and Future Directions	247
References	256
Appendix	265
Publications	349
Vita	350

Synopsis

In recent years the chemistry of supramolecular assemblies has advanced extensively for their diverse structural aesthetics and for a variety of potential applications in catalysis, separation, sensors, gas storage, luminescent materials, ion exchange, magnetism, etc. Formation of infinite one-, two-, and three dimensional (1D, 2D, and 3D) supramolecular assemblies requires highly organized structures - both with and without metal ions - held together through various interactions, such as metal-donor atom coordinate bonds (in case of those with metal ions), strong and/or weak hydrogen bonds, π-π stacking of aromatic moieties, C-H…O interactions, etc. These assemblies are prepared from a variety of molecular building blocks, also termed as secondary building units (SBUs). The use of metal centers or metal atom clusters as the building blocks gives advantages due to availability of different coordination numbers that also vary from metal to metal. The selection of ancillary ligands and the multi-atom organic linkers is crucial in making such assemblies with varied dimensionality. The role of ancillary ligands that surround and protect the metal cores leaving open sites for the linkers is of great importance in making such frameworks. Furthermore, combining ancillary ligands with multitopic carboxylates and/or neutral linkers is less common in the literature.

This thesis focuses on the strategic design and development of metal organic coordination networks (MOCNs) through reproducible synthesis under ambient as well as hydrothermal conditions. Over one hundred new MOCNs comprised of divalent transition metal ions, polydentate ancillary ligands and mostly multi-atom carboxylate linkers have been synthesized in good to high yields. For making these MOCNs several ancillary ligands (with improved yields and purity) have also been synthesized and characterized. Through systematic studies, such MOCNs with well-defined structures and tunable metrics are obtained. These have diverse structures and topologies, are chemically and thermally stable, have a variety of functions. These are characterized by elemental analysis, FT-IR, Raman and UV-Vis spectroscopy, single crystal and powder X-ray diffraction, and ESI-MS analysis as well as are studied for their redox behavior by cyclic voltammetry, and thermal properties by thermogravimetric analysis. Their photoluminescent properties are established by fluorescence spectroscopy in the solid state. Several of these MOCNs are found to be porous (termed as MOFs) and have been tested for their

potential applications in water adsorption studies. There are four chapters in this thesis. Below are the short summaries of each chapter.

In Chapter I (Introduction), based on a thorough literature search that is discussed to cite prior work and current trend in the field of this research work, it is noted that the combining polydentate ancillary ligands with multitopic carboxylates and/or neutral linkers is less common. In most cases, the hydrothermal/solvothermal method has been employed to synthesize such materials. Use of this method has some limitations, such as poor stability of some carboxylate linkers at high temperature. On the other hand, the use of ancillary ligands provides a way to have better solubility of the MOCNs than those with mostly carboxylates. However, it is a challenge with a polydentate ancillary ligand, which itself can satisfy the usual hexacoordination of a divalent transition metal ion, to prevent the formation of a 1:1 (for a hexadentate ligand) or 1:2 (for a tridentate ligand) discrete molecule instead of the desired polymeric MOCN. Thus the selection of ancillary ligands along with the multi-atom organic linkers is crucial in forming the MOCNs. Furthermore, making MOCNs under ambient conditions is an attractive route for its simplicity as well as generalization for similar systems. Utilizing a scheme, the hitherto well-defined MOCNs is outlined to clearly classify the subsets studied in this work. This chapter outlines the rationale for the need of the current work with a plan to expand the field of metal ions with organic linkers in the presence various ancillary ligands, particularly the systematic studies in finding and exploiting the factors influencing the formation of MOCNs.

In Chapter II (Experimental Section), synthesis protocols of all ancillary ligands and the MOCNs are described. Several general methods were developed to synthesize twenty-five ancillary ligands. Three major synthetic procedures, namely self-assembly under ambient conditions, hydrothermal, were employed in making the MOCNs; however, majority of these were obtained by the first method. Procedures for their characterization by various analytical techniques mentioned above are detailed.

In Chapter III (Results and Discussion), one subsection has been created for each type of ancillary ligand based on its denticity. Within each subsection, variation of other factors, such as divalent metal ion, carboxylate linker or reaction conditions, are categorized to give an organized comparative study. In each case, full structural characterization, properties and any possible

applications are discussed and compared with those reported in the literature for similar systems. Further details are provided below:

Complexes with Tridentate Ligands

Using the tridentate bpxa (where bpxa = N,N-bis(2-pyridylmethyl)alkylamine) ligands, thirty compounds comprised of divalent metal ion, such as Mn(II), Co(II), Ni(II), Cu(II), Zn(II) and Cd(II), and dicarboxylate linkers, such as acetylene dicarboxylate (adc), fumarate, succinate, and thiophene dicarboxylate (tdc), have been prepared mostly via the self-assembly reactions under ambient conditions while a few isolated from the hydrothermal reactions. In order to identify the factors affecting the formation of such complexes with diverse structural features and properties, these compounds are grouped with one variation at a time for the Mn(II) complexes: $[Mn_2(bpma)_2(adc)_2(H_2O)_2]$, $[Mn_2(bpea)_2(adc)_2]_n$, $[Mn_2(bpipa)_2(adc)_2(H_2O)_2]$, $[Mn_2(bpta)_2(adc)_2(H_2O)_2]\cdot 5H_2O$, and $[Mn_2(bpba)_2(adc)_2(H_2O)_2]$, where the effect of substitution on the alkyl N of the ligands are observed. For example, just changing from methyl to ethyl group, the bpma derivative is a supramolecular assembly while the bpea derivative is a CP. Furthermore, with a tert-butyl group the bpta ligand forms a 3D supramolecular assembly comprised of coordinated water molecules and lattice water molecules that undergoes de-/rehydration processes in the single crystal to single crystal (SC-SC) transformation. On the other hand, the use of fumarate, succinate or terephthalate as the carboxylate linker instead of adc in $[Mn_2(bpea)_2(fumarate)_2]$, $[Mn_2(bpta)_2(fumarate)(H_2O)_2](ClO_4)_2$, $[Mn_2(bpta)_2(succinate)_2(H_2O)_2]\cdot H_2O$, $[Mn_2(bpta)_2(terephthalate)_2(H_2O)_2]\cdot 2H_2O$, provides further understanding in their structural diversity due to binding differences and similarities of these carboxylates.

As the divalent metal ion is taken as a variable, the bpta analogs of Ni(II), Co(II) and Cu(II), namely $[Ni(bpta)(adc)(H_2O)_2]\cdot 2H_2O$, $[Ni_4(bpta)_4(fumarate)_4(H_2O)_4]\cdot 2H_2O$, $[Ni(bpta)(succinate)(H_2O)_2]\cdot 2H_2O$, $[Co_2(bpta)_2(adc)(H_2O)_4](ClO_4)_2$, $[Cu_2(bpta)_2(fumarate)(H_2O)_2](ClO_4)_2$, and $[Cu_2(bpta)_2(tdc)(ClO_4)](ClO_4)\cdot 2H_2O$ are isolated. Among the Ni(II) complexes, the fumarate derivative is a square while the adc and succinate analogs are rare examples of complexes with monodentate dicarboxylates that form supramolecular assemblies through extensive hydrogen bonding network of lattice water molecules and uncoordinated oxygen atoms of the carboxylate groups. It is clear from this series that both Co(II) and Cu(II) form mono-bridged dinuclear complexes which are further hydrogen bonded to form supramolecular coordination networks.

Thus further work with Ni(II) carried out to generate $[Ni_2(bpma)_2(adc)_2]\cdot 4H_2O$, $[Ni_2(bpea)_2(adc)_2]$, $[Ni(bpma)(fumarate)(H_2O)_2]$ and $[Ni_2(bpea)_2(fumarate)_2]$. Once again the difference in the bpma complexes for the adc and fumarate linkers is due to coordinated water molecules in the latter. Since there is no effect of the dicarboxylate for the bpea ligand, another derivative with 1,1'-ferrocene dicarboxylate (fcdc), $[Ni_2(bpea)_2(fcdc)_2]\cdot 6.5\ H_2O$, was prepared.

When the chemistry of these tridentate ligands is extended to Zn(II) and Cd(II) for the adc linker, water soluble polymers are obtained: $[Zn_2(bpta)_2(adc)_2]_n$, $[Cd_2(bpta)_2(adc)_2]_n$, $[Zn_2(bpma)_2(adc)_2]_n$, $[Cd_2(bpma)_2(adc)_2]_n$, $[Zn_2(bpea)_2(adc)_2]_n$, $[Cd_2(bpea)_2(adc)_2]_n$ $[Zn_2(bpba)_2(adc)_2]_n$, and $[Cd_2(bpba)_2(adc)_2]_n$. These coordination polymers with d^{10} metal centers show enhanced photoluminescence properties compared to the ligands and linkers present in them.

The last series in this category is for the Mn(II) and Cd(II) with the tricarboxylate linker 1,3,5-benzenetricarboxylic acid (BTC) $\{[Mn_3(bpea)_3(BTC)_2]\}_n$, $\{[Cd_3(bpta)_3(BTC)_2(H_2O)]\cdot 5H_2O\}_n$ and $[Cd_2(bpma)_2(HBTC)_2]_n$ that are synthesized by using the hydrothermal method.

Complexes with Tetradentate Ligands

Compared to the chemistry of Mn(II)-adc with tridentate ligands, for a similar tetradentate ligand, N,N,N-tris(2-pyridylmethyl)amine (tpa), it is expected to have no coordinated water molecule on the hexacoordinated Mn(II) center, for example, and thus the formation of a supramolecular assembly with this ligand will depend on the lattice water cluster. Indeed, it is found that the restriction on the coordinated water molecule for the tetradentate tpa ligand has resulted in the formation of a 3D supramolecular assembly of the dimanganese subunit, $[Mn_2(adc)_2(tpa)_2]$, and a cluster of six water molecules in $[Mn_2(adc)_2(tpa)_2]\cdot 6H_2O$. In addition to this change in the ancillary ligand, the dicarboxylate linker is varied with a triple bond (adc) to double bond (fumarate) to single bond (succinate) in the aliphatic chain structure between the carboxylate groups to show any further effect on the stability and properties of such supramolecular assemblies, particularly the structural diversity in the water clusters. In doing so, respective supramolecular assemblies of $[Mn_2(fumarate)_2(tpa)_2]\cdot 8H_2O$ and $[Mn_2(succinate)_2(tpa)_2]\cdot 6H_2O$ have been isolated and characterized, where the unusual stability of the fumarate analog compared to other two is observed due to the presence of a cyclic quasiplanar hexamer water cluster formed through hydrogen bonding interactions. While a

similar supramolecular assembly of Ni(II)-adc, $[Ni_2(tpa)_2(adc)_2]\cdot 7H_2O$, is obtained but those with Zn(II) and Cd(II), $\{[Zn_2(tpa)_2(adc)_2].6H_2O\}_n$ and $[Cd_2(tpa)_2(adc)_2]_n$ are found to be 1D CPs.

Complexes with Hexadentate Ligands

In this study, the hexadentate ligands with variation in the methylene chain length (2 to 7) between the alkyl nitrogens act as bis(tridentate) ligands and thus provide the dimetal subunit for connecting with various linkers to demonstrate diversity of product formation for the MOCNs outlined in Chapter I. Utilizing such ligands and various linkers (mostly carboxylates), over fifty new MOCNs have been prepared applying the same strategy for the tridentate ligands. These MOCNs have been grouped into various categories depending on the metal center, the carboxylate linker and the polypyridyl ligand used. It should be noted that one of the ligands, tpbn, has been utilized more than the others due to the results obtained with it. Similarly, majority of the MOCNs are made with Mn(II) and Cu(II) while a few examples are there with Zn(II) and Cd(II).

Using Mn(II) ion and adc linker, seven new MOCNs are reported where the formation of discrete to supramolecular to coordination polymers is effected by the methylene chain length in these ligands. $[Mn_2(tpen)_2(adc)](ClO_4)_2$ and $[Mn_2(1,2\text{-}tppn)_2(adc)[(ClO_4)_2$ are the first examples of heptacoordinated Mn(II) complexes with a dicarboxylate where the hexadentate ligand with two methylene groups has wrapped around each Mn(II) center and adc bridges two such Mn(II) centers. Using the tppn ligand with three methylene groups, a 3D supramolecular assembly of $[Mn_2(tppn)(H_2O)_6](adc)_2\cdot 3H_2O$ is obtained; this is one of the rarest example of Mn(II) coordinated to three water molecules or where adc is acting as a counter anion. On the other hand, $\{[Mn_2(adc)_2(tpbn)(H_2O)_2]\cdot 2CH_3OH\}_n$ is a neutral 2D spiral CP where further hydrogen bonding and $\pi-\pi$ interactions make it a 3D MOCN. With 5-7 methylene groups, 1D CP $\{[Mn_2(adc)(tppen)_2(H_2O)_4](adc)\cdot 4H_2O\}_n$, $\{[Mn_2(adc)(tphxn)_2(H_2O)_4](adc)\cdot 2H_2O\}_n$ and $\{[Mn_2(adc)(tphn)_2(H_2O)_4](adc)\cdot 5H_2O\}_n$, which are rare examples of having adc as a linker and a counter anion in the same structure, are obtained; the 1D chains in these three compounds are further connected via both hydrogen bonding and $\pi-\pi$ interactions.

Further to the crucial role played by the ancillary ligand in the Mn(II)-adc chemistry described above, there are four cases where the carboxylate linker is also responsible for self-assembled product formation: (i) the fumarate analog of the tppn ligand is a discrete dinuclear compound,

$[Mn_2(tppn)_2(fumarate)](ClO_4)_2$, different from that for the adc while there is no change in product formation for the tpbn ligand, $\{[Mn_2(fumarate)_2(tpbn)(H_2O)_2]\cdot 4H_2O\}_n$, due to the change from adc to fumarate; (ii) the oxalate linker with no aliphatic chain between the carboxylate groups provides a 1D CP for the tpbn ligand; (iii) the anion directed formation of $\{[Mn_2(tpbn)](ClO_4)_2\}_n$ and $[Mn_2(tpbn)(H_2O)_6](tdc)_2\cdot 4H_2O$, where the same metal salt $Mn(ClO_4)_2$ is used as the starting material in both cases, is really unusual as the latter is the adc analog of the tppn ligand mentioned above; (iv) for the cycloaliphatic dicarboxylate, cdc, a 2D MOF with very different structure compared to those with other dicarboxylates is obtained though the reaction was carried out under hydrothermal conditions.

Utilizing hydrothermal reaction conditions, for H_3BTC and its cycloaliphatic analog, H_3CTC, different products are obtained: a 3D coordination polymer $[Mn_2(tpbn)(HBTC)]_n$ forming a chair like structure with Mn(II) centers acting as nodes; a tetrameric $[Mn_4(tpbn)_2(HCTC)_2(SO_4)_2]$ synthon, where the SO_4^{2-} anion and $HCTC^{2-}$ are bridging between the two Mn(II) centers, for the supramolecular assembly. In both cases, out of the three carboxylic acid groups two are de-protonated and the remaining acid group plays a crucial role in their hydrogen bonding interactions.

Using several aliphatic dicarboxylates, such as fumarate, maleate, succinate, glutarate and adipate, the chemistry of Cu(II) was explored with the polypyridyl ligands. For the tpen ligand, 1D CPs are obtained for succinate, glutarate and adipate, namely $\{[Cu_2(tpen)(succinate)(H_2O)_2](ClO_4)_2\cdot 2H_2O\}_n$. In case of the tppn ligand, similar 1D CPs are formed for glutarate and adipate while an unusual discrete tetrameric compound, $[\{Cu_2(tppn)(H_2O)_2(ClO_4)\}_2(succinate)](ClO_4)_4$, where the dicopper subunit is bridged by the succinate, is formed. For the tpbn ligand, dicarboxylate dependent product formation is observed: only the adipate gives the 1D CP while the succinate and glutarate provide molecular rectangles, $[Cu_4(tpbn)_2(succinate)_2(H_2O)_4](ClO_4)_4$ and $[Cu_4(tpbn)_2(glutarate)_2(H_2O)_4](ClO_4)_4\cdot 4H_2O$. To understand this difference further, derivatives of these three carboxylates are used with the tpbn ligand. With unsaturated derivatives of succinate (fumarate and maleate), 1D CPs $\{[Cu_2(tpbn)(fum)(H_2O)_2](ClO_4)_2\cdot 3H_2O\}_n$ and $\{[Cu_2(tpbn)(maleate)(H_2O)_2](ClO_4)_2\cdot 3H_2O\}_n$, where the alternative Cu(II) centers in the polymeric chain are penta- and tetra-coordinated, respectively, are obtained. Molecular rectangles are obtained for the substituted succinates (mercaptosuccinate and malate). Two derivatives of glutarate, where the central carbon atom in

the chain is replaced with O or S (namely diglyconate and 2,2'-dithioacetate), provide a spiral 1D CP, $\{[Cu_2(tpbn)(digylconate)(H_2O)_2](ClO_4)_2\cdot 2H_2O\}_n$, and a molecular rectangle, $[Cu_4(tpbn)_2(2,2'\text{-dithioacetate})_2(H_2O)_4](ClO_4)_4$, respectively. Similarly, with unsaturated derivatives of adipate (namely c,c-muconate and t,t-muconate) no effect on the product formation is found as both provides the similar 1D CPs, $\{[Cu_2(tpbn)(t,t\text{-muconate})(H_2O)_2](ClO_4)_2\}_n$ and $\{[Cu_2(tpbn)(t,t\text{-muconate})(H_2O)_2](ClO_4)_2\cdot 3H_2O\}_n$. Interestingly, with the tphxn ligand a 1D CP, $\{[Cu_2(tphxn)(succinate)(H_2O)_2](ClO_4)_2\cdot 4H_2O\}_n$, is obtained. The effect of the methylene chain length is further demonstrated in $\{[NaCu_2(tppn)(O,O'\text{-oxydiethylenediglyconate})(ClO_4)(H_2O)_3](ClO_4)_2\}_n$ and $\{[NaCu_2(tpbn)(O,O'\text{-oxydiethylenediglyconate})(H_2O)(ClO_4)](ClO_4)_2\}_2$.

Varying the dicarboxylate from aliphatic to aromatic for the same polypyridyl ligand, namely tpbn, the terephthalate provides the similar 1D CP $\{[Cu_2(tpbn)(tere)(H_2O)_2](ClO_4)_2\cdot 4H_2O\}_n$ while the tetrafluoroterephthalate affords a 2D CP $\{[Cu_4(F_4\text{-tere})_3(tpbn)_2](ClO_4)_2\cdot 4H_2O\}_n$. Another aromatic dicarboxylate, 2,6-pyridinedicarboxylate (2,6-PDC), affords a 1D CP $\{[Cu_2(tpbn)(2,6\text{-PDC})(H_2O)_2](ClO_4)_2\cdot 4H_2O\}_n$ similar to terephthalate. On the other hand, using the cycloaliphatic derivative of terephthalate, CDC, with the tpen ligand a 2D CP $\{[Cu_4(tpen)_2(CDC)_3](ClO_4)_2\cdot 8H_2O\}_n$ is obtained.

The most fascinating chemistry for Cu(II) is obtained with a heterocyclic dicarboxylate, i.e., 2,5-thiophenedicarboxylate (tdc). With tpen, the formation of a octanuclear discrete MOF $[Cu_8(tpen)_4(tdc)_4(H_2O)_4](ClO_4)_8\cdot 4H_2O$ is different from those with tppn, tpbn and tppen where molecular rectangles are obtained $[Cu_4(tppn)_2(tdc)_2(H_2O)_4](ClO_4)_4\cdot 2H_2O$, $[Cu_4(tpbn)_2(tdc)_2(H_2O)_4](ClO_4)_4$ and $[Cu_4(tppen)_2(tdc)_2(H_2O)_4](ClO_4)_4\cdot 4H_2O$. These rectangles show excellent photoluminescence properties arising from the ligand (tdc) to metal charge transfer. On the other hand, a 2D coordination polymer $[Cu_2(tphn)(tdc)_2]_n$ is obtained in which binding of tdc is similar to that of adc found in $\{[Mn_2(tpbn)(adc)_2(H_2O)_2]\cdot 2CH_3OH\}_n$.

While no Cu(II)-adc chemistry could be developed with these ligands, the Zn(II) and Cd(II) derivatives $[Zn_2(tpbn)(adc)_2(H_2O)_2]\cdot 4H_2O$, $[Cd_2(tppn)(adc)_2]$ and $\{[Cd_6(tpbn)_3(adc)_3(H_2O)_3]\}_n$ are obtained. On the other hand, $\{[Cd_2(tpbn)(tdc)_2]\cdot 2H_2O\}_n$ exemplifies the diversity of the chemistry of tdc.

In order to show diversity of MOCNs with H_3BTC and H_3CTC, a few examples of Cu(II), Co(II) and Zn(II) are included: $\{[Cu_6(tpen)_3(CTC)_2](ClO_4)_6\cdot 5H_2O\}_n$ and

$\{[Cu_4(tpbn)_2(BTC)_2(H_2O)_2](ClO_4)_2\}_n$, $[Co_2(tpbn)(HBTC)_2]_n$, $[Zn_2(tpbn)(H_2BTC)(NO_3)_2]$ and $[Zn_2(tpbn)(HBTC)_2]_n$. In the Zn(II) derivatives, anion in the starting material assisted formation of different products under same conditions – a supramolecular assembly of a dinuclear synthon vs. a 3D CP is observed.

Extending the chemistry of dicarboxylates, disulphonates are utilized as linkers for Cu(II) and the hexadentate ligands. Three such compounds are reported here: $[Cu_2(tpen)_2(2,6\text{-}NDS)_2(H_2O)_4]\cdot 8H_2O$, $\{[Cu_4(tppn)_2(Cl)_2(H_2O)_4](2,6\text{-}NDS)_2\cdot 14H_2O\}_n$, $\{[Cu_2(tpbn)(2,6\text{-}NDS)(Cl)_2]\cdot 5H_2O\}_n$, where 2,6-NDS = 2,6-naphthalene disulphonate. In this series the most notable difference is the binding of 2,6-NDS. In case of tpen, it is a dinuclear Cu(II) compound with NDS binding in a monodentate fashion; in case of tppn, a Cl-bridged cationic polymer with NDS acting as a counter anion is obtained; in case of tpbn, NDS is binding in a bis(monodentate) fashion resulting in a 1D CP.

Finally, using a few nitrogen linkers two 1D CPs $\{[Cu_2(tpbn)(4,4'\text{-}bpy)(H_2O)_2](ClO_4)_2\cdot 3H_2O\}_n$ $\{[Cu_2(tpbn)(N_3)_2(H_2O)_2](ClO_4)_2\}_n$ are obtained. It is notable that a similar product with bis(pyridyl)ethene (bpe) could not be isolated under the conditions tried.

In Chapter IV (Conclusions and Future Directions), based on the study described in this thesis conclusions are drawn and comments on future directions are made. In this work the role of ancillary ligands in generating diverse MOCNs with the same or different linker carboxylate is demonstrated in many ways. Both porous and non-porous MOCNs are obtained depending on the ancillary ligand. Supramolecular assemblies are formed in various cases via strong hydrogen bonding. For a tetradentate ligand encapsulation of hexamer of water is the result of a specific carboxylate linker in the system. Structural diversity of MOCNs is also established based on the length of the methylene link between the alkyl nitrogens of the hexadentate ligands. Due to changes in the carboxylate linker different MOCNs are formed. The solid-state structures were determined by single crystal XRD while bulk purity was confirmed by powder XRD. Spectroscopic and thermal properties of these compounds were studied by FTIR, Raman, DSC and TGA, respectively. Their redox behavior by cyclic voltammetry and photoluminescent properties by fluorescence spectroscopy in the solid state were studied. Applications of these MOCNs in gas adsorption, host-guest chemistry, etc., were explored. Using some of these MOCNs water adsorption studies has indicated their suitability in desiccant and adsorbent

cooling applications but can be optimized to show their real use compared to zeolites and silica gels. Based on the photoluminescent properties of selected MOCNs, further studies, particularly with Lanthanides, will provide a new direction in this field. With a database of compounds from this work, chemical modifications of the ligands and linkers should focus on their use in various applications.

CHAPTER I

Introduction

Coordination compounds with or without polymeric structures showing zeolite-like properties to reversibly absorb small molecules have long been known dating back to the reports for the use of Werner complexes [β-M(4-methylpyridyl)$_4$(NCS)$_2$] (where M(II) = Ni(II) or Co(II)), Prussian blue compounds $Fe_4[Fe(CN)_6]_3 \cdot xH_2O$, and Hofmann clathrates and their derivatives $M(NH_3)_2M'(CN)_4 \cdot 2G$, where M = Ni, Mn or Cd, M′ = Ni or Pd, while G is benzene or thiophene.[1-4] However, this field did not get much attention for a long time. On the other hand, a tremendous growth in the chemistry of supramolecules since the discovery of crown ethers about 45 years ago has enabled researchers from various fields to utilize the learnings from it.[5-7] Although there is an early report on the use of organic bridging ligands to form the porous coordination polymer, $[Cu(NO_3)(adiponitrile)_2]_n$, with a diamond net,[8] an upsurge in the chemistry of metal ions and organic linkers was seen only about 15 years ago in search for materials that can mimic porous materials, such as zeolites, metallophosphates, activated carbons or mesoporous solids.[9-10] This started with the seminal work by Robson et al. in 1990 for a porous coordination polymer capable of an anion exchange.[11] Subsequently, the catalytic properties of the 2D coordination polymer $\{[Cd(4,4'\text{-bpy})_2]^{2+}\}_n$ were studied by Fujita et al. in 1994[12] followed by the adsorption of guest molecules studied by the groups of Yaghi[13], Moore[14], and Kitagawa[15] in next few years. Thus in recent years a large number of such compounds has been synthesized and crystallographically characterized for their diverse structural aesthetics[16-28] and for a variety of potential applications in catalysis,[29-43] separation,[44-48] sensors,[49-52] gas storage,[53-65] luminescent materials,[66-71] ion exchange,[72-73] magnetism,[74-83] etc. In all such cases, in addition to the metal-donor atom coordinate bonds a special consideration of supramolecular interactions,[5,84-93] such as strong and/or weak hydrogen bonds, π-π stacking of aromatic moieties, C-H…O interactions, etc., has been given to describe the formation of infinite one-, two-, and three dimensional (1D, 2D, and 3D) networks. While the terms coordination polymers (CPs) and metal organic frameworks (MOFs) have been used for the corresponding compounds, there is a

lack of a general term to include all networks arising from further interactions of discrete metal subunits including those forming triangles, squares, rectangles, etc., as well as CPs and MOFs. Therefore, a general term metal organic coordination networks (MOCNs) is used in our research group to describe all these as classified below.[94]

Components of MOCNs

In order to understand the background of this research, an MOCN is defined first with respect to its components. As shown schematically in Figure 1.1, major components of an MOCN are a metal ion, a linker and an ancillary ligand. The metal ion is usually a transition metal ion (or a lanthanide) with varied coordination numbers providing different dimensionalities of the MOCNs. A metal ion in combination with an ancillary ligand forms the metal center which is also called a secondary building unit (SBU).[20,95-101] A linker joins the metal centers to form a framework - proper design of such linkers add flexibility and diversity to the overall structure of the framework. While neutral and anionic organic linkers are the most widely used, a few examples of cationic organic linkers are also known. Examples of neutral linkers are nitrogen-based organic moieties, such as pyrazine, 4,4'-bipyridine. Anionic linkers are mostly di-, tri-, and tetra-carboxylates, such as acetylene dicarboxylate, terephthalate, 1,3,5- benzenetricarboxylate.

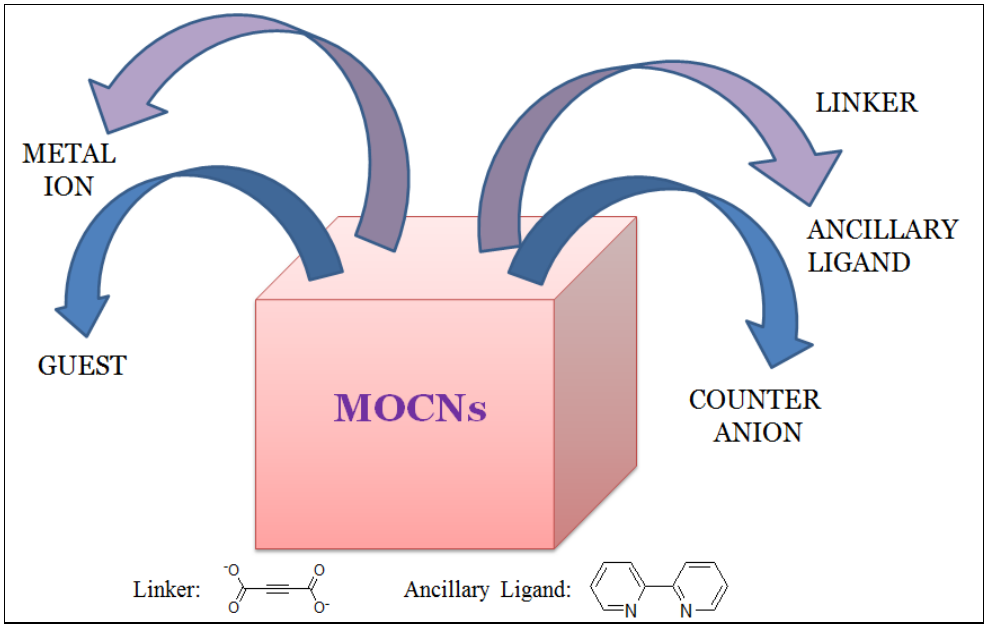

Figure 1.1. Components of MOCNs.

Cationic linkers are based on N-aryl pyridinium and 4,4'-bipyridinium derivatives. The nature of the organic linkers determines the size and shape of the pores in the framework. The longer organic linkers allow the formation of much larger pores than what is accessible through single oxygen linkers (as in the case of zeolites). Most of the MOCNs are neutral or cationic in nature. If the MOCN is cationic, the charge is balanced by the presence of a counter anion. Lastly, the presence of guest molecules in it is due to the fact that pores are usually filled with solvent molecules, such as water.

Proposed Classification of MOCNs

In the literature the use of different terminologies for the products reported has been confusing to some extent. There is a proposal[102] to have a consensus for it but no official recommendation by the IUPAC has come out yet. In order to cover all products made from the combinations of metal ions (or metal centers) and organic linkers, these MOCNs can be classified into three categories as shown in Figure 1.2 - CPs, MOFs (which are porous in nature) and supramolecular coordination networks (SCNs). The last category, SCNs, can be formed by CPs, squares and rectangles, dimers and monomers with various supramolecular interactions, such as hydrogen bonding and π–π interactions.

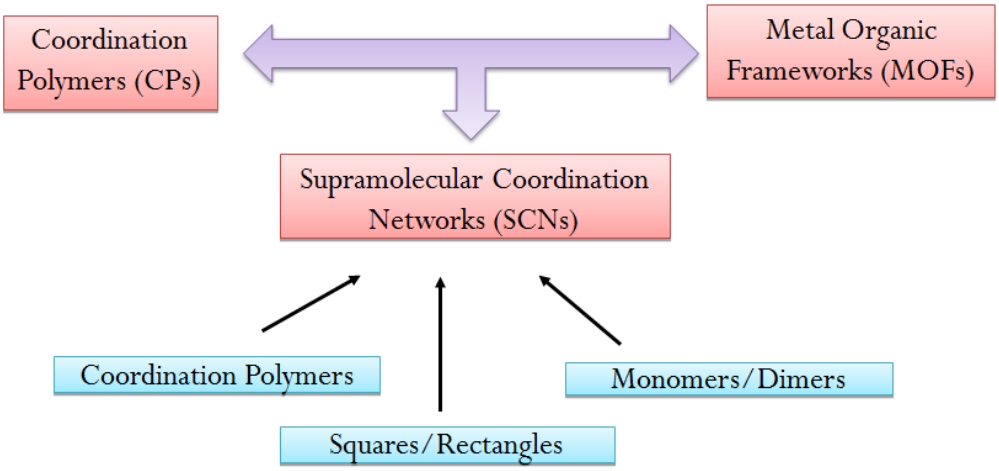

Figure 1.2. Proposed Classification of MOCNs.

Various combinations of the components that are unlimited can provide a large number of MOCNs with flexibility in their supramolecular interactions and pore sizes. Structural diversity

arising from the variable coordination numbers of the metal centers as well as different binding modes of linkers has resulted in new topologies.[103-108] Modulation of physical properties is the key to improving the target parameters for their applications. Some of these MOCNs provide examples of 2D or 3D coordination architectures with very unusual topologies.

In the schematic representation below, the formation of various MOCNs are considered (the red filled oval represents a metal center whereas the blue small oval represents an open site on the metal center). If a hexacoordinated metal center has two open sites at an angle of 180°, then with a bifunctional linker it will form a 1D CP (linear type). Whereas if the two open sites at the hexacoordinated metal center are at an angle of 90°, then either a 1D CP (zig-zag type) or a square can be the product with a bifunctional linker. This is shown in Figure 1.3. In the above two cases for hexacoordinated metal center providing CPs, the geometry is expected to be octahedral and a choice of ancillary ligand with respect to denticity (two or four) and flexibility will make it possible to have the open sites at an angle of 180° or 90°. It should be noted that (a) a metal center having two open sites at an angle of 90° and two bifunctional linkers connecting

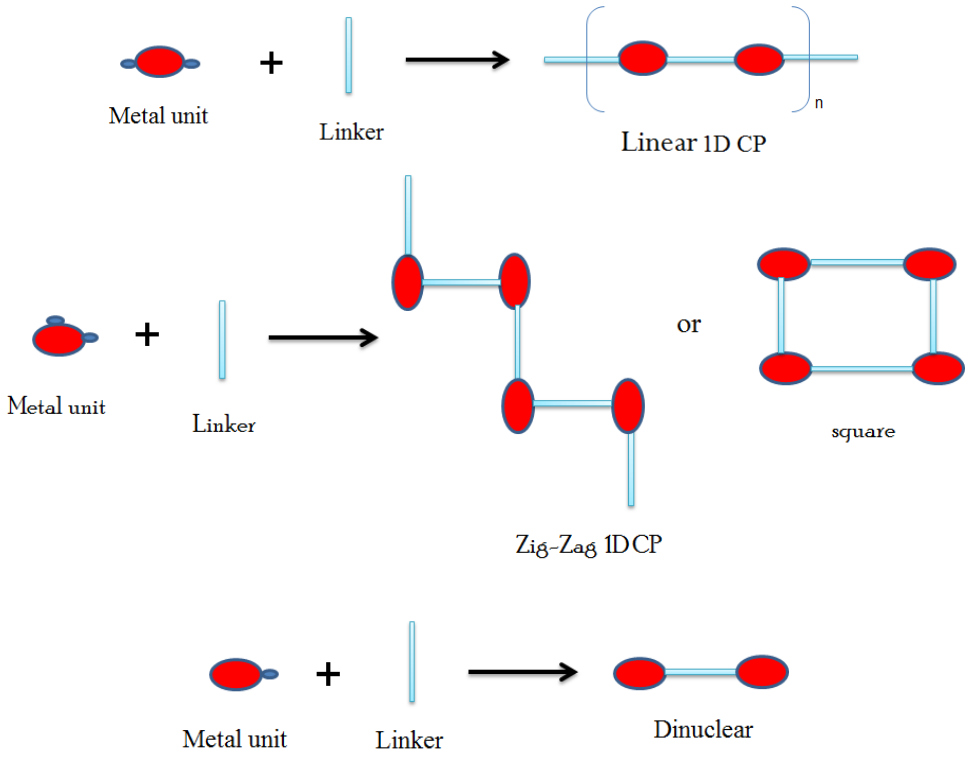

Figure 1.3. Schematic representation of the formation of various products including 1D CPs (linear or zig-zag type) and squares.

two such metal centers will form a rectangle or square, (b) a metal center with only one open site with a bifunctional linker connecting two such metal centers will yield a dinuclear compound. Thus the ratio of the components as well as number of linkers between the metal centers are also important. While the literature is filled with a large number of examples of the linear-style 1D CP,[109-110] there are only a limited number of step-style 1D CP.[111-112] There are numerous examples of squares with square-planar metal centers[113-114] but a few could be found with the square pyramidal metal centers.[115-116] On the other hand, the formation of squares by the octahedral metal center is rare.

With one open site on each metal center in a dimetal subunit (which can be a metal-metal bonded[117-118] or two metal centers connected by a spanning ligand[119-120]) a bifunctional linker will give either a 1D CP if the open sites are at trans position or a square/rectangle if the open sites are at cis position. All these combinations are shown in Figure 1.4.

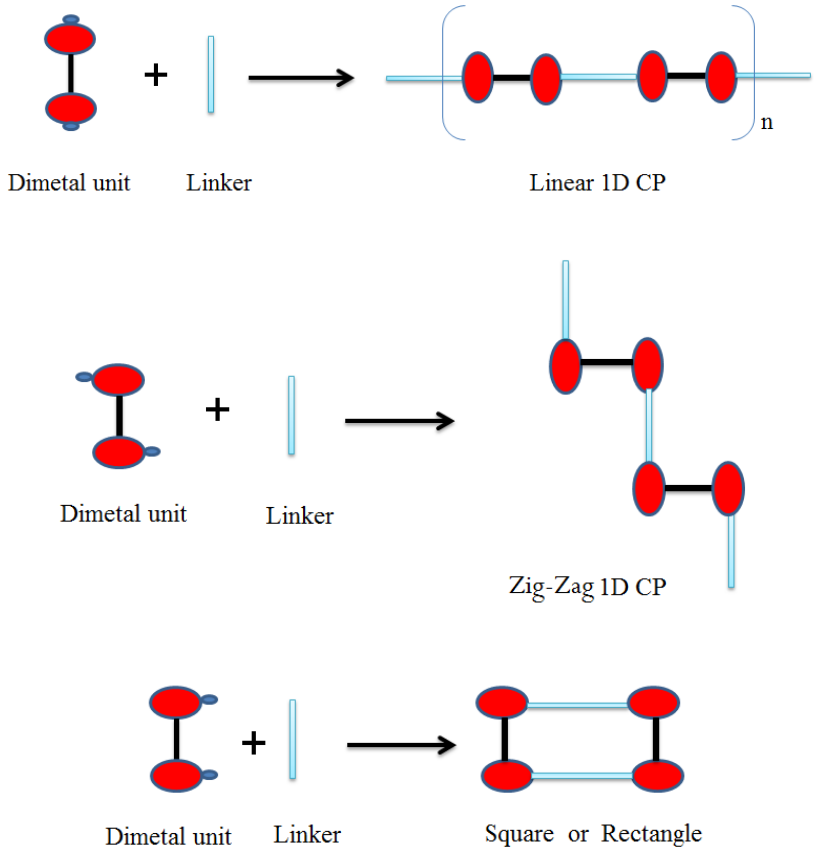

Figure 1.4. Schematic representation of the formation of various products including 1D CPs and squares/rectangles.

Similarly, if a metal center has three open sites it will form a 2D MOF whereas a 3D MOF will be formed by a metal center with four open sites (see Figure 1.5). In the literature there are many examples of 2D and 3D MOFs but with mostly carboxylates.[16,121-122]

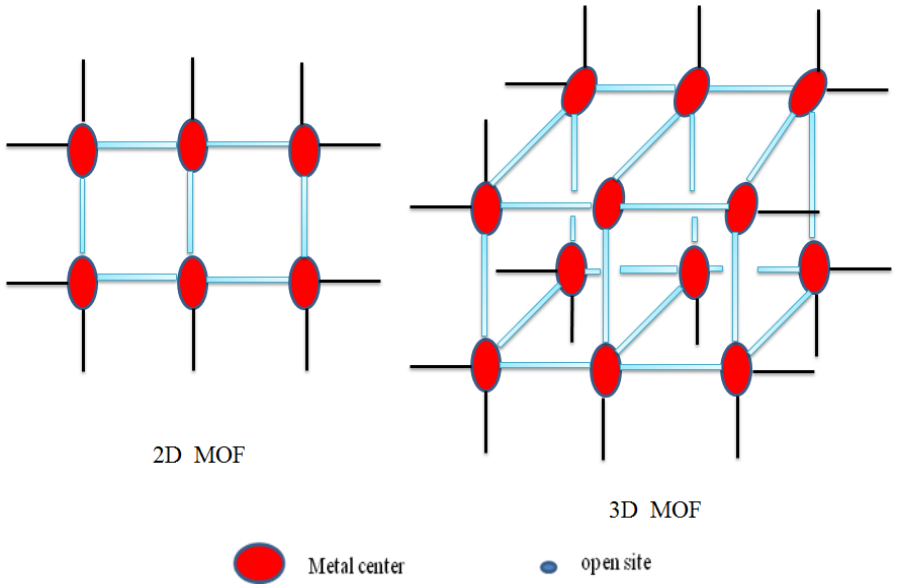

Figure 1.5. Schematic representation of the formation of 2D and 3D MOFs.

Further association of the 1D or 2D MOCNs through strong and/or weak hydrogen bonds, π-π interactions of aromatic moieties or C-H…O interactions, etc., generates supramolecular assemblies of higher dimensions. Two layers of a coordination polymer can form a supramolecular coordination network via weak interaction, such as hydrogen bonding, π–π, and other weak interactions (see Figure 1.6).

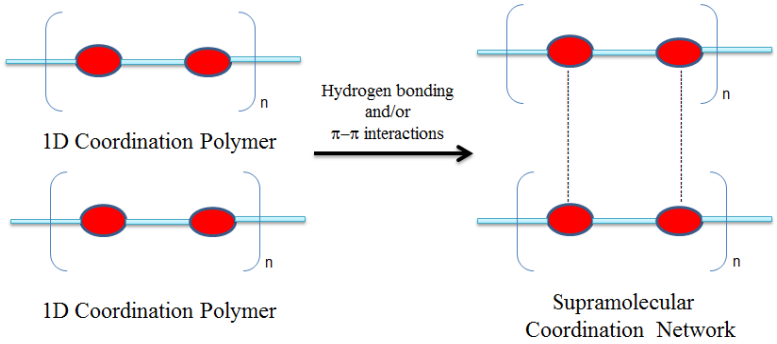

Figure 1.6. Formation of an SCN of 1D CPs.

With functionalities, such as coordinated water molecules and/or aromatic rings from the ligands, available for viable supramolecular interactions, squares/rectangles can also form supramolecular coordination network as shown in Figure 1.7.

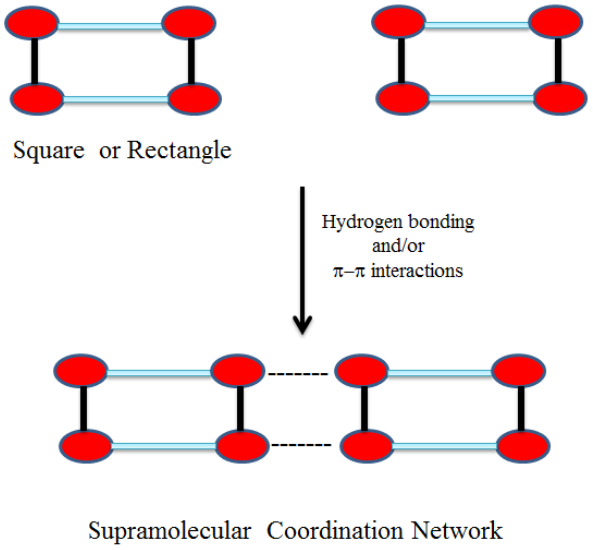

Figure 1.7. Formation of a SCN of Squares/Rectangles.

Motivation for Research in This Field

Until mid 1990, there were basically two types of porous materials, namely, carbon-based materials[123-124] and inorganic materials.[9-10] Zeolites, which are hydrated alkaline or alkaline-earth aluminosilicates with the general formula $M^{n+}_{x/n}[(AlO_2)_x(SiO_2)_y]_x \cdot wH_2O$ (M = metal), belong to one of the major classes among the inorganic materials. Due to their microporous and crystalline nature, zeolites are used in water treatment, separation and catalysis. The maximum size of the molecular or ionic species that can enter the pores of a zeolite is controlled by the dimensions of the channels. The porosity is then provided through the elimination of the water molecules while the framework usually remains unaffected by this.

However, there are less than 200 unique zeolite frameworks identified to date, and over 40 naturally occurring zeolite frameworks are known. Futhermore, these are 100% inorganic in nature, have rigid and small pores with very little flexibility, and lack further modifications, if required. Since the number of zeolites is limited, the need for synthetic porous materials has

prompted researchers to start the new field that uses both organic and inorganic components bridging the gap between the two classes of porous materials mentioned above.

Synthetic Methods for MOCNs

MOCNs are prepared from a variety of metal centers or metal atom clusters and multiatom organic linkers.[16b,21,101,125] Ancillary ligands that are part of metal centers play an important role in the formation of MOCNs as the number of open sites available at the metal center depends on the denticity and binding of the ancillary ligand which determines the dimensionality of the MOCN. Additionally, the use of ancillary ligands provides a way to have better solubility of the MOCNs than those with mostly carboxylates.[16, 121-122]

Although a large number of MOCNs are reported in the literature, development of general methods that can be used for similar systems is required. One of the reasons the traditional one pot synthesis at room temperature to make MOFs is less favored is the difficulty in crystallizing the MOFs which often are not soluble in most of the solvents. In overcoming this issue, various methods of crystallization have also been used to obtain suitable single crystals of MOCNs directly; one of these is slow diffusion of reactants into each other from the layering of solutions of reactants,[126] and the second is solvent evaporation in which crystals can be easily grown by evaporation of excess solvent.[127]

Over the years, the most used method is the hydro/solvothermal synthesis[125a] where the reaction takes place in a closed vessel under autogenous pressure above the boiling point of the solvent.[16b] In this method, all the reactants are placed with a solvent (or a mixture of solvents), preferably water, in a bomb reactor which is then put inside a programmable oven under high temperature (120-180 ^{o}C) for 2-3 days; the bomb is allowed to cool slowly over 10-24 hours affording good quality crystals of MOCNs directly. However, this method often suffers from a few drawbacks - irreproducibility of products and insoluble nature of products do not allow any studies in the solution state.

Other methods that have also been reported are microwave-assisted synthesis,[16b,128a-d] sonochemical synthesis,[16b,129] mechanochemical synthesis,[16b,130] and electrochemical synthesis.[16b,131] In recent times,[128e] microwave-assisted synthesis has attracted a lot of attention

due to its green nature as well as much shorter reaction time through acceleration of the rate of chemical reactions in presence of microwave-absorbing solvents. In this case, direct interaction of the microwave radiation with the reactants in the solvent occurs making it an energy-efficient method. Similarly, in the sonochemical synthesis high-energy ultrasound waves which produce very high local temperatures (greater than 5000 K) resulting in extremely fast heating and cooling rates yield small MOCN crystals with decreased reaction times. Lastly, the mechanochemical synthesis which involves grinding the metal salt with the linker together in a ball mill to produce the desired MOCN is used for a selected examples.[130c,132]

Many groups in the world are involved in the generation of MOCNs but most of them use only carboxylates[16,121-122] and to some extent phosphonates[133,134] and sulphonates[134] or in combination with neutral N-donor linkers based on pyridyl, imidazole, nitrile groups.[135] Several thousands of MOCNs have been reported until now. The use of many bidentate ancillary ligands, like 2,2′-bpy or 1,10-phenanthroline, has been reported but only a limited number of tridentate or tetradentate ligands is used prior to this work.[119-120,136] More imporantly, MOCNs with the tridentate and tetradendate ligands[137]chelating to the same metal center is rare.

Applications of MOCNs

In addition to their structural diversity, MOCNs with porous nature can offer a number of potential applications in the fields of energy, environment, medicine, industry and host-guest studies. Their use in these fields as storage materials, separators, sensors and catalysts has been the key motivations for researchers around the world to design and develop such species. A few such applications are discussed further for relevance to this work. For demonstrating their viability in storing gases, such as hydrogen and methane which are potential alternate fuel source, MOCNs have been studied in gas adsorption experiments at low temperatures.[138-139] Similarly, separation of gases by MOCNs is crucially important in purification and sequestration of carbon dioxide that is a major area of interest from an environmental point of view; this is demonstrated through selectivity in gas adsorption experiments.[16d,21,140]

Adsorption of mositure by the MOCNs and MOFs in particular drives several important applications. Two such examples are: *sensors* and *drug delivery agents*. Achmann et al. demonstrated the use of an iron-trimesic acid based MOF as humidity sensor. Morris et al.

showed the adsorption of NO at room temperature and its release when exposed to moisture by Co(II) and Ni(II) based MOFs.[141a] The main principle behind these applications is adsorption of water molecules from the environment causes a change in impedance of the MOF.[141b] On the other hand, the use of MOCNs for *desiccant and adsorbent coolant* applications are based on the ability for reversible adsorption of water at room temperature.[142]

Thus the porosity is one of the most targeted properties of supramolecular assemblies as there exist channels and cavities required for a number of applications mentioned earlier. Due to the existence of such large channels and cavities, these are expected to mimic the functions of traditional zeolites and clays, which are limited in the literature.[9-10] In this respect, removal or exchange of guest molecules in the host assemblies through the solid state transformations, such as single crystal to single crystal (SC-SC) transformation, is a difficult but achievable route where formation of a stable lower dimensional assembly is unique. If this structural transformation is reversible in nature, then investigation of the dehydrated and rehydrated species not only allows one to understand its formation but more importantly provide an opportunity to use it in various applications ranging from molecular recognition and separation to gas storage and sensing.[16-24] Although there are several examples reported in the literature where the 2D and 3D assemblies are generated from with or without metal subunits and water clusters via supramolecular interactions but these normally break down upon dehydration.[143-146]

Water plays a very important role in many biological and chemical processes and has received continued scientific investigations, both experimental and theoretical, to unravel its unique properties with a special focus on structure-function relationships.[147-149] Thus, the study of water has attracted researchers from numerous fields to gain insights into its diverse structural modifications found in these processes.[150] In addition to the continued study of its bulk properties, some of which are considered anomalous,[151] a considerable effort has been put into the structural investigations of various water clusters including tetramers, hexamers, octamers, etc., for probing the stabilization and functionalization of biomolecules as well as developing new functional materials.[152] Water clusters (discrete and polymeric)[153] are formed through hydrogen bonding interactions between the water molecules and the diversity in their structural arrangement originates from the surroundings that provide the most stable geometry. The key to understanding the behavior of these water clusters is to determine the precise structural

parameters that also include the interactions with the surroundings and to compare with those observed in water and ice.[147] In recent years, an upsurge of scientific papers reporting the formation of such assemblies of various nuclearity with different structural networks has come from the study of water clusters encapsulated (or enclathrated) in the metal organic frameworks (MOFs). Numerous groups including ours are involved in such study that is aimed at designing new materials for their possible applications in magnetochemistry, chemical technology and host-guest chemistry.[5,16-24,74,94,154] Furthermore, the formation of supramolecular assemblies due to the hydrogen bonding interactions of water clusters of various sizes with metal subunits provides excellent opportunities for host-guest chemistry. Modulation of the water clusters with respect to their structural diversity is a way to generate materials with varied properties required in various applications ranging from molecular recognition and separation to gas storage and sensing. Additionally, their use in water adsorption applications such as desiccant and adsorbent coolant are sought to develop materials as an alternative to zeolites and silica gel, for example. However, examples of 3D supramolecular assemblies constructed from metal subunits (termed as SCNs in this thesis) and water clusters are still limited in the literature.[155-156]

Scope of the Present Research

Although a large number of MOCNs has been reported, continued interests in this field are due to obtaining functional mimics of those existing materials, such as zeolites and silica gel. Thus the plan for the proposed research was as follows:

- Utilization of tri-, tetra-, and hexadentate ancillary ligands (shown in Figure 1.8) in combination with various linkers (shown in Figure 1.9) for the synthesis of new MOCNs at ambient conditions
- Generation of selected MOCNs under hydrothermal conditions with reproducible results
- Systematic studies to identify the factors responsible for the formation of these materials
- Further modifications in the ancillary ligands to show structural diversity of the product with new topologies
- Their structural characterization, spectroscopic and thermal properties
- Demonstration of their use in some applications, like water adsorption, photoluminescence, etc.

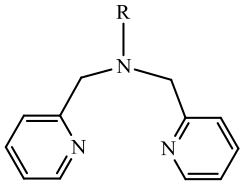

R = CH_3, bpma = N, N'-bis(2-pyridylmethyl)-methylamine
R = C_2H_5, bpea = N, N'-bis(2-pyridylmethyl)-ethylamine
R = $CH(CH_3)_2$, bpipa = N, N'-bis(2-pyridylmethyl)-isopropylamine
R = $C(CH_3)_3$, bpta = N, N'-bis(2-pyridylmethyl)-t-butylamine
R = $CH_2C_6H_5$, bpba = N, N'-bis(2-pyridylmethyl)-benzylamine

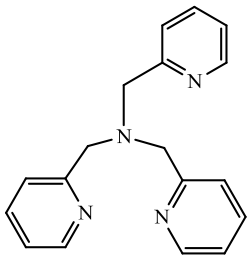

N,N',N''-tris(2-pyridylmethyl)-amine (tpa)

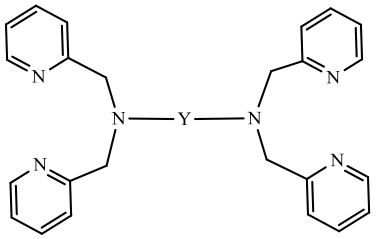

Y = CH_2, tpen = N,N, N',N'-tetrakis(2-pyridylmethyl)-1,2-diaminoethane
Y = CH_2-$CH(CH_3)$, 1,2-tppn = N,N, N',N'-tetrakis(2-pyridylmethyl)-2-methyl-1,2-diaminoethane
Y = $(CH_2)_3$, tppn = N,N, N',N'-tetrakis(2-pyridylmethyl)-1,3-diaminopropane
Y = $(CH_2)_4$, tpbn = N,N, N',N'-tetrakis(2-pyridylmethyl)-1,4-diaminobutane
Y = $(CH_2)_5$, tppen = N,N, N',N'-tetrakis(2-pyridylmethyl)-1,5-diaminopentane
Y = $(CH_2)_6$, tphxn = N,N, N',N'-tetrakis(2-pyridylmethyl)-1,6-diaminohexane
Y = $(CH_2)_7$, tphn = N,N, N',N'-tetrakis(2-pyridylmethyl)-1,7-diaminoheptane

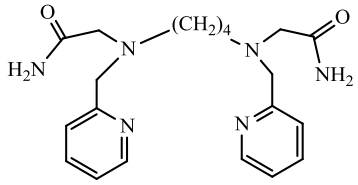

bpbg = N,N'-bis(2-pyridylmethyl)-N,N'-bis(glutamate)-1,4-diaminobutane

Figure 1.8. Ancillary ligands used in this study.

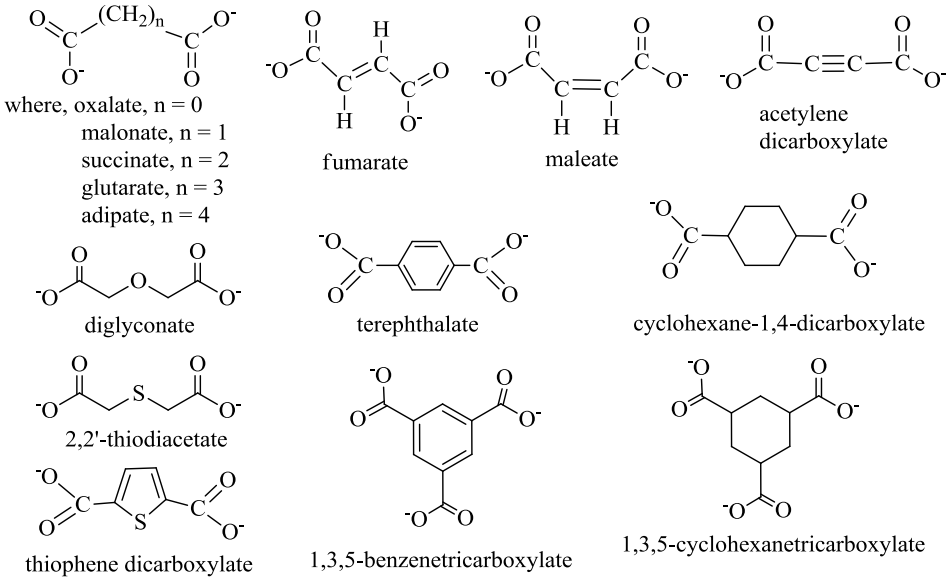

Figure 1.9. Structures of the carboxylates used in this study.

There are several challenges for the above plan. Some of these are listed below:

- For a six-coordinated metal ion, as shown in Figure 1.10, the formation of a 1:2 complex (for the tridentate ligands) or 1:1 complex (for the hexadentate ligands) will prohibit the isolation of the desired polymeric MOCN in good yields and high purity. Thus the selection of ancillary ligands along with the multiatom organic linkers is crucial.
- As the molecular structures of the MOCNs are the keys to establishing their structure-property-function relationship, solubility of the MOCNs in common organic solvent could be a hurdle to grow suitable crystals for carrying out single crystal X-ray studies.
- For a systematic change in organic linkers, obtaining diverse MOCNs with the same framework structure or for the same ligand, constructing MOCNs with several different structures are limited in the literature.

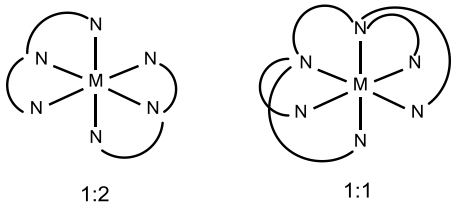

where M = metal center and N represents donor atoms from the ligand.

Figure 1.10. Schematic drawings of the 1:2 and 1:1 complexes.

Outcome of the Present Research

In the present work, the strategic design and development of a variety of MOCNs are reported. Three general methods - two at ambient conditions and one at hydrothermal conditions - have been developed to prepare over 100 MOCNs comprised of divalent transition metal ions, polydentate ancillary ligands and mostly multiatom carboxylate linkers have been synthesized in good to high yields. The majority of them are prepared by the methods at ambient conditions while the rest under hydrothermal conditions are reproducible. For making these MOCNs several ancillary ligands (with improved yields and purity) have also been synthesized and characterized. All MOCNs were characterised by elemental analysis, FTIR spectroscopy, UV-visible spectroscopy, mass spectrometry, single crystal and powder X-ray diffractometry. These are studied for their redox behavior by cyclic voltammetry, and thermal properties by thermogravimetric analysis. Their photoluminescent properties are established by fluorescence spectroscopy in the solid state. Several of these MOCNs are found to be porous (termed as MOFs) and have been tested for their water adsorption.

CHAPTER II

Experimental Section

2.1 Materials and Methods. All chemicals and solvents used for synthesis were obtained from commercial sources and were used as received, without further purification. All reactions were carried out under aerobic conditions unless otherwise stated. Ancillary ligands were prepared either by modifying[94b] or following procedures reported in the literature.[157-160]

2.2 Physical Measurements.

^{1}H NMR spectra of the ligands were obtained in $CDCl_3$ solution at 25 ℃ on a Bruker ARX-400 spectrometer; chemical shifts are reported relative to the residual solvent signals (e.g., $CDCl_3$: δ = 7.26 ppm). Each sample was prepared taking 5-10 mg of the compound in approx. 1 mL of the deuterated solvent. Each data obtained was analyzed and plotted using either TOPSPIN software by Bruker or Spinworks.

Melting points (M.p.) were measured on a *Büchi Melting and Boiling Point apparatus*. All melting points have been measured in open melting point capillaries.

Elemental analysis (C, H, N) was carried out using a Mettler CHNS analyzer at NIPER Mohali, a Varian at CSMCRI-Bhavnagar and a ThermoFisher at PU Chandigarh.

IR spectra were recorded in the 4000−400 cm^{-1} range on a Perkin-Elmer Spectrum I spectrometer with samples prepared as KBr pellets. The solid sample was grounded with predried KBr in a 2:98 w/w ratio and the pellet was made using a die set and a hydraulic press. The pressure in hydraulic press was kept at 150 Kg/cm^2 for a minute. Few IR spectra were recorded using ATR attached to the Agilent Cary 650 Spectrometer. For ATR neat solid sample was used. Spectra for oily samples were collected using KBr plates. Each data set obtained was analyzed with either Spectrum v5.3.1 software by Perkin Elmer or ResPro by Agilent technologies.

UV-Visible spectra were recorded in the solution state using either a Perkin Elmer Lambda 25 UV-Vis spectrometer or a Cary 60 by Agilent Technology. A 1 to 2 mM solution of the sample was prepared in an appropriate solvent. Each data set obtained was analyzed with either Perkin Elmer UV WinLab 5.2 or Cary 60 software.

Electrochemical measurements were carried out using the Epsilon model by Bioanalytical Systems with a three-elctrode set-up. In each case, for a 2 mM solution of the compound in a solvent, a solution of 0.2 M tetrabutyl ammonium perchlorate in the same solvent is used as the supporting eletrolyte. The scan rate was between 50-100 mVs^{-1}. A blank run is always done with the supporting electrolyte to show a narrow (indicating minimum current) scan in the range of +1.5 V to -1.0 V confirming the proper functioning of the instrument. Under the conditions each measurement was done, the instrument was calibrated with ferrocene that provided an $E_{1/2}$ value of 0.53 V for Fc/Fc^{+} (with ΔE = 70 mV and i_a/i_c = 1) against the SCE.

Thermogravimetric analysis was carried out using either a Mettler Toledo 851 E or a TA Shimadzu instrument. The sample to be analyzed was weighed using an analytical balance, put in a pan and weighed again using the microbalance of the instrument to avoid any discrepancy. The samples were heated from 25 to 500 °C at a rate of 10 °C/min under nitrogen atmosphere. The data obtained was analyzed using TA 60 software.

Solid State fluorescence spectra were measured using HORIBA Fluorolog-3 spectrofluorometer. The data was analyzed with FluorEssence^{TM} software.

Raman spectra were recorded on a Renishaw InVia Raman microscope equipped with a 785 nm high-power near-infrared laser working at 300 mW power and a Renishaw CCD detector. Analysis of the Raman spectra was performed in reflection mode on powder samples placed on the sample stage and aligned in the optical path by using a camera, with 10−50% laser power and by using 20−50× optics in the range 200−4000 cm^{-1}. The data obtained was analyzed using the software provided with the instrument.

Water adsorption measurements were measured for pressures in the range 0–1.2 bar by the volumetric method using a BELSORP instrument. Each solid sample was transferred to pre-weighed analysis tubes, which were capped with transeals and evacuated by heating at a temperature between 110-150 °C (based on thermal profile obtained from TGA) under dynamic

vacuum until an outgas rate of less than 2 mTorr min^{-1} (0.27 Pa min^{-1}) was achieved (ca. 12-24 hrs). The evacuated analysis tubes containing the degassed sample was then carefully transferred to an electronic balance and weighed again to determine the mass of sample. The tube was then placed back on the analysis port of the gas adsorption instrument. The outgas rate was again confirmed to be less than 2 mTorr min^{-1} (0.27 Pa min^{-1}). For all isotherms, warm and cold free-space (dead volume) correction measurements were performed using ultra-high-purity He gas (UHP grade 5.0, 99.999% purity). The change of the pressure was monitored and the degree of adsorption was determined by the decrease in pressure at the equilibrium state via computer controlled automatic operations that are set up at the start of each measurement. Oil-free vacuum pumps and oil-free pressure regulators were used for all measurements to prevent contamination of the samples during the evacuation process or of the feed gases during the isotherm measurements.

Single Crystal X-ray Studies were performed on a Kappa APEX II diffractometer equipped with a CCD detector (with the crystal-to-detector distance fixed at 60 mm) and sealed-tube monochromated MoKα radiation. Crystals of MOCNs suitable for the single crystal X-ray study were grown from various methods, such as slow evaporation, slow cooling, layering and direct layering of the reactants. Crystals of the compounds were transferred from mother liquor to mineral oil for manipulation, selection and mounting, and were then transferred to a thin glass fiber or nylon loop on a goniometer head. Those studied at non-ambient temperature were placed under a cold stream of nitrogen gas at 296 K followed by slow cooling or heating to the desired temperature for the experiment in each case. The diffractometer was interfaced to a PC that controlled the crystal centering, unit cell determination, refinement of the cell parameters and data collection through the program APEX2.[162] For each sample, three sets of frames of data were collected with 0.30° steps in ω and an exposure time of 10 s within a randomly oriented region of reciprocal space surveyed to the extent of 1.3 hemispheres to a resolution of 0.85 Å. By using the program SAINT[162] for the integration of the data, reflection profiles were fitted, and values of F^2 and $\sigma(F^2)$ for each reflection were obtained. Data were also corrected for Lorentz and polarization effects. The subroutine XPREP[162] was used for the processing of data that included determination of space group, application of an absorption correction (SADABS),[162] merging of data, and generation of files necessary for solution and refinement. The crystal

structures were solved and refined using SHELX 97.[163] In each case, the space group was chosen based on systematic absences and confirmed by the successful refinement of the structure. Positions of most of the non-hydrogen atoms were obtained from a direct methods solution. Several full-matrix least-squares/difference Fourier cycles were performed, locating the remainder of the non-hydrogen atoms. In certain structures, occupancy factors of some atoms were adjusted to have reasonable thermal parameters and converged refinement resulting in the lowest residual factors and optimum goodness of fit. All non-hydrogen atoms, except where indicated otherwise, were refined with anisotropic displacement parameters. All hydrogen atoms were placed in ideal positions and refined as riding atoms with individual isotropic displacement parameters. Crystallographic parameters and basic information pertaining to data collection and structure refinement for all compounds are summarized in Appendix (Tables A1-A37). All figures were drawn using Mercury V 3.0,[164] OLEX2,[165] and ORTEP[166] and hydrogen bonding parameters were generated using PLATON.[167] The topological analysis of some compounds was done using the TOPOS software.[168]

Powder X-ray Studies were done on a Rigaku Ultima IV diffractometer equipped with a 3 KW sealed tube Cu Kα X-ray radiation (generator power settings: 40 kV and 40 mA) and a DTex Ultra detector using parallel beam geometry (2.5° primary and secondary solar slits, 0.5° divergence slit with 10 mm height limit slit). Each sample grounded into a fine powder using a mortar and a pestle was placed on a glass sample holder that was placed on the sample rotation stage (120 rpm) attachment. The data were collected over an angle range 5° to 50° with a scanning speed of 1 to 2° per minute with 0.001° step with XRF reduction for metal complexes.

2.3 Synthesis of Ancillary Ligands

2.3.1 Tridentate ligands

N,N′-bis-(2-pyridylmethyl)-methylamine (bpma). To a solution of 0.54 g (0.08 mmol) of methylamine hydrochloride in 5 mL water placed in 50 mL RBF, 0.32 g (0.08 mmol) of sodium hydroxide was added. The solution was stirred for 5 minutes followed by the addition of 2.62 g (0.016 mmol) of 2-picolylchloridehydrochloride in 15 mL water. A solution of 1.28 g of sodium hydroxide in 6 mL water was added to the above solution in a dropwise manner and the resulting reaction mixture was allowed to stir for a day at RT. The oily product obtained was extracted

with chloroform. The chloroform layer was dried over anhydrous sodium sulphate for an hour, filtered and evaporated to dryness; yellow oil was obtained. Yield: 52% (0.88 g). ^{1}H NMR ($CDCl_3$): δ 2.20 (s, 3H), 3.66 (s, 4H), 7.03 (t, 2H), 7.41 (d, 2H), 7.55 (t, 2H), 8.55 (d, 2H).

N,N′-bis-(2-pyridylmethyl)-ethylamine (bpea). To a solution of 0.5 g (0.1 mol) ethylamine in 7 mL water placed in a 50 mL RBF, a solution of 3.64 g (0.2 mol) of 2-picolylchloridehydrochloride in 7 mL water was added. A solution of sodium hydroxide (1.76 g in 4.5 mL water) was added to the above reaction mixture in a dropwise manner and the reaction mixture was allowed to stir at RT for 24 hrs. The oily product obtained was extracted with chloroform. The chloroform layer was dried over anhydrous sodium sulphate for an hour, filtered and evaporated to dryness; brown oil was obtained which was purified by column filtration over neutral alumina using ethyl acetate as a solvent. Removal of ethyl acetate afforded yellow oil. Yield: 59% (1.48 g). ^{1}H NMR ($CDCl_3$): δ 1.070 (t, 3H), 2.582 (q, 2H), 3.778 (s, 4H), 7.068 (t, 2H), 7.286 (d, 2H), 7.575 (t, 2H), 8.470 (d, 2H). B.p.: 292 °C.

N,N′-bis-(2-pyridylmethyl)-isopropylamine (bpipa). To a solution of 2.78 g (0.017 mmol) of 2-picolylchloridehydrochloride in 15 mL water placed in a 50 mL RBF, 0.5 g (0.008 mmol) of isopropylamine was added through a funnel at once. A solution of 1.35 g of sodium hydroxide in 3.5 mL water was added to the above solution in a dropwise manner over a period of 20 minutes and the resulting reaction mixture was stirred for a day at RT. A white solid that separated out was washed with water and dried under vacuum. Yield: 58% (1.20 g). ^{1}H NMR ($CDCl_3$): δ 1.02 (d, 6H), 2.76 (m, 1H), 3.79 (s, 4H), 7.03 (t, 2H), 7.19 (d, 2H), 7.49 (t, 2H), 8.43 (d, 2H). M.p.: 69.7 °C.

N,N′-bis-(2-pyridylmethyl)-t-butylamine (bpta). To a solution of 16.9 g (0.1 mol) of 2-picolylchloridehydrochloride in 80 mL water in a three neck RBF 4.0 mL of tertiarybutylamine was added through a funnel at once. The mixture was heated to 50 °C using a water bath. 20 mL of 10 M sodium hydroxide taken in a 25 mL side-arm addition funnel was added to the above reaction mixture at 50-60 °C over an hour with continuous stirring. After complete addition of sodium hydroxide, the solution was allowed to cool to room temperature with continuous stirring for an hour. Extraction of the product with chloroform followed by drying over anhydrous sodium sulphate and evaporation of solvent provided a brown semi-solid. A mixture of hexane and water was added to it and allowed to stir for half an hour. A brown solid that separated out

was filtered, washed with water and vacuum dried. Yield: 37% (4.82 g). ^{1}H NMR ($CDCl_3$): δ 1.458 (4H, q), 2.20 (3H, s), 3.66 (4H, s), 7.03 (2H, t), 7.30 (4H, d), 7.55 (4H, t), 8.55 (4H, d). M.p.: 89.7 °C.

N,N′-bis-(2-pyridylmethyl)-methylamine (bpba). To a solution of 1.64 g (10 mmol) of 2-picolylchloridehydrochloride in 25 mL water placed in a 100 mL two-neck RBF 535 mg (5.75 mmol) of benzylamine was added through a funnel at once. A solution of 0.540 g of sodium hydroxide in 8 mL water was added to the above solution dropwise and the resulting reaction mixture was stirred for a day at RT. The oily product obtained was extracted with chloroform. The chloroform layer was dried over anhydrous sodium sulphate over an hour, filtered and evaporated to dryness to obtain a yellow oil. Yield: 72% (1.04 g). ^{1}H NMR ($CDCl_3$): δ 3.63 (s, 2H), 3.80 (s, 4H), 7.05 (d, 2H), 7.32 (d, 2H), 7.53 (d, 2H), 8.49 (d, 2H).

2.3.2 Tetradentate ligands

N,N,N-tris-(2-pyridylmethyl)-amine (tpa). *Step 1,* **Synthesis of N,N′-bis-(2-pyridylmethyl)-amine (bpa).** In a 100 mL RBF 13.9 g (10 mmol) of 2-(aminomethyl)-pyridine was added to 10 mL methanolic solution of 13.14 g (10 mmol) of 2-pyridinecarboxaldehyde and the reaction mixture was stirred for half an hour. An excess (1.5 equivalents) of solid sodium borohydride was added slowly in portions to the above solution and stirred for one and half hour. The reaction mixture was evaporated to dryness and the slurry obtained was dissolved in water to extract the product with chloroform. The chloroform layer was dried over anhydrous sodium sulphate for an hour and evaporated to dryness; an orange oil was obtained. Yield: ^{1}H NMR ($CDCl_3$): δ 4.151 (4H, s), δ 7.346 (2H, t), 7.555 (2H, d), 7.760 (2H, t), 8.5693 (4H, d).

Step 2, To a solution of 0.74 g (3.72 mmol) of bpa in 8 mL water placed in a 25 mL two-neck RBF, 0.152 g (0.93 mmol) 2-picolylchloridehydrochloride was added. 1.98 g of sodium hydroxide in 5 mL of water was added in a dropwise manner to the above reaction mixture over a period of 20 minutes with continuous stirring. The reaction mixture was allowed to stir for 24 hours. An off-white solid product was obtained via filtration, washed with water and vacuum dried. Yield: 30% (0.326 g). ^{1}H NMR ($CDCl_3$): δ2.553 (6H, s), 7.062 (4H, t), 7.449 (4H, d), 7.557 (4H, t), 8.430 (4H, d). M.p.: 82.6 °C.

2.3.3 Hexadentate ligands

N,N,N′,N′-tetrakis-(2-pyridylmethyl)-1,2-diaminoethane (tpen). To a solution of 16.9 g (0.1 mol) of 2-picolylchloride hydrochloride in 85 mL water in a three neck round bottom flask 1.6 mL (0.02 mmol) of ethylenediamine was added through a funnel at once. The mixture was heated to 40 °C using a water bath. 20 mL of 10 M sodium hydroxide taken in a side-arm addition funnel was added dropwise to the above reaction mixture at 40-50°C over an hour with continuous stirring. It was allowed to cool to room temperature with continuous stirring for one and half an hour. The red colored solution was decanted off and 50 mL fresh water was added to the black colored lumps to stir for another half an hour. An off-white solid product was obtained via filtration, washed with water and vacuum dried. Yield: 44.2% (4.62 g). ^{1}H NMR ($CDCl_3$): δ 2.45 (2H, q), 3.86 (8H, s), 7.33 (4H, t), 7.50 (4H, d), 7.55 (4H, t), 8.64 (4H, d). M.p.: 116 °C.

N,N,N′,N′--tetrakis-(2-pyridylmethyl)-1,2-diaminopropane (**1,2-tppn**)**.** It was prepared following the method described above for tpen except 2.2 mL (0.03 mmol) of 1,2-diaminopropane was used. Yield: 37.3% (4.18 g). ^{1}H NMR ($CDCl_3$): δ 1.20 (3H, d), 2.42 (2H, t), 3.20 (1H, m), 4.05 (8H, s), 7.06 (4H, t), 7.45 (4H, d), 7.56 (4H, t), 8.53 (4H, d). M.p.: 161 °C.

N,N,N′,N′-tetrakis-(2-pyridylmethyl)-1,3-diaminopropane (tppn). To a solution of 16.4 g (0.1 mol) of 2-picolylchloride hydrochloride in 85 mL water in a 250 mL three-neck RBF, 2.5 mL (0.03 mmol) of 1,3-diaminopropane was added through a funnel at once. The mixture was heated to 40 °C using a water bath. 20 mL of 10 M sodium hydroxide taken in a 25 mL side-arm addition funnel was added to the above reaction mixture over an hour with continuous stirring at 40-50 °C. The reaction mixture was allowed to cool to room temperature with continuous stirring for 1.5 hours. The product obtained was extracted with chloroform. The chloroform layer was dried over anhydrous sodium sulphate for an hour and evaporated to dryness. The dark brown oily substance obtained was purified by column separation over neutral Al_2O_3 using EtOAc as solvent. The ethyl acetate layer was evaporated to dryness and an orange solid was obtained. Yield: 45% (4.92 g). ^{1}H NMR ($CDCl_3$): δ1.458 (4H, q), 2.20 (3H, s), 3.66 (4H, s), 7.03 (2H, t), 7.30 (4H, d), 7.55 (4H, t), 8.55 (4H, d). M.p.: 79 ºC.

N,N,N′,N′--tetrakis-(2-pyridylmethyl)-1,4-diaminobutane (tpbn). To a solution of 16.9 g (0.1 mol) of 2-picolylchloride hydrochloride in 85 mL water in a 250 mL three-neck RBF, 2.5 mL

(0.03 mmol) of 1,4-diaminobutane was added through a funnel at once. The mixture was heated to 40 °C using a water-bath. 20 mL of 10 M sodium hydroxide taken in a 25 mL side-arm addition funnel was added to the above reaction mixture over an hour with continuous stirring and maintaining the temperature between 40-50°C. The reaction mixture was allowed to cool to room temperature with continuous stirring for 1.5 hours. The resulting red mother liquor was decanted off and 50 mL water was added to the dark brown lumps in the flask. After stirring for half an hour, an off-white solid product was obtained via filtration, washed with water and vacuum dried. Yield: 82% (9.26 g). ^{1}H NMR ($CDCl_3$): δ1.458 (4H, q), 2.099 (4H, t), 3.725 (8H, s), 7.062 (4H, t), 7.449 (4H, d), 7.557 (4H, t), 8.430 (4H, d). M.p.: 127 °C.

N,N,N′,N′-tetrakis-(2-pyridylmethyl)-1,5-diaminopentane (tppen). Step 1: To a methanolic solution of 2-pyridinecarboxaldehyde (432 mg (4 mmol) in 6 mL methanol) in a 25 mL two neck RBF, 234 μL (2 mmol) of 1,5-diaminopentane was added and stirred for two hours. An excess of sodium borohydride (1.5 equivalents) was added slowly to the above solution at 0 °C and stirred for another two and half an hour. The resulting reduced schiff base was isolated from the reaction mixture by extracting with chloroform followed by drying with MgSO4 and removal of solvent. Step 2: To an aqueous solution of the reduced schiff base obtained in step 1 (568 mg (1.97 mmol) in 10 mL water) in a 25 mL RBF, 652.5 mg (3.95 mmol) of solid 2-picolylchloridehydrochloride was added. A sodium hydroxide solution (0.32 g in 2 mL water) was added to the above mixture in a dropwise manner and was stirred for a day. Extraction of the product with chloroform followed by the removal of the solvent under vacuum resulted in a light orange solid. Yield: 70% (0.648 g). ^{1}H NMR (CDCl3): δ 1.291 (m, 2H), 1.490 (m, 4H), 2.501 (t, 4H), 4.685 (s, 8H), 7.230 (t, 4H), 7.470 (d, 4H), 7.707 (t, 4H), 8.581 (d, 4H). M.p.: 59 °C.

N,N,N′,N′-tetrakis-(2-pyridylmethyl)-1,6-diaminohexane (tphxn). To a solution of 1.00 g (0.006 mmol) of 2-picolylchloridehydrochloride in 8 mL water in a 25 mL RBF, 0.180 g (1.52 mmol) of 1,6-diaminohexane was added. A solution of 1.95 g of sodium hydroxide in 5 mL water was added in a dropwise manner to the above reaction mixture over a period of 20 minutes with continuous stirring. The reaction mixture was allowed to stir for 24 hours at RT. An off-white solid product was obtained via filtration, washed with water and vacuum dried. Yield: 73% (0.54 g). ^{1}H NMR ($CDCl_3$): δ 1.20 (4H, q), 1.504 (4H, q), 2.515 (4H, t), 3.811 (8H, s), 7.134 (4H, t), 7.542 (4H, d), 7.646 (4H, t), 8.515 (4H, d). M.p.: 77 °C.

N,N,N′,N′-tetrakis-(2-pyridylmethyl)-1,7-diaminoheptane (**tphn**)**.** To a solution of 4.20 g (0.025 mol) of 2-picolylchloridehydrochloride in 22 mL water in a 100 mL three-neck RBF, 0.725 g (0.00625 mol) of 1,7-diaminoheptane was added through a funnel at once. The reaction mixture was heated to 40 ℃ using a water bath. 5 mL of 10 M sodium hydroxide taken in a 25 mL side-arm addition funnel was added to the above reaction mixture over an hour with continuous stirring at 40-50 ℃. The reaction mixture was allowed to cool to room temperature with continuous stirring for 2.5 hours. The product was extracted with chloroform, dried over anhydrous sodium sulphate for an hour. The chloroform layer was evaporated to dryness, and a brown oil was obtained which solidified upon cooling. Yield: 83% (2.63 g). ^{1}H NMR ($CDCl_3$): δ1.30 (6H, m), 1.45 (4H, t), 2.46 (4H, t), 3.72 (8H, s), 7.06 (4H, t), 7.44 (4H, d), 7.55 (4H, t), 8.43 (4H, d). M.p.: 55 ℃.

N,N′-bis-(2-pyridylmethyl)-1,4-diaminobutane (bpbn). In a 100 mL RBF, a solution of 4.28 g (0.04 mol) of 2-pyridinecarboxaldehyde in 20 mL methanol was added to a 10 mL methanolic solution of 1.76 g (10 mmol) of 1,4-diaminobutane at 10-15 ℃ and stirred for an hour. An excess of sodium borohydride (2 equivalents) as solid was added slowly in portions to the above solution at 0 ℃ and stirred for two hours. The reaction mixture was evaporated to dryness, the residue obtained was dissolved in water and the product was extracted with chloroform. The chloroform layer was dried over anhydrous sodium sulphate for an hour and evaporated to dryness. A yellow oil was obtained. Yield: 90% (5.27 g). ^{1}HNMR ($CDCl_3$): δ 1.44 (4H, t), 1.95 (2H, t) 2.56 (4H, t), 3.79 (4H, m), 7.04 (2H, t), 7.30 (2H, d), 7.54 (2H, t), 8.44 (2H, d).

N,N'-bis-(2-pyridylmethyl)-N,N'-bis-(glutamate)-1,4-diaminobutane (bpbg). In a 50 mL two-neck RBF 0.5 g (0.0019 mmol) of bpbn was added along with 10 mL ethanol to obtain a clear light yellow solution. To this was added anhydrous sodium carbonate (4 equivalent) and tetrabutyl ammonium bromide (40-50 mg) followed by the addition of 0.37 g (0.004 mmol) of 2-chloroacetamide. Additionally, 15 mL ethanol was added to it. The reaction mixture was refluxed for 96 h with continuous stirring (the reaction was followed by TLC using a 9:1 dichloromethane and methanol mixture). It was cooled to room temperature and filtered, and the solution obtained was evaporated to dryness. A brown semi-solid compound was obtained. To this semi-solid substance dry acetonitrile was added to separate out an off-white solid which was filtered through a G4 crucible, washed with acetonitrile and dried under vacuum. Yield: 42%

(0.304 g). Selected FTIR peaks (KBr, cm^{-1}): 3376, 3188, 2939, 2818, 1653, 1589, 1402, 1112, 760. ^1H NMR ($CDCl_3$): δ 1.34 (4H, t), 2.42 (4H, t), 3.09 (4H, s), 3.67 (4H,s), 7.15 (2H, t), 7.59 (2H, d), 8.01 (2H, t), 8.51 (2H, d). M.p.: 157-158°C.

2.4 Synthesis of Metal Organic Coordination Networks (MOCNs)

Caution! In this study metal perchlorates were used without any problem but special care should be taken while handling such salts, which are dangerous.

General Methods

For the preparation of all MOCNs two general methods at ambient conditions and one method under hydrothermal conditions were developed. These methods are described below:

Method 1. Upon addition of x mmol of dicarboxylic acid to a clear 3 to 6 mL methanolic solution of x mmol of $M(OAc)_2$ and x mmol of the tri- or tetra-dentate ligand (or x/2 mmol of the hexadentate ligand), a white precipitate appeared immediately. The reaction mixture was stirred for another 3 to 4 hours at RT. The resulting slurry was evaporated to dryness, treated with 2 mL of acetonitrile-toluene mixture (50:50 v/v) to completely remove the acetic acid affording a pure solid. The value of x was varied from 0.125-0.25 mmol.

Method 2. In a RBF, y mmol of $M(ClO_4)_2$ and y mmol of the tridentate ligand (or y/2 mmol of the hexadentate ligand),were dissolved in 1.5 to 3 mL of methanol with stirring. To this was added a clear solution of disodium salt of a dicarboxylate (Na_2dc) which was prepared using y/2 mmol of the dicarboxylic acid and y mmol of sodium or potassium hydroxide in 1 mL methanol and 1 mL to a minimum amount of water. With an initial cloudiness in the reaction mixture, a precipitate started to form as the stirring was continued. The reaction mixture was stirred for another 3 to 4 hours at room temperature. Precipitates were obtained in almost all cases except wherever mentioned via filtration, washed with a solvent (in which the product was insoluble), and vacuum dried. The value of y was varied from 0.125-0.25 mmol.

Method 3. In Teflon-lined (7-15 mL) stainless steel reactors starting materials (in an appropriate ratio) were taken along with 1 to 5 mL of distilled water. The reaction mixture was heated to 120

°C over 3h, held for 48 h, then brought to RT at the rate of 10 °C/h. The crystals obtained were collected, washed with methanol and ether, and dried under vacuum.

$[Mn_2(bpma)_2(adc)_2(H_2O)_2]$ (1). It was synthesized following Method 1 using 14 mg (0.125 mmol) of acetylene dicarboxylic acid, 31 mg (0.125 mmol) of $Mn(OAc)_2{\cdot}4H_2O$ in 3 mL methanol and 26.5 mg (0.125 mmol) of bpma. A colorless solid was obtained. Yield: 37 mg (74.4%). Single crystals were obtained by slow evaporation of its aqueous solution. Anal. Calcd for $C_{34}H_{34}N_6Mn_2O_{10}$ (MW 796): C, 51.25; H, 4.27; N, 10.55. Found: C, 51.40; H, 4.33; N, 10.81. Selected FTIR peaks (KBr, cm^{-1}): 3423, 1623, 1602, 1379, 1348, 1016, 770, 680. Selected Raman peaks (cm^{-1}): 2213, 1607, 1574, 1373, 1052, 1015, 846, 642.

$[Mn_2(bpea)_2(adc)_2]_n$ (2). It was synthesized following Method 1 using 14 mg (0.125 mmol) of acetylene dicarboxylic acid, 31 mg (0.125 mmol) of $Mn(OAc)_2{\cdot}4H_2O$ in 3 mL methanol and 28 mg (0.125 mmol) of bpea. A colorless solid was obtained. Yield: 40 mg (81.3%). Single crystals were obtained by slow evaporation of its aqueous solution. Anal. Calcd for $C_{36}H_{34}Mn_2N_6O_8$ (MW 788): C, 54.82; H, 4.31; N, 10.65. Found: C, 54.33; H, 4.54; N, 10.39. Selected FTIR peaks (KBr, cm^{-1}): 3407, 1646, 1607, 1571, 1376, 1318, 1016, 773, 758, 661. Selected Raman peaks (cm^{-1}): 2185, 1626, 1380, 1057, 1016, 861.

$\{[Mn_2(bpipa)_2(adc)_2]{\cdot}2H_2O\}_n$ (3). It was synthesized following Method 1 using 14 mg (0.125 mmol) of acetylene dicarboxylic acid, 31 mg (0.125 mmol) of $Mn(OAc)_2{\cdot}4H_2O$ in 3 mL methanol and 29 mg (0.125 mmol) of bpipa. A colorless solid was obtained. Yield: 36 mg (67.7%). Anal. Calcd for $C_{38}H_{42}Mn_2N_6O_{10}$ (MW 852) C, 53.52; H, 4.92; N, 9.85. Found: C, 53.80; H, 4.58; N, 9.41. Selected FTIR peaks (KBr, cm^{-1}): 3431, 1628, 1617, 1605, 1579, 1438, 1364, 1320, 1160, 779, 693. Selected Raman peaks (cm^{-1}): 2211, 1626, 1377, 1379, 1057, 1018, 862.

$[Mn_2(bpta)_2(adc)_2(H_2O)_2]{\cdot}5H_2O$ (4·$5H_2O$**).** It was synthesized following Method 2 using sodium salt of acetylene dicarboxylic acid {14 mg (0.125 mmol) of acetylene dicarboxylic acid and 10 mg (0.25 mmol) of sodium hydroxide}, 32 mg (0.125 mmol) of $Mn(ClO_4)_2$ in 3 mL methanol and 32 mg (0.125 mmol) of bpta. A colorless solid was obtained. Yield: 32 mg (54.5%). Single crystals were obtained by the slow evaporation of its hot aqueous solution. Anal. Calcd for $C_{40}H_{56}N_6Mn_2O_{15}$ (MW 970.79): C, 49.48; H, 5.77; N, 8.65. Found: C, 48.82; H, 5.73;

N, 8.22. Selected FTIR peaks (KBr, cm^{-1}): 3386, 3216, 2978, 1625, 1599, 1351, 774, 668. Selected Raman peaks (cm^{-1}): 2215, 1576, 1385, 1021. It was also synthesized using Method 1. Direct layering of the starting materials provided $[Mn_2(adc)_2(bpta)_2(H_2O)_2]\cdot 4H_2O\cdot CH_3OH$ (**4**$\cdot 4H_2O\cdot CH_3OH$) with a yield of 45.4%.

$[Mn_2(bpba)_2(adc)_2(H_2O)_2]$ (**5**)**.** It was synthesized following Method 1 using 14 mg (0.125 mmol) of acetylene dicarboxylic acid, 31 mg (0.125 mmol) of $Mn(OAc)_2{\cdot}4H_2O$ in 3 mL methanol and 36 mg (0.125 mmol) of bpba. A colorless solid was obtained. Yield: 31 mg (46%). Anal. Calcd for $C_{50}H_{42}Mn_3N_6O_{14}$ (MW 1166.8): Calc. C, 53.81; H, 3.77; N, 7.53. Found: C, 54.73; H, 4.06; N, 7.78. It should be noted that one molecule of [Mn(adc)] was added to the formula to do the CHN calculation. Selected FTIR peaks (KBr, cm^{-1}): 3422, 3063, 2923, 1603, 1585, 1438, 1351, 1016, 769, 757, 672. Selected Raman peaks (cm^{-1}): 2198, 1604, 1391, 1054, 1018, 1006, 816.

$[Mn_2(bpea)_2(fumarate)_2]_n$ (**6**)**.** It was synthesized following Method 1 using 14.5 mg (0.125 mmol) of fumaric acid, 31 mg (0.125 mmol) of $Mn(OAc)_2{\cdot}4H_2O$ in 3 mL methanol and 28 mg (0.125 mmol) of bpea. A colorless solid was obtained. Yield: 41 mg (77.5%). Anal. Calcd for $C_{36}H_{44}Mn_2N_6O_{11}$ (MW 846): Calc. C, 51.06; H, 5.20; N, 9.92. Found: C, 50.48; H, 5.04; N, 9.32. Selected FTIR peaks (KBr, cm^{-1}): 3422, 1647, 1606, 1376, 1319, 1016, 773, 759, 661.

$[Mn_2(bpta)_2(fumarate)](ClO_4)_2$ (7). It was synthesized following Method 2 using sodium salt of fumaric acid {14.5 mg (0.125 mmol) of fumaric acid and 10 mg (0.25 mmol) of sodium hydroxide}, 32 mg (0.125 mmol) of $Mn(ClO_4)_2$ in 3 mL methanol and 32 mg (0.125 mmol) of bpta. A colorless solid was obtained. Yield: 40 mg (71%). Anal. Calcd for $C_{36}H_{46}Mn_2N_6O_{16}Cl_2$ (MW 933): Calc. C, 46.30; H, 4.93; N, 9.00. Found: C, 46.27; H, 4.40; N, 8.53. Selected FTIR peaks (KBr, cm^{-1}): 3434, 1636, 1603, 1574, 1485, 1436, 1380, 1094, 766, 657, 623.

$[Mn_2(bpta)_2(succinate)_2(H_2O)_2]\cdot H_2O$ (**8**)**.** It was synthesized following Method 1 using 15 mg (0.125 mmol) of succinic acid, 31 mg (0.125 mmol) of $Mn(OAc)_2{\cdot}4H_2O$ in 3 mL methanol and 28 mg (0.125 mmol) of bpea. A colorless solid was obtained. Yield: 40 mg (81%). Anal. Calcd for $C_{40}H_{56}Mn_2N_6O_{11}$ (MW 888): Calc. C, 52.98; H, 6.18; N, 9.27. Found: C, 52.36; H, 6.04; N, 8.27. Selected FTIR peaks (KBr, cm^{-1}): 3434, 1604, 1574, 1568, 1424, 1402, 1017, 765, 650.

$[Mn_2(bpta)_2(tere)_2(H_2O)_2]\cdot H_2O$ (9). It was synthesized following Method 2 using sodium salt of terephthalic acid {21.5 mg (0.125 mmol) of terephthalic acid and 10 mg (0.25 mmol) of sodium hydroxide}, 32 mg (0.125 mmol) of $Mn(ClO_4)_2$ in 3 mL methanol and 32 mg (0.125 mmol) of bpta. A colorless solid was obtained. Yield: 40 mg (62%). Anal. Calcd for $C_{48}H_{56}Mn_2N_6O_{11}$ (MW 1014): C, 56.80; H, 5.52; N, 8.28. Found: C, 56.73; H, 5.42; N, 7.67. Selected FTIR peaks (KBr, cm^{-1}): 3400, 3069, 3028, 2990, 1603, 1582, 1487, 1439, 1383, 1378, 1095, 784, 766, 754, 638.

$[Mn_3(bpea)_3(BTC)_2(H_2O)]_n$ (10). It was prepared following Method 1 using 18 mg (0.083 mmol) of 1,3,5-benzenetricarboxylic acid, 31 mg (0.125 mmol) of $Mn(OAc)_2\cdot 4H_2O$ in 3 mL methanol and 28 mg (0.125 mmol) of bpea. A colorless solid was obtained. Yield: 48 mg (78%). Anal. Calcd for $C_{60}H_{42}N_9Mn_3O_{12}$ (MW 1485): C, 50.10; H, 3.97; N, 8.48. Found: C, 50.18; H, 4.07; N, 8.48. Selected FTIR peaks (KBr, cm^{-1}): 3418, 3072, 2971, 1623, 1605, 1563, 1435, 1372, 1098, 763, 711, 676.

$[Ni(bpma)(adc)(H_2O)_2]$ (11). It was prepared following Method 1 using 14 mg (0.125 mmol) of acetylene dicarboxylic acid, 31 mg (0.125 mmol) of $Ni(OAc)_2\cdot 4H_2O$ in 3 mL methanol and 26.5 mg (0.125 mmol) of bpma. A green solid was obtained. Yield: 43 mg (70%). Anal. Calcd for $C_{17}H_{19}N_3NiO_6$ (MW 420): C, 48.57; H, 4.52; N, 10.00. Found: C, 48.42; H, 4.19; N, 9.13. Selected FTIR peaks (KBr, cm^{-1}): 3380, 3233, 3076, 1607, 1590, 1483, 1440, 1342, 1024, 768, 676.

$[Ni(bpea)(adc)(H_2O)_2]$ (12). It was prepared following Method 1 using 14.5 mg (0.125 mmol) of fumaric acid, 31 mg (0.125 mmol) of $Ni(OAc)_2\cdot 4H_2O$ in 3 mL methanol and 28 mg (0.125 mmol) of bpea. A green solid was obtained. Yield: 27 mg (84%). Anal. Calcd for $C_{18}H_{21}N_3NiO_6$ (MW 434): C, 49.76; H, 4.83; N, 9.67. Found:C, 49.44; H, 5.13; N, 8.95. Selected FTIR peaks (KBr, cm^{-1}): 3404, 3208, 1607, 1585, 1430, 1413, 1351, 1024, 767, 668.

$[Ni(bpta)(adc)(H_2O)_2]\cdot 2H_2O$ (13). It was prepared following Method 1 using 31 mg (0.125 mmol) of $Ni(OAc)_2$ in 3 mL methanol and 32 mg (0.125 mmol) of bpta and 14 mg (0.125 mmol) of acetylene dicarboxylic acid. A green solid was obtained. Yield: 53 mg (81%). Single crystals were grown by the slow cooling of its methanolic solution. Anal. Calcd for $C_{20}H_{29}N_3NiO_8$ (MW 498): C, 39.980; H, 3.718; N, 8.479. Found: C, 39.852; H, 3.658; N, 8.652. Selected FTIR peaks

(KBr, cm^{-1}): 3484, 2975, 1605, 1591, 1343, 1026, 777, 767, 676. Selected Raman Peaks (cm^{-1}): 2208, 1610, 1570, 1373, 1229, 1029, 831, 614.

$[Ni_4(bpma)_4(fumarate)_4(H_2O)_4]\cdot 8H_2O$ (14). It was prepared following Method 1 using 14.5 mg (0.125 mmol) of fumaric acid, 31 mg (0.125 mmol) of $Ni(OAc)_2\cdot 4H_2O$ in 3 mL methanol and 26.5 mg (0.125 mmol) of bpea. A green solid was obtained. Yield: 20 mg (31%). Anal. Calcd for $C_{68}H_{92}N_{12}Ni_4O_{28}$ (MW 1760): C, 46.36; H, 5.23; N, 9.54. Found:C, 45.95; H, 5.55; N, 9.69. Selected FTIR peaks (KBr, cm^{-1}): 3401, 1608, 1575, 1558, 1384, 1374, 1023, 765, 677, 649.

$[Ni_4(bpea)_4(fumarate)_4(H_2O)_4]\cdot 4H_2O$ (15). It was prepared following Method 1 using 14.5 mg (0.125 mmol) of fumaric acid, 31 mg (0.125 mmol) of $Ni(OAc)_2\cdot 4H_2O$ in 3 mL methanol and 28 mg (0.125 mmol) of bpea. A green solid was obtained. Yield: 27 mg (86%). Anal. Calcd for $C_{72}H_{92}N_{12}Ni_4O_{24}$ (MW 1744): C, 49.54; H, 5.27; N, 9.63. Found: C, 49.26; H, 5.34; N, 9.20. Selected FTIR peaks (KBr, cm^{-1}): 3419, 3257, 1608, 1574, 1568, 1435, 1385, 1024, 765, 677.

$[Ni_4(bpta)_4(fumarate)_4(H_2O)_4]\cdot 4H_2O$ (16). It was prepared following Method 1 1using 14.5 mg (0.125 mmol) of fumaric acid, 31 mg (0.125 mmol) of $Ni(OAc)_2\cdot 4H_2O$ in 3 mL methanol and 32 mg (0.125 mmol) of bpta. A blue solid was obtained. Yield: 46 mg (80%). Single crystals were grown by slow evaporation of its aqueous solution. Anal. Calcd for $C_{80}H_{104}N_{12}Ni_4O_{23}$ (MW 1838): C, 52.23; H, 5.76; N, 9.14. Found: C, 52.23; H, 5.70; N, 8.66. It should be noted that the formula used for CHN analysis was with three water moleucle although other charcaterization techniques including X-ray crystallography indicated it had four water molecules. Selected FTIR peaks (KBr, cm^{-1}): 3402, 3024, 2967, 2918 1607, 1578, 1567, 1490, 1434, 1375, 1189, 1023, 987, 774, 764, 670, 652. Selected Raman Peaks (cm^{-1}): 1654, 1608, 1571, 1574, 1449, 1403, 1260, 832, 644.

$[Ni(bpta)(succinate)(H_2O)_2]\cdot 3H_2O$ (17). It was prepared following Method 1 using 15 mg (0.125 mmol) of succinic acid, 31 mg (0.125 mmol) of $Ni(OAc)_2\cdot 4H_2O$ in 3 mL methanol and 32 mg (0.125 mmol) of bpta. A green solid was obtained. Yield: 41 mg (56%). Single crystals were grown by slow evaporation of its methanolic solution. Anal. Calcd for $C_{20}H_{31}N_3NiO_7$ (MW 500): C, 49.79; H, 6.43; N, 8.71. Found: C, 49.84; H, 6.37; N, 8.83. It should be noted that the formula used for CHN analysis was with one water moleucle although other charcaterization techniques including X-ray crystallography indicated it had three water molecules. Selected FTIR peaks

(KBr, cm^{-1}): 3406, 1608, 1565, 1487, 1254, 1024, 769, 659. Selected Raman Peaks (cm^{-1}):1610, 1575, 1451, 1228, 1028, 853, 831, 710, 645.

$[Ni_2(bpea)_2(fcdc)_2]\cdot 6.5H_2O$ (18). It was prepared following Method 1 using 34 mg (0.125 mmol) of ferrocene dicarboxylic acid, 31 mg (0.125 mmol) of $Ni(OAc)_2\cdot 4H_2O$ in 3 mL methanol and 28 mg (0.125 mmol) of bpea. A dark red solid was obtained. Yield: 33 mg (35%). Anal. Calcd for $C_{56}H_{67}N_6Ni_2Fe_1O_{15}$ (MW 1285): C, 52.29; H, 5.21; N, 6.53. Found: C, 52.65; H, 6.09; N, 5.53. Selected FTIR peaks (KBr, cm^{-1}): 3418, 1607, 1560, 1467, 1383, 1351, 1022, 769, 654.

$[Co_2(bpta)_2(adc)(H_2O)_2](ClO_4)_2$ (19). It was prepared following Method 2 using sodium salt of acetylene dicarboxylic acid {14 mg (0.125 mmol) of acetylene dicarboxylic acid and 10 mg (0.25 mmol) of sodium hydroxide}, 48 mg (0.125 mmol) of $Co(ClO_4)_2$ in 3 mL methanol and 32 mg (0.125 mmol) of bpta. Yield: 39 mg (54%). There was no precipitate obtained in this case; the pink filtrate was evaporated to dryness to obtain a solid which was recrystallised from a methanol-water mixture to afford the product from sodium perchlorate. Single crystals were grown by the slow evaporation of a solution of the compound in a methanol-water mixture. Anal. Calcd for $C_{36}H_{54}N_6Co_2Cl_2O_{14}$ (MW 1163.36): C, 37.13; H, 4.64; N, 7.22. Found: C, 37.52; H, 4.68; N, 7.09. Selected FTIR peaks (KBr, cm^{-1}): 3404, 1567, 1435, 1345, 1096, 764, 621.

$[Cu_2(bpta)_2(fumarate)(H_2O)_2](ClO_4)_2$ (20). It was prepared following Method 2 using sodium salt of fumaric acid {14.5 mg (0.125 mmol) of acetylene dicarboxylic acid and 10 mg (0.25 mmol) of sodium hydroxide}, 46.5 mg (0.125 mmol) of $Cu(ClO_4)_2$ in 3 mL methanol and 32 mg (0.125 mmol) of bpta. There was no precipitate obtained in this case; a dark blue filtrate was processed as described above for **19** to isolate the product. Yield: 41 mg (69%). Single crystals were grown by slow evaporation of a solution of the compound in a methanol-water mixture. Anal. Calcd for $C_{36}H_{44}N_6Cu_2Cl_4O_{12}$ (MW 950): C, 45.47; H, 4.63; N, 8.84. Found: C, 45.34; H, 4.63; N, 8.38. Selected FTIR peaks (KBr, cm^{-1}): 3438, 1606, 1563, 1481, 1441, 1380, 1077, 762, 698, 619.

$[Cu_2(bpta)_2(tdc)(H_2O)(ClO_4)](ClO_4)\cdot 2H_2O$ (21). It was prepared following Method 2 using sodium salt of thiophene dicarboxylic acid {21.5 mg (0.125 mmol) of thiophene dicarboxylic acid and 10 mg (0.25 mmol) of sodium hydroxide}, 46.5 mg (0.125 mmol) of $Cu(ClO_4)_2$ in 3 mL methanol and 32 mg (0.125 mmol) of bpta. There was no precipitate obtained in this case; a dark

blue filtrate was processed as described above for **19** to isolate the product. Yield: 65 mg (79%). Single crystals were grown by the slow evaporation of a solution of the compound in a water-methanol mixture. Anal. Calcd for $C_{38}H_{50}N_6Cu_2Cl_4S1O_{23}Na_2$ (MW 1304.84): C, 34.97; H, 3.87; N, 6.43. Found: C, 34.50; H, 3.79; N, 6.30. It should be noted that the formula used for CHN analysis was with two sodium perchlorate molecules because this compound was soluble in methanol and water thus separation of sodium perchlorate was difficult. Selected FTIR peaks (KBr, cm^{-1}): 3436, 1611, 1586, 1530, 1378, 1351, 1095, 772, 623.

$[Zn_2(bpma)_2(adc)_2]_n$ (22). It was prepared following Method 1 using 14 mg (0.125 mmol) of acetylene dicarboxylic acid, 27.5 mg (0.125 mmol) of $Zn(OAc)_2{\cdot}2H_2O$ in 3 mL methanol and 26.5 mg (0.125 mmol) of bpma. A colorless solid was obtained. Yield: 24 mg (53%). Single crystals were grown by slow evaporation of its aqueous solution. Anal. Calcd for $C_{34}H_{30}N_6Zn_2O_8$ (MW 780): C, 52.30; H, 3.84; N, 10.76. Found: C, 51.70; H, 3.85; N, 10.74. Selected FTIR peaks (KBr, cm^{-1}): 3421, 1639, 1619, 1603, 1489, 1441, 1351, 1320, 1023, 781, 762, 695, 677. Selected Raman Peaks (cm^{-1}):1610, 1575, 1451, 1228, 1028, 853, 831, 710, 645.

$[Zn_2(bpea)_2(adc)_2]_n$ (23). It was prepared following Method 1 using 14 mg (0.125 mmol) of acetylene dicarboxylic acid, 27.5 mg (0.125 mmol) of $Zn(OAc)_2{\cdot}2H_2O$ in 3 mL methanol and 28 mg (0.125 mmol) of bpea. A colorless solid was obtained. Yield: 35 mg (71%). Single crystals were grown by slow evaporation of its aqueous solution. Anal. Calcd for $C_{36}H_{34}N_6Zn_2O_8$ (MW 809): C, 53.39; H, 4.40; N, 10.38. Found: C, 53.55; H, 3.99; N, 10.14. Selected FTIR peaks (KBr, cm^{-1}):3420, 1636, 1606, 1346, 1314, 1024, 781, 761, 693, 674.

$[Zn_2(bpta)_2(adc)_2{\cdot}2H_2O]_n$ (24). It was prepared following Method 1 using 14 mg (0.125 mmol) of acetylene dicarboxylic acid, 27.5 mg (0.125 mmol) of $Zn(OAc)_2{\cdot}2H_2O$ in 3 mL methanol and 32 mg (0.125 mmol) of bpta. A colorless solid was obtained. Yield: 38 mg (67%). Single crystals were grown by slow evaporation of its aqueous solution. Anal. Calcd for $C_{40}H_{46}N_6Zn_2O_{10}$ (MW 901): C, 53.27; H, 5.10; N, 9.33. Found: C, 53.47; H, 4.77; N, 9.33. Selected FTIR peaks (KBr, cm^{-1}):3451, 2977, 1634, 1609, 1587, 1366, 1321, 1026, 779, 768, 679. Selected Raman Peaks (cm^{-1}): 2212, 1615, 1451, 1362, 1029, 844, 655.

$[Zn_2(bpba)_2(adc)_20{\cdot}5H_2O]_n$ (25). It was prepared following Method 1 using 14 mg (0.125 mmol) of acetylene dicarboxylic acid, 27.5 mg (0.125 mmol) of $Zn(OAc)_2{\cdot}2H_2O$ in 3 mL

methanol and 36.5 mg (0.125 mmol) of bpba. A colorless solid was obtained. Yield: 35 mg (61%).Anal. Calcd for $C_{44}H_{39}N_6Zn_2O_{8.5}$ (MW 918): C, 57.51; H, 4.24; N, 9.15. Found: C, 57.92; H, 4.14; N, 8.76. Selected FTIR peaks (KBr, cm^{-1}): 3436, 1632, 1606, 1573, 1332, 1312, 1024, 769, 756, 681.

$[Cd_2(bpma)_2(adc)_2{\cdot}2H_2O]_n$ (26). It was prepared following Method 1 using 14 mg (0.125 mmol) of acetylene dicarboxylic acid, 33.5 mg (0.125 mmol) of $Cd(OAc)_2{\cdot}2H_2O$ in 3 mL methanol and 26.5 mg (0.125 mmol) of bpma. A colorless solid was obtained. Yield: 36 mg (67%). Single crystals were grown by slow evaporation of its aqueous solution. Anal. Calcd for $C_{34}H_{34}N_6Cd_2O_{10}$ (MW 878): C, 44.63; H, 3.72; N, 9.19. Found: C, 44.68; H, 3.43; N, 9.01. Selected FTIR peaks (KBr, cm^{-1}): 3438, 1611, 1581, 1528, 1356, 770.

$[Cd_2(bpea)_2(adc)_2]_n$ (27). It was prepared following Method 1 using 14 mg (0.125 mmol) of acetylene dicarboxylic acid, 33.5 mg (0.125 mmol) of $Cd(OAc)_2{\cdot}2H_2O$ in 3 mL methanol and 28 mg (0.125 mmol) of bpea. A colorless solid was obtained. Yield: 49 mg (88%). Single crystals were grown by slow evaporation of its aqueous solution. Anal. Calcd for $C_{36}H_{34}N_6Cd_2O_8$ (MW 902): C, 47.89; H, 3.76; N, 9.31. Found: C, 47.43; H, 3.79; N, 9.14. Selected FTIR peaks (KBr, cm^{-1}): 3441, 1605, 1582, 1346, 1018, 761, 690, 641.

$[Cd_2(bpta)_2(adc)_2{\cdot}2H_2O]_n$ (28). It was prepared following Method 1 using 14 mg (0.125 mmol) of acetylene dicarboxylic acid, 33.5 mg (0.125 mmol) of $Cd(OAc)_2{\cdot}2H_2O$ in 3 mL methanol and 32 mg (0.125 mmol) of bpta. A colorless solid was obtained. Yield: 58 mg (93%). Single crystals were grown by slow evaporation of its aqueous solution. Anal. Calcd for $C_{40}H_{46}N_6Cd_2O_{10}$ (MW 995): C, 48.24; H, 4.62; N, 8.44. Found: C, 48.06; H, 4.54; N, 8.39. Selected FTIR peaks (KBr, cm^{-1}): 3570, 3475, 3071, 2971, 1630, 1605, 1560, 1377, 1328, 1096, 775, 765, 690.

$[Cd_2(bpba)_2(adc)_2]_n$ (29). It was prepared following Method 1 using 14 mg (0.125 mmol) of acetylene dicarboxylic acid, 33.5 mg (0.125 mmol) of $Cd(OAc)_2{\cdot}2H_2O$ in 3 mL methanol and 36 mg (0.125 mmol) of bpba. A colorless solid was obtained. Yield: 45 mg (57%). Single crystals were grown by slow evaporation of its aqueous solution. Anal. Calcd for $C_{50}H_{38}N_6Cd_2O_{12}$ (MW 1250): C, 48.00; H, 3.04; N, 6.72. Found: C, 48.65; H, 3.40; N, 6.99. It should be noted that one molecule of [Cd(adc)] was added to the formula to do the CHN calculations. Selected FTIR peaks (KBr, cm^{-1}): 3444, 1600, 1574, 1562, 1378, 1344, 1017, 776, 768, 755, 688.

$[Zn_2(bpma)_2(HBTC)_2]_n$ (30a). It was prepared following Method 3 using 18 mg (0.125 mmol) of 1,3,5-benzene tricarboxylic acid, 27.5 mg (0.125 mmol) of $Zn(OAc)_2 \cdot 2H_2O$ in 1 mL water and 26.5 mg (0.125 mmol) of bpma. There were two types of crystals obtained from this reaction. In addition to **30a**, the second crytsal was found to be $[Zn_3(BTC)_2(H_2O)_{12}]_n$ (**30b**).

$[Cd_2(bpma)_2(HBTC)_2]_n$ (31). It was prepared following Method 3 using 27 mg (0.125 mmol) of 1,3,5-benzene tricarboxylic acid, 33.5 mg (0.125 mmol) of $Cd(OAc)_2 \cdot 2H_2O$ in 1 mL water and 26.5 mg (0.125 mmol) of bpma. Colorless crystals were obtained. Yield: 36 mg (68%). Selected FTIR peaks (KBr, cm^{-1}): 3368, 3221, 1630, 1605, 1557, 1541, 1442, 1372, 1349, 1029, 766, 728, 736.

$\{[Cd_3(bpea)_3(BTC)_2(H_2O)] \cdot 10H_2O\}_n$ (32). It was prepared following Method 3 using 18 mg (0.083 mmol) of 1,3,5-benzene tricarboxylic acid, 33.5 mg (0.125 mmol) of $Cd(OAc)_2 \cdot 2H_2O$ in 1 mL water and 28 mg (0.125 mmol) of bpea. Colorless crystals were obtained. Yield: 31 mg (52%). Anal. Calcd for $C_{60}H_{57}N_9Cd_3O_{12}$ (MW 1449): C, 49.68; H, 3.91; N, 8.138. Found: C, 49.66; H, 3.87; N, 7.88. It should be noted that the formula used for CHN analysis was with no water molecule although X-ray crystallography indicated it had ten water molecules. The reason for this could be: fresh single crystals were used for structure analysis but the crystals were washed with methanol and dried using ether to do CHN analysis. TGA also indicated it had no water molecule in the dried sample. Selected FTIR peaks (KBr, cm^{-1}): 3418, 1705, 1615, 1603, 1576, 1552, 1440, 1434, 1367, 1276, 1017, 768, 756, 732, 686.

$\{[Cd_6(bpta)_6(BTC)_2(H_2O)] \cdot 5H_2O\}_n$ (33). It was prepared following Method 3 using 9 mg (0.042 mmol) of 1,3,5-benzene tricarboxylic acid, 33.5 mg (0.125 mmol) of $Cd(OAc)_2 \cdot 2H_2O$ in 1 mL water and 32 mg (0.125 mmol) of bpta. Colorless crystals were obtained. Yield: 30.8 mg (47%). Anal. Calcd for $C_{66}H_{77}N_9Cd_3O_{16}$ (MW 1587.08): C, 49.90; H, 4.85; N, 7.93. Found: C, 49.76; H, 4.58; N, 7.01. It should be noted that the formula used for CHN analysis was with three water molecules although X-ray crystallography indicated it had five water molecules. Selected FTIR peaks (KBr, cm^{-1}): 3448, 3081, 2923, 2976, 1615, 1569, 1542, 1442, 1370, 1021, 770, 758, 717, 680.

$[Mn_2(tpa)_2(adc)_2] \cdot 6H_2O$ (34). It was prepared following Method 1 using 14 mg (0.125 mmol) of acetylene dicarboxylic acid, 31 mg (0.125 mmol) of $Mn(OAc)_2 \cdot 4H_2O$ in 3 mL methanol and 36.5

mg (0.125 mmol) of tpa. A colorless solid was obtained. Yield: 55 mg (86%). Single crystals were obtained by slow evaporation of its aqueous solution. Anal. Calcd for $C_{44}H_{48}N_8Mn_2O_{14}$ (MW 1022): Calc. C, 51.66; H, 4.69; N, 10.95. Found: C, 51.13; H, 4.50; N, 10.51. Selected FTIR peaks (KBr, cm^{-1}): 3408, 3330, 1619, 1602, 1590, 1361, 1101, 777, 763, 688. Selected Raman peaks (cm^{-1}): 2214, 1574, 1383, 1057, 1019, 861, 660.

$[Mn_2(tpa)_2(fumarate)_2]\cdot 8H_2O$ (35). It was synthesized following Method using 14.5 mg (0.125 mmol) of fumaric acid, 31 mg (0.125 mmol) of $Mn(OAc)_2\cdot 4H_2O$ in 3 mL methanol and 36.5 mg (0.125 mmol) of tpa. A colorless solid was obtained. Yield: 46 mg (74%). Single crystals were obtained by slow evaporation of its aqueous solution. Anal. Calcd for $C_{44}H_{54}N_8Mn_2O_{15}$ (MW 1044): Calc. C, 50.57; H, 5.17; N, 10.72. Found: C, 50.89; H, 4.86; N, 10.69. It should be noted that the formula used for the calculation of CHN analysis was with seven water molecules although other characterizations including X-ray crystallography indicated to have eight water molecules. Selected FTIR peaks (KBr, cm^{-1}): 3400, 3275, 2916, 1602, 1574, 1481, 1380, 1087, 773, 763, 670. Selected Raman peaks (cm^{-1}): 1662, 1604, 1576, 1407, 1278, 1227, 1019, 860.

$[Mn_2(succinate)_2(tpa)_2]\cdot 6H_2O$ (36). It was prepared following Method 1 using 15 mg (0.125 mmol) of succinic acid, 31 mg (0.125 mmol) of $Mn(OAc)_2\cdot 4H_2O$ in 3 mL methanol and 36.5 mg (0.125 mmol) of tpa. A colorless solid was obtained. Yield: 44 mg (64%). Single crystals were obtained by slow evaporation of its aqueous solution. Anal. Calcd for $C_{44}H_{56}N_8Mn_2O_{14}$ (MW 1030): Calc. C, 51.26; H, 5.43; N, 10.87. Found: C, 51.40; H, 5.20; N, 10.91. Selected FTIR peaks (KBr, cm^{-1}): 3400, 3293, 2977, 2928 1601, 1574, 1561, 1479, 1398, 1419, 1012, 768, 761, 666. Selected Raman peaks (cm^{-1}): 1603, 1576, 1225, 1056, 1016, 862.

$[Ni_2(tpa)_2(adc)_2]\cdot 7H_2O$ (37). It was prepared following Method 1 using 14 mg (0.125 mmol) of acetylene dicarboxylic acid, 31.2 mg (0.125 mmol) of $Ni(OAc)_2\cdot 4H_2O$ in 3 mL methanol and 36.5 mg (0.125 mmol) of tpa. There was no precipitate; a purple filtrate was processed as described above for **19** to isolate the product. Yield: 42 mg (64%). Anal. Calcd for $C_{44}H_{36}N_8Mn_2O_{15}$ (MW 1048): Calc. C, 50.38; H, 4.77; N, 10.68. Found: C, 50.50; H, 4.72; N, 10.31. Selected FTIR peaks (KBr, cm^{-1}): 3382, 3230, 1606, 1583, 1568, 1484, 1446, 1370, 1322, 1024, 768, 681, 646, 618.

$[Fe_2(tpa)_2(adc)](ClO_4)_4 \cdot 2 \cdot 5H_2O$ (38). It was prepared following Method 2 using sodium salt of acetylene dicarboxylic acid {14 mg (0.125 mmol) of acetylene dicarboxylic acid and 10 mg (0.25 mmol) of sodium hydroxide}, 44.5 mg (0.125 mmol) of $Fe(ClO_4)_3$ in 3 mL methanol and 36.5 mg (0.125 mmol) of tpa. A brown solid was obtained. Yield: 30 mg (42%). Anal. Calcd for $C_{44}H_{41}N_8Fe_2O_{18.5}$ (MW 1160): Calc. C, 45.52; H, 3.53; N, 9.65. Found: C, 45.34; H, 3.51; N, 10.45. Selected FTIR peaks (KBr, cm^{-1}): 3400, 3275, 2916, 1638, 1607, 1487, 1444, 1276, 1111, 1073, 1024, 825, 770, 760, 656, 622.

$\{[Zn_2(tpa)_2(adc)_2] \cdot 6H_2O\}_n$ (39). It was prepared following Method 1 using 14 mg (0.125 mmol) of acetylene dicarboxylic acid, 27.5 mg (0.125 mmol) of $Zn(OAc)_2 \cdot 2H_2O$ in 3 mL methanol and 36.5 mg (0.125 mmol) of tpa. A colorless solid was obtained. Yield: 42 mg (64%). Anal. Calcd for $C_{46}H_{50}N_8Zn_2O_{14}$ (MW 1042.88): Calc. C, 52.97; H, 4.84; N, 10.73. Found: C, 52.51; H, 4.94; N, 10.93. Selected FTIR peaks (KBr, cm^{-1}): 3401, 3074, 1614, 1581, 1482, 1441, 1352, 1337, 1050, 776, 765, 675.

$[Cd_2(tpa)_2(adc)_2]_n$ (40). It was prepared following Method 1 using 14 mg (0.125 mmol) of acetylene dicarboxylic acid, 33.5 mg (0.125 mmol) of $Cd(OAc)_2 \cdot 2H_2O$ in 3 mL methanol and 36.5 mg (0.125 mmol) of tpa. A colorless solid was obtained. Yield: 46 mg (72%). Single crystals were obtained by the slow evaporation of its aqueous solution. Anal. Calcd for $C_{46}H_{36}N_8Cd_2O_8$ (MW 1028): Calc. C, 50.98; H, 3.50; N, 10.89. Found: C, 50.71; H, 3.45; N, 10.68. Selected FTIR peaks (KBr, cm^{-1}): 3431, 1605, 1581, 1568, 1364, 1349, 1011, 777, 754, 693, 686.

$\{[Mn_2(tpbn)(adc)_2(H_2O)_2] \cdot 2CH_3OH\}_n$ (41). It was prepared using Method 2 using 127 mg (0.5 mmol) of $Mn(ClO_4)_2$ in 6 mL MeOH, a solution of K_2adc (prepared by taking 57.0 mg (0.5 mmol) of acetylene dicarboxylic acid and 56 mg (0.1 mmol) of potassium hydroxide in 2 mL of MeOH and 8 mL of water) and 113 mg (0.25 mmol) of solid tpbn. A white precipitate was obatined. Yield: 123 mg (56%). It was also prepared using Method 1 using 60.5 mg (0.25 mmol) of $Mn(OAc)_2$ was dissolved in 6 mL methanol, 56.5 mg (0.125 mmol) of solid tpbn and 14.5 mg (0.125 mmol) of H_2adc yielding a white precipitate. Yield: 60 mg (54%). The white solid obtained from both procedures was analyzed and confirmed to be the same. Anal. Calcd for $C_{36}H_{38}Mn_2\ N_6O_{12}$ (MW 856): C, 50.50; H, 4.44; N, 9.81. Found: C, 50.11; H, 4.51; N, 9.84.

Selected FTIR peaks (KBr, cm^{-1}): 3392, 3203, 1622, 1600, 1570, 1351, 779, 767, 671. Selected Raman peaks (cm^{-1}): 2216, 1573, 1379, 1053, 1016, 846, 812.

Since the compound was practically insoluble in most of the solvents, single crystals of $\{$**41**$\cdot 2CH_3OH\}_n$ (**41b**) were obtained by direct layering of reactants. Thus the formula obtained from the X-ray single crystal studies differs only in terms of solvates from that for all other characterizations done with the white solid collected from either Method 1 or 2.

$[Mn_2(tppn)(H_2O)_6](adc)_2\cdot 3H_2O$ (**42**)**.** It can be prepared following either Method 1 or Method 2 described above for **41**. As is the case for **41**, the product formation is independent of the Mn(II) salt used. Therefore, one method is reported here, i.e., Method 1 using 14 mg (0.125 mmol) of acetylene dicarboxylic acid, 31 mg (0.125 mmol) of $Mn(OAc)_2\cdot 4H_2O$ in 3 mL methanol and 27.5 mg (0.0625 mmol) of tppn. A colorless solid was obtained. Yield: 41.5 mg (69.0%). Single crystals were obtained by slow cooling of its aqueous solution. Anal. Calcd for $C_{35}H_{48}Mn_2N_6O_{17}$ (MW 934.67): C, 44.96; H, 5.13; N, 8.99. Found: C, 44.48; H, 4.67; N, 8.61. Selected FTIR peaks (KBr, cm^{-1}): 3387, 3230, 1603, 1330, 775, 665.

$[Mn(1,2\text{-}tppn)(H_2O)[(ClO_4)_2$ (**43**)**.** It was prepared following Method 2 using 31 mg (0.125 mmol) of $Mn(OAc)_2$, 55 mg (0.125 mmol) of 1,2-tppn and 7.5 mg (0.0625 mmol) of H_2adc were dissolved in 3 mL methanol, 30.5 mg (0.5 mmol) of sodium perchlorate was added to initiate precipitation. A white solid was obtained. Yield: 40 mg (47%). Single crystals were obtained by slow evaporation of its acetonitrile solution. Anal. Calcd for $C_{58}H_{62}Cl_2Mn_2N_{12}O_{15}$ (MW 1351): C, 51.52; H, 4.589; N, 12.43. Found: C, 51.90; H, 4.644; N, 12.34. Selected FTIR peaks (KBr, cm^{-1}): 3430, 2926, 1615, 1602, 1570, 1436, 1319, 1087, 763, 675, 622.

$[Mn_2(tpen)_2(adc)](ClO_4)_2$ (**44**)**.** It was synthesized following Method 2 using 30.6 mg (0.125 mmol) of $Mn(OAc)_2$, 53 mg (0.125 mmol) of tpen and 7.5 mg (0.0625 mmol) of H_2adc were dissolved in 3 mL methanol, 30.5 mg (0.5 mmol) of sodium perchlorate was added to initiate precipitation. A white solid was obtained. Yield: 57 mg (68%). Single crystals were obtained by the slow evaporation of an acetonitrile solution of the compound. Anal. Calcd. for $C_{56}H_{56}Cl_2Mn_2N_{12}O_{14}$ (MW 1305): C, 51.49; H, 4.41; N, 12.89. Found: C, 51.26; H, 4.40; N, 12.59. Selected FTIR peaks (KBr, cm^{-1}): 3446, 3067, 2921, 1617, 1602, 1571, 1436, 1322, 1087, 766, 758, 675, 623.

$[Mn_2(tppen)(adc)(H_2O)_4](adc)\cdot 4H_2O\}_n$ (45). It was synthesized following Method 1 using 14 mg (0.125 mmol) of acetylene dicarboxylic acid, 31 mg (0.125 mmol) of $Mn(OAc)_2\cdot 4H_2O$ in 3 mL methanol and 29 mg (0.0625 mmol) of tppen. A colorless solid was obtained. Yield: 41 mg (74%). Single crystals were obtained by slow evaporation of a mixture of acetonitrile-water solution of the compound. Anal. Calcd. for $C_{37}H_{44}Mn_2N_6O_{13}$ (MW 890): C, 49.92; H, 4.94; N, 9.43. Found: C, 49.72; H, 4.41; N, 8.74. It should be noted that the formula used for the calculation of CHN analysis was with one water molecule although other characterizations including X-ray crystallography indicated to have four water molecules. Selected FTIR peaks (KBr, cm^{-1}): 3392, 3220, 2935, 1626, 1604, 1570, 1482, 1443, 1329, 1016, 777, 767, 665.

$[Mn_2(tphxn)(adc)(H_2O)_4](adc)\cdot 2H_2O\}_n$ (46). It was synthesized following Method 1 using 14 mg (0.125 mmol) of acetylene dicarboxylic acid, 31 mg (0.125 mmol) of $Mn(OAc)_2\cdot 4H_2O$ in 3 mL methanol and 30 mg (0.0625 mmol) of tphxn. A colorless solid was obtained. Yield: 45 mg (79%).Anal. Calcd. for $C_{38}H_{44}Mn_2N_6O_{14}$ (MW 926): C, 49.24; H, 4.75; N, 9.07. Found: C, 49.36; H, 4.73; N, 8.51. Selected FTIR peaks (KBr, cm^{-1}): 3382, 3065, 2936, 1627, 1604, 1575, 1482, 1442, 1337, 1016, 776, 767, 665.

$[Mn_2(tphn)(adc)(H_2O)_4](adc)\cdot 5H_2O\}_n$ (47). It was synthesized following Method 1 using 14 mg (0.125 mmol) of acetylene dicarboxylic acid, 31 mg (0.125 mmol) of $Mn(OAc)_2\cdot 4H_2O$ in 3 mL methanol and 31 mg (0.0625 mmol) of tphn. A colorless solid was obtained. Yield: 45 mg (76%). Single crystals were obtained by slow evaporation of a solution of the compound in a mixture of acetonitrile-water. It should be noted that the formula used for CHN analysis was with two and half water molecules although other characterizations including X-ray crystallography indicated it had five water molecules. Anal. Calcd. for $C_{39}H_{42}Mn_2N_6O_{14.5}$ (MW 949): C, 49.31; H, 4.95; N, 8.85. Found: C, 49.10; H, 4.96; N, 8.75. Selected FTIR peaks (KBr, cm^{-1}): 3434, 2930, 1627, 1603, 1441, 1345, 777, 668.

$\{[Mn_2(bpbg)(adc)_2]\cdot 4H_2O\}_n$ (48). It was synthesized following Method 1 using 14 mg (0.125 mmol) of acetylene dicarboxylic acid, 31 mg (0.125 mmol) of $Mn(OAc)_2\cdot 4H_2O$ in 3 mL methanol and 26 mg (0.0625 mmol) of bpbg. A colorless solid was obtained. Yield: 32 mg (65%). Anal. Calcd. for $C_{28}H_{36}Mn_2N_6O_{14}$ (MW 794): C, 42.32; H, 4.53; N, 10.57. Found: C, 42.50; H, 4.91; N, 9.03. Selected FTIR peaks (KBr, cm^{-1}): 3423, 1676, 1607, 1571, 1443, 1342, 769, 676.

$[Mn_2(tppn)_2(fumarate)](ClO_4)_2$ (49). It was synthesized following Method 2 using sodium salt of fumaric acid {7.2 mg (0.0625 mmol) of fumaric acid and 5 mg (0.25 mmol) of sodium hydroxide}, 32 mg (0.125 mmol) of $Mn(ClO_4)_2$ in 3 mL methanol and 27 mg (0.0625 mmol) of tppn. A white solid was obtained. Yield: 54 mg (67%). Single crystals were obtained by the slow evaporation of an acetonitrile solution of the compound. Anal. Calcd. for $C_{58}H_{62}Mn_2N_{12}O_{12}$ (MW 1299): C, 53.57; H, 4.77; N, 12.93. Found: C, 53.33; H, 4.99; N, 12.25. Selected FTIR peaks (KBr, cm^{-1}): 3434, 1604, 1571, 1437, 1406, 1379, 1089, 770, 675, 625.

$\{[Mn_2(tpbn)(fumarate)_2(H_2O)_2]\cdot 6H_2O\}_n$ (50). Like **41**, it was synthesized following both Method 1 and Method 2. The final product obtained was same from both the methods. Single crystals were grown from the direct layering of the reactants. Yield: 43 mg (83%). Anal. Calcd. for $C_{36}H_{44}Mn_2N_6O_{12}$ (MW 880): C, 49.09; H, 5.22; N, 9.54. Found: C, 49.73; H, 4.93; N, 9.87. Selected FTIR peaks (KBr, cm^{-1}): 3367, 3239, 2941, 1604, 1570, 1483, 1440, 1373, 1191, 765, 666.

$\{[Mn_2(tpbn)(oxalate)(H_2O)_2](ClO_4)_2\}_n$ (51). It was prepared following Method 2 using 23 mg (0.25 mmol) potassium oxalate, 64 mg (0.25 mmol) of $Mn(ClO_4)_2$ in 4 mL acetonitrile and 57 mg (0.125 mmol) of tpbn. A colorless solid was obtained. Yield: 63 mg (59%). Single crystals were obtained by the slow evaporation of an acetonitrile solution of the compound. Anal. Calcd. for $C_{28}H_{36}Mn_2N_6O_{12}$ (MW 886): C, 39.26; H, 3.69; N, 9.28. Found: C, 39.26; H, 3.69; N, 9.28. It should be noted that in the single crystal structure analysis four water molecules are found but elemental analysis showed no water. Selected FTIR peaks (KBr, cm^{-1}): 3468, 2946, 1649, 1606, 1572, 1484, 1444, 1313, 1093, 765, 622.

$\{[Mn(tpbn)](ClO_4)_2\cdot CH_3OH\}_n$ (52). It was prepared following Method 2 using 32 mg (0.125 mmol) of $Mn(ClO_4)_2$ in 3 mL methanol and 28 mg (0.0625 mmol) of tpbn. A colorless solid was obtained. Yield: 72 mg (81%). Single crystals were obtained by direct layering of the reactants. It should be noted that crystals had one molecule of methanol. Anal. Calcd. for $C_{28}H_{32}Mn_2N_6Cl_2O_8$ (MW 706): C, 47.59; H, 4.53; N, 11.89. Found: C, 47.30; H, 4.35; N, 11.35. Selected FTIR peaks (KBr, cm^{-1}): 3189, 2619, 1649,1603, 1591, 1516, 1460, 1393, 1107, 750, 663, 623.

$[Mn_2(tpbn)(H_2O)_6](tdc)_2\cdot 4H_2O\}_n$ (53). It was prepared following Method 1 using 21.5 mg (0.125 mmol) of thiophene dicarboxylic acid, 31 mg (0.125 mmol) of $Mn(OAc)_2\cdot 4H_2O$ in 3 mL

methanol and 28 mg (0.0625 mmol) of tpbn. A colorless solid was obtained. Yield: 53 mg (74%). Single crystals were obtained by slow evaporation of its aqueous solution. Anal. Calcd. for $C_{37}H_{44}Mn_2N_6O_{13}$ (MW 890): C, 49.92; H, 4.94; N, 9.43. Found: C, 49.72; H, 4.41; N, 8.74. Selected FTIR peaks (KBr, cm^{-1}): 3392, 3220, 2935, 1626, 1604, 1570, 1482, 1443, 1329, 1016, 777, 767, 665.

$[Mn_4(tpbn)_2(CDC)_4(H_2O)_4]_n$ (54). It was prepared following Method 3 using 22 mg (0.125 mmol) of 1,4-cyclohexanedicarboxylic acid, 21.2 mg (0.125 mmol) of $MnSO_4 \cdot H_2O$ in 5 mL water and 28 mg (0.0625 mmol) of tpbn. Colorless crystals were obtained. Yield: 40 mg (68%). Anal. Calcd. for $C_{72}H_{92}Mn_5N_{12}S_1O_{16}$ (MW 1687): C, 51.12; H, 5.45; N, 9.95. Found: C, 50.72; H, 5.41; N, 9.74. It should be noted that the elemnetal analysis is done adding one molecule of manganese sulphate which is also evident from its FTIR spectrum. Selected FTIR peaks (KBr, cm^{-1}): 3403, 3076, 2944, 1719, 1654, 1604, 1482, 1443, 1396, 1123 (sulphate), 766, 618 (sulphate).

$[Mn_2(tpbn)(HBTC)_2]_n$ (55). It was prepared following Method 3 using 27 mg (0.125 mmol) of 1,3,5-benzene tricarboxylic acid, 21.5 mg (0.125 mmol) of $MnSO_4 \cdot H_2O$ in 5 mL water and 28 mg (0.0625 mmol) of tpbn. Colorless crystals were obtained. Yield: 33 mg (50%). Anal. Calcd for $C_{46}H_{48}N_6Mn_2O_{16}$ (MW 1050): Calc. C, 52.57; H, 4.57; N, 8.00. Found: C, 52.08; H, 4.60; N, 8.38. It should be noted that the formula used for CHN analysis was with four water molecules although X-ray crystallography indicated it had no water molecules. Selected FTIR peaks (KBr, cm^{-1}): 3448, 2923, 1717, 1618, 1605, 1444, 1370, 758, 678.

$[Mn_4(tpbn)_2(HCTC)_2(SO_4)_2]$ (56). It was prepared following Method 3 using 26 mg (0.125 mmol) of 1,3,5-cyclohexane tricarboxylic acid, 21.5 mg (0.125 mmol) of $MnSO_4 \cdot H_2O$ in 1 mL water and 28 mg (0.0625 mmol) of tpbn. Colorless crystals were obtained. Yield. 38 mg (53%). Anal. Calcd for $C_{74}H_{80}N_{12}Mn_5S_1O_{24}$ (MW 1681): Calc. C, 52.82; H, 4.75; N, 9.99. Found: C, 51.92; H, 4.96; N, 9.60. It should be noted that the elemnetal analysis is done adding one molecule of manganese sulphate which is also evident from its FTIR spectrum. Selected FTIR peaks (KBr, cm^{-1}): 3421, 1636, 1610, 1574, 1448, 1364, 1182, 1116, 1054, 1026, 975, 772, 626.

$[Mn_2(tphxn)(HBTC)_2(H_2O)_2]_n$ (57). It was prepared following Method 3 using 27 mg (0.125 mmol) of 1,3,5-benzene tricarboxylic acid, 21.5 mg (0.125 mmol) of $MnSO_4 \cdot H_2O$ in 5 mL water

and 30 mg (0.0625 mmol) of tphxn. Colorless crystals were obtained. Yield: 36 mg (55%). Anal. Calcd for $C_{48}H_{46}N_6Mn_2O_{14}$ (MW 1042): Calc. C, 55.27; H, 4.41; N, 8.06. Found: C, 55.68; H, 4.74; N, 7.83. Selected FTIR peaks (KBr, cm^{-1}): 3479, 1707, 1613, 1570, 1481, 1449, 1382, 765.

$\{[Cu_2(tpen)(succinate)(H_2O)_2](ClO_4)_2{\cdot}2H_2O\}_n$ (58). It was prepared following Method 2 using sodium salt of succinic acid {7.5 mg (0.0625 mmol) of succinic acid and 5 mg (0.25 mmol) of sodium hydroxide}, 46.5 mg (0.125 mmol) of $Cu(ClO_4)_2$ in 3 mL methanol and 26.5 mg (0.0625 mmol) of tpen. A blue solid was obtained. Yield: 51 mg (87%). Single crystals were grown from the slow evaporation of a solution of the compound in a mixture of acetonitrile-water. Anal. Calcd for $C_{30}H_{40}N_6Cu_2O_{14}$ (MW 938): Calc. C, 38.37; H, 4.26; N, 8.95. Found: C, 37.36; H, 3.86; N, 8.60. Selected FTIR peaks (KBr, cm^{-1}): 3473, 3216, 2923, 1612, 1556, 1480, 1449, 1386, 1094, 767, 623.

$\{[Cu_2(tpen)(glutarate)(H_2O)_2](ClO_4)_2{\cdot}2H_2O\}_n$ (59). It was prepared following Method 2 using sodium salt of glutaric acid {8.5 mg (0.0625 mmol) of glutaric acid and 5 mg (0.25 mmol) of sodium hydroxide}, 46.5 mg (0.125 mmol) of $Cu(ClO_4)_2$ in 3 mL methanol and 26.5 mg (0.0625 mmol) of tpen. A blue solid was obtained. Yield: 41.6 mg (74%). Single crystals were obtained by slow evaporation of its aqueous solution. Anal. Calcd for $C_{31}H_{38}N_6Cu_2O_{14}$ (MW 952): Calc. C, 39.07; H, 4.41; N, 8.82. Found: C, 38.76; H, 4.29; N, 8.44. Selected FTIR peaks (KBr, cm^{-1}): 3435, 2929, 1611, 1577, 1568, 1558, 1449, 1396, 1091, 769, 624.

$\{[Cu_2(tpen)(adipate)(H_2O)_2](ClO_4)_2\}_n$ (60). It was prepared following Method 2 using sodium salt of adipic acid {9 mg (0.0625 mmol) of adipic acid and 5 mg (0.125 mmol) of sodium hydroxide}, 46.5 mg (0.125 mmol) of $Cu(ClO_4)_2$ in 3 mL methanol and 26.5 mg (0.0625 mmol) of tpen. A blue solid was obtained. Yield: 37.6 mg (65%). Single crystals were obtained by slow evaporation of a solution of the compound in a mixture of acetonitrile-water. Anal. Calcd for $C_{32}H_{40}N_6Cu_2O_{14}$ (MW 930): Calc. C, 41.29; H, 4.30; N, 9.03. Found: C, 41.17; H, 4.10; N, 8.97. Selected FTIR peaks (KBr, cm^{-1}): 3392, 3220, 2935, 1611, 1576, 1558, 1540, 1482, 1448, 1395, 1092, 767, 623.

$[\{Cu_2(tppn)(H_2O)_2(ClO_4)\}_2(succinate)](ClO_4)_4$ (61). It was prepared following Method 2 using sodium salt of succinic acid {15 mg (0.125 mmol) of succinic acid and 10 mg (0.25 mmol) of sodium hydroxide}, 46.5 mg (0.125 mmol) of $Cu(ClO_4)_2$ in 3 mL methanol and 27 mg (0.0625

mmol) of tppn. There was no precipitate; a dark blue filtrate was processed as described above for **19** to isolate the product. Yield: 45 mg (75%). Single crystals were obtained by the slow evaporation of the methanolic solution. Anal. Calcd for $C_{58}H_{74}N_{12}Cu_4Cl_6O_{30}$ (MW 1933.24): Calc. C, 36.00; H, 3.82; N, 8.69. Found: C, 35.30; H, 3.58; N, 8.19. Selected FTIR peaks (KBr, cm^{-1}): 3448, 2927, 1711, 1622, 1370, 758, 678.

{[Cu_2(tppn)(glutarate)(H_2O)$_2$](ClO_4)$_2$·2H_2O}$_n$ (62). It was prepared following Method 2 using sodium salt of glutaric acid {8 mg (0.0625 mmol) of glutaric acid and 5 mg (0.25 mmol) of sodium hydroxide}, 46.5 mg (0.125 mmol) of $Cu(ClO_4)_2$ in 3 mL methanol and 27 mg (0.0625 mmol) of tppn. A blue solid was obtained. Yield: 28 mg (81%). Single crystals were obtained by the slow evaporation of a solution of the compound in a mixture of acetonitrile-water. Anal. Calcd for $C_{32}H_{42}N_6Cu_2Cl_2O_{16}$ (MW 964): Calc. C, 39.83; H, 4.35; N, 8.71. Found: C, 39.18; H, 4.12; N, 8.41. Selected FTIR peaks (KBr, cm^{-1}): 3436, 2925, 1611, 1576, 1447, 1393, 1284, 1093, 764, 624.

{[Cu_2(tppn)(adipate)(H_2O)$_2$](ClO_4)$_2$·2H_2O}$_n$ (63). It was prepared following Method 2 using sodium salt of adipic acid {9 mg (0.0625 mmol) of adipic acid and 5 mg (0.25 mmol) of sodium hydroxide}, 46.5 mg (0.125 mmol) of $Cu(ClO_4)_2$ in 3 mL methanol and 27 mg (0.0625 mmol) of tppn. A blue solid was obtained. Yield: 32 mg (55%). Single crystals were obtained by slow evaporation of a solution of the compound in a mixture of acetonitrile-water. Anal. Calcd for $C_{33}H_{44}N_6Cu_2Cl_2O_{16}$ (MW 978): C, 40.49; H, 4.49; N, 8.58. Found: C, 39.52; H, 4.34; N, 8.12. Selected FTIR peaks (KBr, cm^{-1}): 3419, 2952, 2923, 1612, 1575, 1570, 1560, 1448, 1417, 1091, 768, 623.

[Cu_4(tpbn)$_2$(succinate)$_2$(H_2O)$_4$](ClO_4)$_4$·2H_2O (64). It was prepared following Method 2 using sodium salt of succinic acid {7.5 mg (0.0625 mmol) of succinic acid and 5 mg (0.125 mmol) of sodium hydroxide}, 46.5 mg (0.125 mmol) of $Cu(ClO_4)_2$ in 3 mL methanol and 28 mg (0.0625 mmol) of tpbn. A blue solid was obtained. Yield: 39 mg (81%). Single crystals were obtained by slow evaporation of a solution of the compound in a mixture of acetonitrile-water. Anal. Calcd for $C_{64}H_{80}N_{12}Cu_4Cl_4O_{30}$ (MW 1925): C, 39.89; H, 4.15; N, 8.72. Found: C, 39.69; H, 4.14; N, 9.11. Selected FTIR peaks (KBr, cm^{-1}): 3484, 3429, 1611, 1566, 1483, 1375, 1093, 767, 624.

$[Cu_4(tpbn)_2(glutarate)_2(H_2O)_4](ClO_4)_4 \cdot 4H_2O$ (65). It was prepared following Method 2 using sodium salt of glutaric acid {8.5 (0.0625 mmol) of glutaric acid and 5 mg (0.125 mmol) of sodium hydroxide}, 46.5 mg (0.125 mmol) of $Cu(ClO_4)_2$ in 3 mL methanol and 28 mg (0.0625 mmol) of tpbn. A blue solid was obtained. Yield: 44 mg (65%). Single crystals were obtained by slow evaporation of a solution of the compound in a mixture of acetonitrile-water. Anal. Calcd for $C_{66}H_{88}N_{12}Cu_4Cl_4O_{28}$ (MW 1925.24): C, 41.17; H, 4.51; N, 8.72. Found: C, 40.94; H, 4.34; N, 9.04. Selected FTIR peaks (KBr, cm^{-1}): 3429, 1609, 1595, 1483, 1375, 1101, 764, 624.

$\{[Cu_2(tpbn)(adipate)(H_2O)_2](ClO_4)_2 \cdot 4H_2O\}_n$ (66). It was prepared following Method 2 using sodium salt of adipic acid {18.5 mg (0.125 mmol) of adipic acid and 10 mg (0.25 mmol) of sodium hydroxide}, 93 mg (0.25 mmol) of $Cu(ClO_4)_2$ in 6 mL methanol and 57 mg (0.125 mmol) of tpbn. A blue solid was obtained. Yield: 93 mg (72%). Single crystals were obtained by slow evaporation of an acetonitrile solution of the compound. Anal. Calcd. for $C_{34}H_{50}N_6Cu_2Cl_2O_{18}$ (MW 1030.68): C, 39.57; H, 4.84; N, 8.14. Found: C, 39.00; H, 4.73; N, 7.80. Selected FTIR peaks (KBr, cm^{-1}): 3435, 1610, 1580, 1568, 1484, 1446, 1092, 765, 626.

$[Cu_2(tpbn)(fumarate)](ClO_4)_2 \cdot 3H_2O\}_n$ (67). It was prepared following Method 2 using sodium salt of fumaric acid {14.5 mg (0.125 mmol) of succinic acid and 10 mg (0.125 mmol) of sodium hydroxide}, 93 mg (0.25 mmol) of $Cu(ClO_4)_2$ in 6 mL methanol and 57 mg (0.125 mmol) of tpbn. A blue solid was obtained. Yield: 95 mg (80%). Single crystals were obtained by slow evaporation of an acetonitrile-water solution of the compound. Anal. Calcd for $C_{32}H_{40}N_6Cu_2Cl_2O_{15}$ (MW 946.56): C, 40.60; H, 4.26; N, 8.87. Found: C, 40.84; H, 3.96; N, 8.74. Selected FTIR peaks (KBr, cm^{-1}): 3479, 1613, 1587, 1570, 1481, 1449, 1384, 1101, 765, 623.

$\{[Cu_2(tpbn)(maleate)(H_2O)_2](ClO_4)_2 \cdot 2H_2O\}_n$ (68). It was prepared following Method 2 using sodium salt of maleic acid {14.5 mg (0.125 mmol) of maleic acid and 10 mg (0.25 mmol) of sodium hydroxide}, 93 mg (0.125 mmol) of $Cu(ClO_4)_2$ in 6 mL methanol and 57 mg (0.125 mmol) of tpbn. A blue solid was obtained. Yield: 85 mg (71%). Single crystals were obtained by slow evaporation of a solution of the compound in a mixture of acetonitrile-water. Anal. Calcd for $C_{32}H_{38}N_6Cu_2Cl_2O_{14}$ (MW 960.56): C, 40.00; H, 3.99; N, 8.74. Found: C, 40.64; H, 3.72; N, 8.70. Selected FTIR peaks (KBr, cm^{-1}): 3435, 1609, 1574, 1564, 1487, 1448, 1381, 1100, 770, 624.

$[Cu_4(tpbn)_2(mercaptosuccinate)_2(H_2O)_4](ClO_4)_4 \cdot 2H_2O$ (69). It was prepared following Method 2 using sodium salt of mercaptosuccinic acid {19 mg (0.125 mmol) of mercaptosuccinic acid and 10 mg (0.25 mmol) of sodium hydroxide}, 46.5 mg (0.125 mmol) of $Cu(ClO_4)_2$ in 3 mL methanol and 28 mg (0.0625 mmol) of tpbn. A blue solid was obtained. Yield: 42 mg (69%). Single crystals were obtained by the slow evaporation of its aqueous solution. Anal. Calcd for $C_{66}H_{84}N_{12}Cu_4Cl_4S_2O_{30}$ (MW 1984): C, 39.91; H, 4.23; N, 8.46. Found: C, 40.09; H, 4.34; N, 8.76. Selected FTIR peaks (KBr, cm^{-1}): 3422, 1610, 1589, 1447, 1376, 1290, 1092, 768, 624.

$[Cu_4(tpbn)_2(malate)_2(H_2O)_2(ClO_4)_2](ClO_4)_2 \cdot 5H_2O$ (70). It was prepared following Method 2 using sodium salt of malic acid {17 mg (0.125 mmol) of malic acid and 10 mg (0.25 mmol) of sodium hydroxide}, 46.5 mg (0.125 mmol) of $Cu(ClO_4)_2$ in 3 mL methanol and 28 mg (0.0625 mmol) of tpbn. A blue solid was obtained. Yield: 45.6 mg (75%). Single crystals were obtained by the slow evaporation of an aqueous solution of the compound. Anal. Calcd for $C_{64}H_{82}N_{12}Cu_4Cl_4O_{33}$ (MW 1946): C, 39.14; H, 4.38; N, 8.56. Found: C, 39.37; H, 4.29; N, 8.26. Selected FTIR peaks (KBr, cm^{-1}): 3421, 1608, 1587, 1482, 1444, 1331, 1016, 778, 670.

$\{[Cu_2(tpbn)(t,t\text{-muconate})(H_2O)_2](ClO_4)_2 \cdot 3H_2O\}_n$ (71). It was prepared following Method 2 using sodium salt of t,t-muconic acid {18 mg (0.125 mmol) of t,t-muconic acid and 10 mg (0.25 mmol) of sodium hydroxide}, 93 mg (0.25 mmol) of $Cu(ClO_4)_2$ in 6 mL methanol and 57 mg (0.125 mmol) of tpbn. A blue solid was obtained. Yield: 95 mg (75%). Single crystals were obtained by slow evaporation of aceonitrile solution of the compound. Anal. Calcd for $C_{34}H_{46}N_6Cu_2Cl_2O_{17}$ (MW 1008.66): C, 40.48; H, 4.60; N, 8.33. Found: C, 39.08; H, 4.52; N, 7.78. Selected FTIR peaks (KBr, cm^{-1}): 3386, 1610, 1556, 1483, 1447, 1366, 1337, 1092, 767, 623.

$\{[Cu_2(tpbn)(c,c\text{-muconate})(H_2O)_2](ClO_4)_2 \cdot 2H_2O\}_n$ (72). It was prepared following Method 2 using sodium salt of c,c-muconic acid {18 mg (0.125 mmol) of c,c-muconic acid and 10 mg (0.125 mmol) of sodium hydroxide}, 93 mg (0.25 mmol) of $Cu(ClO_4)_2$ in 6 mL methanol and 57 mg (0.0625 mmol) of tpbn. A blue solid was obtained. Yield: 88 mg (72%). Anal. Calcd for $C_{34}H_{44}N_6Cu_2Cl_2O_{16}$ (MW 990.64): C, 41.22; H, 4.48; N, 8.48. Found: C, 41.08; H, 4.26; N, 8.23. Selected FTIR peaks (KBr, cm^{-1}): 3412, 1603, 1544, 1483, 1447, 1392, 1098, 769, 623.

{[Cu_2(tphxn)(succinate)(H_2O)$_2$](ClO_4)$_2$·4H_2O}$_n$ (73). It was prepared following Method 2 using sodium salt of succinic acid {7.5 mg (0.0625 mmol) of succinic acid and 5 mg (0.25 mmol) of sodium hydroxide}, 46.5 mg (0.125 mmol) of $Cu(ClO_4)_2$ in 3 mL methanol and 30 mg (0.0625 mmol) of tphxn. A blue solid was obtained. Yield: 56 mg (88%). Single crystals were obtained by slow evaporation of aqueous and acetonitrile solution of the compound. Anal. Calcd for $C_{34}H_{48}N_6Cu_2Cl_2O_{14}$ (MW 1030): C, 39.61; H, 4.66; N, 8.15. Found: C, 39.39; H, 4.37; N, 8.12. Selected FTIR peaks (KBr, cm^{-1}): 3420, 1608, 1557, 1449, 1364, 1098, 767, 734, 623.

{[Cu_2(tpbn)(digylconate)(ClO_4)(H_2O)](ClO_4)·H_2O}$_n$ (74). It was prepared following Method 2 using sodium salt of diglyconic acid {8.5 mg (0.0625 mmol) of diglyconic acid and 5 mg (0.25 mmol) of sodium hydroxide}, 46.5 mg (0.125 mmol) of $Cu(ClO_4)_2$ in 3 mL methanol and 28 mg (0.0625 mmol) of tpbn. A blue solid was obtained. Yield: 41.6 mg (81.2%). Single crystals were obtained by slow evaporation of an aceonitrile solution of the compound. Anal. Calcd for $C_{32}H_{40}N_6Cu_2Cl_2O_{15}$ (MW 946.78): C, 40.59; H, 4.26; N, 8.87. Found: C, 40.52; H, 4.18; N, 8.69. Selected FTIR peaks (KBr, cm^{-1}): 3429, 1609, 1595, 1483, 1375, 1101, 764, 624.

[Cu_4(tpbn)$_2$(2,2′-dithioacetate)$_2$(H_2O)$_4$](ClO_4)$_4$ (75). It was prepared following Method 2 using sodium salt of 2,2′-dithioacetic acid {19 mg (0.125 mmol) of 2,2′-dithioacetic acid and 10 mg (0.25 mmol) of sodium hydroxide}, 46.5 mg (0.125 mmol) of $Cu(ClO_4)_2$ in 3 mL methanol and 28 mg (0.0625 mmol) of tpbn. A blue solid was obtained. Yield: 41 mg (68%). Single crystals were obtained by slow evaporation of an aqueous solution of the compound. Anal. Calcd for $C_{64}H_{80}N_{12}Cu_4Cl_4S_2O_{28}$ (MW 1924): C, 39.91; H, 4.15; N, 8.73. Found: C, 39.45; H, 3.96; N, 8.08. Selected FTIR peaks (KBr, cm^{-1}): 3386, 1610, 1594, 1587, 1449, 1381, 1365, 1100, 1071, 1054, 770, 622.

{[Cu_2(tpbn)(tere)(H_2O)$_2$](ClO_4)$_2$·4H_2O}$_n$ (76). It was synthesized following Method 2 using sodium salt of terephthalic acid {17 mg (0.125 mmol) of terephthalic acid and 10 mg (0.25 mmol) of sodium hydroxide}, 93 mg (0.25 mmol) of $Cu(ClO_4)_2$ in 6 mL methanol and 57 mg (0.0125 mmol) of tpbn. A blue solid was obtained. Yield: 119 mg (96%). Single crystals were obtained by slow evaporation of an acetonitrile solution of the compound. Anal. Calcd for $C_{36}H_{44}N_6Cu_2Cl_2O_{14}$ (MW 1050): C, 41.14; H, 4.19; N, 8.00. Found: C, 41.34; H, 3.96; N, 7.61.

Selected FTIR peaks (KBr, cm^{-1}): 3434, 1611, 1586, 1570, 1483, 1447, 1398, 1381, 1374, 1094, 769, 623.

{[$Cu_4(F_4$-tere$)_3$(tpbn$)_2$](ClO$_4)_2$·4H$_2$O}$_n$ (77). It was prepared following Method 2 using 24 mg of lithium salt of tetrafluoroterephthalic acid, 46.5 mg (0.125 mmol) of $Cu(ClO_4)_2$ in 3 mL methanol and 28 mg (0.0625 mmol) of tpbn. A blue solid was obtained. Yield: 44 mg (66%). Single crystals were obtained by slow evaporation of solution of the compound in a mixture of acetonitrile-water. Selected FTIR peaks (KBr, cm^{-1}): 3434, 1611, 1586, 1570, 1483, 1447, 1398, 1381, 1374, 1094, 769, 623.

{[Cu_2(tpbn)(2,6-PDC)(H$_2$O)$_2$](ClO$_4)_2$·4H$_2$O}$_n$ (78). It was prepared following Method 2 using sodium salt of 2,6-PDC acid {11 mg (0.0625 mmol) of 2,6-PDC acid and 5 mg (0.125 mmol) of sodium hydroxide}, 46.5 mg (0.125 mmol) of $Cu(ClO_4)_2$ in 3 mL methanol and 28 mg (0.0625 mmol) of tpbn. A blue solid was obtained. Yield: 47 mg (74%). Anal. Calcd for $C_{35}H_{41}N_6Cu_2O_{16}$ (MW 1015): Calc. C, 41.37; H, 4.04; N, 9.65. Found: C41.91; H, 3.91; N, 9.65. Selected FTIR peaks (KBr, cm^{-1}): 3523, 3402, 3086, 2952, 1700, 1628, 1485, 1450, 1369, 1291, 1096, 766, 655, 622.

{[$NaCu_2$(tppn)(O,O′-oxydiethylenediglyconate)(ClO$_4$)(H$_2$O)$_3$](ClO$_4)_2$}$_n$ (79). It was prepared following Method 2 using sodium salt of O,O′-diethylenediglyconic acid {14 mg (0.0625 mmol) of O,O′-diethylenediglyconic acid and 5 mg (0.125 mmol) of sodium hydroxide}, 46.5 mg (0.125 mmol) of $Cu(ClO_4)_2$ in 3 mL methanol and 27.5 mg (0.0625 mmol) of tppn. A dark blue filtrate was processed as described above for **19** to isolate the product. Yield: 52 mg (73%) . Single crystals were obtained by layering of methanolic solution of the compound with diethylether. It should be noted that the formula used for the calculation of CHN analysis was without any water molecule. Anal. Calcd. for $C_{35}H_{46}N_6Cu_2Na_1Cl_3O_{21}$ (MW 1142): C, 36.77; H, 4.02; N, 7.35. Found: C, 36.30; H, 3.58; N, 7.69. Selected FTIR peaks (KBr, cm^{-1}): 3464, 1614, 1486, 1448, 1317, 1100, 768, 623.

{[$NaCu_2$(tpbn)(O,O′-oxydiethylenediglyconate)(H$_2$O)(ClO$_4$)](ClO$_4)_2$}$_2$ (80). It was prepared following Method 2 using sodium salt of O,O′-diethylenediglyconic acid {14 mg (0.0625 mmol) of O,O'-diethylenediglyconic acid and 5 mg (0.125 mmol) of sodium hydroxide}, 46.5 mg (0.125 mmol) of $Cu(ClO_4)_2$ in 3 mL methanol and 28 mg (0.0625 mmol) of tpbn. A dark blue

filtrate was processed as described above for **19** to isolate the product. Yield: 25 mg (46%). Single crystals were obtained by the slow evaporation of a methanolic solution of the compound. Anal. Calcd for $C_{72}H_{88}N_{12}Cu_4Cl_4O_{30}$ (MW 1996): C, 41.14; H, 4.19; N, 8.00. Found: C, 41.34; H, 3.96; N, 7.61. Selected FTIR peaks (KBr, cm^{-1}): 3435, 1610, 1432, 1445, 1320, 1145, 1110, 768, 636, 626. It should be noted that the formula used for the calculation of CHN analysis was without any water molecule.

$\{[Cu_4(tpen)_2(CDC)_3](ClO_4)_2 \cdot 8H_2O\}_n$ (81). It was prepared following Method 2 using sodium salt of cyclohexane dicarboxylic acid {15.5 mg (0.094 mmol) of 1,4-cyclohexane dicarboxylic acid and 8 mg (0.19 mmol) of sodium hydroxide}, 46.5 mg (0.125 mmol) of $Cu(ClO_4)_2$ in 3 mL methanol and 26 mg (0.0625 mmol) of tpen. A blue solid was obtained. Yield: 33 mg (58%). Single crystals were grown from a solution of the compound in a hot acetonitrile and water mixture. Selected FTIR peaks (KBr, cm^{-1}): 3430, 1610, 1542, 1449, 1410, 1444, 1358, 1092, 767, 734, 625.

$[Cu_8(tpen)_4(tdc)_4(H_2O)_4](ClO_4)_8 \cdot 4H_2O$ (82). It was prepared following Method 2 using sodium salt of thiophene dicarboxylic acid {11 mg (0.0625 mmol) of thiophene dicarboxylic acid and 5 mg (0.125 mmol) of sodium hydroxide}, 46.5 mg (0.125 mmol) of $Cu(ClO_4)_2$ in 3 mL methanol and 26 mg (0.0625 mmol) of tpen. A blue solid was obtained. Yield: 34 mg (57%). Single crystals were obtained by slow evaporation of solution of the compound in a mixture of acetonitrile-water. Anal. Calcd for $C_{128}H_{136}N_{24}Cu_8O_{56}S_4$ (MW 3824): Calc. C, 39.71; H, 3.62; N, 8.68. Found: C, 39.68; H, 3.52; N, 8.50. Selected FTIR peaks (KBr, cm^{-1}): 3423, 1613, 1589, 1577, 1486, 1449, 1354, 1341, 1091, 775, 761, 623.

$[Cu_4(tppn)_2(tdc)_2(H_2O)_4](ClO_4)_4 \cdot 2H_2O$ (83). It was prepared following Method 2 using sodium salt of thiophene dicarboxylic acid {11 mg (0.0625 mmol) of thiophene dicarboxylic acid and 5 mg (0.125 mmol) of sodium hydroxide}, 46.5 mg (0.125 mmol) of $Cu(ClO_4)_2$ in 3 mL methanol and 27 mg (0.0625 mmol) of tppn. A blue solid was obtained. Yield: 50 mg (81%). Single crystals were obtained by slow evaporation of solution of the compound in a mixture of acetonitrile-water. Calcd for $C_{66}H_{73}N_{12}Cu_4Cl_4S_2O_{30}$ (MW 1982.63): C, 39.980; H, 3.718; N, 8.479. Found: C, 39.852; H, 3.658; N, 8.652. Selected FTIR peaks (KBr, cm^{-1}): 3435, 1612, 1577, 1530, 1358, 1097, 769, 632. Selected Raman Peaks (cm^{-1}): 3077, 1611, 1573, 1457, 1029, 927, 655.

$[Cu_4(tpbn)_2(tdc)_2(H_2O)_4](ClO_4)_4$ (84). It was prepared following Method 2 using sodium salt of thiophene dicarboxylic acid {11 mg (0.0625 mmol) of thiophene dicarboxylic acid and 5 mg (0.125 mmol) of sodium hydroxide}, 46.5 mg (0.125 mmol) of $Cu(ClO_4)_2$ in 3 mL methanol and 28 mg (0.0625 mmol) of tpbn. A blue solid was obtained. Yield: 47 mg (74.5%). Single crystals were obtained by slow evaporation of a hot aqueous solution of the compound. Anal. Calcd for $C_{68}H_{78}N_{12}Cu_4Cl_4S_2O_{31}$ (MW 2019.67): C, 40.430; H, 3.900; N, 8.324. Found: C, 39.964; H, 3.722; N, 7.652. Selected FTIR peaks (KBr, cm^{-1}): 3430, 1610, 1578, 1528, 1359, 1088, 768, 625. Selected Raman Peaks (cm^{-1}): 3079, 1611, 1571, 1461, 1030, 929, 810, 658, 621.

$[Cu_4(tppen)_2(tdc)_2(H_2O)_4](ClO_4)_4 \cdot 4H_2O$ (85). It was prepared following Method 2 using sodium salt of thiophene dicarboxylic acid {11 mg (0.0625 mmol) of thiophene dicarboxylic acid and 5 mg (0.125 mmol) of sodium hydroxide}, 46.5 mg (0.125 mmol) of $Cu(ClO_4)_2$ in 3 mL methanol and 29 mg (0.0625 mmol) of tppen. A blue solid was obtained. Yield: 50 mg (77%). Single crystals were obtained by the slow evaporation of an acetonitrile solution of the compound. Anal. Calcd for $C_{70}H_{80}N_{12}Cu_4Cl_4S_2O_{30}$ (MW 2065.08): C, 40.71; H, 3.91; N, 8.14. Found: C, 40.09; H, 3.90; N, 8.39. Selected FTIR peaks (KBr, cm^{-1}): 3438, 1611, 1581, 1528, 1356, 1091, 770, 624. Selected Raman Peaks (cm^{-1}): 1468, 1033, 931, 854.

$[Cu_4(tphxn)_2(tdc)_2(H_2O)_4](ClO_4)_4 \cdot 4H_2O$ (86). It was prepared following Method 2 using sodium salt of thiophene dicarboxylic acid {11 mg (0.0625 mmol) of thiophene dicarboxylic acid and 5 mg (0.125 mmol) of sodium hydroxide}, 46.5 mg (0.125 mmol) of $Cu(ClO_4)_2$ in 3 mL methanol and 30 mg (0.0625 mmol) of tphxn. A blue solid was obtained. Yield: 38 mg (60%). Anal. Calcd for $C_{72}H_{80}N_{12}Cu_4Cl_4S_2O_{30}$ (MW 2024): C, 45.05; H, 4.15; N, 8.30. Found: C, 45.22; H, 3.53; N, 8.36. Selected FTIR peaks (KBr, cm^{-1}): 3439, 3074, 2935, 2856, 1611, 1594, 1447, 1352, 1094, 771, 624.

$\{[Cu_2(tphn)(tdc)_2] \cdot 2NaClO_4\}_n$ (87). It was prepared following Method 2 using sodium salt of thiophene dicarboxylic acid {21 mg (0.125 mmol) of thiophene dicarboxylic acid dicarboxylic acid and 10 mg (0.25 mmol) of sodium hydroxide}, 46.5 mg (0.125 mmol) of $Cu(ClO_4)_2$ in 3 mL methanol and 31 mg (0.0625 mmol) of tphn. Dark green filtrate was processed as described above for **19** to isolate the product. Yield: 50 mg (77%). Single crystals were obtained by slow evaporation of a methanolic solution of the compound. Anal. Calcd for $C_{43}H_{40}N_6Cu_2Cl_2S_2Na_1O_{16}$ (MW 1208): C, 42.71; H, 3.31; N, 6.90. Found: C, 42.55; H, 3.24; N, 6.82. In the single crystal

structure analysis two molecules of acetonitrile were also found. Selected FTIR peaks (KBr, cm^{-1}): 3468, 2929, 1662, 1612, 1528, 1448, 1369, 1090, 769, 623.

$\{[Cu_6(tpen)_3(CTC)_2](ClO_4)_6 \cdot 5H_2O\}_n$ (88). It was prepared following Method 2 using sodium salt of 1,3,5-cyclohexanetricarboxylic acid {18 mg (0.083 mmol) of 1,3,5-cyclohexanetricarboxylic acid and 5 mg (0.125 mmol) of sodium hydroxide}, 46.5 mg (0.125 mmol) of $Cu(ClO_4)_2$ in 3 mL methanol and 28 mg (0.0625 mmol) of tpbn. A blue solid was obtained. Yield: 42 mg (73%). Single crystals were obtained by slow evaporation of a solution of the compound in a mixture of acetonitrile and water. Anal. Calcd for $C_{96}H_{112}N_{18}Cu_6O_{41}$ (MW 2772): C, 41.55; H, 4.04; N, 9.09. Found: C, 40.92; H, 4.17; N, 9.65. Selected FTIR peaks (KBr, cm^{-1}): 3401, 1611, 1576, 1567, 1447, 1389, 1093, 796, 625.

$\{[Cu_4(tpbn)_2(BTC)_2(H_2O)_2](ClO_4)_2\}_n$ (89). It was prepared following Method 2 using sodium salt of 1,3,5-benzenetricarboxylic acid {18 mg (0.083 mmol) of 1,3,5-benzenetricarboxylic acid and 14 mg (0.25 mmol) of potassium hydroxide}, 93 mg (0.25 mmol) of $Cu(ClO_4)_2$ in 2 mL methanol and 4 mL water and 56.5 mg (0.125 mmol) of tpbn except after stirring at RT the reaction mixture was refluxed for 4 hrs. A blue solid was obtained. Yield: 65 mg (59%). Single crystals were obtained by layering of a DMSO solution of the compound with acetonitrile. Selected FTIR peaks (KBr, cm^{-1}): 3428, 1610, 1562, 1483, 1444, 1358, 1092, 767, 734, 625.

$[Cu_2(tpen)(2,6\text{-}NDS)_2(H_2O)_4] \cdot 8H_2O$ (90). It was prepared following Method 2 using 42 mg (0.125 mmol) sodium salt of naphthalene disulphonic acid, 46.5 mg (0.125 mmol) of $Cu(ClO_4)_2$ in 3 mL methanol and 26.5 mg (0.0625 mmol) of tpen. A green solid was obtained. Yield: 40 mg (48%). Single crystals were obtained by slow evaporation of a solution of the compound in a mixture of acetonitrile-water. Anal. Calcd for $C_{46}H_{60}N_6Cu_2S_2O_{24}$ (MW 1339): C, 41.22; H, 4.48; N, 6.27. Found: C, 40.12; H, 4.49; N, 6.06. Selected FTIR peaks (KBr, cm^{-1}): 3401, 1609, 1446, 1234, 1194, 1183, 1029, 908, 763, 664, 627.

$\{[Cu_4(tppn)_2(Cl)_2(H_2O)_4](2,6\text{-}NDS)_2 \cdot 14H_2O\}_n$ (91). It was prepared following Method 2 using 21 mg sodium salt of naphthalene disulphonic acid, 46.5 mg (0.125 mmol) of $Cu(ClO_4)_2$ in 3 mL methanol and 27 mg (0.0625 mmol) of tppn. A blue solid was obtained. Yield: 42 mg (63%). Single crystals were obtained by slow evaporation of its aqueous solution. Anal. Calcd for $C_{74}H_{100}N_{12}Cu_4Cl_4O_{22}S_4$ (MW 2138): C, 41.53; H, 4.67; N, 7.85. Found: C, 41.68; H, 4.58; N,

7.86. Selected FTIR peaks (KBr, cm^{-1}): 3525, 3459, 1609, 1440, 1196, 1184, 1028, 908, 772, 664, 626.

$\{[Cu_2(tpbn)(2,6\text{-}NDS)(Cl)_2]\cdot 4\cdot 5H_2O\}_n$ (92). It was prepared following Method 2 using 21 mg (0.0625 mmol) sodium salt of naphthalene disulphonic acid, 46.5 mg (0.125 mmol) of $Cu(ClO_4)_2$ in 3 mL methanol and 28 mg (0.0625 mmol) of tpbn. A blue solid was obtained. Yield: 45 mg (71%). Single crystals were obtained by slow evaporation of its aqueous solution. Anal. Calcd for $C_{38}H_{45}N_6Cu_2Cl_2O_6S_2$ (MW 1018): C, 44.79; H, 4.42; N, 8.25. Found: C, 45.17; H, 4.58; N, 8.29. Selected FTIR peaks (KBr, cm^{-1}): 3392, 1609, 1480, 1469, 1439, 1234, 1195, 1183, 1028, 774, 664, 628.

$\{[Cu_2(tpbn)(4,4'\text{-}bpy)](ClO_4)_2\cdot 3H_2O\}_n$ (93). It was prepared following Method 2 using 10 mg (0.0625 mmol) 4,4′-bipy, 46.5 mg (0.125 mmol) of $Cu(ClO_4)_2$ in 3 mL methanol and 28 mg (0.0625 mmol) of tpbn. A purple solid was obtained. Yield: 52 mg (67%). Single crystals were obtained by slow evaporation of a solution of the compound in a mixture of acetonitrile-water. Anal. Calcd for $C_{38}H_{46}N_6Cu_2Cl_4O_{21}$ (MW 1223): C, 37.28; H, 3.92; N, 9.15. Found: C, 37.07; H, 3.47; N, 9.17. Selected FTIR peaks (KBr, cm^{-1}): 3445, 1613, 1483, 1449, 1292, 1091, 771, 626.

$\{[Cu_2(tpbn)(N_3)_2(H_2O)_2](ClO_4)_2\}_n$ (94). It was prepared following Method 2 using 4.5 mg (0.0625 mmol) sodium azide, 46.5 mg (0.125 mmol) of $Cu(ClO_4)_2$ in 3 mL methanol and 28 mg (0.0625 mmol) of tpbn. A dark green solid was obtained. Yield: 40 mg (74%). Single crystals were obtained by slow evaporation of an acetonitrile solution of the compound. Anal. Calcd for $C_{28}H_{30}N_{12}Cu_2Cl_2O_8$ (MW 862): C, 38.97; H, 3.48; N, 19.48. Found: C, 37.79; H, 3.66; N, 20.24. Selected FTIR peaks (KBr, cm^{-1}): 3420, 2947, 2074, 1612, 1573, 1449, 1292, 1103, 766, 623.

$[Co_2(tpbn)(HBTC)_2]_n$ (95). It was prepared following Method 3 using using 27 mg (0.125 mmol) of 1,3,5-benzene tricarboxylic acid, 37 mg (0.125 mmol) of $Co(NO_3)_2$ in 5 mL water and 28 mg (0.0625 mmol) of tpbn. Block shaped violet crystals were obtained. Yield: 16 mg (26%). Anal. Calcd for $C_{46}H_{38}N_6Co_2O_{12}$ (MW 988): C, 55.87; H, 4.04; N, 8.50. Found: C, 55.75; H, 4.03; N, 8.79. Selected FTIR peaks (KBr, cm^{-1}): 3431, 2954, 2922, 1707, 1614, 1608, 1441, 1431, 1371, 1245, 1097, 756, 721, 677.

$[Zn_2(tpbn)(adc)_2(H_2O)_2]\cdot 4H_2O$ (96). It was prepared following Method 1 using 14 mg (0.125 mmol) of acetylene dicarboxylic acid, 27.5 mg (0.125 mmol) of $Zn(OAc)_2\cdot 2H_2O$ in 3 mL

methanol and 28 mg (0.0625 mmol) of tpbn. A colorless solid was obtained. Yield: 51.6 mg (98%). Single crystals were obtained by slow evaporation of its aqueous solution. Anal. Calcd for $C_{36}H_{36}N_6Zn_2O_{10}$ (MW 847): Calc. C, 51.00; H, 4.25; N, 9.91. Found: C, 51.09; H, 4.41; N, 9.48. It should be noted that four water molecules were found in the crystal structure which is also evident from thermogravimetric analysis. Selected FTIR peaks (KBr, cm^{-1}):3448, 2937, 1627, 1608, 1486, 1445, 1325, 1025, 774, 680, 649.

$\{[Cd_6(tpbn)_3(adc)_3(H_2O)_3]\}_n$ (97). It was prepared following Method 1 using 14 mg (0.125 mmol) of acetylene dicarboxylic acid, 33.5 mg (0.125 mmol) of $Cd(OAc)_2{\cdot}2H_2O$ in 3 mL methanol and 28 mg (0.0625 mmol) of tpbn. A colorless solid was obtained. Yield: 37 mg (74%). This compound had a very low solubility in water and insoluble in other organic solvents. Single crystals were obtained by evaporation of its aqueous solution. Anal. Calcd for $C_{36}H_{32}N_6Cd_2O_8$ (MW 900): Calc. C, 48.00; H, 3.55; N, 9.33. Found: C, 47.82; H, 3.66; N, 9.21. Selected FTIR peaks (KBr, cm^{-1}): 3437, 3210, 3072, 2941, 2881, 1623, 1603, 1580, 1483, 1444, 1351, 1328, 1019, 774, 760, 683. Selected Raman peaks (cm^{-1}): 2213, 1607, 1574, 1373, 1052, 1015, 846, 642.

$[Cd_2(tppn)(adc)_2]_n$ (98). It was prepared following Method 1 using 14 mg (0.125 mmol) of acetylene dicarboxylic acid, 33. 5 mg (0.125 mmol) of $Cd(OAc)_2{\cdot}2H_2O$ in 3 mL methanol and 27 mg (0.0625 mmol) of tppn. A colorless solid was obtained. Yield: 54 mg (87%). Anal. Calcd for $C_{35}H_{38}N_6Cd_2O_{12}$ (MW 958): Calc. C, 43.84; H, 3.96; N, 8.76. Found: C, 43.64; H, 3.67; N, 8.65. Selected FTIR peaks (KBr, cm^{-1}): 3401, 1604, 1572, 1483, 1410, 1442, 1369, 767, 724, 690.

$[Cd_2(bpbg)(adc)_2(H_2O)_3]_n$ (99). It was prepared following Method 1 using 14 mg (0.125 mmol) of acetylene dicarboxylic acid, 33.5 mg (0.125 mmol) of $Cd(OAc)_2{\cdot}2H_2O$ in 3 mL methanol and 24 mg (0.0625 mmol) of bpbg. A colorless solid was obtained. Yield: 38 mg (72%). Single crystals were obtained by slow evaporation of its aqueous solution. Anal. Calcd for $C_{26}H_{32}N_6Cd_2O_{12}$ (MW 844): Calc. C, 36.96; H, 3.79; N, 9.95. Found: C, 36.55; H, 3.56; N, 9.93. Selected FTIR peaks (KBr, cm^{-1}): 3446, 2949, 2923, 1678, 1623, 1614, 1601, 1579, 1569, 1379, 1342, 763, 759, 683.

$[Cd_2(tpbn)(tdc)_2{\cdot}2H_2O]_n$ (100). It was prepared following Method 1 using 12 mg (0.125 mmol) of thiophene dicarboxylic acid, 33.5 mg (0.125 mmol) of $Cd(OAc)_2{\cdot}2H_2O$ in 3 mL methanol and

28 mg (0.0625 mmol) of tpbn. A colorless solid was obtained. Yield: 53 mg (80%). Anal. Calcd for $C_{40}H_{40}N_6Cd_2O_{10}S_2$ (MW 1052): Calc. C, 45.62; H, 3.80; N, 7.98. Found: C, 45.98; H, 3.55; N, 8.25. Selected FTIR peaks (KBr, cm^{-1}): 3434, 1604, 1589, 1568, 1379, 1368, 1016, 818, 772.

$[Zn_2(tpbn)(H_2BTC)_2(NO_3)_2]$ (101). It was prepared following Method 3 using 18 mg (0.125 mmol) of 1,3,5-benzene tricarboxylic acid, 37.5 mg (0.125 mmol) of $Zn(NO_3)_2 \cdot 6H_2O$ in 5 mL water and 28 mg (0.0625 mmol) of tpbn. Colorless crystals were obtained. Yield: 35 mg (49%). Selected FTIR peaks (KBr, cm^{-1}): 3408, 3072, 2944, 2925, 1715, 1694, 1609, 1575, 1462, 1383, 1292, 1108, 764, 686.

$[Zn_2(tpbn)(HBTC)_2]_n$ (102). It was prepared following Method 3 using 18 mg (0.125 mmol) of 1,3,5-benzene tricarboxylic acid, 37 mg (0.125 mmol) of $ZnSO_4 \cdot 7H_2O$ in 5 mL water and 28 mg (0.0625 mmol) of tpbn. Colorless crystals were obtained. Yield: 42 mg (65%). Selected FTIR peaks (KBr, cm^{-1}): 3392, 1715, 1609, 1576, 1462, 1383, 1292, 1025, 764, 685.

$\{[Cd_2(tpbn)(HBTC)_2(H_2O)_2] \cdot 4H_2O\}_n$ (103). It was prepared following Method 3 using 18 mg (0.125 mmol) of 1,3,5-benzene tricarboxylic acid, 33.5 mg (0.125 mmol) of $Cd(OAc)_2 \cdot 2H_2O$ in 1 mL water and 28 mg (0.0625 mmol) of tpbn. Colorless crystals were obtained. Yield: 44 mg (63%). Selected FTIR peaks (KBr, cm^{-1}): 3391, 1681, 1626, 1605, 1574, 1556, 1371, 1354, 1017, 765, 678.

CHAPTER III

Results and Discussion

In this chapter synthesis, isolation (in good to high yields and purity), and structural characterization of ancillary ligands are discussed first. Based on the strategic design for systematic studies, reproducible syntheses in good to high yields of over one hundred MOCNs comprised of divalent transition metal ions, ancillary ligands and multiatom organic linkers are conducted under ambient as well as hydrothermal conditions. These are characterized by elemental analysis, FT-IR, Raman and UV-Vis spectroscopy, single crystal and powder X-ray diffraction, and ESI-MS analysis as well as are studied for their redox behavior by cyclic voltammetry, and thermal properties by thermogravimetric analysis. Their photoluminescent properties are established by fluorescence spectroscopy in the solid state. A few MOCNs have been used to demonstrate their viability in water adsorption applications.

3.1 Ancillary ligands

As discussed in the 'Introduction' section, ancillary ligands play an important role in the generation of MOCNs. The denticity of the ancillary ligand dictates the number of open sites on the metal center, the main criteria in generating MOCNs of different dimensions.

In order to carry out a systematic study, a series of ancillary ligands varying the denticity from three to six has been prepared and their effect on the formation of MOCNs has been studied with different metal centers and carboxylate linkers. The tridentate ligands can occupy three sites of the metal center leaving two or three open sites depending on the preferred coordination number for the metal ion used. For studying the effect of N-alkyl substituent in the tridentate ligands on the formation of MOCNs, the substitution on the alkyl nitrogen has been varied from methyl to ethyl to isopropyl to t-butyl to benzyl. When the substitution on the alkyl nitrogen of the tridentate ligand is changed to a methylpyridyl group, it forms a tetradentate ligand. Several hexadentate ligands varying the methylene chain length between the two alkyl nitrogens have been synthesized. This is aimed at exploring the effect of methylene chain length on the

formation of product. A pyridyl-amide derivative with four methylene groups between alkyl nitrogens is also synthesized to understand any difference in the product formation compared to the corresponding polypyridyl ligand.

3.1.1 Tridentate ligands.

Five different tridentate ligands are prepared in this work. A few of these ligands have been known in the literature for their use in bioinorganic chemistry over decades but for the first time their utilization in supramolecular chemistry for the generation of MOCNs is demonstrated in this work. These are synthesized by modifying the literature procedure[157-158] from the corresponding primary amine and 2-picolylchloride hydrochloride (in a 1:2 ratio) in the presence of an appropriate amount of base in water. Their yields vary from 38% to 60%. The chemical reaction involved in the synthesis of the tridentate ligands is generalized in Scheme 1.

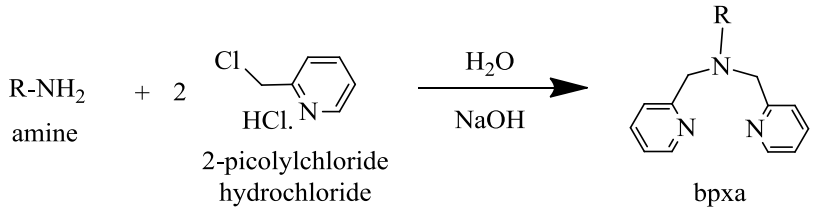

R = CH_3, bpma = N, N'-bis(2-pyridylmethyl)-methylamine
R = C_2H_5, bpea = N, N'-bis(2-pyridylmethyl)-ethylamine
R = $CH(CH_3)_2$, bpipa = N, N'-bis(2-pyridylmethyl)-isopropylamine
R = $C(CH_3)_3$, bpta = N, N'-bis(2-pyridylmethyl)-t-butylamine
R = $CH_2C_6H_5$, bpba = N, N'-bis(2-pyridylmethyl)-benzylamine

Scheme 1. General synthesis of tridentate ligands.

3.1.2 Tetradentate ligands. The well-studied tetradentate ligand, tpa, in bioinorganic chemistry is prepared in two steps.[159] First, the secondary amine 'bpa' was synthesised which was then reacted with 2-picolylchloride hydrochloride to form the ligand. The chemical reaction involved in its synthesis is shown in Scheme 2.

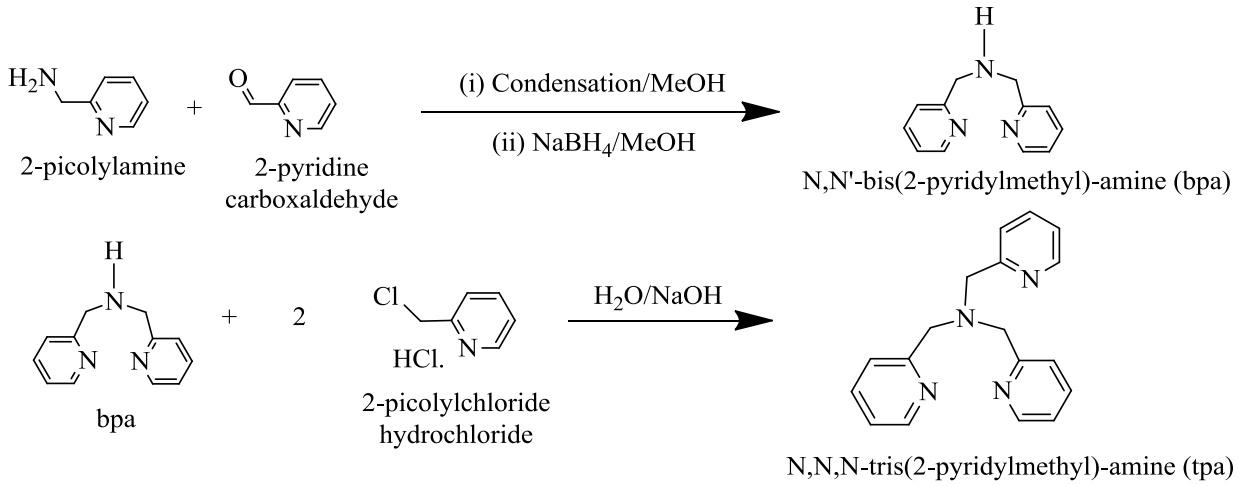

Scheme 2. Synthesis of tpa.

3.1.3 Hexadentate ligands

3.1.3a Polypyridyl ligands

Although the syntheses of the hexadentate ligands used in this study were reported in the literature,[160] improved syntheses of tpen, 1,2-tppn and tppn resulted in the isolation of solid products in shorter time. Interestingly, the synthesis of tpbn utilizing the method described in this thesis was never described fully with respect to its yield and purity as it was always referred to the method for tppn.[160d] All other reports[161] for the synthesis of tpbn in good yields required either (a) the use of halogenated solvents and handling of expensive tris-(acetoxy) borohydrides under inert conditions as well as extensive work-up including column chromatography, or (b) an expensive phase transfer catalyst and a long reaction time (days). On the other hand, for a total of 2.5 h reaction time (see the 'Experimental Section'), tpbn is isolated in 82% yield (with no detectable impurity based on ^{1}H NMR data and a sharp melting point) using water as solvent and more importantly, without the use of column chromatography. Similarly, tppen, tphxn and tphn are prepared and isolated in good yields and purity under ambient conditions and without further purification. The general synthesis of these ligands is summarized in Scheme 3.

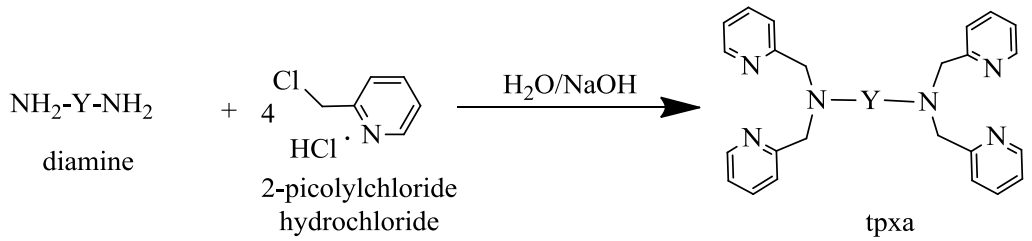

Y = CH_2, tpen = N,N, N',N'-tetrakis(2-pyridylmethyl)-1,2-diaminoethane
Y = CH_2-$CH(CH_3)$, 1,2-tppn = N,N, N',N'-tetrakis(2-pyridylmethyl)-2-methyl-1,2-diaminoethane
Y = $(CH_2)_3$, tppn = N,N, N',N'-tetrakis(2-pyridylmethyl)-1,3-diaminopropane
Y = $(CH_2)_4$, tpbn = N,N, N',N'-tetrakis(2-pyridylmethyl)-1,4-diaminobutane
Y = $(CH_2)_5$, tppen = N,N, N',N'-tetrakis(2-pyridylmethyl)-1,5-diaminopentane
Y = $(CH_2)_6$, tphxn = N,N, N',N'-tetrakis(2-pyridylmethyl)-1,6-diaminohexane
Y = $(CH_2)_7$, tphn = N,N, N',N'-tetrakis(2-pyridylmethyl)-1,7-diaminoheptane

Scheme 3. General synthesis of polypyridyl hexadentate ligands.

3.1.3b Pyridyl-Amide ligand

Most of the MOCNs reported in this thesis are with the polypyridyl ligands and are soluble in water. A new amide ligand was synthesized to understand the effect of flexible amide group on the formation of MOCNs as well as its added hydrogen bonding capability compared to the polypyridyl hexadentate ligands. Its synthesis involves two steps which are summarized in Scheme 4 below.

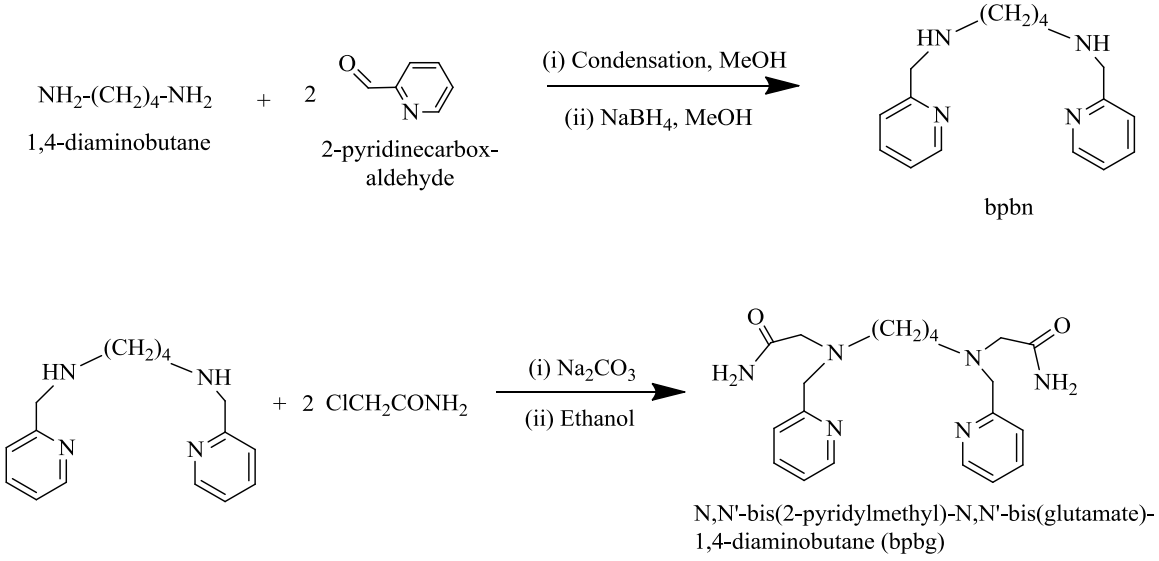

Scheme 4. Synthesis of the bpbg ligand.

3.2 Metal Organic Coordination Networks (MOCNs)

For the synthesis of the MOCNs, three general methods - two at ambient conditions and one at hydrothermal conditions - were developed (see Scheme 5). These methods are one-pot self-assembly reactions of starting materials in an appropriate ratio designed for a particular product. About 90% of the MOCNs were prepared by the methods at ambient conditions. Method 1 involves the use of metal acetates with ancillary ligand and carboxylic acid in methanol at room temperature; in this case, acetic acid (AcOH) is the by-product which is completely removed using a 1:1 acetonitrile:toluene mixture yielding 100% pure product. Method 2 involves the use of metal perchlorates with ancillary ligand and sodium salt of carboxylic acid in a methanol-water mixture at room temperature; usually a precipitate is obtained as the product and thus the by-product sodium perchlorate ($NaClO_4$) can easily be separated out due to its solubility in both methanol and water. Method 3 is the reaction of metal salts, like metal acetates, nitrates, sulphates etc., with the ancillary ligand and carboxylic acid in a 5-15 mL Teflon-lined stainless steel bomb reactor under hydrothermal conditions (raising temperature from 25 °C to 120 °C over 3 hours, holding at 120 °C for two days and cooling to room temperature over 24 hrs); the corresponding inorganic acid is the by product in these reactions which is soluble in water and a pure crystalline product which is thoroughly washed with water is obtained.

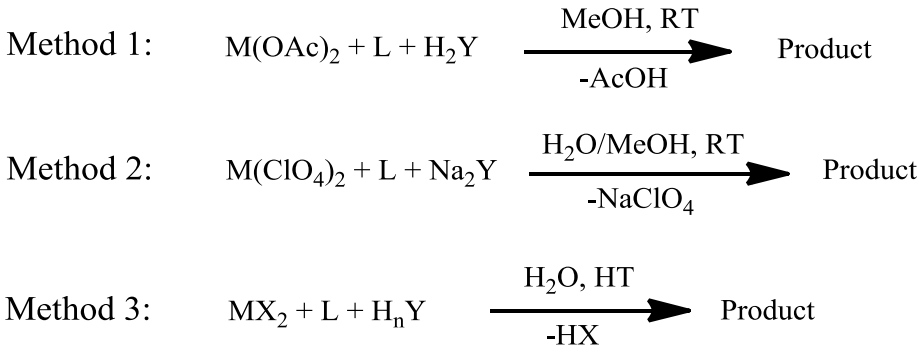

Scheme 5. General methods for the synthesis of MOCNs.

3.2.1 MOCNs with Tridentate ligands

Using the tridentate ligands discussed above, several MOCNs with a number of divalent metal ions, such as Mn(II), Co(II), Ni(II), Cu(II), Zn(II) and Cd(II), and dicarboxylate linkers, such as acetylene dicarboxylate (adc), fumarate (fum), succinate (succ), terephthalate (tere) and thiophene dicarboxylate (tdc), have been prepared mostly via the self-assembly reactions under ambient conditions. Few MOCNs with Mn(II) and Cd(II) using a tricarboxylate linker, such as BTC, are also prepared. The main problem with the BTC linker is that the product obtained is normally insoluble in most of the common organic solvents. In case of Mn(II), the product isolated under ambient conditions was insoluble and thus its single crystal structure could not be obtained, whereas crystals were obtained for those with Zn(II) and Cd(II) under hydrothermal reactions and hence these were crystallographically characterized. In order to identify the factors affecting the formation of such products with diverse structural features and properties, these MOCNs are grouped together in various sections based on the metal center used.

3.2.1.1 *Mn(II) Chemistry*

Dicarboxylate and Tricarboxylate linkers

Synthesis. In Mn(II) chemistry, **1**-**5** have been prepared using Method 1 and Method 2 for the five tridentate ligands with the same dicarboxylate linker adc (see Scheme **6**). On the other hand, the use of fumarate, succinate or terephthalate as the carboxylate linker instead of adc in $[Mn_2(bpea)_2(fumarate)_2]_n$ (**6**), $[Mn_2(bpta)_2(fumarate)(H_2O)_2](ClO_4)_2$ (**7**), $[Mn_2(bpta)_2(succinate)_2(H_2O)_2]\cdot H_2O$ (**8**), and $Mn_2(bpta)_2(terephthalate)_2(H_2O)_2]\cdot 2H_2O$ (**9**) provides further understanding in their structural diversity due to binding differences and similarities of these carboxylates. All these compounds are soluble in water at RT except **4** which is soluble in hot water. As shown in Scheme **7**, a reaction has been done with a tricarboxylate linker and bpea resulting in the formation of $[Mn_3(bpea)_3(BTC)_2(H_2O)]_n$ (**10**), which is insoluble in almost all organic solvents. Due to the solubility issue, no other reaction with tridentate ligands and tricarboxylate linkers was carried out at ambient conditions.

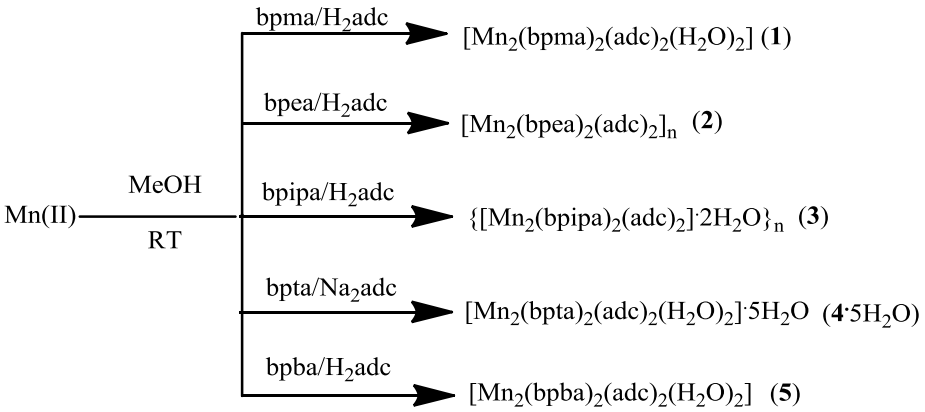

Mn(II) = $Mn(OAc)_2$ for bpma, bpea, bpipa, bpba
Mn(II) = $Mn(ClO_4)_2$ for bpta

Scheme 6. Synthesis of **1**-**5**.

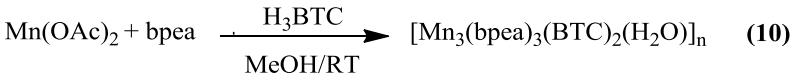

Scheme 7. Synthesis of **10**.

Single Crystal Structure Analysis. Crystals of **1** and **2** were grown from slow evaporation of their aqueous solutions. Single crystals of **4**·$5H_2O$ were grown from its hot aqueous solution. Single crystals of **3**, **5**, **6**, **7**, **8**, **9** and **10** could not be grown despite numerous attempts.

$[Mn_2(bpma)_2(adc)_2(H_2O)_2]$ (1). It crystallizes in the orthorhombic *Pbca* space group. Each Mn(II) center is hexacoordinated, three sites are occupied by nitrogen atoms of the ligand, two sites are occupied by O atoms of adc and one site is occupied by a water molecule forming a small cavity where Mn---Mn distance is 8.055 Å (see Figure 3.1). The geometry around each Mn(II) center is distorted octahedron. The Mn-N_{alkyl} and Mn-N_{py} distances are in the range as found in other similar type of complexes. There are two adc linkers in **1**, where each adc is binding in a bis(mondentate) syn-syn fashion to two Mn(II) centers. This type of bis(adc) core with such binding mode in **1** is unprecedented despite several metal-adc[169-175] complexes without any ancillary ligand showing 2D and 3D networks as well as Mn(II) complexes of adc with bidentate pyridyl ligands, such as 2,2′-bipy[176] and 1,10-phenanthroline[177] are known in the literature. The values observed for the acetylene group confirm that its triple bond character is

kept in all these complexes angles are close to linearity (ranges from 177.2(2)° to 178.0(2)°), and C−C triple bond distances range is 1.195(3) Å. The selected bond distances and angles for **1** are listed in Table A38. These parameters are similar to those observed in hexacoordinated Mn(II) complexes of similar ancillary ligands.[176-178]

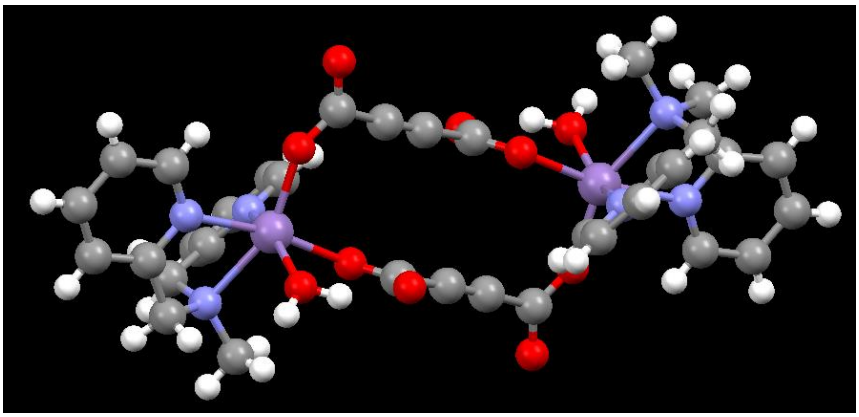

Figure 3.1 The dinuclear unit, $[Mn_2(bpma)_2(adc)_2(H_2O)_2]$, in **1**.

Four dimanganese subunits of **1** are strongly hydrogen bonded through the coordinated water of one unit to the uncoordinated oxygen atom of adc of the next subunit resulting in the formation of a tetrameric synthon. In Figure 3.2, a different color for each dimanganese unit was chosen for clarity. All hydrogen bonding parameters for **1** are listed in Table 3.1 and are found to be very close to those in ice.[147,150] This tetrameric synthon repeats itself to form a 3D supramolecular

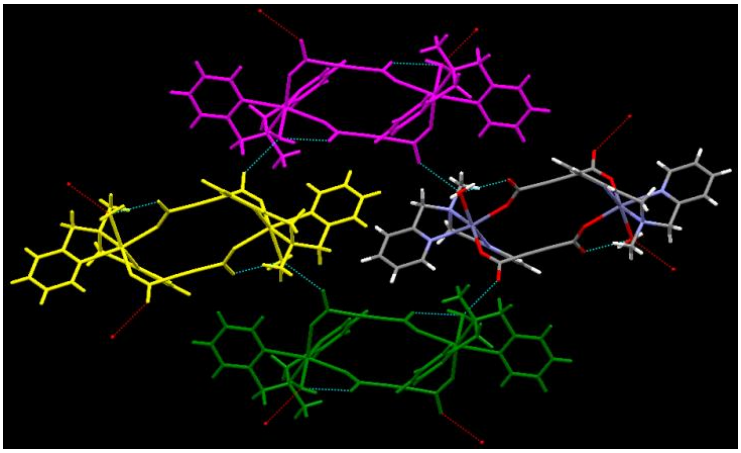

Figure 3.2 The Tetrameric synthon of **1**.

assembly as shown in Figure 3.3. Different colors for the repeat tetrameric synthon have been used in Figure 3.3 for clarity.

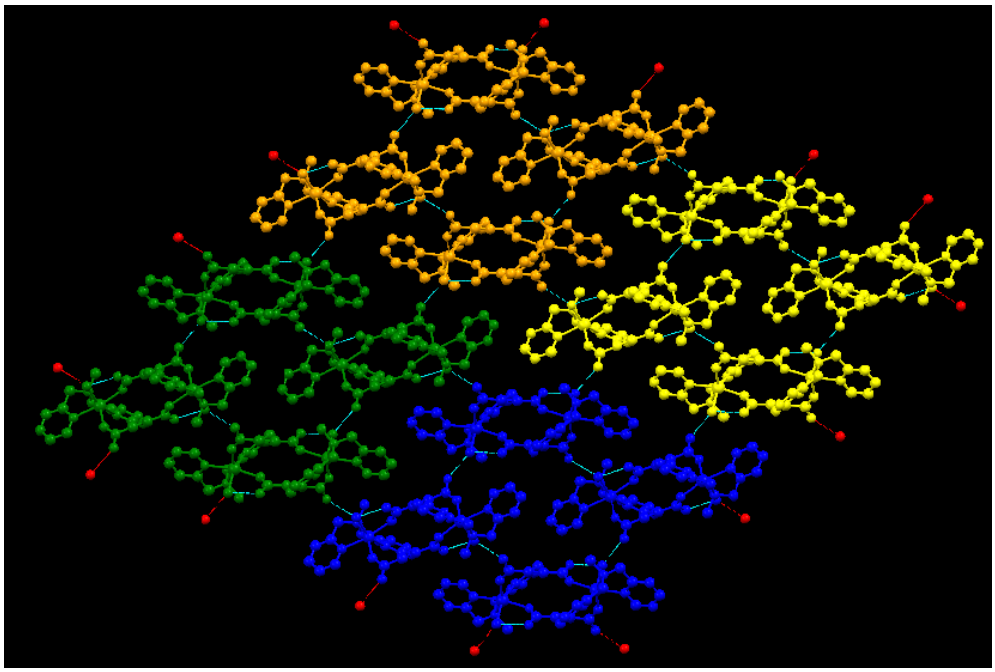

Figure 3.3 3D Supramolecular Assembly of tetrameric synthon in **1**.

Table 3.1. Hydrogen bonding parameters for **1**.[a]

D–H…A	r (D-H) (Å)	r (H…A) (Å)	r (D…A) (Å)	∠D-H…A (deg)	Symmetry
O(5)--H(1A)...O(3)	0.91(3)	1.79(3)	2.657(2)	158(2)	1-x,1-y,1-z
O(5)--H(1B)...O(1)	0.90(3)	1.78(3)	2.669(2)	172(3)	1-x,1/2+y,1/2-z
C(2)--H(2)...O(3)	0.93	2.49	3.234(2)	137	x,1/2-y,-1/2+z

[a]Numbers in parenthesis are estimated standard deviations in the last significant digits.

$[Mn_2(adc)_2(bpea)_2]_n$ (2). It is a 1D CP that crystallizes in the monoclinic $P2_1/c$ space group. A subtle change from methyl to ethyl group on the alkyl nitrogen resulted in the formation of **2** under the same reaction conditions. It is to be noted that both compounds **1** and **2** have the same solubility in water despite the nature of their structures. Like **1**, in **2** Mn(II) centers are hexacoordinated with similar coordination environment (N_3O_3) but the binding of adc is different. One end of adc is bridging between Mn(II) centers and the other end is binding in a monodentate fashion (see Figure 3.4). The two binding modes of adc are also evident from FTIR

stretching frequencies described below. There are two kinds of Mn….Mn distances present in **2**. The Mn(II) centers bridged by the carboxylate groups of two adc are part of cavity where Mn---Mn distance is 4.796 Å. On the other hand, a 14-membered cavity with a Mn---Mn distance of 8.143 Å is similar to that found in the subunit of **1**. Two chains of 1D polymer in **2** has moderate π–π interactions which result in the formation of a ladder shaped supramolecular assembly (see Figure 3.5). The centroid-centroid distance between two corresponding pyridine rings of two different polymer units is 3.659 Å.[182] The selected bond distances and angles for **2** are listed in Table A39.

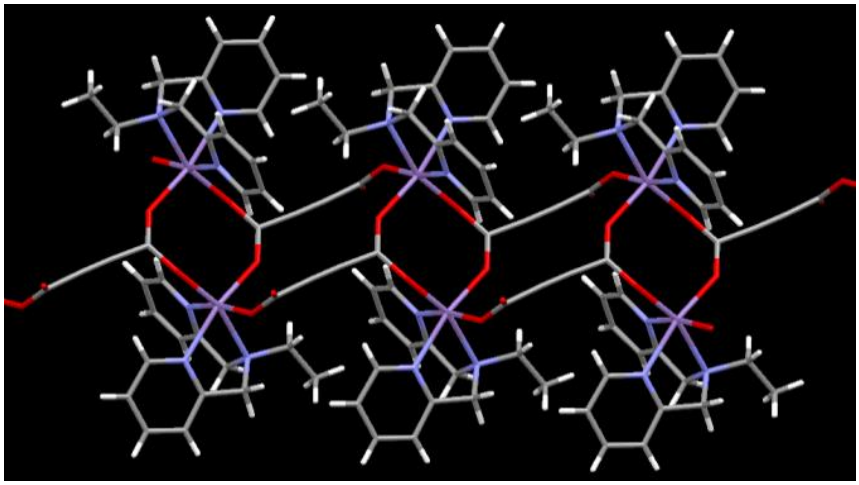

Figure 3.4. A schematic drawing of **2**.

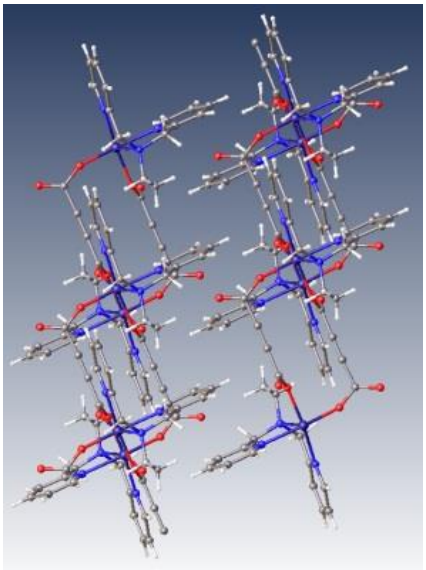

Figure 3.5. Ladder shaped supramolecular assembly in **2** through π–π interactions.

[$Mn_2(bpta)_2(adc)_2(H_2O)_2$]·$5H_2O$ **(4**·$5H_2O$**).** It is a hydrated bpta analogue of **1** and crystallizes in the monoclinic $P2_1/n$ space group. The dimetal subunit, $[Mn_2(adc)_2(bpta)_2(H_2O)_2]$, has an inversion center that generates the full molecule in the asymmetric unit is similar to **1** with some variations in structural parameters which are listed in Table A40. A perspective view of the subunit in **4**·$5H_2O$ is shown in Figure 3.6. Like **1**, the Mn(II) centers bridged by two adc groups, each of which binds in a bis-monodentate fashion. The tridentate ligand bpta binds each Mn atom in a facial configuration with the aliphatic nitrogen positioned trans to the oxygen atom of the carboxylate groups of adc. One of the two py groups in the bpta ligand is trans to the other carboxylate group of adc while the other py group is trans to the bound water molecule. In **4**·$5H_2O$, the $Mn-N_{alkyl}$ distances (2.4420 Å) are longer than the $Mn-N_{py}$ distances (2.2468(19)−2.2580(19) Å). The $Mn-O_{carb}$ distances are 2.1378(14) Å and 2.1512(13) Å, and the $Mn-O_{water}$ distance is 2.1564(16) Å. The octahedral geometry at each manganese center in **4**·$5H_2O$ is highly distorted with the $O-Mn-N_{py}$ angles 172.03(6)° and 165.67(6)°. The $O-Mn-N_{amine}$ angles are in the range from 100.09(6)° to 105.78(5)°. These bond distances are similar to the values usually observed in hexa-coordinated Mn(II) complexes of similar ancillary ligands and **1**.[176-178]

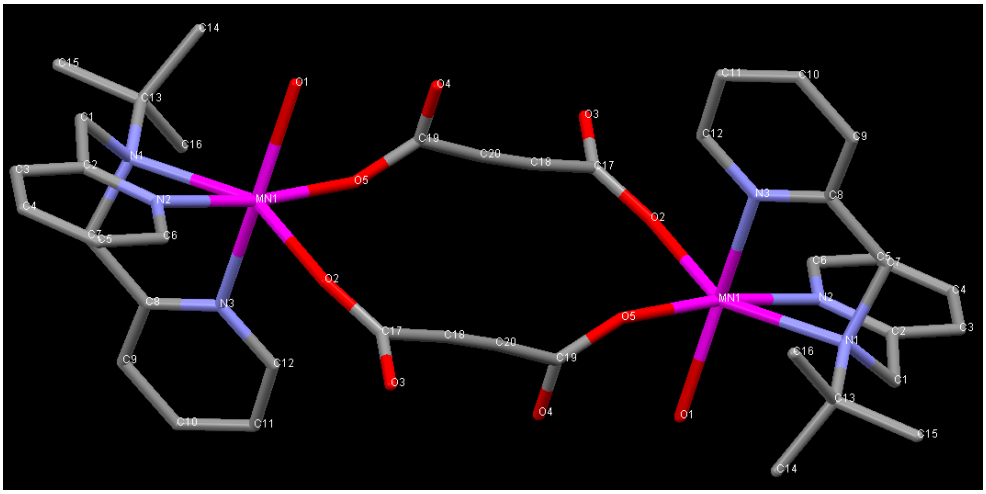

Figure 3.6. A view of the dinuclear subunit in the 2D supramolecular assembly of **4**·$5H_2O$.

The presence of five lattice water molecules forms a supramolecular assembly different from **1**. The perspective view of the 3D supramolecular assembly of **4**·$5H_2O$ is shown in Figure 3.7. The cluster of five water molecules in the channel shows strong hydrogen bonding (see Table 3.2).

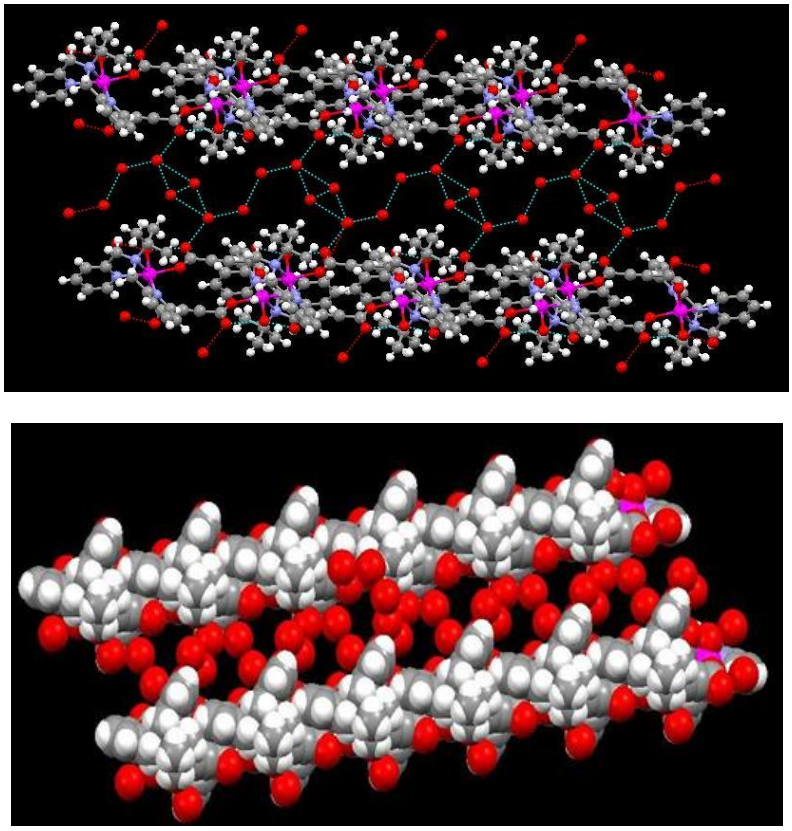

Figure 3.7. A perspective view of the 2D supramolecular assembly of **4**·$5H_2O$ (top); its space-filling representation showing the water channel (bottom).

When the single crystal structure of **4**·$5H_2O$ was determined at 120 K, a cluster of six water molecules (**4**·$6H_2O$) were found between the 2D layers of the dimetal subunit. In **4**·$6H_2O$, the O−Mn−N_{py} angles are 172.03(6)° and 165.67(6)°. The O−Mn−N_{amine} angles are in the range from 100.09(6)° to 105.78(5)°. The values observed for the acetylene group confirm that its triple bond character is kept in all these complexes: (C17−C18−C19 and C18−C19−C20) angles are close to linearity (ranges from 175.8(2)° to 178.5(7)°), and C−C triple bond distances range from 1.186(5) Å to 1.201(8) Å. A perspective view of the 3D supramolecular assembly of **4**·$6H_2O$ is shown in Figure 3.8. The cluster of six water molecules in the channel shows strong hydrogen bonding (see Table 3.2).

Increasing the temperature from 120 K to 296 K induced changes in the water cluster while the 3D supramolecular assembly remains the same. In order to prove this difference in the water layers of the two structures, the water molecule that was not found in **4**·$5H_2O$, based on the coordinates of the oxygen atoms of water molecules in the channel between the 2D layers in

4·6H_2O and **4**·5H_2O, was deleted in the redrawn space-filling representation of **4**·6H_2O (Figure 3.9).

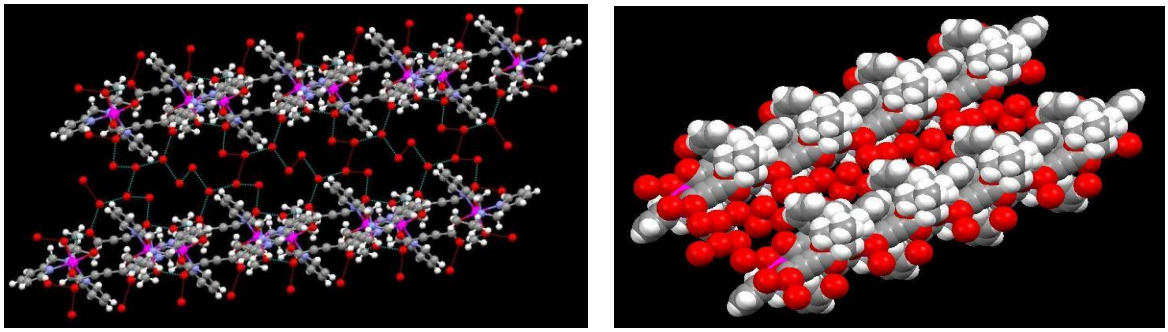

Figure 3.8. A perspective view of the 2D supramolecular assembly of **4**·6H_2O (left); its space-filling representation showing the water channel (right).

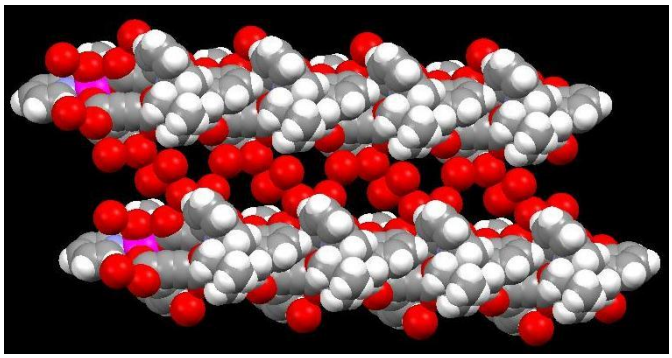

Figure 3.9. For comparison, the structure of **4**·6H_2O after deleting one water molecule.

Just considering the hydrogen bonding interactions in the water clusters along with the adc molecules in **4**·6H_2O and **4**·5H_2O (Figure 3.10), it is very clear that the positions of the water molecules are distinct to create different topologies, indicating their temperature dependency. It is equally important to note that such differences could be correlated to the formation of 3D supramolecular assemblies that can act as synthons for the reversible processes, such as dehydration and rehydration, to generate new entities with unusual stabilities.

Various hydrogen bonding parameters relevant to the water cluster are listed in Table 3.2. In all complexes, there exists the O−H···O intermolecular hydrogen bonding that occurs between the oxygen atoms of the coordinated water molecules and the oxygen atoms of the carboxylic groups. The D···A distances and D−H···A angles fall in the ranges of 2.678−2.681 Å and 143−175°, respectively, which are in agreement with the normal range of hydrogen bonding

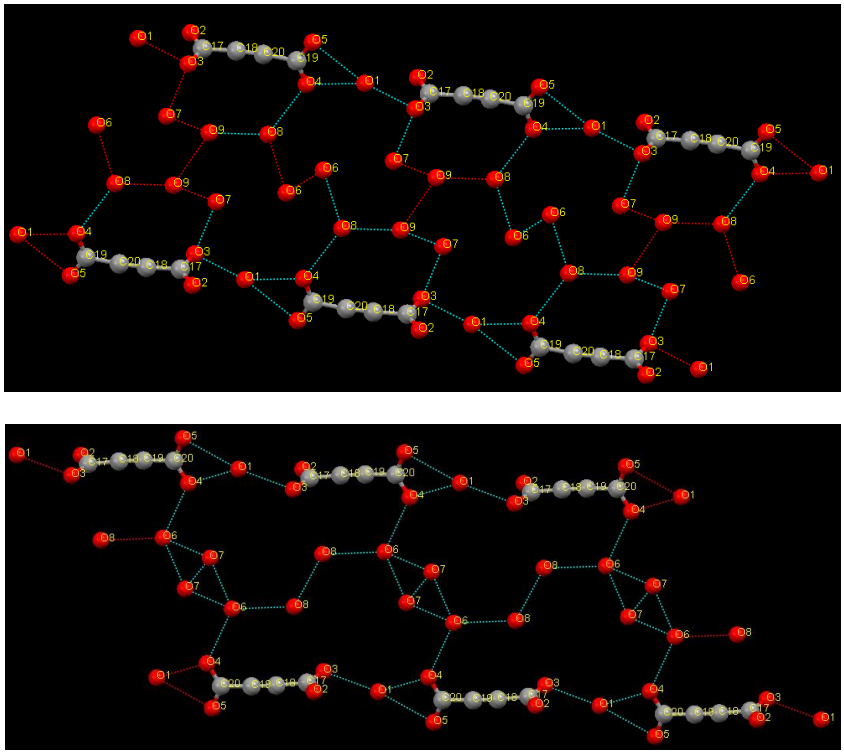

Figure 3.10. Representation of water clusters in **4**·6H_2O (top) and **4**·5H_2O (bottom), respectively. Contacts between water molecules (coordinated and free) and the carboxylate oxygen atoms of adc are considered. For clarity all hydrogen atoms are omitted.

between coordinated water molecule and uncoordinated oxygen atom of a carboxylate found in some compounds reported in the literature.[179,180] Besides those in **4**, two other O−H···O intermolecular hydrogen bonding interactions exist, namely (i) the O−H···O intermolecular hydrogen bonding between the oxygen atoms of the carboxylic groups and the oxygen atoms of the free water molecules with the D···A distances and D−H···A angles in the range of 2.782−2.714 Å and 107−149°, respectively; (ii) the O−H···O intermolecular hydrogen bonding between the oxygen atoms of the uncoordinated water molecules with the D···A distances and D−H...A angles in the range of 2.04−2.881 Å and 101−177°, respectively. Inclusion of methanol molecules in addition to water molecules in the channel forms a similar 3D supramolecular assembly **4**·4H_2O·CH_3OH (Figure 3.11). In this case, two methanol molecules are found to be tightly held between the two layers of four water molecules that are propagating the 3D assembly perpendicular to the 2D layers. Each OH group of the methanol molecules is strongly hydrogen bonded with one of four water molecules. These methanol molecules can be considered guests within the water clusters that are forming parallel chains. The pore sizes in different forms are

listed in Table 3.3. The change of the pore sizes is more complex and nonsystematic in nature due to several factors involved.

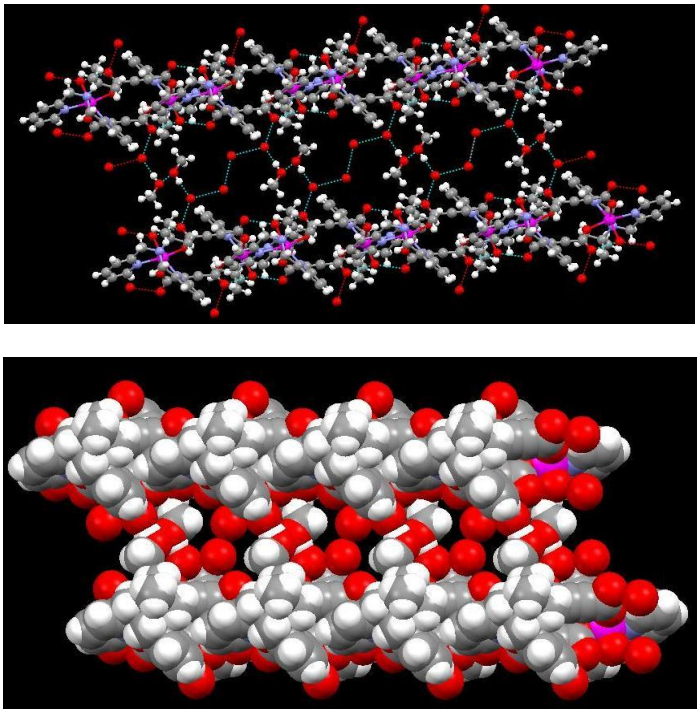

Figure 3.11 (a) A schematic view of the 2D supramolecular assembly of **4**·4H_2O·CH_3OH (left); (b) its space-filling representation showing the channel filled with water and methanol between the one-dimensional layers (right).

Table 3.2. Hydrogen bonding parameters for **4**·6H_2O, **4**·5H_2O, **4**, **4**·4H_2O·CH_3OH and **4**·4H_2O.[a]

D–H…A	r (D-H) (Å)	r (H…A) (Å)	r (D…A) (Å)	∠D-H…A (deg)	Symmetry
4·6H_2O					
O(1)--H(1A)...O(5)	0.73(3)	1.96(3)	2.681(2)	167(3)	-x, -y, -z
O(1)--H(1B)...O(3)	0.84(3)	1.89(3)	2.670(2)	153(3)	
O(6)--H(6A)...O(7)	0.86(8)	1.74(10)	2.555(11)	156(11)	-x, -y, 1-z
O(6)--H(6B)...O(9)	0.85(11)	2.46(11)	3.072(12)	129(9)	
O(7)--H(7C)...O(8)	0.86(5)	2.00(4)	2.799(4)	137(4)	
O(7)--H(7D)...O(7)	0.84(4)	1.99(4)	2.804(4)	160(4)	-x, -y, 1-z
O(8)--H(8A)...O(3)	0.858(13)	2.01(2)	2.782(3)	149(3)	1-x, -y, 1-z
O(8)--H(8B)...O(9)	0.86(3)	2.18(4)	3.035(6)	173(4)	1-x,-y,1-z
O(9)--H(9A)...O(6)	0.85(6)	2.23(5)	3.072(12)	169(8)	
O(9)--H(9A)...O(8)	0.85(2)	2.00(5)	2.659(5)	134(6)	
C(12)--H(12)...O(4)	0.95(3)	2.51(3)	3.097(3)	120(3)	

4·5H_2O					
O(1)--H(1)...O(3)	0.87(8)	1.81(7)	2.678(5)	175(6)	1-x, 1-y, 1-z
O(1)--H(2)...O(4)	0.88(7)	1.85(7)	2.677(5)	157(7)	
O(6)--H(6A)...O(8)	0.85(8)	2.22(7)	2.888(13)	135(8)	
O(6)--H(6B) ...O(4)	0.85(7)	2.11(9)	2.888(7)	135(8)	½-x, -½+y, ½-z
O(7)--H(7C)...O(6)	0.87(12)	2.31(4)	3.009(17)	137(10)	1-x, -y, 1-z
O(7)--H(7D)...O(6)	0.86(8)	1.84(1)	2.696(17)	177(15)	1-x, -y, 1-z
O(8)--H(8B) ...O(6)	0.86(18)	2.31(19)	2.888(13)	125(14)	
C(6)--H(6)...O(2)	0.93(5)	2.53(5)	3.110(5)	121(5)	
4					
O(1)--H(1)...O(3)	0.84(11)	1.93(11)	2.716(10)	156(10)	1-x, -y, -z
O(1)--H(2)...O(4)	1.10(11)	1.59(12)	2.621(9)	152(9)	
4·4H_2O·CH_3OH					
O(1)--H(1A)...O(4)	0.85(3)	1.82(3)	2.659(5)	171(4)	1-x, -y, -z
O(1)--H(1B)...O(3)	0.85(5)	1.95(4)	2.680(5)	143(4)	
O(6)--H(6A)...O(7)	0.84(5)	1.71(4)	2.554(13)	177(4)	½+x, ½-y, ½+z
O(7)--H(7C)...O(8)	0.85(9)	2.10(7)	2.919(13)	161(11)	½-x, ½+y, ½-z
O(7)--H(7D)...O(3)	0.85(5)	2.02(8)	2.774(8)	147(9)	3/2-x, ½+y, ½-z
C(12)--H(12)...O(2)	0.95(6)	2.51(6)	3.097(6)	120(6)	
C(21)--H(21B)...O(1)	0.98(2)	2.54(2)	3.29(2)	133(2)	
4·4H_2O					
O(1)--H(1A)...O(3)	0.84(3)	1.92(3)	2.710(7)	156(5)	1-x, -y, -z
O(1)--H(1B)...O(4)	0.85(4)	1.90(5)	2.607(8)	140(4)	
O(7)--H(7B)...O(3)	0.87(19)	2.32(18)	2.32(18)	156(2)	1-x, -y, 1-z

[a]Numbers in parenthesis are estimated standard deviations in the last significant digits.

Table 3.3. Pore Sizes within the dimetal subunits in **1**, **2** and **4**·6H_2O and its various forms.

	1	**2**	**4**·6H_2O	**4**·5H_2O	anhydrous **4**	**4**·4H_2O·CH_3OH	rehydrated **4** (**4**·4H_2O)
L (Å)	8.005	8.143	8.225	8.181	8.139	8.187	7.867
W (Å)	4.110	4.290	4.048	4.163	4.010	4.122	4.277

where, L = Mn···Mn distance and W = distance between two acetylene moieties of the adc groups

Powder X-ray Data Analysis. To confirm whether the single crystal structure corresponds to the bulk material or not, the powder X-ray diffraction pattern was recorded for **1**, **2**, **3**, **4**·5H_2O, **4**·4H_2O·CH_3OH, **4**, **5**, **6**, **7** and **9**. The experimental and simulated X-ray patterns (wherever single crystal structures are obtained) were similar to each other for respective MOCNs as shown in Figures 3.12 to 3.14. The patterns obtained confirm that the single crystal and bulk material

properties are the same. Combining all other characterization for these species, this study also confirms the phase purity of the bulk sample. The experimental powder patterns for **3** and **6** resembles with **2** which shows that these two are isostructural with **2**, which is in good agreement with FTIR and TGA analysis (*vide infra*).

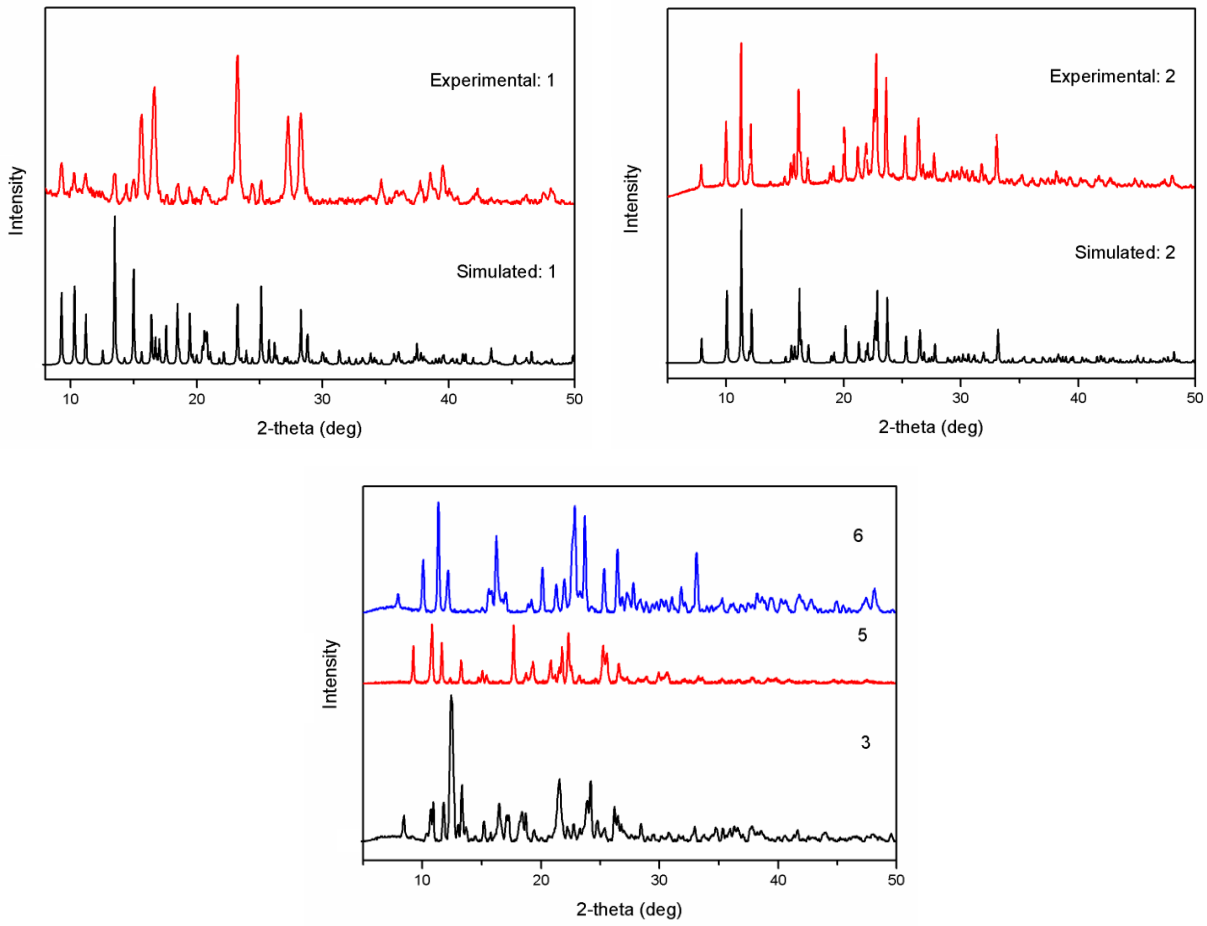

Figure 3.12. Experimental and simulated powder patterns for **1** and **2** (top); experimental powder patterns for **3, 5** and **6** (bottom).

The powder patterns for **4**·$5H_2O$ and its various forms are similar to each other which shows that these are isostructural. The experimental powder patterns of **5** and **9** match with the experimental powder pattern for **1** indicating that these two compounds are isostructural with the latter. Thus powder diffraction was very useful in determining the structural similarities in addition to characterization by FTIR spectroscopy and TGA (vide infra). The powder patterns for **8** and **10** (not shown) indicates that these materials are amorphous.

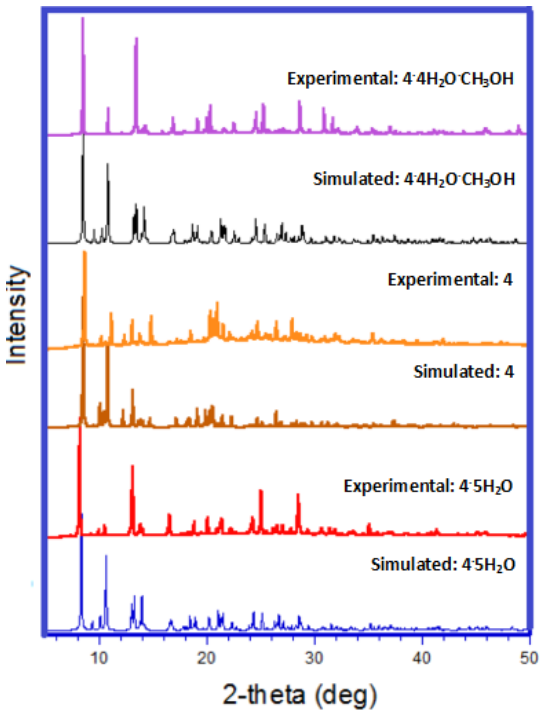

Figure 3.13. Simulated and experimental powder patterns for **4**·5H_2O and its various forms.

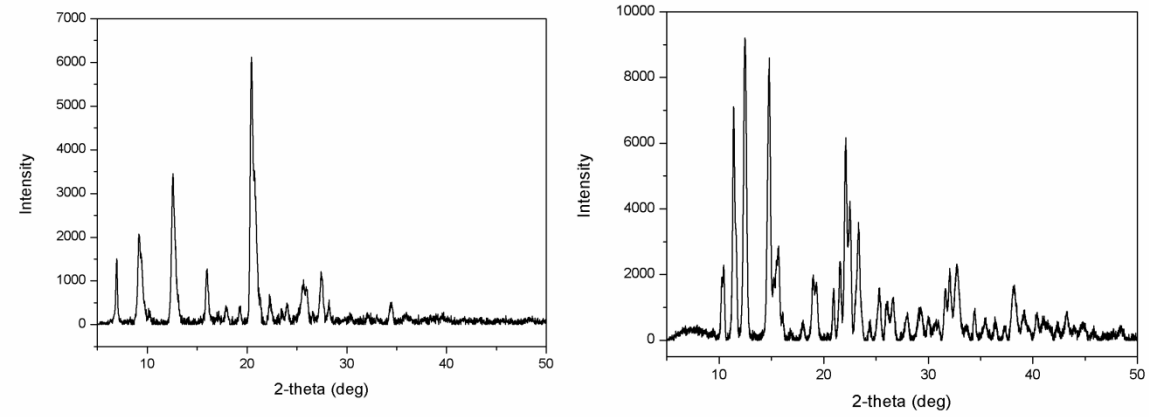

Figure 3.14. Experimental powder patterns for **7** (left) and **9** (right).

FTIR and Raman Spectroscopy. The IR spectra of **1**, **2**, **3**, **4**·5H_2O, **5**, **6**, **7**, **8**, **9** and **10** recorded in the solid state show broad bands centered at 3423 cm^{-1} (**1**), 3407 cm^{-1} (**2**), 3431 cm^{-1} (**3**), 3386 and 3216 cm^{-1} (**4**·5H_2O), 3422 cm^{-1} (**5**), 3422 cm^{-1} (**6**), 3434 cm^{-1} (**7**), 3434 (**8**), 3400 (**9**) and 3418 cm^{-1} (**10**). Out of all these compounds only **4**·5H_2O showed two kinds of O-H stretching frequencies. Generally, the IR spectrum of water shows the O−H stretching frequency at 3490 cm^{-1} and 3280 cm^{-1} while that for ice is at 3220 cm^{-1}.[147c] This suggests that the water

cluster in **4**·$5H_2O$ shows O−H stretching vibrations similar to those of liquid water with deviations due to the difference in local environments.

All compounds also show a series of bands between 1610 and 1310 cm^{-1}. While some of these features are due to the ligands, the bands at 1623 and 1348 cm^{-1} (**1**), 1646 and 1376 cm^{-1}; 1571 and 1318 cm^{-1} (**2**), 1628 and 1364 cm^{-1}; 1579 and 1320 cm^{-1} (**3**), 1599 and 1351 cm^{-1} (**4**·$5H_2O$), 1578 and 1351 cm^{-1} (**5**), 1647 and 1376 cm^{-1} ; 1578 and 1319 cm^{-1} (**6**), 1574 and 1424 cm^{-1} (**7**), 1574 and 1402 cm^{-1} (**8**), 1569 and 1367 cm^{-1} (**9**) and 1623 and 1435 cm^{-1}; 1563 and 1372 cm^{-1} (**10**) are due to the asymmetric and symmetric stretching modes of the carboxylate groups of carboxylate, respectively. A value of 248 cm^{-1} for the difference in the asymmetric and symmetric stretching modes is indicative of monodentate binding of the carboxylate groups as found in the crystal structure and a value of 253 cm^{-1} is indicative of bridging mode of carboxylate groups. The stretching frequencies in **2**, **3** and **6** are very close to each other which show the same binding mode of carboxylate in these compounds whereas stretching frequencies of carboxylate found in **5**, **9** is similar to that of **4**·$5H_2O$. The carboxylate stretching frequencies in **10** suggests two binding modes of BTC – monodentate and chelated.

On the other hand, the Raman spectra of few selected compounds were recorded because of the presence of adc in these compounds. Compounds **1**, **2**, **3** and **4**·$5H_2O$, **4**·$4H_2O$·CH_3OH, **4** and **5** (see Figure 3.15) show a peak at 2215 cm^{-1} for the C−C triple bond, and other features for the bpta ligand and the carboxylate groups of adc (1576 and 1385 cm^{-1}) similar to those of the FTIR spectra. As expected, there is no difference in the Raman spectra for all these species for 4·$5H_2O$ (see Figure 3.16). The observed value for the C−C triple bond is very close to those (2239 and 2220 cm^{-1}) in the Cd(II) complexes, $[Cd(adc)(H_2O)_3]\cdot H_2O$ and $[Cd(adc)(H_2O)_{2.3}]$, respectively.[181] Results from FTIR and Raman spectroscopy show good agreement with the X-ray structure analysis of **4**·$5H_2O$ and its other forms.

Thermoanalytical Investigations. In order to understand the thermal stability and its structural variation as a function of temperature, thermogravimetric analyses (TGA) were recorded for the single-phase polycrystalline sample of **1**, **2**, **3**, **4**·$5H_2O$, **5**, **6**, **7**, **9** and **10**. The TGA scans are shown in Figures 3.17-3.21. TGA of **8** was not carried out as it contains perchlorate anion. TGA between 25 and 500 °C shows the multistep weight loss profile for the compounds with the adc linker. It is clearly evident that free solvent molecules are lost first followed by the coordinated

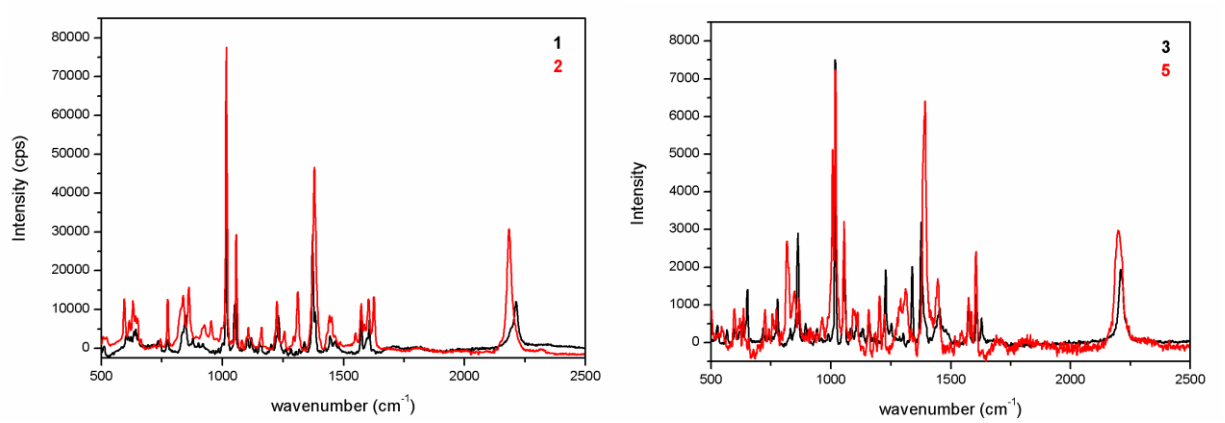

Figure 3.15. Raman spectra of **1**, **2**, **3** and **5**.

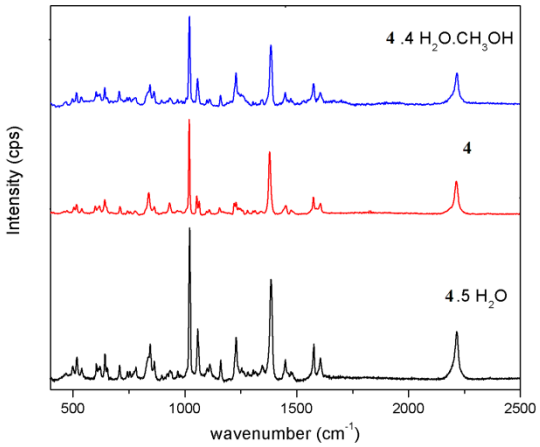

Figure 3.16. Raman Spectra of **4**·5H_2O, **4** and **4**·H_2O·CH_3OH.

water molecules and the adc linker. For **1**, the first weight loss of 20.91% between 30-125 °C corresponds to two coordinated water molecules and one acetylene dicarboxylic acid molecule (ca. 18.84%). The second weight loss of 41.1% between 125-210 °C corresponds to loss of second acetylene dicarboxylic acid molecule and one bpma molecule (ca. 40%). Further loss of 31.8% between 210-280 °C is indicative of subsequent decomposition of the product(s) from the first two steps. On the other hand, **2** is stable up to 150 °C and then shows a continuous weight loss of 73.4% between 150-400 °C accounting for two bpea ligands and one acetylene dicarboxylic acid (ca. 72.2%). Like powder patterns TGA scans for **3** and **6** are similar to each other, **3** was stable up to 150 °C while **6** was stable up to 175 °C followed by loss of carboxylic acid. For **4**, the first weight loss of 8.40% between 50 and 100 °C corresponds to five uncoordinated water molecules (ca. 9.10%). The second weight loss of 18.65% between 125 and

175 °C corresponds to two bound water molecules and one acetylene dicarboxylic acid linker. Two further steps showing weight loss of 37.59% between 175 and 300 °C and 14.80% between 300 and 450 °C indicate loss of the remaining organic ligands. This thermal study is in full agreement with single crystal X-ray studies, where an exceptional stability of **4** was observed for 18 h at 77 °C, and the FTIR data described above. For **5**, like FTIR and powder TGA is also similar to **1**. The TGA scan of **10** shows a continuous loss.

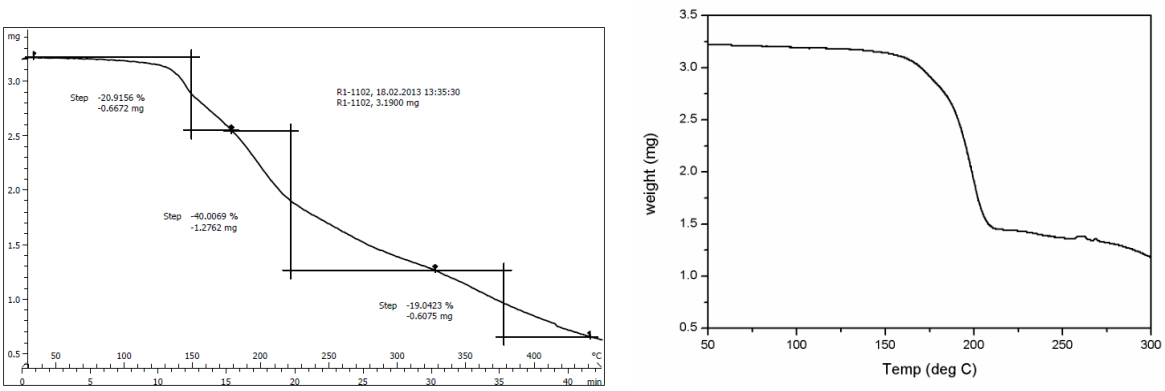

Figure 3.17. TGA scans for **1** (left) and **2** (right).

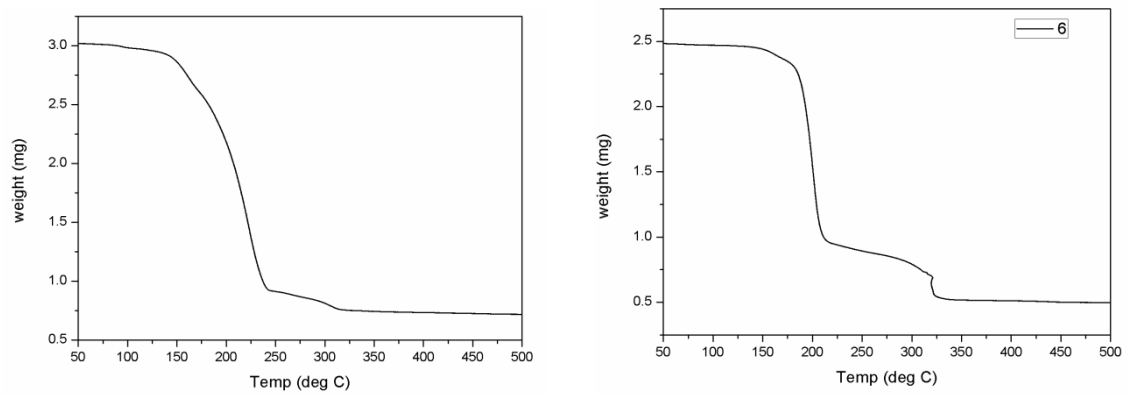

Figure 3.18. TGA scan for **3** (left) and **6** (right).

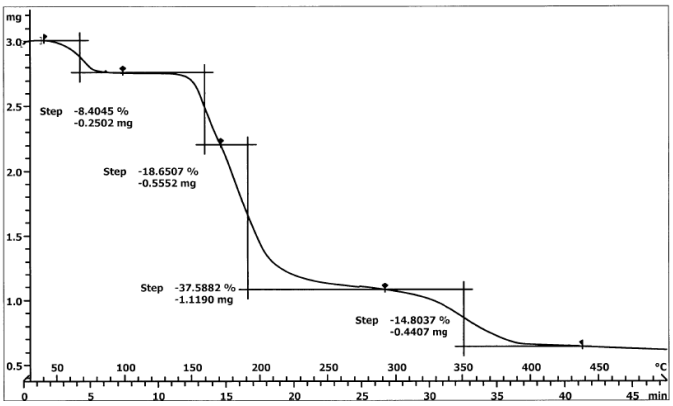

Figure 3.19. TGA scan for **4**·5H_2O.

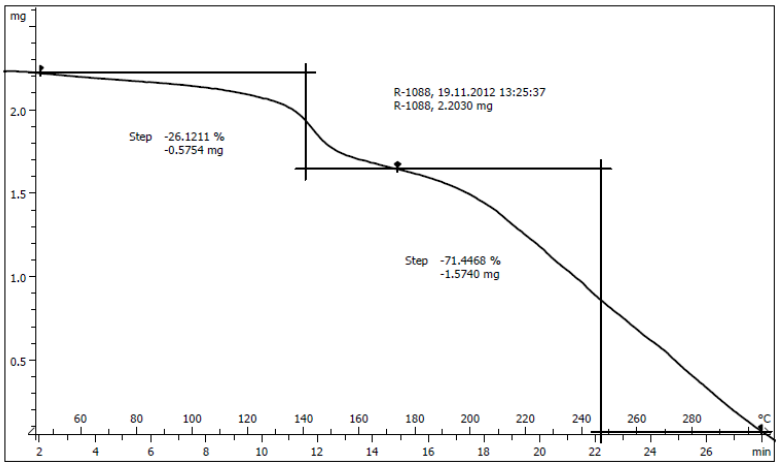

Figure 3.20. TGA scan for **5**.

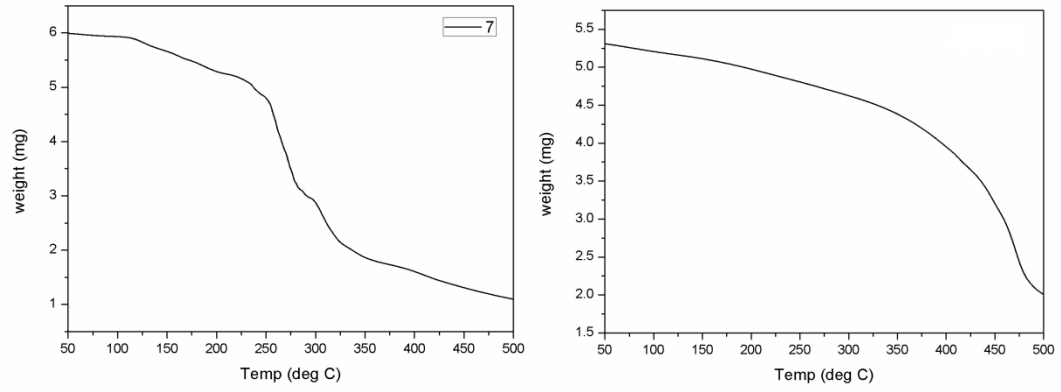

Figure 3.21. TGA scans for **7** (left) and **10** (right).

Single Crystal to Single Crystal (SC-SC) transformation. Through thermal dehydration and rehydration processes, the crystals of **4**·$5H_2O$ undergo a reversible solid-state structural transformation (see Figure 3.22). When a single crystal of **4**·$5H_2O$ is slowly dehydrated to 350 K (77 °C), it undergoes a phase transition to form a 2D framework $[Mn_2(bpta)_2(adc)_2(H_2O)_2]$ (**4**). The crystals of **4** were kept under ambient conditions for couple of weeks which absorbed four water molecules to form **4**·$4H_2O$. This phenomenon shows these are breathing crystals.

Since the basic dimetal unit is same in **1** and **4**, experiment was done to get the anhydrous analogue of **4.** To achieve this hydrated sample was heated to 350 K for few hours and the anhydrous analogue of **4**·$5H_2O$ was obtained which was confirmed by determining the unit cell. Thus, SC-SC transformation was achieved converting hydrated species to the anhydrous one.

The structure of the dehydrated species of **4** done at 350 K is one of the few examples where its integrity was intact over the period of 18 h during the data collection. The uncoordinated oxygen atoms O(3) and O(4) of the carboxylate groups of adc dianions in **4** are also oriented toward the coordinated water molecules (O(1)) of neighbouring units via hydrogen bonding. In **4**, one hydrogen atom on each of the coordinated water molecule makes an intramolecular hydrogen bond (1.93 Å) to each of the non-coordinated oxygen atoms of adc (Figure 3.22).

Rehydration of **4** over a few weeks under ambient conditions generates the 3D supramolecular assembly, $[Mn_2(bpta)_2(adc)_2(H_2O)_2]\cdot 4H_2O$ (**4**$\cdot 4H_2O$) (Figure 3.22), where the water molecules reoccupy the channel between the 2D layers. In this 3D assembly, in addition to strong hydrogen bonding, a closer view indicates the involvement of the water molecules in moderate C−H···O interactions with the pyridine rings of the bpta ligand, for example C(3)−H(3)···O(3) (distance, 3.413(9) Å; angle, 161°).

It should be noted here that such C−H···O interactions are also present in **4**$\cdot 6H_2O$ (distance, 3.101(4) Å; angle, 120°), **4**$\cdot 5H_2O$ (distance, 3.112(5) Å; angle, 121°), and **4**$\cdot 4H_2O\cdot CH_3OH$ (distance, 3.096(5) Å; angle, 120°; distance, 3.29(2) Å; angle, 133°). The dehydration and rehydration processes have been verified several times by unit cell measurements of the single crystals used in this study. The change in unit cell volume due to a decrease or increase in temperature at which the crystal structure is performed is also coupled with dehydration/rehydration processes; for example, an increase in measurement temperature and the dehydration process have opposite effects on the unit cell volume change. Considering a change (3.2%) in the unit cell volume of **4**$\cdot 6H_2O$ at 120 K over **4**$\cdot 5H_2O$ at 296 K would give a volume of 2416.96 $Å^3$ for **4**$\cdot xH_2O$ at 350 K. However, due to loss of the water cluster (the dehydration process), the unit cell volume of **4**$\cdot 5H_2O$ shows a 7.01% increase over that of **4**, which indicates that the framework structure is fairly flexible upon removal of the water molecules. This is further indicated by the increase in the unit cell volume for **4**$\cdot 4H_2O\cdot CH_3OH$ over **4**$\cdot 6H_2O$ at the same temperature (120 K) as the total number of non-hydrogen atoms per asymmetric unit is the same in both cases. Similarly, there is a decrease (4.18%, considering a 19 $Å^3$ volume loss for one less non-hydrogen atom in **4**$\cdot 4H_2O$) in the unit cell volume for the rehydrated species **4**$\cdot 4H_2O$ over **4**$\cdot 5H_2O$ at the same temperature (296 K) due to different supramolecular (vide infra) interactions between the 2D layers found in the former. Thus, the calculated densities for

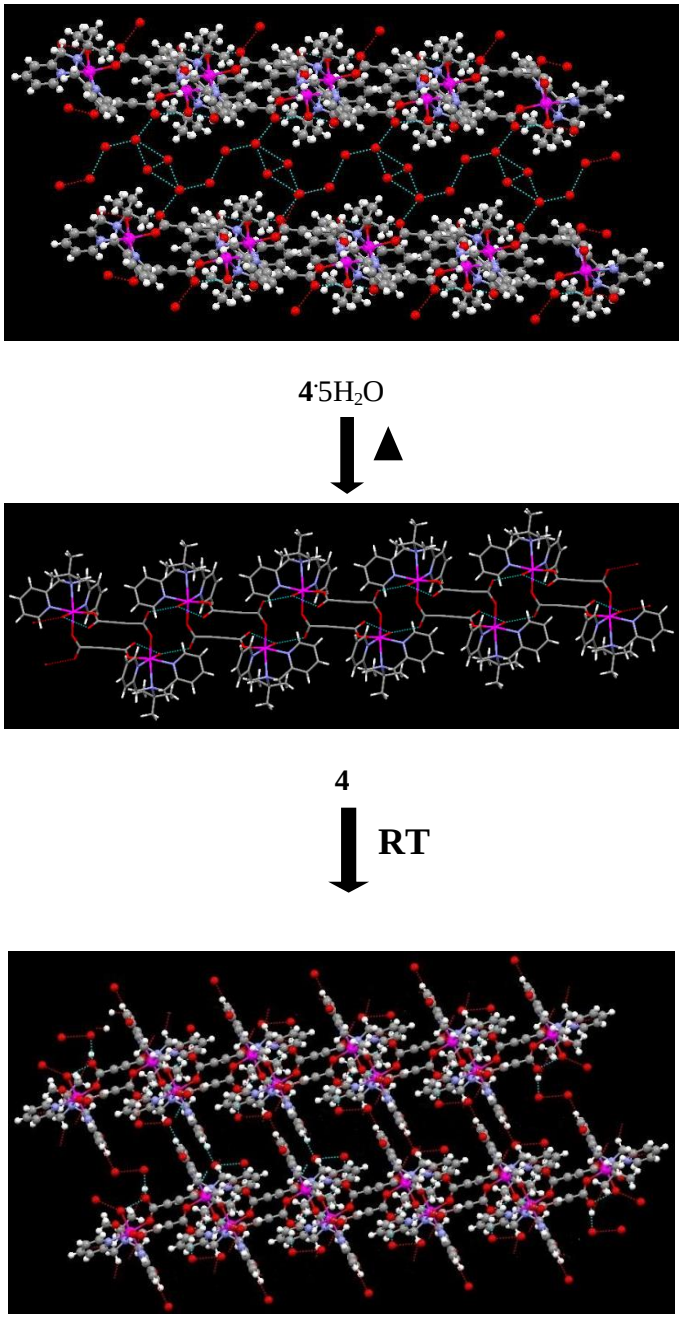

Figure 3.22. Schematic representation of the solid-state structural transformation of **4**·$5H_2O$ to 2D and 3D supramolecular assemblies **4** and **4**·$4H_2O$, respectively, during the dehydration and rehydration processes.

all these species are consistent with that being the lowest for **4**. Another interesting feature in this respect (dehydration/rehydration processes) is the decrease (2.249°) in the β angle of the unit cell for **4**·$4H_2O$ compared to **4** while other unit cell parameters are very similar to each other

(considering the opposite effect of an increase in measurement temperature and the dehydration process). Based on the above discussion, the 3D supramolecular assemblies reported here can be compared to channels filled with water (and methanol) where each side of the channel is the 2D supramolecular network of **4**. The diameters of the channel for the 3D supramolecular assemblies in **4**·$6H_2O$, **4**·$5H_2O$, **4**·$4H_2O$·CH_3OH, and **4**·$4H_2O$ are 13.845 Å, 14.191 Å, 14.364 Å, and 13.393 Å, respectively.

Considering the temperature (at which these structures were determined) alone, an increase of 0.519 Å in the channel diameter between **4**·$6H_2O$ and **4**·$4H_2O$·CH_3OH (both structures are done at 120 K) clearly indicates the change in the spatial orientation of the water cluster vs the water/methanol cluster, respectively. On the other hand, a change (0.173 Å) in the channel diameter between **4**·$5H_2O$ and **4**·$4H_2O$·CH_3OH (structures were done at 296 and 120 K, respectively) does not reflect the same. In this context the pore size within the dimetal subunit for all the compounds listed in Table 3.3 can be considered, e.g., in **4**·$6H_2O$, it is 8.225 Å × 4.048 Å, where the length is the Mn...Mn distance and the width is the distance between two acetylene moieties of the adc groups.

This SC-SC was also followed by FTIR using the powder sample. The sample was heated at 80 °C under vacuum and IR was obtained after every one hour. It was found as shown in Figure 3.23 that the feature at 3216 cm^{-1} reduces on heating at 80 °C over time and disappears completely after 3h. This indicates that the feature at 3386 cm^{-1} is for the coordinated water molecules in case of **4**·$5H_2O$.

Water adsorption studies. In order to demonstrate their affinity towards water (lattice and coordinated) that controlled the solid state structures of the supramolecular assemblies **1, 2** and **4** described above, water adsorption studies were carried out. Absorption isotherms of **1**, **2** and **4** are presented in Figure 3.24. Based on the discussion of the dehydration/rehydration of **4** in the previous sections, it was clear that this compound could be a good candidate for water adsorption studies for its affinity towards water. The sample was pretreated for 24 hours at 100 °C under vacuum followed by purging with nitrogen to use in this study. In doing so, anhydrous **4** was generated. At p/po = 1 (where po is the vapor pressure at saturation), it adsorbed approx. 160 cm^3 water per g of sample. This value is much more than the amount in the fully hydrated form of **4** indicating the presence of adsorbate-adsorbate interactions via hydrogen bonding at higher p/po.

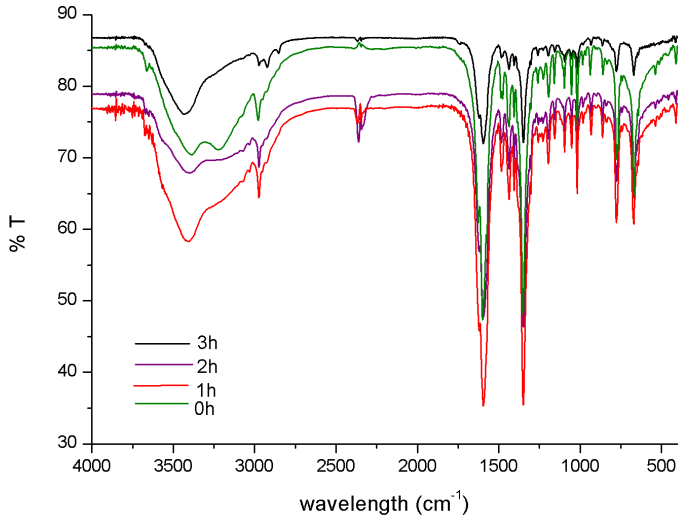

Figure 3.23. FTIR spectra of **4**·5H_2O at 80 °C under vacuum at intervals.

Its desorption curve does not follow the adsorption one generating a prominent hysteretic profile that is indicative of hydrophilic nature of the pore surfaces in **4**. On desorption it showed retention of water confirming the fact that at ambient conditions it retains two-third of the water upon rehydration. Furthermore, a stepwise adsorption profile is observed. The stepwise adsorption profile for **4** is indicative of its structural flexibility as well as certain structural changes (maybe metastable states) due to the host-guest interactions. Utilizing PXRD and FTIR it was found that **4** is stable towards water. This result is very encouraging and is being considered further for desiccant and absorbent coolant applications. On the other hand, **1** with only coordinated water molecules is already in an anhydrous form (no lattice water) shows different water adsorption behavior - it adsorbed approx. 190 cm^3 water per g of sample in gradual uptake of water - conforming to the difference in their solid state crystal structures. Interestingly, the solvated form of **1** like that of **4** (**4**·5H_2O) was not isolated when it was crystallized from water. In addition to measuring with a pretreated sample of **1**, another measurement was done with a sample of **1** as prepared without any pretreatment. As can be seen from Figure 3.24, the maximum of water (90 cm^3 water per g of sample) adsorbed by the untreated sample of **1** is less than the value of the water retained (110 cm^3 water per g of sample) on desorptyion by the treated sample of **1**. Furethermore, the hysteresis of the untreated sample

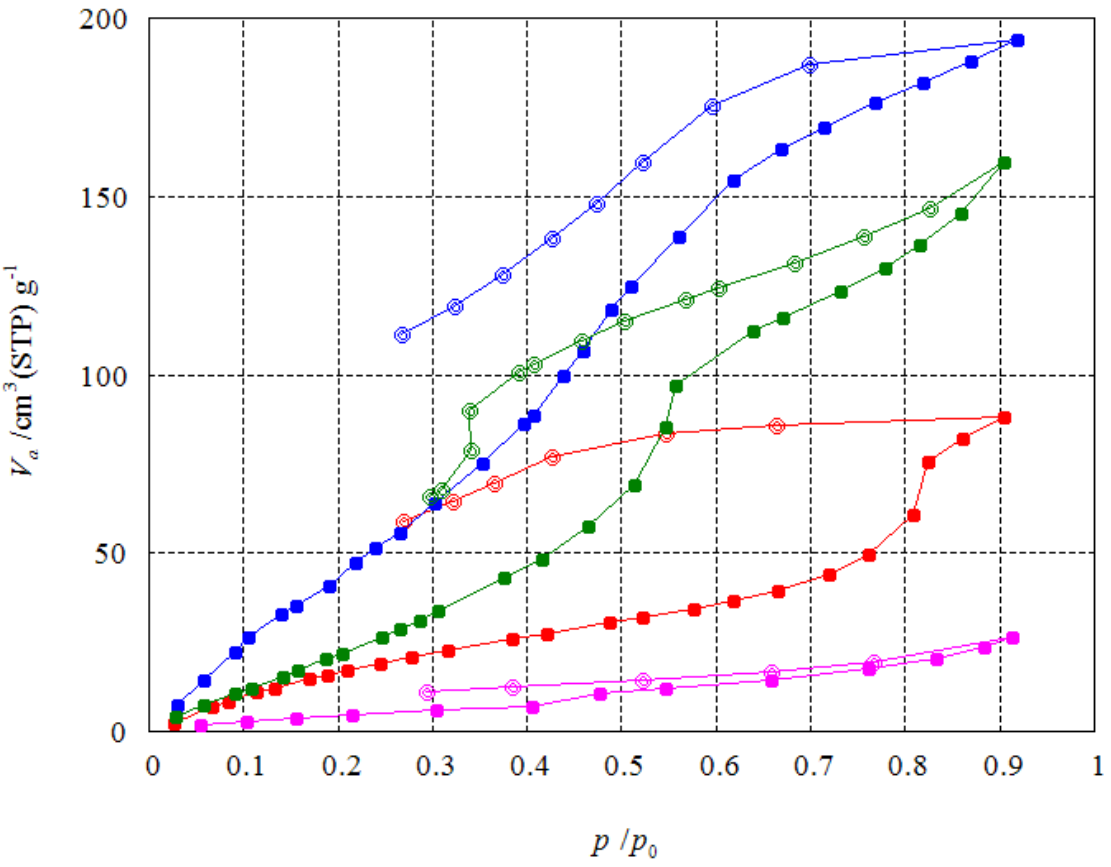

Figure 3.24. Water adsorption isotherms for **1**, **2** and **4** (Bluelines: **1** after pretreatment, Redlines: **1** without pretreatment, Pinklines: **2**; Greenlines: **4**; filled squares, adsorption and circles, desorption).

shows more area than that of the treated sample. This shows the effect of the activation of the sample of **1** on its water adsorption behavior and thus the change in the hydrophilic nature of the pores in it. This dynamic behavior of **1** can be due to the structural flexibility in response to the host-guest interactions. In case of **2** with no water in it (even coordinated), it shows the least affinity towards water. This study further indicates how their structures control the affinity of water whether during synthesis in water or crystallization in water.

3.2.1.2 *Ni(II) Chemistry*

The metal center was changed from Mn(II) to Ni(II) to study the effect of ligand as well as carboxylate linker on the formation of the product. For example, in the Ni(II)-bpta system, variation of carboxylates afforded diverse MOCNs. The fumarate analogue is a square while the

adc and succinate analogs are rare examples of Ni(II) monomeric subunit with only one end of the dicarboxylate coordinated. The monomeric subunits form supramolecular assemblies through extensive hydrogen bonding network of lattice water, coordinated water and uncoordinated oxygen atoms of the carboxylate groups.

Synthesis. All Ni(II) compounds are synthesized via a one pot self-assembly reaction of $Ni(OAc)_2$/bpxa/dicarboxylic acid with a ratio of 1:1:1 in methanol. Acetic acid that was the by-product in all reactions was removed completely with a mixture of toluene:acetonitrile (1:1) added to the reaction mixture. The synthesis of all the compounds of Ni(II) is summarized in Scheme 8.

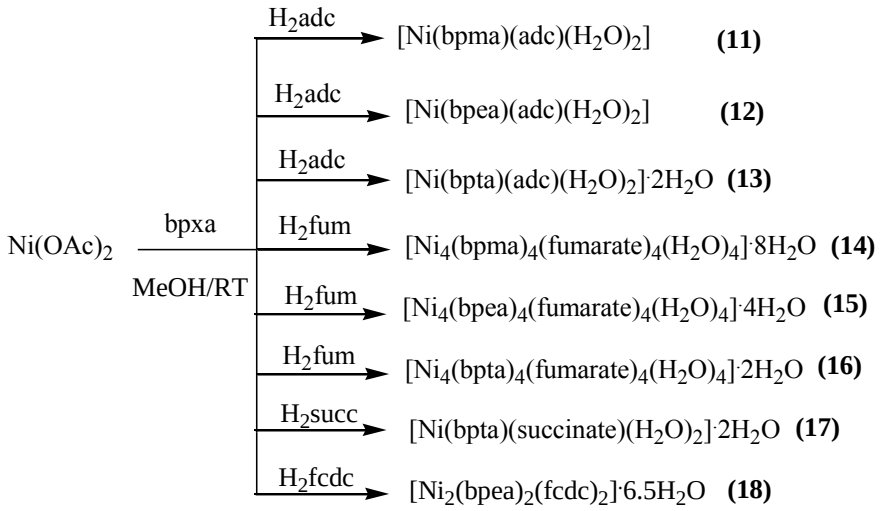

Scheme 8. Synthesis of **11**-**18**.

Single Crystal Structure Analysis. For the single crystal X-ray study, crystals were grown from slow cooling of methanolic solutions of **13** and **17** and slow evaporation of aqueous solution for **16**. Single Crystals of other compounds could not be obtained.

$[Ni(bpta)(adc)(H_2O)_2]\cdot 2H_2O$ (**13**). It crystallizes in the orthorhombic *Pbca* space group. A discrete unit of **13** is shown in Figure 3.25. The coordination environment around the Ni(II) center is N_3O_3, where the ligand 'bpta' wraps around the Ni(II) center leaving three open sites for two water molecules and one monodentate adc. The selected bond distances and angles around Ni(II) center are shown in Table A41. The bond distances are similar to those found in

nickel(II) bpta complex.[183] This is an example of a monomeric synthon forming a supramolecular assembly. Although a dicarboxylate is used, only one carboxylate group binds in a monodentate mode to the Ni(II) center allowing water molecules to coordinate to the Ni(II) center. This is one of the rarest examples where only one end of a dicarboxylate is binding to a metal center. Lang et al. has reported a similar binding mode of ferrocene dicarboxylate (fcdc) in [Cu(pmdta)(fcdc)(H_2O) (CH_3OH)], where pmdta is pentamethyldiethylenetriamine, which forms a supramolecular network similar to compound **13**.[184] The reason for the other end of the dicarboxylate not binding to another Ni(II) center is the strong hydrogen bonding between carboxylate group and two coordinated water molecules on Ni(II) as shown in Figure 3.26. The O-H...O distances between the coordinated water molecules (O1 and O2) and the oxygen atom (O3 and O4) of the free end of carboxylate are 2.736 Å and 2.796 Å which are close to those found in water.[147,150] This results in the formation of a 1D supramolecular assembly of **13** as shown in Figure 3.26. The presence of two lattice water molecules makes it a 2D supramolecular assembly through further hydrogen bonding of lattice water molecules with coordinated water molecules and uncoordinated oxygen atoms of adc. This resulted in the formation of three motifs - a heptagon $R_7^7(7)$ labeled as 1 and two $R_4^4(10)$ motifs labeled as 2 and 3 in Figure 3.27. Motif 1 comprised of O2…O5…O8…O4…O1…O6…O7, Motif 2 has O5…O8…O7…O2…Ni…O3 and 4 carbons of adc and Motif 3 has O8…O7…O6..carbon atoms of adc…O4. All hydrogen bonding parameters are listed in Table 3.4 Further, this supramolecular assembly is also stabilized by C-H…O interactions. In order to make the dehydrated analogue a single crystal was slowly heated to 320 K (47 °C) at the rate of 60 K/h using the Oxford LT device attached to

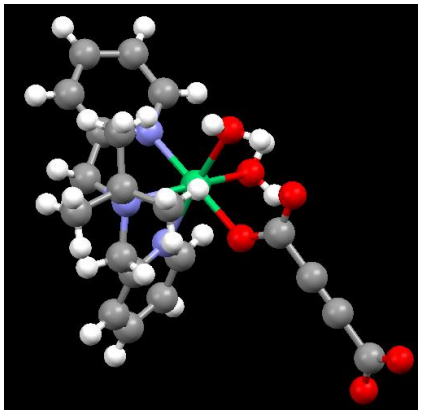

Figure 3.25. A ball and stick presentation of **13**.

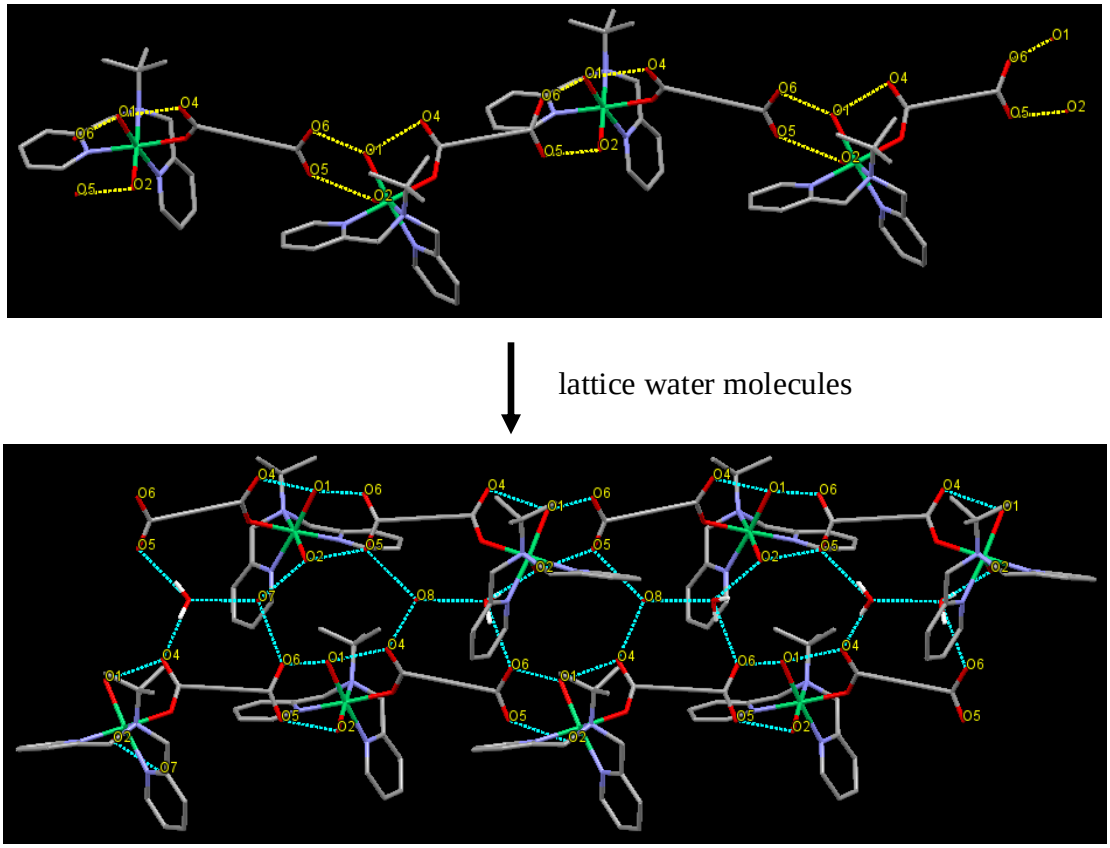

Figure 3.26. Formation of a 2D Supramolecular assembly from the 1D Supramolecular assemblies and lattice water molecules in **13**.

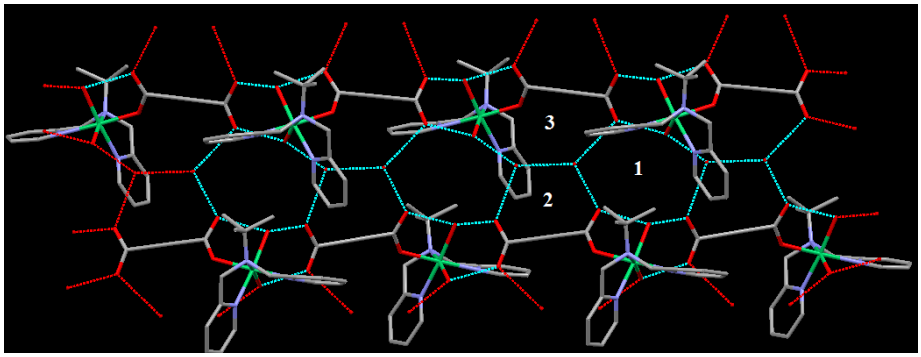

Figure 3.27. Hydrogen bonded network in **13** showing three different motifs.

the diffractometer. The full data collection was carried on this crystal at 320 K for 8 hrs. Based on the structure deduced from this data, it was found that the crystal did not lose its integrity and more importantly both lattice water molecules were found to be intact even after an 8-hour long exposure at 320 K. This shows the strength of hydrogen bonding in this molecule.

Table 3.4. Hydrogen bonding parameters for **13**. [a]

D–H...A	r (D-H) (Å)	r (H…A) (Å)	r (D…A) (Å)	∠D-H…A (deg)	Symmetry
O(1)--H(1B)...O(4)	0.88	1.93	2.656(3)	140	x,1/2-y,-1/2+z
O(2)--H(2A)...O(5)	0.88	1.95	2.796(3)	161	x,1/2-y,-1/2+z
O(7)--H(7A)...O(6)	0.87	2.06	2.891(4)	159	1/2+x,y,1/2-z
O(8)--H(8A)...O(4)	0.87	1.95	2.818(4)	173	x,1/2-y,-1/2+z
O(8)--H(8B)...O(5)	0.87	2.06	2.919(4)	168	
C(3)--H(3C)...O(1)	0.98	2.59	3.57(4)	145	
C(4)--H(4A)...O(1)	0.98	2.52	3.50(4)	147	x,1/2-y,-1/2+z
C(8)--H(8)...O(5)	0.95	2.35	3.250(4)	158	½-x, -1/2+y, z
C(11)--H(11)...O(7)	0.95	2.57	3.384(5)	143	

[a]Numbers in parenthesis are estimated standard deviations in the last significant digits.

$[Ni_4(bpta)_4(H_2O)_4(fum)_4]\cdot 4H_2O$ (16). It crystallizes in the triclinic *P-1* space group. Unlike the adc (vide supra) and succinate (vide infra) analogs, the fumarate analogue is structurally different. It is a square with sides made up of bridging fumarates. The pore size of the square is 12.805 Å x 13.693 Å (Figure 3.28). Each hexacoordinated Ni(II) center is surrounded by one bpta ligand, one water molecule and two oxygens from two fumarate that binds in bis(monodentate) syn-syn fashion. The geometry around Ni(II) centers is distorted octahedron. The selected bond distances and angles are listed in Table A42. The orientation of coordinated water moleucles on Ni(II) centers are different - two are pointing inside the cavity while the other two are pointing outside the cavity. A few tetranuclear Ni(II) squares are reported in the literature with a tetradentate carboxylate-appended pyridyl ligand where each Ni(II) center is pentacoordinated as well as with nitrogen based ligands where each Ni(II) center is hexacoordinated similar to **16**.[185]

These squares are further associated via hydrogen bonding between lattice water molecules, uncoordinated oxygen atoms of the fumarate and the coordinated water molecule on Ni(II) center forming a six membered hexagonal motif $R_6^6(6)$ labeled as 1 in Figure 3.29. All hydrogen bonding parameters are listed in Table 3.5. On each corner of the square, the coordinated water molecule is intramolecularly hydrogen bonded to uncoordinated oxygen atoms of the carboxylate group, e.g., O7 is intramolecularly hydrogen bonded to O10 and O11 (distances: 2.589(4) and 2.624(5) Å). Further, this supramolecular assembly is also stabilized by C—H…O interactions listed in Table 3.5.

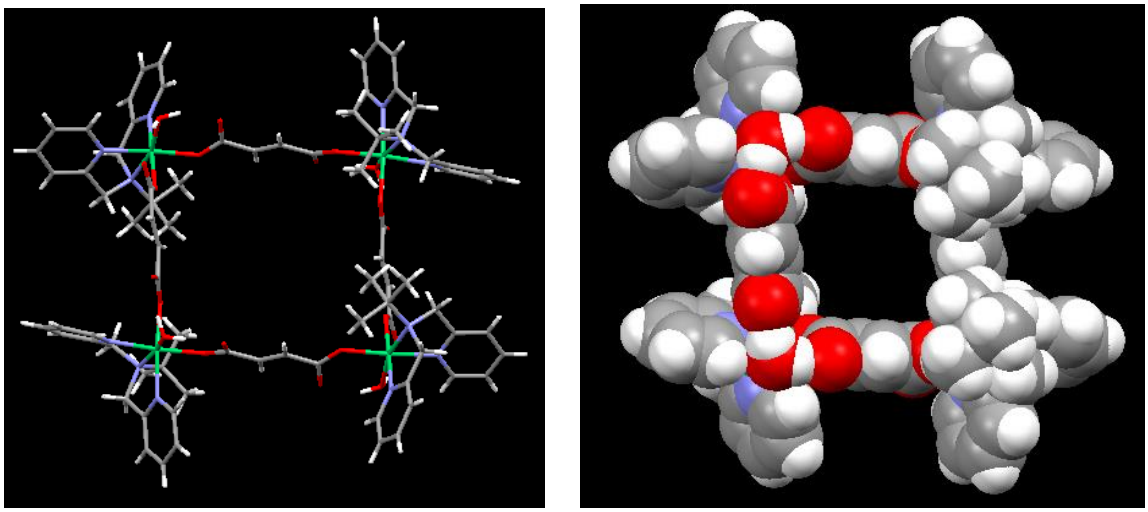

Figure 3.28. A perspective view of **16** (left) and its space-filling model (right).

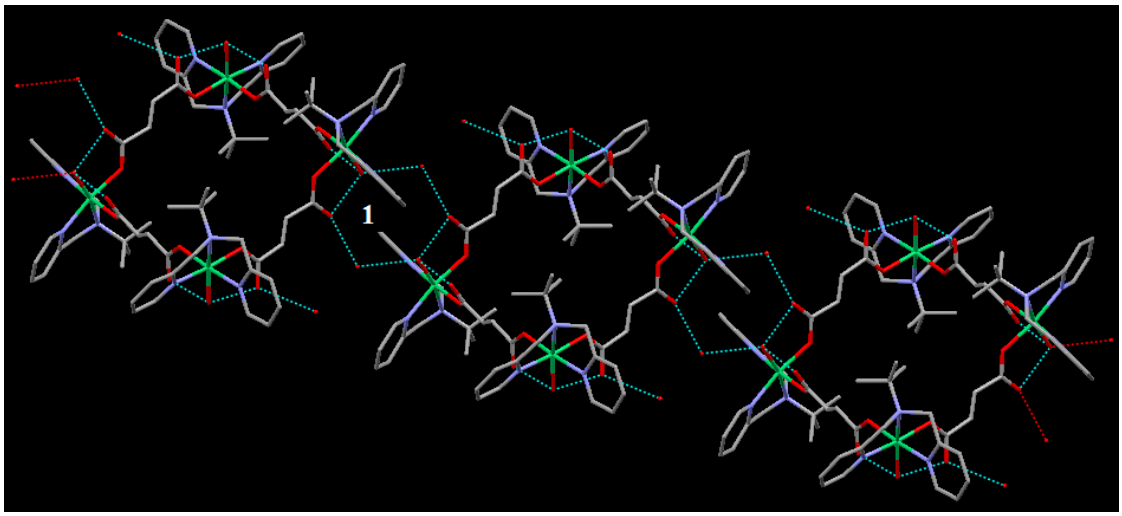

Figure 3.29. Supramolecular assembly of squares in **16** showing a hexameric motif.

Table 3.5. Hydrogen bonding parameters for **16**.[a]

D–H...A	r (D-H) (Å)	r (H…A) (Å)	r (D…A) (Å)	∠D-H…A (deg)	Symmetry
O(5)--H(5A)...O(2)	0.86	1.93	2.661(7)	142	
O(5)--H(5B)...O(10)	0.86	1.77	2.563(7)	153	1-x,1-y,-z
O(6)--H(6B)...O(8)	0.86	1.81	2.592(7)	151	
O(11)--H(11A)...O(5)	0.85	2.04	2.885(8)	171	1-x,1-y,1-z
O(11)--H(11B)...O(2)	0.85	1.98	2.821(8)	173	

[a]Numbers in parenthesis are estimated standard deviations in the last significant digits.

[Ni(bpta)(succ)(H_2O)$_2$]·3H_2O (17). It crystallizes in the monoclinic *P*ca2$_1$ chiral space group. None of the components in this compound is chiral in nature. Chirality in it is due to the orientation of the succinate linker. The succinate linker can have three rotamers - eclipsed, anti and gauche.[186-187] The gauche form is chiral and can form chiral compound from achiral components.[188-189] The coordination environment around Ni(II) is similar to that in **13** (see Figure 3.30) but the hydrogen bonding interactions are different. The selected bond distances and angles are listed in Table A41. Like in **13**, only one end of the succinate binds to the Ni(II) center in a mondentate fashion and other end is strongly hydrogen bonded with the coordinated water molecules resulting in the formation of 1D supramolecular assembly (see Figure 3.31). Because of the hydrogen bonding interactions, four different motifs are formed. Motif 1 is $R_8^8(12)$ involving the uncoordinated O atom of succinate, coordinated water molecules and the lattice water molecules. Motif 2 is $R_7^7(12)$ and motif 3 is $R_4^4(6)$. The hydrogen bonding parameters are listed in Table 3.6.

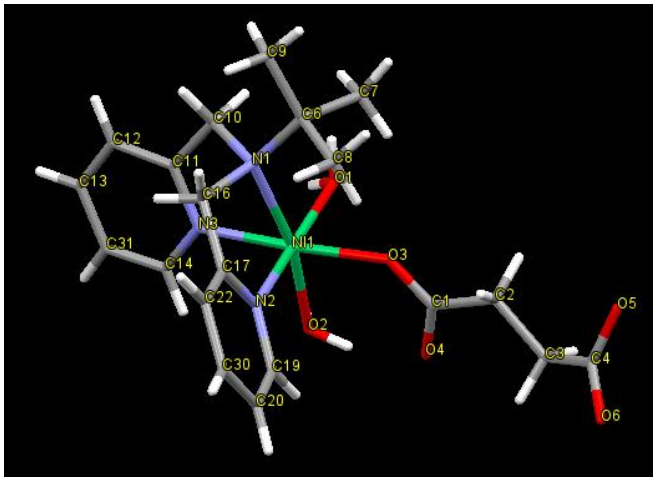

Figure 3.30. A capped stick presentation of **17**.

FTIR and Raman Spectroscopy. The IR spectra of all the compounds were recorded in the solid state as KBr pellets. In **11**, **12** and **13**, there are two broad peaks centered at 3380 and 3233 cm^{-1}; 3384 and 3200 cm^{-1}; 3484 cm^{-1}, respectively, indicating the presence of two different kinds of water molecules. These show asymmetric and symmetric stretching frequencies at 1590 and 1342 cm^{-1} (**11**), 1591 and 1343 cm^{-1} (**12**), 1591 and 1343 cm^{-1} (**13**) for the carboxylate group. For **14**, **15** and **16**, the peaks at 3401 cm^{-1}, 3419 cm^{-1} and 3402 cm^{-1}, respectively, correspond to the

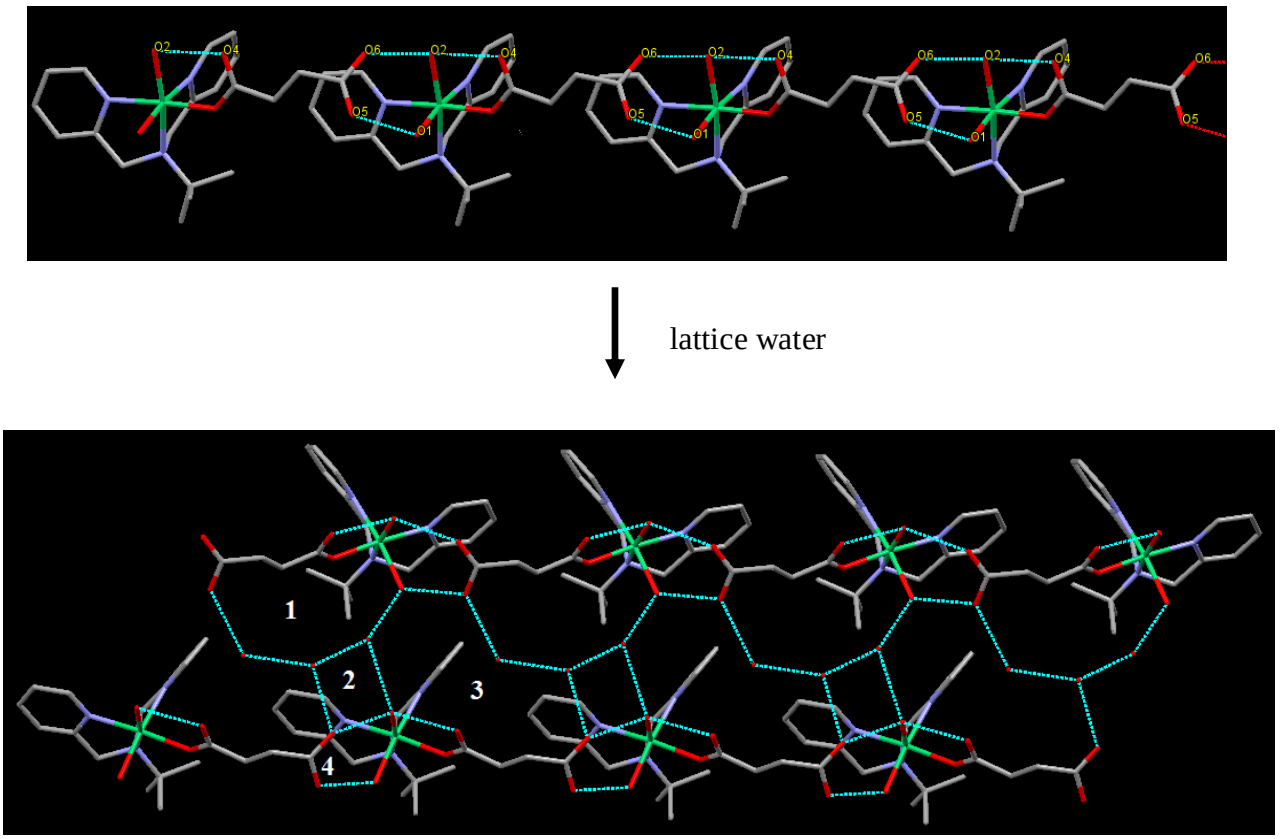

Figure 3.31. Hydrogen bonded network showing motifs in **17** (Hanging contacts and hydrogens are deleted for clarity).

Table 3.6. Hydrogen bonding parameters for **17**.[a]

D–H...A	r (D-H) (Å)	r (H…A) (Å)	r (D…A) (Å)	∠D-H…A (deg)	Symmetry
O(2)—H(3A)...O(6)	0.85	1.90	2.736(4)	169	
O(2)—H(3B)...O(4)	0.85	1.83	2.611(4)	152	x,-1+y,z
O(1)—H(4A)....O(5)	0.85	1.88	2.676(4)	155	
O(7)—H(7D)...O(9)	0.85	1.97	2.757(4)	154	x,-1+y,z
O(8)—H(8D)…O(4)	0.85	2.31	3.085(4)	152	
O(9)—H(9D)…O(6)	0.85	1.91	2.756(4)	174	
O(9)—H(9E)…O(8)	0.85	1.93	2.765(4)	169	
C(7)—H(7B)...O(3)	0.96	2.46	3.287(5)	144	
C(8)—H(8A)...O(3)	0.96	2.46	3.293(6)	145	

[a]Numbers in parenthesis are estimated standard deviations in the last significant digits.

O-H stretch of the water molecules while the bands at 1575 and 1384 cm^{-1} (**14**), 1574 and 1384 cm^{-1} (**15**) and 1567 and 1375 cm^{-1} (**16**) corresponds to asymmetric and symmetric stretch of the carboxylate group. In case of **17**, a peak at 3406 cm^{-1} corresponds to the O-H stretch, a peak at

2976 cm^{-1} corresponds to the C-H stretch (succinate), and two peaks at 1565 cm^{-1} and 1405 cm^{-1} correspond to the asymmetric and symmetric stretch of the carboxylate group, respectively. For **18**, the peaks observed at 1560 cm^{-1} and 1383 cm^{-1} are due to the asymmetric and symmetric stretch of the carboxylate group, respectively. The peaks at 1607, 768, 676 cm^{-1} are due to the tridentate ligand and are common in all the compounds with a shift by few wave numbers.

Compounds **13**, **16** and **17** were also studied by Raman spectroscopy. The peak at 2200 cm^{-1} correspond to the C-C triple bond in **13** which is absent in **16** and **17** (see Figure 3.32).

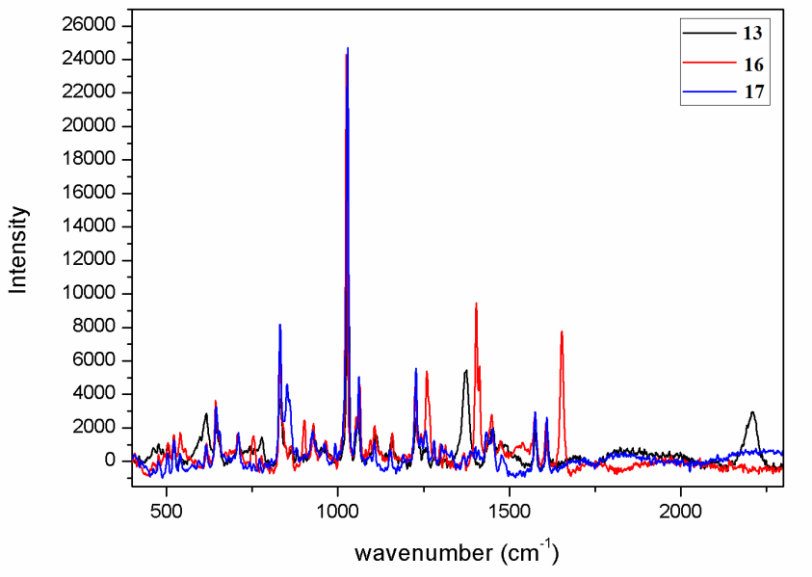

Figure 3.32. Raman spectra of **13**, **16** and **17**.

Thermoanalytical Investigations. The thermal stability of these compounds has been studied by TGA. The TGA scans were recorded from 25-450 °C at the rate of 10 °C/min under a nitrogen atmosphere. As shown in Figures 3.33 and 3.34, **16** is more stable than **13** and **17** which corroborates well with the structural differences found in their single crystal structures. The TGA scan of **13** is a three step profile. For **13**, the first weight loss of 10.13% between 50-150 °C corresponds to loss of two lattice water molecules and one coordinated water molecules (ca. 10.84%). The second loss of 20.51% between 175-270 °C corresponds to the loss of one coordinated water molecule and acetylene dicarboxylic acid molecule followed by continuous decomposition of the molecule. The TGA scan of **16** is a two-step profile. The first weight loss of 3.88% between 150-175 °C corresponds to loss of four lattice water molecules (ca. 3.85%).

After the loss of lattice water molecules the compound was stable up to ca. 300 °C followed by decomposition due to loss of fumaric acid. This shows its unusual stability. The TGA scan of **17** is a two-step profile. The first loss of 7.54% corresponds to the loss of three lattice water molecules (ca. 10.42%). Further weight loss pattern of **17** is different from that of **13** and corresponds to the loss of coordinated water molecules and succinic acid.

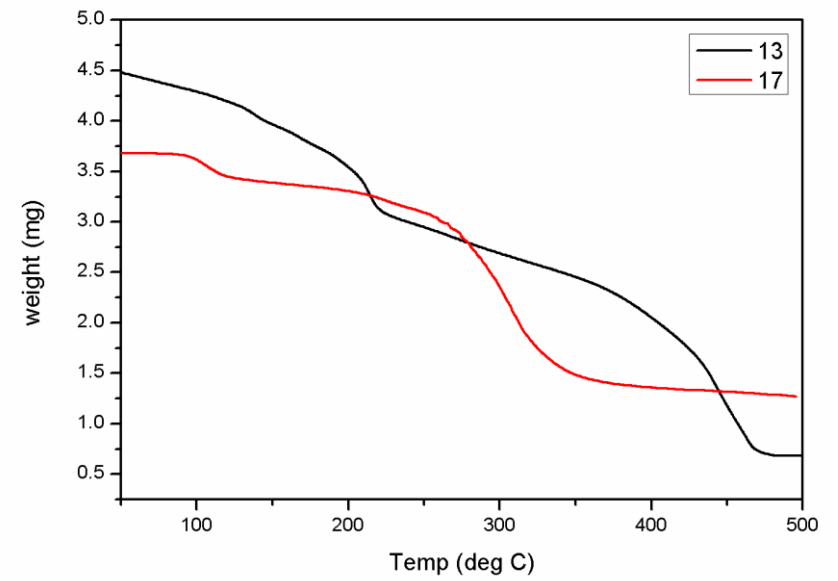

Figure 3.33. TGA scans of **13** and **17**.

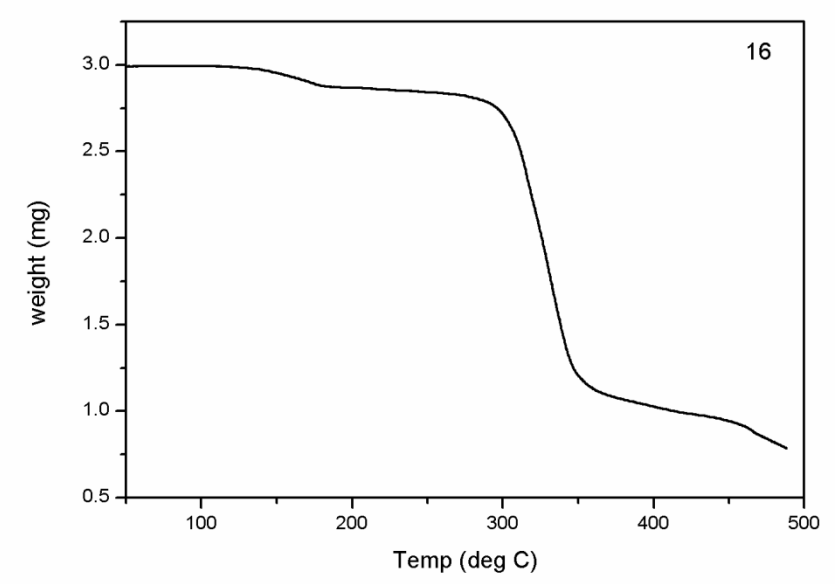

Figure 3.34. TGA scan of **16**.

3.2.1.3 *Co(II) and Cu(II) Chemistry*

The chemistry of the tridentate ligands was extended to Co(II) and Cu(II) metal ions using the bpta ligand while varying the carboxylate. The interest in bpta ligand was due to its affinity for water as was seen in Mn(II) and Ni(II) chemistry. In all cases, discrete binuclear compounds were obtained which formed supramolecular coordination networks via hydrogen bonding.

Synthesis. All these complexes are prepared using the metal perchlorate salt, bpta and sodium salt of dicarboxylic acid in a ratio of 1:1:0.5 in a methanol-water mixture. These compounds were obtained as solutions due to their solubility in the methanol-water mixture. Sodium perchlorate was the by-product in all the cases, the compounds were purified by re-crystallization but in case of **21** sodium perchlorate could not be separated from the bulk sample.

$$M(ClO_4)_2 + bpta + Na_2X \xrightarrow[-NaClO_4]{H_2O/MeOH,\ RT} [M_2(bpta)_2(X)(H_2O)_n](ClO_4)_2$$

where M(II) = Co(II) or Cu(II); X = dicarboxylate, n = 4, (**19**); n = 2, (**20**); n = 2, (**21**)

Scheme 9. General synthesis of **19**-**21**.

Single Crystal structure analysis. Single crystals of all three compounds were grown by slow evaporation of their methanolic solutions.

$[Co_2(bpta)_2(adc)(H_2O)_4](ClO_4)_2 \cdot 4H_2O$ (**19**). It is a dinuclear cobalt(II) complex that crystallizes in the monoclinic $P2_1/c$ space group. There are two independent molecules in the asymmetric unit. Each hexacoordinated Co(II) center is surrounded by three nitrogens of the bpta ligand, two coordinated water molecules and one oxygen of the adc (Figure 3.35). The carboxylate binds to the Co(II) center in a bis(monodentate) syn-syn fashion which is different from those found in the Mn(II)-adc complex of the same ligand (described above). The selected bond distances and angles are listed in Table A43.

Two discrete dinuclear units are hydrogen bonded with each other via coordinated and lattice water molecules to form a supramolecular assembly as shown in Figure 3.36. All the hydrogen bonding parameters are listed in Table 3.7. The coordinated water molecule O8 of one discrete dinuclear unit is hydrogen bonded to the O26 (perchlorate oxygen atom), O7 is hydrogen bonded

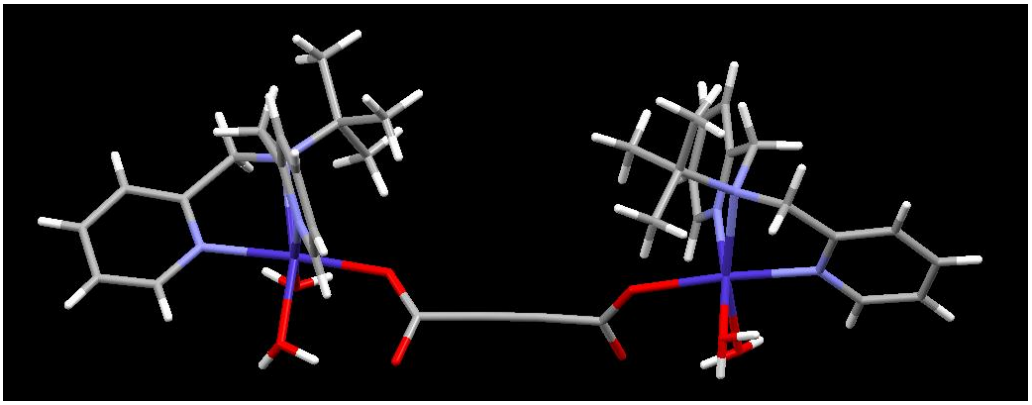

Figure 3.35. Structure of the cation in **19**.

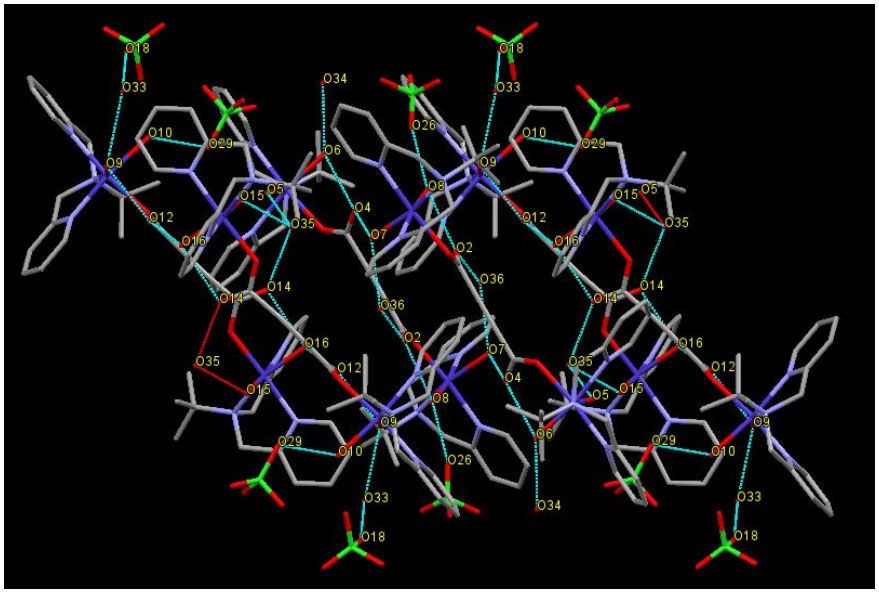

Figure 3.36. Supramolecular assembly in **19**.

to with O4 (uncoordinated oxygen atom of adc of next same subunit), O6 is intramolecularly hydrogen bonded to O4 (uncoordinated oxygen atom of adc of same subunit), O5 is hydrogen bonded to O35 (lattice water molecule) which is further hydrogen bonded to O15 (coordinated water molecule on second subunit) thus connecting two subunits. Similar hydrogen bonding pattern is found for second dinuclear unit.

$[Cu_2(bpta)_2(fum)(H_2O)_2](ClO_4)_2$ (**20**). It is a discrete dinuclear Cu(II) complex in which both Cu(II) centers are pentacoordinated. The fumarate binds in a bis(monodentate) syn-anti mode. Similar types of complexes are reported with 1,10-phenanthroline but with no coordinated water molecule on the Cu(II) center.[190] The selected bond distances and angles are listed in Table A44.

Table 3.7. Hydrogen bonding parameters for **19**.[a]

D–H…A	r (D-H) (Å)	r (H…A) (Å)	r (D…A) (Å)	∠D-H…A (deg)	Symmetry
O(5)--H(5B)...O(35)	0.88	2.14	2.895(6)	144	x,1/2-y,-1/2+z
O(6)--H(6A)...O(4)	0.86	2.22	2.779(8)	123	
O(6)--H(6B)...O(34)	0.86	1.92	2.702(8)	151	x,1/2-y,-1/2+z
O(7)--H(7A)...O(4)	0.85	1.92	2.732(7)	160	1-x,-y,-z
O(7)--H(7B)...O(36)	0.85	1.84	2.692(6)	175	
O(8)--H(8A)...O(2)	0.87	1.92	2.628(7)	138	
O(8)--H(8B)...O(26)	0.86	2.26	2.924(11)	134	1-x,-1/2+y,1/2-z
O(9)--H(9D)...O(12)	0.86	1.89	2.653(9)	148	
O(10)--H(10D)...O(29)	0.86	2.31	2.96(2)	133	x,1/2-y,-1/2+z
O(10)--H(10E)...O(18)	0.86	2.57	3.325(13)	147	
O(10)--H(10E)...O(19)	0.86	2.29	3.056(14)	148	
O(15)--H(15B)...O(35)	0.85	2.21	2.784(7)	125	1-x,-1/2+y,1/2-z
O(16)--H(16A)...O(12)	0.86	1.87	2.700(7)	162	
O(16)--H(16B)...O(14)	0.86	1.81	2.605(8)	153	
O(33)--H(33B)...O(31)	0.85	2.38	3.19(3)	160	
O(34)--H(34A)...O(21)	0.85	2.3	3.057(8)	148	1-x,-1/2+y,1/2-z
O(35)--H(35A)...O(5)	0.85	2.12	2.895(6)	151	x,1/2-y,1/2+z
O(35)--H(35B)...O(14)	0.85	1.83	2.672(7)	174	-1+x,1/2-y,1/2+z
O(36)--H(36A)...O(2)	0.85	1.89	2.687(7)	156	1-x,-y,-z
C(9)--H(9C)…O(8)	0.96	2.6	3.432(9)	146	
C(10)--H(10A)...O(8)	0.96	2.51	3.373(10)	149	
C(11)--H(11A)...O(20)	0.97	2.53	3.367(11)	144	1-x,-1/2+y,1/2-z
C(14)--H(14)...O(32)	0.93	2.47	3.36(2)	161	
C(21)--H(21A)...O(20)	0.97	2.53	3.327(10)	139	
C(23)--H(23)...O(32)	0.93	2.48	3.34(3)	155	x,1/2-y,-1/2+z
C(28)--H(28A)...O(6)	0.96	2.52	3.395(11)	152	
C(44)--H(44C)...O(17)	0.96	2.49	3.222(13)	133	1-x,-1/2+y,1/2-z
C(45)--H(45C)...O(13)	0.96	2.51	3.364(9)	149	
C(47)--H(47B)...O(22)	0.97	2.47	3.263(11)	139	
C(59)--H(59)...O(24)	0.93	2.6	3.355(12)	139	1-x,1-y,-z
C(61)--H(61A)...O(19)	0.97	2.29	3.108(11)	142	1-x,1-y,-z
C(63)--H(63A)...O(11)	0.96	2.51	3.364(10)	148	
C(64)--H(64C)...O(11)	0.96	2.52	3.369(9)	147	
C(65)--H(65A)...O(22)	0.97	2.47	3.369(11)	155	

[a]Numbers in parenthesis are estimated standard deviations in the last significant digits.

Due to the orientation of the coordinated water molecules on the Cu(II) centers, which are trans to each other (see Figure 3.37), O1 (coordinated water molecule) is hydrogen bonded to the uncoordinated oxygen O3 of the fumarate of next dinuclear unit forming a ladder shaped

supramolecular assembly shown in Figure 3.38. The hydrogen bonding parameters are listed in Table 3.8.

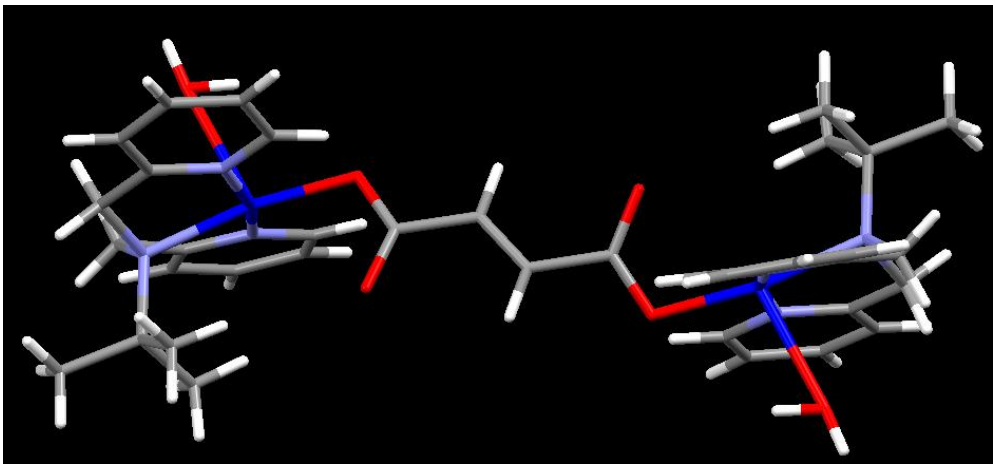

Figure 3.37. Structure of the cation in **20**.

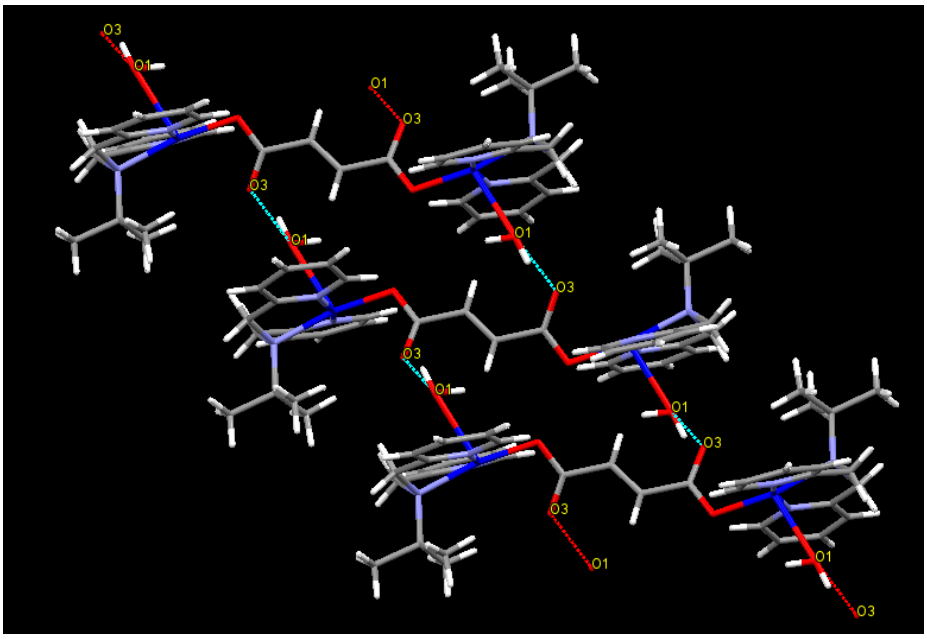

Figure 3.38. Supramolecular assembly in **20**.

Table 3.8. Hydrogen bonding parameters for **20**.[a]

D–H…A	r (D-H) (Å)	r (H…A) (Å)	r (D…A) (Å)	∠D-H…A (deg)	Symmetry
O(1) --H(1A)...O(3)	0.85	2.20	2.730(8)	120	x,-y,-1/2+z
C(13 --H(13)...O(6)	0.93	2.33	3.23(3)	161	1/2-x,1/2-y,1-z

[a]Numbers in parenthesis are estimated standard deviations in the last significant digits.

$[Cu_2(bpta)_2(tdc)(H_2O)(ClO_4)](ClO_4)\cdot 2H_2O$ (21). The Cu (II) centers in **21** are pentacoordinated and inequivalent. One Cu(II) center is surrounded by three nitrogens of the ligand, one coordinated water molecule and one oxygen of tdc while the other does not have coordinated water molecule and its fifth site is occupied by the perchlorate oxygen. The tdc binds in a bis(monodentate) syn-syn mode between the two Cu(II) centers as shown in Figure 3.39, similar to the ones with 1,10-phenanthroline and imidazole ligands reported in the literature.[191-193] The selected bond distances and angles are listed in Table A45.

The dinuclear unit is growing in one direction due to hydrogen bonding of perchlorate oxygen (O10) with uncoordinated oxygen atom of tdc (O2) via a lattice water molecule (O16) as shown in Figure 3.40. O16 is further hydrogen bonded to another lattice water molecule O14. Two such layers of dinuclear units are further connected with each other via O54, the coordinated water molecule on Cu(II). The hydrogen bonding parameters are listed in Table 3.9.

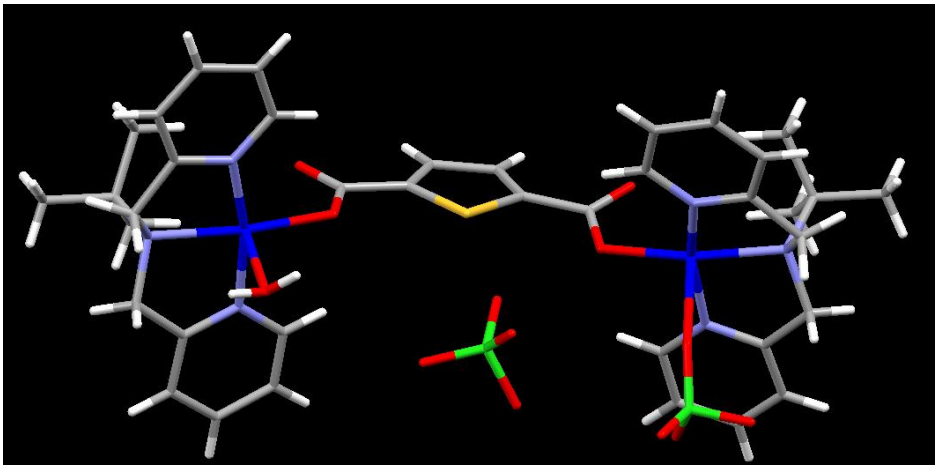

Figure 3.39. Structure of **21**.

FTIR Spectroscopy. The IR spectra of all three compounds **19**, **20** and **21** were recorded in the solid state as KBr pellets. The peaks at 3404 cm^{-1} (**19**), 3438 cm^{-1} (**20**) and 3434 cm^{-1} (**21**) corresponds to the O-H stretching frequencies of lattice water molecules. The asymmetric and symmetric stretching frequencies for the carboxylate group appears at 1567 and 1345 cm^{-1} (**19**), 1563 and 1380 cm^{-1} (**20**) and 1586 and 1378 cm^{-1} (**21**). A difference of approx. 200 cm^{-1} between the two stretching frequencies corresponds to the monodentate binding mode of the carboxylate. The peaks at 1606, 1441, 762 cm^{-1} are due to the ligand; these peaks are common in all

compounds with a shift by few wave numbers. The peaks at 1095 and 621 cm^{-1} (**19**), 1077 and 619 cm^{-1} (**20**) and 1095 and 623 cm^{-1} (**21**) are due to the perchlorate anion.

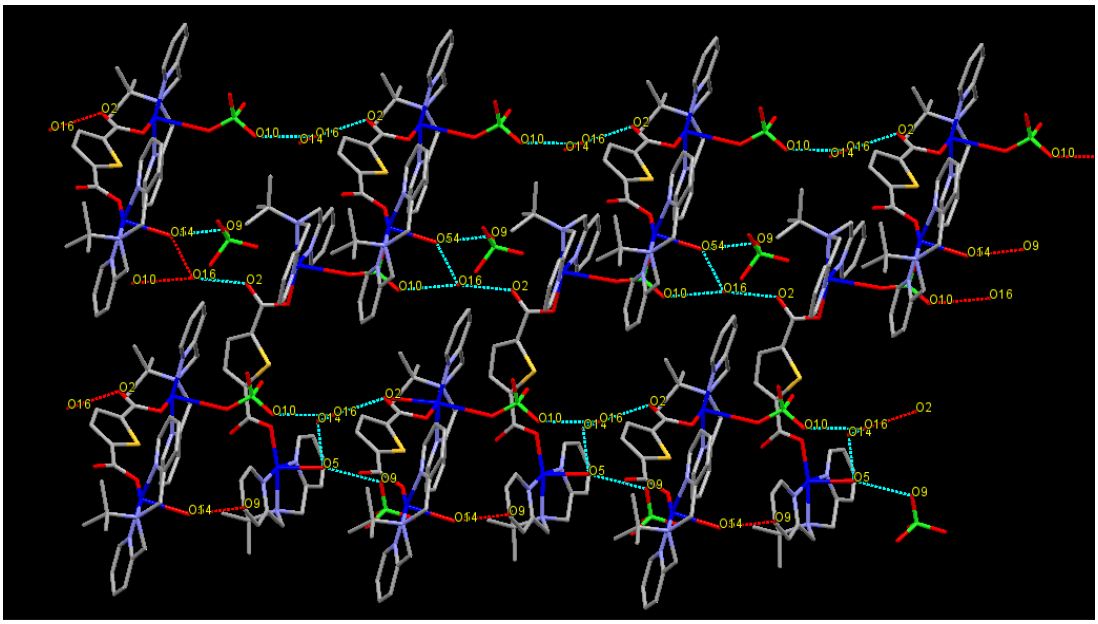

Figure 3.40. Supramolecular assembly in **21**.

Table 3.9. Hydrogen bonding parameters for **21**.[a]

D–H…A	r (D-H) (Å)	r (H…A) (Å)	r (D…A) (Å)	∠D-H…A (deg)	Symmetry
O(14) --H(14D)...O(16)	0.85	2.33	2.953(10)	130	
O(16) --H(16A)...O(10)	0.85	2.07	2.826(8)	147	-1+x,y,z
C(24) --H(24)...O(6)	0.93	2.52	3.370(9)	152	

[a]Numbers in parenthesis are estimated standard deviations in the last significant digits.

3.2.1.4 *Zn(II) and Cd(II) Chemistry*

Dicarboxylate linker

Zn(II) and Cd(II) chemistry with adc as a linker and all the tridentate ligands resulted in the formation of 1D water soluble CPs. Out of all the elements used in this study with tridentate ligands and dicarboxylates, only Zn(II) and Cd(II) form the CPs. This shows the diversity in the formation of products just by changing metal center from Mn(II) to Ni(II) to Co(II) to Cu(II) to Zn(II) and Cd(II) with the same ligand and linker.

Synthesis. All Zn(II) and Cd(II) compounds are synthesized via one-pot self assembly reaction of $Zn(OAc)_2$ or $Cd(OAc)_2$/bpxa/dicarboxylic acid in a ratio of 1:1:1 in methanol. Acetic acid was the by-product in all the reactions, which was removed as an azeotropic mixture using a 1:1 mixture of toluene and acetonitrile. Their synthesis is summarized in Schemes 10 and 11, respectively.

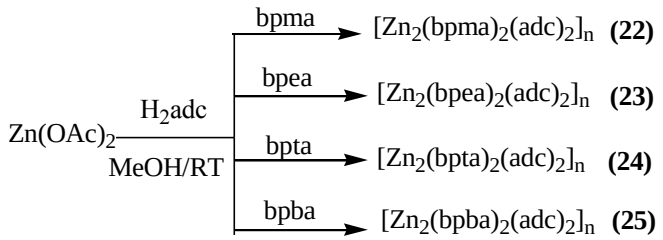

Scheme 10. Synthesis of **22-25**.

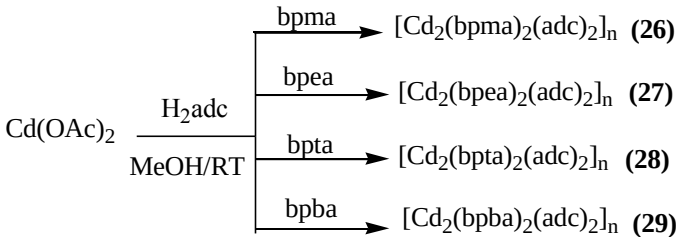

Scheme 11. Synthesis of **26-29**.

Single Crystal structure Analysis. Crystals of all Zn(II) and Cd(II) compounds suitable for the single crystal X-ray study were grown from slow evaporation of aqueous solution of the respective compounds.

$[Zn_2(bpma)_2(adc)_2]_n$ (22). It is a 1D CP that crystallizes in the monoclinic *$P2_1/n$* space group. In this 1D CP, Zn(II) centers are pentacoordinated and surrounded by three nitrogens of the ligand and two oxygens from two ends of two adc linkers (see Figure 3.41). The adc binds in a bis(monodentate) syn-anti fashion. The Zn-O distances are 2.013(4) and 1.974(4) Å. The C-C triple bond varies from 1.175(11) to 1.177(11) Å. The other selected bond distances and bond angles are listed in Table A46. Many CPs with Zn(II) have been reported in the literature with rigid dicarboxylates and neutral linkers, such as 4,4-bphdc, 1,10-phenanthroline, bpe, imidazole

containing ligands but most of these polymers are insoluble in common organic solvents.[194] Recently, Ruschewitz et al. has reported the first CP of Zn and Tl containing adc, $[Tl_2Zn(adc)_2(H_2O)_2]_n$.[195]

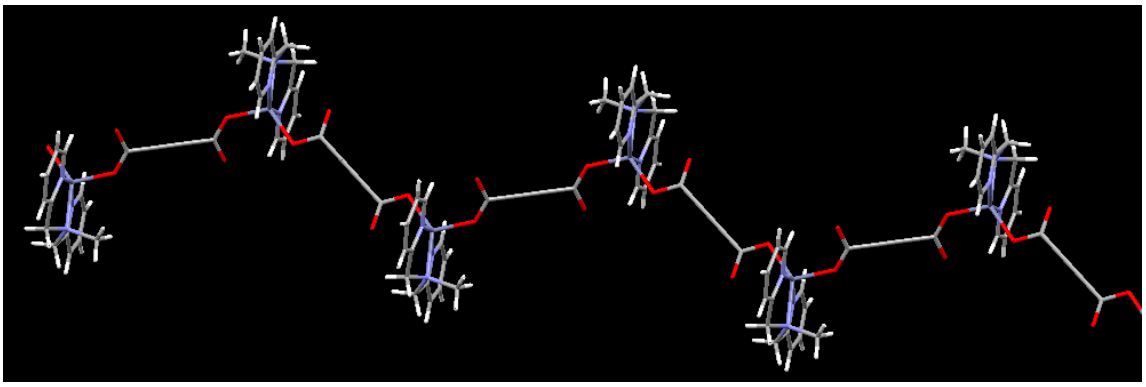

Figure 3.41. A perspective view of **22**.

$[Zn_2(bpea)_2(adc)_2]_n$ (**23**). It is a 1D CP crystallized in the monoclinic $P2_1/n$ space group and is isostructural with **22**. In this 1D polymer, Zn(II) centers are penta-coordinated and surrounded by three nitrogens of the ligand and two oxygens from two ends of two adc linkers (Figure 3.42). The adc binds in a bis(mondentate) syn-anti fashion. The Zn-O distances are 2.0315(16) and 1.9833(16)°. The C-C triple bond varies from 1.188(5) to 1.192(4) Å. The selected bond distances and angles are listed in Table A46.

Unlike **22**, moderate π–π interactions present in **23** resulting in a chair type supramolecular assembly as shown in Figure 3.43. The centroid –centroid distance is 3.879 Å. It should be noted that MOCNs containing the bpea ligand shows π–π interactions (also found in **2**).[182]

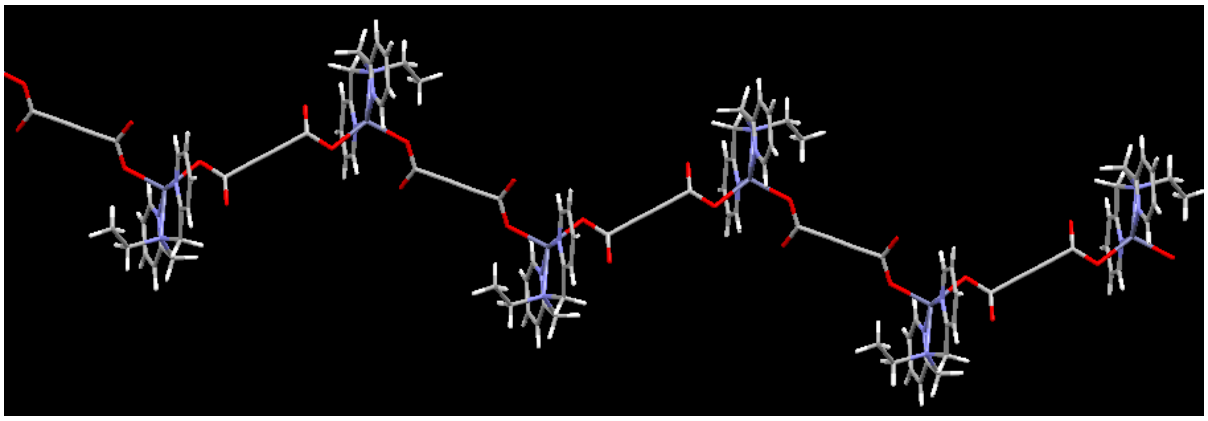

Figure 3.42. A perspective view of **23**.

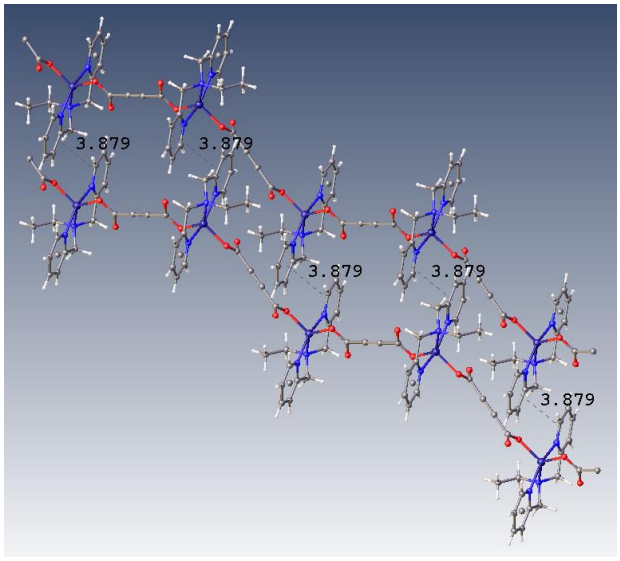

Figure 3.43. Chair-shaped supramolecular assembly in **23**.

$[Zn_2(bpta)_2(adc)_2 \cdot 2H_2O]_n$ (**24**). It is a 1D CP similar to bpma (**22**) and bpea (**23**) analogs but in this case the adc linker binds in a bis(monodentate) syn-syn fashion to Zn(II) (see Figure 3.44). The presence of two lattice water molecules in the crystal structure also makes it different from **22** and **23**. This also shows that bpta analogs irrespective of metal center have more affinity for water molecules over the others. The selected bond distances and angles for **24** are listed in Table A46.

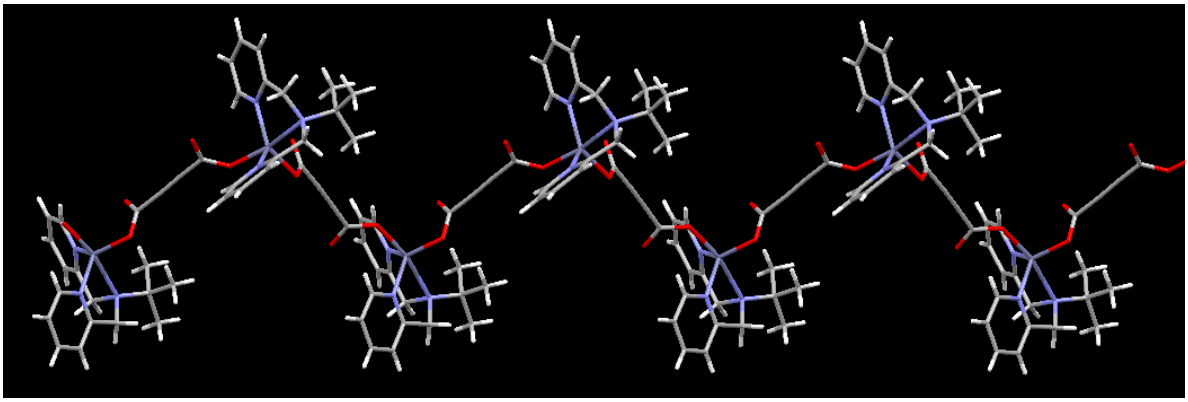

Figure 3.44. A perspective view of **24**.

The lattice water molecules connect two 1D CP chains to form a 2D supramolecular assembly (Figure 3.45). For example, the oxygen of one water molecule, O5, connects the two layers

together via hydrogen bonding with uncoordinated oxygen atoms of the linker. All other hydrogen bonding parameters are listed in Table 3.10.

Table 3.10. Hydrogen bonding parameters for **24**.[a]

D–H...A	r (D-H) (Å)	r (H…A) (Å)	r (D…A) (Å)	∠D-H…A (deg)	Symmetry
O(5)--H(5A)...O(2)	0.85	1.99	2.834(5)	175	1/2+x,y,1/2-z
O(5)--H(5B)...O(3)	0.85	1.96	2.806(5)	173	1+x,y,z
C(6)--H(6)...O(5)	0.93	2.54	3.329(6)	143	
C(7)--H(7)...O(4)	0.93	2.57	3.487(5)	168	-x,1/2+y,1/2-z
C(13)--H(13)...O(4)	0.93	2.54	3.135(5)	122	-1/2-x,1/2+y,z
C(16)--H(16)...O(4)	0.93	2.51	3.407(5)	161	-x,-y,-z
C(19)--H(19A)...O(1)	0.96	2.45	3.348(5)	155	

[a]Numbers in parenthesis are estimated standard deviations in the last significant digits.

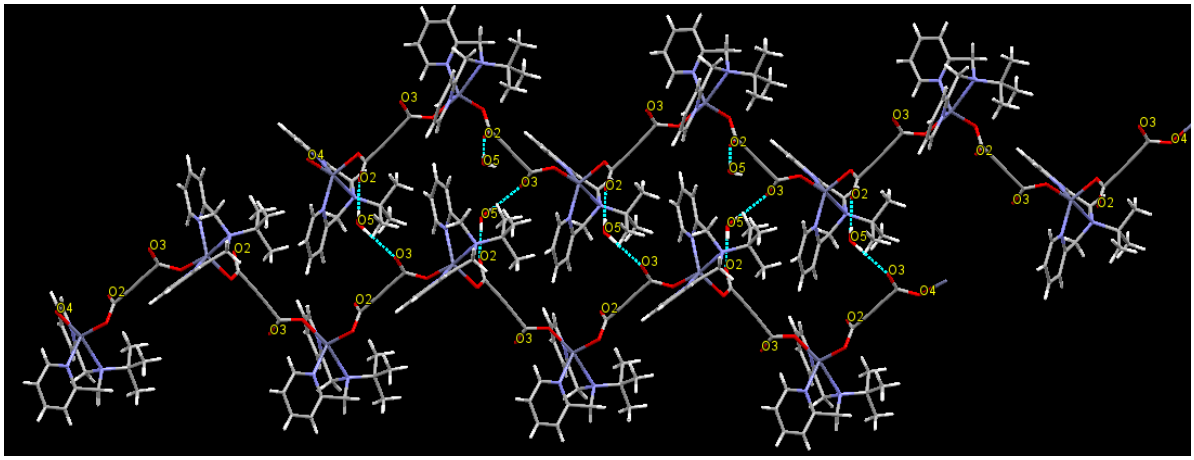

Figure 3.45. 2D supramolecular assembly in **24**.

$[Cd_2(bpea)_2(adc)_2]_n$ (**27**). The 1D CP of **27** is V-shaped and crystallizes in the triclinic *P*-1 (No. 2) space group. There are two independent CP chains in the asymmetric unit. In one of the polymeric chain Cd(II) centers are heptacoordinated surrounded by three nitrogens of the ligand, four oxygen atoms from the two chelated adc as shown in Figure 3.46a. The Cd-O distances for chelated carboxylate in this polymeric chain ranges from 2.268 -2.616 Å. In second polymeric chain shown in Figure 3.46b one Cd(II) center is hexacoordinated surrounded by three nitrogens of the ligand and three oxygens from one chelated and monodentate adc whereas second Cd(II) center is heptacoordinated having similar coordination environment as found in the first polymeric chain. The Cd-O distances for chelated carboxylate in this polymeric chain are 2.241 and 2.616 Å. The selected bond distances and angles are listed in Table A47.

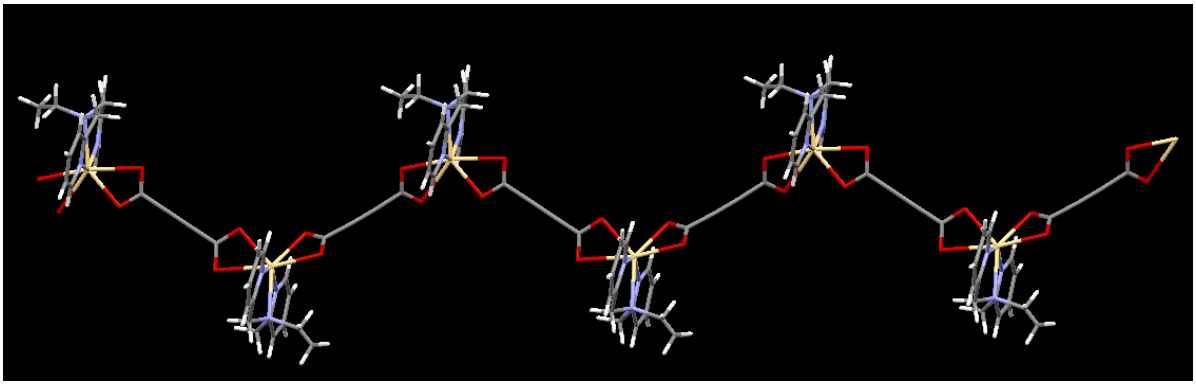

Figure 3.46a. A perspective view of the polymeric chain 1 in **27**.

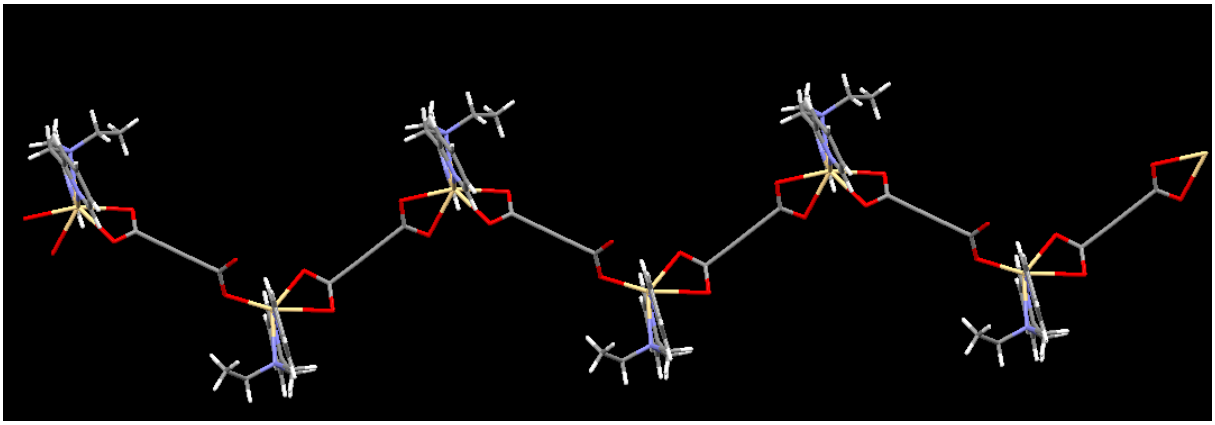

Figure 3.46b. A perspective view of the polymeric Chain 2 in **27**.

The two layers of 1D CP are stacked together with moderate π–π interactions found in one plane (Figure 3.47). The centroid-centroid distance is 3.903 Å.[182] This proves again that only the bpea analogue shows π–π interactions. Similar π–π interactions are found in polymeric chain 2 of **27**.

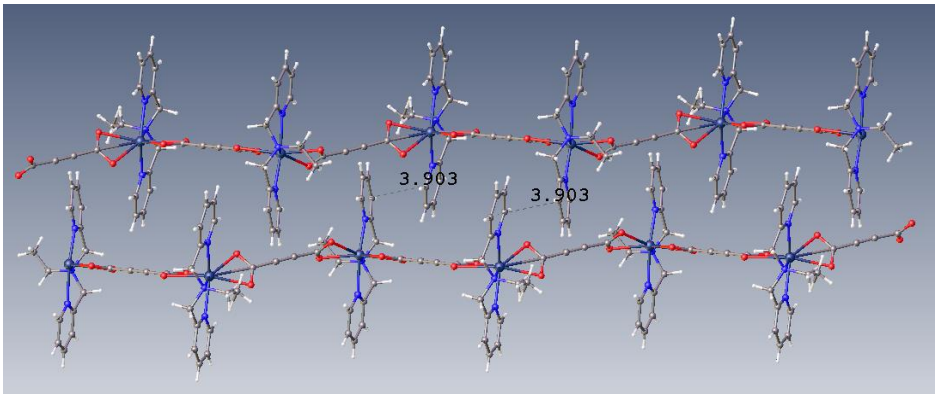

Figure 3.47. 2D Supramolecular assembly in **27** via π–π interactions.

$[Cd_2(bpta)_2(adc)_2 \cdot 2H_2O]_n$ (**28**). It is a V-shaped 1D coordination polymer (see Figure 3.48) similar to **24** except one end of adc is chelating while other one is monodentate. Cd(II) centers are hexacoordinated surrounded by three nitrogens of the ligand and three oxygens of the two adc linkers. The selected bond distances and angles are listed in Table A48. The lattice water molecules connect the two 1D polymeric chains to form a 2D supramolecular assembly via hydrogen bonding (see Figure 3.49). The supramolecular assembly is further stabilized by the presence of C-H…O interactions. All the hydrogen bonding parameters are listed in Table 3.11.

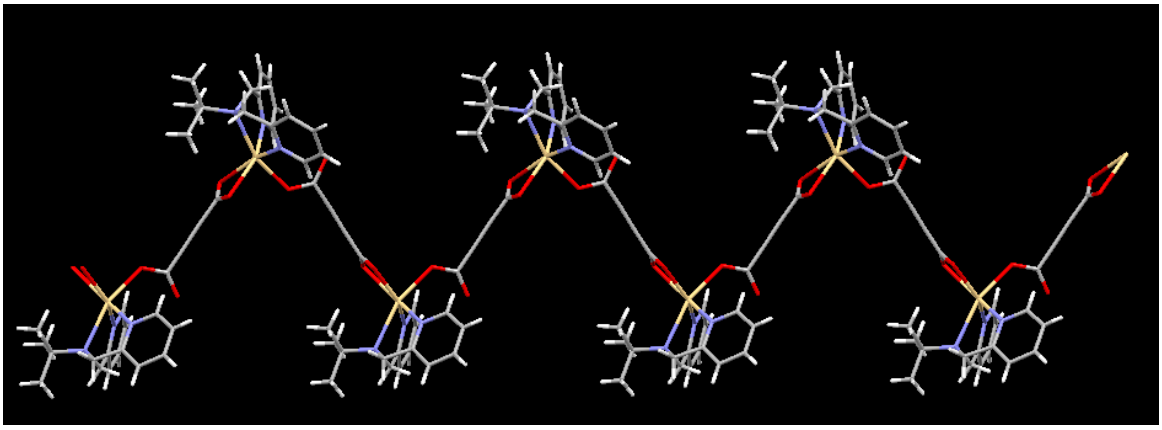

Figure 3.48. V-shaped 1D coordination polymer of **28**.

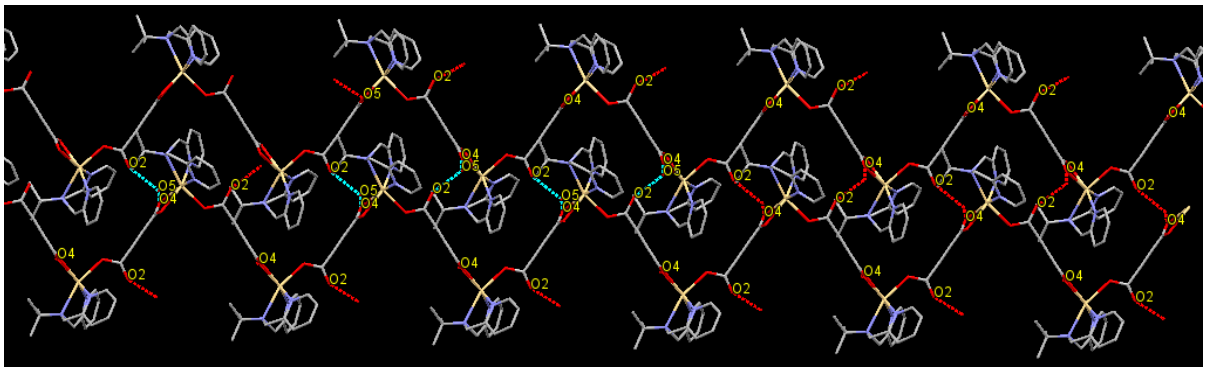

Figure 3.49. 2D supramolecular assembly in **28**.

Table 3.11. Hydrogen bonding parameters for **28**.[a]

D–H...A	r (D-H) (Å)	r (H…A) (Å)	r (D…A) (Å)	∠D-H…A (deg)	Symmetry
C(6)--H(6)...O(5)	0.93	2.55	3.345(9)	143	1/2+x,y,1/2-z
C(7)--H(7)...O(1)	0.93	2.42	3.338(9)	169	1/2+x,y,1/2-z
C(11)--H(11A)...O(3)	0.97	2.57	3.452(8)	152	1/2+x,1/2-y,-z
C(16)--H(16)...O(1)	0.93	2.57	3.456(8)	161	1/2+x,1/2-y,-z

[a]Numbers in parenthesis are estimated standard deviations in the last significant digits.

$[Cd_2(bpba)_2(adc)_2]_n$ (**29**). It is a 1D CP that crystallizes in the orthorhombic *Pbca* space group (Figure 3.50). Each hexacoordinated Cd(II) center is surrounded by three nitrogens of the ligand and three oxygen atoms (from one monodentate carboxylate group of an adc and one chelated carboxylate group of another adc). The selected bond distances and angles around Cd(II) center is listed in Table A49.

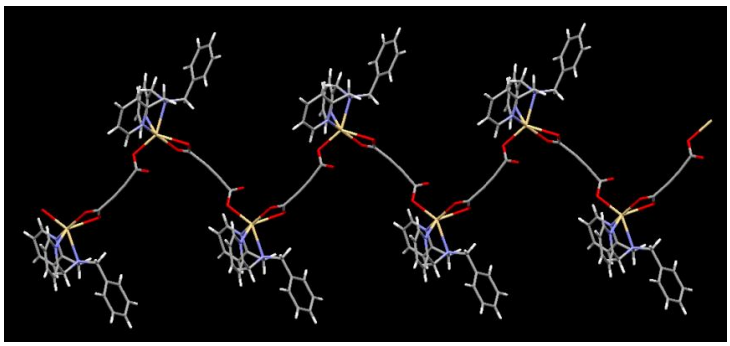

Figure 3.50. V-shaped 1D CP of **29**.

Powder X-ray Analysis. All samples (**22-29**) were studied by powder X-ray diffraction for their bulk purity. The experimental powder patterns obtained for **22**, **23** and **24** are in good agreement with the simulated powder patterns which shows that the bulk sample represents the single crystal. The experimental powder pattern for **25** is similar to **24** (see Figure 3.51) with a shift of peaks which suggests that these two might be isostructural. Similarly, the experimental patterns for **27**, **28** and **29** are in good agreement with their respective simulated powder patterns (see Figure 3.52).

FTIR Spectroscopy. Further characterization of **22-29** was done by FTIR in the solid state using KBr pellets. For Zn(II) compounds, the peaks at 1639 and 1320 cm^{-1}(**22**); 1634 and 1321 cm^{-1} (**23**); 1634 and 1321 cm^{-1} (**24**); 1632 and 1322 cm^{-1} (**25**) correspond to the asymmetric and symmetric stretch of the carboxylate group, respectively. For Cd(II) compounds, the peaks at 1594 and 1349 cm^{-1} (**26**); 1582 and 1345 cm^{-1} (**27**); 1630, 1560, 1328, 1340 cm^{-1} (**28**); 1574, 1562, 1378, 1344 cm^{-1} (**29**) corresponds to the asymmetric and symmetric stretch of the carboxylate group, respectively. The peaks at 1603, 1489, 1023, 781, 695, 677 cm^{-1} are the ligand peaks which are common in all compounds with a shift of few wave numbers.

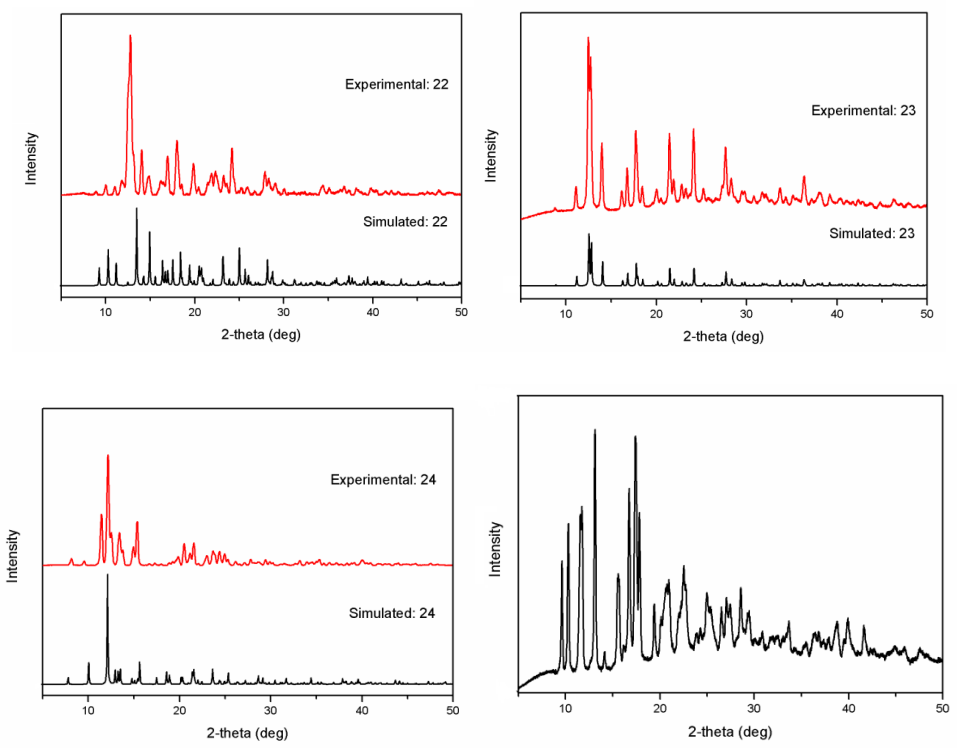

Figure 3.51. Experimental and simulated powder patterns for **22**, **23**, **24** and **25**.

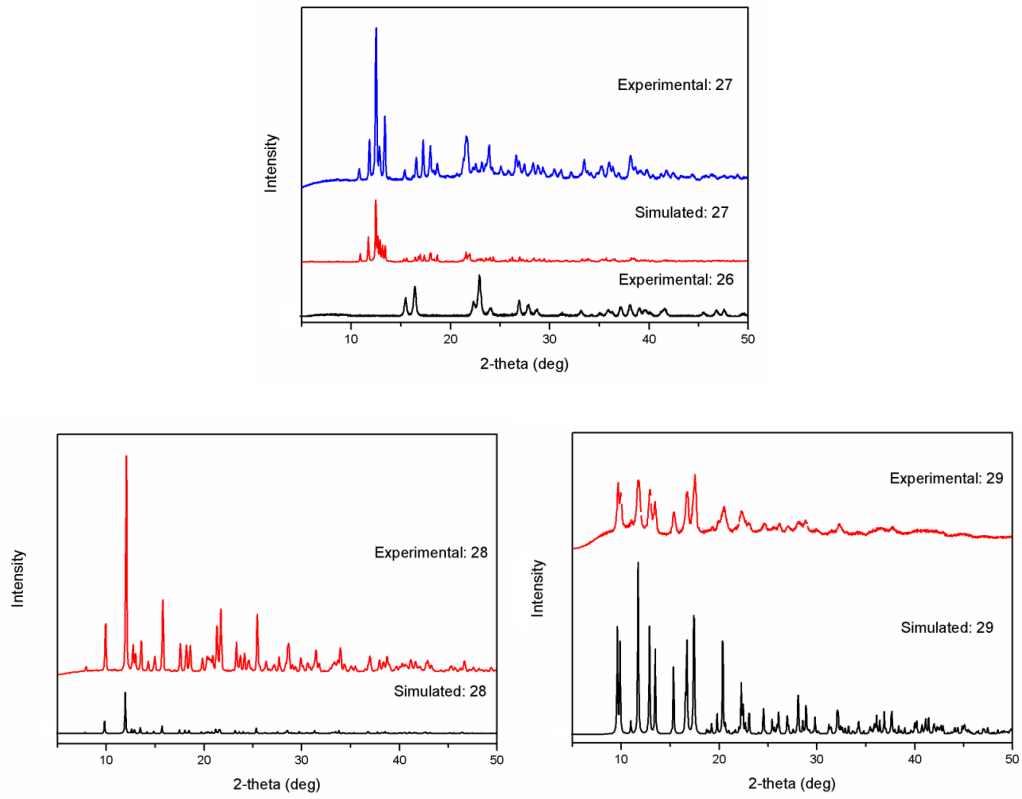

Figure 3.52. Experimental and simulated powder patterns for **26**, **27**, **28** and **29**.

Thermoanalytical Investigations. Thermal stability of all these polymers was studied by Thermogravimetric analysis from 50 to 500 °C under a nitrogen atmosphere. All Zn(II) containing CPs (**22-25**) are stable up to 175 °C followed by loss of acetylene dicarboxylic acid. On the other hand, there is a variability in the temperature up to which the Cd(II) containing polymers are stable: 125 °C (**26**), 175 °C (**27**), 150 °C (**28**) and 200 °C (**29**) followed by loss of acetylene dicarboxylic acid.

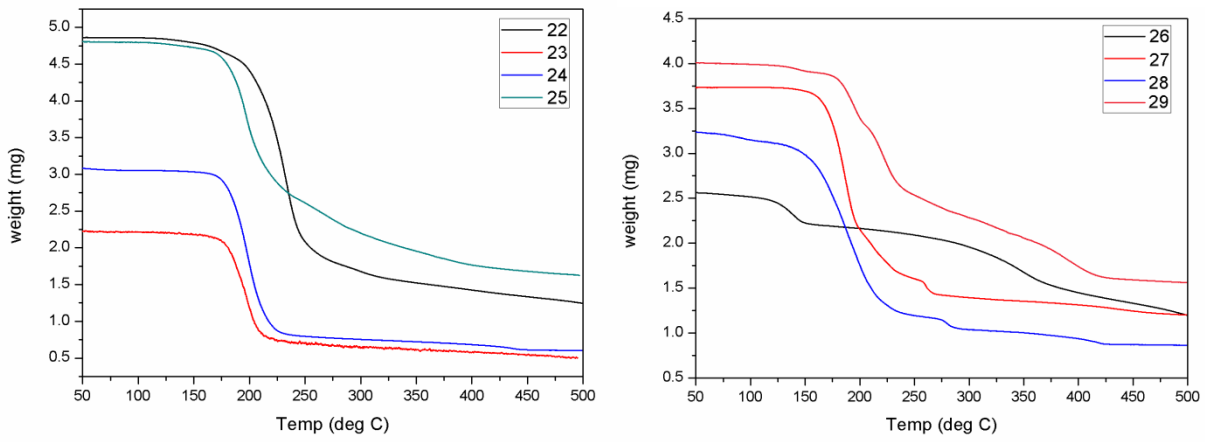

Figure 3.53. TGA scans for **22-25** (left) and **26-29** (right).

Tricarboxylate linker

Synthesis. Few reactions were done with Zn(II) or Cd(II), bpxa and H_3BTC under hydrothermal conditions because products obtained with BTC at ambient conditions are not generally soluble in common organic solvents as mentioned earlier. With its rigid structural feature, BTC has been used in generating many novel structures.[121]The Cd(II) compounds with BTC and nitrogen linkers, such as bpe, acridine etc., has been reported in the literature[121] but not with a chelating tridentate ligand. Massoud et al. has reported the use of tridentate ligands including bpma with benzene tetracarboxylate but with all such ligands only discrete molecules were obtained.[121d]

The reaction of Zn(II) with H_3BTC and bpma resulted in the formation of two kinds of crystals (see Figure 3.54). It was difficult to manually separate the crystals. Based on the single crystal structure determination, the rectangular crystals were found to be a polymer containing both bpma and HBTC (**30a**) whereas rod shaped crystals contained only BTC (**30b**). For reactions of the Cd(II)-H_3BTC system, the ligand was varied from methyl to ethyl to t-butyl. Their synthesis is summarized in Scheme 12.

Single Crystal Structure Analysis. Crystals of **30**, **31**, **32** and **33** were obtained from hydrothermal reaction.

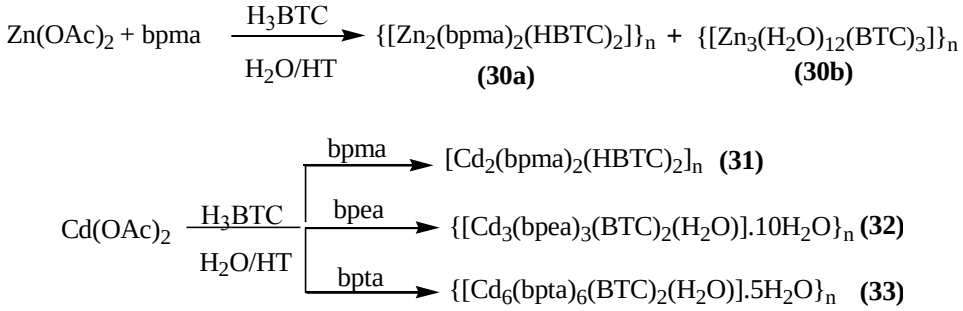

Scheme 12. Synthesis of **30-33** under hydrothermal conditions.

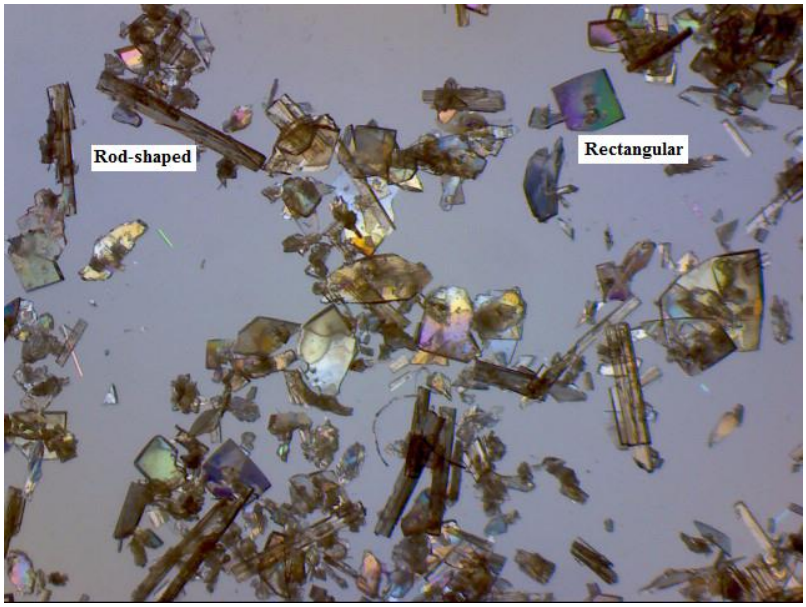

Figure 3.54. Rectangular (**30a**) and rod shaped (**30b**) crystals from the reaction mixture.

{[Zn$_2$(bpma)$_2$(HBTC)$_2$]}$_n$ (**30a**). It is a 1D coordination polymer that crystallizes in the monoclinic *P2$_1$/c* space group. Each Zn(II) center is pentacoordinated with three sites occupied by three nitrogens of bpma and other two sites occupied by oxygen atoms from the two carboxylate groups of one HBTC. A perspective view of 1D CP of **30a** is shown in Figure 3.55. The selected bond distances and bond angles are listed in Table A50. While two ends of HBTC binds to Zn(II) in a bis(monodentate) syn-syn fashion, the carboxylic acid group of BTC that was not deprotonated under the hydrothermal conditions provides strong hydrogen bonding (2.537 to 2.566 Å) interaction to form the 2D supramolecular assembly shown in Figure 3.56. In addition

to hydrogen bonding, the supramolecular assembly is further stabilized by C-H…O interactions. The hydrogen bonding parameters are listed in Table 3.12.

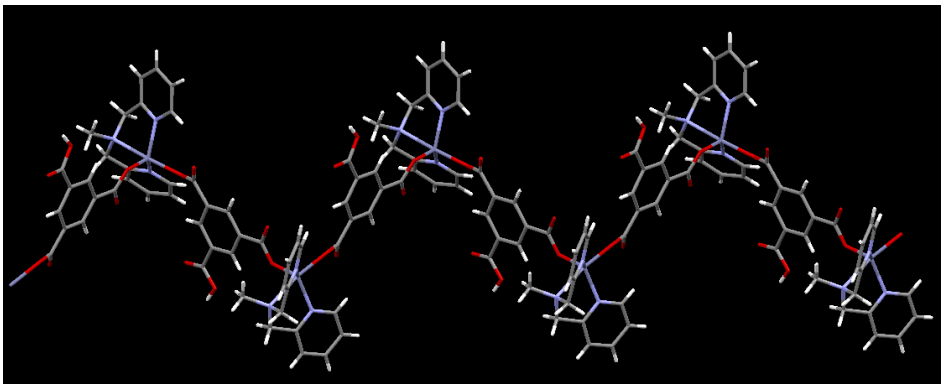

Figure 3.55. A perspective view of **30a**.

Table 3.12. Hydrogen bonding parameters for **30a**.[a]

D–H…A	r (D-H) (Å)	r (H…A) (Å)	r (D…A) (Å)	∠D-H…A (deg)	Symmetry
O3--H3...O2	0.82	1.75	2.5370	161	x,1/2-y,-1/2+z
O12--H10...O7	0.82	1.76	2.5669	169	x,1/2-y,1/2+z
C10--H10B...O4	0.97	2.51	3.1902	127	1-x,-1/2+y,1/2-z
C12--H12...O7	0.93	2.53	3.1249	122	
C14--H14...O9	0.93	2.48	3.2779	144	1-x,-1/2+y,1/2-z
C39--H39...O2	0.93	2.52	3.3717	153	
C41--H41...O13	0.93	2.54	3.1677	125	1-x,-1/2+y,1/2-z

[a]Numbers in parenthesis are estimated standard deviations in the last significant digits.

[$Zn_3(BTC)_2(H_2O)_{12}$] (30b). Its single crystal structure is not reported in the literature. While O. M. Yaghi et al. has proposed the structure of this compound similar to that of Co(II) reported in the same paper, Ling-Guang Qiu et al. has reported the structure of this compound by Rietveld analysis of the powder X-ray diffraction (XRD) patterns using WinPLOTR and Fullprof. [121b,196] It crystallizes in the monoclinic *Cc* chiral space group. Chirality can be due to the helicity of the polymeric chain.[188-189] In **30b**, all Zn(II) centers are hexacoordinated but one center is different from the other two with respect to the coordination environment (Figure 3.57). The selected bond distances and angles are listed in Table A52. Two Zn(II) are coordinated by four water molecules and two carboxylate oxygens from two different BTC linkers. The third one is surrounded by

two oxygens of the chelated carboxylate of the BTC linker in addition to four water molecules. Thus each BTC provides two monodentate carboxylate and one chelated carboxylate for coordination with Zn(II) ions.

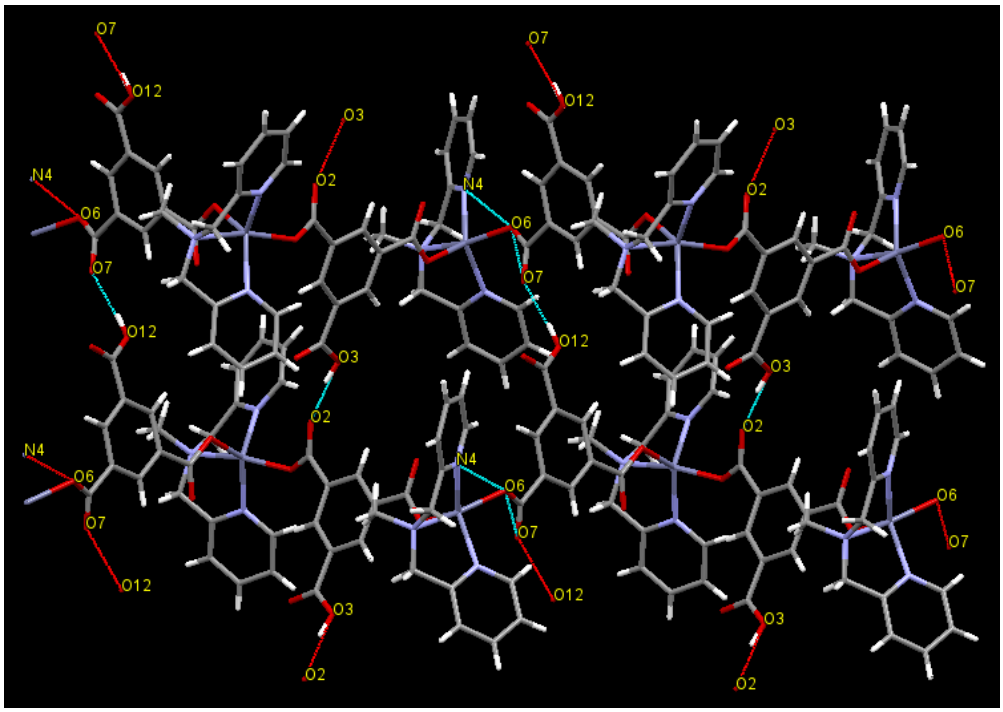

Figure 3.56. 2D Supramolecular assembly in **30a**.

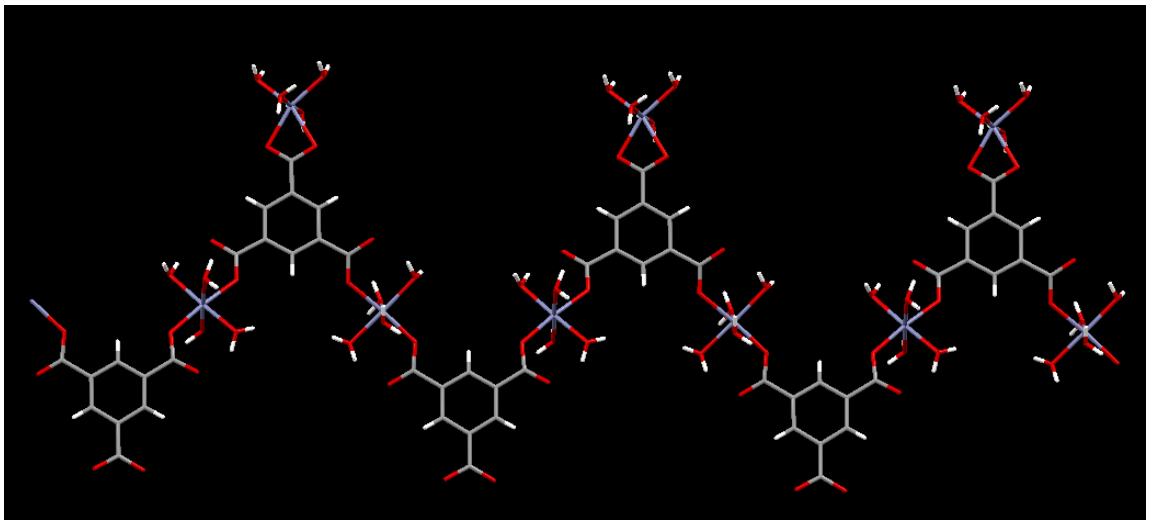

Figure 3.57. A perspective view of **30b**.

The coordinated water molecules on Zn(II) center are hydrogen bonded with the coordinated water molecules on Zn(II) center of the next polymeric chain thus forming a supramolecular assembly with large supramolecular cavities shown in Figure 3.58. The hydrogen bonding parameters are listed in Table 3.13.

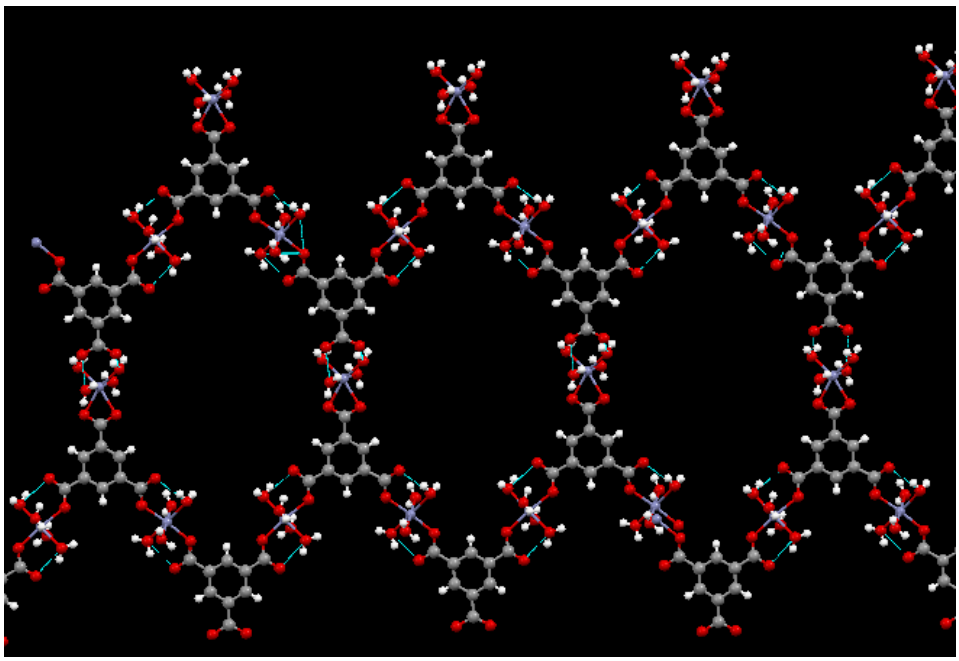

Figure 3.58. 2D Supramolecular assembly in **30b**.

Table 3.13. Hydrogen bonding parameters for **30b**.[a]

D–H…A	r (D-H) (Å)	r (H…A) (Å)	r (D…A) (Å)	∠D-H…A (deg)	Symmetry
O(4)--H(4A)...O(9)	0.86	1.95	2.751(8)	154	1/2-x,-1/2+y,2-z
O(4)--H(4B)...O(7)	0.86	2.43	3.269(8)	165	x,y,1+z
O(5)--H(5A)...O(3)	0.87	2.06	2.826(7)	147	1/2-x,1/2+y,1-z
O(5)--H(5B)...O(2)	0.87	1.79	2.569(8)	148	
O(6)--H(6A)...O(10)	0.85	2.1	2.918(7)	161	1/2-x,-1/2+y,2-z
O(6)--H(6B)...O(11)	0.85	2.06	2.895(8)	167	1/2-x,-1/2+y,1-z
O(7)--H(7A)...O(10)	0.85	2.14	2.918(8)	151	1/2-x,-1/2+y,1-z
O(7)--H(7B)...O(4)	0.85	2.45	3.269(8)	162	x,y,-1+z
O(11)--H(11A)...O(6)	0.87	2.58	2.895(8)	103	1/2-x,1/2+y,1-z
O(11)--H(11B) ...O(3)	0.87	2.04	2.888(9)	164	
O(12)--H(12A)...O(5)	0.85	1.81	2.659(9)	177	-x,1+y,1-z
O(12)--H(12B)...O(3)	0.85	2.22	2.852(9)	131	-1/2+x,3/2+y,-1+z

[a]Numbers in parenthesis are estimated standard deviations in the last significant digits.

$[Cd_2(bpma)_2(HBTC)_2]_n$ (31). It is a linear 1D CP where Cd(II) centers are heptacoordinated and surrounded by two chelated carboxylates of HBTC leaving a carboxylic acid group intact (see Figure 3.59). This allows the two linear polymeric chains to form a hydrogen bonded (O4-H...O2) supramolecular assembly shown in Figure 3.60. This is further supported by FTIR results discussed below. The hydrogen bonding parameters are listed in Table 3.14. In addition to hydrogen bonding, C-H…O interactions further stabilizes this supramolecular assembly. The selected bond distances and angles are listed in Table A52.

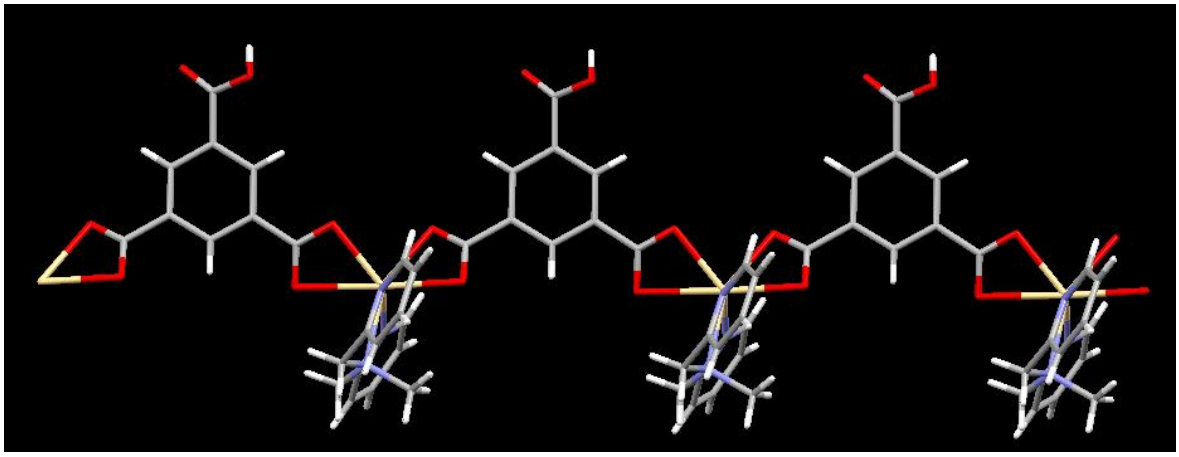

Figure 3.59. A perspective view of **31**.

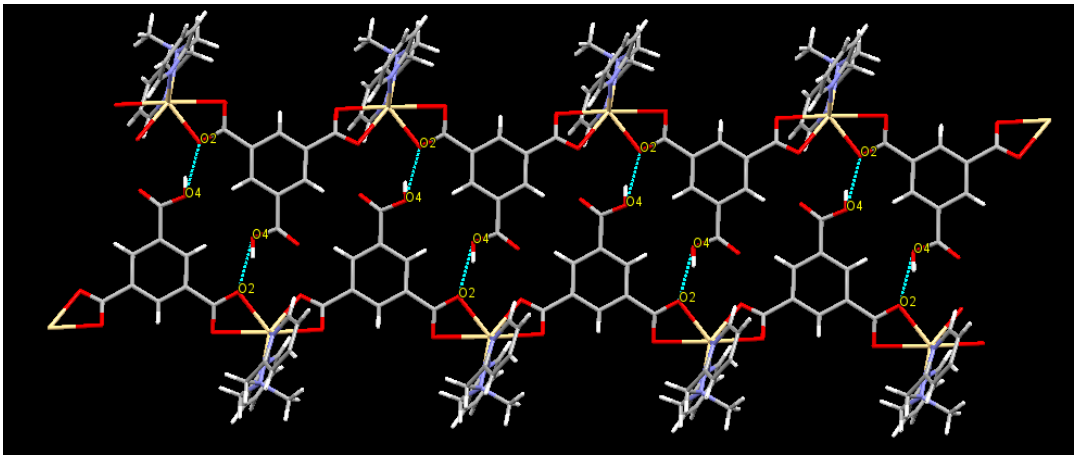

Figure 3.60. 2D Supramolecular Assembly in **31**.

$\{[Cd_3(bpea)_3(BTC)_2(H_2O)]\cdot 10H_2O\}_n$ (32). It crystallizes in the monoclinic chiral *Cc* space group. In the asymmetric unit there are three Cd(II) centers out of which two centers are hepatcoordinated and one is hexacoordinated. The linker BTC binds in chelated fashion around

Table 3.14. Hydrogen bonding parameters for **31**.[a]

D–H…A	r (D-H) (Å)	r (H…A) (Å)	r (D…A) (Å)	∠D-H…A (deg)	Symmetry
O(4)--H(4)...O(2)	0.82	1.86	2.594(6)	149	2-x,1-y,-z
C(10)--H(10)...O(4)	0.93	2.47	3.289(6)	147	2-x,1-y,-z
C(19)--H(19)...O(6)	0.93	2.47	3.317(8)	152	1/2-x,-1/2+y,1/2-z

[a]Numbers in parenthesis are estimated standard deviations in the last significant digits.

heptacooridnated Cd(II) center whereas it binds in monodentate fashion around hexacoordinated Cd(II) centers as shown in Figure 3.61. The Cd-O distances for the chelated carboxylate (2.403(6) Å and 2.379(6) Å) are longer than those for the monodentate carboxylates (2.259(6) Å and 2.262(6) Å). All other selected bond distances and bond angles are listed in Table A53. A triangular shaped pore is formed; the sides of the triangle are 10.068 Å, 9.542 Å and 9.243 Å which can be clearly seen in Figure 3.61 in the space fill model.

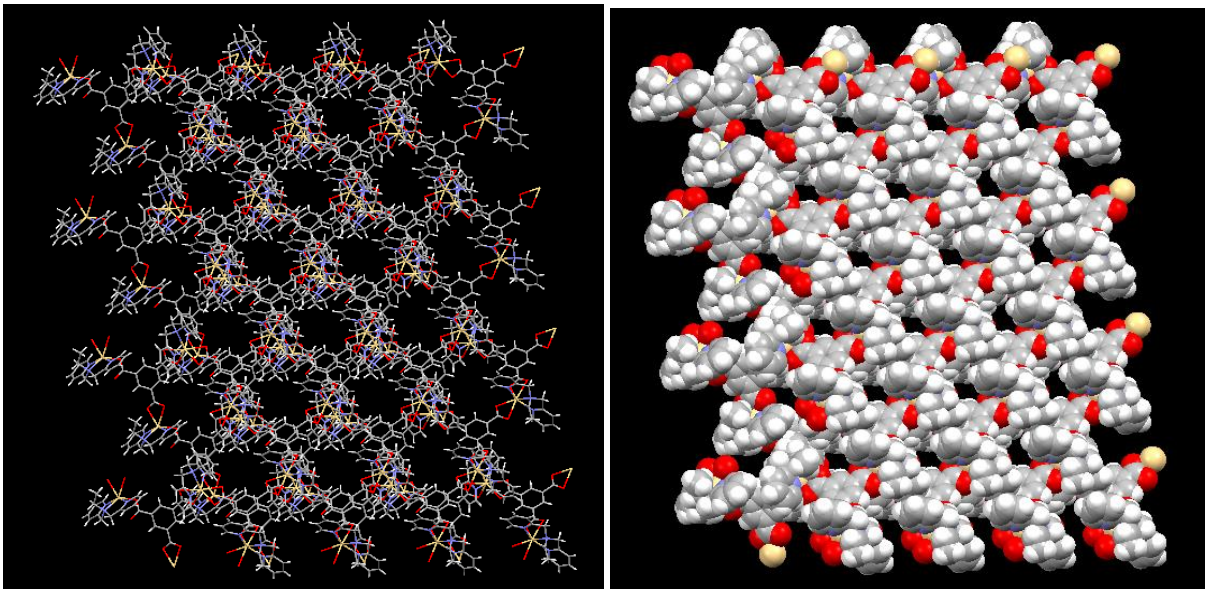

Figure 3.61. A perspective view of **32** and its space-filling model.

The lattice water molecules are found to be present inside the triangular pores as shown in Figure 3.62. These water molecules are strongly hydrogen bonded to the coordinated oxygen atoms of BTC. The hydrogen bonding parameters are listed in Table 3.15.

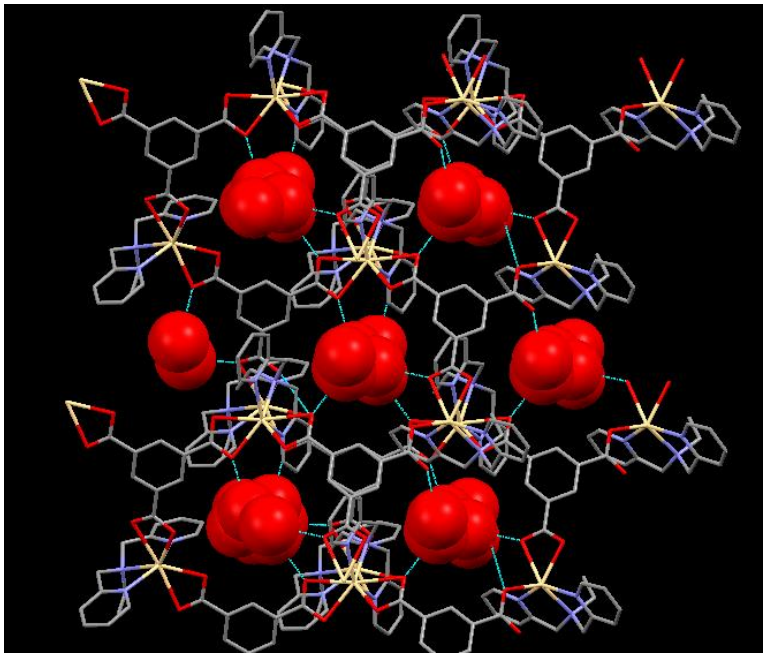

Figure 3.62. A part of 3D MOF showing pores filled with lattice water molecules in **32**.

Table 3.15. Hydrogen bonding parameters for **32**.[a]

D–H…A	r (D-H) (Å)	r (H…A) (Å)	r (D…A) (Å)	∠D-H…A (deg)	Symmetry
O17--H2SA...O32	0.85	1.88	2.731(13)	173	
O17--H2SB...O7	0.85	1.92	2.748(11)	166	1/2+x,1/2+y,z
O18--H5SA...O28	0.85	2.12	2.855(10)	144	
O18--H5SB...O29	0.85	2.31	2.827(10)	120	
O19--H6SA...O27	0.85	2.46	3.284(13)	163	x,1-y,-1/2+z
O19--H6SB...O20	0.85	1.96	2.703(13)	145	
O32--H7SA...O21	0.85	2.08	2.736(9)	134	
O32--H7SB...O24	0.85	2.16	2.803(12)	132	
O23--H18A...O1	0.85	2.51	3.103(12)	128	
O21--H19B...O23	0.85	1.98	2.774(11)	156	
O29--H20B...O18	0.85	2.02	2.827(10)	158	
O25--H21A...O18	0.85	1.96	2.735(11)	152	
O25--H21B...O20	0.85	2.02	2.839(9)	162	

[a]Numbers in parenthesis are estimated standard deviations in the last significant digits.

{[$Cd_6(bpta)_6(BTC)_2(H_2O)]\cdot 5H_2O\}_n$ (33). It is a 3D MOF of Cd(II), bpta and BTC obtained under hydrothermal conditions. It crystallizes in the triclinic *P-1* (No. 2) space group. In this structure, all three Cd(II) centers are crystallographically inequivalent. Cd(1) is surrounded by

three nitrogens of the ligand and four oxygen atoms from the two ends of two BTC which binds in a chelated fashion. Cd(3) is surrounded by three nitrogens of the ligand, one chelated carboxylate group and one monodentate carboxylate group. Cd(2) located in the center of this MOF is surrounded by three nitrogens of the ligand and three oxygens out of which two are from two monodentate carboxylates of BTC and the third one belongs to the coordinated water molecule. Thus Cd(1) is heptacoordinated whereas Cd(2) and Cd(3) are hexacoordinated (see Figure 3.63). Like **32**, the Cd-O distances for the chelated carboxylate distances (2.378 Å and 2.404 Å) are longer than those for the monodentate carboxylates (2.260-2.245 Å). The Cd(2)-O_{water} distance is 2.328 Å. Other selected bond distances and angles around Cd centers are listed in Table A54. The pore size is 11.873 Å x 10.048 Å which can be clearly visible in the space-filling model shown in Figure 3.64.

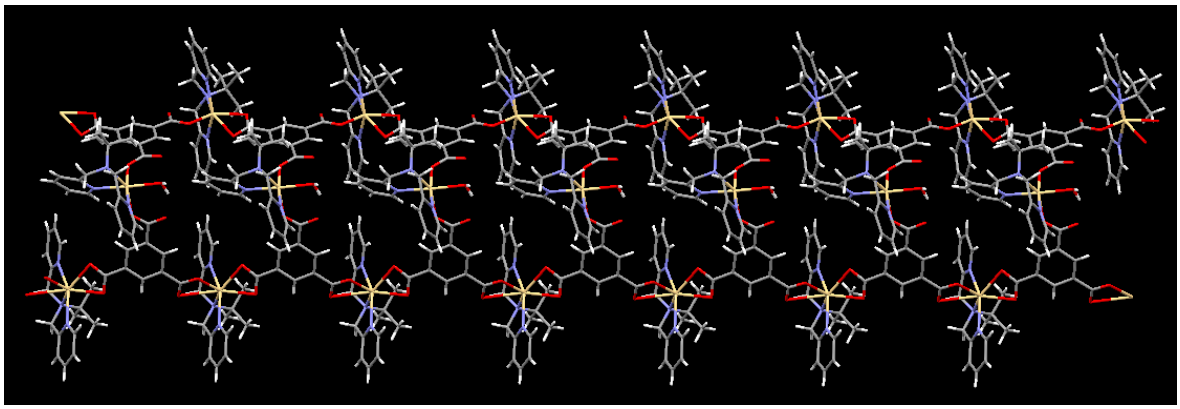

Figure 3.63. A perspective view of **33**.

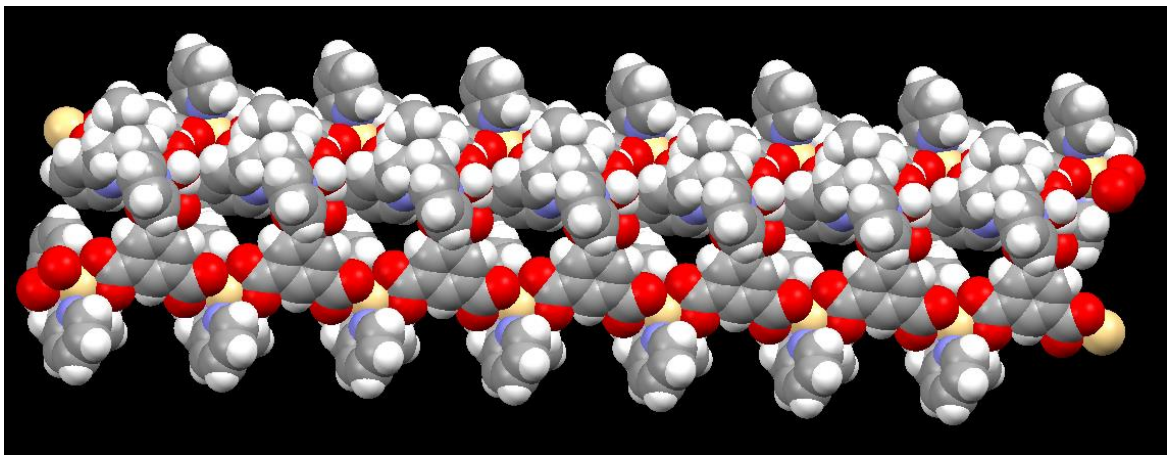

Figure 3.64. A space-filling model of **33**.

Table 3.16. Hydrogen bonding parameters for **33**.[a]

D–H…A	r (D-H) (Å)	r (H…A) (Å)	r (D…A) (Å)	∠D-H…A (deg)	Symmetry
O(7)--H(7A)...O(16)	0.90	2.01	2.900(8)	172	1-x,-y,1-z
O(7)--H(7B)...O(5)	0.90	1.9	2.645(10)	139	
O(15)--H(15C)...O(18)	0.87	1.93	2.769(6)	161	
O(15)--H(15D) ...O(14)	0.87	2.00	2.850(6)	164	
O(18)--H(18A)...O(9)	0.87	1.9	2.753(8)	165	1-x,-y,1-z
O(19)--H(19D)...O(10)	0.87	2.23	2.979(9)	145	
C(10)--H(10)...O(1)	0.95	2.47	3.069(12)	121	
C(12)--H(12)...O(3)	0.95	2.39	3.237(11)	148	1-x,-y,-z
C(15)--H(15B)...O(17)	0.99	2.56	3.387(12)	141	1-x,1-y,-z
C(22)--H(22)...O(11)	0.95	2.56	3.483(12)	163	1-x,-y,-z
C(24)--H(24)...O(2)	0.95	2.51	3.459(12)	176	1-x,-1-y,-z
C(34)--H(34A)...O(8)	0.98	2.51	3.425(11)	155	
C(51)--H(51)...O(19)	0.95	2.54	3.309(12)	138	
C(56)--H(56A)...O(4)	0.99	2.33	3.284(11)	161	-1+x,1+y,z
C(59)--H(59A)...O(4)	0.98	2.44	3.413(11)	174	-1+x,1+y,z
C(61)--H(61A)...O(11)	0.99	2.53	3.171(11)	122	-1+x,y,z
C(64)--H(64)...O(16)	0.95	2.55	3.285(11)	135	-x,1-y,1-z

[a]Numbers in parenthesis are estimated standard deviations in the last significant digits.

The presence of five lattice water molecules connects two MOFs via hydrogen bonding to form a supramolecular assembly. The hydrogen bonding parameters are listed in Table 3.16. As shown in Figure 3.65 lattice water molecules are hydrogen bonded among themselves and with coordinated water on Cd(II) and uncoordinated oxygen atoms of the BTC to form a 3D framework. A hexamer of water is entrapped between the two layers of the MOF. This hexamer of water is further hydrogen bonded to lattice water molecules and uncoordinated oxygen atom of the carboxylate group. This uncoordinated oxygen atom of the BTC is also hydrogen bonded to the coordinated water molecule on Cd(II). This can be viewed as a pentagon. A hexamer of water cluster is supported by two pentagons on each side between the two layers of MOF. This is an example of an MOF forming an SCN through extensive hydrogen bonding due to the lattice water molecules.

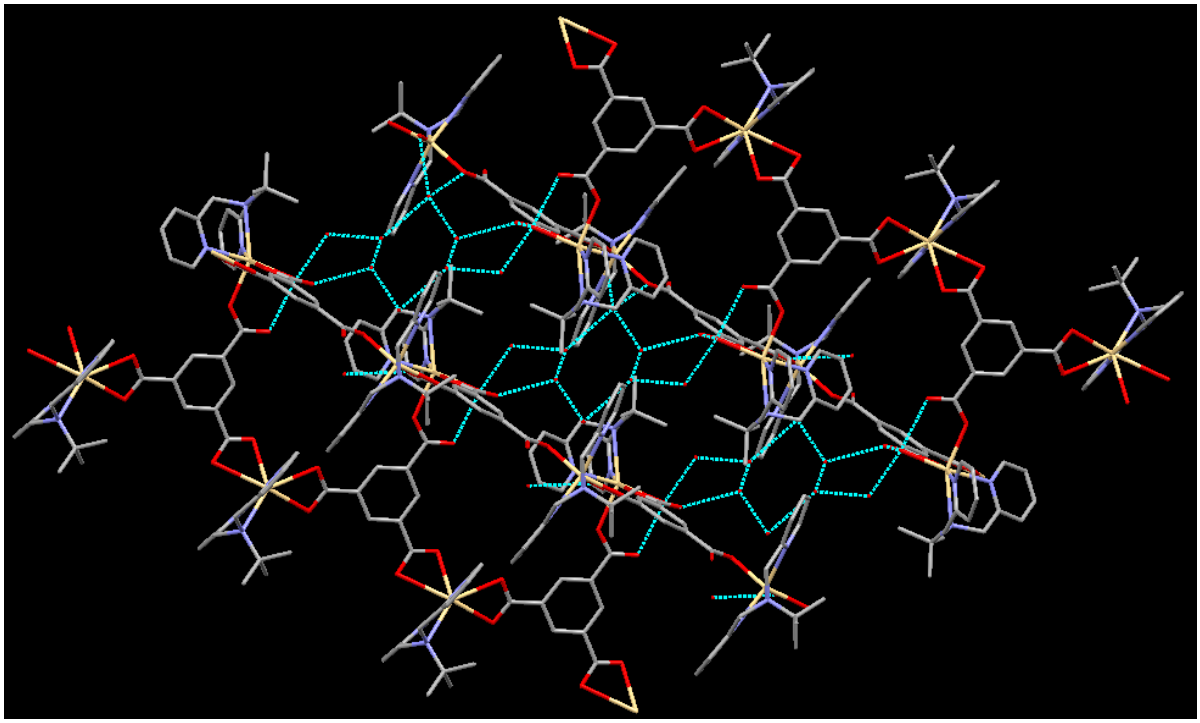

Figure 3.65. Supramolecular coordination network: encapsulation of hexamer of water in **33**.

Powder X-ray Analysis. The MOCNs (**31** and **32**) obtained via hydrothermal reactions were also studied by powder X-ray diffraction as shown in Figure 3.66. The experimental pattern for **31** is in good agreement with the simulated one which shows the bulk purity of the sample. On the other hand, the experimental powder pattern for **32** has peaks similar to the simulated powder pattern but the peaks are shifted.

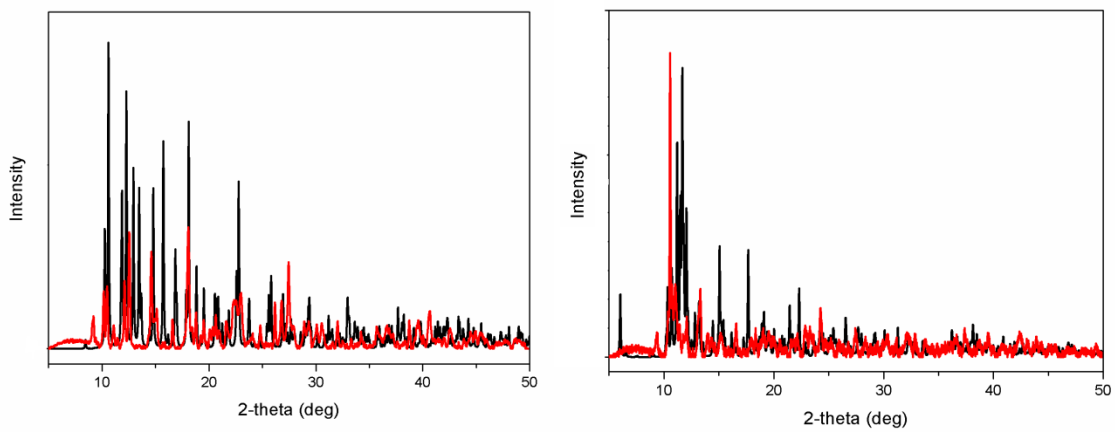

Figure 3.66. Experimental (red) and simulated (black) powder patterns for **31** (left) and **32** (right).

FTIR Spectroscopy. The IR spectra of all compounds recorded in the solid state as KBr pellets show peaks at 3368 cm^{-1} (**31**), 3418 cm^{-1} (**32**), 3448 cm^{-1} (**33**) corresponding to the O-H stretching frequency of water present in these. A peak at 3221 cm^{-1} in **31** is also observed which can be due to O-H stretching frequency of protonated carboxylic acid group. The peak at 1630 cm^{-1} is due to the protonated carboxylic acid group in **31** whereas peaks at 1557, 1541, 1372, 1349 cm^{-1} (**31**), 1615, 1576, 1552, 1434, 1367 cm^{-1} (**32**), 1615, 1569, 1542, 1370 cm^{-1} (**33**) correspond to the asymmetric and symmetric stretch of monodentate and chelated carboxylate, respectively. The peaks at 1603, 1489, 1023, 781, 695, 677 cm^{-1} are the peaks for the ligand which are common in all the compounds with a shift of few wave numbers.

Thermoanalytical Investigations. All hydrothermal products obtained were studied for their thermal stability. From the TGA scans shown below in Figure 3.67, it is clear that **32** and **33** are more stable than **31** which shows a two-step weight loss profile. The first step corresponds to the loss of removal of surface moisture, after this loss compound was stable up to 300 °C. Compound **32** is stable up to 350 °C followed by its decomposition whereas **33** shows a two-step weight loss profile and is stable up to 250 °C.

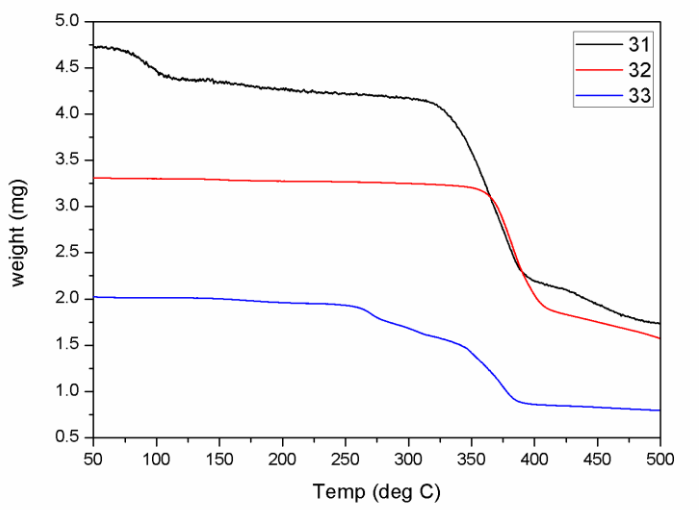

Figure 3.67. TGA scans for **31**, **32** and **33**.

Photoluminescence Studies. An added interest in the Zn(II) and Cd(II) MOCNs was due to their ability to show good photoluminescence properties. Out of all the Zn(II) and Cd(II) compounds described above a few has been tested for photoluminescence in the solid state. The emission

spectra for both are shown in Figure 3.68. Compound **24** showed an intense fluorescence with an emission maximum at ca. 450 nm upon excitation at 400 nm. On the other hand, the emission maximum for compound **28** is red-shifted at 550 nm upon excitation at 380 nm. The ligand bpta has very weak fluorescence. For Zn(II) and Cd(II), which are d^{10} ions, these observed emission may be attributed to the chelation of the ligand to the metal center. This enhances the ‘‘rigidity” of the ligand and thus reduces the loss of energy through a radiationless pathway.[197-198] Therefore, the bpta/adc system can be considered as a sensor media for these two ions.

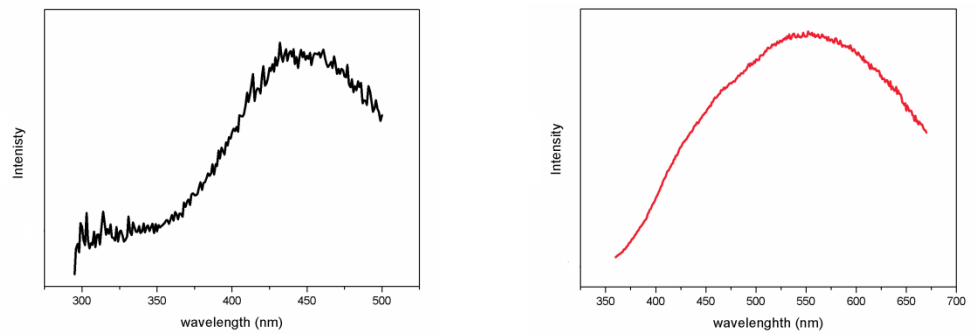

Figure 3.68. Emission spectra of **24** (left) and **28** (right).

Compound **27** and **33** was also studied for its photoluminescence properties. The emission spectra for **27** and **33** are shown in Figure 3.69. Both compounds showed an emission at ca. 525 nm upon an excitation at 350 nm.

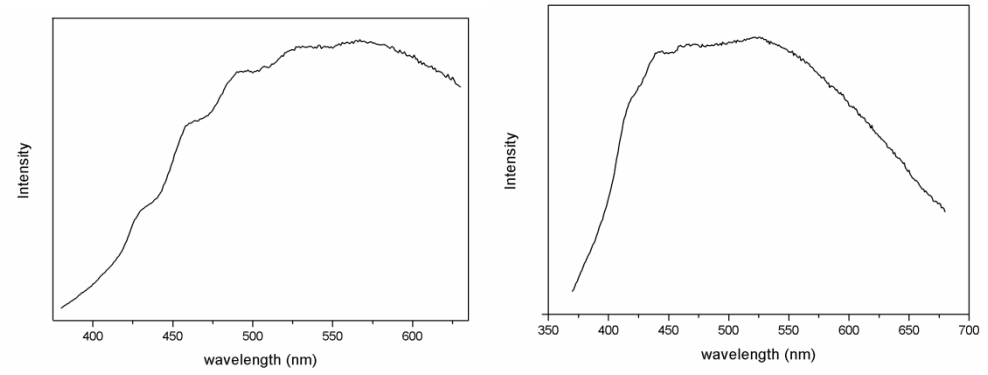

Figure 3.69. Emission spectra of **27** (left) and **33** (right).

3.2.2 MOCNs with Tetradentate ligands.

With tridentate ligands it has been established how a subtle change in the N-substitution of the ligand effects the formation of different kinds of MOCNs. Based on the results presented, it can be generalized that only bpea analogs show π–π interactions and bpta analogs have more affinity for water than other derivatives at ambient conditions. On the other hand, under hydrothermal conditions both bpta and bpea analogs have showed an affinity for water. The importance of coordinated water molecule on Mn(II) center was shown in **4** (dehydrated). Due to the presence of coordinated water molecules the formation of supramolecular assembly was possible in **4.** Thus, with a similar tetradentate ligand, N,N,N-tris(2-pyridylmethyl)-amine (tpa), it is expected to have no coordinated water molecule on the hexacoordinated Mn(II) center and thus the formation of a supramolecular assembly with this ligand will depend on the lattice water cluster.

3.2.2.1 *Mn(II) Chemistry*

Synthesis. 3D supramolecular assemblies with the general formula $[Mn_2(dicarboxylate)_2(tpa)]\cdot xH_2O$ (where tpa = N,N,N-tris(2-pyridylmethyl)-amine; dicarboxylate = acetylene dicarboxylate (adc) and x = 6 (**34**); fumarate and x = 8 (**35**) and succinate and x = 6 (**36**) were prepared and isolated in high yields from the one-pot self-assembly reaction of $Mn(OAc)_2\cdot 4H_2O$, tpa and the corresponding dicarboxylic acid (in a 1:1:1 ratio) in methanol under ambient conditions. In all cases, acetic acid is the by-product which was removed through evaporation of the solvent that was added with a mixture of acetonitrile and toluene to form an azeotrope. Thus, the one-pot synthesis followed by a very simple yet effective work-up afforded pure compounds in high yields without any further purification steps. Scheme 13 below summarises the synthesis of these SCNs.

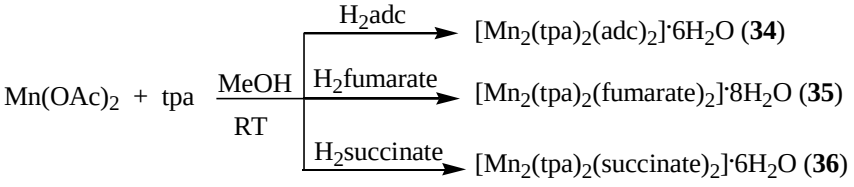

Scheme 13. Synthesis of **34-36**.

Single Crystal Structure Analyses. Crystals of **34, 35** and **36** suitable for the single crystal X-ray study were grown from slow evaporation of aqueous solution of the compounds. With a variation in the extent of hydration, these are isomorphous compounds crystallized in the monoclinic *C2/c* space group with an inversion center situated in the middle of the asymmetric unit. **34** and **35** are isomorphous while **36** is iso-skeletal to **34** and **35**. Considering the formula of **34** and **35**, this isomorphism can be considered as addition isomorphism where two more water molecules are there in **35**; however, the arrangement (positions) of the water molecules in **34** is different from that in **35** (see below). On the other hand, the dinuclear subunit in **36** has a similar structure with those of **34** and **35**, except the location of one of the oxygen atoms of the carboxylate group (on each end of the dicarboxylate group) which is also bound to the Mn(II) center in **36**.

$[Mn_2(tpa)_2(adc)_2]\cdot 6H_2O$ (34). The crystal structure of **34** consists of a dinuclear Mn(II) subunit and a cluster of six water molecules. Each Mn(II) center is hexacoordinated with four nitrogen atoms of the tetradentate tpa ligand and two oxygen atoms from two adc. Thus, the two Mn(II) centers capped by the tpa ligand are connected by two adc resulting in the formation of a discrete dinuclear unit with a 14-membered ring (dimensions: 7.738 Å x 4.129 Å) constructed of two manganese atoms, four oxygen atoms and eight carbon atoms. Each adc binds to two Mn(II) ions in a monodentate syn-anti fashion. The dimanganese subunit in **34** is shown in Figure 3.70. Two of the three Mn-N_{py} distances are similar to each other (2.2354(14), 2.3108(14), 2.3112(14) Å) while all are shorter than the Mn-N_{alkyl} distance (2.3347(13)). This trend has been observed for the Mn(II)-tpa complexes.[159,199] The geometry around the Mn(II) center is highly distorted. The alkyl nitrogen of the tpa ligand is cis to one carboxylate group and is trans to the other carboxylate group; O_{carb}-Mn-N_{alkyl} angles are 87.43(5)° and 154.05(5)°, respectively. On the other hand, the O_{carb}-Mn-N_{py} angles (cis to a carboxylate group) range from 83.97(5)° to 129.13(5)° and the O_{carb}-Mn-N_{py} angles (trans to a carboxylate group) is 162.20(5)°. The two Mn-O_{carb} distances are: Mn1-O1, 2.1240 (12) Å and Mn1-O2, 2.1416 (13) Å. The values observed for the acetylene group confirm that its triple bond character is not affected; C20-C21-C22 and C21-C20-C19 angles are close to linearity [ranges from 172.17(17)° to 175.58(18)°] and C20-C21 triple bond distance is 1.197 Å (see the 'FTIR and Raman Spectroscopy' section below). The selected bond distances and angles for **34** are summarized in Table A55.

Six lattice water molecules in **34** are encapsulated between the dinuclear units through extensive and strong hydrogen bonding interactions forming a supramolecular assembly. Hydrogen bonding interactions involved in **34** are shown in Figure 3.71. All Hydrogen bonding distances and angles are listed in Table 3.17. All hydrogen bonding parameters found in **34** are very close to those found in water and ice (2.888 Å and 2.759 Å).[147,150] In **34**, there are two kinds of hydrogen bonding motifs. In the first motif $R_2^2(4)$ (O4---O5---O4'---O5', with distances 2.8132(18) Å - 2.8104(18) Å), two water molecules and two uncoordinated oxygen atoms of adc from two discrete dimanganese subunits are involved in forming a tetramer. Similarly, the second motif $R_5^5(9)$ that involves three water molecules (O5, O6 and O7) and two uncoordinated oxygen atoms of one adc (O3 and O4) (average O---O distance: 2.83 Å) shares one side (O4---O5) of motif 1 and connects to another such motif via O6. Two adjacent dimanganese subunits in the supramolecular assembly of **34** are oriented perpendicular to each other (see Figure 3.72). Only motif 2 is connected to the alternative dinuclear subunit. Two such motifs involved with the prependicular (along y axis) subunit are connected via two water molecules, O6 and O6' (distance: 2.839 Å). Two adjacent dinuclear units of similar kinds are also connected with each other via O3 (uncoordianted O atom of adc) of one subunit to the O3 of another subunit via a chain of five water molecules O6---O7---O7'---O6'---O6'', distances: 2.835 Å, 2.916 Å and 2.839 Å, respectively. Similarly, next two adjacent units are connected via O4 (uncoordinated oxygen atom of adc) of one subunit to the O4 of the next adjacent subunit via a chain of four water molecules O5---O7---O7'---O5', distance: 2.813 Å, 2.903 Å, 2.7868 Å. Thus the subunits with different orientation are not only connected through the motifs described above but also through the layer of lattice water molecules. The arrangement of water clusters with the oxygen atoms of adc is shown in Figure 3.82. It can be viewed as pockets where dimangnanese subunits sit.

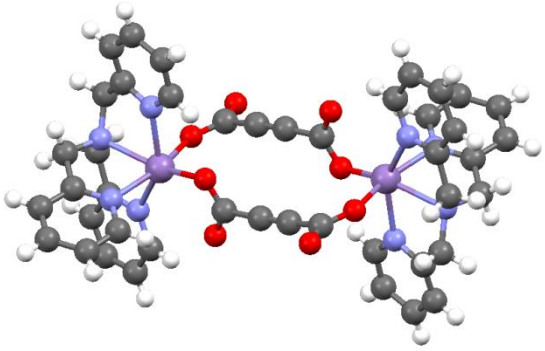

Figure 3.70. A ball and stick representation of the dimanganese subunit in **34**.

In addition to hydrogen bonding interactions described above, numerous C-H…O interactions (listed in Table 3.17) are also present in **34** which further stabilizes it. The C-H...O distances range from 3.055 Å to 3.527 Å.

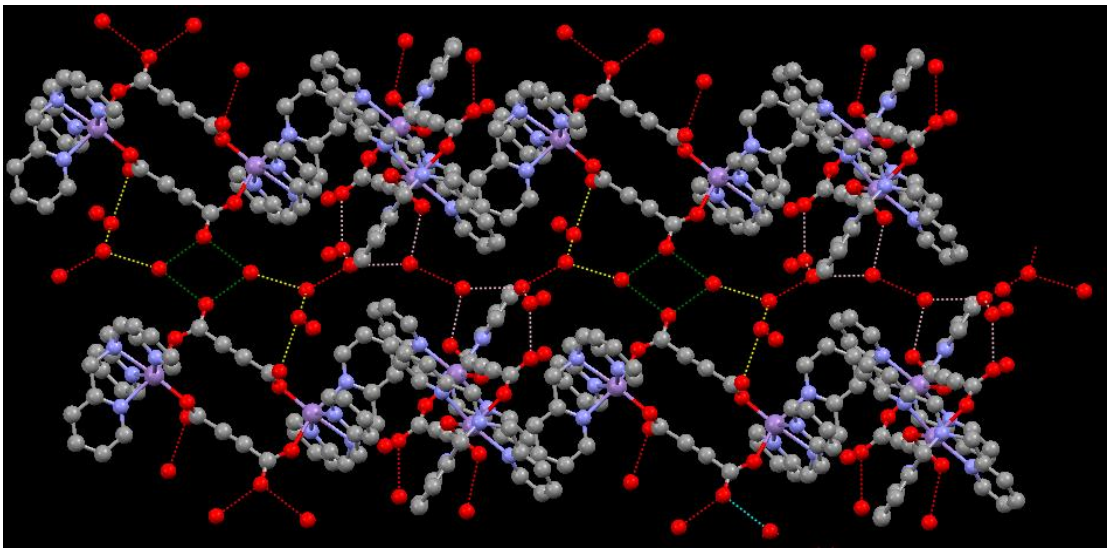

Figure 3.71. A perspective view of the hydrogen bonded network in **34**.

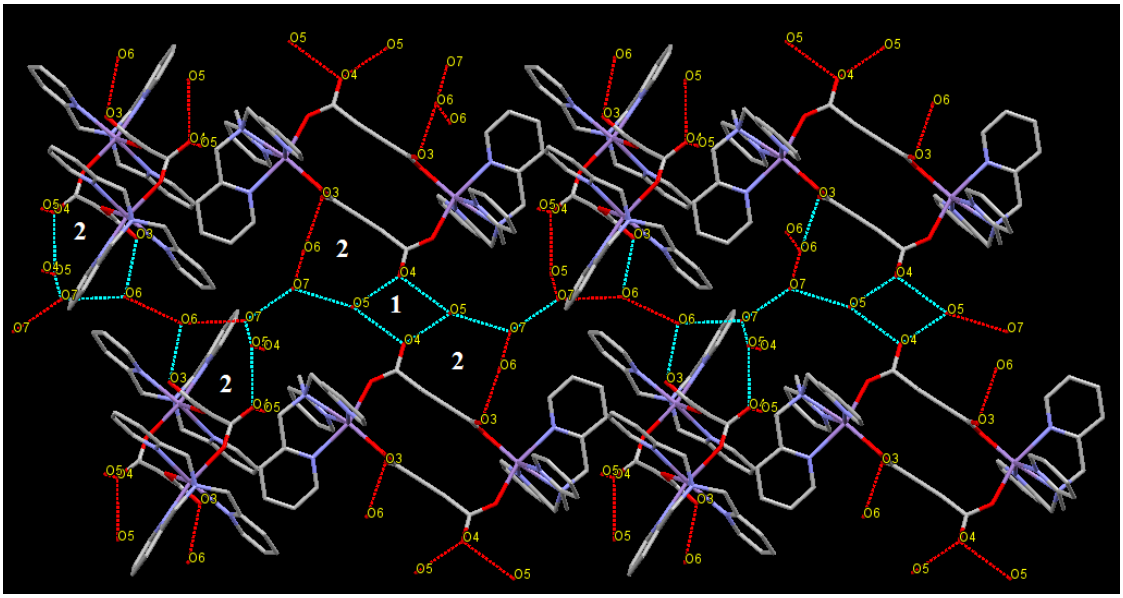

Figure 3.72. Hydrogen bonded network in **34** showing motifs.

Table 3.17. Hydrogen bonding parameters for **34**, **35**, **35a** and **36**.[a]

34

D--- H….A	r (D-H) Å	r (H…A) Å	r (D…A) Å	∠D-H…A(deg)	Symmetry
O(5)--H(5A)...O(4)	0.87(3)	1.97(2)	2.8105(18)	162(2)	1-x,y,1/2-z
O(5)--H(5B) ...O(4)	0.84(2)	2.04(2)	2.8142(17)	154 (2)	x,1-y,-1/2+z
O(7)--H(7B) ...O(6)	0.95	1.90	2.845(3)	172	
O(7)--H(7B) ...O(5)	0.89(3)	1.90	2.783(3)	172	-1/2+x,1/2+y,z
C(2) --H(2B) ...O(5)	0.99	2.57	3.526(2)	161	-1/2+x,1/2+y,z
C(3) --H(3A)...O(4)	0.99	2.59	3.570(2)	171	1/2-x,-1/2+y,1/2-z
C(7)--H(7)...O(3)	0.95	2.56	3.200(2)	125	x,-y,-1/2+z
C(11) --H(11)...O(3)	0.95	2.40	3.159(2)	136	

35

D--H….A	r (D-H) Å	r (H…A) Å	r (D…A) Å	∠D-H…A(deg)	Symmetry
O(5)--H(5A) ...O(4)	0.87	1.89	2.724(3)	161	1/2-x,-1/2+y,1/2-z
O(5)--H(5B) ...O(4)	0.87	1.91	2.760(4)	166	1/2+x,1/2-y,-1/2+z
O(6)--H(6A)...O(5)	0.87	1.89	2.743(3)	166	1-x,y,1/2-z
O(6)--H(6B) ...O(7)	0.87	2.13	2.772(4)	131	1/2-x,1/2-y,1-z
O(7)--H(7C) ...O(6)	0.87	1.92	2.772(4)	168	1/2-x,1/2-y,1-z
O(7)--H(7D) ...O(3)	0.87	2.02	2.844(3)	158	
O(8)--H(8A) ...O(7)	0.87	1.89	2.728(3)	160	-x,-y,1-z
O(8)--H(8B) ...O(3)	0.88	2.2	2.982(3)	149	
C(3) --H(3)...O(4)	0.95	2.59	3.498(4)	159	-x,y,1/2-z
C(10) --H(10)...O(3)	0.95	2.41	3.285(4)	153	1/2-x,1/2+y,1/2-z
C(20) --H(20)...O(2)	0.95	2.45	3.262(4)	143	1/2-x,1/2-y,1-z

35a

D--H….A	r (D-H) Å	r (H…A) Å	r (D…A) Å	∠D-H…A(deg)	Symmetry
O(5)--H(9A) ...O(3)	0.84(3)	1.93(3)	2.722(2)	156(3)	x, -y, -1/2+z
O(5)--H(10A)...O(3)	0.80(3)	1.97(3)	2.755(3)	165(3)	1-x, y, ½-z
O(6)--H(11A) ...O(5)	0.79(4)	2.00(4)	2.770(3)	172(4)	
C(3) --H(3)...O(3)	0.95	2.50	3.393(3)	157	-1/2+x,1/2-y,-1/2+z
C(10) --H(10)...O(4)	0.95	2.39	3.287(3)	158	x,1-y,-1/2+z
C(18) --H(18)...O(4)	0.95	2.49	3.337(3)	148	
C(20) --H(20)...O(1)	0.95	2.43	3.243(3)	144	1/2-x,1/2-y,1-z

36

D--- H….A	r (D-H) Å	r (H…A) Å	r (D…A) Å	∠D-H…A(deg)	Symmetry
O(5)--H(5A)...O(7)	0.87	1.94	2.81(3)	168	-x,y,1/2-z
O(5)--H(5B) ...O(6)	0.87	2.05	2.92(4)	165	-x,y,1/2-z
O(7)--H(7A) ...O(3)	0.84(4)	2.03(4)	2.806(3)	155(4)	x,-y,1/2+z
O(7)--H(7B) ...O(3)	0.83(4)	1.94(4)	2.760(3)	171(4)	-x,y,1/2-z
C(6)--H(6B)...O(1)	0.99	2.54	3.472(4)	157	1/2-x,1/2+y,1/2-z
C(7)--H(7)...O(4)	0.95	2.37	3.062(4)	129	

[a]Numbers in parentheses are estimated standard deviations in the last significant digits.

Furthermore, the presence of π–π interactions[182] in **34** makes it different from the bpta analogue mentioned earlier. It shows π–π interactions in two different planes due to the orientation of the subunits in it. Two out of three pyridine rings have π–π interactions in two different planes as shown in Figure 3.73. Plane 1 formed by N3-C14-C15-C16-C17-C18 atoms of one pyridine ring has a centroid–centroid distance of 3.798 Å with the corresponding pyridine ring of adjacent dimanganese subunit; plane 2 formed by N4-C11-C10-C9-C8-C7 atoms of the second pyridine ring has centroid–centroid distance of 3.854 Å with the corresponding pyridine ring of the adjacent dimanganese unit.

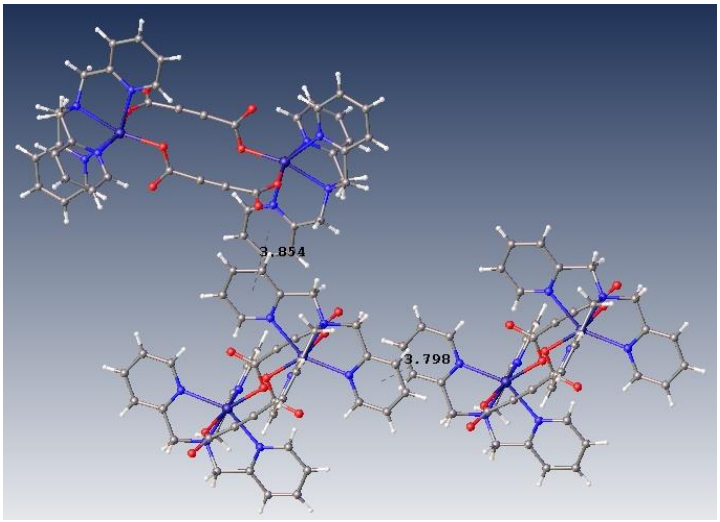

Figure 3.73. A perspective view of **34** showing π–π interactions between two pyridine rings in two different planes.

$[Mn_2(tpa)_2(fumarate)_2]\cdot 8H_2O$ (35). The crystal structure of **35** consists of a dimanganese unit and eight water molecules. Each of the Mn(II) center is wrapped by the tpa ligand occupying four sites and the other two sites are occupied by oxygen atoms of two fumarate molecules forming a cavity of 7.268 Å X 4.828 Å as shown in Figure 3.74. Thus, each hexacoordinated Mn(II) center has an N_4O_2 environment. As found in **34** and other tpa complexes,[159,199] the Mn-N_{alkyl} distance (2.354(5) Å) is longer than the Mn-N_{py} (2.243(4) Å to 2.304(5) Å). The binding mode of fumarate to the Mn(II) center of **35** is different from that of adc; fumarate binds in a syn-syn fashion while adc in **34** binds in a syn-anti fashion. The Mn-carboxylate distances are: Mn-O1, 2.091(4) Å and Mn-O2, 2.131(4) Å. The Mn(II) is in distorted octahedral geometry with O--Mn--N_{py} angles varying from 87.34(15)° to 118.11(17)° and 164.01 (15)° to 165.33(17)°, and

O--Mn--N_{alkyl} angles are 88.05(15)° and 165.33(17)°. The selected bond distances and angles are listed in Table A55.

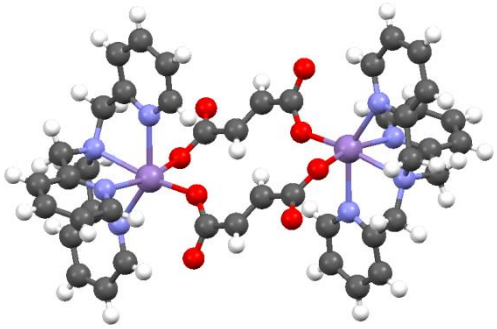

Figure 3.74. A ball and stick representation of the dimanganese subunit in **35**.

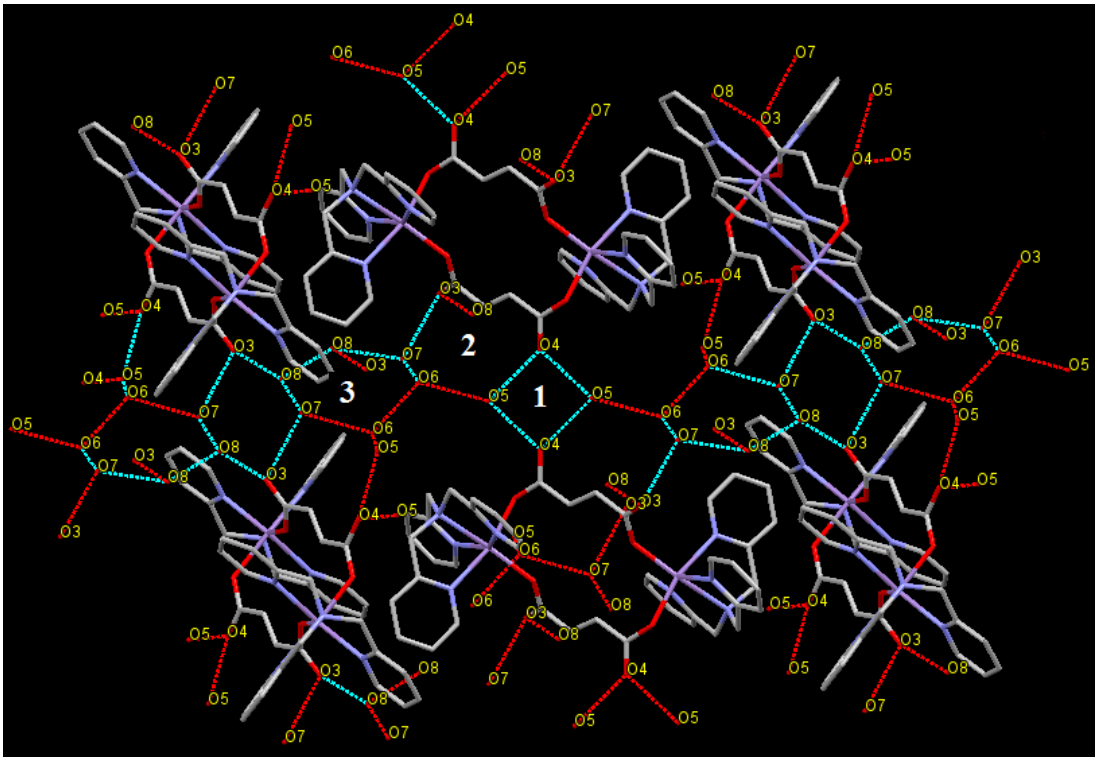

Figure 3.75. 2D supramolecular assembly showing hexamer of encapsulated water molecules in **35**.

Like **34**, extensive hydrogen bonding interactions are present in **35** due to the presence of a cluster of eight lattice water molecules (see Figure 3.75). Hydrogen bonding distances (2.681(18)-2.747(8) Å) listed in Table 3.17 indicate very strong interactions in it and are found to be very close to those of ice (2.759 Å).[147,150] These eight lattice water molecules and two uncoordinated O atoms of fumarate form three different motifs. Motif 1, $R_2^2(4)$, is very similar to

that found in **34** comprised of two uncoordinated O atoms of fumarate (O4, O4') and two water molecules (O5, O5'); distances 2.715(6) Å and 2.752 Å. Motif 2, $R_5^5(9)$, involves three water molecules (O5, O6 and O7) and two uncoordinated O atoms (O3 and O4) of fumarate and four carbons of fumarte. The O---O distances vary from 2.715 Å to 2.747 Å. In motif 3, $R_6^6(6)$, six lattice water molecules are hydrogen bonded to form a hexamer, which is not present in **34** (vide supra) and **36** (vide infra). The motif 3 gives more stability to the supramolecular assembly found in **35** (see TGA section). Motif 1 connects two Motif 3 through O5 and O7, respectively. This connectivity as well as the sides of motif 1 and motif 3 is part of motif 2. The strength of hydrogen bonding and their arrangement can be correlated to FTIR spectral data and TGA (see below). For example, the six water molecules involved in motif 3 are different from the other two water molecules which are lost first in the TGA of **35**. As shown in Figure 3.82, the arrangement of water cluster is remarkably different from those found in **34** and **36**. The C-H…O interactions listed in Table 3.17 are also found in **35** which strengthen this supramolecular assembly further.

The hexamer of water is a very important subject of study. Saykally et al. stated in their paper "*Cyclic structure is important because of its similarity to the structure of ice",*[200] after 15 years of research people are still interested in studying the hexamer of water theoretically as well experimentally. It is evident from few recent publications. Wang et al. stated in a recent publication[201] "*The hexamer has thus been referred to as the "smallest drop of water",*[202] *serving as the prototypical system to understand the molecular structure and dynamics of the water hydrogen-bond network in the bulk phases."*

Our interest was not only to encapsulate and identify structural features of the rare quasi-planar cyclic hexamer of water but also to try to understand its formation. The formation of hexamer of water molecules was monitored during the crystallization process. The first few crystals (appeared after 3 days) bigger in size were collected and used for single crystal X-ray studies. The dimetal subunit was same as in **35** but the number of lattice water molecules were 6 (**35a**). When hydrogen bonding interactions were analyzed for **35a**, it was found that two water molecules were missing from the hexamer (see Figure 3.76), thus the pre-hexamer formation of water was crystallographically caught.

In addition to the hydrogen bonding interactions described above, moderate π–π interactions are also present in **35** and **35a**. Unlike **34**, the π–π interactions in **35** are found to be in only one plane formed by one of the pyridine rings (N3-C14-C15-C16-C17-C18) of the ligand but in **35a** it is found to be in two planes like **34**. The centroid-centroid distance between two corresponding pyridine rings of two different dimanganese subunits is 3.862 Å (Figure 3.77) in **35** and 3.976 Å and 3.733 Å in **35a** (Figure 3.78).[182] This shows that **35a** behaves like **34**.

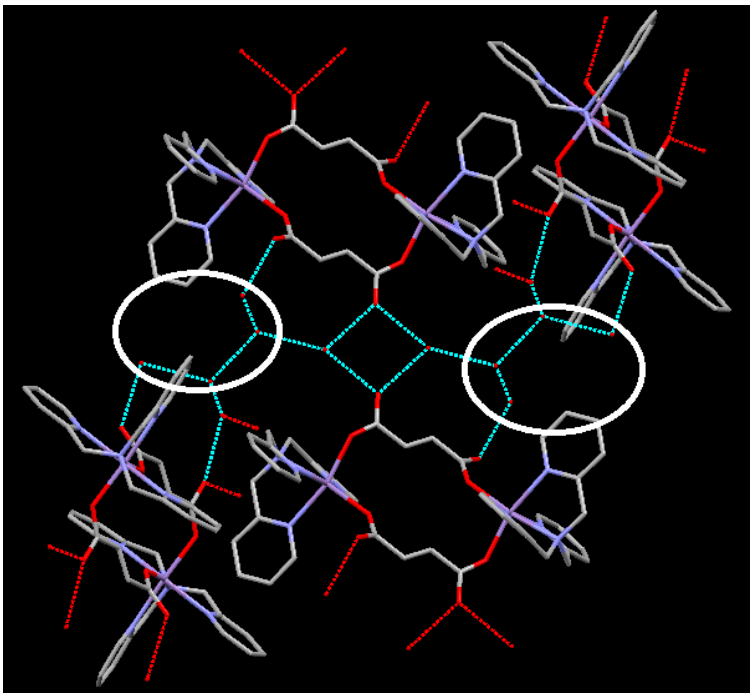

Figure 3.76. A view of pre-hexamer formation of water in **35a**.

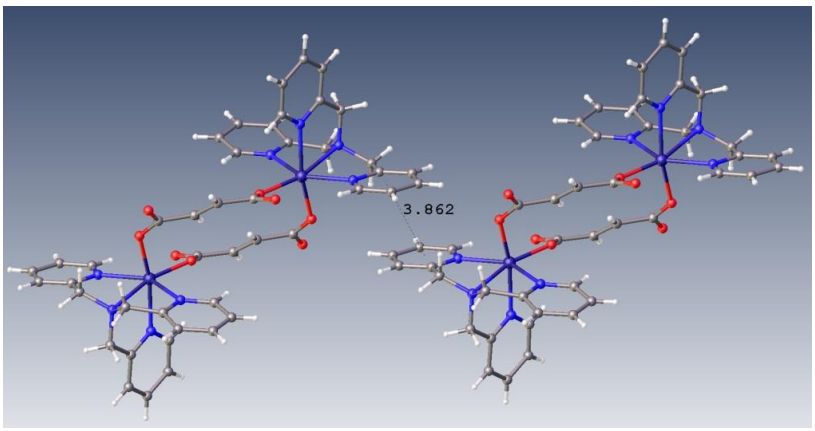

Figure 3.77. A perspective view showing π–π interactions between two pyrdine rings of two dimangenese subunits in **35**.

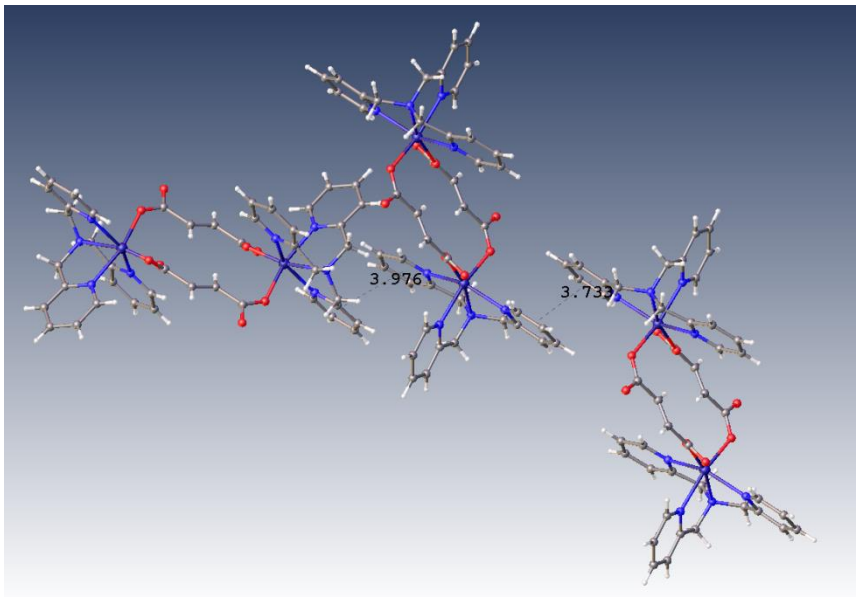

Figure 3.78. A perspective view showing π–π interactions between two pyridine rings of two dimangenese subunits in **35a**.

$[Mn_2(tpa)_2(succinate)_2]\cdot 6H_2O$ (36). Unlike **34** and **35**, in the crystal structure of **36** the most interesting feature is that the Mn(II) centers are heptacoordinated. The dimanganese subunit is shown in Figure 3.79. The coordination environment around Mn(II) centers in **36** is N_4O_3, with four sites occupied by four N atoms of the tpa ligand and three sites occupied by O atoms of the two succinate groups. Two $[Mn(tpa)]^{2+}$ units are connected by two succinate molecules forming a small cavity of dimensions: 7.512 Å X 4.170 Å. The Mn-N_{alkyl} distance (2.383(2) Å) is longer than two Mn-N_{py} distances (2.255(2) Å and 2.250(3) Å) but very close to the third Mn-N_{py} distance (2.369(2) Å). All these distances are similar to those found in **34**, **35** and other tpa complexes.[159, 199] The mode of carboxylate binding is different in **36**; each succinate shows two types of binding mode to the Mn(II) centers - one carboxylate group binds in chelating mode and the other in monodentate mode. The Mn-O_{carb} distances for the chelated carboxylate are different: 2.250 Å and 2.530 Å; the longest Mn-O_{carb} distance is within the range reported in the literature.[203] The monodentate Mn-O_{carb} distance is 2.112 Å. The O_{carb}-Mn-N_{alkyl} angles are 87.78(8)° [for monodentate] and 149.57(9)° and 150.05(4)° [for chelated carboxylate]. The O_{carb}-Mn-N_{py} angles range from 81.029(9)° to 135.06(9)° for the ones which are cis to a carboxylate and 163.30(8)° for the one which is trans to the carboxylate. The selected bond distances and angles for **36** are summarized in Table A55.

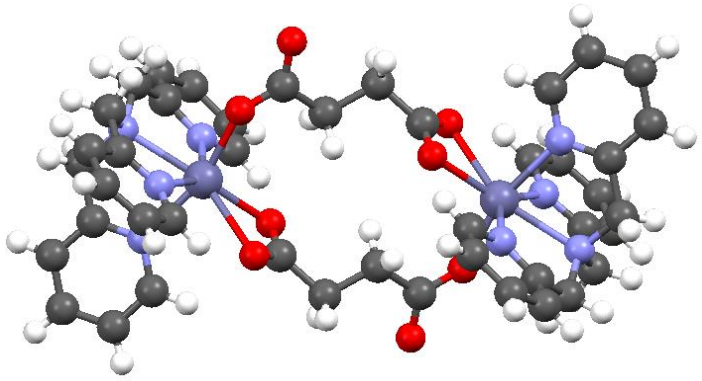

Figure 3.79. A ball and stick representation of the dimanganese subunit in **36**.

Like **34** and **35**, extensive hydrogen bonding interactions are present in **36**. The hydrogen bonding distances are comparable to those found in ice (2.759 Å) and water (2.888 Å).[147, 150] All hydrogen bonding distances are listed in Table 3.17. The hydrogen bonding interactions in **36** resulted in the formation of two different motifs, $R_2^2(4)$ and $R_5^5(9)$, which are very similar to those found in **34** (see Figure 3.80). In motif 1, two dinuclear subunits are connected via hydrogen bonding between two uncoordinated oxygen atoms of the succinate (O3 and O3') and two water molecules (O7 and O7') with O---O distances 2.762 Å and 2.808 Å. Motif 2 comprised of three water molecules (O5, O6 and O7) and two uncoordinated oxygen atoms (O3 and O4) of succinate. Motif 2 shares a common side (O3---O7, distance: 2.762 Å) with motif 1 as found in **34**. Figure 3.80 also shows two alternative diamanganese subunits are perpendicular to each other. This arrangement in **36** has an effect on the π–π interactions (see below). Only motif 2 is connected to the alternative dinuclear subunit. Two such motifs involved with the prependicular (along y axis) subunit are connected via two water molecules. The O6---O6' distance is 2.829 Å, which is very similar to that found in water. Two adjacent dinuclear units are also connected with each other via O3 (uncoordinated O atom of succinate) of one subunit to the O3 of another subunit via a chain of four water molecules O7---O5---O5'---O7', distances: 2.808 Å, 2.794 Å and 2.848 Å, respectively. In case of **34**, five water molecules were connecting such two subunits. Similarly, next two adjacent units are connected via O4 (chelated oxygen atom of succinate) of one subunit to the O4 of the next adjacent subunit via a chain of five water molecules O6---O5---O5'---O6'---O6". The average distance is 2.88 Å. Thus the subunits with different orientation are not only connected through the motifs described above but also through

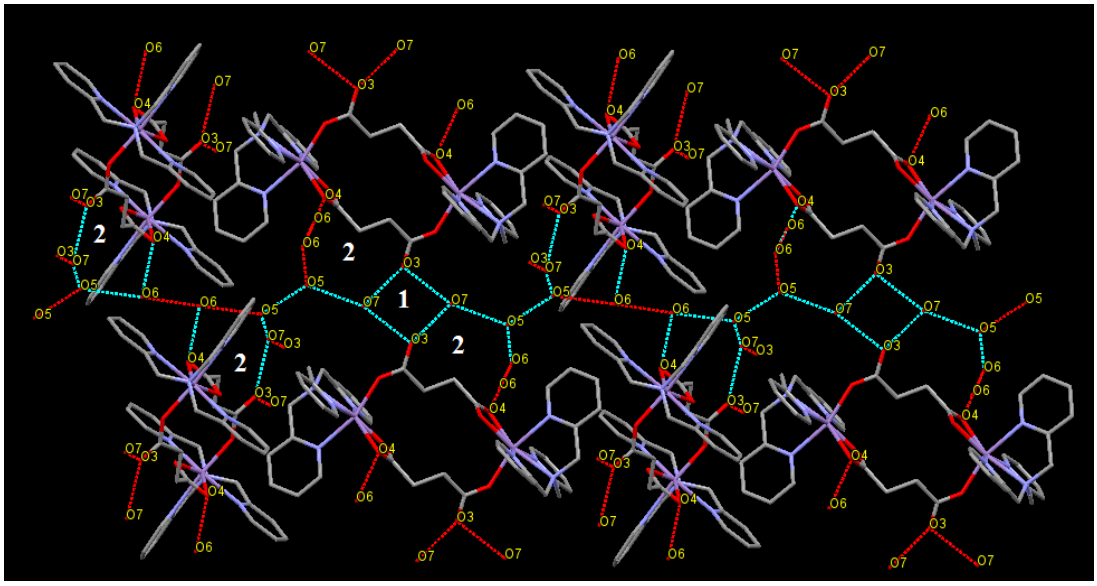

Figure 3.80. A perspective view of the hydrogen bonded network in **36**.

these layers of lattice water molecules. If we not consider the motifs, these lattice water molecules are making a 1D chain of these dimanganese subunits. Motifs are making it grow in other direction thus increasing its dimensionality. The arrangement of water clusters with the oxygen atoms of succinate is shown in Figure 3.81. The arrangement is very similar to that found in **34**. In addition to hydrogen bonding interactions described above, numerous C--H…O interactions (listed in Table 2) are also present in **36** which stabilizes the supramolecular assembly further in **36**. The C...O distances range from 2.836 Å to 3.472 Å.

Like hydrogen bonding, the π–π interactions found in **36** are also similar as found in **34**. The π–π interactions are found in two planes which stabilize the supramolecular assembly further. Two out of three pyridine rings are showing π–π interactions like **34** due to the orientation of subunits in the supramolecualr assembly as shown in Figure 3.82. Plane 1 constructed by atoms N4-C7-C8-C9-C10-C11 shows π–π interactions with the corresponding pyridine ring of the next dimanganese subunit having a centroid-centroid distance of 3.712 Å and Plane 2 constructed by atoms N3-C14-C15-C16-C17-C18 shows π–π interactions with pyridine ring N4-C7-C8-C9-C10-C11 of next dimanganese subunit, the centroid-centroid distance found in this plane is 3.884 Å. These values are in good agreement with those reported in the literature.[182]

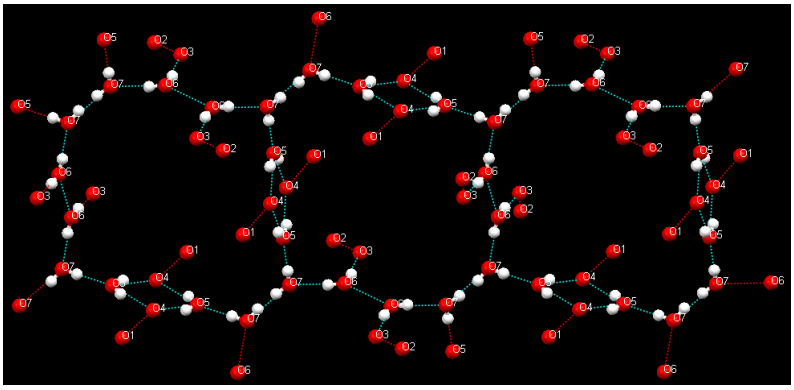

(a)

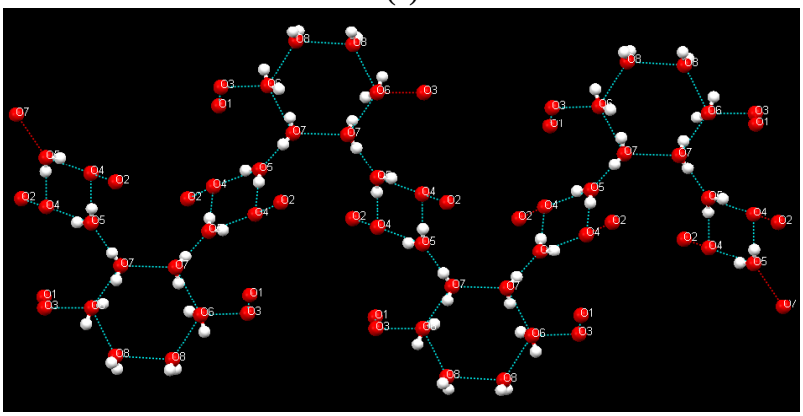

(b)

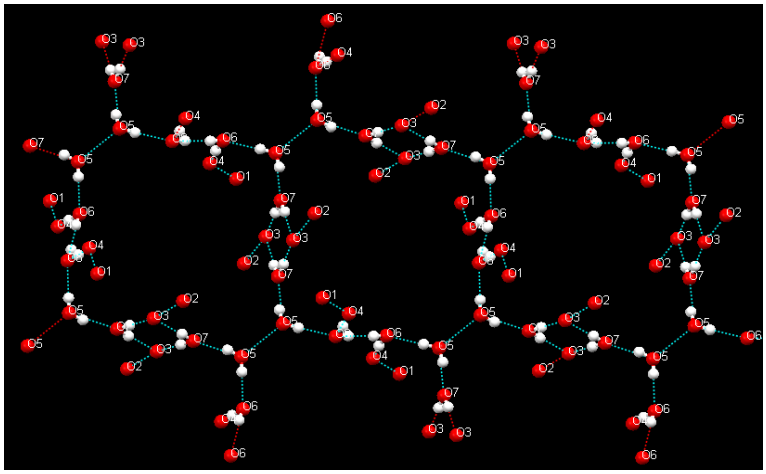

(c)

Figure 3.81. A comparison of the motifs formed through hydrogen bonding interactions of encapsulated water molecules and uncoordinated carboxylate oxygens in **34**, **35** and **36**.

Powder X-ray data analysis. To confirm whether the single crystal structure corresponds to the bulk material or not, powder X-ray diffraction patterns were recorded for **34**, **35** and **36** at room temperature. The experimental and simulated (from the single crystal data) patterns were similar

to each other as shown in Figure 3.83. The patterns obtained confirm that the single crystal and bulk material properties are the same. It also confirms the phase purity of the bulk sample.

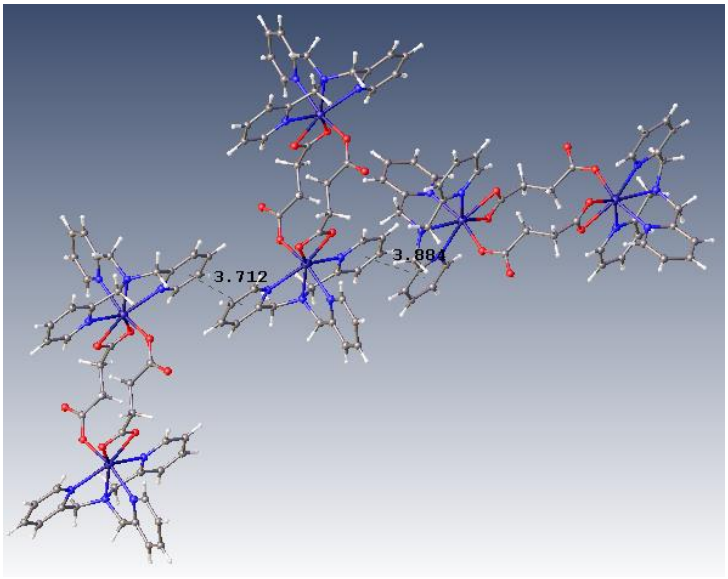

Figure 3.82. A perspective view of **36** showing π–π interactions between two pyridine rings in two different planes.

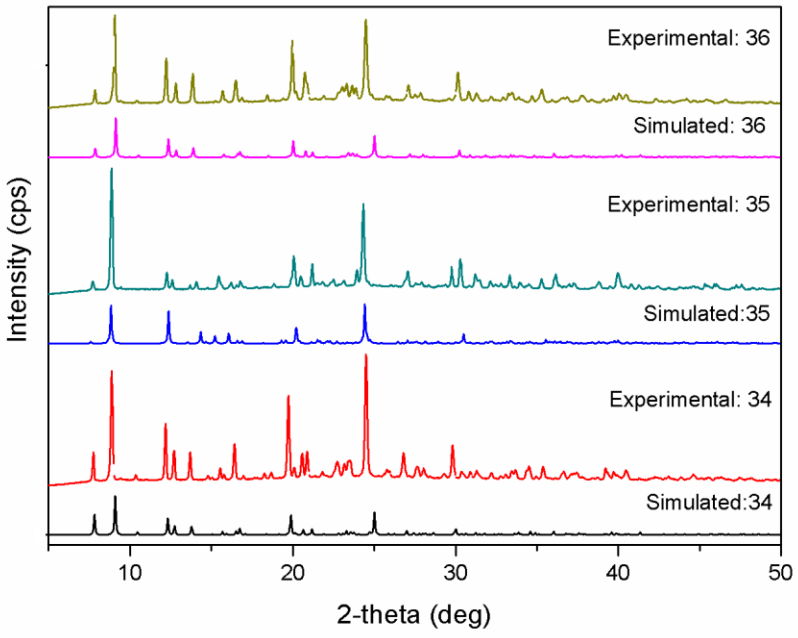

Figure 3.83. Experimental and simulated powder patterns for **34**, **35** and **36**.

FT-IR and Raman Spectroscopy. The IR spectra of **34**, **35** and **36** recorded in the solid state show two broad bands centered at 3408 and 3300 cm^{-1}, 3392 and 3272 cm^{-1}, 3394 and 3293 cm^{-1}, respectively. This pattern (two broad bands) is a characteristic feature for the O-H stretching frequency of water molecules. Generally, the IR spectrum of water shows the O−H stretching frequency at 3490 $cm^{-1}$and 3280 cm^{-1} while that for ice is at 3220 cm^{-1}.[147c] This suggests that the water cluster in all three shows O−H stretching vibrations similar to those of liquid water with deviations due to the difference in local environments. It is important to note that in **35** the two bands are clearly separated but in **34** and **36** second band appeared as a shoulder to the first one indicating there is some difference in water environment in all these assemblies as can be seen from their solid state structures. In **34** and **36** arrangement of encapsulated water molecules within the dimanganese subunits is very similar whereas in **35** the arrangement of encapsulated waters is different, six out of eight water molecules are behaving differently, six water molecules are forming a hexamer (shown in Figure). For all three assemblies, a series of bands between 1610 and 1310 cm^{-1} are also observed. While some of these features are due to the tpa ligand, bands at 1590 and 1361 cm^{-1} (**34**), 1574 and 1380 cm^{-1} (**35**) and 1574, 1561 and 1398 cm^{-1} (**36**) are due to asymmetric and symmetric stretching modes of the carboxylate groups, respectively. The different values of carboxylate stretch for these three complexes suggest different binding mode of carboxylates as can be seen from their solid state crystal structures e.g., a value of 229 cm^{-1} for the difference in the asymmetric and symmetric stretching modes is indicative of monodentate binding of the carboxylate groups of adc as found in the crystal structure of **34**, a value of 194 cm^{-1} is indicative of monodentate binding as found in the crystal structure of **35** and in **36** values at 176 cm^{-1} indicates monodentate carboxylate binding. A value of 163 cm^{-1} for the difference in the asymmetric and symmetric stretching modes indicates chelated carboxylate binding of other carboxylate of succinate. Clearly, the values for **36** indicates the binding modes of chelated and monodentate of the succinate to two different Mn(II) centers as found in its crystal structure.

These compounds were also studied by Raman spectroscopy as shown in Figure 3.84. The Raman spectrum of **34** shows a peak at 2216 cm^{-1} for the C-C triple bond which is absent in those for **35** and **36**. The other features for the tpa ligand and the carboxylate groups of adc (1573 and 1389 cm^{-1}), fumarate (1576 and 1407) and succinate (1576 and 1225) are similar to the IR spectrum of each compound.

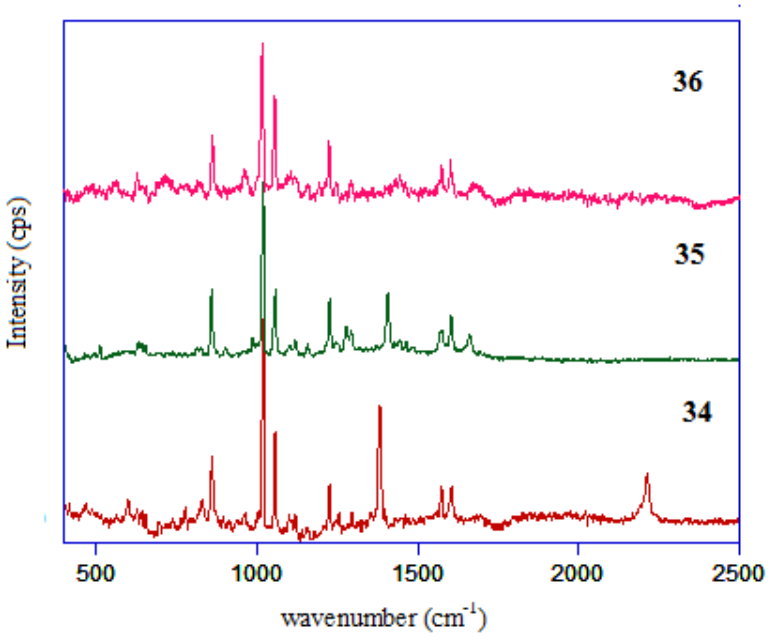

Figure 3.84. Raman spectra of **34**, **35** and **36**.

Thermogravimetric Analyses. The strength of H-bonding in these supramolecular assemblies is also studied by thermogravimetric analysis. Figures 3.85 and 3.86 summarize the result. For **34**, the first weight loss of 25.2% between 30-125 ℃ corresponds to six lattice water molecules and one acetylene dicarboxylic acid molecule (ca. 21.5%). The second weight loss of 40.6% between 125-210 ℃ corresponds to loss of second acetylene dicarboxylic acid molecule and one tpa molecule (ca. 39.3%). Further loss of 31.8% between 210-280 ℃ is indicative of subsequent decomposition of the product(s) from the first two steps. On the other hand, **35** show a three-step profile distinct from **34**. The first weight loss of 3.2% between 50-75 ℃ corresponds to two lattice water molecules (ca. 3.4%). Between 75-175 ℃ there was no loss indicating the strength of hydrogen bonding of the lattice water molecules with the dimanganese subunit. The second weight loss of 47% between 175-365 ℃ corresponds to six water molecules, one tpa molecule and one fumaric acid (ca. 50%). This can be correlated to the FTIR spectrum and the solid state crystal structure of **35** described above. All eight water molecules are uncoordinated but their arrangement in the supramolecular assembly is different. The hexamer of water molecules, which is absent in **34** and **36**, provides extra stability to the supramolecular assembly in **35**. The third weight loss of 9.1% between 365-400 °C corresponds to the loss of second fumaric acid molecule (ca. 10.9%). Further steps indicate decomposition of the compound at 450 ℃. For **3**,

the first weight loss of 11.0% between 25-150 ℃ corresponds to six water molecules (ca. 10.2%) while the second weight loss of 7.8% corresponds to loss of one succinic acid molecule (ca. 10.9%). The third weight loss of 34.5% corresponds to loss of one succinic acid molecule and one tpa molecule (ca. 38.2%). In the last step, a weight loss of 24.8% is due to loss of a second tpa molecule (ca. 27.2%). The TGA analyses of **34**-**36** not only support the findings of other characterization techniques but show the distinct behavior of **35** from those of **34** and **36**.

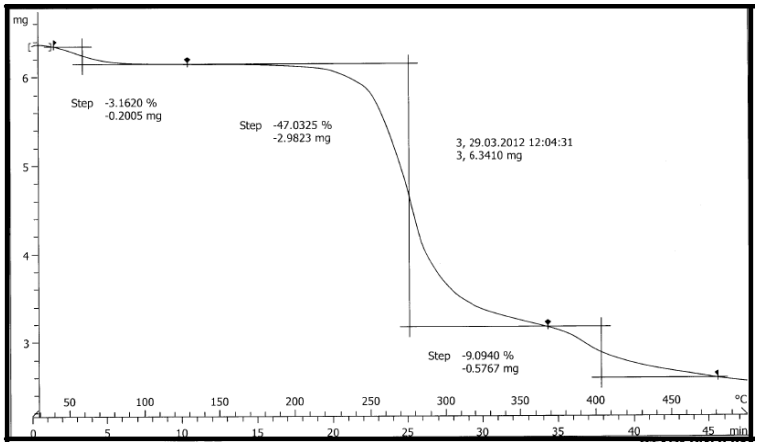

Figure 3.85. TGA scan of **35**

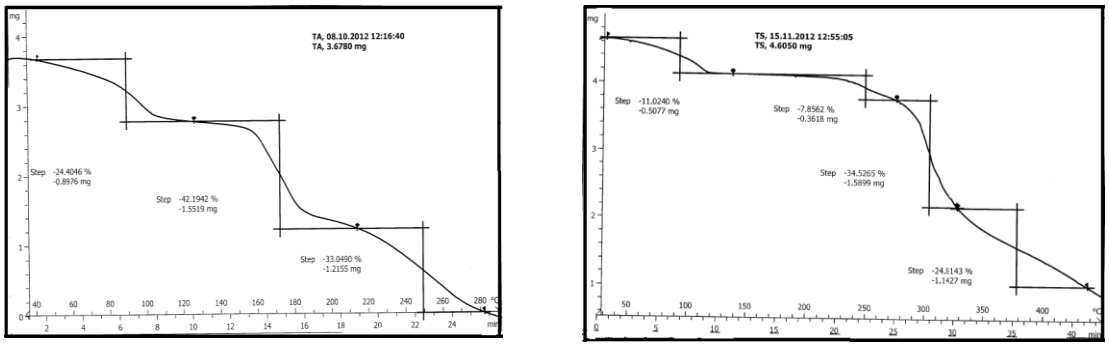

Figure 3.86. TGA scans of **34** (left) and **36** (right).

3.2.2.2 *Ni(II) and Fe(III) Chemistry*

Synthesis. Using adc as a linker the chemistry of Ni(II) and Fe(III) was also conducted. $Ni(OAc)_2$ was used for **37** while $Fe(ClO_4)_3$ was the starting material for **38**. Scheme 14 summarizes their synthesis.

$$Ni(OAc)_2 + tpa \xrightarrow[MeOH,\ RT]{H_2adc} [Ni_2(tpa)_2(adc)_2]\cdot 7H_2O\ (\mathbf{37})$$

$$Fe(ClO_4)_3 + tpa \xrightarrow[MeOH,\ RT]{H_2adc} [Fe_2(tpa)_2(adc)](ClO_4)_4\cdot 2.5H_2O\ (\mathbf{38})$$

Scheme 14. Synthesis of **37** and **38**.

FTIR Spectroscopy. The IR spectra of both compounds were recorded in solid state as KBr pellets. The IR spectra are shown in Figure 3.87. The IR spectrum of **37** shows two broad bands at 3382 and 3230 cm^{-1} while that of **38** shows a band at 3435 cm^{-1}, all corresponding to the O-H stretching frequency of water present in these MOCNs. The two bands indicate that there two kinds (with respect to the environment around it) of water in **37** (Figure 3.87). The peaks at 1568 and 1370 cm^{-1} (**37**) and 1638 and 1276 cm^{-1} (**38**) are due to asymmetric and symmetric stretching modes of the carboxylate group, respectively. The peaks at 1073 and 622 cm^{-1} for **38** confirms the presence of the perchlorate anion. The peaks at 1606, 1442, 760, 656 cm^{-1} are common in both spectra with a shift by few wave numbers.

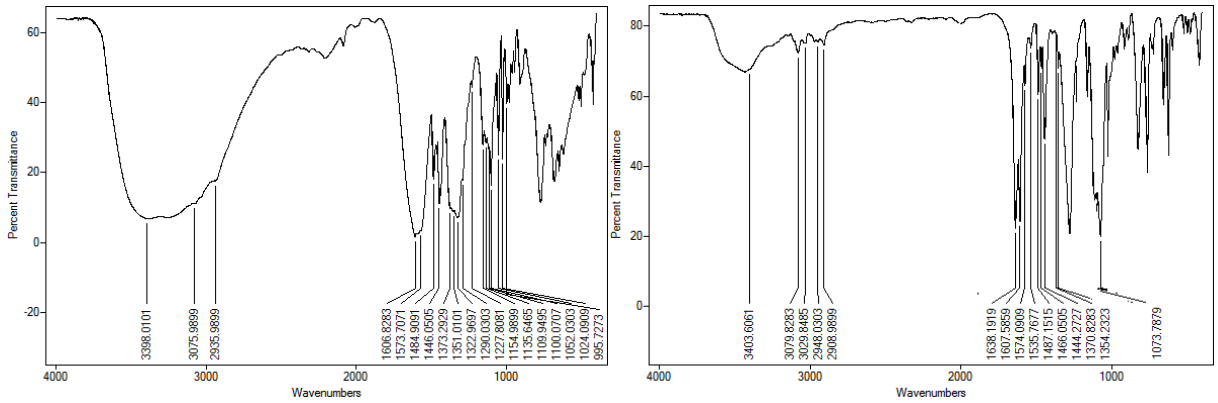

Figure 3.87. FTIR spectra of **37** (left) and **38** (right).

Thermogravimetric analysis. The TGA scan of **37** shown in Figure 3.88 clearly indicates the loss of lattice water in the first step. The loss of acetylene dicarboxylic acid in the second step at 150 °C is followed by a continuous weight loss due to its further decomposition. The TGA of **38** is not done as it contains perchlorate anions.

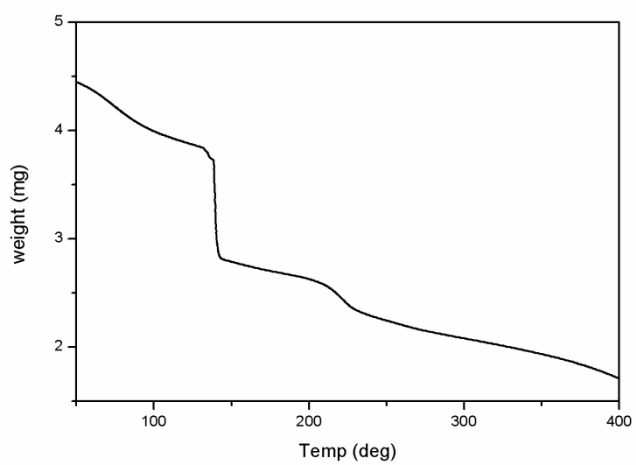

Figure 3.88. TGA scan of **37**.

3.2.2.3 *Zn(II) and Cd(II) Chemistry*

In case of Zn(II) and Cd(II), water soluble CPs were obtained with the tridentate ligands (section 3.2.1.4), and thus a similar chemistry was done with the tetradentate ligand, tpa, to see if there would be any effect on the formation of MOCN.

Synthesis. These are prepared in a similar way reported above for the Mn(II) compounds. Scheme 15 summarises their synthesis.

$$M(OAc)_2 + tpa \xrightarrow[MeOH,\ RT]{H_2adc} [M_2(tpa)_2(adc)_2]_n$$

where M = Zn (**39**)
M = Cd (**40**)

Scheme 15. Synthesis of Zn and Cd(II) compounds.

Single Crystal Structure Analysis. Single crystals of **40** were obtained by slow evaporation of its aqueous solution whereas single crystals of **39** could not be obtained.

$[Cd_2(tpa)_2(adc)_2]_n$ (40). Unlike the Mn(II) complex of tpa, a CP was obtained with Cd(II) as shown in Figure 3.89. This is similar to those with the tridentate ligands except the Cd(II) centers are octacoordinated in **40**. In this case, both adc ends bind in a chelated fashion around Cd(II) centers and tpa ligand is wrapping around each Cd(II) center with four nitrogen donor atoms. The selected bond distances and angles are listed in Table A56.

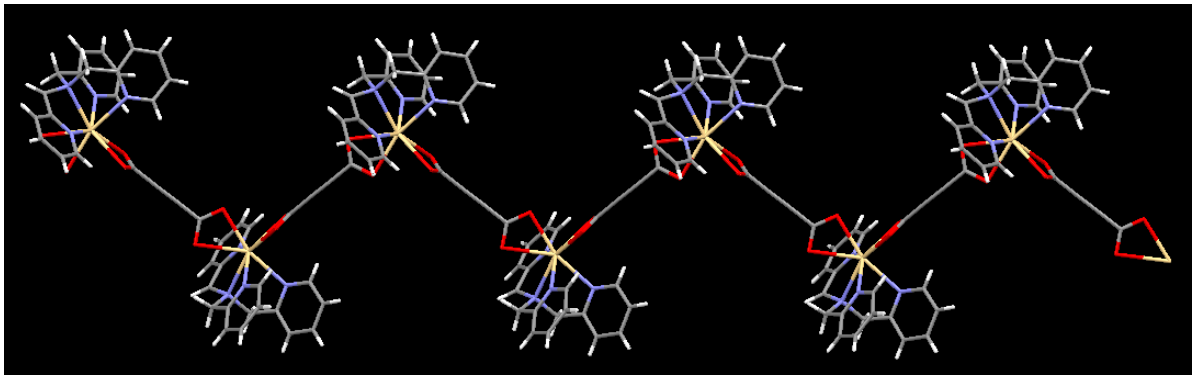

Figure 3.89. V-shaped 1D CP of **40**.

It forms a 2D Supramolecular assembly via π–π interactions (see Figure 3.90) that are found to be in two different planes. The centroid-centroid distances in two planes are 3.731 Å and 3.707 Å.[182]

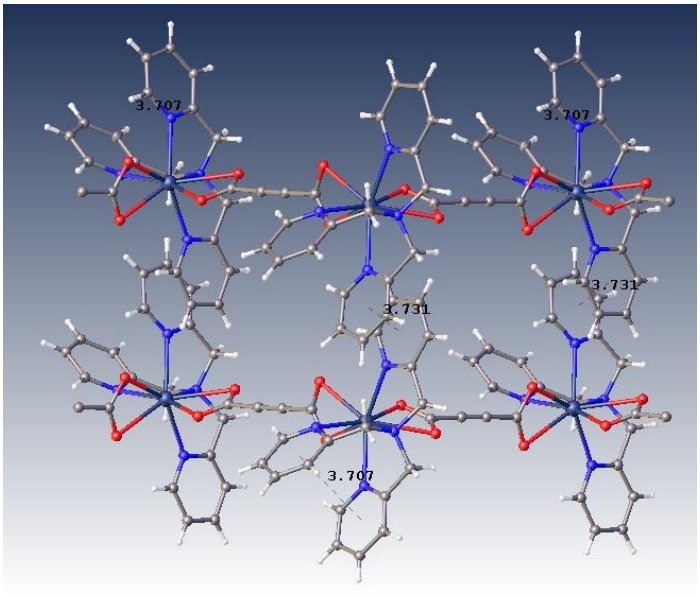

Figure 3.90. Supramolecular assembly in **40**.

Powder X-ray data analysis. Both **39** and **40** were studied by powder diffraction to confirm the bulk purity of the samples. The powder patterns are shown in Figure 3.91.The experimental powder pattern for **40** is in good agreement with its simulated powder pattern thus and confirms the bulk purity of the sample.

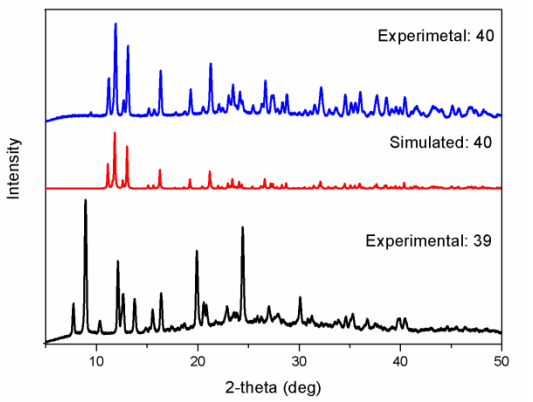

Figure 3.91. Simulated and experimental powder patterns for **39** and **40**.

FTIR Spectroscopy. The IR spectra of **39** and **40** show peaks at 3402 and 3431 cm^{-1} corresponding to the O-H stretch of water present in these MOCNs. The peaks at 1614, 1581, 1352, 1337 cm^{-1} for **39** and 1581, 1568, 1364, 1349 cm^{-1} for **40** correspond to the asymmetric and symmetric stretching modes of the carboxylate group, respectively.

Thermogravimetric Analysis. The thermal stability of both compounds was determined by TGA. The TGA scans shown below in Figure 3.92 clearly indicate that **40** is more stable than **39** although both are 1D CP. The reason for this is **39** has lattice water molecule whereas **40** has no lattice water molecules.

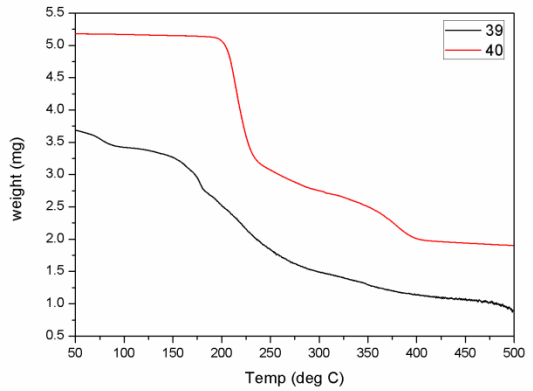

Figure 3.92. TGA scans of **39** and **40**.

3.2.3 MOCNs with Hexadentate ligands

The hexadentate ligands comprises of two tridentate units connected with each other with an alkyl chain. The number of methylene groups in this series was varied from 2 to 7 to understand if there would be any effect on the formation of MOCNs. Most of the fascinating results in this series were obtained with tpbn where number of methylene groups were 4. Since all these ligands were polypyridyl, an amide ligand with n = 4 was prepared and few complexes were synthesized to see the difference in the formation of products due to the flexible amide group as compared to the pyridyl group.

3.2.3.1 *Mn(II) Chemistry*

Dicarboxylate linkers

Using adc linker Mn(II) chemistry was done with all seven polypyridyl ligands and one amide-pyridyl ligand. An effect of the methylene chain length between the alkyl nitrogens in these ligands was observed on the formation of the diverse nature of the products. Two MOCNs were made from the reactions of the Mn(II)-fumarate system with the tppn and tpbn ligands. The reaction of Mn(II) with the oxalate linker with no aliphatic chain between the carboxylate groups provides a 1D CP for the tpbn ligand. The anion directed formation of $\{[Mn_2(tpbn)](ClO_4)_2\}_n$ and $[Mn_2(tpbn)(H_2O)_6](tdc)_2{\cdot}4H_2O$, where the same metal salt $Mn(ClO_4)_2$ is used as the starting material in both cases, is really unusual as the latter is the adc analog of the tppn ligand mentioned above. With the amide analogue of tpbn, $\{[Mn_2(bpbg)(adc)_2]{\cdot}4H_2O\}_n$ is obtained. For the cycloaliphatic dicarboxylate, cdc, a 2D MOF with very different structure compared to those with other dicarboxylates is obtained though the reaction carried out under hydrothermal conditions.

Synthesis. Scheme 16 summarizes the synthesis of seven compounds from the Mn(II) and H_2adc (Method 1 and/or Method 2) for all the hexadentate polypyridyl ligands. $\{[Mn_2(adc)_2(tpbn)(H_2O)_2]{\cdot}2H_2O\}_n$ (**41**) was prepared and isolated as a colorless solid from the self-assembly reaction of $Mn(ClO_4)_2{\cdot}6H_2O$ and dipotassium acetylene dicarboxylate (in a 1:1 ratio) in a methanol-water mixture followed by the addition of half equivalent of tpbn under ambient conditions. Alternatively, **41** can be prepared using $Mn(OAc)_2$ as the starting material indicating no effect of the Mn(II) source on the product formation. When the same procedure

similar to **41** using $Mn(OAc)_2$ was followed for the tpen, 1,2-tppn, tppn and tppen ligands, different products are formed. However, products for tphxn and tphn are similar to that obtained for tppen. A supramolecular assembly $[Mn_2(tppn)(H_2O)_6](adc)_2{\cdot}3H_2O$ (**42**), consisting of $Mn_2(tppn)(H_2O)_6$ dinuclear subunits, lattice water molecules and adc anions through strong hydrogen bonding interactions, is the product for the tppn ligand. Discrete dinulcear complexes $[Mn_2(adc)(1,2\text{-tppn})_2](ClO_4)_2{\cdot}3H_2O$ (**43**) and $[Mn_2(adc)(tpen)_2](ClO_4)_2{\cdot}2H_2O$ (**44**) are formed where each Mn(II) center is heptacoordinated. On the other hand, for the tppen ligand a 3D supramolecular assembly $\{[Mn_2(adc)(tppen)(H_2O)_4](adc){\cdot}4H_2O\}_n$ (**45**) is isolated where adc is found to be a linker as well as a counter anion in the same structure. It should be noted here that the use of $Mn(ClO_4)_2$ as the starting material for **41**, **42**, **43** and **45** gives the same product and only reduces the isolated yield by a few %. Therefore, the appropriate method is described in the experimental section that suited the final work-up for isolating the product with the best yields. This difference in their formulation can be easily observed by comparing their FTIR spectra and solubility behavior. **41** is a neutral species with two adc ligands bridging the Mn(II) ions in a bis(monodentate) fashion. Although the formula of **41** and **42** contain two adc molecules, the FTIR spectra clearly show the difference in its stretching frequencies indicating its inclusion in the primary coordination sphere in **42** while it acting as a counter anion in **42**. In **45**, the presence of both coordinated (in a monodentate fashion) adc and uncoordinated adc in its FTIR spectrum could be compared to those for **41** and **42**. Dinuclear complexes **43** and **44** have two perchlorate counter anions, which show characteristic features in the FTIR spectroscopy. Compound **41** was found to be insoluble in almost all organic solvents whereas **42** and **45** were soluble in water, and **43** and **44** were soluble in acetonitrile. Further evidence for the diversity of such product formation due to a subtle change in the methylene chain length between the alkyl nitrogens of these ligands is provided with the help of X-ray crystallography which is discussed next.

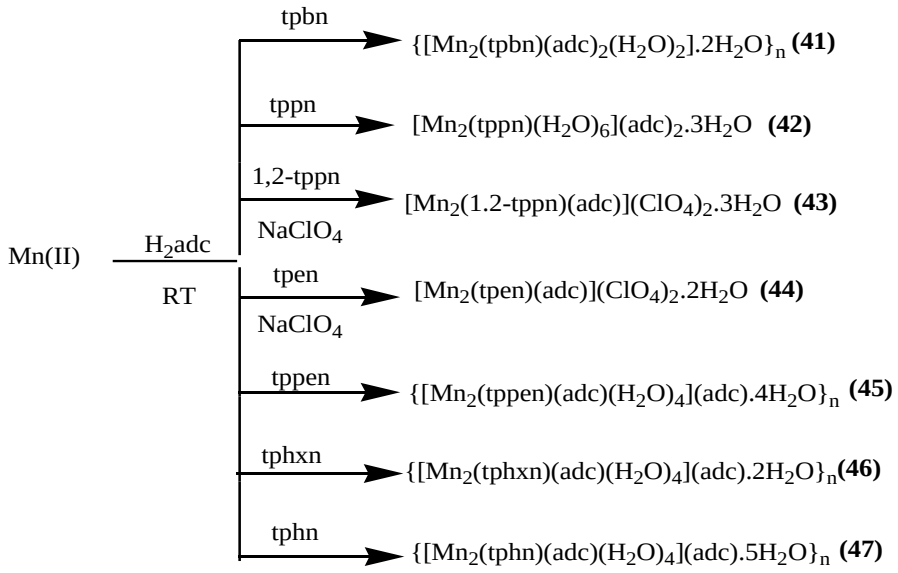

Scheme 16. Synthesis of **41**-**47**.

Compound **48** was synthesized in similar way as **41**. Scheme 17 summarises its synthesis. Unlike **41**, **48** is soluble in water. The reason for it could be the amide group instead of pyridine in the ligand.

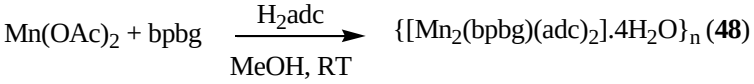

Scheme 17. Synthesis of **48**.

Compound **49** was synthesized in a similar way to **43** and **44** whereas **50** was synthesized following **41**. Like **41**, **50** was also insoluble in almost all organic solvents. The starting material was same for both the compounds but **49** was soluble in methanol that's why sodium perchlorate was used to precipitate out the product whereas **50** was obtained as solid. Scheme 18 summarises their synthesis.

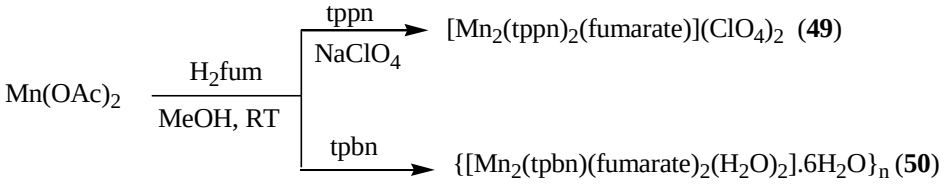

Scheme 18. Synthesis of **49**-**50**.

Compounds **51** and **53** were obtained using $Mn(ClO_4)_2$ as the starting material. For **51**, the potassium salt of oxalate was used. Compound **52** was obtained in a similar way to **43** using H_2tdc instead of H_2adc. Compound **54** was obtained under hydrothermal conditions with CDC using $MnSO_4$ as the starting material.

$$MnSO_4 + tpbn \xrightarrow[H_2O,\ HT]{H_2CDC} [Mn_4(tpbn)_2(CDC)_2]_n \quad (\mathbf{54})$$

Scheme 19. Synthesis of **54**.

Single crystal structure analysis. Single Crystals of **41**, **50** and **53** were obtained by direct layering of the reactants, single crystals for **42**, **45**, and **47** were obtained by slow evaporation of an aqueous solution of the respective compound, single crystals for **43**, **44**, **49**, **51** and **52** were obtained by slow evaporation of an acetonitrile solution of the respective compound. Single crystals of **54** were obtained directly from the hydrothermal synthesis. Single crystals of **46** and **48** suitable for X-ray studies could not be obtained even after several tries.

$\{[Mn_2(tpbn)(adc)_2(H_2O)_2]\cdot 2CH_3OH\}_n$ (41b). It crystallizes in the triclinic *P*-1 space group (No. 2) with an inversion center in the middle of the dinuclear unit consisting two Mn(II) centers bridged by two adc groups, each of which binding in a monodentate syn-syn fashion. The geometry around each Mn(II) center is distorted octahedral and is surrounded by three nitrogens of tpbn, one water molecule and two oxygen atoms of two adc (see Figure 3.93). As mentioned earlier for **4** and its derivatives, prior to this work bis(adc) core in **41** was not observed even though several metal-adc[204-210] 2D and 3D networks without any ancillary ligand were reported in the literature.

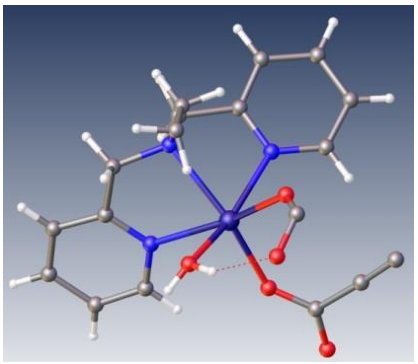

Figure 3.93. Coordination environment around Mn(II) in **41b**.

The tpbn ligand spans between two such dinuclear subunits forming the spiral coordination polymer. A perspective view of **41b** is shown in Figure 3.94 (left). A space filling model of **41b** depicting the repeated pores (size: 7.662 Å X 4.530 Å) in the polymeric structure is also shown in Figure 3.94 (right). The alkyl nitrogen of each half of the tpbn ligand is trans to one of the adc whereas one of the pyridine nitrogens is trans to the coordinated water molecule and the other pyridine nitrogen is trans to the second adc. The selected bond distances and angles are summarized in Table A57. The Mn-N_{py} distance [2.2870(15)- 2.2901(16) Å] is shorter than Mn-N_{alkyl} distance [2.3381(15) Å]. The two Mn-O_{carb} distances are found to be different; Mn-O2 (2.1644(13) Å) and Mn-O4 (2.1029(13) Å). The Mn-O_{water} (2.1697(13) Å) distances are similar to the values usually observed in hexacoordinated Mn(II) complexes of similar ancillary ligands.[176-178] The O-Mn-N_{py} angles are 160.69(5)° and 162.73(5)°. The O-Mn-N_{amine} angles are all in the same range, from 94.88 (5)° to 154.12(5)°. The values observed for the acetylene group confirm that its triple bond character is kept in **41b**: C16-C18-C17 and C18-C16-C15 angles are close to linearity (ranges from 176.71(19)° to 176.82(19)°) and C-C triple bond distance is 1.195(3) Å (see the FTIR and Raman Spectroscopy section below).

The coordinated water molecule (O1) on the Mn center of **41b** is strongly hydrogen bonded in an intramolecular fashion (O---O distance: 2.670 (2) Å) to the uncoordinated O atom of the adc molecule (O3), which is further hydrogen bonded (O---O distance: 2.770(2) Å) to the O atom (O6) of methanol (see Figure 3.95). Through intermolecular hydrogen bonding, the coordinated water molecule (O1) further connects the uncoordinated O atom of the adc molecule (O5) of the next asymmetric unit (O---O distance: 2.649(2) Å) forming the supramolecular network of the polymeric $Mn_2(adc)_2(tpbn)(H_2O)_2$ layer in a direction with an angle of 45° to the latter. Hydrogen bonding distances found in **41b** are summarized in Table 3.18. There is π–π interactions between the pyridine rings of the tpbn ligands (centroid-centroid distance: 3.766)[182] of the two spiral 2D chains resulting in the formation of 3D supramolecular assembly as shown in Figure 3.96. For demonstrating the strength of hydrogen bonding in **41b**, its single crystal was subjected to variable temperature X-ray studies. In order to make it methanol solvent free, a single crystal was slowly heated to 323 K (50 °C) at the rate of 40 K/hr using the Oxford LT device attached to the diffractometer. When the temperature was raised above 323 K, it was found that the crystal lost its integrity. The full data collection was carried on this crystal at 323 K and it was found

that one of the two methanol molecules remained within the lattice. Its dehydration upon heating can further be followed from the TGA (*vide infra*).

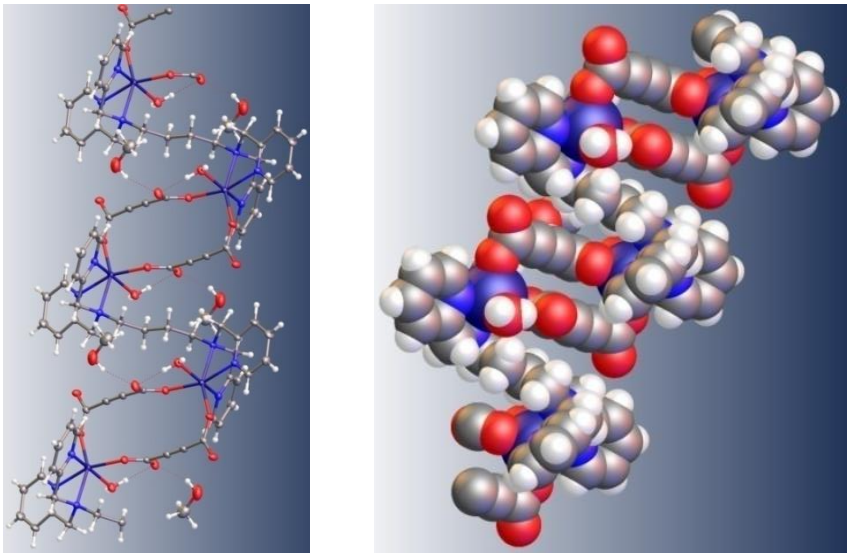

Figure 3.94. A perspective view of 2D spiral **41b** (left) and its space-filling representation (right).

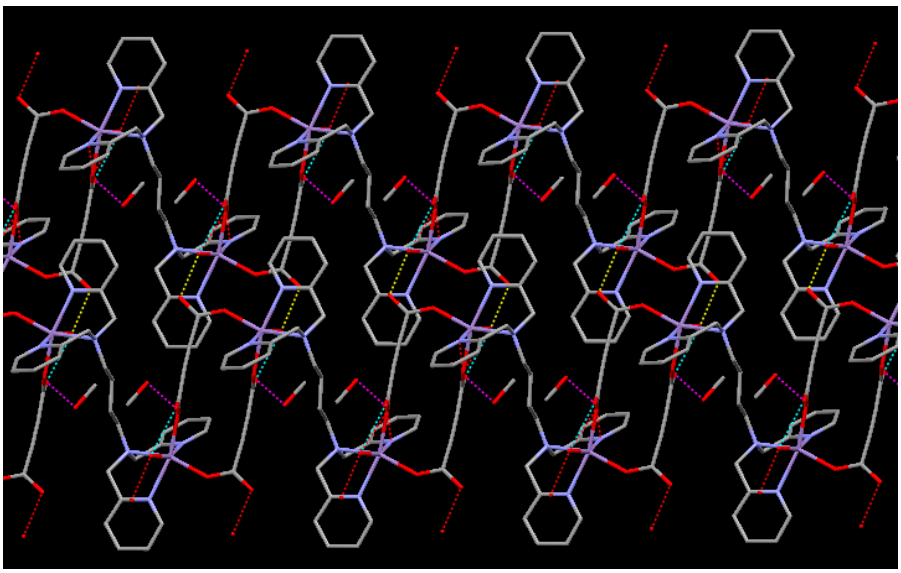

Figure 3.95. Representation of hydrogen bonding in the 3D assembly of **41b**. Hydrogen atoms are omitted for clarity.

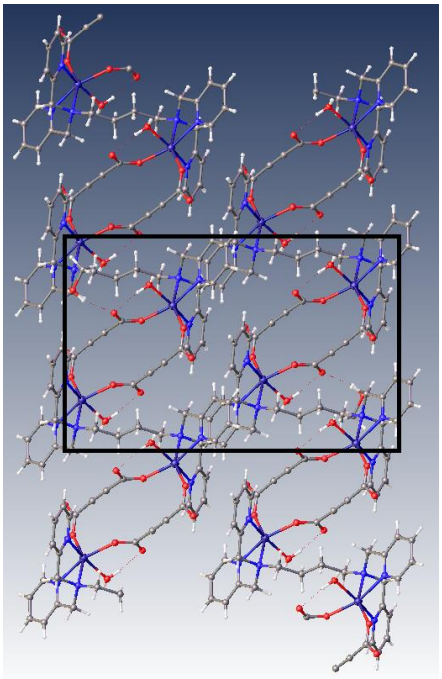

Figure 3.96. Formation of the 3D network via π–π interactions in **41b**.

$[Mn_2(tppn)(H_2O)_6](adc)_2{\cdot}3H_2O$ (42). It crystallizes in the monoclinic $P2_1/n$ space group (No. 14). Like **41b**, the tppn ligand in **42** is spanning between two Mn(II) centers, which are hexacoordinated (Mn···Mn distance: 7.037 Å). Each Mn(II) center is coordinated with three water molecules and three nitrogen atoms from one-half of the tppn ligand as shown in Figure 3.97. The selected bond distances and angles are summarized in Table A58. The Mn-N_{py} distance [2.237(3)-2.262(3) Å] is shorter than Mn-N_{alkyl} distance [2.336(3)-2.362(3) Å]. The Mn-O_{water} (2.144(3) - 2.222(3) Å) distances are similar to the values found in **41b**. The O-Mn-$N_{pyridine}$ angles ranges from 84.73(12)° to 91.25 (13)° and 153.74(12)° to 177.17(13)°. The O-Mn-N_{amine} angles are in the range of 86.94 (12)° to 108.48 (12)° and 161.59(13)° to 166.84(13)°. The values observed for the acetylene group in **42** are similar to those found in **41b**: C30-C29-C28 and C34-C33-C32 angles are close to linearity (ranges from 174.3° to 179°) and C-C triple bond distances range from 1.187 Å to 1.200 Å. Very few examples are known in which a Mn(II) center has three or more water molecules.[211] The coordinated water molecules prohibit adc anions to coordinate to the Mn(II) centers in **42**. Unlike **41b**, the adc is acting as counter anions in **42**. Prior to this work, there is only two reports[212] in the literature where the adc is not part of the first coordination sphere of the transition metal ion. However, the reported examples are coordination polymers where the $[Mn(H_2O)_4]^{2+}$ moieties are connected with the 1,2-bis(4-

pyridyl)ethane or 4,4'-bpy ligand. Thus the coordination of three water molecules to each Mn(II) center of **42** in the presence of a hexadentate ligand is unprecedented. These three coordinated water molecules, adc anions and lattice water molecules are connected through extensive hydrogen bonding as shown in Figure 3.98. Hydrogen bonding parameters found in **42** are summarized in Table 3.18. The orientation of coordinated water molecules on each Mn(II) center is different. This resulted in different hydrogen bonding mode of two adc anions with coordinated water molecules. In order to show the difference in the two types of binding modes of the adc anions in **42**, these are colored in green and yellow in Figure 3.98.

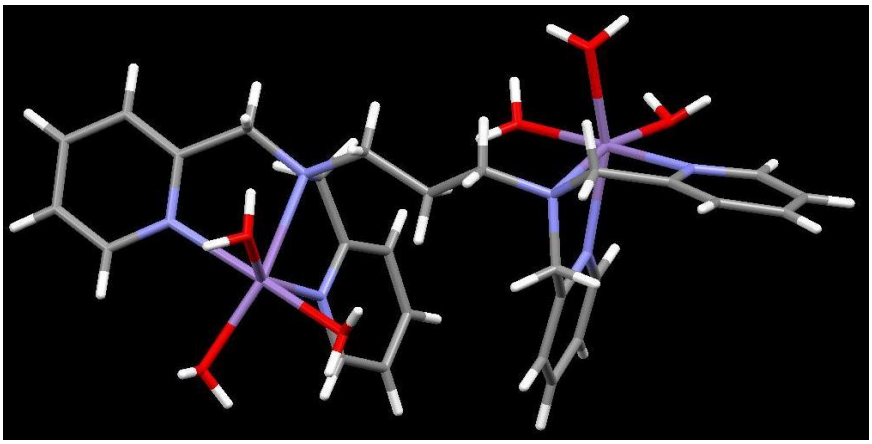

Figure 3.97. A perspective view of the $Mn_2(tppn)(H_2O)_6$ subunits in **42**.

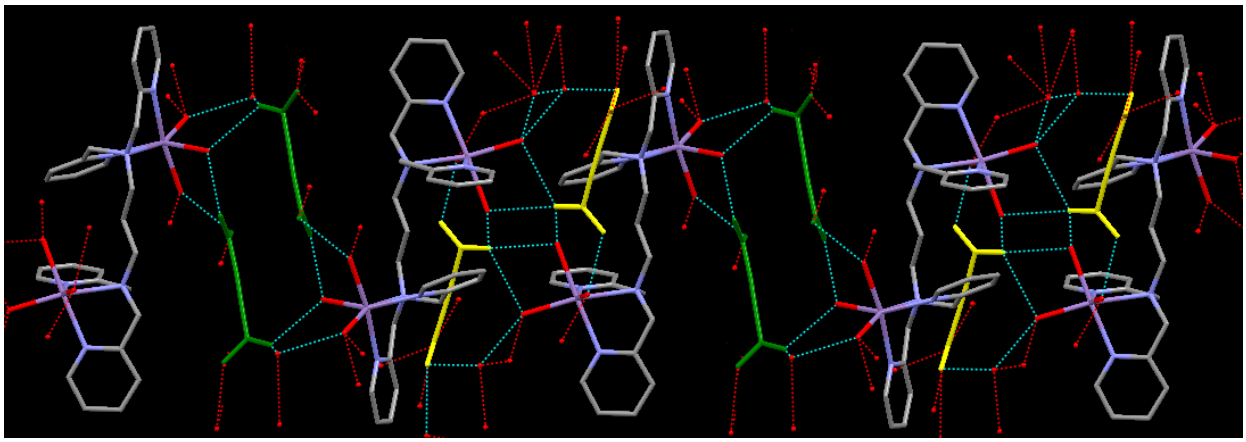

Figure 3.98. Formation of the 3D supramolecular assembly of **42** via hydrogen bonding. Only one of the disordered oxygen of a carboxylate group of the adc group is shown. Hydrogen atoms are omitted for clarity.

The bonding of the adc anions in green color to the coordinated water molecules can be visualized as the two adc anions connect two dimanganese subunits together resulting in the

formation of a channel (Mn¨Mn distance: 12.026 Å). On the other hand, the adc anions in yellow color are hydrogen bonded to the coordinated water molecules to generate totally different motifs (Mn¨Mn distance: 8.952 Å). In the second mode, one of the carboxylate groups of each adc anion is hydrogen bonded to the lattice water molecules. Considering the fact that the direct coordination of the adc anions in **41** allows only one coordinated water molecule per Mn(II) center compared to three water molecules in **42**, the formation of **41** can be through an intermediate similar to **42**. Thus the isolation of **42** with one less methylene group in tppn compared to tpbn indicates that only the former can stabilize such a 3D supramolecular assembly. As mentioned in the next sections, reducing the methylene chain length less than 3 which is the case for 1,2-tppn or tpen, or increasing the methylene chain length more than 4 like in tppen gives different products. This finding is helpful to understand the formation of the supramolecular assemblies, such as **41** and **42**.

$[Mn_2(1,2\text{-tppn})_2(adc)][(ClO_4)_2$ (43) and $[Mn_2(tpen)_2(adc)](ClO_4)_2$ (44). These are isostructural and crystallize in the monoclinic *C*2/*c* space group. The structure of cations in **43** and **44** are shown in Figure 3.99 and 3.100 respectively. In both cases, the Mn(II) centers are heptacoordinated. Although there are many mononuclear heptacoordinated Mn(II) complexes reported in the literature,[213] carboxylato bridged dinuclear species are limited. An example of acetate bridged dinulcear compound with both Mn(II) centers being heptacoordinated (N_6O environment) was reported for the tpen ligand several years ago.[214] Thus **43b** and **44b** are the first examples of heptacoordinated dinuclear Mn(II) complexes with a combination of dicarboxylates and polydentate ancillary ligands. The striking feature in these two compounds is that even with a hexadentate ligand, such as 1,2-tppn and tpen, the Mn(II) centers are bridged by the adc linker in bis(monodentate) anti-anti fashion. The selected bond distances and angles are listed in Table A59. The Mn-N_{alkyl} distances in **43b** and **44b** range from 2.385(2) to 2.360(1) Å and 2.462(3) to 2.450(2) Å, respectively. These distances are comparable to those found in Mn(II) complexes of similar ancillary ligands.[213]

The C-C triple bond distance of adc in **43b** and **44b** falls in the range 1.196-1.200 Å and is slightly shorter than that found in **41b**. This shows that the triple bond character of adc remains intact in these molecules and is not much affected by the increase in coordination number of the Mn(II) centers in **41b** and **43b** or **44b**.

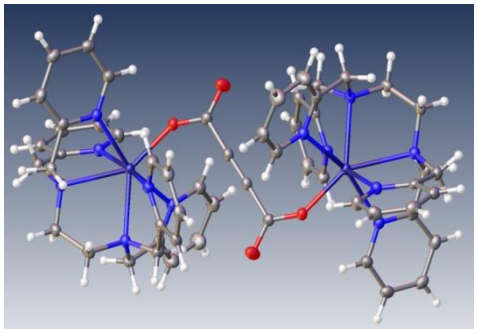

Figure 3.99. Crystal structure of the cation in **43**.

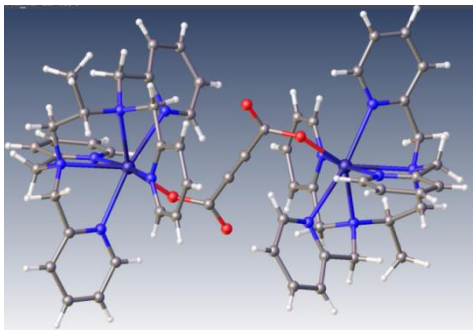

Figure 3.100. Crystal structure of the cation in **44**.

$[Mn_2(tppen)(adc)(H_2O)_4](adc).4H_2O\}_n$ (45). It crystallizes in the monoclinic *P*2/*c* space group. Unlike **43** and **44b**, it is a 1D coordination polymer where the adc group links the $Mn_2(tppen)(H_2O)_4$ dinuclear subunits (Mn···Mn distance: 9.468 Å) with the tppen ligand spanning between two Mn(II) centers (Mn···Mn distance: 10.980 Å). Each hexacoordinated Mn(II) center is surrounded by three nitrogens of tppen, two water molecules and one oxygen atom of one monodentate adc as shown in Figure 3.101 (top). The alkyl nitrogen of each half of the tppen ligand is trans to the bridging adc whereas both pyridine nitrogens are trans to the bound water molecules. The selected bond distances and angles for **45** summarized in Table A60 are similar to those for **41b** and **42**. Two coordinated water molecules, coordinated adc, uncoordinated adc anions and lattice water molecules are linked through extensive hydrogen bonding as shown in Figure 3.101 (bottom). Two layers of polymeric $Mn_2(adc)(tppen)(H_2O)_4$ are connected to generate 2D supramolecular network with two types of Mn---Mn distances due to different connectivity of the adc; the Mn---Mn distance is 8.839 Å for 1D polymer connected via uncoordinated adc and lattice water molecules while it is 8.410 Å for two layers that are connected via coordinated adc and lattice water molecules. Hydrogen bonding parameters found

in **45** are summarized in Table 3.18. There are π–π interactions between the pyridine rings of the tppen ligands (centroid-centroid distance: 3.631 Å)[182] of the two spiral 2D chains resulting in the formation of 3D supramolecular assembly as shown in Figure 3.102.

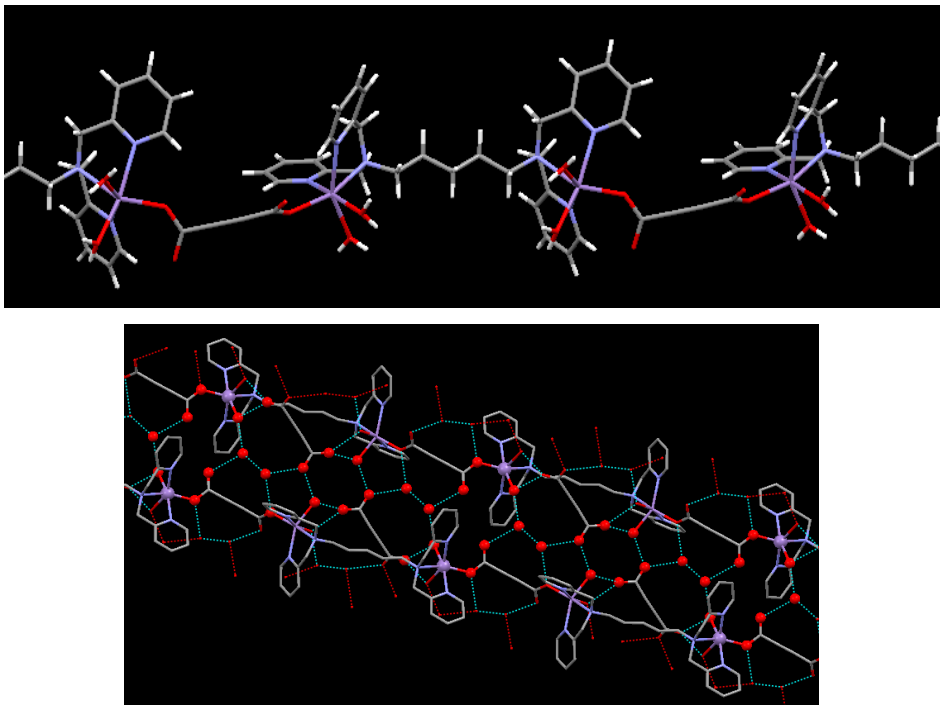

Figure 3.101. 1D chain structure of **45** (top) and hydrogen bonding interactions in **45** (bottom).

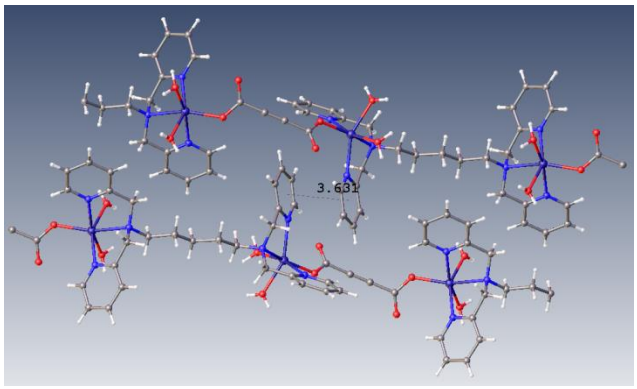

Figure 3.102. Formation of the 3D network via π–π interactions in **45**. For clarity, lattice water molecules and adc anions are omitted.

$\{Mn_2(tphn)(adc)(H_2O)_2](adc)\cdot 5H_2O\}_n$ (47). Its structure is similar to **45** (see Figure 3.103). Each Mn(II) center is hexacooridnated surrounded by three nitrogens of the ligand, two oxygens of the coordinated water molecule and one oxygen of the adc. Like **45**, one of the adc is acting as counter anion. The selected bond distances and angles are listed in Table A61.

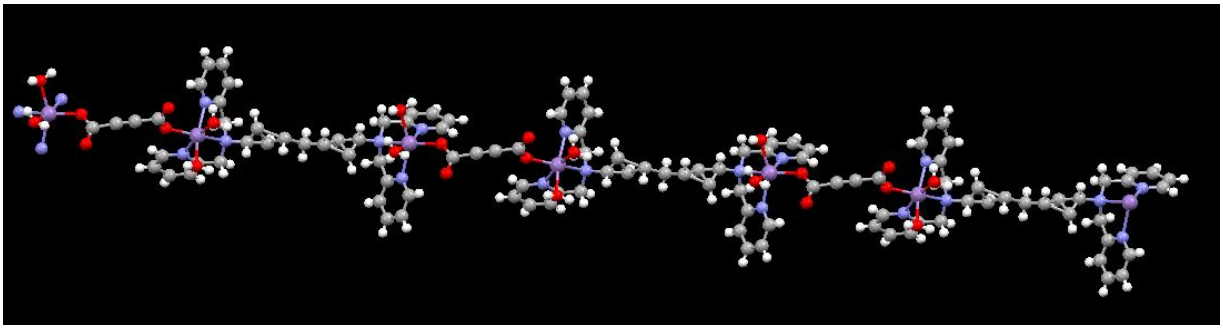

Figure 3.103. A perspective view of **47**.

Due to the presence of lattice water molecules the two 1D CP layers are connected to each other via hydrogen bonding as shown in Figure 3.104. In addition to Hydrogen bonding, this supramolecular assembly is further stabilized by C-H…O interactions. The hydrogen bonding parameters are listed in Table 3.18.

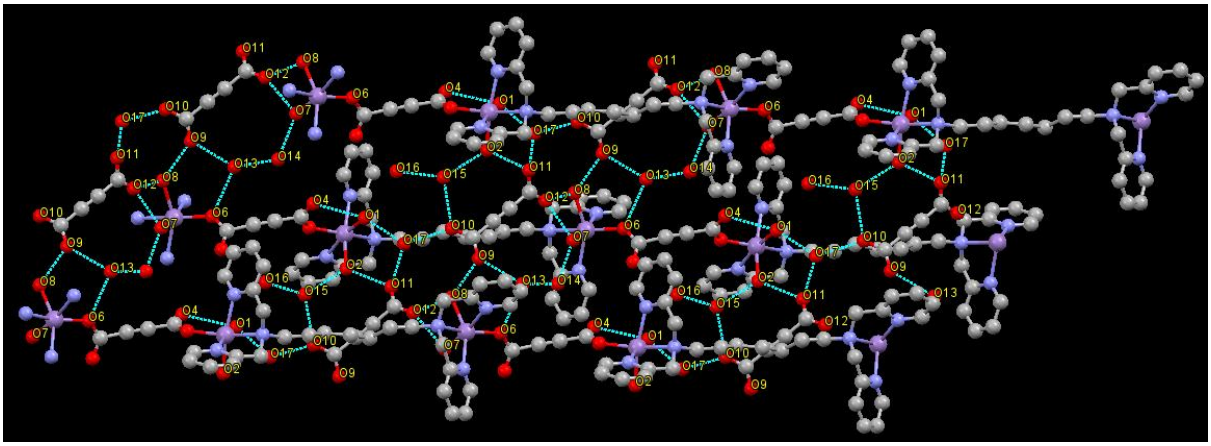

Figure 3.104. Hydrogen bonded network of **47**. For clarity, hydrogens are omitted.

Furthermore, this supramolecular assembly is stabilized by moderate π-π interactions (see Figure 3.105). The π-π interactions were found in two planes like **45.** The centroid-centroid distances are 3.728 Å and 3.898 Å.

Compounds **45** and **47** are unexpected for two reasons: with more than 4 methylene chain length one would expect a derivative of **41b** and if the odd number of methylene groups has any effect a derivative of **42** should be the product.

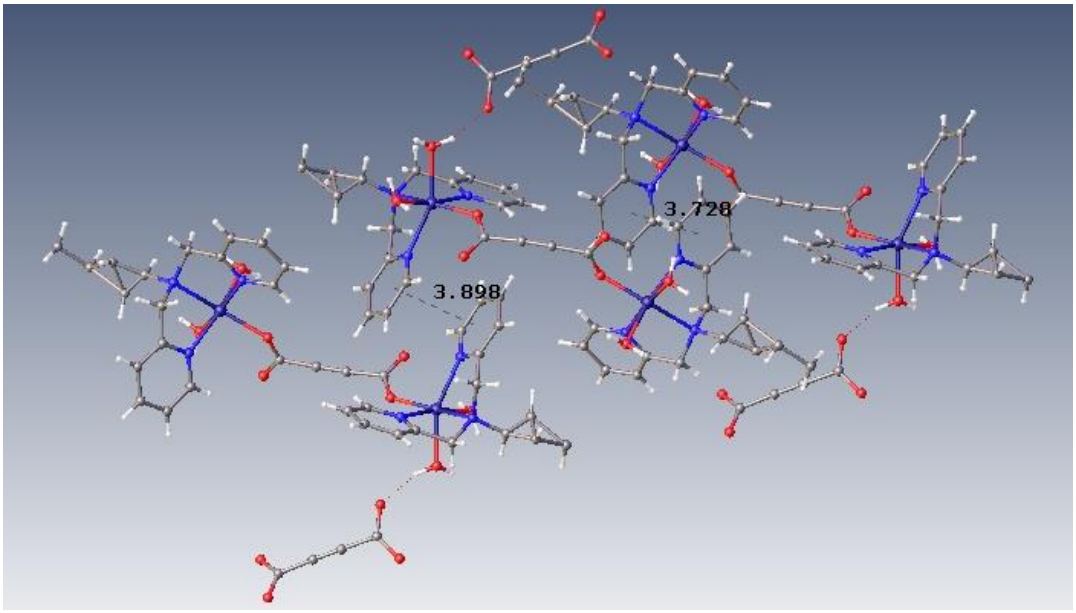

Figure 3.105. Formation of the 3D network via π–π interactions in **47**.

Table 3.18. Hydrogen bonding parameters for **41b**, **42**, **45** and **47**.[a]

41b

D–H…A	r (D-H) (Å)	r (H…A) (Å)	r (D…A) (Å)	∠D-H…A (deg)	Symmetry
O(1) --H(1A) ..O(5)	0.808(15)	1.868(16)	2.6494(18)	162(2)	1-x,-y,1-z
O(1) --H(1B) ..O(3)	0.81(2)	1.91(2)	2.6701(19)	155(2)	
O(6) --H(6) ..O(3)	0.84	1.97(2)	2.770(2)	158	

42

D–H…A	r (D-H) (Å)	r (H…A) (Å)	r (D…A) (Å)	∠D-H…A (deg)	Symmetry
O(1) --H(1A)..O(17)	0.88	1.82	2.702(5)	176	3/2-x,-1/2+y,1/2-z
O(1) --H(1B)..O(15)	0.89	1.73	2.505(6)	144	
O(2) --H(2B)..O(13)	0.87	1.85	2.678(6)	159	3/2-x,-1/2+y,1/2-z
O(3) --H(3B)..O(11)	0.88	1.87	2.703(4)	158	1/2+x,1/2-y,1/2+z
O(4) --H(4A) ..O(8)	0.88	1.85	2.697(5)	161	
O(4) --H(4B) ..O(8)	0.88	1.87	2.741(5)	170	1-x,1-y,1-z
O(5) --H(5A) ..O(10)	0.86	1.91	2.661(5)	145	2-x,1-y,1-z
O(5) --H(5B)..O(7)	0.86	1.89	2.706(4)	159	
O(6) --H(6A)..O(18)	0.87	1.98	2.848(7)	178	1-x,1-y,1-z
O(16) --H(16C)..O(9)	0.85	2.29	2.972(7)	137	
O(18) --H(18A)..O(10)	0.85	1.90	2.715(7)	159	-1+x, y, z
C(2) --H(2C) ..O(4)	0.97	2.39	3.242(5)	146	
C(2) --H(2D) ..O(3)	0.97	2.53	3.425(5)	153	
C(6) --H(6) ..O(14)	0.93	2.54	3.418(9)	158	1/2+x,1/2-y,1/2+z
C(10) --H(10B) ..O(17)	0.97	2.56	3.408(4)	146	-1/2+x,1/2-y,1/2+z

45

D—H…A	r (D-H) (Å)	r (H…A) (Å)	r (D…A) (Å)	∠D-H…A (deg)	Symmetry
O(1) --H(1)...O(5)	0.75(4)	1.88(4)	2.624(4)	176(5)	x,1-y,1/2+z
O(1)--H(2)...O(6)	0.88(4)	1.90(4)	2.741(4)	159(4)	-x,1+y,1/2-z
O(2)--H(2C)...O(8)	0.88(7)	1.78(6)	2.658(5)	173(7)	
O(2)--H(2D)...O(6)	0.87(4)	1.91(4)	2.770(4)	169(4)	-x,1+y,1/2-z
O(7)--H(7A)...O(5)	0.97(4)	1.80(4)	2.745(4)	164(4)	
O(7) --H(7B)...O(3)	0.83(6)	2.09(6)	2.920(4)	173(5)	x,1-y,-1/2+z
O(8)--H(8C)...O(7)	0.77(6)	2.01(6)	2.773(4)	170(6)	x,1+y,z
O(8)--H(8D)...O(4)	0.91(6)	1.91(6)	2.822(5)	177(7)	1-x,2-y,1-z

47

D–H…A	r (D-H) (Å)	r (H…A) (Å)	r (D…A) (Å)	∠D-H…A (deg)	Symmetry
O1--H1B...O16	0.86	2.29	3.036(7)	145	x,1/2-y,1/2+z
O2--H2B...O11	0.88	1.76	2.624(6)	164	1+x,y,z
O7--H7A...O12	0.86	1.83	2.680(8)	168	x,1/2-y,-1/2+z
O8--H8A...O9	0.88	1.83	2.625(5)	150	
O8--H8B...O12	0.88	1.83	2.683(8)	163	x,1/2-y,-1/2+z
O13--H13A...O6	0.85	2.1	2.940(6)	168	
O14--H14A...O13	0.85	1.95	2.793(7)	174	
O14--H14B...O4	0.85	2.19	3.041(8)	174	
O15--H15A...O2	0.85	2.18	2.760(7)	126	
O16--H15B...O1	0.85	2.36	3.036(7)	137	x,1/2-y,-1/2+z
O16--H16A...O5	0.85	2.24	3.008(7)	151	
O15--H16B...O10	0.85	1.96	2.787(6)	164	1+x,y,z
O17--H17A...O10	0.85	1.9	2.723(6)	162	1+x,y,z
O17--H17B...O11	0.85	1.99	2.754(6)	149	1+x,1/2-y,-1/2+z
C7--H7C...O17	0.98	2.57	3.432(8)	147	1-x,1-y,-z
C18--H18...O5	0.94	2.39	3.260(7)	154	
C36--H32...O13	0.94	2.5	3.423(8)	167	1-x,1-y,1-z
C20--H20A...O10	0.99	2.44	3.393(16)	162	-x, y-1, -z

[a]Numbers in parenthesis are estimated standard deviations in the last significant digits.

$[Mn_2(tppn)_2(fumarate)](ClO_4)_2$ (49). In this tppn is acting as a pentadentate ligand where one of the pyridyl ring was hanging as shown in Figure 3.106. The five sites on Mn(II) center is surrounded by five nitrogens of the ligand and sixth site was occupied by oxygen of the carboxylate. The fumarate binds in a bis(monodentate) syn-anti fashion. The selected bond distances and angles are listed in Table A62. This example shows how the product formation depends on the ligand as well as the carboxylate used.

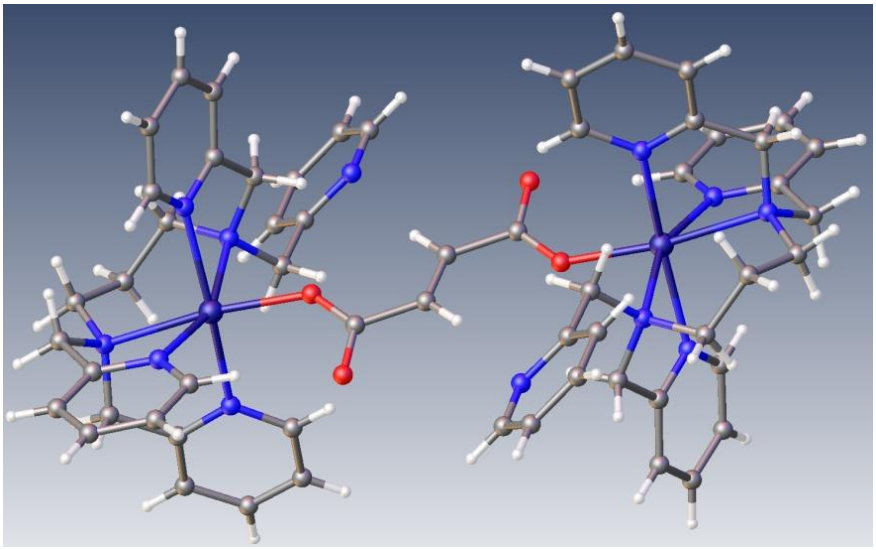

Figure 3.106. Structure of $[Mn_2(tppn)_2(fumarate)]^{2+}$ in **49**.

{[Mn_2(tpbn)(fumarate)$_2$(H_2O)$_2$]·6H_2O}$_n$ (**50**). It is similar to **41b** except it has six lattice water molecules instead of methanol. It crystallises in the monoclinic *C2/c* space group. Each Mn(II) center is hexacoordinated and surrounded by three nitrogens of the ligand, one coordinated water molecule and two oxygens of the fumarate. The selected bond distances and angles are listed in Table A62. Two Mn(II) centers are connected with a bis(fumarate) core and the tpbn ligand spans between two such cores making it a 1D polymer as in case of **41**. The fumarate binds in a bis(monodentate) syn-syn fashion.

The presence of four lattice water molecules has resulted in the formation of a 3D supramolecular assembly of **50** via strong Hydrogen bonding interactions shown in Figure 3.108. The hydrogen bonding parameters are listed in Table 3.19.

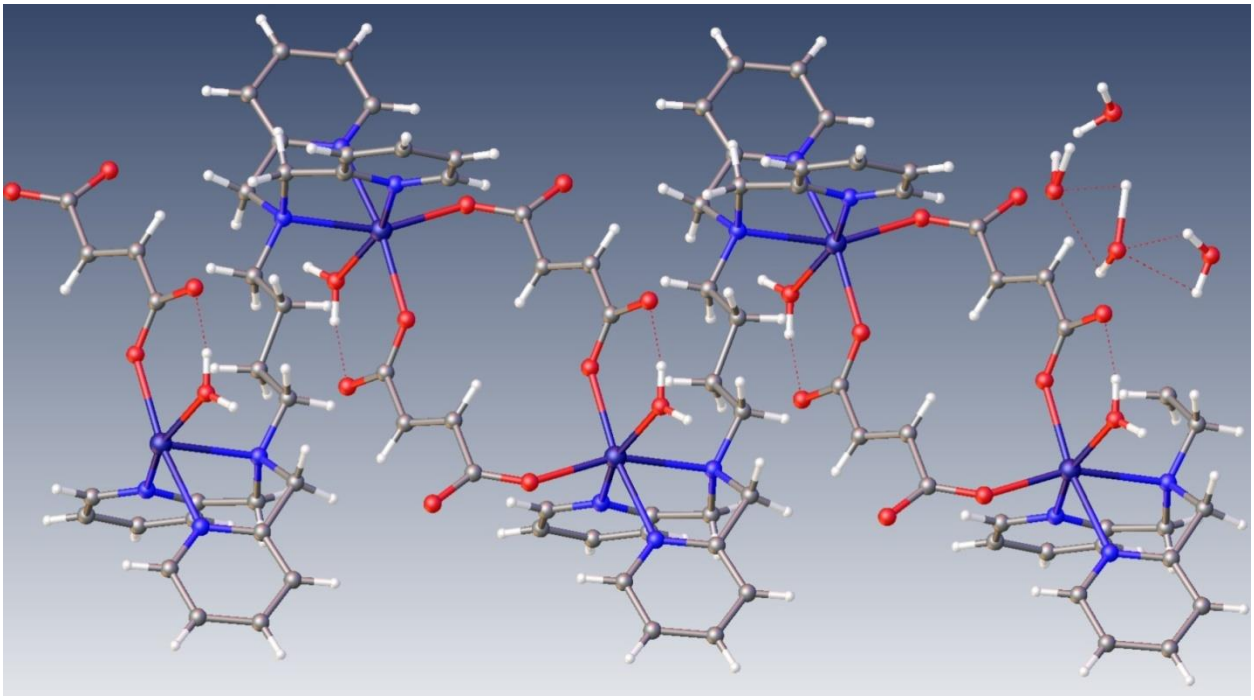

Figure 3.107. A perspective view of **50**.

Table 3.19. Hydrogen bonding parameters for **50**.[a]

D–H...A	r (D-H) (Å)	r (H…A) (Å)	r (D…A) (Å)	∠D-H…A (deg)	Symmetry
O(1)--H(1A)...O(2)	0.88	2.04	2.622(4)	122	
O(1)--H(1B). ..O(5)	0.88	2.02	2.710(5)	134	1/2-x,1/2+y,1/2-z
O(7)--H(6E)...O(9)	0.87	2.13	2.899(12)	147	-x,1-y,1-z
O(8)--H(8A)...O(5)	0.87	2.02	2.832(6)	155	x,1+y,z
O(8)--H(8B)...O(8)	0.87	2.09	2.803(6)	138	
O(9)--H(9A)...O(2)	0.87	2.00	2.844(8)	163	1/2-x,1/2-y,1-z
C(7) --H(7A) ..O(4)	0.99	2.52	3.238(6)	129	1/2-x,1/2+y,1/2-z
C(9) --H(9) ..O(1)	0.95	2.56	3.423(6)	151	1/2-x,1/2+y,1/2-z
C(11) --H(11) ..O(6)	0.95	2.57	3.260(8)	130	x,-1+y,z
C(14) --H(14A) ..O(3)	0.99	2.52	3.339(5)	140	
C(17) --H(17) ..O(3)	0.95	2.55	3.246(5)	130	1/2-x,-1/2-y,1-z

[a]Numbers in parenthesis are estimated standard deviations in the last significant digits.

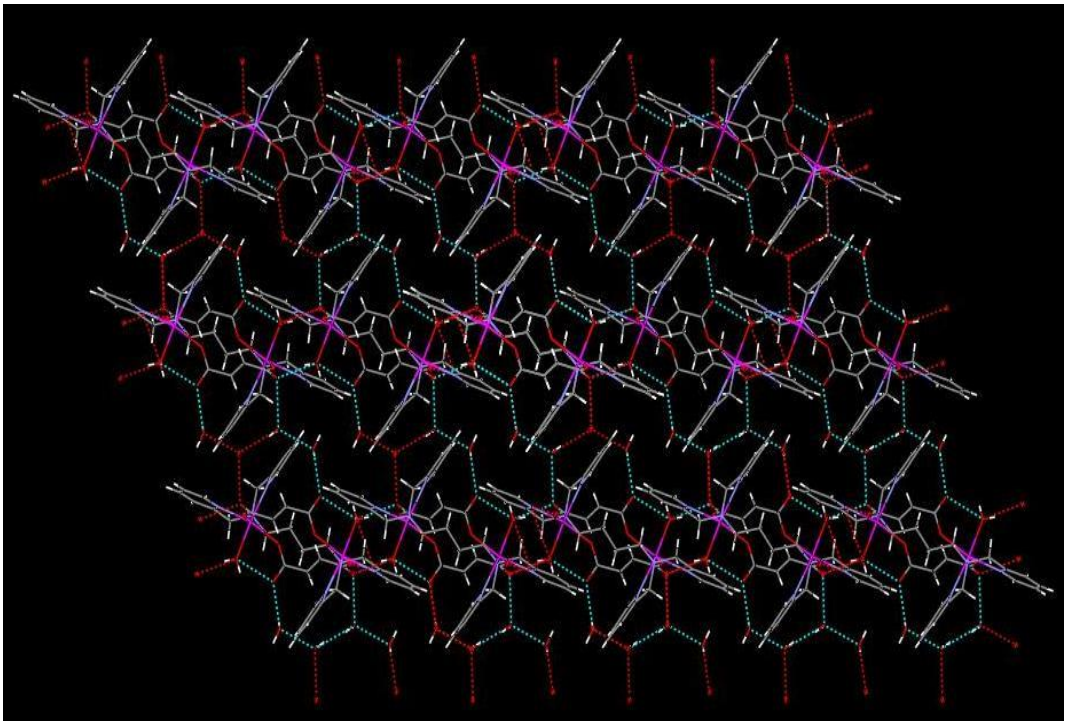

Figure 3.108. 3D Supramolecular assembly in **50**.

Effect of N-Donor Ligands. In this study, seven hexadentate polypyridyl ancillary ligands differing in methylene chain lengths between the alkyl nitrogens have been used to investigate the formation of products in the Mn(II)-adc system under similar reaction conditions. With two methylene groups for the tpen and 1,2-tppn ligands, it is anticipated due to chelating effect to have a 1:1 complex with the Mn(II) ion; thus, the formation of **43a** and **44a** is not a surprise. As the chain length increased from three to four to five (tppn, tpbn and tppen, respectively) which reduces the chelating effect, the spanning of the hexadentate ligands between two Mn(II) centers is the result in **41a, 42** and **45**. However, the remaining three coordination sites on each Mn(II) center have different ligand binding (adc and/or water) providing the diversity of product formation. With four methylene groups in tpbn, a polymeric bis(monodentate adc) bridged structure of **41** is obtained where each Mn(II) center has one water molecule. On the other hand, each Mn(II) center in **42** and **45** has three and two coordinated water molecules, respectively, allowing no coordinated adc in **42** and one coordinated adc in **45**; in both cases adc acts as a counter anion. Interestingly, upon further increase in the methylene chain length (tpxn and tphn) products (**46** and **47**, respectively) similar to **45** are obtained. For the tppn and tppen ligands, the

role of the adc anion in the product formation is important and further demonstrates the effect of the methylene chain length in determining the structure of such MOCNs.

$\{[Mn_2(tpbn)(oxalate)(H_2O)_2](ClO_4)_2\}_n$ (**51**). It is a cationic 1D CP that crystallizes in the triclinc *P-1* space group shown in Figure 3.109. The hexacoordinated Mn(II) center is surrounded by three nitrogens of the ligand, one coordinated water molecule and two oxygens of the oxalate. The oxalate binds in a bis(chelated) fashion. The selected bond distances and angles are listed in Table A64.

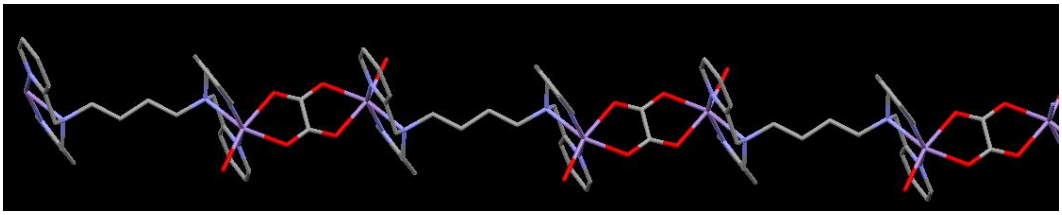

Figure 3.109. A perspective view of **51** (perchlorates and hydrogens are omitted for clarity).

Two chains of 1D Coordination polymers are connected to each other via hydrogen bonding between lattice water molecules, coordinated water molecule on Mn(II) and the uncoordinated carboxylate oxygen as shown in Figure 3.110. In this hydrogen bonding arrangement there are two kinds of hydrogen bonding motifs: $R_6^6(8)$ comprising of O3-O8-O1-Mn-O3′-O8′-O1′-Mn′ and a tetrameric motif $R_4^4(4)$ comprising of O9-O7-O9′-O7′. In the tetrameric motif, two lattice water molecules are hydrogen bonded to perchlorates. As shown in Figure 3.110 below it can be viewed as a small motif sitting inside a big cavity with walls made up of a big motif. The hydrogen bonding distances are listed in Table 3.20.

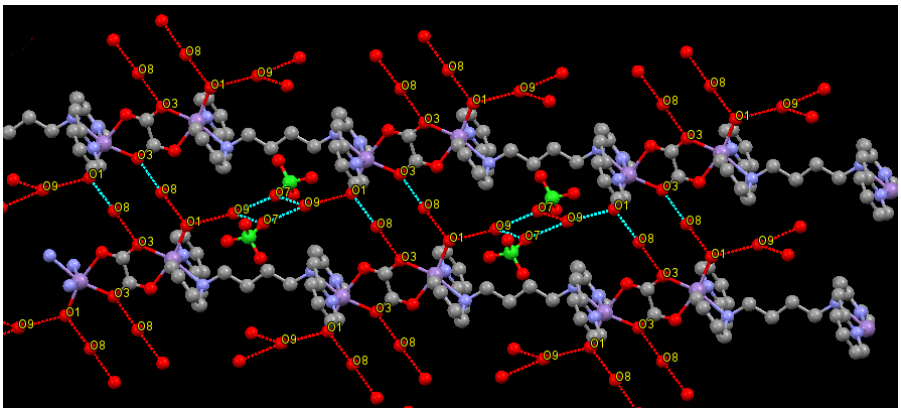

Figure 3.110. Supramolecular Assembly in **51**.

Table 3.20. Hydrogen bonding parameters for **51**.[a]

D–H…A	r (D-H) (Å)	r (H…A) (Å)	r (D…A) (Å)	∠D-H…A (deg)	Symmetry
O(1)--H(1A)...O(8)	0.85	1.93	2.697(6)	150	x,-1+y,z
O(8)--H(8B)...O(6)	0.85	2.4	3.051(7)	134	-x,1-y,1-z
O(9)--H(9A)...O(4)	0.85	2.38	3.064(6)	137	-x,1-y,1-z
O(9)--H(9A)...O(7)	0.85	2.1	2.912(6)	160	-x,1-y,1-z
O(9)--H(9B)...O(1)	0.85	2.18	2.800(5)	130	
C(3)--H(3)...O(9)	0.93	2.47	3.351(7)	157	1-x,-y,-z
C(4)--H(4)...O(6)	0.93	2.59	3.332(7)	137	1+x,y,-1+z

[a]Numbers in parenthesis are estimated standard deviations in the last significant digits.

Furthermore, the 1D polymer chains in **51** have π–π interactions in two planes as shown in Figure 3.111. The centroid-centroid distances are 3.659 Å and 3.745 Å.[182]

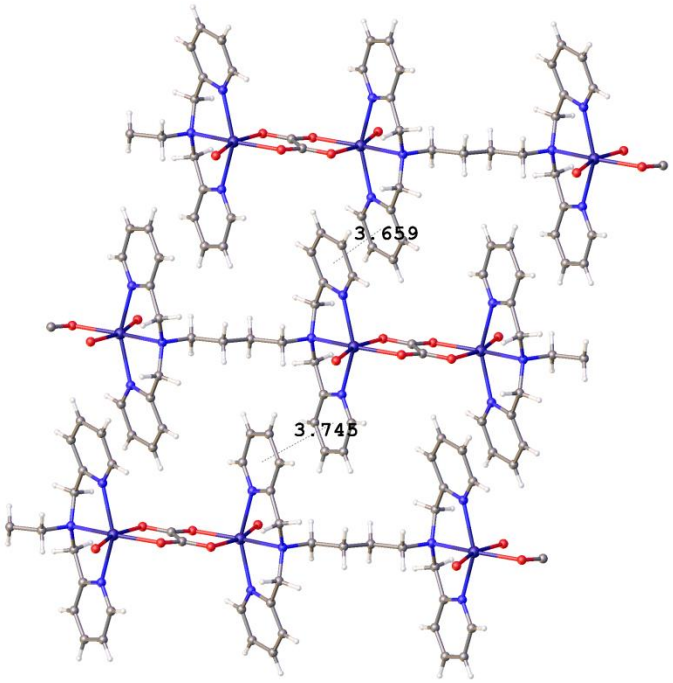

Figure 3.111. Supramolecular assembly in **51** via π–π interactions.

{[Mn(tpbn)](ClO$_4$)$_2$·CH$_3$OH}$_n$ (52). In the literature the structure of Mn(II)-tpbn is not reported. It was predicted to be a mononuclear where its synthesis and spectroscopic characterization was reported.[160d] Based on the structure of **52**, it is found to be a 1D CP that crystallizes in the

monoclinic $P2_1/n$ space group (see Figure 3.112). Each Mn(II) center is hexacoordinated with an N_6 environment due to the spanning tpbn ligand. The selected bond distances and angles are listed in Table A65.

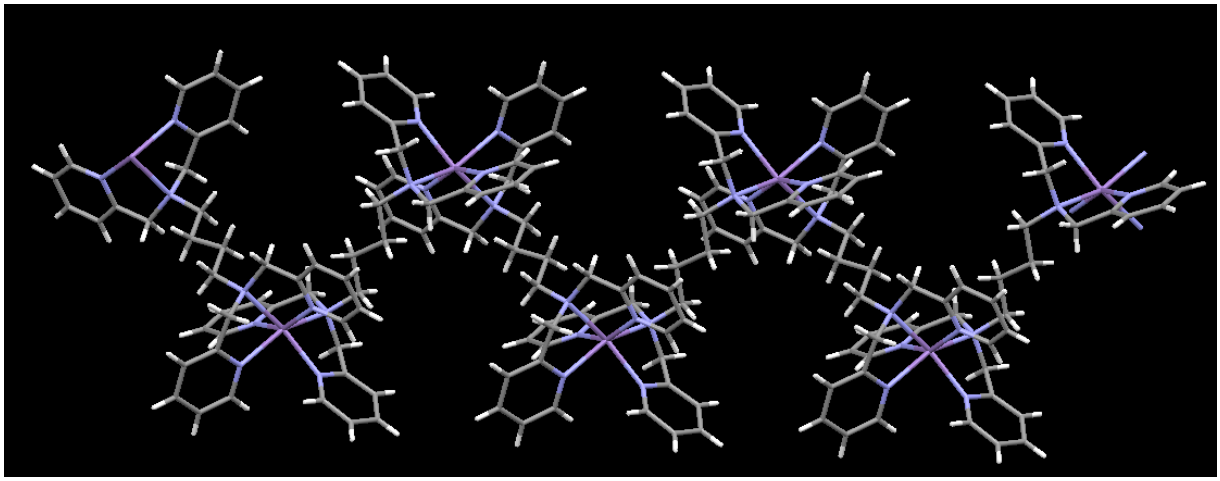

Figure 3.112. A perspective view of **52**.

$[Mn_2(tpbn)(H_2O)_6](tdc)_2.4H_2O\}_n$ (53). It is a discrete dinuclear compound that crystallises in the triclinic *P-1* space group. There are two independent molecules in the asymmetric unit. The dinuculear unit is similar to the one obtained in **42** as can be seen in Figure 3.113. Both the Mn(II) centers are surrounded by three nitrogens of the ligand and three coordinated water molecules. The selected bond distances and angles are listed in Table A66. The orientation of coordinated water molecule is different on the Mn(II) centers. Both thiophene dicarboxylate acts as counter anion. Very few examples are known in the literature having tdc as a counter-anion.[191, 215]

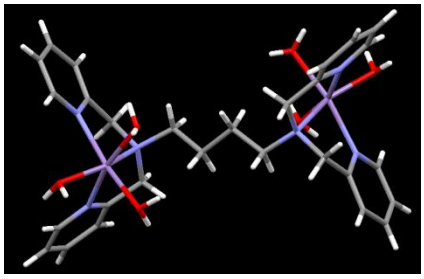

Figure 3.113. Structure of the **[**$Mn_2(tpbn)(H_2O)_6$] subunit in **53**.

A part of supramolecular assembly in **53** is shown in Figure 3.114. Two dinuclear subunits are connected with each other via hydrogen bonding between coordinated and lattice water molecules and tdc anion. The hydrogen bonding between these results in the formation of two

pentagons (sharing a common side) between the two dinuclear subunits. The hydrogen bonding parameters are listed in Table. In addition to Hydrogen bonding, the supramolecular assembly is further stabilized by C-H…O interactions listed in Table 3.21.

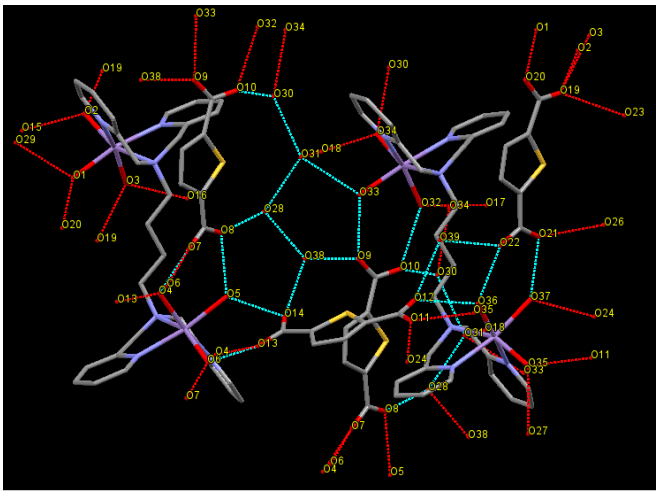

Figure 3.114. Hydrogen bonded network in **53**.

$[Mn_4(tpbn)_2(CDC)_4(H_2O)_4]_n$ (54). It is a porous 2D MOF that crystallizes in the monoclinic $P2_1/c$ space group. A perspective view of **54** is shown in Figure 3.115 Each Mn(II) center of a tetrameric repeat unit is hexacoordianted and surrounded by three nitrogen of the ligand, two oxygen atoms of the carboxylate and one water molecule. Coordinated water molecules on the Mn(II) centers points towards the cavity. The pores can be seen in space-filling model in Figure 3.116. CDC binds in a bis(monodentate) syn-syn fashion bridging between two Mn(II) centers in one direction and the ligand tpbn is spanning between two Mn(II) centers in another direction. This view is better seen in the topological drawing (Figure 3.117); its topology is SP 1-periodic net. The two layers parallel to each other are shown in red and green colors. The other orientations of the layers in **54** are shown in Figure 3.118. Selected bond distances and angles are listed in Table A67. Few examples of CP and MOF containing the CDC linker have been reported in the literature for Cu(II), Ni(II), Co(II), Zn(II), Cd(II), etc. with nitrogen based ligands, like 4,4'-bpy, 1,10-phenanthroline.[122a-f] Ma et al. has reported the 3D hydrogen bonding network of CP of Mn(II)-cdc with an imidazole ligand.[122g]

Table 3.21. Hydrogen bonding parameters for **53**.[a]

D–H…A	r (D-H) (Å)	r (H…A) (Å)	r (D…A) (Å)	∠D-H…A (deg)	Symmetry
O1--H1B...O29	0.87	1.98	2.821(8)	162	x,-1+y,z
O2--H2A ...O15	0.87	1.86	2.701(7)	162	x,-1+y,z
O3--H3A...O19	0.87	2.2	2.891(9)	136	1-x,-y,1-z
O3--H3A...O20	0.87	2.41	3.211(10)	154	1-x,-y,1-z
O4--H4A...O13	0.88	2.12	2.725(6)	125	1-x,-y,1-z
O4--H4B...O7	0.88	1.99	2.631(7)	129	
O5--H5B...O8	0.89	1.91	2.770(7)	162	
O6--H6B...O13	0.87	1.76	2.592(6)	158	
O23--H23B...O16	0.87	2.13	2.921(7)	151	x,-1+y,1+z
O24 --H24B...O11	0.87	1.88	2.740(8)	170	2-x,1-y,1-z
O25 --H25B...O20	0.87	2.47	3.086(14)	129	1-x,1-y,1-z
O26 --H26A...O25	0.87	1.77	2.636(14)	175	
O26--H26B...O29	0.87	2.03	2.848(11)	156	
O27 --H27...O35	0.84	2.01	2.793(17)	154	
O29--H29C...O23	0.87	2.04	2.784(8)	143	
O30--H30C...O34	0.87	1.97	2.811(7)	161	1-x,1-y,-z
O30--H30D...O10	0.87	2.03	2.849(7)	156	
O31--H31C...O28	0.87	1.85	2.708(8)	166	
O31--H31D...O18	0.87	1.92	2.741(6)	158	1-x,1-y,-z
O32--H32A...O17	0.87	1.94	2.681(6)	143	1+x,y,z
O33--H33B...O9	0.88	1.84	2.684(6)	160	1+x,y,z
O34--H34B...O18	0.88	1.82	2.654(6)	159	1-x,1-y,-z
O35 --H35A...O11	0.87	1.91	2.637(8)	140	2-x,1-y,1-z
O36--H36A ...O22	0.87	1.81	2.588(8)	147	
O36--H36B...O35	0.87	2.33	3.103(7)	147	2-x,1-y,1-z
O38--H38C...O14	0.87	1.96	2.804(8)	163	
O39--H39A...O22	0.87	1.88	2.65(2)	146	
C9 --H9...O16	0.95	2.4	3.323(8)	165	
C15--H15...O20	0.95	2.59	3.316(11)	134	x,y,-1+z
C21--H21...O7	0.95	2.57	3.422(8)	149	1-x,-y,1-z
C28--H28A...O17	0.99	2.39	3.363(8)	166	1+x,y,z
C31 --H31B...O12	0.99	2.48	3.458(8)	168	
C36--H36...O12	0.95	2.59	3.515(12)	164	1+x,y,z
C49 --H49...O32	0.95	2.6	3.522(8)	164	2-x,1-y,-z
C54 --H54...O17	0.95	2.46	3.196(8)	134	
C76 --H76 ...O25	0.95	2.3	3.238(16)	167	1-x,1-y,1-z
C80 --H80...O11	0.95	1.91	2.75(2)	146	

[a]Numbers in parenthesis are estimated standard deviations in the last significant digits.

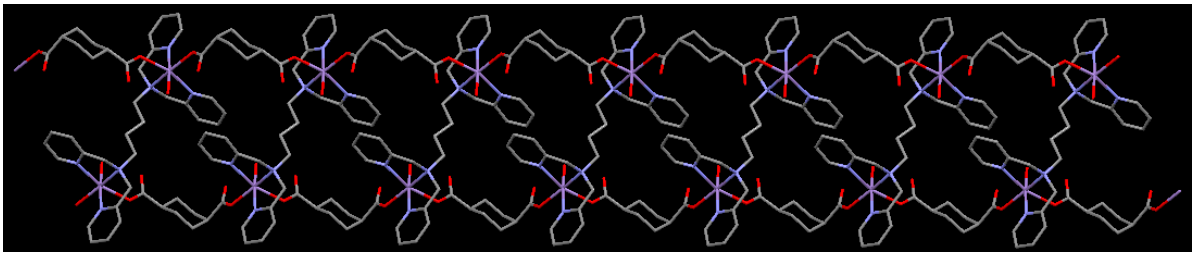

Figure 3.115. A perspective view of **54**.

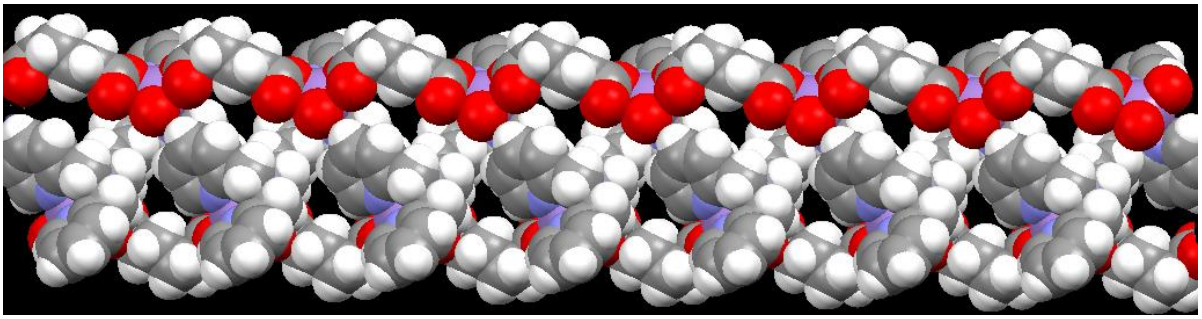

Figure 3.116. Space-filling model of 2D MOF of **54** showing pores.

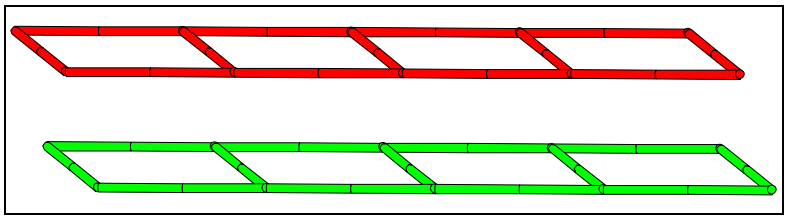

Figure 3.117. A topological view of **54**.

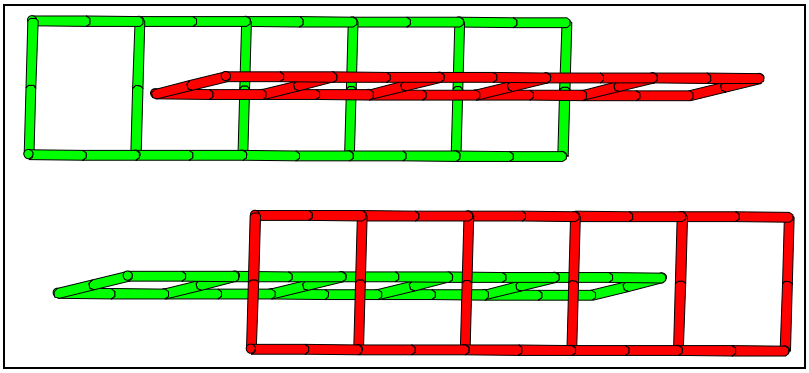

Figure 3.118. Another topological view of **54.**

Powder X-ray data Analysis. In order to confirm whether the single crystal structure corresponds to the bulk material and phase purity, powder X-ray diffraction patterns for all were

recorded at room temperature. The experimental and simulated X-ray patterns for **41a, 41b** and **42** are shown in Figure 3.119a. The simulated pattern for **41b** matches with the experimental patterns for **41a** and **41b**. This confirms that the single crystal and bulk material are the same and the compound with water (**41a**) and methanol (**41b**) as solvent of crystallization are isostructural. The experimental and simulated X-ray patterns for **43a**/**43b** and **44a**/**44b** are compared to show their isostructural behavior.

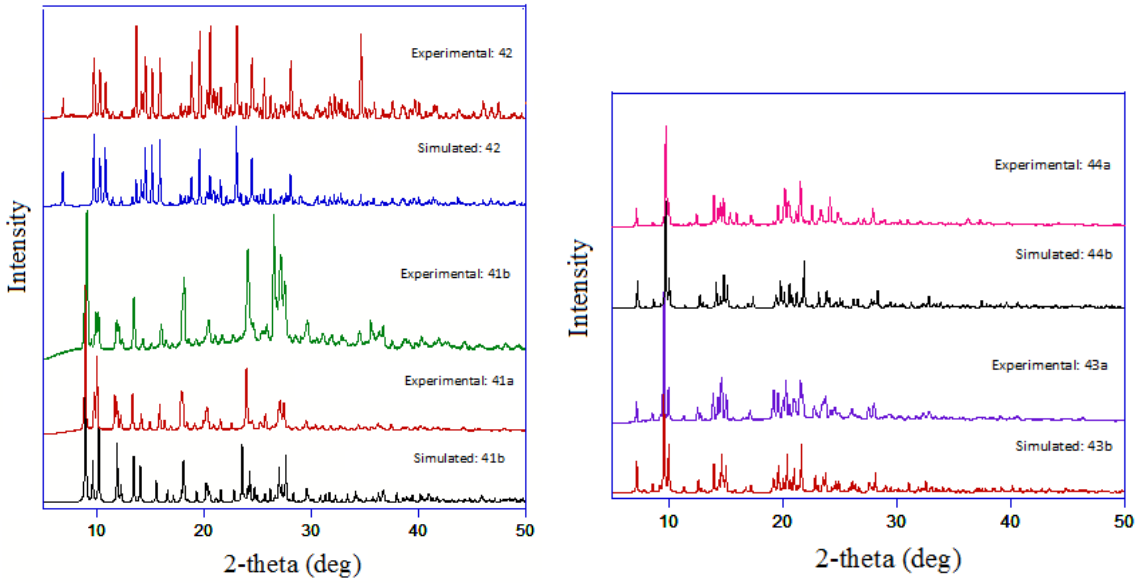

Figure 3.119a. Experimental and simulated X-ray powder patterns of **41, 42, 43** and **44**.

The experimental powder pattern for **50** is shown in Figure 3.119b. There appears to have a shift of the peaks as well as appearance of a couple of new peaks compared to the simulated one. This could be due to different solvation of the bulk sample compared that found in the single crystal.

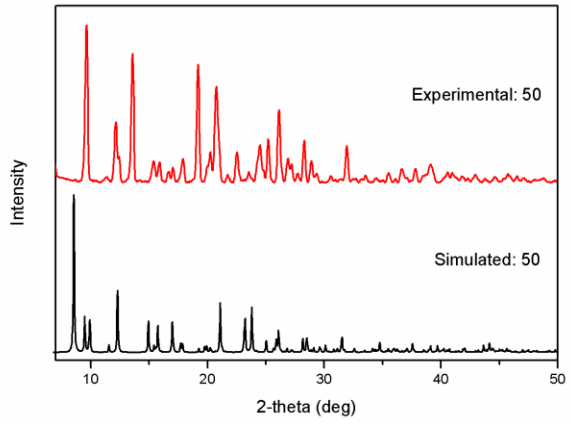

Figure 3.119b. Experimental and simulated X-ray powder patterns of **50**.

FTIR and Raman Spectroscopy. The IR spectra of **41, 42** and **45** were recorded in the solid state show a band centered at 3392 cm^{-1} which is a characteristic feature for O-H stretching frequency of the lattice water molecule. Another band in this region centered at 3203 cm^{-1} (**41**), 3230 cm^{-1} (**42**) and 3220 cm^{-1} (**45**) is due to coordinated water molecules. In contrast, there is only one band centered at 3430 and 3446 cm^{-1} for **43** and **44**, respectively, due to lattice water molecules clearly indicating that in both these compounds Mn(II) does not have a bound water molecule. These spectra also have a series of bands between 1610 and 1310 cm^{-1}. While some of these features are due to the tpbn ligand, bands at 1570 and 1351 cm^{-1} are due to asymmetric and symmetric stretching modes of the carboxylate groups of adc, respectively, in case of **41**. A value of 219 cm^{-1} for the difference in the asymmetric and symmetric stretching modes is indicative of monodendate binding of the carboxylate groups of adc in **43** as found in the crystal structure. For **44**, the asymmetric and symmetric stretching frequencies for the carboxylate group of the uncoordinated adc are at 1572 and 1330 cm^{-1}, respectively. Other features in the spectra for **43** and **44** are similar to those in **41** with a shift of few wave numbers in each case. For **45**, the asymmetric and symmetric stretching frequencies for the carboxylate group are at 1626, 1570 and 1329 cm^{-1}, respectively, for the uncoordinated and coordinated adc. The second most important difference in the FTIR spectra for the complexes is the absence of perchlorate ion peaks in **41** (a neutral compound), **42** and **45** (with adc as counter ions in both) whereas in **42** and **43** perchlorate peaks are found to be present at 1090, 623 and 1087, 623 cm^{-1}, respectively. For **46** and **47** the peaks at 3433, 3226 cm^{-1} and 3434 cm^{-1} corresponds to the O-H stretching frequency. The peaks at 1627, 1587 and 1333 cm^{-1} (**46**) and 1627 and 1345 cm^{-1} (**47**) correspond to the asymmetric and symmetric stretching frequencies for the carboxylate group, respectively. The IR spectrum of **49** showed peaks at 3434 cm^{-1} (O-H stretch), 1571 and 1379 cm^{-1} are due to asymmetric and symmetric stretch of the carboxylate, 1089 and 625 are due to the perchlorate anions. The IR spectrum for **51** showed peaks at 3468 cm^{-1} (O-H stretch), 2946 cm^{-1} (C-H stretch), 1572 and 1313 cm^{-1} are due to asymmetric and symmetric stretch of the carboxylate, the peaks at 1606, 1484, 1444 and 765 cm^{-1} are due to the ligand and peaks at 1093 and 622 cm^{-1} corresponds to the perchlorate anion. The IR spectrum of **53** showed peaks at 3392 and 3220 cm^{-1} correspond to two kinds of O-H stretch which also suggest two kinds of water molecules as evident from its solid state structure, the peaks at 1570 and 1482 cm^{-1} correspond to the asymmetric and symmetric stretch of the carboxylate. The IR spectrum of **54** showed a peak at

3403 cm^{-1} is due to the O-H stretching frequency, peaks at 1654, 1396 correspond to the asymmetric and symmetric stretch of the carboxylate. Although **54** is a neutral compound, IR shows peak at 1122 cm^{-1} and 618 cm^{-1} that can be due to the $MnSO_4$ left as found from elemental analysis too.

All but **45, 46 and 47** were studied by Raman spectroscopy (see Figure 3.120); several attempts failed to obtain the Raman spectra of **45, 46** and **47**. For **41** it shows a peak at 2216 cm^{-1} for the C-C triple bond while the other features for the tpbn ligand and the carboxylate groups of adc (1573 and 1389 cm^{-1}) are similar to its IR spectrum. Similarly, Raman spectra of **42**, **43** and **44** show peaks at 2206, 2207 and 2213 cm^{-1}, respectively, for the C-C triple bond.[94a,181] However, the intensity of the peak is much lower for **42**, **43** and **44** compared to **41**. This may be explained for the fact that the association of the adc is different in these complexes. While **41** is a polymer with two adc molecules bridging between the two Mn(II) ions, **42** is a supramolecular assembly with adc not bound to the Mn(II) ions and **43** and **44** are discrete dinuclear complexes with one bridging adc between the two Mn(II) ions. This study correlates well with findings from other characterization techniques.

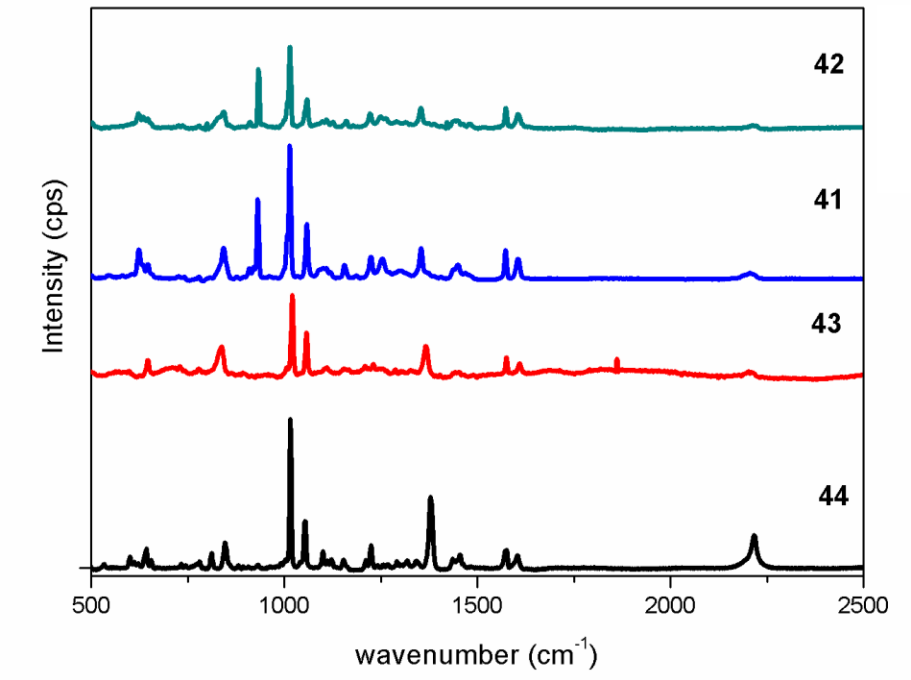

Figure 3.120. Raman spectra for **41, 42, 43** and **44**.

Thermogravimetric Analyses. For studying the thermal stability as a function of temperature, thermogravimetric analyses (TGA) were conducted for the single phase polycrystalline samples of **41a** and **42** between 25-500 °C under dinitrogen atmosphere. From the multi-step decomposition process for **41a** (Figure 3.121), it is clearly evident that lattice water molecules are lost first followed by the coordinated water molecules and the adc linker. The first weight loss of 3.08% between 50-100 °C corresponds to one and a half lattice water molecules (ca. 3.15%). The second weight loss of 5.02 % between 100-175 °C corresponds to one half lattice water molecule and two coordinated water molecules (ca. 5.45%). The third weight loss of 33.95% between 175-450 °C indicates further decomposition of the dehydrated species. For **42** (Figure 3.122), the first weight loss of 10.90% observed between 45-105 °C corresponds to three free and three coordinated water molecules (ca. 11.61%). The second weight loss of 11.07% between 105-155 °C corresponds to decomposition one acetylene dicarboxylic acid (ca. 12.20%). The third weight loss of 50.33% between 155-450 °C corresponds to three coordinated water molecules and one tppn ligand (ca. 52.67%). This shows how strongly water molecules are hydrogen bonded with acetylene dicarboxylates in **2**. For **45** (Figure 3.123), the first weight loss of 7.99% observed between 35-80 °C corresponds to loss of four lattice water molecules (ca. 7.77%). The second weight loss of 21.14% between 80-190 °C corresponds to four coordinated water molecules and one acetylene dicarboxylic acid (ca. 19.70%). The third weight loss of 41.32% between 190-400 °C indicates further decomposition of the dehydrated species. Thermal behavior of all these compounds is in very good agreement with the X-ray studies as well as the FT-IR spectroscopic data. The TGA scan of **54** is a three step profile shown in Figure 3.126 (right). After the loss of water molecules in Step-1, this compound is stable up to ca. 250 °C followed by further decomposition. The TGA scan of 50 (Figure 3.126 left) is a two step profile. First step corresponds to the loss of water molecules followed by loss of fumaric acid molecule in step 2. The TGA scan of **53** shown in Figure 3.125 is a two-step profile, the first loss of 25.39 % between 25–160 °C corresponds to the loss of four lattice water molecules and one molecule of thiophene dicarboxylic acid (ca. 27%) followed by decomposition of the molecule in second step. TGA of **42a**, **43a**, **49**, **51** and **52** were not carried out as these contain perchlorate anions.

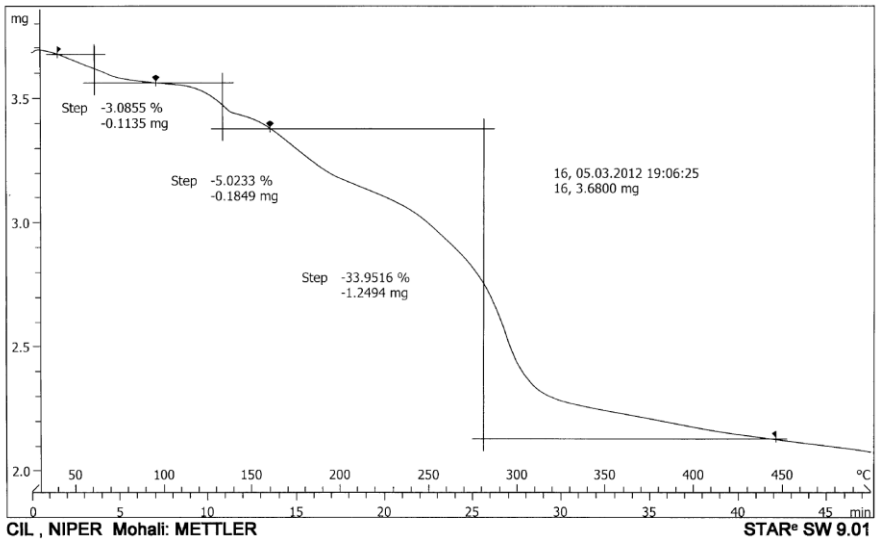

Figure 3.121. TGA scan of **41a**.

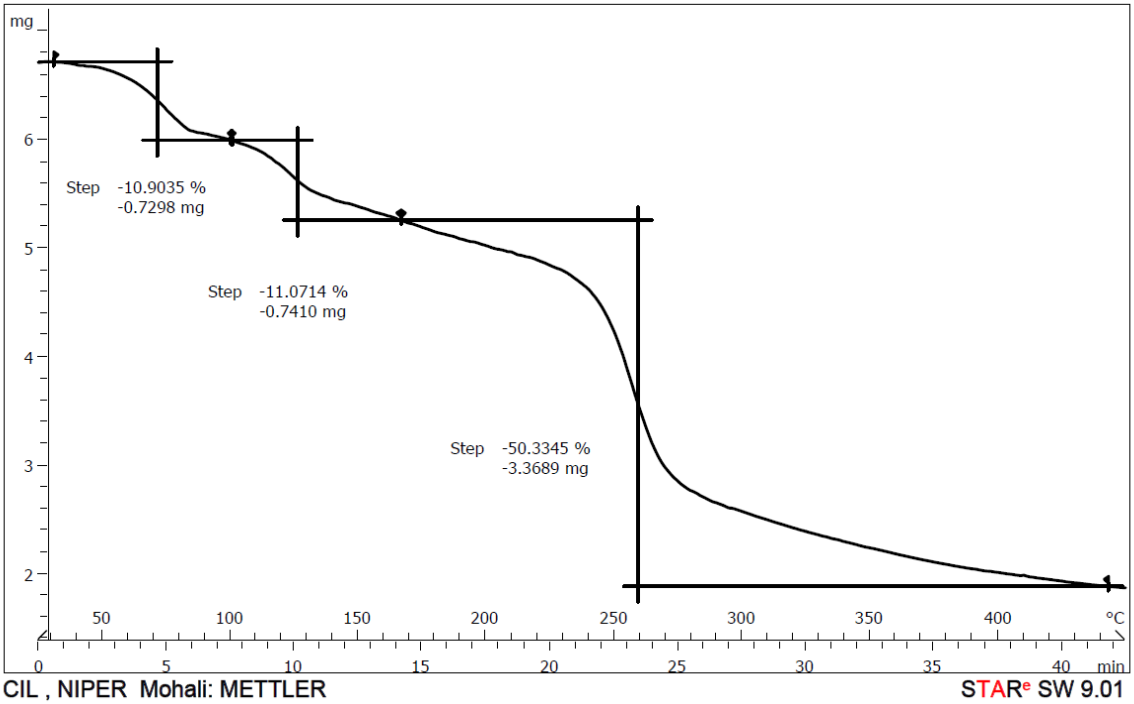

Figure 3.122. TGA scan of **42**.

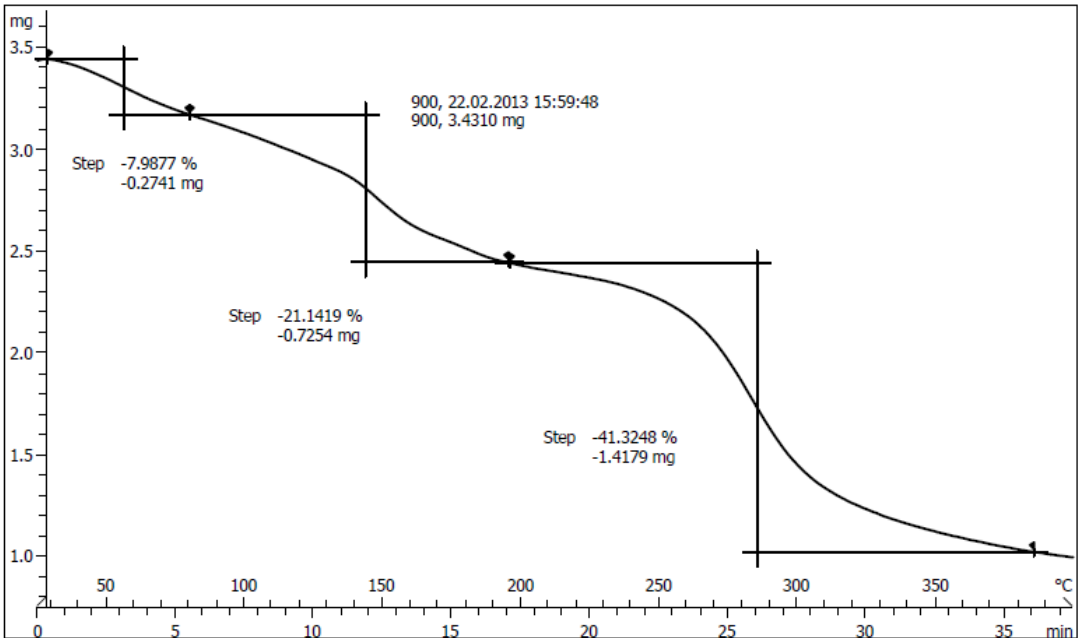

Figure 3.123. TGA scan of **45**.

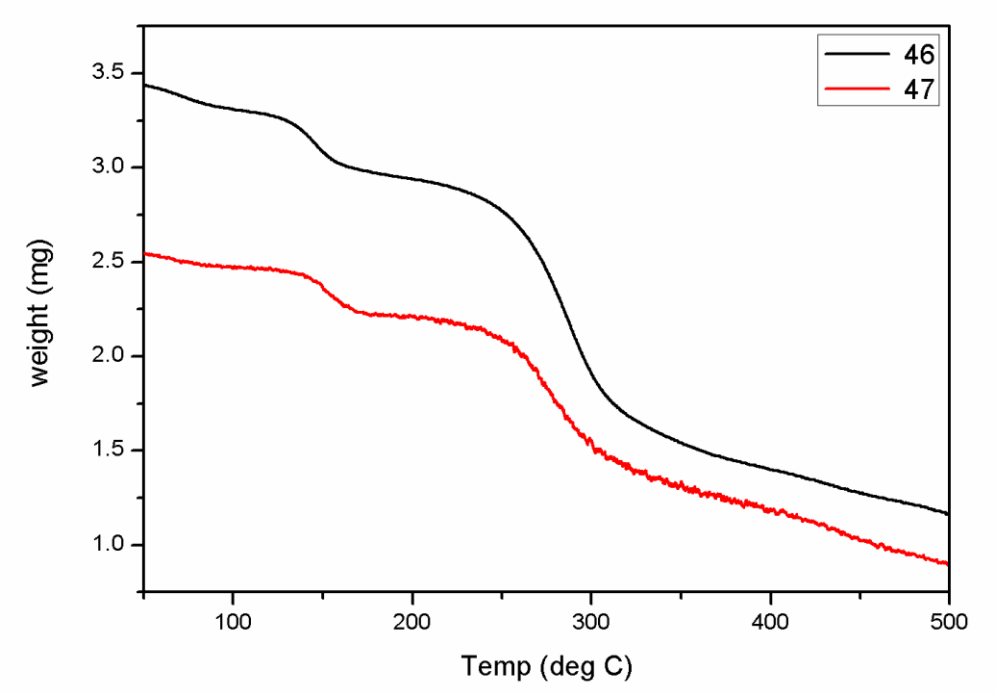

Figure 3.124. TGA scans of **46** and **47**.

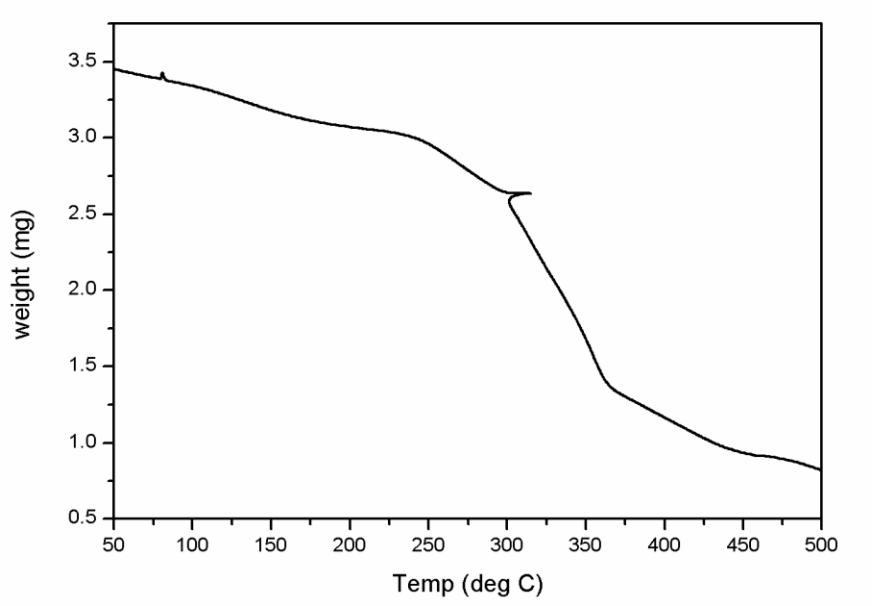

Figure 3.125. TGA scan of **53**.

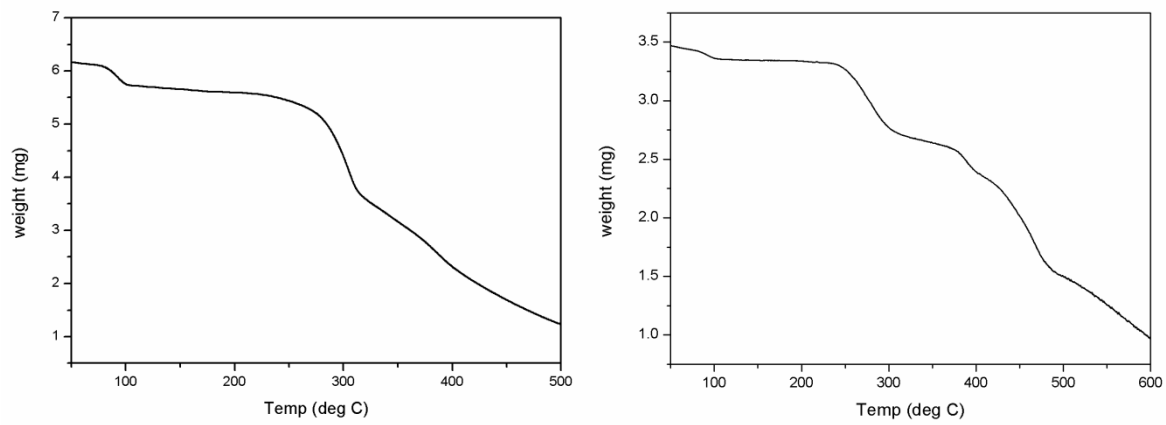

Figure 3.126. TGA scans of **50** (left) and **54** (right).

Tricarboxylate linker

Utilizing hydrothermal reaction conditions, for H_3BTC and its cycloaliphatic analog, H_3CTC, different products are obtained: a 3D coordination polymer $[Mn_2(tpbn)(HBTC)]_n$ forming a chair like structure with Mn(II) centers acting as nodes; a tetrameric compound, $[Mn_4(tpbn)_2(HCTC)_2(SO_4)_2]$, that forms a supramolcular assembly.

Synthesis. Reactions of Mn(II)/tricarboxylates were done under hydrothermal conditions and products were obtained in the crystalline form. The crystals obtained were collected, washed with methanol and ether, and dried under vacuum. Scheme 20 summarizes their syntheses.

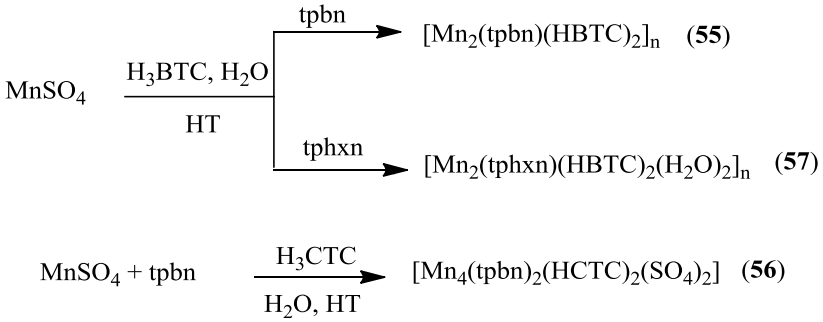

Scheme 20. Synthesis of **55-57**.

Single Crystal Structure Analysis. Single crystals obtained from hydrothermal reactions were suitable for X-ray studies.

$[Mn_2(tpbn)(HBTC)_2]_n$ (55). It is a 3D CP that crystallises in the monoclinic *$P2_1/n$* space group. Each hexacoordinated Mn(II) center is surrounded by three nitrogens of the ligand, one monodentate carboxylate and one chelated carboxylate. The third carboxylate end of BTC is protonated. The selected bond distances and angles are listed in Table A68. As shown in Figure 3.127, this coordination polymer grows in such a way that it forms a chair like configuration. On each corner of this chair is occupied by a Mn(II) and arms of this chair is constituted by the alkyl chain of the ligand and two carboxylate ends of BTC alternatively. An Mn(II)-BTC compound is reported in the literature[121e] but none of these has a chair-like configuration which was obtained using a spanning hexadentate ligand in **55**.

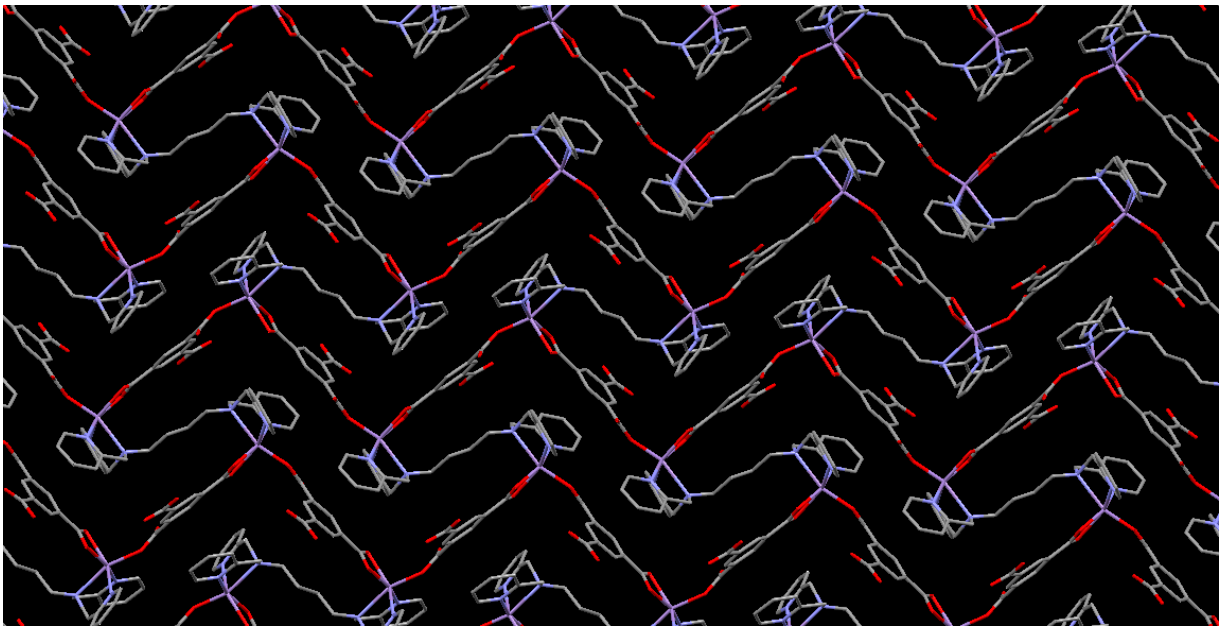

Figure 3.127. A perspective view of **55**.

[Mn_4(tpbn)(HCTC)$(SO_4)_2$] (**56**). It is a discrete tetrameric bis(μ-dicarboxylato)(μ-sulphato) Mn(II) complex that crystallizes in the monoclinic $P2_1/n$ space group. Each Mn(II) center is surrounded by three nitrogens of the ligand, two oxygens from two bridging carboxylate ends of the CTC and one oxygen of the bridging sulphate (see Figure 3.128). The selected bond distances and angles are listed in Table A69. Most of the compounds reported in the literature with CTC are with lanthanides.[216] Qiu et al. has reported Zn(II) and Cd(II) containing MOFs: $[Cd_3(CTC)_2(TED)(H_2O)_2\cdot(H_3O)_2Cl_2]$, $[Cd_3(CTC)_2(bpy)(DMF)_2\cdot(DMF)(H_2O)_2]$, $[Cd_3(CTC)_2(bpe)(DMF)_2\cdot(DMF)(H_2O)_2]$, $[Zn_3(CTC)_2(4,4'\text{-bpy})\cdot(DMF)(H_2O)_2]$, and $[Zn_3(CTC)_2(bpe)\cdot(DMF)(H_2O)_2]$.[217] A Mn(II) containing MOF is also reported $[Mn_3(tib)_2(CTC)_2]$, where tib is 1,3,5-tris(1-imidazolyl)benzene.[218] All these compounds are polymeric in nature. To the best of our knowledge, a discrete molecule with CTC is not reported in the literature.

One end of the $HCTC^{2-}$ is strongly hydrogen bonded to the uncoordinated sulphate oxygens (distance: 2.605 Å, angle: 168°) resulting in a 3D supramolecular assembly shown in Figure 3.129.

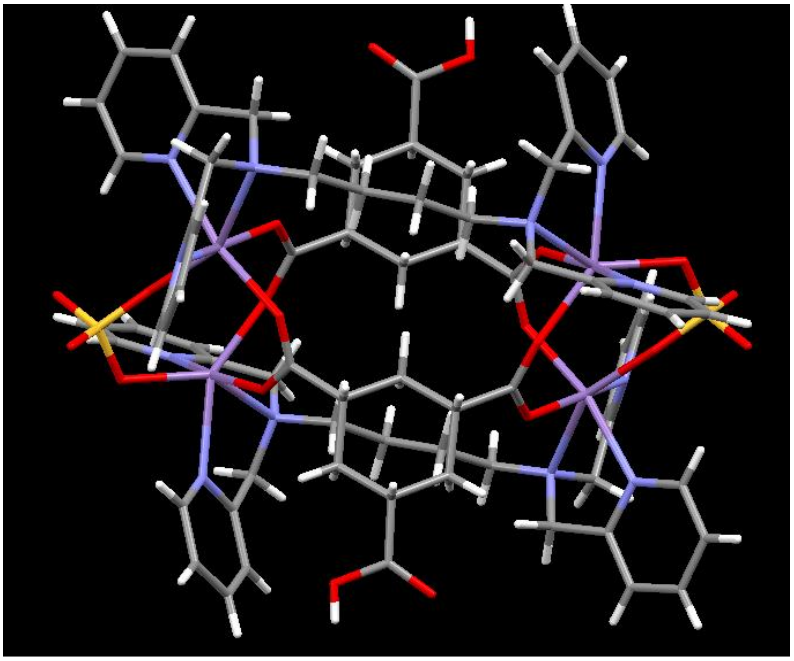

Figure 3.128. A view of the discrete tetranuclear Mn(II) complex, **56**.

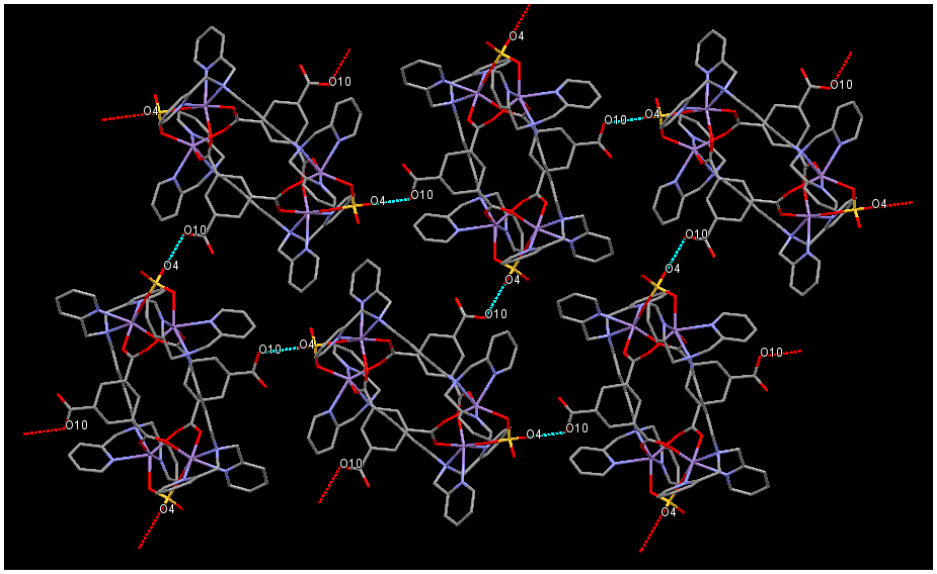

Figure 3.129. Supramolecular assembly of the discrete tetranuclear unit in **56**.

$[Mn_2(tphxn)(HBTC)_2(H_2O)_2]_n$ (**57**). Its overall structure is similar to $[Mn_2(tpbn)(HBTC)]_n$ with a difference in the Mn(II) coordination environment (Figure 3.131). In this case, the Mn(II) center is surrounded by three nitrogens of the ligand, two oxygen atoms of the two monodentate carboxylates and one coordinated water molecule which is absent in **55**. This example again

shows the importance of methylene chain length between the alkyl nitrogens of the ligand. The selected bond distances and angles are listed in Table A70. A part of **57** is shown in Figure 3.130, where O6 and O4 belongs to the BTC and O5 is coordinated water.

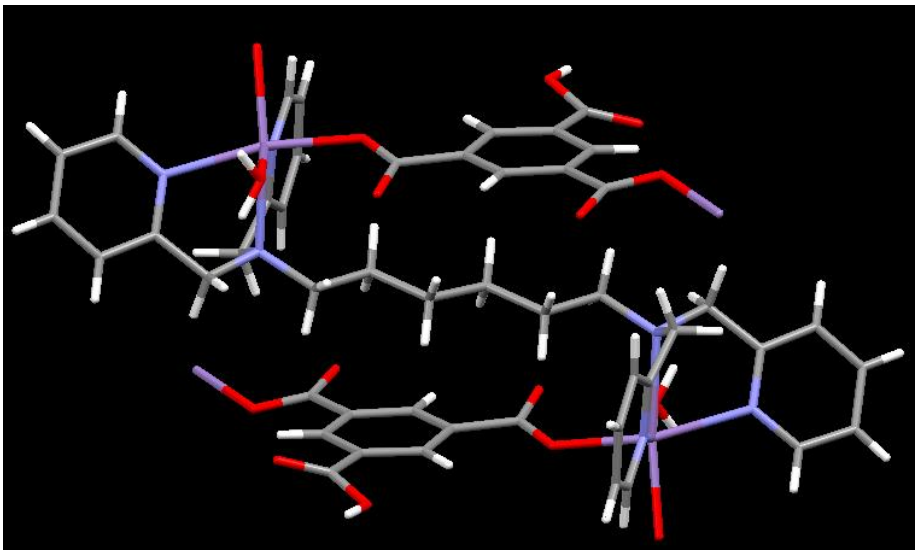

Figure 3.130. Coordination environment around Mn(II) in **57**.

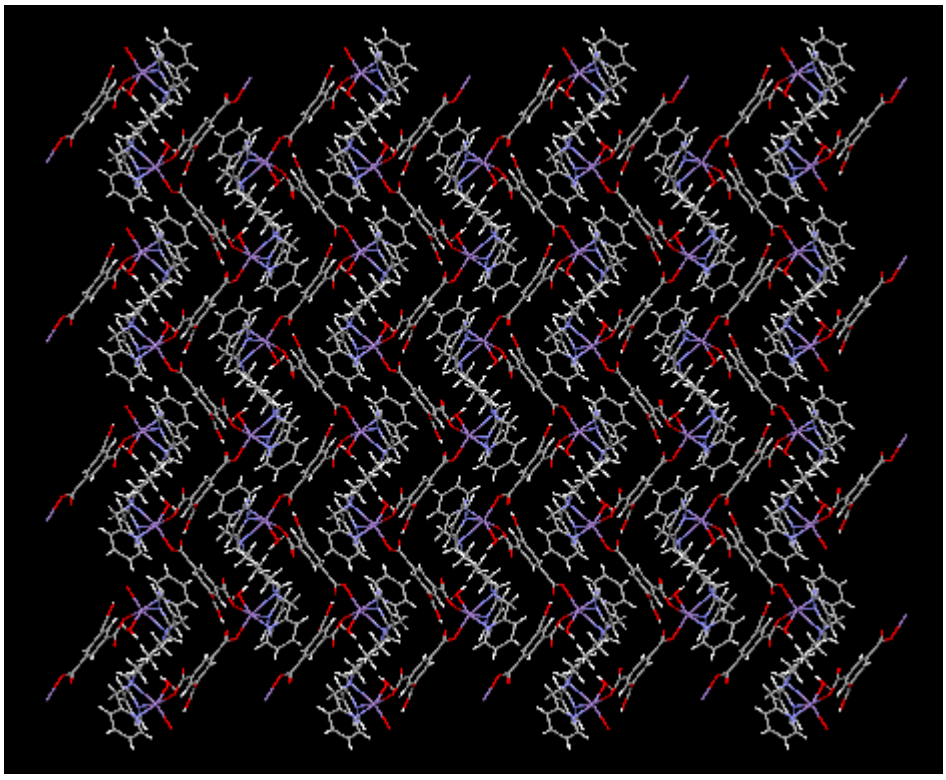

Figure 3.131. A perspective view of **57**.

Its Topology is hcb; Shubnikov hexagonal plane net shown in Figure 3.132. As described above, its chair shaped configuration gives the followings: Mn point symbol is {6^3} and extended point symbol is [6.6.6]; point symbol for net is {6^3},3-c net - uninodal net.

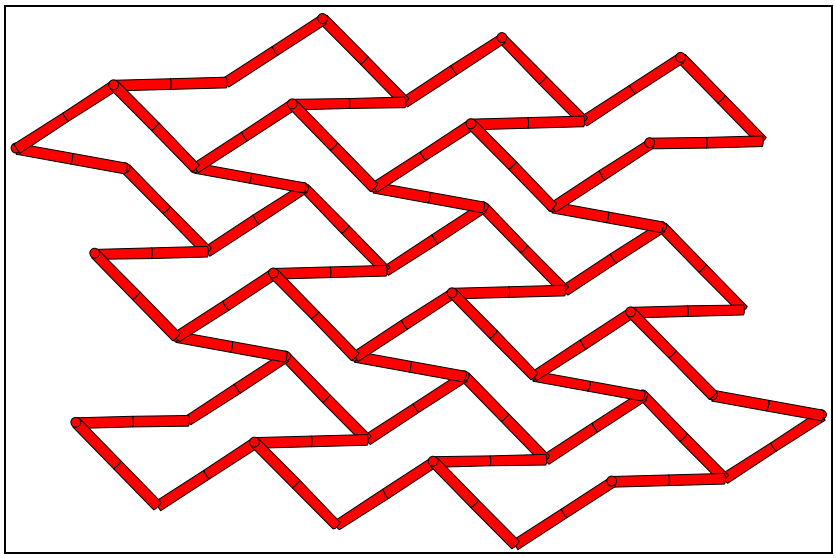

Figure 3.132. A topological view of **57**.

FTIR Spectroscopy. The IR spectra of all three compounds was recorded in solid state as KBr pellets. The peaks at 3448 cm^{-1} (**55**), 3421 cm^{-1} (**56**) and 3479 cm^{-1} (**57**) correspond to the O-H stretching frequency. FTIR was very helpful in determining the protonated carboxylic acid group in all three compounds. The peaks at 1717 cm^{-1} (**55**), 1636 cm^{-1} (**56**) and 1707 cm^{-1} (**57**) correspond to the stretching frequency of the protonated carboxylic acid group. The peaks at 1659, 1618, 1382, 1372 cm^{-1} (**55**); 1574, 1364 cm^{-1} (**56**); 1570 and 1382 (**57**), correspond to the asymmetric and symmetric stretch frequency of the carboxylate. The peaks at 1605, 1292, 767, 678 cm^{-1} with a shift by few numbers are common in all the three spectra due to the ligand.

Thermogravimetric analysis. The stability of these compounds were determined by thermogravimetric analysis. The CP **55** and **57** were analysed between 50-500 °C whereas **56** was analysed between 50-450 °C. All TGA scans are shown in Figure 3.133. Compound **55** was stable up to ca. 250 °C wheras for **57** after loss of water molecules between 100 to 150 °C is stable up to 250 °C followed by continuous loss. The TGA scan of **56** is a two step profile, after loss of surface mositure in Step-1 it is stable up to 300 °C followed by decomposition.

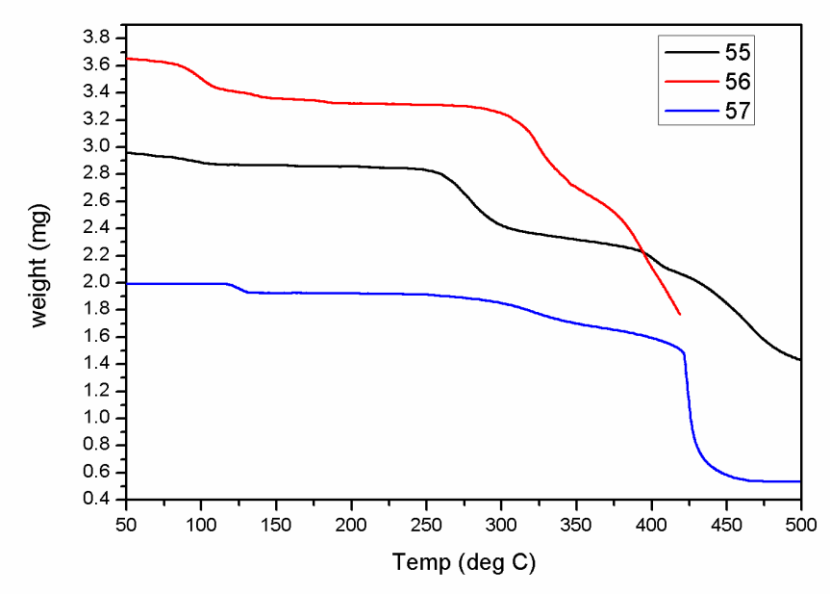

Figure 3.133. TGA scans of **55**, **56** and **57**.

3.2.3.2 *Cu(II) Chemistry*

Dicarboxylate linkers

Synthesis. All copper (II) compounds with different polypyridyl ligands and dicarboxylates have been prepared by one pot self-assembly reaction of a copper salt, the ligand and the respective carboxylate in an appropriate ratio at ambient conditions. All products were obtained as precipitates except **61**, **79**, and **80**. Schemes 21- 29 summarize their synthesis.

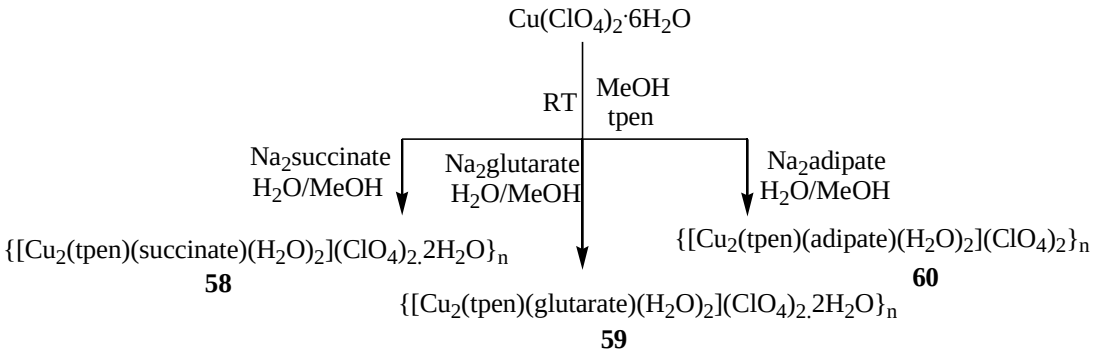

Scheme 21. Synthesis of **58-60**.

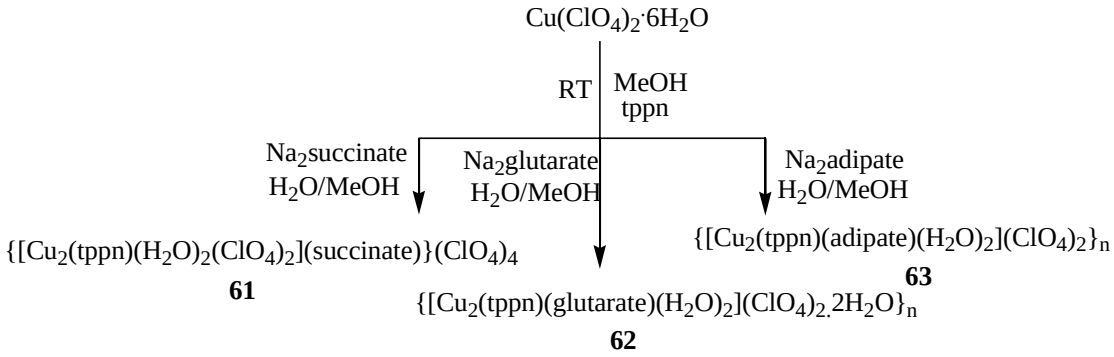

Scheme 22. Synthesis of **61-63**.

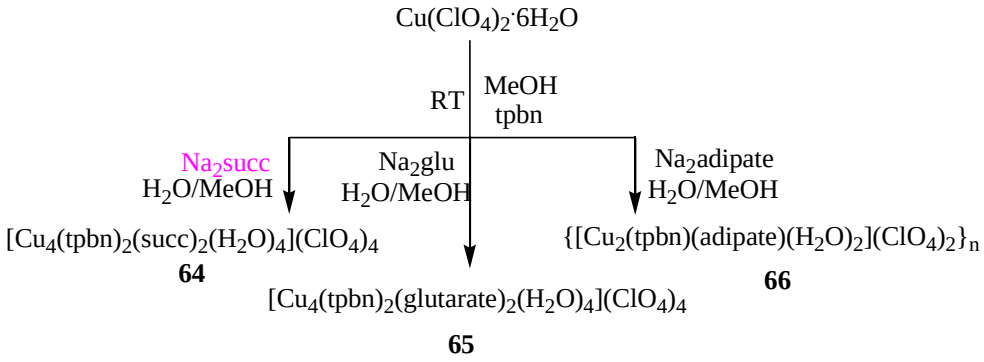

Scheme 23. Synthesis of **64-66**.

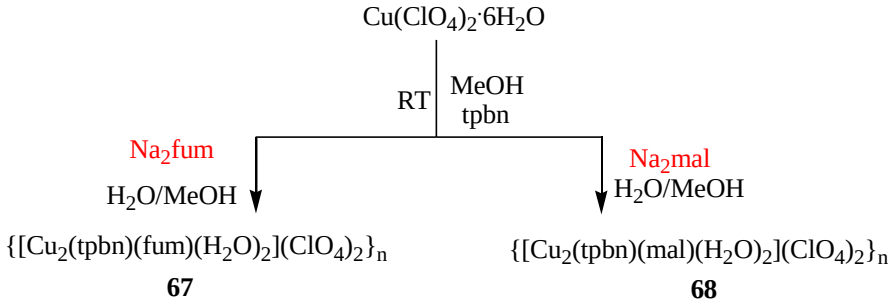

Scheme 24. Synthesis of **67-68**.

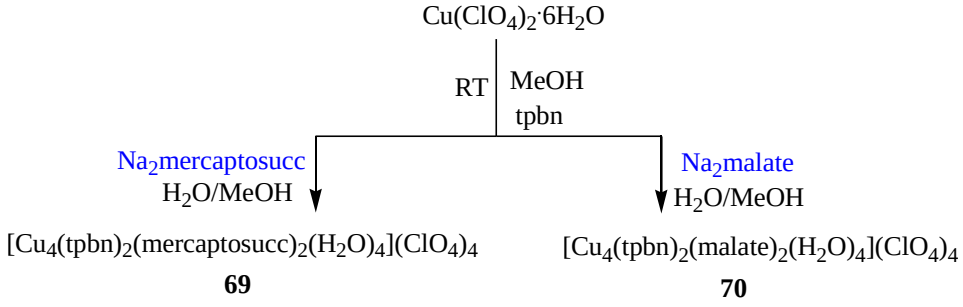

Scheme 25. Synthesis of **69-70**.

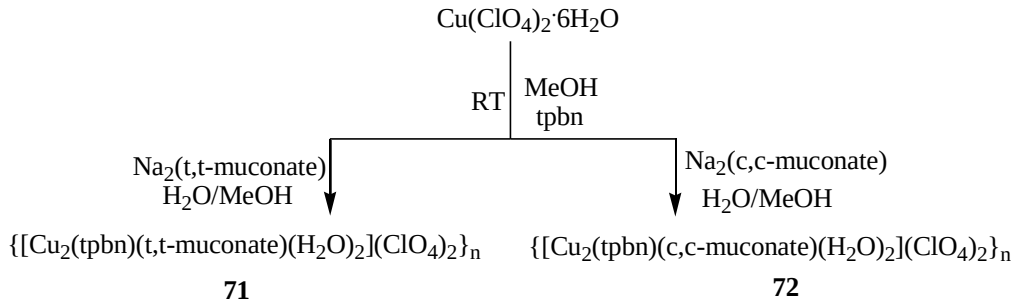

Scheme 26. Synthesis of **71-72**.

Using the tphxn ligand, **73** was synthesized in a similar way to **64**.

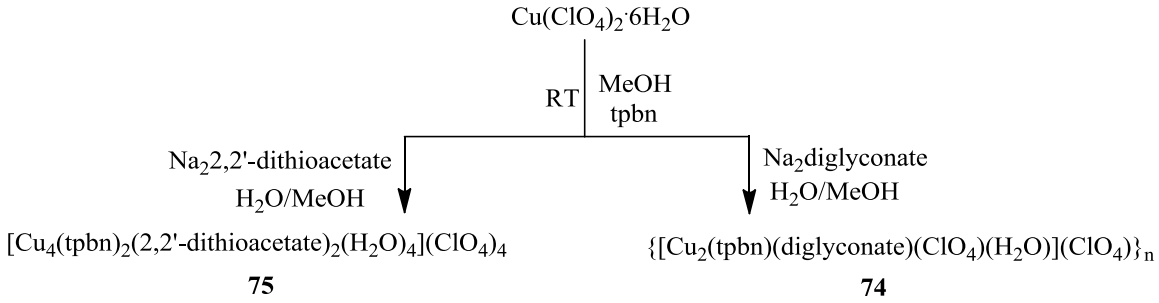

Scheme 27. Synthesis of **74-75**.

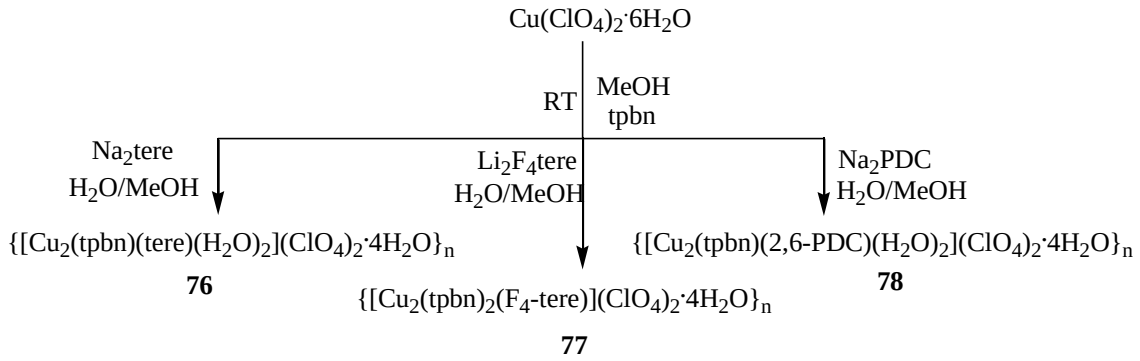

Scheme 28. Synthesis of **76-78**.

Using the corresponding sodium salt of the dicarboxylate, **79**, **80** and **81** were prepared in a similar way as described above for **76**.

Cu(II)-tdc compounds are synthesized with all six polypyridyl ligands (Scheme 29). Several Cu(II)-tdc compounds are reported in the literature with nitrogen based linkers, such as bpy,

1,10-phenanthroline, imidazole but those are either discrete molecules or 1 D CP.[191] On the other hand, tetranuclear compounds with Cu(II) are reported with nitrogen-based polydentate ligands.[115, 116, 185a]

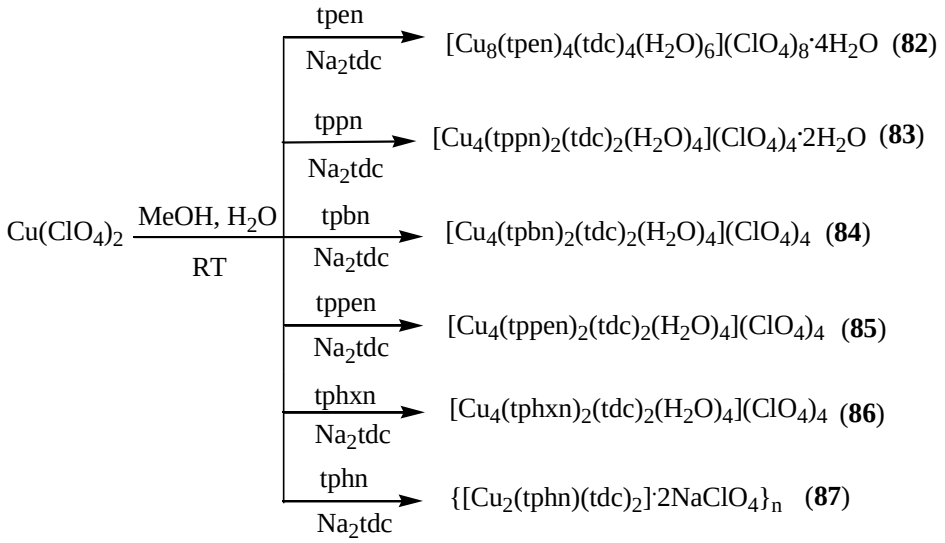

Scheme 29. Synthesis of **82-87**.

Single Crystal Structure Analysis.

Single crystal of **58** was obtained by slow evaporation of its acetonitrile solution. Single crystals for **59** and **60** could not be obtained. However, based on elemental analysis and comparison of the IR spectroscopic data **58-60** containing succinate, glutarate and adipate, respectively, are all 1D CPs. With the Cu(II)-tpen system, there is no CP reported in the literature. For the first time, CPs and an octanuclear compound with Cu(II)-tpen system were obtained using a linker, where tpen spans between the two Cu(II) centers.

{[Cu_2(tpen)(succinate)(H_2O)$_2$](ClO_4)$_2$·2H_2O}$_n$ (**58**). It crystallizes in the monoclinic $P2_1/c$ space group. Each Cu(II) center is pentacoordinated and surrounded by three nitrogens of the ligand, one coordinated water molecule and one oxygen of the succinate shown in Figure 3.134. The tpen ligand spans between the two Cu(II) centers forming a dimetal subunit which is connected to similar dimetal subunit with the succinate linker thus forming a 1D CP. The succinate binds in a bis(monodentate) anti-anti mode. The selected bond distances and angles around Cu(II) center are listed in Table A71.

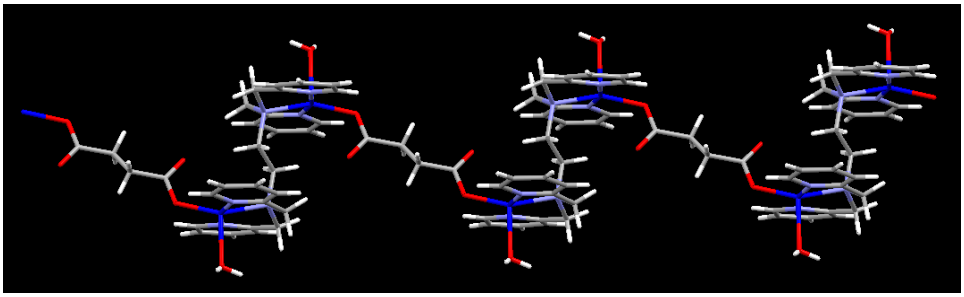

Figure 3.134. A perspective view of **58** (perchlorates anions are omitted for clarity).

The uncoordinated oxygen atom of the succinate is hydrogen bonded to the coordinated water molecule thus connecting two 1D CPs forming a supramolecular assembly as shown in Figure 3.135. In addition to Hydrogen bonding, the supramolecular assembly is further stabilized by C-H…O intercations. All hydrogen bonding parameters are listed in Table 3.22.

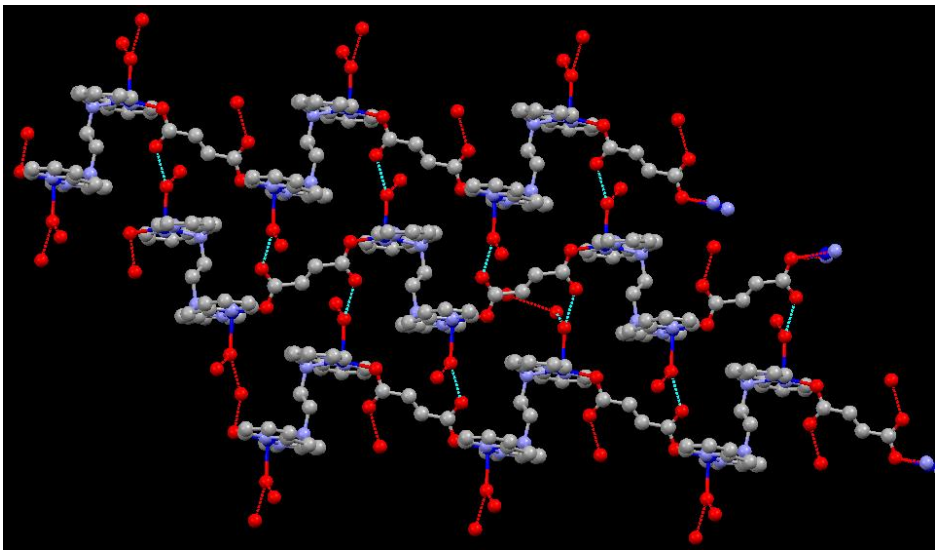

Figure 3.135. Supramolecular assembly in **58**.

Table 3.22. Hydrogen bonding parameters for **58**.[a]

D–H...A	r (D-H) (Å)	r (H…A) (Å)	r (D…A) (Å)	∠D-H…A (deg)	Symmetry
O(1) --H(1A) ..O(8)	0.86	2.18	2.768(7)	125	
O(1) --H(1B) ..O(3)	0.86	2.09	2.788(6)	138	x,1/2-y,1/2+z
C(8) --H(8B) ..O(3)	0.97	2.54	3.393(7)	146	1-x,-y,-z
C(9) --H(9A) ..O(3)	0.97	2.58	3.505(7)	161	1-x,-y,-z
C(9) --H(9B) ..O(2)	0.97	2.41	3.053(6)	124	1-x,-1/2+y,1/2-z

[a]Numbers in parenthesis are estimated standard deviations in the last significant digits.

One of the lattice water molecules is hydrogen bonded to the coordinated water molecule, which is further hydrogen bonded to the perchlorate anion. Through second lattice water molecule perchlorate anions are hydrogen bonded forming a network that runs through the 1D CP chain (see Figure 3.136).

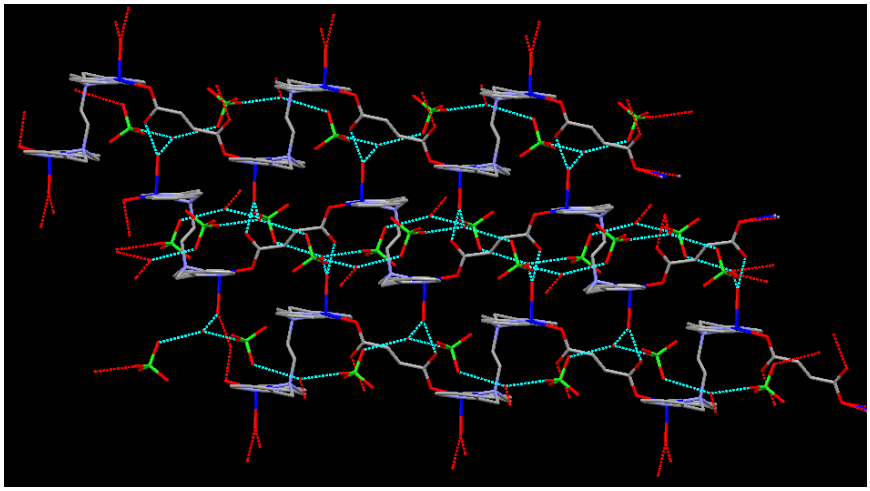

Figure 3.136. An arrangement of the perchlorate anions in supramolecular assembly of **58**.

In case of the tppn ligand, similar 1D CPs are formed for glutarate and adipate while an unusual discrete tetrameric compound is formed for the succinate, $[\{Cu_2(tppn)(H_2O)_2(ClO_4)\}_2(succinate)](ClO_4)_4$ (**61**), where the dicopper subunit is bridged by the succinate. Single Crystals of **62** could not be obtained despite many attempts.

$[\{Cu_2(tppn)(H_2O)_2(ClO_4)\}_2(succinate)](ClO_4)_4\cdot 4H_2O$ (**61**). It is a discrete tertanuclear compound that crystallizes in the monoclinic $P2_1/c$ space group. All copper(II) centers are not equivalent (see Figure 3.137). Two central Cu(II) centers are surrounded by three nitrogen of the ligand and one oxygen from the bis(monodentate) succinate which binds in a syn-anti mode and the fifth site is occupied by the perchlorate oxygen. Terminal Cu(II) centers are surrounded by three nitrogens of the ligand and two coordinated water molecules. The selected bond distances and angles are listed in Table A72. This compound is quite interesting because even in the presence of a dicarboxylate it prefers to have a discrete molecule unlike **58**.

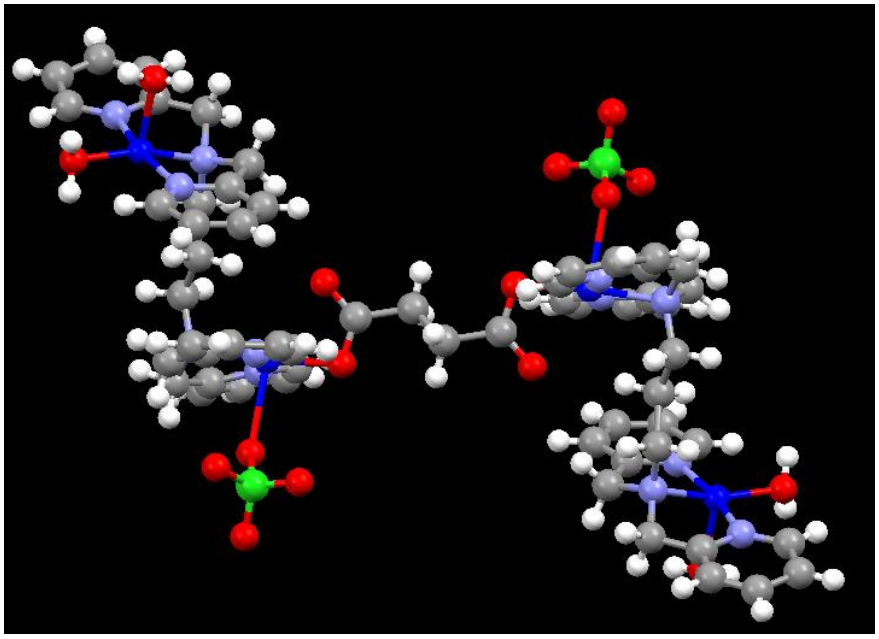

Figure 3.137. Structure of $[\{Cu_2(tppn)(H_2O)_2(ClO_4)\}_2(succinate)]^{4+}$ in **61**.

The tetranuclear unit in **61** is hydrogen bonded to the next units as shown in Figure 3.138. The hydrogen bonding parameters are listed in Table 3.23. The uncoordinated oxygen atom of succinate of one unit is hydrogen bonded to the coordinated water molecule on copper(II) center of the next unit through lattice water molecule. The second coordinated water molecule on copper(II) center of one unit is hydrogen bonded to the coordinated oxygen atom of succinate of next unit forming a 11-membered ring. The second coordinated water molecule is also hydrogen bonded to the coordinated perchlorate anion forming a 6-membered ring. The free perchlorate anion is found to be in 11-membered ring via hydrogen bonding.

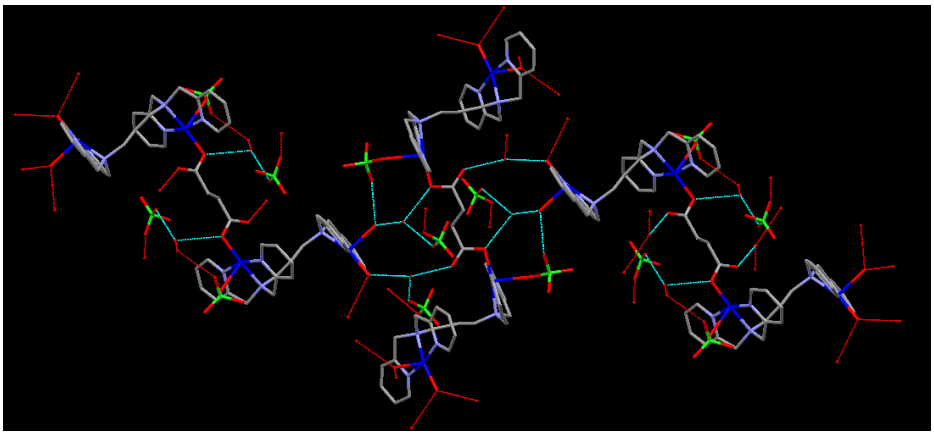

Figure 3.138. Supramolecular assembly in **61.**

Table 3.23. Hydrogen bonding parameters for **61.**[a]

D–H…A	r (D-H) (Å)	r (H…A) (Å)	r (D…A) (Å)	∠D-H…A (deg)	Symmetry
O(3)--H(3C)...O(9)	0.87	2.27	2.83(2)	122	x,1/2-y,1/2+z
O(4)--H(4A)...O(17)	0.88	2.08	2.64(2)	121	
O(17)--H(17A) ...O(1)	0.87	2.23	2.84(2)	127	1-x,1/2+y,1/2-z
O(17)--H(17B)...O(5)	0.87	2.25	2.82(2)	123	x,1/2-y,1/2+z
O(18)--H(18B)...O(7)	0.87	2.04	2.80(3)	144	
C(1)--H(1A)...O(12)	0.99	2.57	3.35(2)	136	x,1/2-y,1/2+z
C(2)--H(2A)...N(5)	0.99	2.62	3.29(2)	125	
C(3)--H(3A)...O(18)	0.99	2.59	3.497(19)	153	
C(4)--H(4C)...O(14)	0.99	2.41	3.36(3)	163	1-x,1/2+y,1/2-z
C(8)--H(8)...O(10A)	0.95	2.37	3.27(4)	159	1+x,1/2-y,1/2+z
C(13)--H(13)...O(15)	0.95	2.33	3.19(4)	150	-x,1/2+y,1/2-z
C(14)--H(14)...O(17)	0.95	2.35	3.20(3)	149	-1+x,y,z
C(16)--H(16A)...O(10)	0.99	1.94	2.74(3)	135	
C(19)--H(19)...O(4)	0.95	2.48	3.26(3)	140	
C(22)--H(22B)...O(11)	0.99	2.54	3.40(2)	145	x,1/2-y,1/2+z
C(24)--H(24)...O(16)	0.95	2.24	3.18(3)	169	1-x,-y,1-z
C(25)--H(25)...O(10)	0.95	2.42	3.35(3)	164	1+x,1/2-y,1/2+z
C(29)--H(29B)...O(17)	0.99	2.52	3.44(3)	156	x,1/2-y,-1/2+z

[a]Numbers in parenthesis are estimated standard deviations in the last significant digits.

{[Cu_2(tppn)(adipate)(H_2O)$_2$(ClO_4)$_2$]·2CH_3CN}$_n$ (63). It crystallizes in the monoclinic *C*2/*c* space group. Each Cu(II) center in this 1D CP is tetracoordinated and surrounded by three nitrogens of the ligand and one oxygens from carboxylate. The tppn ligand spans between the two copper centers like the tpen analogue, which is further connected by the adipate linker and thus forms a polymer (Figure 3.139). The adipate binds in a bis(monodentate) syn-anti mode. The selected bond distances are listed in Table A73.

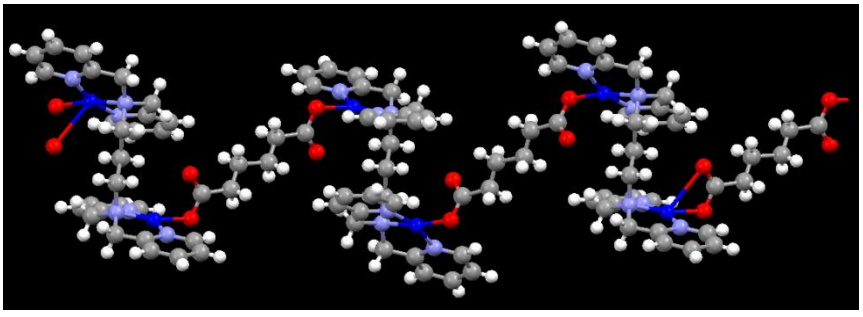

Figure 3.139. A perspective view of **63**.

The Cu(II)-tpbn is a dinuclear species reported in the literature where tpbn spans between the two Cu(II) centers, the two sites on each Cu(II) center is either occupied by water or halide ion depending upon the copper(II) salt used for the study. With Cu(II)-tpbn system CPs and molecular rectangles were obtained depending on the linker used.

For the tpbn ligand, the dicarboxylate-dependent product formation is observed: only the adipate gives the 1D CP while the succinate and glutarate provide molecular rectangles, $[Cu_4(tpbn)_2(succinate)_2(H_2O)_4](ClO_4)_4$ (**64**) and $[Cu_4(tpbn)_2(glutarate)_2(H_2O)_4](ClO_4)_4.4H_2O$ (**65**).

$[Cu_4(tpbn)_2(succinate)_2(H_2O)_2(ClO_4)_2](ClO_4)_2$ (**64**). It crystallizes in the triclinic *P-1* space group. There are two independent molecules in the asymmetric unit which differs in the orientation of methylene chain of the tpbn ligand shown in Figure 3.140. The selected bond distances and angles are listed in Table A74. Molecule A has a zig-zag conformation of the chain whereas Molecule B has step up-down conformation of the chain. These are also evident from the value of the torsion angles. In Molecule A, the value of the torsional angle between four carbon atoms of the chain is -168.05° whereas in Molecule B the value is 89.44°. Due to the different orientation of the methylene chain in the tpbn ligand, the pore sizes were different, in Molecula A pore size is 11.968 Å x 11.402 Å while the pore size is 12.357 Å x 10.971 Å in Molecule B. In these molecular rectangles two Cu(II) centers are connected by spanning tpbn ligand in one direction and succinate in the another direction. Out of four copper(II) centers, two are different from the other two. The coordination environment around each Cu(II) is N_3O_2; however, two Cu(II) centers have coordinated water molecule while other two have bound perchlorate. The Cu-$O_{perchlorate}$ distance varies from 2.359 to 2.505 Å. The succinate binds in a bis(monodentate) syn-syn fashion.

The molecular rectangles A and B in **64** also differ in forming supramolecular coordination networks due to hydrogen bonding. Molecule A forms a supramoecular assembly due to hydrogen bonding between the coordinated and lattice water molecuels as shown in Figure 3.141. Inside the cavity of molecule A the lattice water molecules are hydrogen bonded with the coordinated water molecule to form a cubical like structure. Two such recatngles are connected via hydrogen bonding between coordinated water molecule and coordinated oxygen atom of

succinate forming a supramolecular assembly. This supramolecular assembly is further stabilized by C-H…O interactions. The hydrogen bonding parameters are listed in Table 3.24.

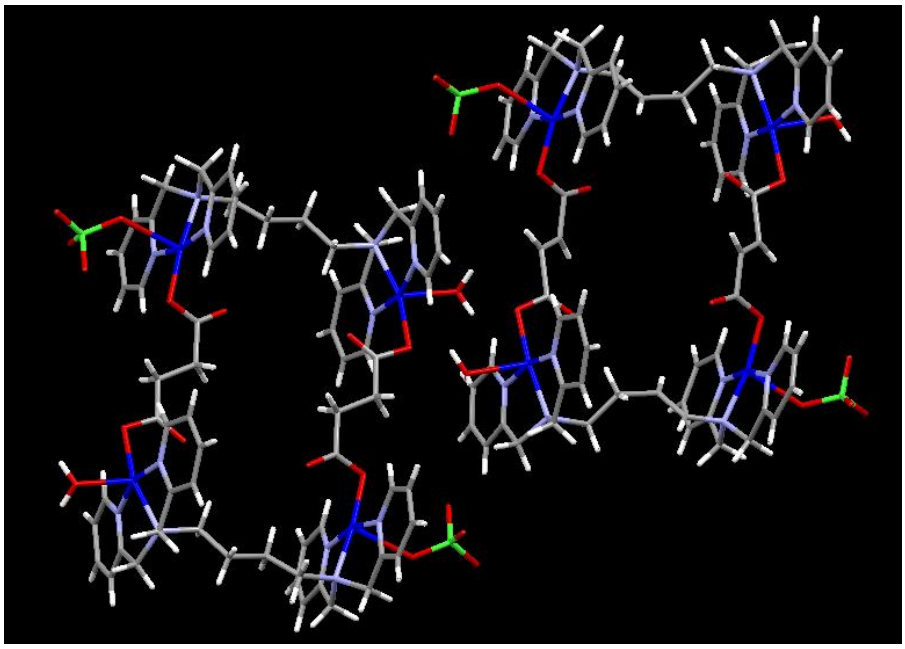

Figure 3.140. Molecules A (left) and B (right) in **64**.

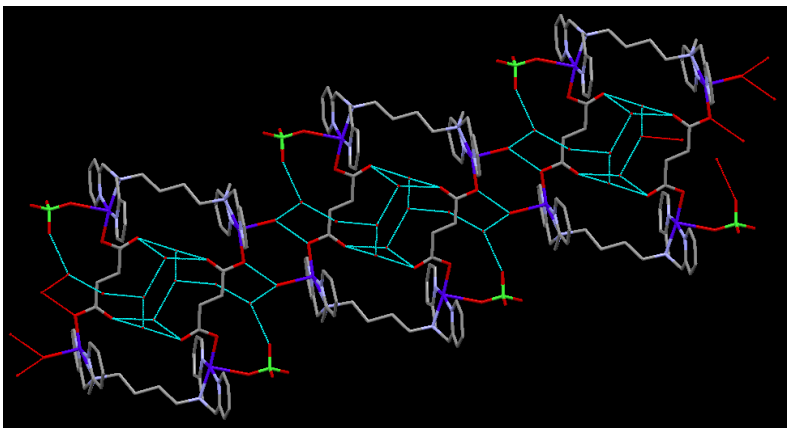

Figure 3.141. Supramolecular assembly of molecule A in **64.**

Molecule B shows hydrogen bonding only between coordinated perchlorate anions and coordianted water molecules; this resulted in the formation of a small box where the unbound perchlorate anions sit as shown in Figure 3.142. The hydrogen bonding distance varies from 2.853 Å to 2.973 Å.

Table 3.24. Hydrogen bonding parameters for **64**.[a]

D–H…A	r (D-H) (Å)	r (H…A) (Å)	r (D…A) (Å)	∠D-H…A (deg)	Symmetry
O1S --H1SA...O31	0.85	2.47	3.07(4)	129	-1+x,y,z
O2S --H2SB...O27	0.85	2.01	2.78(4)	150	-x,-y,1-z
O3S --H3SA...O6	0.85	2.2	2.94(3)	145	x,1-y,1-z
O4S --H4SB...O2S	0.85	2.18	2.80(5)	129	
O5S --H5SB...O26	0.85	2.07	2.72(3)	133	-x,-y,1-z
O29 --H29A...O28	0.89	2.09	2.846(19)	142	-1-x,-y,1-z
O29 --H29B...O3S	0.89	1.9	2.76(3)	162	-1+x,-1+y,z
O34 --H34C...O4	0.93	2.16	2.97(3)	146	-1+x,y,z
O34 --H34D...O19	0.93	2.24	2.85(4)	123	
C107 --H10D...O10	0.97	2.43	3.37(4)	165	1-x,1-y,1-z
C106 --H10E...O26	0.97	2.55	3.49(2)	166	
C106 --H10F. ..O13	0.97	2.36	3.14(4)	138	1-x,1-y,1-z
C108 --H10G...O12	0.97	2.54	3.39(4)	146	1-x,1-y,1-z
C108 --H10H...O6	0.97	2.54	3.50(3)	169	1+x,y,z
C105 --H10I ...O3	0.97	2.48	3.35(3)	150	
C105 --H10I...O4	0.97	2.47	3.39(4)	156	
C105 --H10J...O16	0.97	2.44	3.35(5)	157	1-x,1-y,-z
C14 --H14...O25	0.93	2.58	3.10(3)	116	
C17 --H17...O9	0.93	2.6	3.15(4)	119	x,y,1+z
C18 --H18B...O3	0.97	2.32	3.20(3)	151	-1+x,y,1+z
C20 --H20 ...O8	0.93	2.5	3.37(3)	156	-x,-y,2-z
C21 --H21...O1	0.93	2.55	3.25(3)	133	1-x,-y,1-z
C27 --H27...O4	0.93	2.37	3.22(4)	152	2-x,1-y,1-z
C36 --H36 ...O9	0.93	2.13	3.03(5)	162	1-x,1-y,-z
C37 --H37...N9	0.93	2.61	3.24(4)	126	
C38 --H38B...O32	0.97	2.47	3.38(4)	155	
C39 --H39A...O15	0.97	2.59	3.47(4)	150	
C46--H46 ...O8	0.93	2.51	3.31(3)	144	
C48 --H48B...O3	0.97	2.49	3.27(3)	137	
C51--H51...O14	0.93	2.5	3.42(6)	171	
C52 --H52A ...O7	0.97	2.44	3.24(3)	140	1+x,y,-1+z
C52 --H52B...O9	0.97	2.47	3.24(5)	136	1-x,1-y,-z
C52--H52B...O10	0.97	2.49	3.43(5)	162	1-x,1-y,-z

[a]Numbers in parenthesis are estimated standard deviations in the last significant digits.

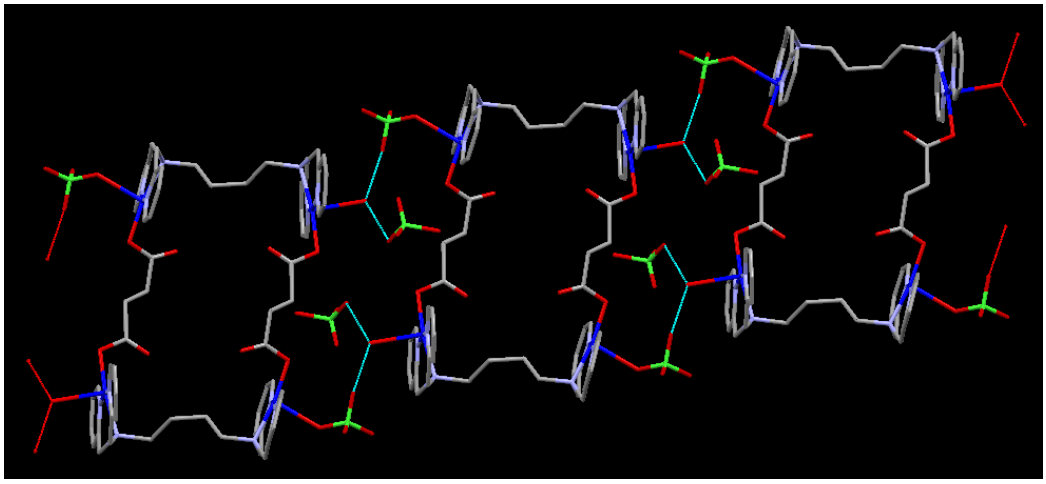

Figure 3.142. Supramolecular assembly of molecule B in **64**.

$[Cu_4(tpbn)_2(glutarate)_2(H_2O)_4](ClO_4)_4 \cdot 4H_2O$ (65). It is a molecular rectangle similar to **64**, crystallizes in the orthorhombic *Pbca* space group. All Cu(II) centers are pentacoordinated and surrounded by three nitrogens of the ligand, one water molecule and fifth site is occupied by monodentate carboxylate. The direction of the coordinated water on copper centers is found to be different. Out of four, two water molecules are found to be inside the cavity and other two points outside the cavity. The selected bond distances and angles are listed in Table A75. Two copper centers are connected via glutarate in one direction (along x-axis) and by the ligand in the other direction (along y-axis) forming a molecular rectangle shown in Figure 3.143. The glutarate binds in bis(monodentate) syn-anti fashion. The lattice water molecules are found to be inside the cavity of the rectangle. These water molecules are hydrogen bonded among themselves, with the coordinated water molecules (those pointing inside the cavity) and uncoordinated oxygen atoms of the carboxylate forming a hexagonal motif ($R_6^6(6)$) as shown in Figure 3.144.

Two such molecular rectangles are connected with each other via two perchlorate anions which are hydrogen bonded to the coordinated water molecules (pointing outside the cavity) of these rectangles in one direction. The perchlorate anions connecting the two molecular rectangles also forms an 8-membered motif $R_6^6(8)$. Further, these perchlorate anions are hydrogen bonded to another molecular rectangle in two directions forming a chair type supramolecular assembly(see Figure 3.145). All the hydrogen bonding parameters are listed in Table 3.25. Furthermore, these rectangles are connected via $\pi-\pi$ interactions in two planes (centroid-centroid distances: 3.633 Å and 3.803 Å) as shown in Figure 3.146.

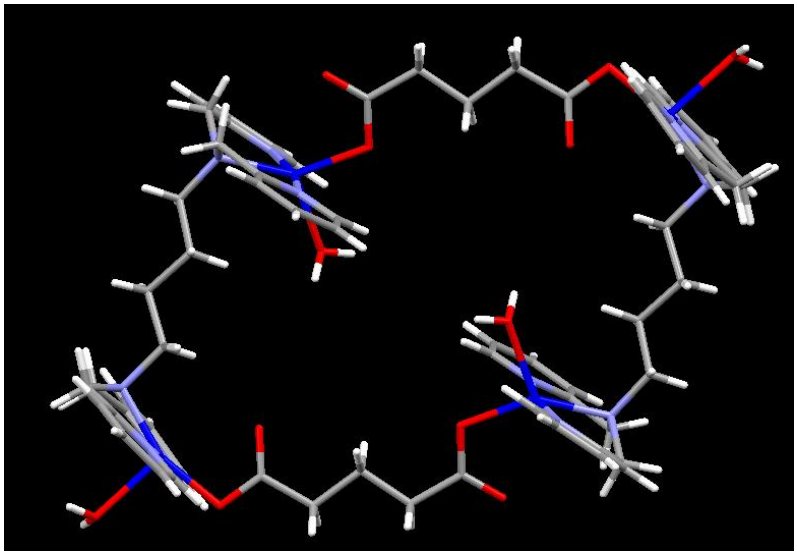

Figure 3.143. A view of molecular rectangle **65**.

Table 3.25. Hydrogen bonding parameters for **65**.[a]

D–H…A	r (D-H) (Å)	r (H…A) (Å)	r (D…A) (Å)	∠D-H…A (deg)	Symmetry
O2S--H2SB...O1S	0.9(2)	1.9(2)	2.748(12)	163(15)	1/2-x,1/2+y,z
O1S--H1SB...O14	0.87(17)	2.0(2)	2.652(10)	136(17)	
O14--H14B...O1S	0.86(7)	1.92(19)	2.652(10)	141	1/2+x,y,1/2-z
O17--H17A...O2	0.86(11)	2.48(13)	3.30(2)	161(12)	1/2-x,-1/2+y,1+z
O17--H17A...O11	0.86(11)	2.5(2)	3.20(2)	140(18)	1/2-x,-1/2+y,1+z
O17--H17B...O11	0.94(11)	2.56(14)	3.392(19)	149(9)	1/2+x,1/2-y,1-z
O17--H17B...O20	0.94(11)	2.02(13)	2.854(19)	147	1/2+x,1/2-y,1-z
C21--H21...O7	0.93	2.55	3.34(3)	143	1/2-x,-1/2+y,z
C26--H26...O16	0.93	2.51	3.19(5)	131	1/2+x,y,1/2-z
C29--H29...O15	0.93	2.53	3.40(2)	156	1-x,-1/2+y,1/2-z
C30--H30B...O23	0.97	2.41	3.35(3)	163	1/2+x,y,1/2-z
C41--H41B...O23	0.97	2.53	3.37(3)	145	1/2+x,y,1/2-z
C44--H44B...O7	0.97	2.54	3.47(3)	159	
C45--H45B...O15	0.97	2.58	3.47(2)	152	x,1/2-y,1/2+z

[a]Numbers in parenthesis are estimated standard deviations in the last significant digits.

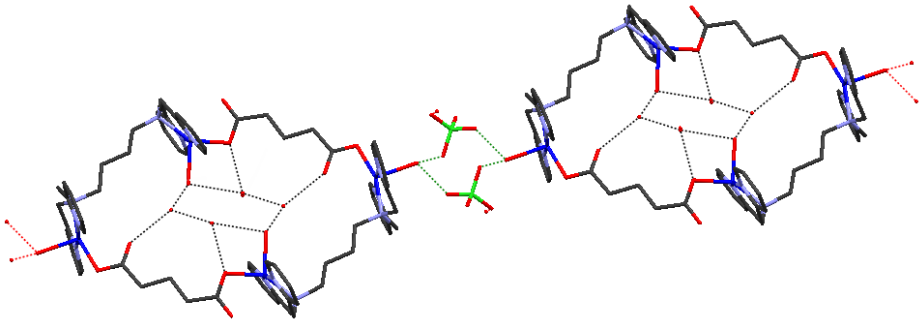

Figure 3.144. Association of molecular rectangles in **65** via hydrogen bonding.

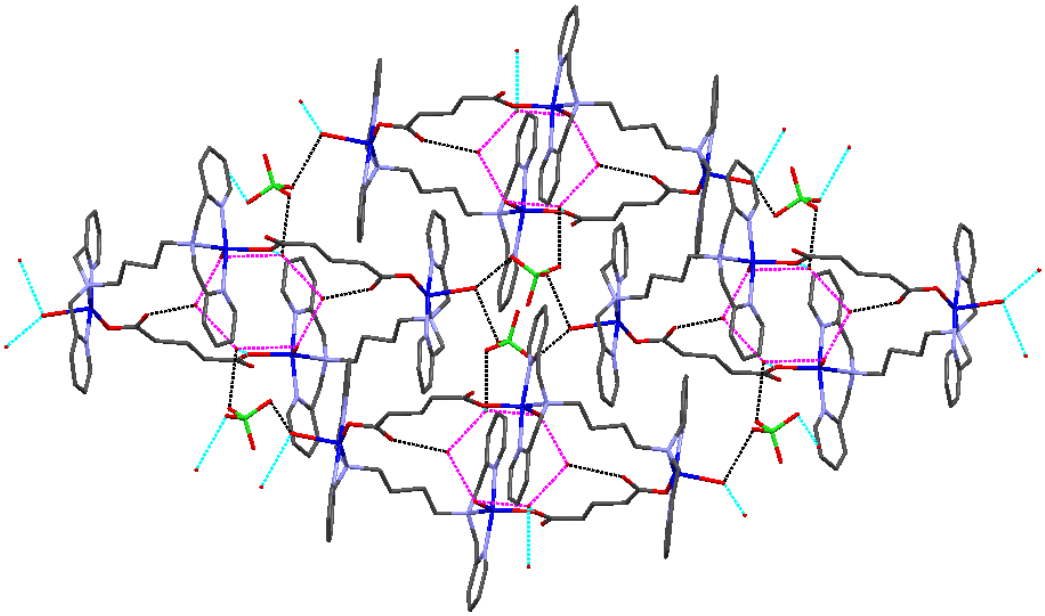

Figure 3.145. Supramolecular assembly in **65**.

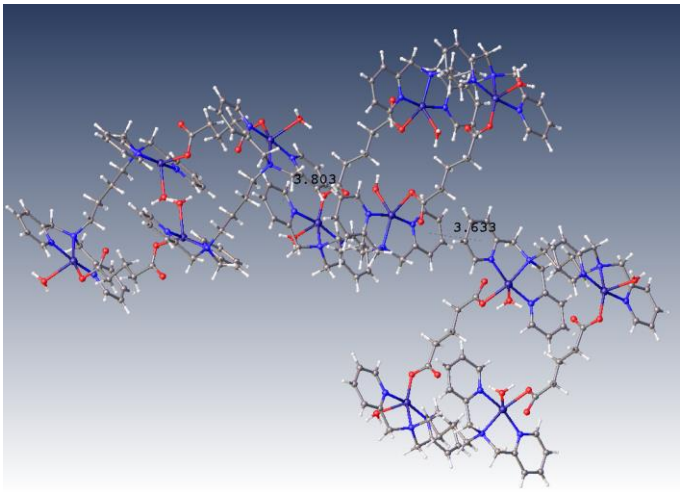

Figure 3.146. A view of π–π interactions in **65**.

{[Cu_2(tpbn)(adipate)(H_2O)$_2$](ClO_4)$_2$}$_n$ (66). It is a 1D coordination polymer crystallizes in the triclinic *P-1* space group (see Figure 3.147). Both Cu(II) centers are pentacoordinated and surrounded by three nitrogens of the tpbn ligand, one oxygen of the carboxylate and one water molecule. The adipate binds in a bis(monodentate) anti-anti fashion. The selected bond distances and angles are listed in Table A76.

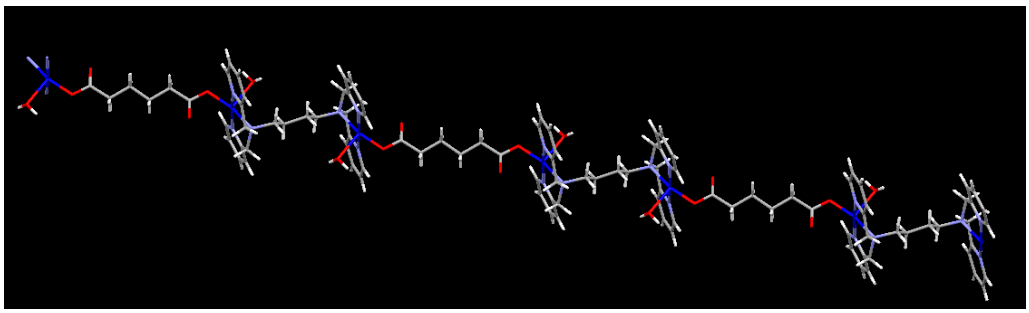

Figure 3.147. A perspective view of 1D CP of **66**.

Hydrogen bonding between two lattice water molecules with the coordinated oxygen atom of the carboxylate and the coordinated water molecule on Cu(II) results in the formation of a supramolecular assembly of the 1D coordination polymer chains as shown in Figure 3.148. The hydrogen bonding parameters are listed in Table 3.26. For example, hydrogen bonding of bound water molecule O1 with the lattice water molecule O8 results in the formation of a 4-membered motif ($R_4^4$4): O1---O8---O1---O8 (O1-O8, 2.858 Å). O8 is further hydrogen bonded to O6 of the perchlorate anion (not shown in Figure because of disorder) (O8-O6, 2.803 Å). Furthermore, the bound oxygen atom O2 of the carboxylate is hydrogen bonded to O8 (O2-O8, 2.692 Å).

Table 3.26. Hydrogen bonding parameters for **66**.[a]

D–H…A	r (D-H) (Å)	r (H…A) (Å)	r (D…A) (Å)	∠D-H…A (deg)	Symmetry
O(1)--H(1B)...O(8)	0.85(3)	2.03(3)	2.858(7)	166(5)	x,-1+y,z
O(8)--H(8A)...O(2)	0.85(5)	1.90(6)	2.692(6)	154(7)	x,1+y,z
O(8)--H(8B)...O(6)	0.85(5)	1.97(5)	2.803(7)	168(6)	
C(7)--H(7)...O(3)	0.93	2.42	3.299(8)	158	-x,-y,1-z
C(8)--H(8)...O(3)	0.93	2.6	3.378(8)	142	
C(11)--H(11B)...O(1)	0.97	2.55	3.342(8)	138	
C(12)--H(12B)...O(7B)	0.97	2.47	3.404(12)	162	

[a]Numbers in parenthesis are estimated standard deviations in the last significant digits.

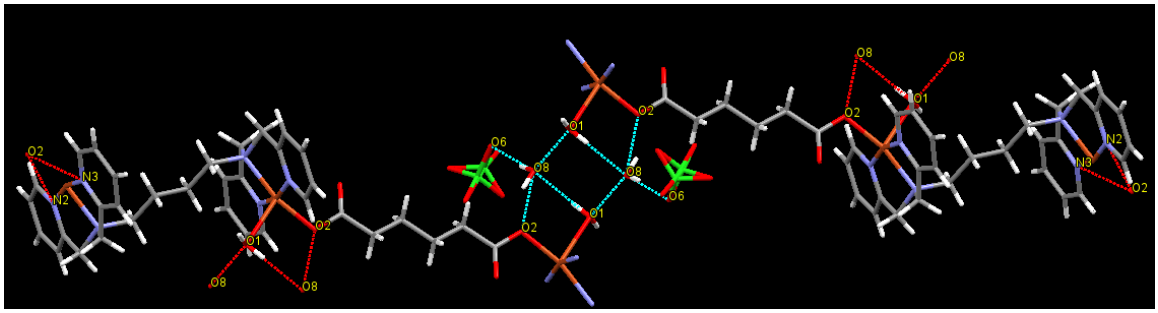

Figure 3.148. A view of supramolecular assembly in **66**.

{[Cu_2(tpbn)(fumarate)(H_2O)$_2$](ClO_4)$_2$}$_n$ (67). It is a 1D CP that crystallizes in the monoclinic $P2_1/n$ space group. The Cu(II) centers are five coordinated and surrounded by three nitrogen of the ligand, one oxygen atom of fumarate (Figure 3.149). Instead of water in other two cases, the fifth site on Cu(II) center is occupied by the perchlorate oxygen. The selected bond distances and angles are listed in Table A77. All four uncoordinated oxygen atoms of fumarate binds to four more polymeric chains via lattice water molecules. These chains are perpendicular to each other as shown in Figure 3.150. The hydrogen bonding parameters are listed in Table 3.27.

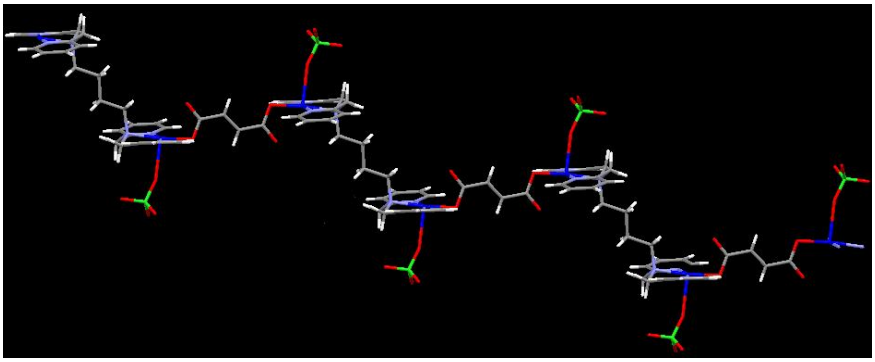

Figure 3.149. A perspective view of **67**.

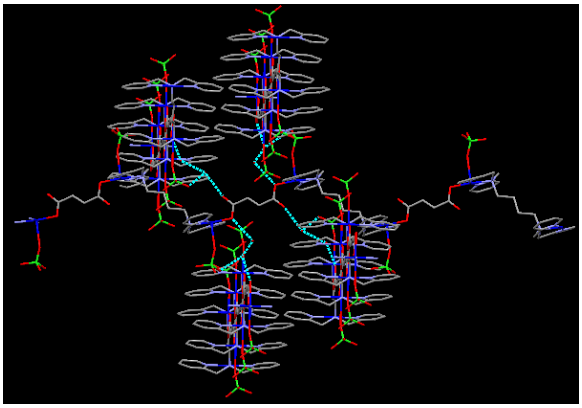

Figure 3.150. Supramolecular assembly in **67** (all hanging contacts are deleted for clarity).

Table 3.27. Hydrogen bonding parameters for **67**.[a]

D–H…A	r (D-H) (Å)	r (H…A) (Å)	r (D…A) (Å)	∠D-H…A (deg)	Symmetry
O2S--H6...O4	0.82(3)	2.08(4)	2.846(6)	156	1+x,y,z
O2S--H7...O6	0.82(5)	1.99(4)	2.798(6)	167	1/2+x,1/2-y,-1/2+z
C6--H6...O2S	0.93	2.49	3.275(6)	142	
C1--H1A...O1S	0.97	2.58	3.365(5)	139	
C3--H3...O3	0.93	2.59	3.409(6)	147	1/2-x,-1/2+y,1/2-z
C4--H4...O4	0.93	2.49	3.301(6)	145	1/2-x,-1/2+y,1/2-z
C5--H5...O1S	0.93	2.53	3.300(6)	140	3/2-x,-1/2+y,1/2-z
C9--H9A...O3	0.97	2.57	3.481(6)	157	
C13--H13...O1	0.93	2.39	3.019(7)	125	-1/2+x,1/2-y,1/2+z

[a]Numbers in parenthesis are estimated standard deviations in the last significant digits.

{[Cu_2(tpbn)(maleate)(H_2O)$_2$](ClO_4)$_2$·2H_2O}$_n$ (68). It is a spiral shaped CP that crystallises in the triclinic *P*-1 space group. The coordination environment around Cu(II) centers is similar to the fumarate analogue (**67**). The selected bond distances and angles are listed in Table A78. Because of the cis orientation of maleate, the shape of 1D CP is different from the fumarate analogue (see Figure 3.151). Two such coordination polymer chains are hydrogen bonded to each other via a zig-zag chain of lattice water molecules as shown in Figure 3.152. The hydrogen bonding parameters are listed in Table 3.28.

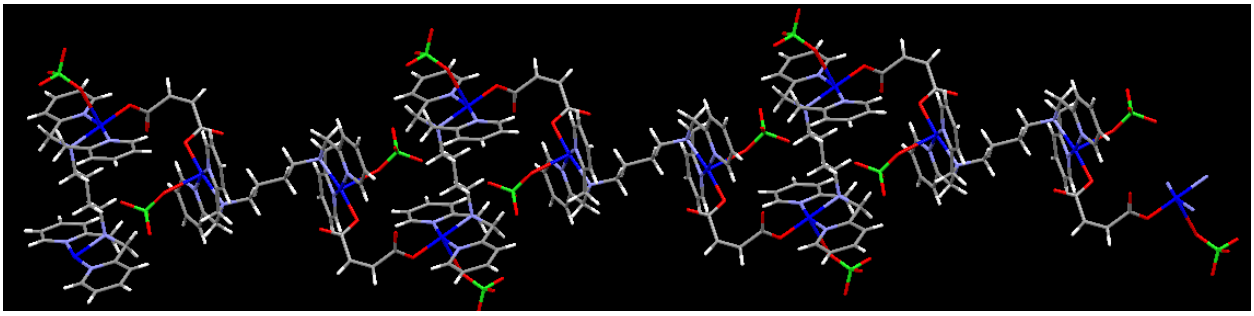

Figure 3.151. A perspective view of **68**.

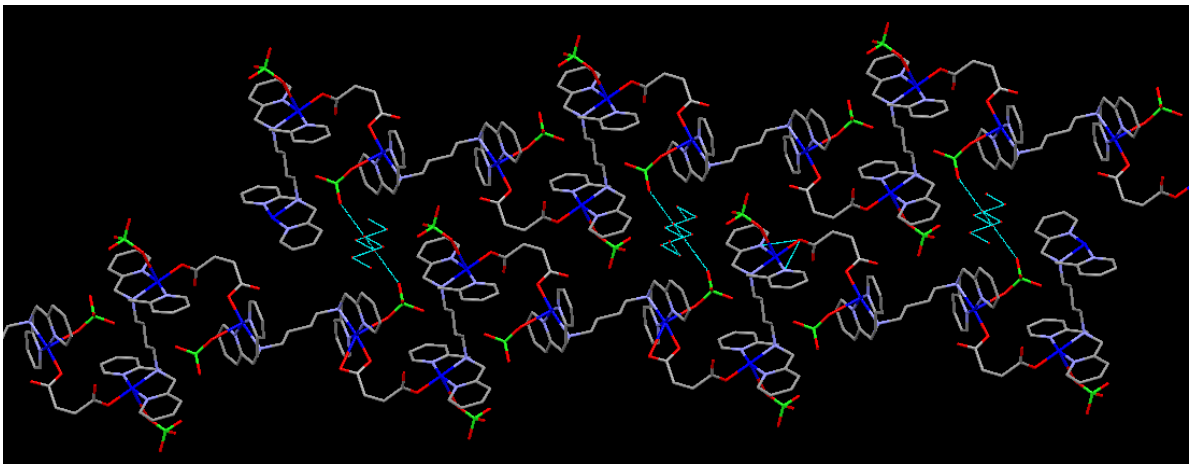

Figure 3.152. Supramolecular assembly in **68**.

Table 3.28. Hydrogen bonding parameters for **68**.[a]

D–H…A	r (D-H) (Å)	r (H…A) (Å)	r (D…A) (Å)	∠D-H…A (deg)	Symmetry
O(13)--H(13A) ..O(14)	0.87	1.91	2.727(15)	155	x,y,-1+z
O(14)--H(14A) ..O(7)	0.87	2.14	3.011(12)	175	
O(14)--H(14B) ..O(13)	0.87	1.92	2.727(15)	154	x,y,1+z
C(5) --H(5)..O(2)	0.95	2.36	3.261(13)	159	
C(11)--H(11A) ..O(7)	0.99	2.45	3.376(15)	156	x,y,-1+z
C(15)--H(15)..O(3)	0.95	2.47	3.250(15)	139	-1+x,y,z
C(18)--H(18A) ..O(3)	0.99	2.4	3.389(14)	176	
C(19)--H(19B) ..O(14)	0.99	2.55	3.365(12)	139	
C(23)--H(23) ..O(5)	0.95	2.52	3.264(16)	136	1+x,y,z
C(25) --H(25A)..O(9)	0.99	2.59	3.485(13)	150	-x,-y,1-z
C(28) --H(28)..O(2)	0.95	2.47	3.149(15)	128	
C(30) --H(30)..O(4)	0.95	2.5	3.389(14)	156	
C(31) --H(31B)..O(9)	0.99	2.5	3.472(14)	167	

[a]Numbers in parenthesis are estimated standard deviations in the last significant digits.

$[Cu_4(tpbn)_2(malate)_2(H_2O)_4](ClO_4)_4 \cdot 5H_2O$ (**70**). It is a molecular rectangle similar to **65** and crystallises in the triclinic *P-1* space group. The coordination environment around Cu(II) centers is different in **70** as compared to **65**. In this rectangle two copper centers are different from the other two in terms of their coordination environment as shown in Figure 3.153. Two copper(II) centers are connected with each other via spanning ligand, fourth site is occupied by oxygen of monodentate carboxylate and fifth site is occupied by a water molecule whereas in other two copper(II) centers fifth site is occupied by perchlorate oxygen atoms. The Cu-$O_{perchlorate}$ distance

is 2.476 Å and Cu-O_{water} distance is 2.505Å. The malate binds in bis(monodentate) syn-anti fashion. All other selected bond distances and angles are listed in Table A79.

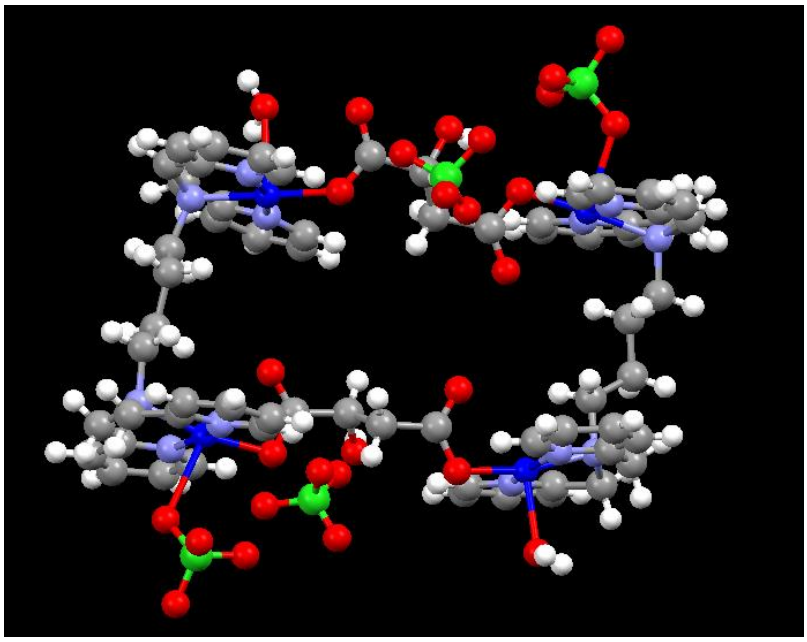

Figure 3.153. Molecular rectangle **70**.

The supramolecular assembly in **70** is shown in Figure 3.154. The molecular rectangles are connected via hydrogen bonding of coordinated water molecule O11 with the hydroxy oxygen atom O3 of the next molecular rectangle and O6 (coordinated oxygen atom of one rectangle) is hydrogen bonded to O33 (coordinated water molecule on copper(II) center) via a lattice water molecule O40. The perchlorates are also hydrogen bonded to these molecular rectangles. The O17 of perchlorate is hydrogen bonded to O8 (hydroxy group of the carboxylate) and second perchlorate is hydrogen bonded to coordinated water molecule O11 via a lattice water molecule O12. The hydrogen bonding parameters are listed in Table 3.29. In addition to Hydrogen bonding, C-H…O interactions further stabilize the supramolecular assembly.

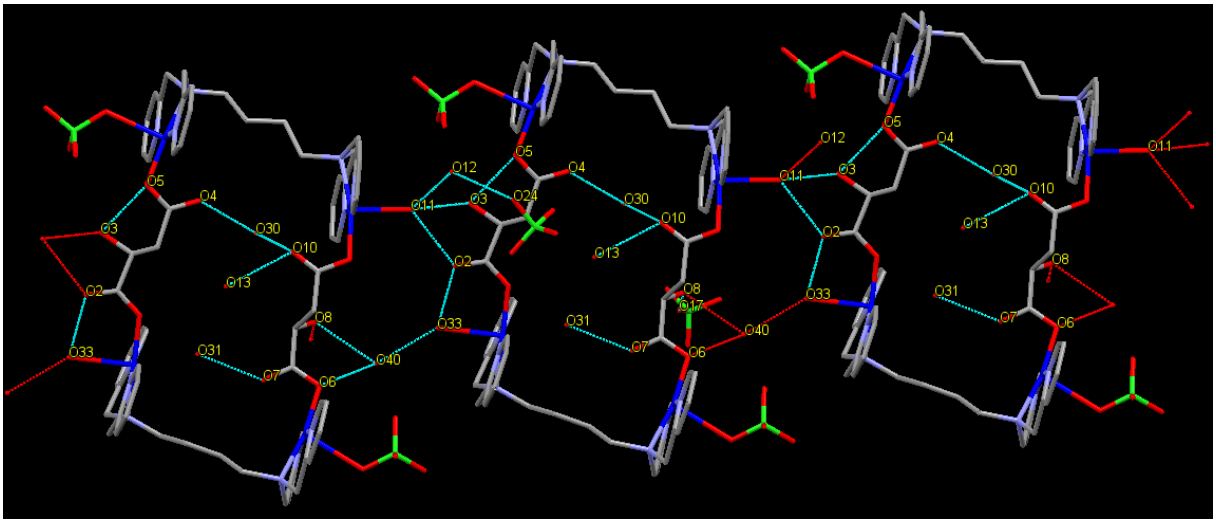

Figure 3.154. Supramolecular assembly in **70**.

Table 3.29. Hydrogen bonding parameters for **70**.[a]

D–H…A	r (D-H) (Å)	r (H…A) (Å)	r (D…A) (Å)	∠D-H…A (deg)	Symmetry
O(3) --H(3A) ..O(5)	0.82	1.85	2.55(2)	141	
O(8) --H(8) ..O(17)	0.82	1.81	2.32(3)	118	1-x,1-y,1-z
O(11) --H(11B) ..O(12)	0.86	2.18	2.874(16)	137	x,1+y,z
O(13) --H(13C) ..O(10)	0.85	2.27	2.988(14)	143	
O(13) --H(13D) ..O(25)	0.85	2.52	3.077(18)	124	
O(31) --H(31) ..O(7)	0.85	1.86	2.684(12)	164	
O(33) --H(33A) ..O(40)	0.85	1.87	2.711(12)	169	
O(40) --H(40B) ..O(21)	0.85	2.37	3.106(14)	144	x,-1+y,z
C(2) --H(2) ..O(14)	0.93	2.46	3.21(2)	137	1-x,1-y,1-z
C(6) --H(6B) ..O(19)	0.97	2.32	3.114(13)	139	2-x,2-y,1-z
C(10) --H(10) ..O(21)	0.93	2.44	3.338(15)	162	
C(14) --H(14B) ..O(7)	0.97	2.5	3.304(12)	140	
C(32) --H(32) ..O(22)	0.93	2.52	3.343(15)	147	
C(34) --H(34) ..O(25)	0.98	2.45	3.407(15)	167	
C(40) --H(40) ..O(2)	0.93	2.44	3.343(15)	165	1-x,1-y,-z
C(61) --H(61) ..O(8)	0.93	2.58	3.48(3)	162	
C(65) --H(65A) ..O(27)	0.97	2.35	3.243(14)	153	

[a]Numbers in parenthesis are estimated standard deviations in the last significant digits

{[Cu_2(tpbn)(t,t-muconate)(H_2O)$_2$](ClO_4)$_2$}$_n$ (71). It is a spiral shaped 1D CP that crystallizes in the triclinic *P*-1 space group. The coordination environment around Cu(II) centers is similar to

66. The spiral chains of the polymer shown in Figure 3.155 (left) are connected with each other via hydrogen bonding between the bound water molecule and bound oxygen of the carboxylate (O1---O2, 2.838 Å) shown in Figure 3.155(right). The selected bond distances and angles are listed in Table A80. The hydrogen bonding parameters are listed in Table 3.29. Unlike adipate, in this case, the uncoordinated oxygen atom of the carboxylate is also involved in hydrogen bonding with the bound water molecule of the next chain. Furthermore, this supramolecular assembly is stabilized by C--H…O interactions listed in Table 3.30.

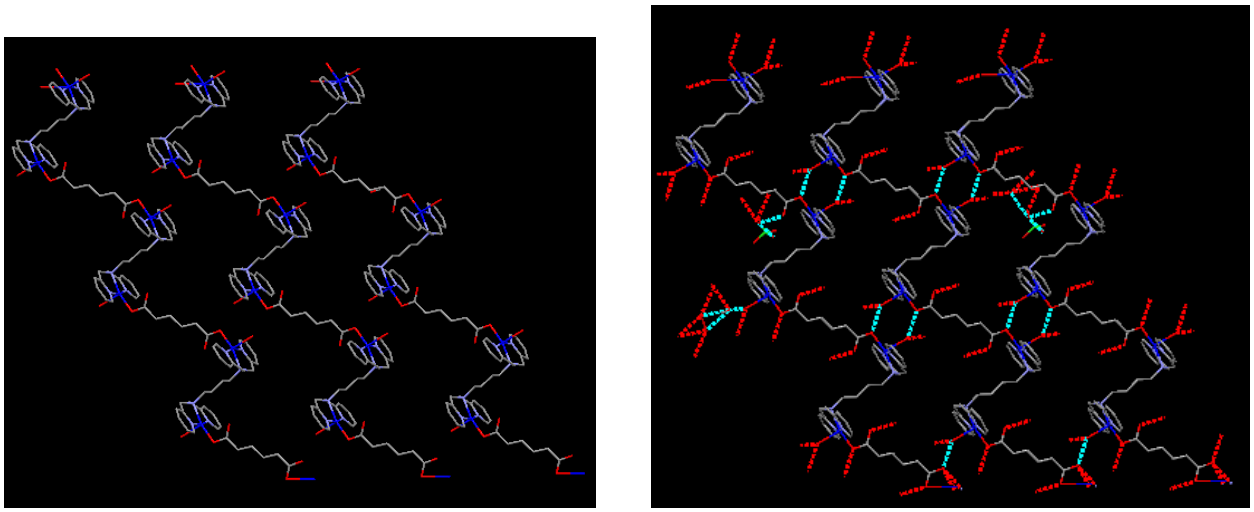

Figure 3.155. A perspective view of 1D chains of **71** (left) and their association via hydrogen bonding (right).

Table 3.30. Hydrogen bonding parameters for **71**.[a]

D–H...A	r (D-H) (Å)	r (H…A) (Å)	r (D…A) (Å)	∠D-H…A (deg)	Symmetry
O(1)--H(1A)...O(9)	0.88	1.95	2.806(5)	164	
O(1)--H(1B)...O(2)	0.88	2.07	2.838(3)	146	1-x,-y,-z
O(10)--H(10C)...O(3)	0.85	2.02	2.845(4)	163	x,1+y,z
O(10)--H(10D)...O(6)	0.85	2.11	2.948(4)	167	1-x,1-y,1-z
C(4)--H(4A)...O(5)	0.99	2.54	3.332(5)	137	1-x,1-y,1-z
C(4)--H(4B)...O(7)	0.99	2.5	3.454(4)	162	1+x,y,z
C(14)--H(14)...O(4)	0.95	2.49	3.440(5)	174	
C(17)--H(17A)...O(3)	0.99	2.51	3.393(3)	149	

[a]Numbers in parenthesis are estimated standard deviations in the last significant digits.

{[Cu_2(tphxn)(succinate)(H_2O)$_2$](ClO_4)$_2$}$_n$ (73). Similar to tpen, the tphxn with succinate also forms a 1D CP. Each Cu(II) center in this coordination polymer is pentacoordinated and surrounded by three nitrogens of the ligand, one water molecule and one oxygen from the carboxylate. The adipate binds in a bis(monodentate) syn-anti mode. The 1D CP is shown in Figure 3.156. The selected bond distances and angles are listed in Table A81.

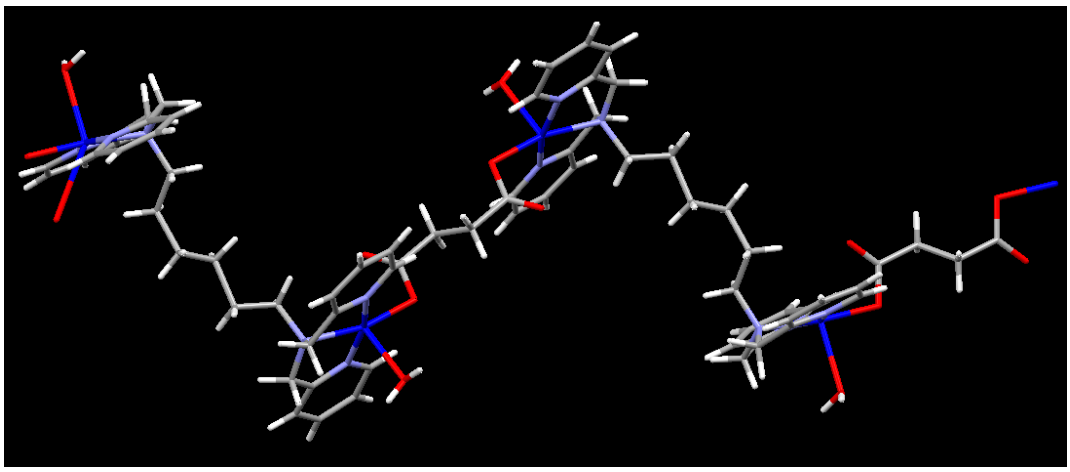

Figure 3.156. A perspective view of **73**.

Figure 3.157 below shows the formation of supramolecular assembly of 1D CP of the {[Cu_2(tphxn)(succinate)(H_2O)$_2$](ClO_4)$_2$}$_n$ via hydrogen bonding. Different colors are chosen for four different polymeric chains for clarity. The chains are connected via hydrogen bonding of coordinated water molecule with the coordinated oxygen atom of the carboxylate. The uncoordinated oxygen atom of succinate is hydrogen bonded to the lattice water molecule. These four polymeric chains are hydrogen bonded in such a way that they form a supramolecular cavity in which lattice water molecules entrapped. Hydrogen bonding parameters are listed in Table 3.31.

Table 3.31. Hydrogen bonding parameters in **73**.[a]

D–H…A	r (D-H) (Å)	r (H…A) (Å)	r (D…A) (Å)	∠D-H…A (deg)	Symmetry
O3--H3B...O11	0.88	2.53	3.29(3)	146	-1+x,y,z
O6--H6A...O14	0.88	2.02	2.87(4)	161	1-x,1-y,1-z
O7--H7A...O1	0.84	2.34	2.89(4)	123	1-x,1-y,1-z

[a]Numbers in parenthesis are estimated standard deviations in the last significant digits.

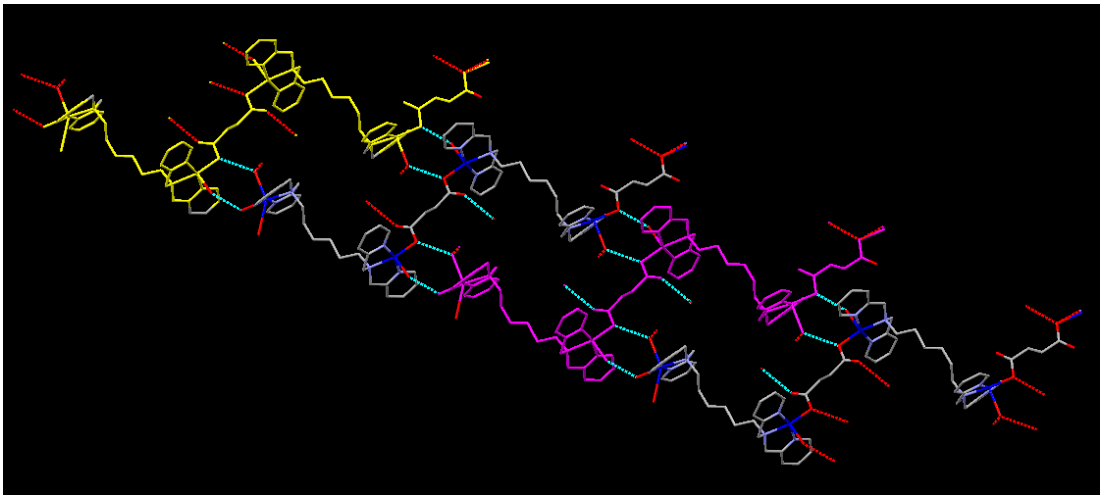

Figure 3.157. Supramolecular assembly in **73**.

{[Cu_2(tpbn)(digylconate)(ClO_4)(H_2O)](ClO_4)·H_2O·CH_3CN}$_n$ (74). A helical shaped 1D Coordination polymer that crystallizes in the monoclinic *P2$_1$* space group. A small change in the spacer atom in the dicarboxylate from CH_2 of glutarate described above (**65**) to O gave a totally different product. In this case, both copper centers are pentacoordinated but the coordination environment around Cu(II) centers is different. One of the Cu(II) is surrounded by three nitrogens of the ligand, one water molecule and one oxygen atom of the carboxylate; second Cu(II) center has a coordinated perchlorate instead of water (see Figure 3.158). In **74**, the

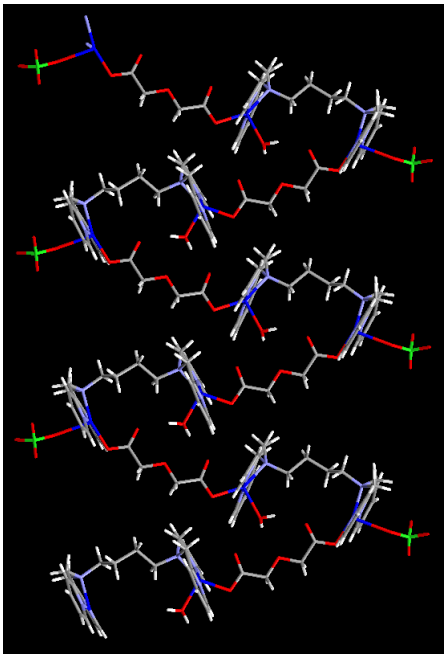

Figure 3.158. A perspective view of 1D helical CP of **74**.

diglyconate binds in a bis(monodentate) syn-syn fashion which is different from the one found in **65**. The selected bond distances and angles are listed in Table A82.

The coordinated water on one of the copper center is intramolecularly hydrogen bonded to the uncoordinated O atom of the carboxylate and O atom of the coordinated carboxylate forming two 5-membered rings sharing a common side (see Figure 3.159). The hydrogen bonding paraemeters are listed in Table 3.32.

Table 3.32. Hydrogen bonding parameters for **74** and **75**.[a]

D--H…A	r (D-H) (Å)	r (H…A) (Å)	r (D…A) (Å)	∠D-H…A (deg)	Symmetry
74					
O(6) --H(6A) ..O(4)	0.85	1.9	2.745	168	
C(1) --H(1A) ..O(16)	0.97	2.51	3.364	147	1+x,y,z
C(4) --H(4) ..O(2)	0.93	2.52	3.4195	162	1+x,y,z
C(11) --H(11) ..O(12)	0.93	2.51	3.1693	128	1-x,1/2+y,-z
C(14) --H(14A) ..O(5)	0.97	2.45	3.3981	165	x,1+y,z
C(16) --H(16) ..O(10)	0.93	2.57	3.309	137	1+x,y,z
C(30) --H(30B) ..O(9)	0.97	2.42	3.2221	139	1+x,-1+y,z
C(34) --H(34C) ..O(7)	0.96	2.4	3.2824	152	1+x,y,z
75					
O(1) --H(1A) ..O(13)	0.85	2.31	3.0979	153	-1/2+x, ½-y, -z
O(1) --H(1A) ..O(14)	0.85	2.54	3.25	141	-1/2+x, ½-y, -z
O(1) --H(1B) ..O(12)	0.85	1.95	2.7965	174	-1/2+x, ½-y, -z
O(2) --H(2A) ..O(15)	0.85	2.09	2.8566	150	1/2-x,-1/2+y,z
O(2) --H(2B) ..O(16)	0.85	1.89	2.6777	154	1/2-x,-y,1/2+z
C(1) --H(1C) ..O(10)	0.97	2.47	3.3215	146	
C(3) --H(3) ..O(10)	0.93	2.6	3.1732	121	
C(6) --H(6) ..O(9)	0.93	2.5	3.3845	159	1/2-x,-1/2+y,z
C(10) --H(10) ..O(16)	0.93	2.55	3.3414	143	-1+x, y, z
C(12) --H(12) ..O(8)	0.93	2.55	3.3649	146	-x,-1/2+y,1/2-z
C(13) --H(13A) ..O(6)	0.97	2.56	3.1699	121	
C(23) --H(23A) ..O(14)	0.97	2.55	3.519	175	-1/2+x,y,1/2-z
C(30) --H(30A) ..O(7)	0.97	2.55	3.4967	164	1/2-x,-1/2+y,z
C(31) --H(31B) ..O(9)	0.97	2.41	3.3036	153	1/2-x,-1/2+y,z

[a]Numbers in parenthesis are estimated standard deviations in the last significant digits.

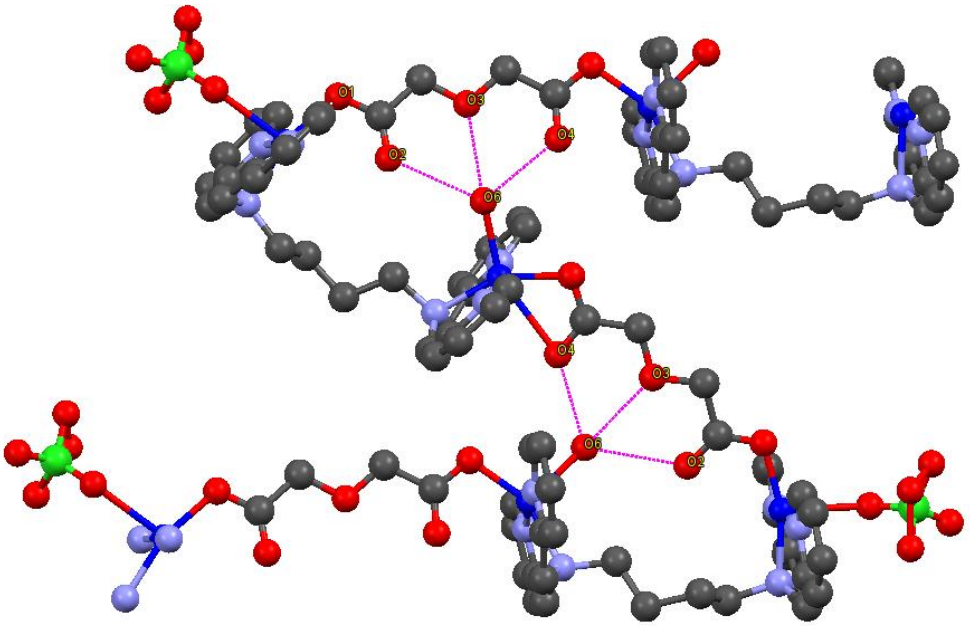

Figure 3.159. Intramoleular hydrogen-bonding in 1D CP of **74**.

The 1D CP chains are stacked together via π–π interactions found in two planes as shown in Figure 3.160. The centroid-centroid distances are 3.782 Å and 3.856 Å.[182]

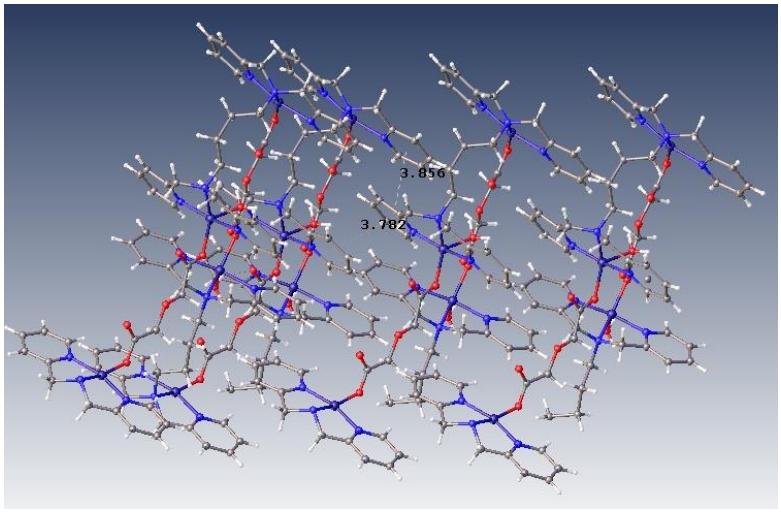

Figure 3.160. 2D Supramolecular assembly via π–π interactions in **74**.

$[Cu_4(tpbn)_2(2,2'\text{-dithioacetate})_2(H_2O)_4](ClO_4)_4$ (75). It is a molecular rectangle similar to **65** shown in Figure 3.161. The pore size is 15.756 Å x 8.662 Å. The dicarboxylate 2,2′-dithioacetate binds to the Cu(II) center in a similar fashion to that of glutarate in **65**. The selected bond distances and angles are listed in Table A83. As seen in **74** the slight change in spacer atom

resulted in a 1D CP. The reason for this could be due to similar electronegativities of C and S while the electronegativity of O is much higher than both C and S. The difference in the products is also evident from the UV-visible spectroscopic studies (vide infra).

These molecular rectangles are associated with each other via perchlorate anions. Inside the cavity of the rectangles the lattice water molecules are hydrogen bonded to the coordinated water molecules those pointing inside the cavity to form a hexameric motif inside the rectangle (shown by pink line in the Figure 3.162). This hexameric motif is hydrogen bonded to the uncoordinated oxygen atoms of the 2,2'-thiodiacetate. The molecular rectangles are connected with each other through coordinated water molecules (those pointing outside the cavity) via perchlorate anions. The hydrogen bonding parameters are listed in Table 3.32. Similar to **64**, these rectangles of **75** are connected via moderate π–π interactions in two planes (centroid-centroid distances: 3.623 Å and 3.841 Å).

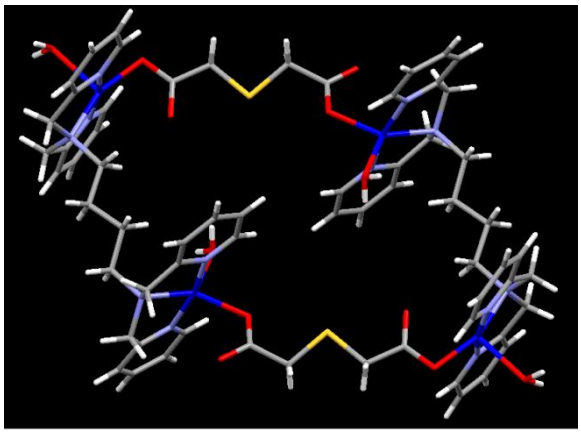

Figure 3.161. Structure of molecular rectangle, **75**.

{[Cu_2(tpbn)(tere)(H_2O)$_2$](ClO_4)$_2$·2H_2O}$_n$ (76). It crystallizes in the orthorhombic *Pbca* space group. Each pentacoordinated Cu(II) center is surrounded by three nitrogens of the ligand, one oxygen from the carboxylate and one water molecule. The carboxylate binds in a bis(monodentate) syn-anti fashion. The tpbn ligand spans between the two Cu(II) centers like in other cases (example) and terephthalate bridges two such subunits making it a 1D CP as shown in Figure 3.163. The selected bond distances and angles are listed in Table A84.

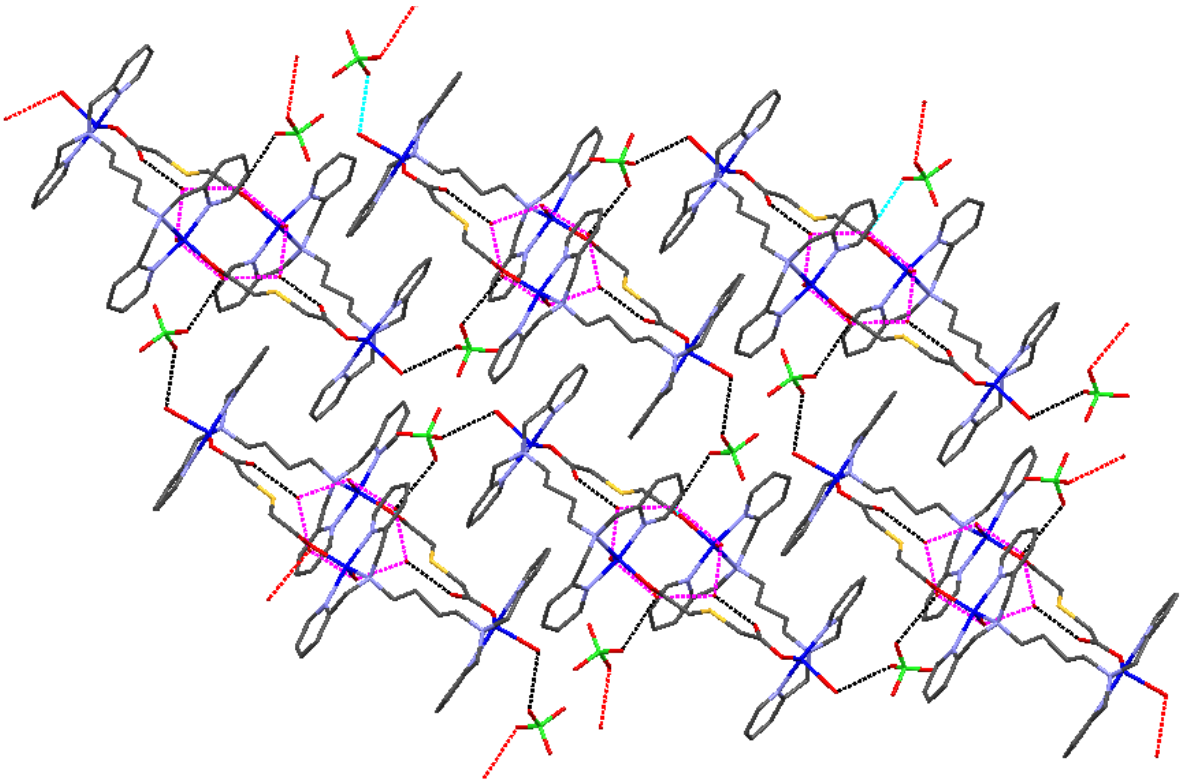

Figure 3.162. 2D supramolecular assembly in **75**.

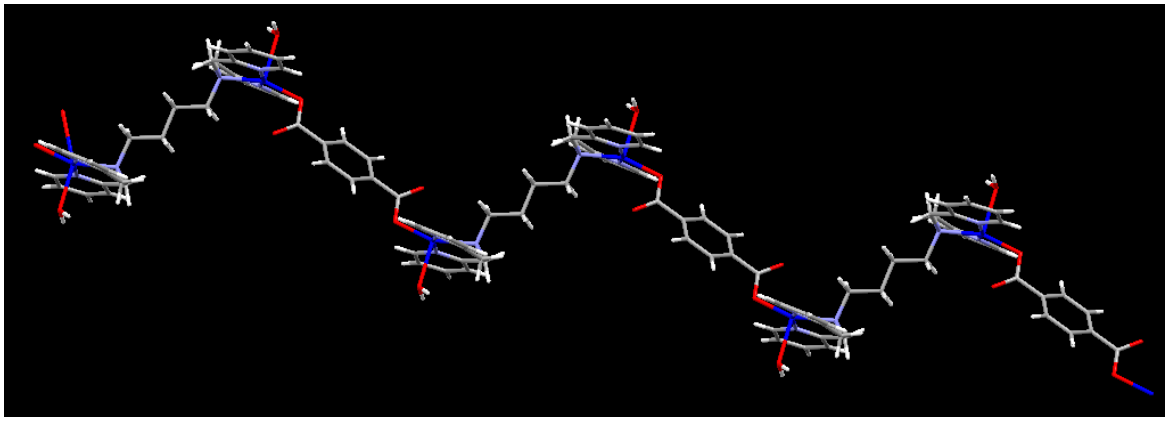

Figure 3.163. A perspective view of **76** (Only cationic part is shown).

The 1D CPs are further connected to form a supramolecular assembly via hydrogen bonding between coordinated water molecule and uncoordinated oxygen atom of terephthalate (distance: 2.762 Å). The hydrogen bonding parameters are listed in Table 3.33. The perchlorate anions are also hydrogen bonded via the lattice water molecules to form a 1D chain as shown in Figure 3.164. Two such chains are embedded within the polymeric chain of **76** as shown in Figure 3.165.

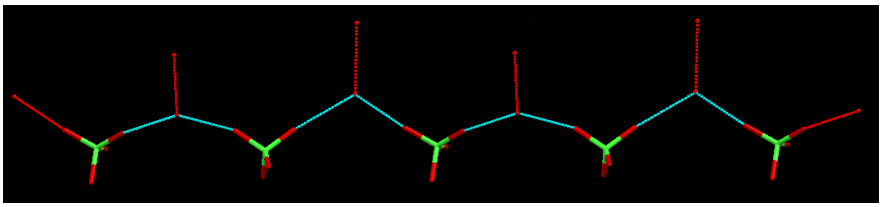

Figure 3.164. An arrangement of perchlorate anions chain in **76**.

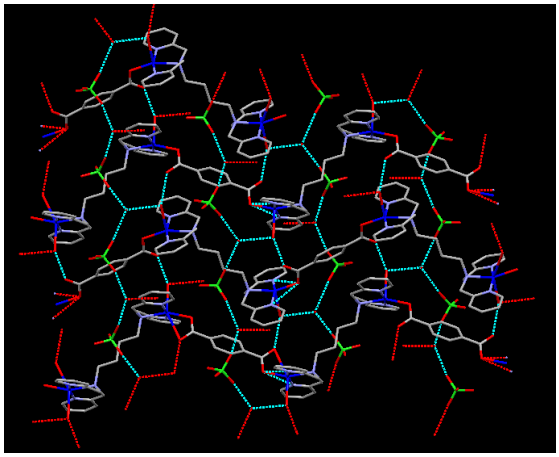

Figure 3.165. Hydrogen bonded network and perchlorate anion arrangement in **76.**

Table 3.33. Hydrogen bonding parameters for **76**.[a]

D–H…A	r (D-H) (Å)	r (H…A) (Å)	r (D…A) (Å)	∠D-H…A (deg)	Symmetry
O(1) --H(1B) ..O(3)	0.87	1.94	2.762(5)	157	-1/2+x,1/2-y,-z
O(8) --H(8A) ..O(1)	0.85	1.97	2.809(6)	169	
O(8) --H(8B) ..O(6)	0.85	2.11	2.918(7)	158	
C(7) --H(7A) ..O(7)	0.99	2.49	3.409(8)	155	x,1/2-y,-1/2+z

[a]Numbers in parenthesis are estimated standard deviations in the last significant digits.

{[Cu$_4$(F$_4$-tere)$_3$(tpbn)$_2$](ClO$_4$)$_2$·4H$_2$O}$_n$ (77). It crystallizes in the monoclinic *C2/c* space group. Due to the substitution on terephthalate, its structure is totally different from **76**. Two Cu(II) centers are connected by a bis(F$_4$-tere) core where F$_4$-tere shows two binding modes: monodentate and bridging. The bridging one binds to the Cu(II) center of the next unit as shown in Figure 3.166. The selected bond distances and angles are listed in Table A85. The third F$_4$-tere binds only in a monodentate fashion which connects one such layer with the other one shown in Figure 3.167.

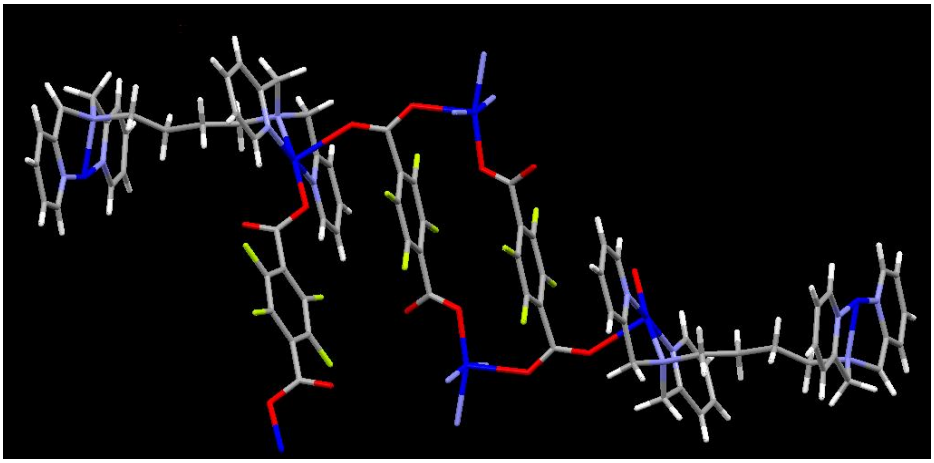

Figure 3.166. A part of the CP in **77**.

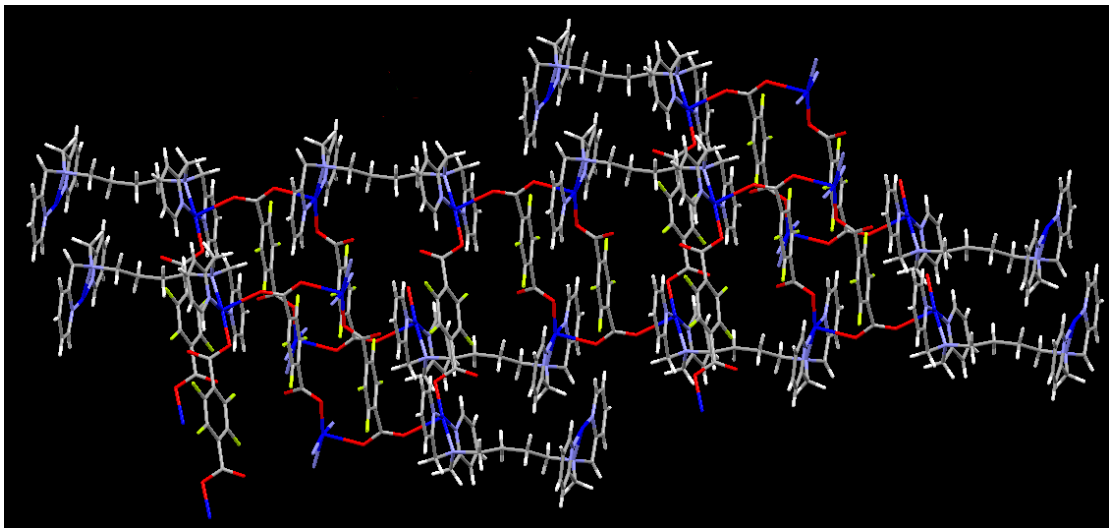

Figure 3.167. A perspective view of 2D CP of **77**.

{[$NaCu_2$(tppn)(O,O′-oxydiethylenediglyconate)(ClO_4)(H_2O)$_3$](ClO_4)$_2$}$_n$ (**79**). It is a 1D CP that crystallizes in the monoclinic chiral *$P2_1$* space group. Each Cu(II) center is pentacoordinated surrounded by three nitrogens of the ligand, one coordinated water molecule and one oxygen from carboxylate. The carboxylate binds in a bis(monodentate) syn-syn fashion. The selected bond distances and angles are listed in Table A86.

Since this compound was soluble in methanol-water mixture one molecule of sodium perchlorate was also found in the crystal structure. The molecule of sodium perchlorate is embedded in the crown made by the carboxylate as shown in Figure 3.168 (top). The sodium ion is bound to oxygens of the carboxylate groups, ether oxygens in the backbone of the carboxylate, one water

molecule and perchlorate ion. Thus the carboxylate which is connecting two Cu(II) centers acts a host to the Na^+ ion like the crown ethers. The Na-O distances vary from 2.338 to 2.643 Å, where those with ether oxygens are the shortest. Thus this 1D CP traps the sodium ion which is a by-product in the reaction. It can be clearly seen in Figure 3.168 (bottom) where sodium ion and the carboxylate atoms are shown in the space-filling model.

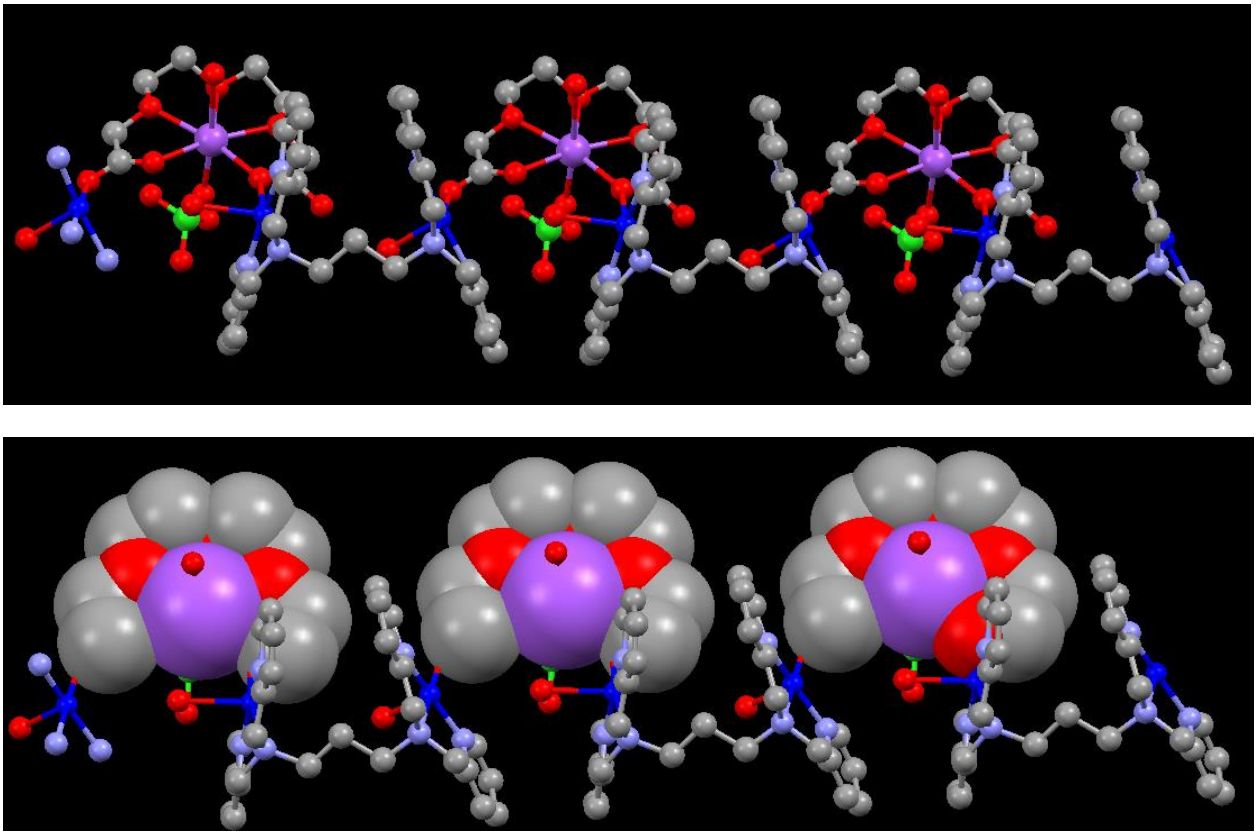

Figure 3.168. A schematic view of **79** (top) and sodium ion inside the CP (bottom).

{**[$NaCu_2$(tpbn)(O,O′-oxydiethylenediglyconate)(H_2O)(ClO_4)](ClO_4)$_2$}$_2$ (**80**). Unlike **79**, it is a dimetallacycle bridged by a perchlorate that crystallises in the monoclinic *P2₁/n* space group (see Figure 3.169). Although the synthesis of **79** and **80** were done at the same conditions, an effect of the methylene chain length produced different products. In this metallacycle copper(II) centers have different coordination environemnts. One Cu(II) center is pentacoordinated surrounded by three nitrogens of the ligand, one water molecule and one oxygen of the carboxylate whereas second Cu(II) center has one bound perchlorate oxygen. Like **79**, in this molecule sodium perchlorate was also found in the crystal structure. The sodium ion is found to be interacting with four oxygens of the carboxylate as shown in Figure 3.169, unlike **79** where sodium ion was

interacting with all the oxygens of the carboxylate. The selected bond distances and angles are listed in Table A87.

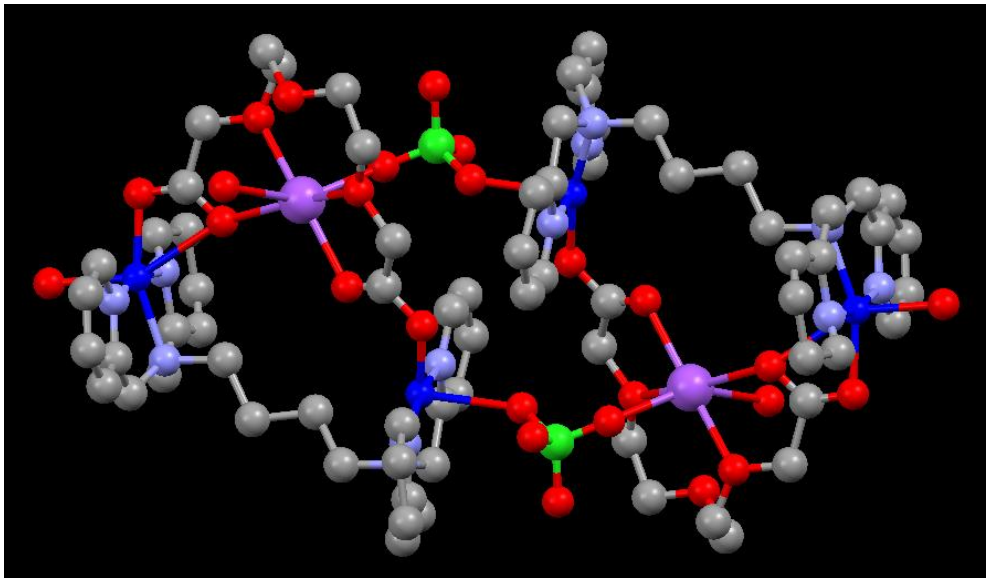

Figure 3.169. A view of the metallacycle in **80**.

{[Cu_4(tpen)$_2$(CDC)$_3$](ClO$_4$)$_2$·8H_2O}$_n$ (81). It crystallizes in the monoclinic *P2$_1$/c* space group. Each Cu(II) center is pentacoordinated and surrounded by three nitrogens of the ligand and two oxygens of the CDC. The role of CDC which shows two binding modes (monodentate and bridging) in this structure is remarkable: the dicopper centers with a bis(CDC) core is connected by a bis(monodendate) CDC to generate a ploymeric structure shown in Figure 3.170. On the other hand, the tpen ligand spans between two Cu(II) centers one of which is from the dicopper subunit with a bis(CDC) core.

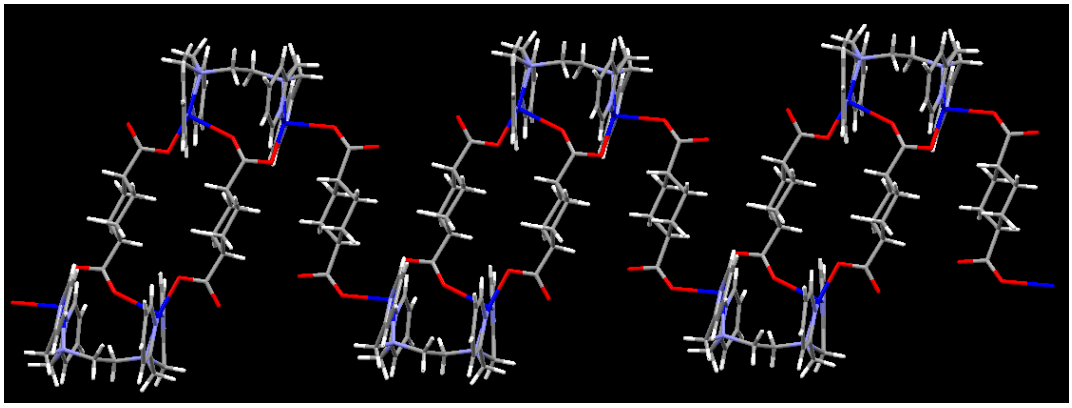

Figure 3.170. A perspective view of **81** (perchlorates and water not included).

Due to the presence of lattice water molecules the CDC which connects the two bis(CDC) core is intramolecularly hydrogen bonded to the uncoordinated oxygen atom of the CDC of the bis(CDC) core thus forming a new bis(CDC) core via hydrogen bonding shown in Figure 3.171. The hydrogen bonding distance is 2.529 Å.

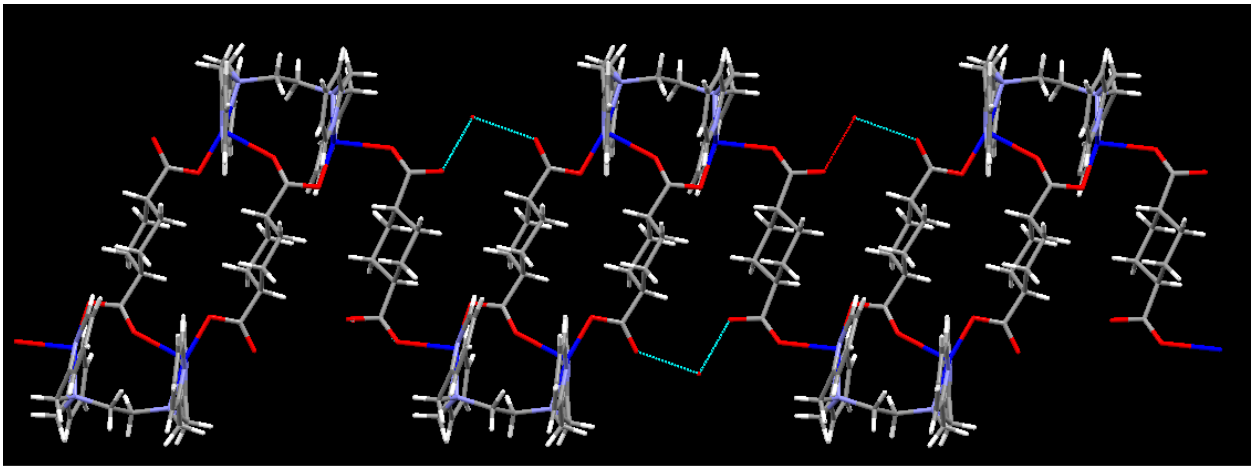

Figure 3.171. Supramolecular assembly in **81**.

$[Cu_8(tpen)_4(tdc)_4(H_2O)_4](ClO_4)_8 \cdot 4H_2O$ (82). It is an octanuclear discrete MOF of Cu(II) that crystallizes in the triclinic *P-1* (No. 2) space group shown in Figure 3.172. The cavity size is 19.478 Å x 18.419 Å. Out of the eight Cu(II) centers, six are equivalent and surrounded by three nitrogens, one water molecule and one oxygen atom of tdc. Among the six coordinated water molecules, two are pointing inside the cavity and all other four are pointing outside the cavity. Other two Cu(II) centers have similar coordination environment (N_3O_2) similar to six Cu(II) centers except an oxygen atom of the tdc coordinates instead of water molecule. Two tdc carboxylates behave differently from the other two in their binding modes: two binds in a syn-syn mondentate fashion and the other two shows monodenate as well as bridging modes. The S atoms of the thiophene rings in all tdc point outside the cavity.

The two rectangles are connected to form a supramolecular assembly shown in Figure 3.173 via hydrogen bonding. The coordinated water molecules on Cu(II) center are hydrogen bonded to the coordinated water molecule of the next unit; and coordinated oxygen atom of tdc of one unit is hydrogen bonded to the uncoordinated oxygen atom of tdc of next unit forming a 6-membered motif. Inside the cavity of this discrete MOF, due to the hydrogen bonding of lattice water

molecules with the coordinated water molecule (the one pointing inside the cavity) and coordinated oxygen atom of tdc a pentagon-shaped motif is formed which is further hydrogen bonded to another similar motif within the same cavity.

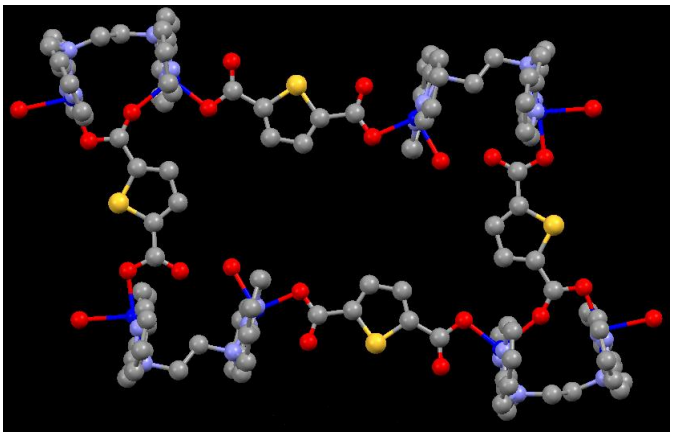

Figure 3.172. An octanuclear discrete MOF of **82**.

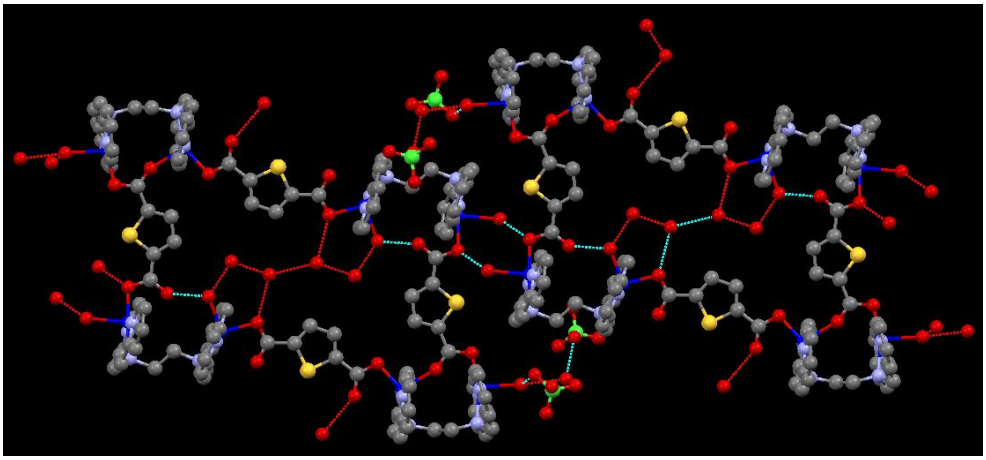

Figure 3.173. Supramolecular assembly in **82**.

$[Cu_4(tppn)_2(tdc)_2(H_2O)_4](ClO_4)_4{\cdot}2H_2O$ (83). It crystallises in the orthorhombic *Pbcn* space group. A discrete unit of **83** and its space-filling diagram are shown in Figure 3.174. The coordination environment around Cu(II) is N_3O_2 where N belongs to the polypyridyl ligand and O belongs to the bound water and carboxylate, respectively. The selected bond distances and angles around Cu1 and Cu2 are shown in Table A88. The tppn ligand spans between two Cu(II) centers and thiophene dicarboxylate binds in a monodentate syn-anti fashion forming a cavity of size 13.361 Å x 6.017Å (as shown in the spacefill diagram, Figure 3.174). The 'S' atom of the thiophene ring points inside the cavity. The Cu1-O6 (H_2O) and Cu2-O1 (H_2O) distances are 2.407 and 2.212 Å, respectively, which show that two Cu(II) centers are inequivalent. All four

Cu(II) centers have water molecules each pointing in opposite direction, two are facing towards the cavity and two are pointing outside the cavity. The lattice water molecules are found inside the cavity, which are strongly hydrogen bonded with the coordinated water molecules and uncoordinated oxygen atoms of thiophene dicarboxylate. This leads to the formation of a 2D supramolecular assembly of **83** as shown in Figure 3.175. All hydrogen bonding parameters are listed in Table 3.34. This supramolecular assembly is further stabilized by C-H…O interactions. As can be seen from Figure 3.175 water molecules inside the cavity are also hydrogen bonded to the perchlorate anions. The orientation of these perchlorates is different in alternative rectangles; these can be viewed as above the plane in one and below the plane in the next one. This supramolecular assembly of rectangles is further stabilized by π–π interactions in two planes which makes it 3D supramolecular assembly (see Figure 3.176). The centroid–centroid distances in plane 1 and plane 2 are 3.863 Å and 3.864 Å, respectively.

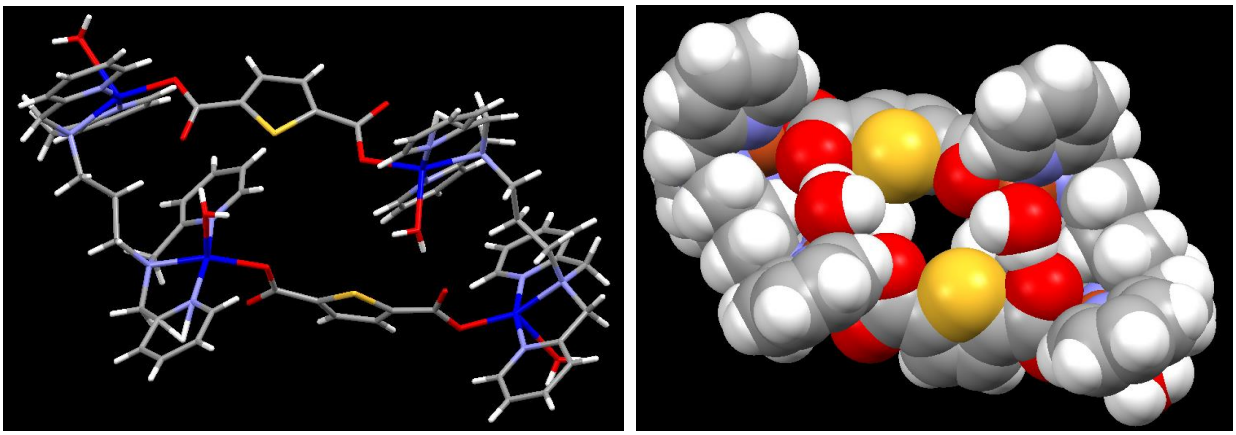

Figure 3.174. Structure of **83** (left) and its space-filling model (right).

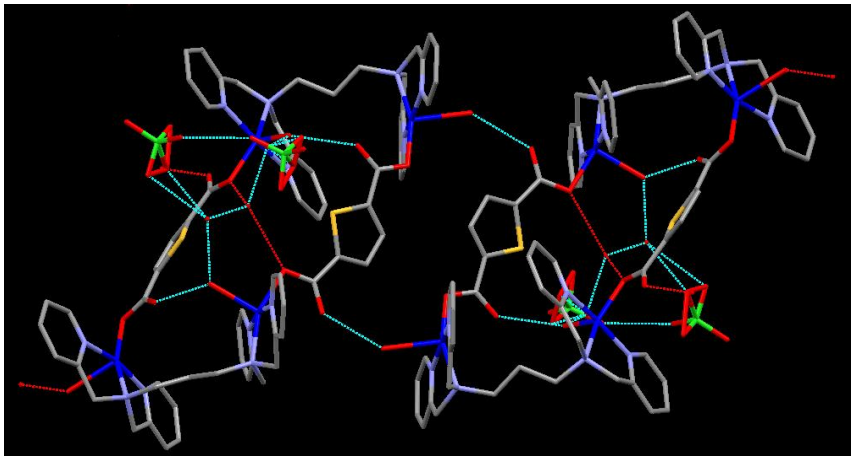

Figure 3.175. 2D network of molecular rectangles in **83** through hydrogen bonding interactions.

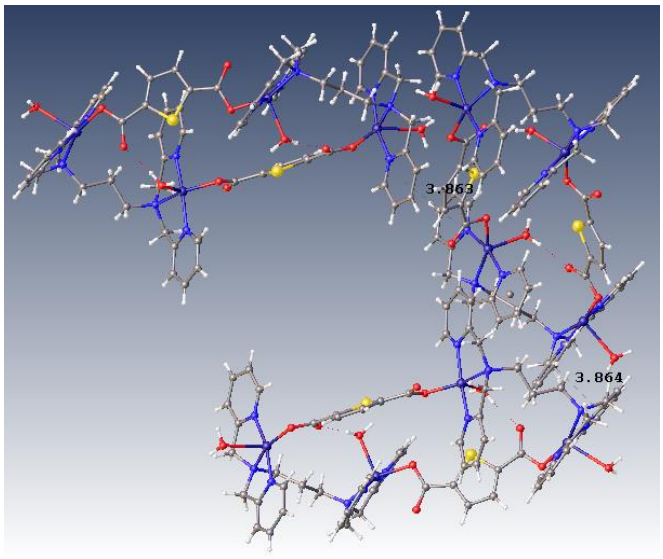

Figure 3.176. A view of π–π interactions in two planes in **83**.

Table 3.34. Hydrogen bonding parameters for **83**, **84** and **85**.[a]

83

D–H…A	r (D-H) (Å)	r (H…A) (Å)	r (D…A) (Å)	∠D-H…A (deg)	Symmetry
O(1)--H(1A)...O(10)	0.86	2.24	3.057(13)	156	-1/2+x,1/2-y,-z
O(2)--H(2A)...O(4)	0.82(4)	1.88(3)	2.699(5)	173(5)	1-x,y,1/2-z
O(2)--H(2B)...O(16)	0.81(4)	2.00(5)	2.702(14)	145(5)	1-x,y,1/2-z
O(16)--H(16A)...O(17)	0.85	1.83	2.579(18)	146	
C(7)--H(7)...O(13)	0.93	2.49	3.232(7)	137	1/2+x,1/2-y,-z
C(8)--H(8)...O(12)	0.93	2.56	3.210(7)	127	1/2+x,1/2-y,-z
C(9)--H(9)...O(5)	0.93	2.58	3.470(6)	160	-1/2+x,1/2-y,-z
C(13)--H(13A)...O(10)	0.97	2.46	3.409(9)	167	-1/2+x,1/2-y,-z
C(16)--H(16)...O(4)	0.93	2.43	3.333(6)	162	1/2-x,1/2+y,z
C(17)--H(17)...O(15)	0.93	2.56	3.167(9)	123	1/2-x,1/2+y,z
C(18)--H(18)...O(15)	0.93	2.6	3.191(8)	122	1/2-x,1/2+y,z
C(20)--H(20B)...O(4)	0.97	2.5	3.385(6)	151	
C(28)--H(28B)...O(11)	0.97	2.43	3.306(11)	150	-1/2+x,1/2+y,1/2-z

84

D–H...A	r (D-H) (Å)	r (H…A) (Å)	r (D…A) (Å)	∠D-H…A (deg)	Symmetry
C(7)--H(3)...O(23)	0.95	2.45	3.11(2)	126	1-x,-y,1-z
C(13)--H(9)...O(15)	0.99	2.58	3.52(4)	158	1-x,1-y,1-z
C(18)--H(14)...O(28)	0.95	2.56	3.42(2)	151	-x,1-y,1-z
C(20)--H(17)...O(6)	0.99	2.47	3.31(2)	143	
C(21)--H(20)...O(24)	0.99	2.57	3.54(2)	166	
C(24)--H(24)...O(13)	0.95	2.52	3.44(2)	163	1-x,-y,1-z
C(32)--H(32)...O(11)	0.95	2.53	3.44(2)	159	-x,1-y,1-z

C(33)--H(33)...O(15)	0.95	2.57	3.45(4)	153	
C(41)--H(37)...O(22)	0.95	2.47	3.30(2)	147	x,1+y,-1+z
C(43)--H(39)...O(10)	0.95	2.48	3.36(2)	153	x,1+y,z
C(46)--H(41)...O(19)	0.99	2.52	3.40(2)	149	x,1+y,z
C(46)--H(42)...O(24)	0.99	2.35	3.30(2)	160	1-x,1-y,1-z
C(51)--H(47)...O(25)	0.95	2.52	3.15(2)	124	1+x,y,-1+z
C(52)--H(48)...O(25)	0.95	2.6	3.21(2)	123	1+x,y,-1+z
C(54)--H(51)...O(24)	0.99	2.5	3.29(2)	136	1-x,1-y,1-z
C(55)--H(53)...O(21)	0.99	2.55	3.50(2)	160	1-x,1-y,1-z
C(60)--H(60)...O(3)	0.95	2.59	3.48(2)	155	x,1+y,z
C(61)--H(61)...O(19)	0.95	2.56	3.43(3)	153	1-x,1-y,-z
C(62)--H(62)...O(30)	0.95	2.58	3.46(2)	154	1-x,1-y,-z
C(63)--H(64)...O(13)	0.99	2.56	3.54(2)	173	

85

D–H…A	r (D-H) (Å)	r (H…A) (Å)	r (D…A) (Å)	∠D-H…A (deg)	Symmetry
O(1)--H(1A)...O(34)	0.85(7)	1.92(7)	2.697(18)	152(7)	
O(1)--H(1B)...O(16)	0.85(9)	2.41(10)	3.074(14)	136(8)	
O(2)--H(2A)...O(31)	0.86(4)	1.98(5)	2.831(18)	170(9)	x,1-y,-1/2+z
O(3)--H(3A)...O(11)	0.85(6)	2.23(8)	2.791(11)	124(5)	
O(3)--H(3B)...O(33)	0.85(5)	2.02(6)	2.763(14)	145(7)	1+x,1+y,z
O(33)--H(33A)...O(18)	0.85(5)	2.22(9)	2.96(2)	146(10)	
O(34)--H(34A) ...O(21)	0.91(12)	2.2(2)	2.83(3)	129(16)	
O(34)--H(34B) ...O(20)	0.90(16)	2.00(15)	2.86(3)	159	
C(12)--H(12B)...O(15)	0.99	2.52	3.453(15)	156	
C(13)--H(13B) ...O(16)	0.99	2.36	3.223(16)	145	
C(17)--H(17)...O(32)	0.95	2.44	3.37(2)	167	x,1-y,1/2+z
C(20)--H(20B)...O(6)	0.99	2.47	3.341(13)	147	
C(24)--H(24A) ...O(24)	0.99	2.29	3.17(2)	148	x,1-y,-1/2+z
C(24)--H(24B) ...O(31)	0.99	2.18	3.17(2)	178	x,1-y,-1/2+z
C(26)--H(26)...O(24)	0.95	2.59	3.20(2)	122	x,1-y,-1/2+z
C(27)--H(27)...O(6)	0.95	2.24	3.165(17)	163	x,2-y,-1/2+z
C(28)--H(28)...O(27)	0.95	2.53	3.18(2)	126	x,1+y,z
C(28)--H(28)...O(29)	0.95	2.59	3.28(3)	130	x,1+y,z
C(52)--H(52)...O(28)	0.95	2.44	3.23(3)	141	x,1-y,1/2+z
C(57)--H(57B)...O(8)	0.99	2.54	3.426(12)	149	
C(62)--H(62)…O(8)	0.95	2.45	3.275(13)	145	x,1-y,1/2+z
C(69)--H(69)...O(29)	0.95	2.37	3.28(3)	161	
C(70)--H(70)...O(30)	0.95	2.58	3.323(18)	136	

[a]Numbers in parenthesis are estimated standard deviations in the last significant digits.

$[Cu_4(tpbn)_2(tdc)_2(H_2O)_4](ClO_4)_4$ (84). It crystallizes in the triclinic *P-1* space group. There are two independent molecules in the asymmetric unit. The tpbn ligand spans between the two Cu(II) centers. The orientation of the methylene chain in tpbn is different in molecule 1 and 2 as found in **64**. In molecule 1 it is zig-zag type and in molecule 2 it is step type, which is a remarkable feature of this molecule. Both molecules are shown in Figure 3.177. The torsional angles are found to be different around tpbn chain in both the molecules which confirms the presence of two different orientation of tpbn. The torsional angles for tpbn chain from one alkyl nitrogen to another in molecule 1 are N2-C19-C20-C21: -165.59°; C20-C21-C22-N5: -169.22° and in molecule 2 are N11-C53-C54-C55 -167.77°; C54-C55-C56-N8: -164.18°. A difference of 2.18° and 5.04° for two corresponding sides is quite significant and is also a good evidence for the existence of two orientations or conformations of the tpbn chain. The coordination environment around copper(II) centers in both molecules is N_3O_2 type where N belongs to the polypyridyl ligand, O belongs to the coordinated water molecule and the carboxylate, respectively. The selected bond distances and angles around Cu1 and Cu2 of molecule 1 and Cu3 and Cu4 of molecule 2 are listed in Table A88. The thiophene dicarboxylate binds in a monodentate syn-anti fashion forming a cavity of 15.07 Å x 6.543 in molecule 1 and 14.42 Å x 6.502 Å in molecule 2. The 'S' atom of the thiophene ring in both the molecules is pointing towards the cavity as seen in **83**. The bond distances and angles listed in Table A88 around Cu(II) centers shows that copper centers are non-equivalent. All four Cu(II) centers have water molecules each pointing in opposite direction, two are facing towards the cavity and two are pointing outside the cavity in both the molecules. The lattice water molecules are found inside the cavity. Strong C-H…O interactions are found in these molecules which are listed in Table 3.34.

In addition to the C-H…O interactions, weak π–π interactions are also found in these molecules which make 2D supramolecular assembly of these rectangles as shown in Figure 3.178.

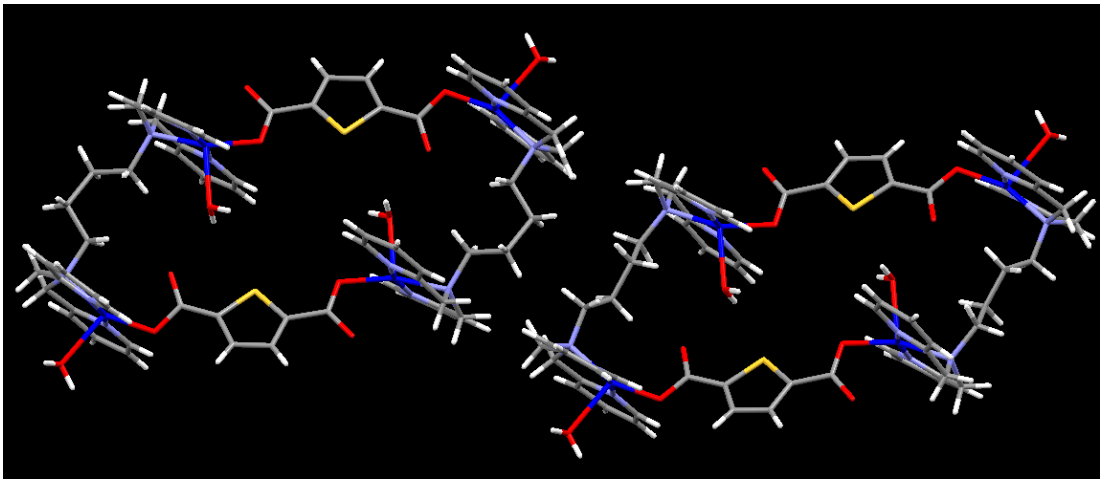

Figure 3.177. Molecular rectangles of **84** showing two conformations of tpbn.

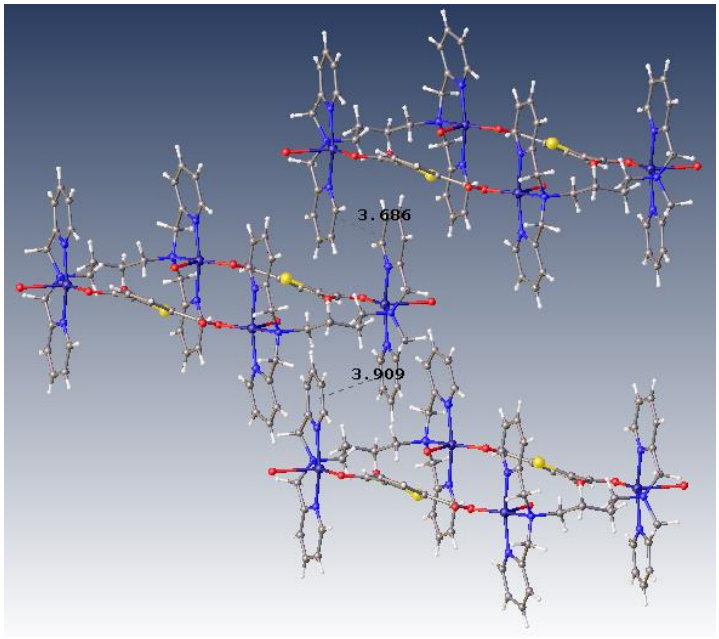

Figure 3.178. Formation of supramolecular assembly via π–π interactions in **84**.

$[Cu_4(tppen)_2(tdc)_2(H_2O)_4](ClO_4)_4$ (**85**). Unlike **83** and **84**, it crystallizes in the monoclinic *P*c chiral space group. A discrete unit of **85** is shown in Figure 3.179. The coordination environment around Cu(II) centers is N_3O_2 similar to that found in **83** and **84** where 'N' belongs to the polypyridyl ligand, 'O' belongs to coordinated water and carboxylate respectively, but the orientations of the thiophene rings and coordinated water molecules are different in **85**. All four Cu(II) centers are inequivalent. The ligand 'tppen' spans between two Cu(II) centers, and unlike **83** and **84** thiophene dicarboxylate binds in a bis(monodentate) syn-syn fashion forming a cavity

of size 11.107 Å x 11.823 Å. The thiophene rings of thiophene dicarboxylate are perpendicular to each other. All four coordinated water molecules on the Cu(II) centers are pointing outside the cavity. The presence of exocyclic lone pair on the thiophene unit imparts the change in environment inside the coordination cage. The selected bond distances and angles around Cu1, Cu2, Cu3 and Cu4 are listed in Table A88.

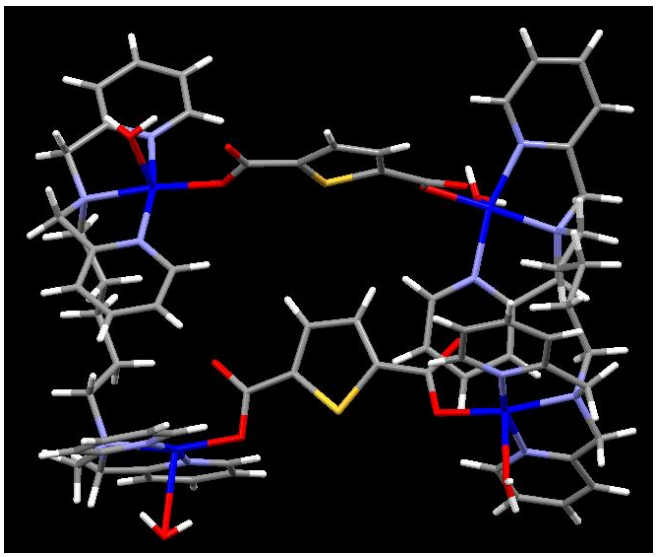

Figure 3.179. Structure of molecular rectangle, **85**.

$[Cu_2(tphn)(tdc)_2{\cdot}2NaClO_4]_n$ (87). With the methylene chain length of 7 in tphn, a 2D coordination polymer that crystallizes in the monoclinic *C2/c* space group is obtained. In this polymeric chain, two Cu(II) centers are connected with a bis(tdc) core where tdc binds in bis(monodentate) syn-syn fashion (see Figure 3.180). To the best of our knowledge, this is the first example having bis(tdc) core. This example shows the importance and effect of methylene chain length between the alkyl nitrogens of the ligand. The selected bond distances and angles are listed in Table A89.

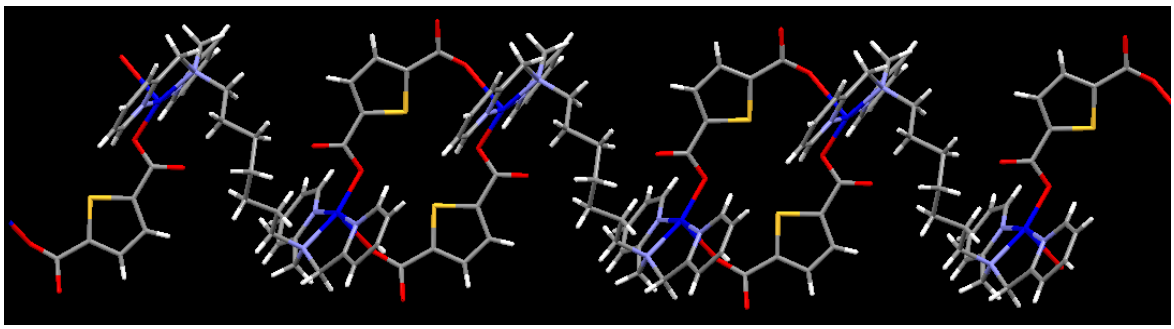

Figure 3.180. A perspective view of **87**.

Out of all the compounds discussed above with tdc (**82-87**), this is the only compound which was soluble in methanol and it was crystallized from methanol. Sodium perchlorate was also crystallized along with the product in the crystal structure. From single crystal X-ray studies, Na^+ was found to be interacting with the uncoordinated oxygen atoms of the tdc as shown in Figure 3.181. In other words, it is a heterometallic CP of s and d block elements. A heterometallic polymeric chain is shown in Figure 3.182.

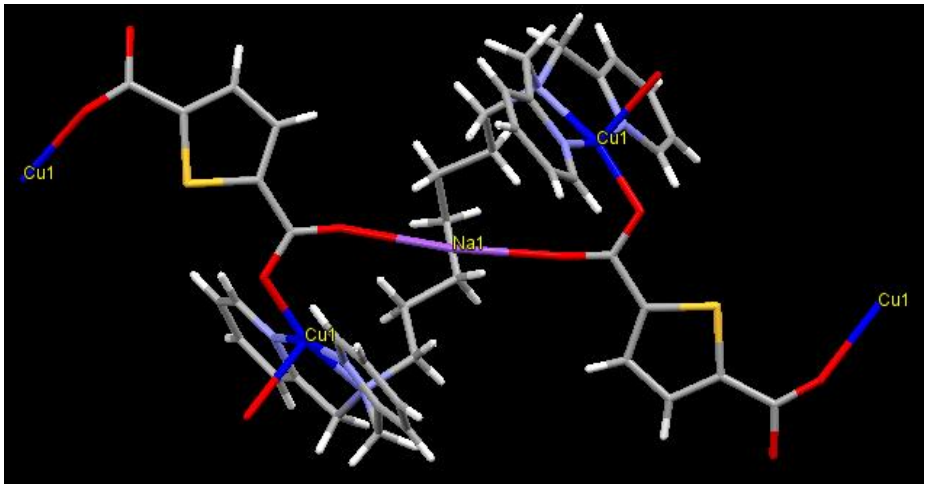

Figure 3.181. A part of CP of **87**.

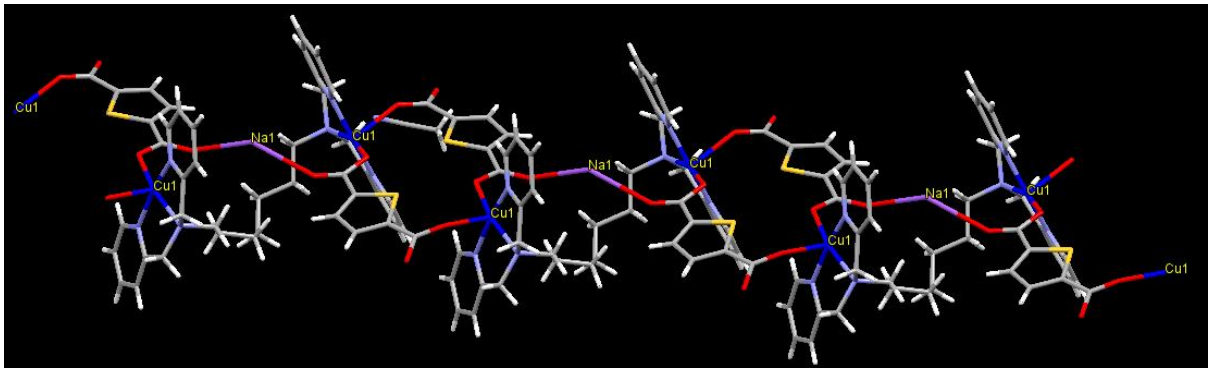

Figure 3.182. A perspective view of heterometallic CP of **87**.

FTIR Spectroscopy. The IR spectra of all the compounds were recorded in the solid state as KBr pellets. The peaks at 3473 cm^{-1} (**58**), 3419 cm^{-1} (**59**) and 3463 cm^{-1} (**60**) correspond to the O-H stretching frequency of coordinated water molecule. The peaks at 1556 and 1386 cm^{-1} (**58**), 1577, 1569, 1560 and 1417 cm^{-1} (**59**), 1576 and 1393 cm^{-1} (**60**) correspond to the asymmetric and symmetric stretch of the carboxylate, respectively. A difference of less than 200 cm^{-1} corresponds to the monodentate binding mode of the carboxylate. The peaks at 1094 and 623 cm^{-1} (**58**), 1091 and 623 cm^{-1} (**59**), and 1093 and 623 cm^{-1} (**60**) correspond to the perchlorate

anion. Similar trends are observed for **61**-**80**. The peaks at 3484 and 3429 cm^{-1} (**64**), 3429 cm^{-1} (**65**) and 3435 cm^{-1} (**66**) correspond to O-H strectching frequency of water molecule. Two kinds of O-H strectching frequencies suggest two different water molecules in **64** - coordinated and lattice water molecules.

The IR spectra of **82**, **83**, **84**, **85**, **86** and **87** show broad bands centered at 3423, 3435, 3429, 3438, 3439 and 3468 cm^{-1}, respectively due to the uncoordinated water molecules. The binding mode of thiophene dicarboxylate in each case is same, which is also evident from their asymmetric and symmetric stretching frequencies: 1589, 1577, 1354, 1341 cm^{-1} (**82**) ; 1578, 1357 cm^{-1} (**83**); 1579, 1359 cm^{-1} (**84**); 1581, 1356 cm^{-1} (**85**); 1594, 1352 cm^{-1} (**86**) and 1662, 1369 cm^{-1} (**87**). In **83**, **84** and **85**, a difference of 220-225 cm^{-1} between the symmetrical and unsymmetrical streching frequencies shows the monodentate binding mode of tdc as found in the crystal structure. The two sets of carboxylate stretching frequencies for **82** is due to the two binding modes of tdc. It also gives a series of bands between 1610 and 1310 cm^{-1}, which are due to the polypyridyl ligand. All complexes have peaks at 1089 and 626 cm^{-1} showing the presence of perchlorate ions with a shift by few numbers.

UV-Vis Spectroscopy. For comparison, selected Cu(II) compounds have also been studied by UV-Vis spectroscopy. It allows to correlate their absorbance differences with the soild state structures described above. From the solid state structures of **65**, **74** and **75**, it has been observed that the change of spacer atom, i.e., CH_2 to O to S in the dicarboxylate linker resulted in the formation of different products. In order to understand the difference in their electronic absorption behavior, these are studied by UV-Vis spectroscopy. Their UV-Vis spectra shown in Figure 3.183 indicate that λ_{max} values for **65** and **75** are close to each other suggesting similar coordination environment around Cu(II) centers whereas for **74** it appeared at 674 nm.

Similarly, the UV-Vis spectra for **83**, **84** and **85** (Figure 3.184) show peaks at 625 nm, 630 nm, 614 nm due to d-d transitions (^2E_g to $^2T_{2g}$) of copper(II). Peaks for **83** and **84** are very close to each other suggesting similar electronic environment around Cu(II), whereas in **85** it appears at 614 nm which clearly indicates the structural differences mentioned earlier, particularly the binding modes of tdc as well as the orientation of its thiophene ring.

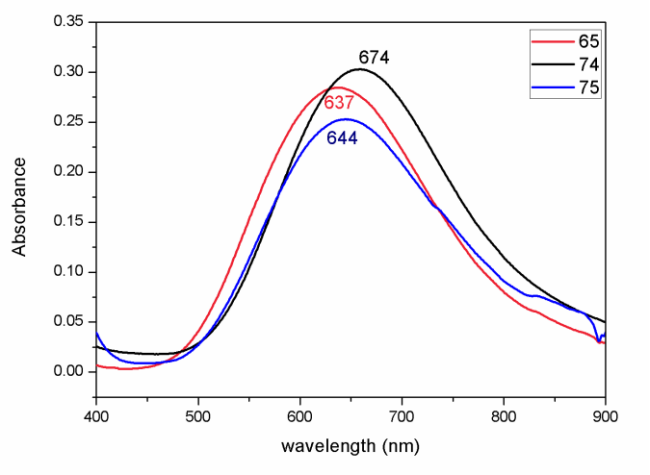

Figure 3.183. UV-Vis spectra of **65**, **74** and **75**.

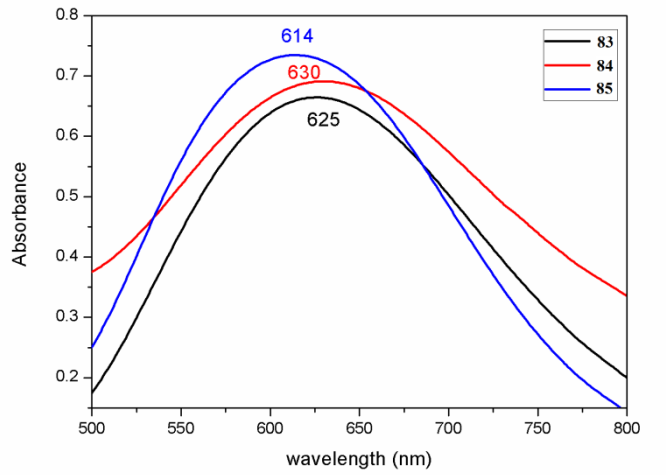

Figure 3.184. UV-Vis spectra of **83**, **84** and **85**.

Mass Spectral Studies. In addition to having single crystal X-ray structures for the rectangles, ESI mass spectroscopy was utilized to confirm the identity of the rectangles in the solution state. As evident from their solid state structures, all these compounds have a perchlorate as an anion. In all the compounds m/z = 1 and m/z = 2 were observed by loss of one and two perchlorate anions, respectively. The parent ion (m/z =1) peak in **64** and **65** differs by 14 units due to the increase in number of methylene group in the linker (from succinate to glutarate). The parent ion (m/z =1) peak differ by approx. 28 units from **83** to **84** to **85** due to the increase in the number of methylene chain length in the polypyridyl ligands. Compound **74** was studied to prove that only one kind of product is formed. These results are in good agreement with the observations based

on the characterization of the species in the solid state by other methods. The mass spectral data is summarized in Table 3.35. It shows that these rectangles are intact in solution state as well. Isotopic patterns due to the presence of perchlorate anions for the parent ions of **83**, **84** and **85** (m/z = 1) are shown in Figure 3.185.

Table 3.35. Mass spectral data for **64**, **65**, **74**, **75**, **83**, **84** and **85**.

Compound	m/z = 1		m/z = 2	
	Calc.	Found	Calc.	Found
64	1715.05	1715.05	807.12	807.20
65	1717.05	1717.05	809.12	809.20
74	811.29	811.09	355.92	355.29
75	1754.05	1752.83	827.30	827.06
83	1769.81	1770.23	835.18	835.40
84	1797.87	1797.27	849.21	849.34
85	1825.93	1825.29	863.24	863.31

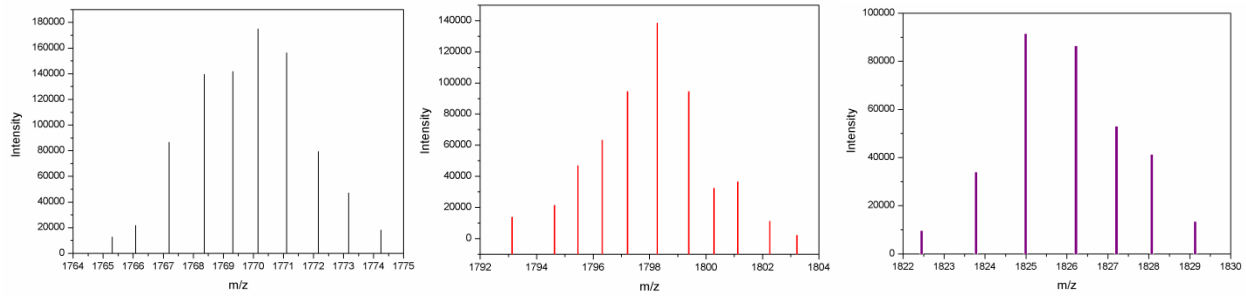

(**83**) (**84**) (**85**)

Figure 3.185. Isotopic patterns for m/z = 1 for **83**, **84** and **85**.

Electrochemical Studies. Cyclic voltammograms of **83**-**85** are shown in Figure 3.186. **83** shows two reductive responses at -0.45 V and at -0.261 V and an oxidation response at -0.183 V. While the first reduction process is irreversible in nature, the second one is quassireversible. **84** shows a reductive response at around -0.35 V and an oxidation response at -0.226 V indicating a

quassireversible process. On the other hand, **85** shows an irreversible reductive response at around -0.336 V. The reductive responses are due to Cu(II) to Cu(I) reduction. From this study, it is further evident that the coordination enviroments around the metal centers in these rectangles are different as observed through other characterization techniques.

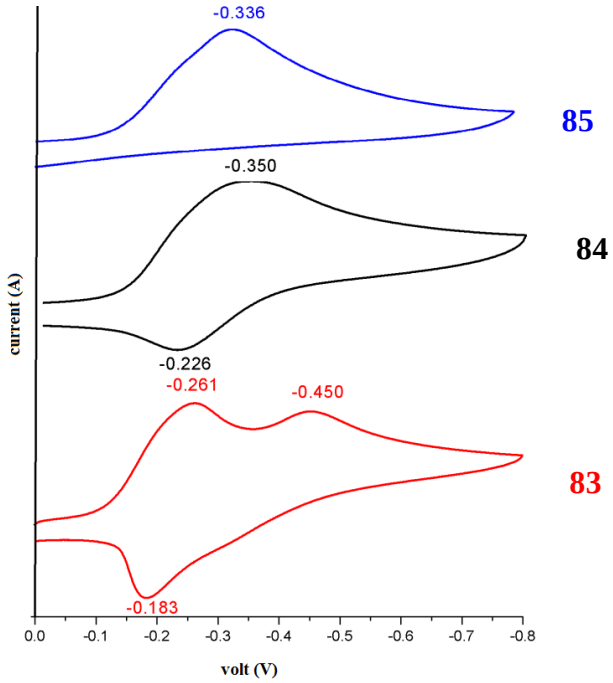

Figure 3.186. Cyclic voltammograms of **83-85**.

Photoluminescence Properties. The molecular rectangles with thiophene dicarboxylates (**83-85**) have been studied for their photoluminescence properties in solid state. Free H_2tdc shows a broad emission band at 440 nm due to the $\pi^*\rightarrow$n transition on excitation at 397 nm.[219a] All three molecular rectangles on excitation upon 380 nm showed two peaks in the emission spectra λ_{em}: 390 nm, 425 nm (tppn); 420 nm, 440 nm (tpbn); 400 nm, 425 nm (tppen). This can be due to the transition within the tdc ligand perturbed by the coordination of the carboxylate groups to the Cu(II) centers.[219b] The emission and excitation spectra for **83-85** are shown in Figure 3.187.

Water Adsorption Studies. Both molecular rectangles (**83** and **84**) were studied for its water adsorption properties due to the presence of cavity in these molecules. These were pretreated at 100 °C under vacuum for 24 hours. Their water adsorption isotherms (solid square, adsorption; open circle, desorption) are shown in Figure 3.188. In **83**, the water uptake was ca. 90 cm^3/g at

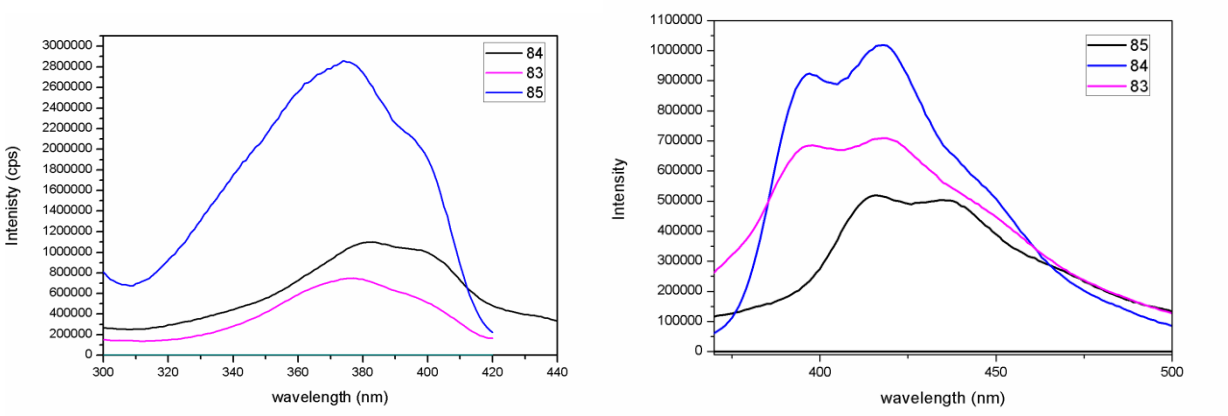

Figure 3.187. Excitation (left) and Emission (right) spectra for **83, 84** and **85**.

p/po = 1 and it retains 80 cm^3/g on desorption at p/po = 0.2. This type of materials which show more adsorption of the adsorbate at lower p/po can be good canditates to use as a desiccant. In **84**, the maximum adsorption of water is 160 cm^3/g at p/po = 1 and on desorption it retains ca. 75 cm^3/g at p/po = 0.3. The area between two curves (adsorption and desorption) shows the degree of hydrophilicity. More the area, the more is the hydrophilicity interactions between adsorbate and adsorbent surface. It is clear that the surface and pore of **84** is more hydrophilic than **83**.

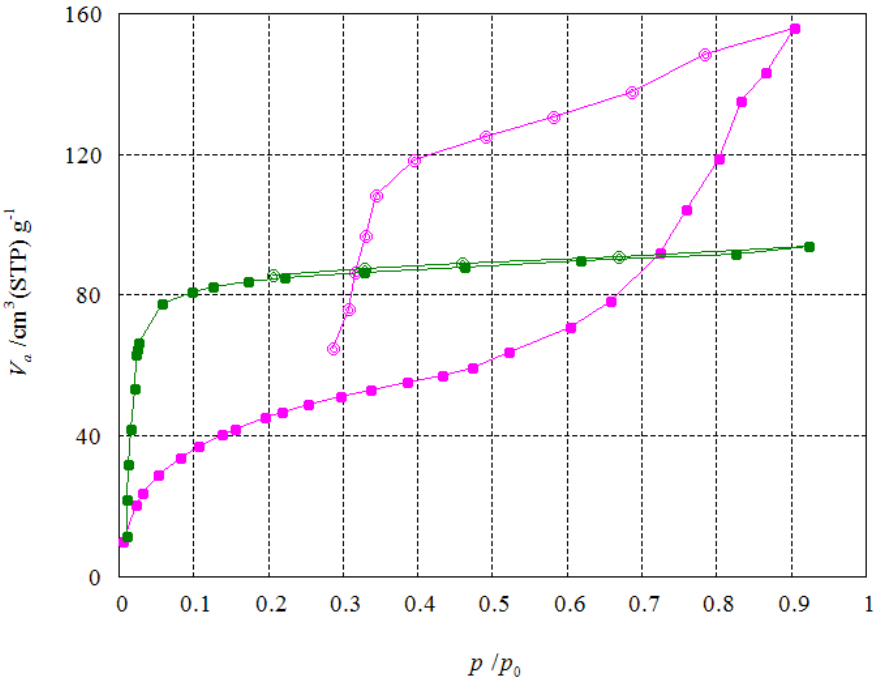

Figure 3.188. Water adsorption isotherms for **83** (green) and **84** (pink).

Tricarboxylates as linkers

Synthesis. Two MOCNs with BTC and CTC have been prepared. The MOCN with CTC-tpen was prepared under ambient conditions whereas that with BTC-tpbn was prepared under reflux conditions in a water-methanol mixture. Scheme 30 summarizes their syntheses.

$$Cu(ClO_4)_2 + tpen + Na_3CTC \xrightarrow[RT]{H_2O/MeOH} \{Cu_6(tpen)_3(CTC)_2](ClO_4)_6\}_n \textbf{(88)}$$

$$Cu(ClO_4)_2 + tpbn + Na_3BTC \xrightarrow[Reflux]{H_2O/MeOH} \{Cu_4(tpbn)_2(BTC)_2(H_2O)_2](ClO_4)_2\}_n \textbf{(89)}$$

Scheme 30. Synthesis of **88** and **89**.

Single Crystal Structure Analysis. Single crystals for **88** were grown by the slow evaporation of its solution in a mixture of water/acetonitrile whereas single crystals for **89** were grown by layering a DMSO solution of the compound with acetonitrile.

$[Cu_6(tpen)_3(CTC)_2](ClO_4)_6 \cdot 4H_2O$ (88). It is a 3D CP that crystallizes in the monoclinic $P2_1/n$ space group (see Figure 3.189). All three carboxylate groups of CTC are coordinated to the copper(II) centers; each copper(II) center is further connected to another copper(II) center via the spanning tpen ligand. The fifth site on each Cu(II) center is occupied by a water molecule. The selected bond distances and angles are listed in Table A90.

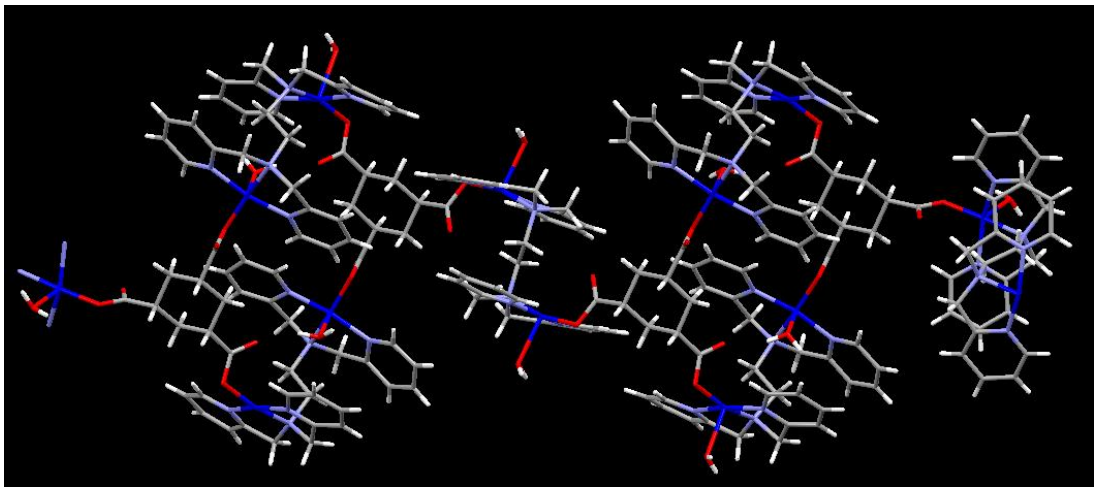

Figure 3.189. A perspective view of 3D CP of **88**; perchlorate anions and water molecules are omitted.

{$Cu_4(tpbn)_2(BTC)_2(H_2O)_2$]$(ClO_4)_2 \cdot 4H_2O \cdot 2DMSO\}_n$ (**89**). It is a 3D MOF comprising of Cu(II), BTC and tpbn as shown in Figure 3.190. In the literature,[121a] the Cu(II)-BTC compound has a paddle wheel structure with dicopper(tetracarboxylato) core, which is absent in **89**. All Cu(II) centers are pentacoordinated surrounded by three nitrogens of the tpbn ligand and two oxygens of the carboxylate group. Eight Cu(II) centers form a loop (colored yellow in Figure 3.191) which can be viewed as two bridges connected by a channel. The length of this channel is 30.261 Å and width is 11.421 Å and 7.655 Å. There is one small pore where two copper centers are bridged by two BTC molecules. The dimension of this pore is 7.529 Å x 5.627 Å. The Copper(II) centers in this pore has no coordinated water molecule. The selected bond distances and angles are listed in Table A91. In the space filling representation of this MOF, distribution of pores can be clearly seen (Figure 3.192).

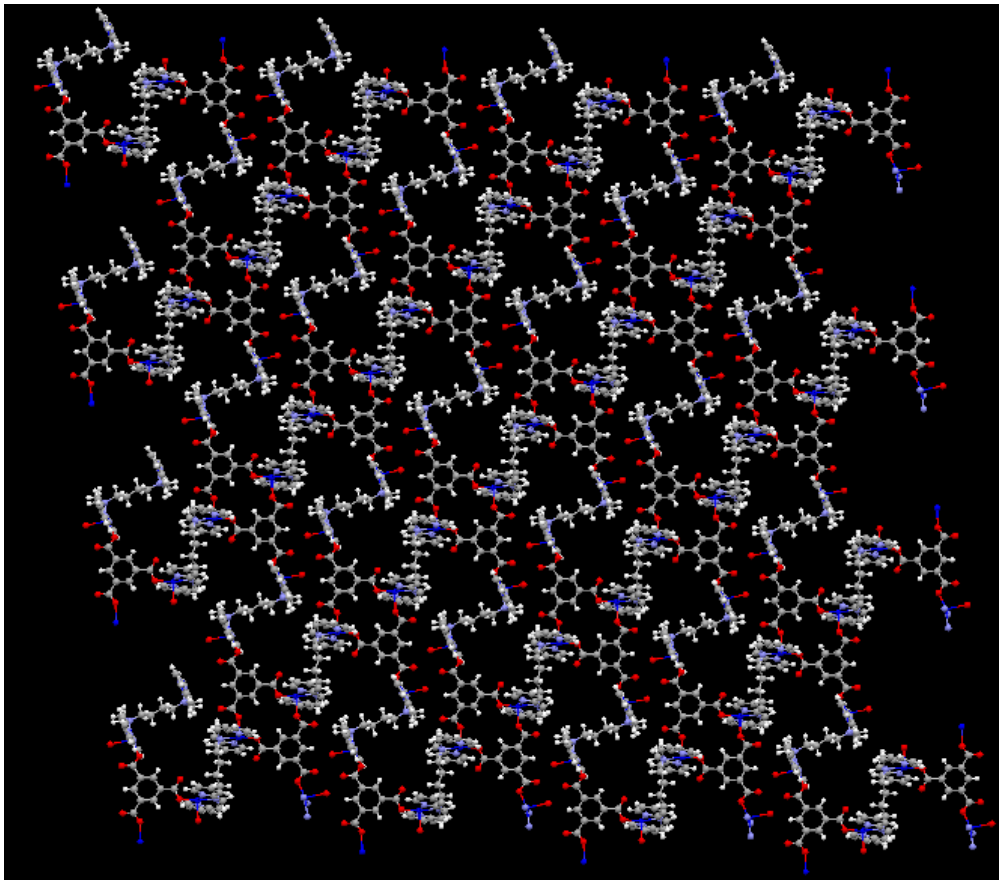

Figure 3.190. A perspective view of **89** (perchlorate anions and lattice water molecules are omitted for clarity).

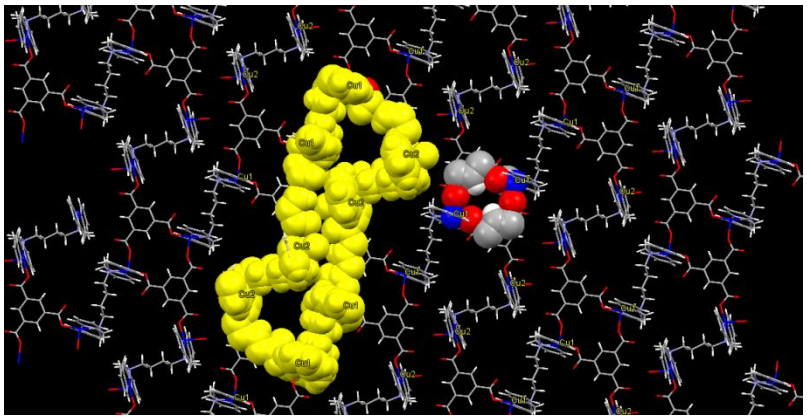

Figure 3.191. A part of 3D MOF of **89** showing two kinds of pores.

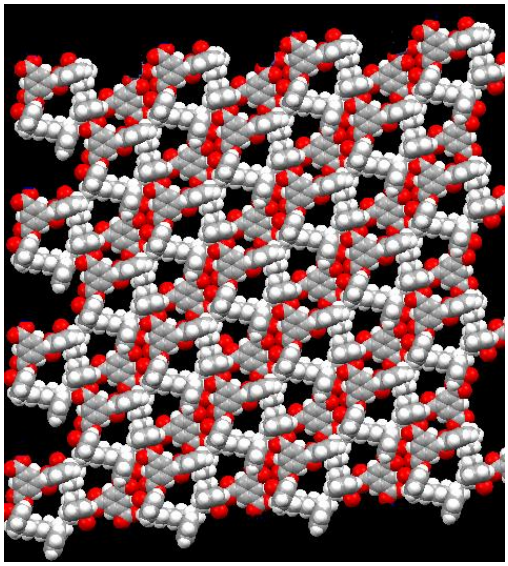

Figure 3.192. Distribution of pores in 3D MOF of **89**.

It is a Shubnikov plane net having feS topology determined by TOPOS. In the topological view shown in Figure 3.193, two kinds of pores can easily be seen. The smaller pores correspond to the Cu(II) centers bridged by BTC whereas the other one represents the larger pore.

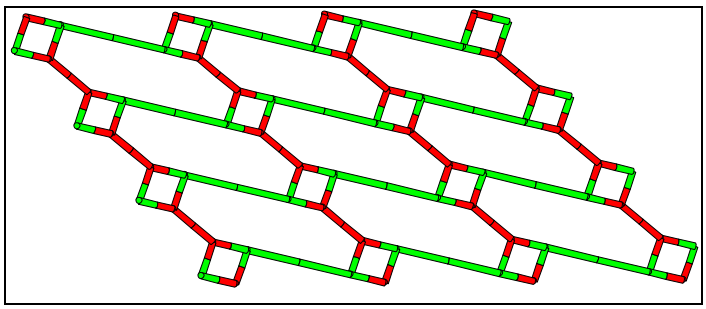

Figure 3.193. A topological view of **89**.

Water Adsorption Measurements. Due to the presence of two kinds of pore in **89**, the sample was studied for water adsorption properties. The sample was pretreated at 100 °C under vacuum for 12 hours. The maximum uptake was 190 cm^3/g and on desorption it retains ca. 150 cm^3/g of water. The isotherm for this material shows two humps (see Figure 3.194) which suggest that one kind of pores is filled first then the next. This material showed very promising results in comparison to zeolites; the maximum uptake by zeolites reported in the literature is 200 cm^3/g.

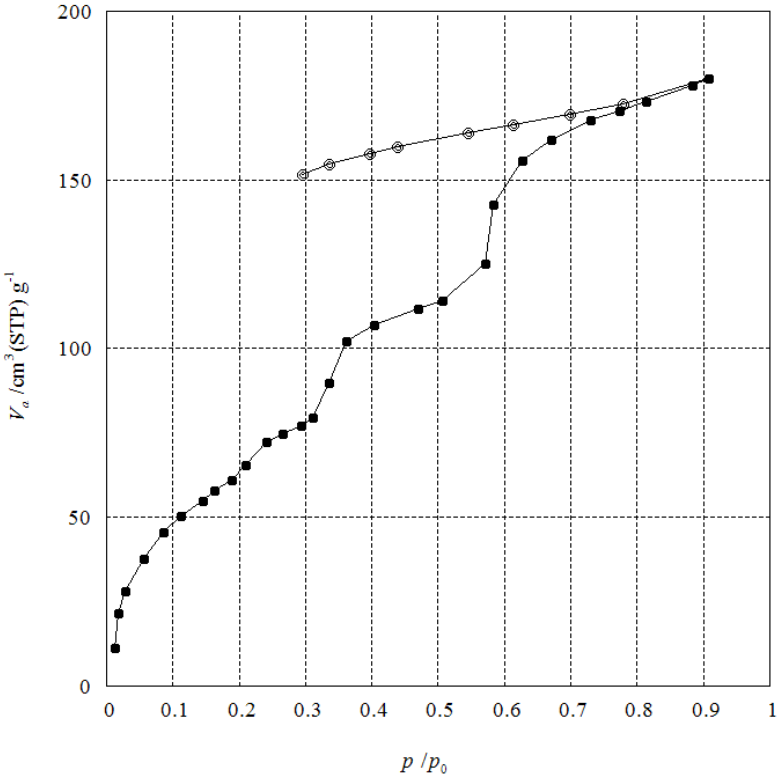

Figure 3.194. Water adsorption isotherm for **89**.

FTIR Spectroscopy. Both the compounds were studied in the solid state as KBr pellets. The peaks at 3401 (**88**) and 3428 (**89**) cm^{-1} correspond to the O-H stretching frequency of the lattice water molecules. The peaks at 1576, 1567, and 1389 cm^{-1} (**88**) and 1562, 1358 cm^{-1}(**89**) correspond to the asymmetric and symmetric stretching frequency of the carboxylate, respectively. The peaks at 1610, 1444, 767 cm^{-1} are due to the polypyridyl ligand; these peaks are common in both with a shift by few wavenumbers. The peaks at 1093 and 625 cm^{-1} are due to the perchlorate anion.

Disulphonate linkers

Extending the chemistry of dicarboxylates, disulphonates are also utilized as linkers for Cu(II) and the hexadentate ligands in this work. Three MOCNs are prepared: $[Cu_2(tpen)_2(2,6\text{-}NDS)_2(H_2O)_4]\cdot 8H_2O$ (**90**), $\{[Cu_4(tppn)_2(Cl)_2(H_2O)_4](2,6\text{-}NDS)_2\cdot 14H_2O\}_n$ (**91**), $\{[Cu_2(tpbn)(2,6\text{-}NDS)(Cl)_2]\cdot 5H_2O\}_n$ (**92**), where 2,6-NDS = 2,6-naphthalene disulphonate. In this series, the most notable difference is the binding of 2,6-NDS. In case of tpen, it is a dinuclear Cu(II) compound with NDS binding in a monodentate fashion; in case of tppn, a Cl-bridged cationic polymer with NDS acting as a counter anion is obtained; in case of tpbn, NDS is binding in a bis(monodentate) fashion resulting in a 1D CP. There are a few reports where disulphonates have been used in the generation of CPs similar to **92**.[134]

Synthesis. All three complexes with NDS are prepared via one pot self-assembly reaction of copper(II) chloride, ligand and sodium salt of NDS. The products were obtained as precipitates and were purified via crystallization. Based on the CHN analyses for both precipitates and crystals in each case, it was found that the precipitate had a molecule of the starting material $CuCl_2$. The yields in the experimental section are reported for the product obtained after crystallization. Scheme 31 summarises their syntheses.

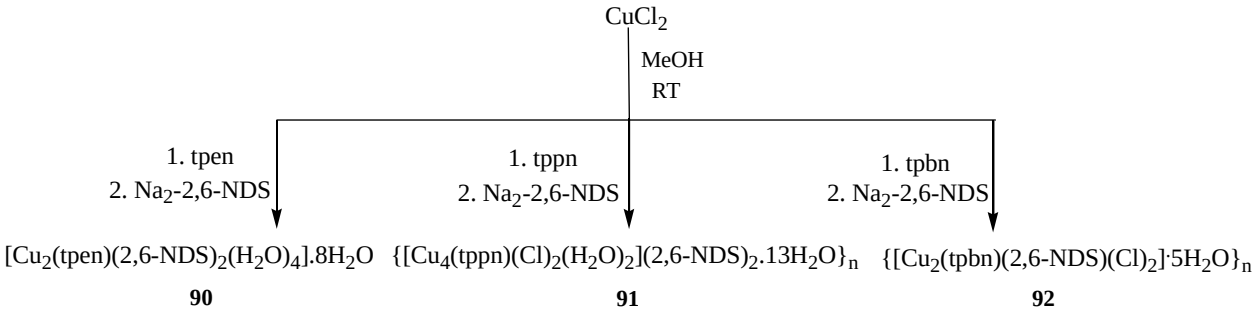

Scheme 31. Synthesis of **90**-**92**.

Single crystal structure analysis. Single crystals for **90**, **91** and **92** are grown from the slow evaporation of the aqueous and acetonitrile mixture solution.

$[Cu_2(tpen)_2(2,6\text{-}NDS)_2(H_2O)_4]\cdot 8H_2O$ (90). It is a dinuclear compound that crystallizes in the monoclinic *C*2/c space group. In the dinuclear unit shown in Figure 3.195, the tpen ligand spans between two hexacoordinated Cu(II) centers, each of which also has three oxygen atoms from

two water molecules and one monodentate 2,6-NDS. The selected bond distances and angles are listed in Table A92.

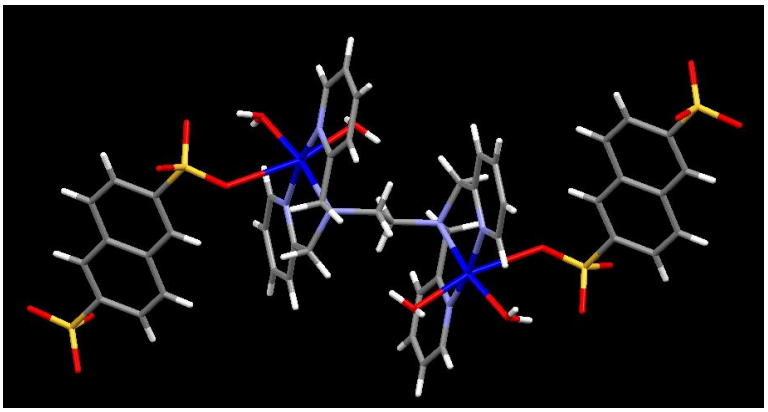

Figure 3.195. A perspective view of **90**.

A 6-membered motif $R_6^6(6)$ is formed via hydrogen bonding of the lattice water molecules with the uncoordinated oxygen atoms of the sulphonate group connects the two dinuclear units to form a supramolecular assembly as shown in Figure 3.196. In addition to this, other lattice water molecules are hydrogen bonded in such a way that it looks like a water channel flowing through the two dinuclear units. The hydrogen bonding parameters for **90** are listed in Table 3.36.

Table 3.36. Hydrogen bonding parameters for **90**.[a]

D–H…A	r (D-H) (Å)	r (H…A) (Å)	r (D…A) (Å)	∠D-H…A (deg)	Symmetry
O(7)--H(7A)...O(4)	0.82	1.99	2.713(8)	147	1-x,y,1/2-z
O(7)--H(7A)...O(5A)	0.82	2.48	3.137(18)	138	1-x,y,1/2-z
O(7)--H(7B)...O(11)	0.78(4)	1.93(5)	2.712(6)	177	
O(8)--H(8A)...O(4A)	0.82	1.95	2.730(13)	159	-1/2+x,-1/2+y,z
O(8)--H(8A)...O(5)	0.82	1.84	2.610(13)	157	-1/2+x,-1/2+y,z
O(8)--H(8B)...O(3)	0.81(5)	1.91(5)	2.685(4)	163	
O(9)--H(9A)...O(12)	0.85	1.75	2.578(15)	166	-x,y,1/2-z
O(10)--H(10A)...O(4)	0.85	2.08	2.876(9)	155	1-x,y,1/2-z
O(10)--H(10A) ...O(6A)	0.85	1.90	2.557(16)	133	1-x,y,1/2-z
O(11)--H(11A) ...O(13)	0.85	2.27	2.965(6)	139	x,-y,-1/2+z
C(16)--H(16)...O(3)	0.93	2.39	3.248(7)	154	1/2-x,-1/2-y,-z
C(18)--H(18)...O(5)	0.93	2.55	3.442(14)	160	-1/2+x,-1/2+y,z
C(19)--H(19A)...O(7)	0.97	2.43	3.215(5)	138	1/2-x,1/2-y,-z
C(22)--H(22)...O(9)	0.93	2.51	3.408(15)	163	1/2+x,1/2+y,z

[a]Numbers in parenthesis are estimated standard deviations in the last significant digits

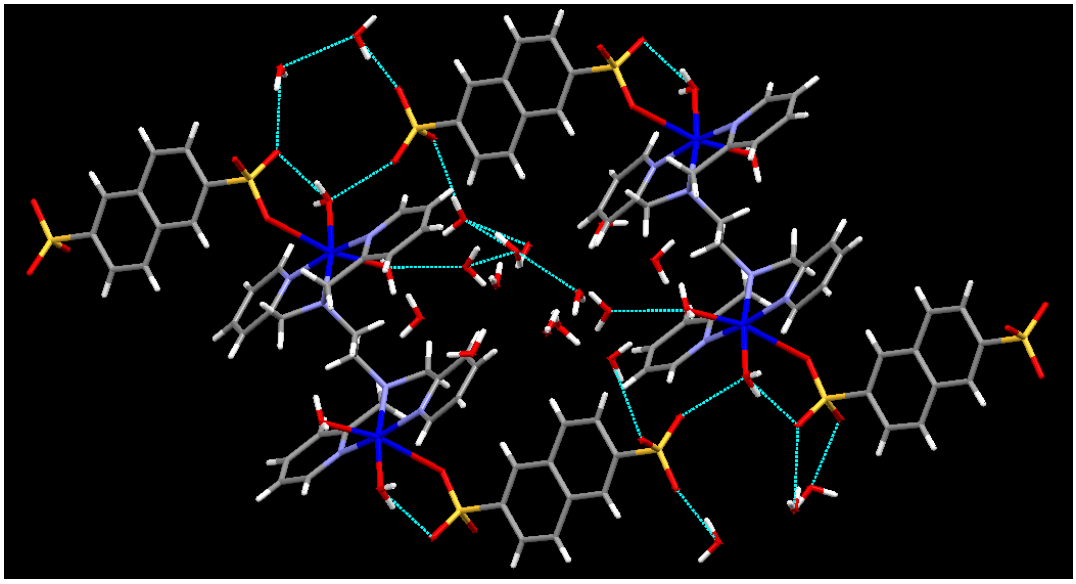

Figure 3.196. The supramolecular network in **90**.

$[Cu_4(tppn)_2(Cl)_4(H_2O)_4](2,6\text{-}NDS)_2 \cdot 14H_2O$ (91). It is a chloride bridged 1D CP that crystallizes in the chiral *P1* space group. Unlike **90** (vide supra) and **92** (vide infra), 2,6-NDS acts as anion in **91**. The copper centers in the polymer have different coordination environments - the fifth site on one copper(II) center is occupied by the chlorine atom whereas on the second copper(II) center it is alternately occupied by a coordinated water molecule (see Figure 3.197). The selected bond distances and angles are listed in Table A93.

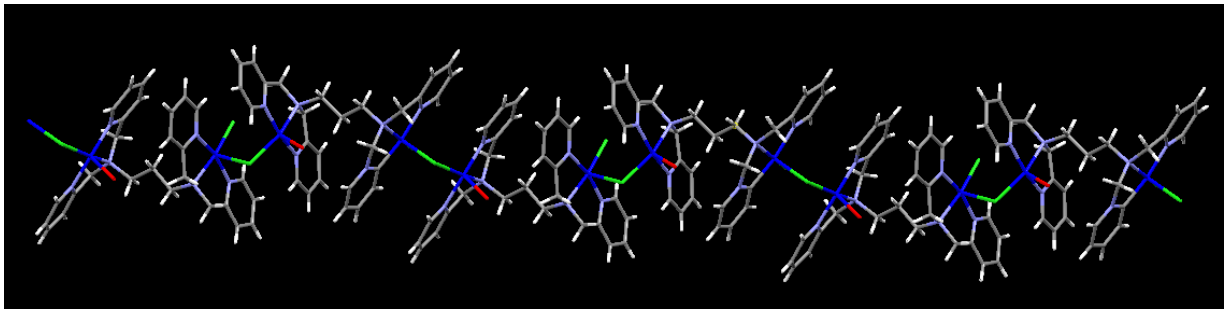

Figure 3.197. A perspective view of **91**.

The suphonate dianions are hydrogen bonded to the coordinated water molecule and lattice water molecules to form a network as shown in Figure 3.198. These 1D CPs are connected via this network to form a 2D supramolecular assembly. The hydrogen bonding parameters for **91** are listed in Table 3.37.

Table 3.37. Hydrogen bonding parameters for **91**.[a]

D–H…A	r (D-H) (Å)	r (H…A) (Å)	r (D…A) (Å)	∠D-H…A (deg)	Symmetry
O(1)--H(1A)...O(24)	0.85	1.93	2.7668	170	
O(2)--H(2A)...O(25)	0.85	2.55	3.2614	142	
O(3)--H(3A)...O(19)	0.85	2.2	2.9353	144	x,1+y,1+z
O(17)--H(17D)...O(29)	0.85	2.27	2.9922	143	
O(18)--H(18C)...Cl(3)	0.85	2.59	3.3791	156	
O(19)--H(19A)...O(28)	0.85	2.03	2.8725	170	x,-1+y,z
O(20)--H(20A)...O(18)	0.85	1.94	2.7652	162	
O(20)--H(20B) ...O(21)	0.85	2.17	2.7506	125	
O(21)--H(21A)…O(20)	0.85	1.9	2.7506	175	
O(22)--H(22A)…O(1)	0.85	2	2.7736	151	
O(22)--H(22B)...O(42)	0.85	2.03	2.7786	146	
O(23)--H(23B) ...O(24)	0.85	2.16	2.7975	131	x,1+y,z
O(24)--H(24A)...O(23)	0.85	1.95	2.7975	174	x,-1+y,z
O(24)--H(24B)…O(1)	0.85	1.96	2.7668	158	
O(25)--H(25A)…O(22)	0.85	2.55	2.8684	103	1+x,y,z
O(26)--H(26B)...O(7)	0.85	2.5	3.2709	152	
O(27)--H(27A)...O(5)	0.85	2.2	2.8459	133	
O(27)--H(27B)...O(25)	0.85	2.21	2.7364	120	
O(28)--H(28A)...O(21)	0.85	2.53	3.069	122	
O(29)--H(29A)...O(17)	0.85	2.46	2.9922	121	
O(42)--H(42C)...O(14)	0.85	1.9	2.751	180	
O(42)--H(42D)...O(22)	0.85	1.93	2.7786	180	
C(6)--H(6A)...O(5)	0.97	2.46	3.1658	129	
C(11)--H(11)...O(4)	0.93	2.34	3.1943	153	x,1+y,z
C(15)--H(15B)...O(1)	0.97	2.39	3.0803	127	
C(17)--H(17B)...O(13)	0.97	2.5	3.4462	165	x,-1+y,z
C(43)--H(43B)...O(3)	0.97	2.41	3.2495	145	
C(45)--H(45)...O(19)	0.93	2.57	3.3671	145	x,1+y,1+z
C(47)--H(47)...O(9)	0.93	2.48	3.2114	136	x,1+y,1+z

[a]Numbers in parenthesis are estimated standard deviations in the last significant digits

{[Cu_2(tpbn)(2,6-NDS)$(Cl)_2$]·4.5H_2O}$_n$ (**92**). In this structure, each Cu(II) center is pentacoordinated and surrounded by three nitrogens of the ligand, one chloride ion and one oxygen from the sulphonate. The sulphonate linker binds in a monodentate fashion bridging between the two Cu(II) centers forming a 1D coordination polymer chain (see Figure 3.199). The selected bond distances and angles are listed in Table A94.

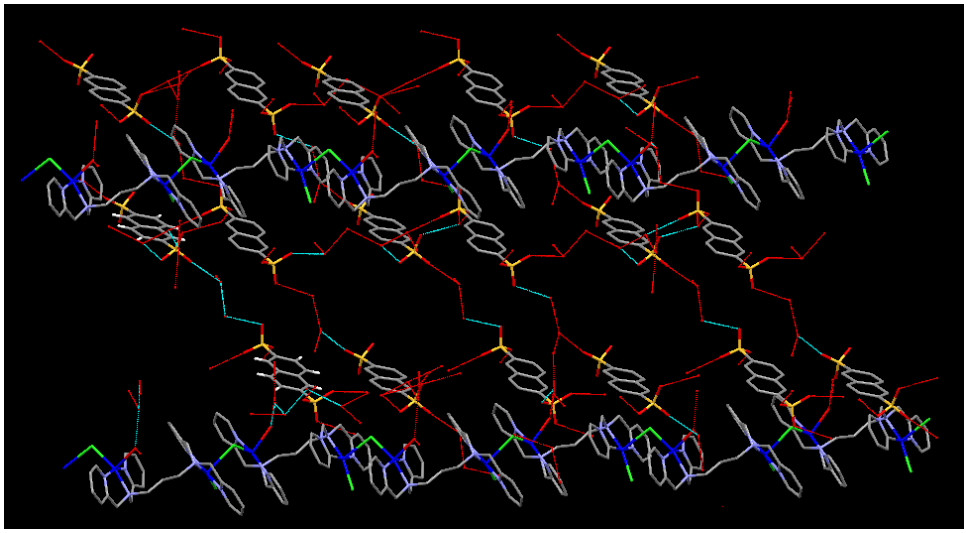

Figure 3.198. An arrangement of the disulphonate anions in the supramoelcular assembly of **91**.

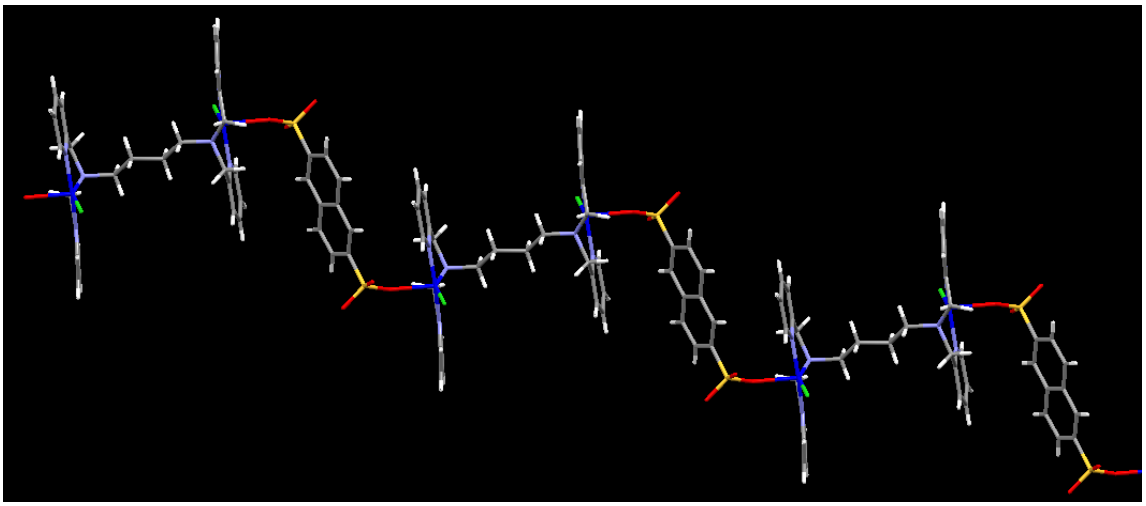

Figure 3.199. A perspective view of **92**.

The two layers of the 1D CP of **92** are connected to each other via lattice water molecules O4 and O5 through hydrogen bonding with sulphonate oxygens O2 and O3 as shown in Figure 3.200. Due to this interactions, two supramolecular cavities are formed - a small cavity with NDS and lattice water, and a big cavity with Cu(II)tpbn subunits. All hydrogen bonding parameters for **92** are listed in Table 3.38.

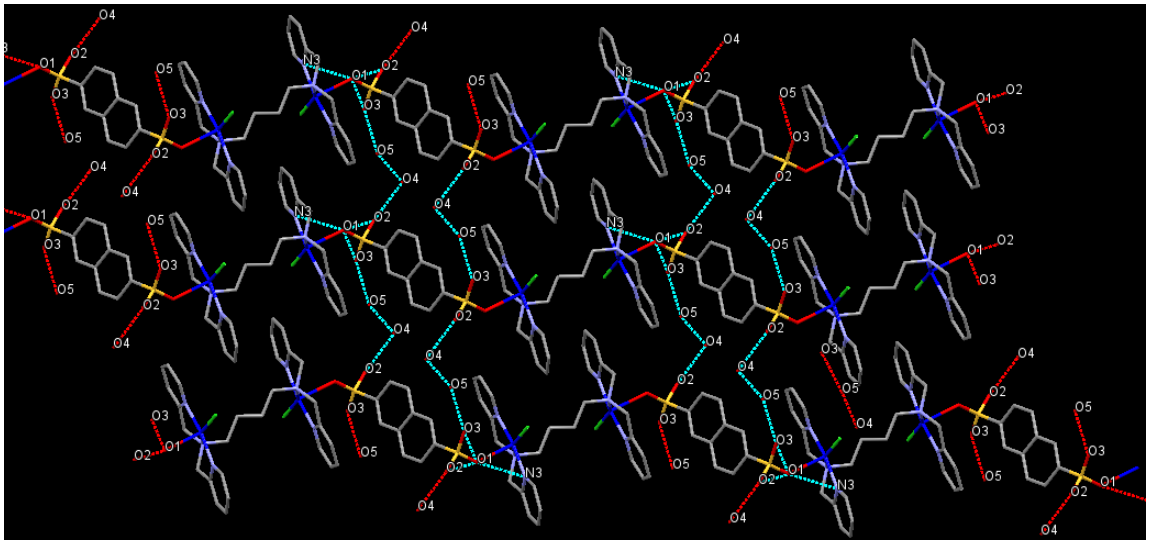

Figure 3.200. A part of the supramolecular assembly in **92**.

Table 3.38. Hydrogen bonding parameters for **92**.[a]

D---H….A	r (D-H) (Å)	r (H…A) (Å)	r (D…A) (Å)	∠D-H…A (deg)	Symmetry
O(4) --H(4A) ..Cl(1)	0.77(3)	2.42(3)	3.185(2)	173(3)	1-x,1-y,-z
O(4) --H(4B) ..O(2)	0.79(3)	1.94(3)	2.716(2)	170(3)	1/2-x,1/2+y,1/2-z
O(5) --H(5A) ..O(4)	0.80(4)	1.95(4)	2.748(3)	175(4)	3/2-x,-1/2+y,1/2-z
O(5) --H(5B) ..O(3)	0.73(4)	2.12(4)	2.845(3)	171(4)	
C(3) --H(3) ...Cl(1)	0.95	2.8	3.659(2)	151	3/2-x,-1/2+y,1/2-z
C(6) --H(6A) ..O(2)	0.99	2.48	3.384(3)	152	1/2-x,-1/2+y,1/2-z
C(9) --H(9B) ..O(3)	0.99	2.56	3.360(2)	138	1/2-x,-1/2+y,1/2-z
C(14) --H(14) ..O(5)	0.95	2.47	3.346(3)	153	1/2-x,-1/2+y,1/2-z
C(18) --H(18) ..O(4)	0.95	2.55	3.344(3)	141	3/2-x,-1/2+y,1/2-z

[a]Numbers in parenthesis are estimated standard deviations in the last significant digits.

FTIR Spectroscopy. The IR spectra of all three compounds were recorded in the solid state as KBr pellets. The peaks at 3401 cm^{-1} (**90**), 3523 and 3459 cm^{-1} (**91**) and 3392 cm^{-1} (**92**) correspond to the O-H strectching frequency of water. Although both **90** and **91** have two kinds of water, only in the spectrum of **91** it is clearly visible. The peaks at 1234, 1194 and 1183 cm^{-1} (**90**), 1222, 1196, 1184 cm^{-1} (**91**), and 1234, 1195, 1183 cm^{-1} (**92**) correspond to the sulphonate stretching frequency. The other peaks at 1609, 664, 627 cm^{-1} are common in all the three spectra due to the polypyridyl ligand with a shift by a few wave numbers.

UV-Visible Spectroscopy. All three MOCNs have been studied by UV-Vis spectroscopy using 1 mM solution of the compound in an acetonitrile-water mixture. Their UV-Vis spectra are shown in Figure 3.201. The λ_{max} values for **90, 91** and **92** correspond to the d-d transition at 692 nm, 667 nm, 659 nm respectively. The difference in λ_{max} values clearly indicates a different coordination environment around copper(II) centers in these compounds, which is also evident from their solid state structure.

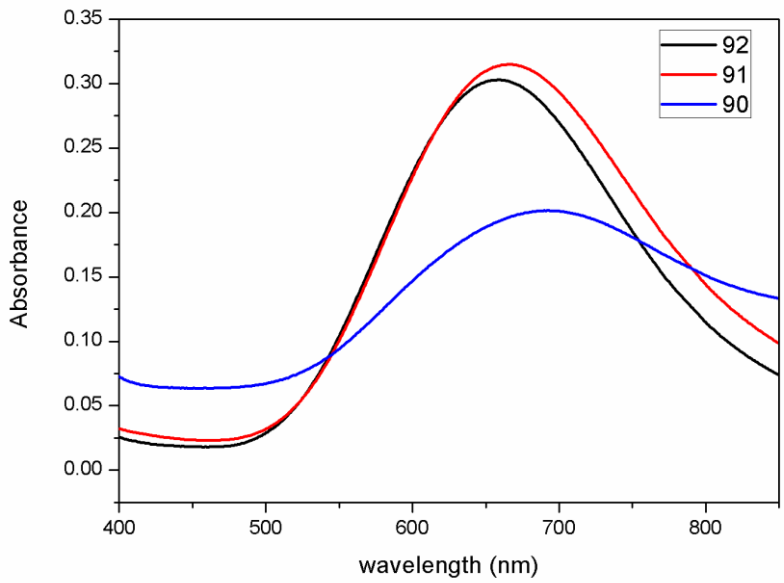

Figure 3.201. UV-vis spectra of **90**, **91** and **92**.

Nitrogen-based linkers

A few neutral and anionic nitrogen linkers were also used with tpbn ligand and two 1D CPs $\{[Cu_2(tpbn)(4,4'\text{-bpy})](ClO_4)_2{\cdot}3H_2O\}_n$ (**93**) and $\{[Cu_2(tpbn)(N_3)_2(H_2O)_2](ClO_4)_2\}_n$ (**94**) were obtained. It is notable that a similar product with bis(pyridyl)ethene (bpe) could not be isolated under the conditions tried.

Synthesis. Both compounds were prepared via one pot self-assembly reaction of $Cu(ClO_4)_2$, tpbn and 4,4′-bpy (**93**) or sodium azide (**94**). Their synthesis is summarized in Scheme 32. Both products were obtained as precipitates in high yield and pure form.

$$Cu(ClO_4)_2 + tpbn \xrightarrow[MeOH,\ RT]{4,4'\text{-bpy}} \{[Cu_2(tpbn)(4,4'\text{-bpy})(H_2O)_2](ClO_4)_2 \cdot 3H_2O\}_n \quad \textbf{(93)}$$

$$Cu(ClO_4)_2 + tpbn \xrightarrow[MeOH,\ RT]{NaN_3} \{[Cu_2(tpbn)(N_3)_2](ClO_4)_2\}_n \quad \textbf{(94)}$$

Scheme 32. Synthesis of **93** and **94**.

{[Cu$_2$(tpbn)(N$_3$)$_2$](ClO$_4$)$_2$}$_n$ (**94**). It is a bis(azide) bridged 1D CP in which each Cu(II) center is hexacoordinated and surrounded by three nitrogens of the tpbn ligand, two nitrogens from two azides and one oxygen from the perchlorate anion. The Cu(II)-perchlorate oxygen distance is 2.633 Å. The selected bond distances and angles are listed in Table A95. In the crystal structure, one of the perchlorate oxygen was disordered over two positions and was refined with 0.5 occupancy factors. In the Figure 3.202, the disordered perchlorate is not shown.

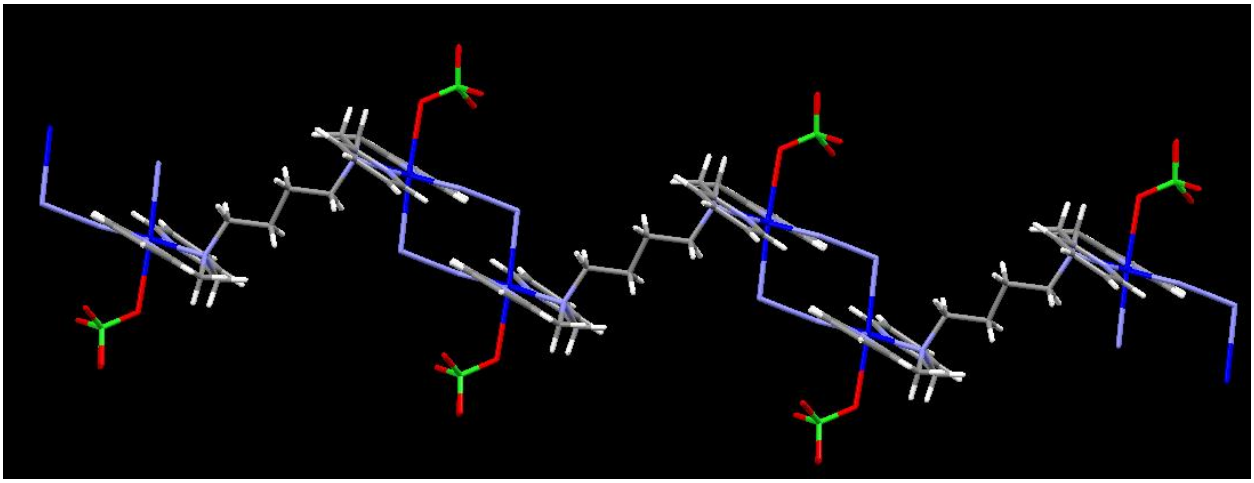

Figure 3.202. A perspective view of **94**.

FTIR Spectroscopy. Both compounds were studied in the solid state as KBr pellets. The peaks at 3445 cm^{-1} (**93**) and 3420 cm^{-1} (**94**) correspond to the O-H stretching frequency of water. The peaks at 1613, 1483, 1449, 1292, 766 cm^{-1} due to the ligand are common in both the compounds with a shift by a few wave numbers. The peaks at 1091 and 626 cm^{-1} (**93**) and 1103 and 623 cm^{-1} (**94**) correspond to the perchlorate anion. A peak at 2074 cm^{-1} is due to the azide group in **94**.

3.2.4 *Co(II) chemistry*

Tricarboxylate linkers

With Co(II), only one reaction was done with tpbn and H_3BTC using different metal salt under hydrothermal conditions to see the difference in product formation with the change of metal salt. This also allowed to compare this chemistry with the Mn(II) chemistry under similar conditions (*vide supra*).

Synthesis. The starting materials were taken in a ratio of 1:1:1 in 5 mL distilled water and heated to 120 ℃ for 2 days under autogeneous pressure and cooled down to RT over 24 hrs. Dark red crystals were obtained. Scheme 33 below summarizes its synthesis.

$$Co(NO_3)_2 + \text{tpbn} \xrightarrow[H_2O/HT]{H_3BTC} [Co_2(\text{tpbn})(HBTC)_2]_n \quad (\mathbf{95})$$

Scheme 33. Synthesis of **95**.

Single Crystal Structure analysis.

$[Co_2(tpbn)(HBTC)_2]_n$ (**95**). It is a porous 3D MOF that crystallizes in the monoclinic $P2_1/c$ space group (see Figure 3.203). Each hexacoordinated Co(II) has N_3O_3 coordination environment where the nitrogens are from the ligand and three oxygens from two carboxylate groups. In it, $HBTC^{2-}$ shows two kinds of binding modes – chelating and monodentate; one of the carboxylic acid group of H_3BTC is not deprotonated. The distances for the chelated carboxylate are 2.2861 Å (Co-O5) and 2.0912 Å (Co-O6), whereas the distance for monodentate carboxylate is 2.0162 Å (Co-O1). All other selected bond distances and angles are listed in Table A96. The tpbn spans between the two Co(II) centers which are further connected by the $HBTC^{2-}$. Six Co(II) centers form a large pore of dimensions 21.866 Å x 17.664 Å, which seems to be divided into two because of the two pyridine rings inside the pore (see the space fill model in Figure 3.204). Yaghi et al. has the reported the Co(II)-BTC, $[Co_3(BTC)_2(H_2O)_{12}]_n$ which is a 1D CP and all carboxylates of BTC were unprotonated.[121b]

The protonated end (O3) of $HBTC^{2-}$ is involved in strong hydrogen bonding with the uncoordinated oxygen atom (O2) of $HBTC^{2-}$ of another polymeric chain; thus a supramolecular assembly connecting two MOFs is formed as shown in Figure 3.205. In addition to this, C-H…O

interactions are also present which stabilizes the supramolecular assembly further. The hydrogen bonding distances are listed in Table 3.39.

Table 3.39. Hydrogen bonding parameters for **95**.[a]

D–H…A	r (D-H) (Å)	r (H…A) (Å)	r (D…A) (Å)	∠D-H…A (deg)	Symmetry
O(3) --H(3) ..O(2)	0.84	1.84	2.623(2)	155	x,1/2-y,1/2+z
C(2) --H(2B) ..O(6)	0.99	2.43	3.053(2)	120	-x,-1/2+y,1/2-z

[a]Numbers in parenthesis are estimated standard deviations in the last significant digits.

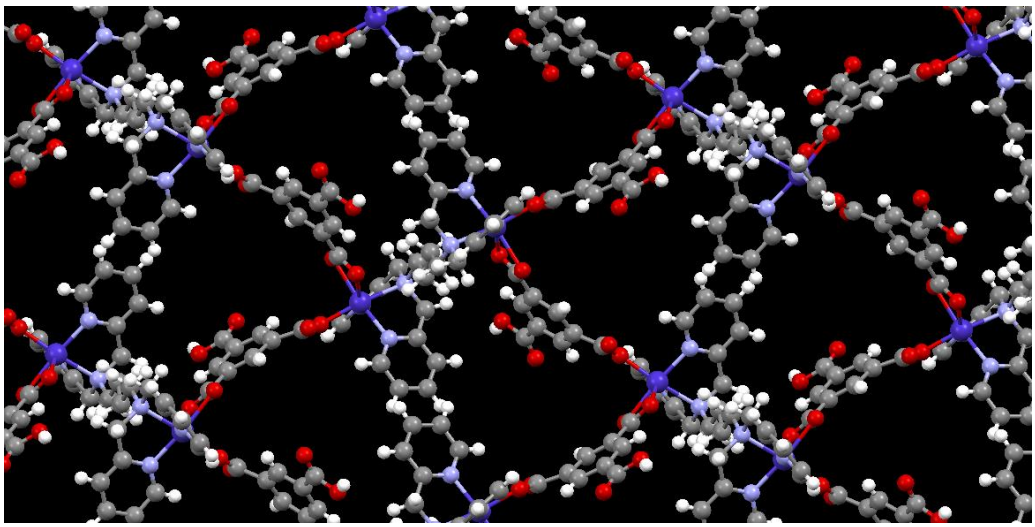

Figure 3.203. A perspective view of **95**.

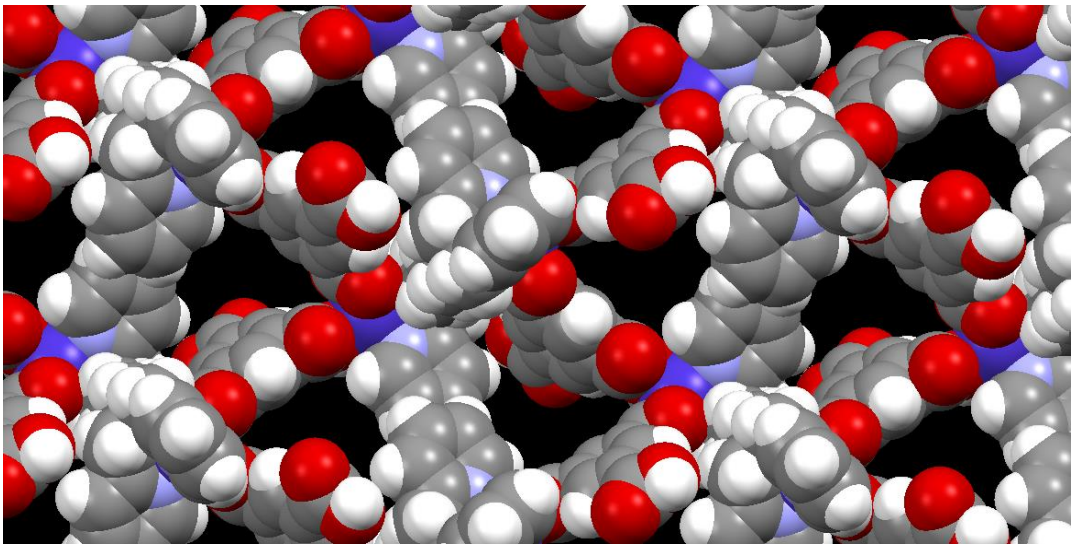

Figure 3.204. A space-filling model of **95**.

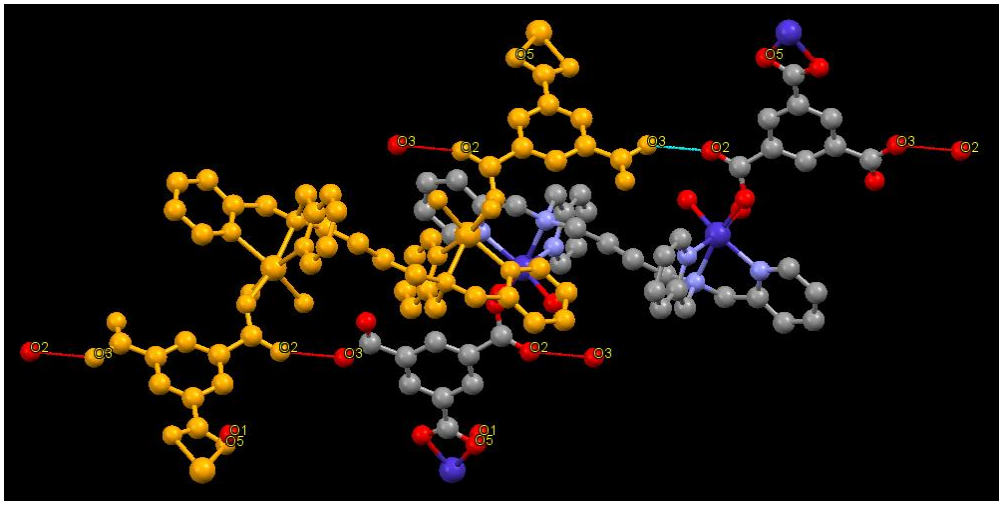

Figure 3.205. A part of the supramolecular assembly in **95** (different color is chosen for clarity).

FTIR Spectroscopy. The IR spectrum of **95** was recorded in the solid state as KBr pellets. As can be seen in Figure 3.206, the peak at 1707 cm^{-1} for the protonated carboxylic acid group of $HBTC^{2-}$ can be identified easily. The peaks at 1618 and 1371 cm^{-1} corresponds to the asymmetric and symmetric stretching frequencies of the carboxylate. The peaks at 3422 and 2922 cm^{-1} corresponds to the O-H and C-H stretching frequencies, respectively. The peaks at 1608, 1442, 756 and 677 cm^{-1} are due to the tpbn ligand.

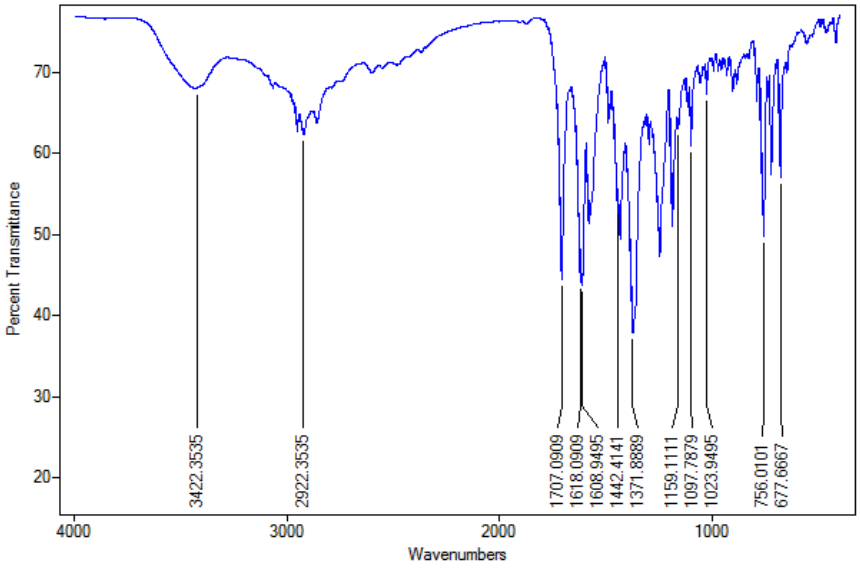

Figure 3.206. FTIR spectrum of **95**.

Thermogravimetric analysis. The thermal stability of **95** was studied from 50 to 500 ℃. From the TGA scan shown in Figure 3.207, it is clear that this compound is stable up to 400 ℃ followed by its decomposition.

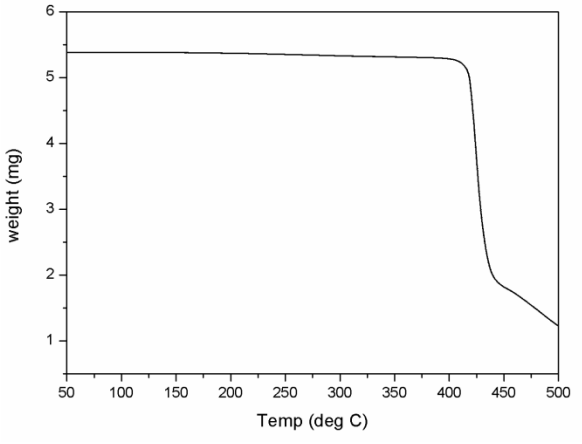

Figure 3.207. TGA scan for **95**.

3.2.3.4 *Zn(II) and Cd(II) chemistry*

Out of all the ligands discussed above, tpbn gave very interesting results and thus the chemistry of Zn(II) and Cd(II) was done with it varying carboxylate linkers.

Dicarboxylate linkers

Synthesis. Both Zn(II) and Cd(II) MOCNs have been prepared via one pot self-assembly reaction of $M(OAc)_2$/tpbn/H_2adc in methanol. The products were different - a water soluble dinuclear compound was obtained for Zn(II) whereas a 3D MOF insoluble in almost all organic solvents was obtained for Cd(II). It is worth mentioning here both reactions were done under similar conditions. Scheme 34 summarizes the synthesis of these MOCNs.

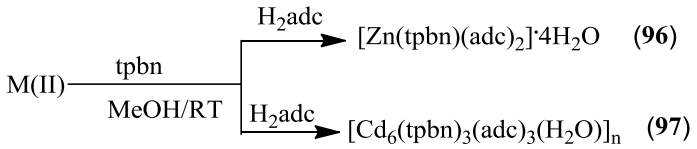

where M(II) = Zn(II) and Cd(II)

Scheme 34. Synthesis of **96** and **97**.

$[Cd_2(tppn)(adc)_2]_n$ (**98**) was prepared in a similar way to **97** but using tppn as the ligand. In order to see the effect of an amide group on the product formation, a reaction was done for the Cd(II)-adc system with bpbg under similar conditions as described for **97.** A change from pyridyl to amide yielded a different product $[Cd_2(bpbg)(adc)_2(H_2O)_2]_n$ (**99**), which is a 1D CP with a dinuclear Cd(II) repeat unit in the polymer. A product similar to **99** was obtained for the tdc. Scheme 35 summarizes the synthesis of **99** and **100**.

$$Cd(OAc)_2 + bpbg + H_2adc \xrightarrow[-AcOH]{MeOH,\ RT} [Cd_2(bpbg)(adc)_2(H_2O)_3]_n\ (\mathbf{99})$$

$$Cd(OAc)_2 + tpbn + H_2tdc \xrightarrow[-AcOH]{MeOH,\ RT} [Cd_2(tpbn)(tdc)_2(H_2O)_4]_n\ (\mathbf{100})$$

Scheme 35. Synthesis of **99** and **100**.

Single Crystal Structure Analysis.

$[Zn_2(tpbn)(H_2O)_2(adc)_2]\cdot 4H_2O$ (**96**). It is a discrete dinuclear compound that crystallizes in the orthorhombic *Pbca* space group. The compound is very interesting because only one end of the dicarboxylate binds while the other end is involved in hydrogen bonding as found in **13** and **17**. Zn(II) centers are hexacoordinated and surrounded by three nitrogens of the ligand, two coordinated water molecules and one oxygen from the monodentate adc (see Figure 3.208). The selected bond distances and angles are listed in Table A97.

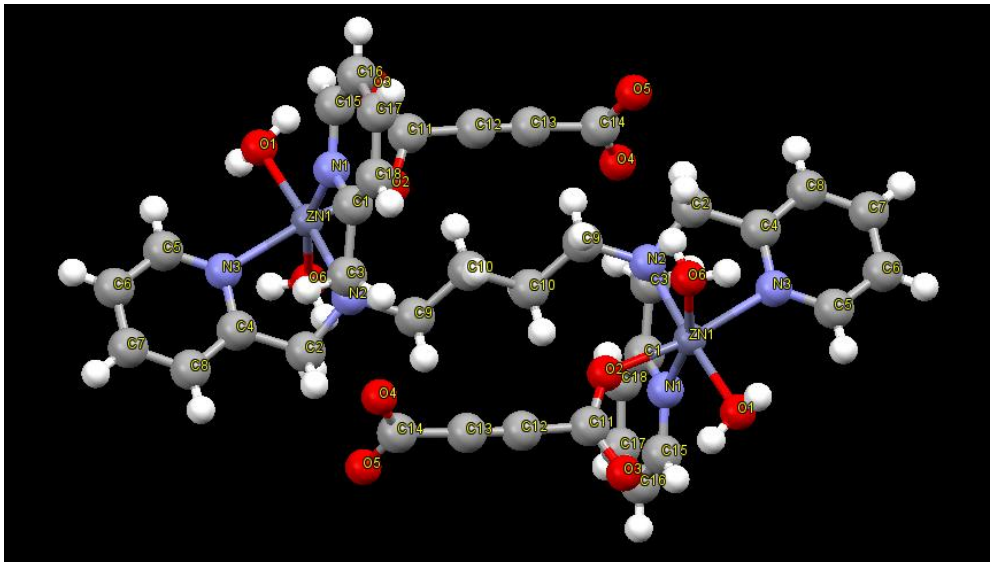

Figure 3.208. A ball and stick representation of **96**.

The reason for a dicarboxylate to bind only from one end is strong hydrogen bonding of the other end with the coordinated water molecules on the metal center and lattice water molecules. As can be seen in Figure 3.209, the end of the carboxylate (O4, O5) which does not bind to Zn(II) is hydrogen bonded to O8 (lattice water molecule) and O1 (coordinated water molecule). The uncoordinated oxygen atom (O3) of the carboxylate end which binds to the Zn(II) center is also hydrogen bonded to O1 and O6 (coordinated water molecules). The hydrogen bonding paraemters are listed in Table 3.40.

Table 3.40. Hydrogen bonding parameters for **96**.[a]

D–H...A	r (D-H) (Å)	r (H…A) (Å)	r (D…A) (Å)	∠D-H…A (deg)	Symmetry
O(5)--H(5A)...O(2)	0.87	1.98	2.764(3)	150	
O(5)--H(5B)...O(4)	0.87	1.91	2.671(4)	145	1/2+x,1/2-y,-z
O(6)--H(6A)...O(2)	0.87	2.07	2.911(3)	161	
O(6)--H(6B)...O(7)	0.88	1.80	2.676(4)	173	
O(7)--H(7D)...O(8)	0.85	1.98	2.786(4)	157	1/2+x,y,1/2-z
O(8)--H(8C)...O(4)	0.85	2.17	2.912(4)	146	x,1/2-y,1/2+z
C(6)--H(6D)...O(3)	0.97	2.50	3.449(5)	166	1-x,1-y,-z
C(8)--H(8A)...O(1)	0.97	2.40	3.134(4)	132	
C(14)--H(14A)...O(8)	0.97	2.55	3.210(4)	126	1-x,1/2+y,1/2-z

[a]Numbers in parenthesis are estimated standard deviations in the last significant digits.

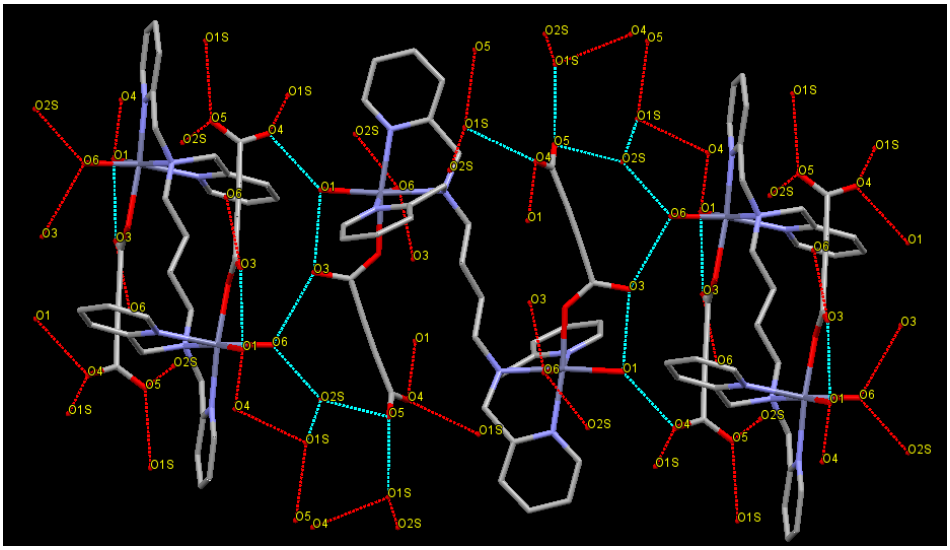

Figure 3.209. Hydrogen bonded network in **96**.

{[$Cd_6(tpbn)_3(adc)_3(H_2O)_3$]·$14.5H_2O$}$_n$ (97). It is a 3D MOF that crystallizes in the triclinic *P-1* space group. All Cd(II) centers are heptacoordinated but out of the six Cd(II) centers in the repeat unit, three are different from the others in terms of their coordination environments. Three Cd(II) centers are surrounded by three nitrogens of the ligand, one coordinated water molecule, one chelated carboxylate and one monodentate carboxylate while the other three centers are surrounded by two chelated carboxylates with no coordinated water molecule. The selected bond distances and angles are listed in Table A98. These Cd(II) centers form a six-membered chair shaped configuration as shown in Figure 3.210. At each corner of the chair a Cd(II) center occupies and arms of the chair are made up of adc and tpbn ligand alternatively.

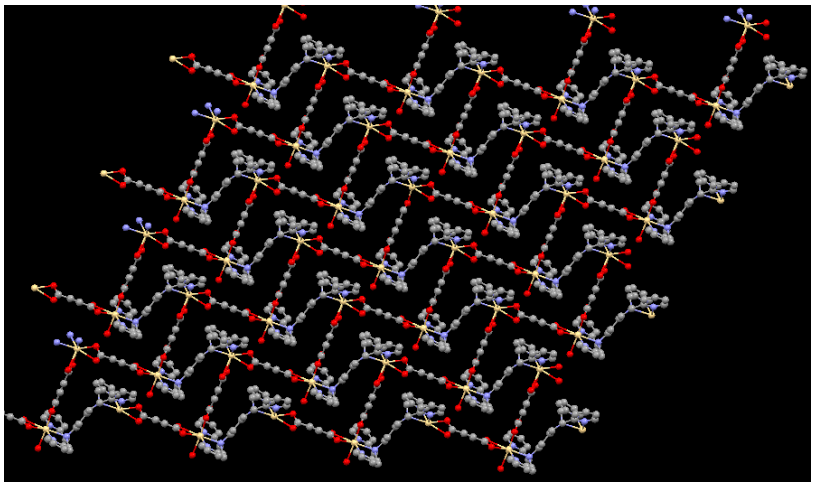

Figure 3.210. A perspective view of **97** (water molecules are omitted for clarity).

Its topology determined by TOPOS is hcb - Shubnikov hexagonal plane. In Figure 3.211, a six-membered chair shaped configuration is clearly visible; the chairs grows in one direction. This can also be viewed as a rhomboid shape in Figure 3.212 Two such polymeric layers are parallel to each other.

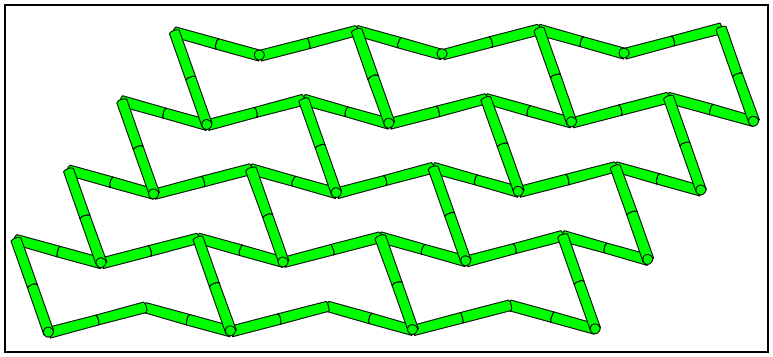

Figure 3.211. A topological view of **97**.

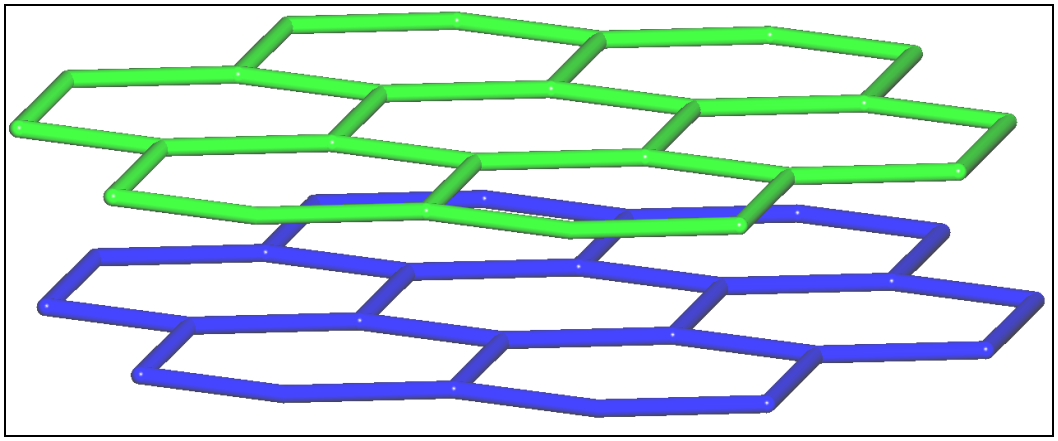

Figure 3.212. Another topological view of **97**.

$[Cd_2(bpbg)(adc)_2(H_2O)_2]_n$ (**99**). It is a 1D CP that crystallizes in the triclinic *P-1* space group. The coordination environment around each Cd(II) center is N_2O_5 but they are unsymmetrical. One Cd(II) center is surrounded by two coordinated water molecule, one chelated carboxylate, two nitrogens of the ligand and one oxygen of the amide group of the ligand while the other Cd(II) center is surrounded by one coordinated water molecule and one oxygen from monodentate carboxylate, two nitrogens of the ligand and one oxygen of the amide group of the ligand. A persepective view of **99** is shown in Figure 3.213. The selected bond distances and angles are listed in Table A99.

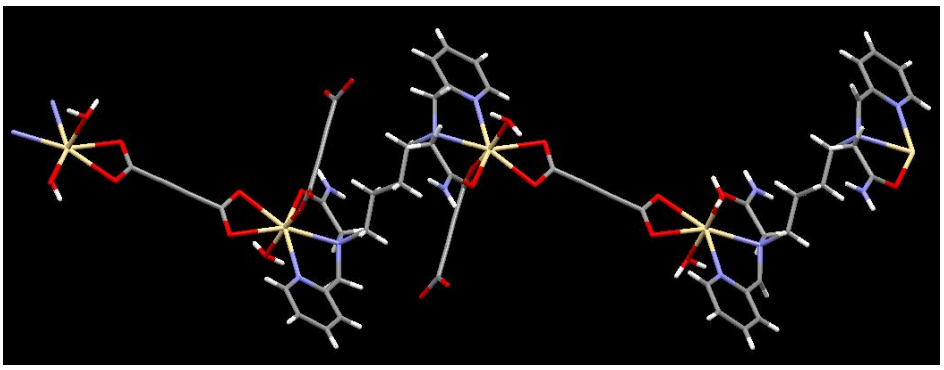

Figure 3.213. A perspective view of **99**.

Table 3.41. Hydrogen bonding parameters for **99**.[a]

D–H…A	r (D-H) (Å)	r (H…A) (Å)	r (D…A) (Å)	∠D-H…A (deg)	Symmetry
O2--H2A...N6	0.85	2.62	3.375(6)	148	-1+x,-1+y,-1+z
O1--H1A...O9	0.87	2.1	2.938(13)	162	x,-1+y,z
O2--H3A...O4	0.85	1.89	2.732(6)	171	1-x,1-y,-z
O7--H7B...O13	0.85	1.88	2.716(6)	169	1-x,1-y,1-z
N6--H11A...O5	0.86	2.16	2.939(7)	151	2-x,2-y,1-z
N6--H11B...O2	0.86	2.59	3.375(6)	152	1+x,1+y,1+z
N1--H12A...O3	0.86	2.11	2.912(7)	156	-x,1-y,-z
O13--H13A...O16	0.85	2.05	2.882(6)	166	-1+x,-1+y,z
O13--H13B...O7	0.85	2.08	2.716(6)	131	1-x,1-y,1-z
O14--H14A...O15	0.85	2.1	2.934(5)	166	
O14--H14B...O2	0.85	1.95	2.693(6)	145	1-x,1-y,-z
C1--H1D...O11	0.97	2.54	3.497(7)	168	2-x,3-y,1-z
C25--H25...O4	0.93	2.58	3.194(7)	124	
C27--H27...O12	0.93	2.55	3.294(11)	137	1-x,-y,-z

[a]Numbers in parenthesis are estimated standard deviations in the last significant digits.

Due to the hydrogen bonding of coordinated water molecule (O5) with the oxygen atom (O6) of the chelated adc, it forms a 2D supramolecular assembly. The hydrogen bonding parameters are listed in Table 3.41. The second coordinated water molecule O2 is also hydrogen bonded to other end of adc (O13) which does not bind to the metal center. The overall view of this supramolecular assembly is similar to **97**, i.e, a chair shaped configuration is formed (see Figure 3.214).

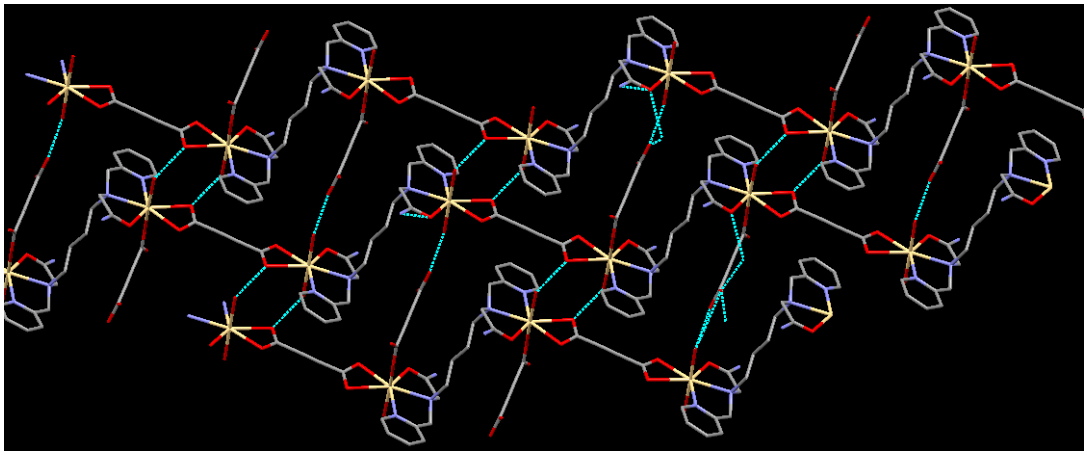

Figure 3.214. 2D Supramolecular assembly in **99**.

FTIR and Raman Spectroscopy. The IR of all the compounds were recorded in the solid state as KBr pellets. The peaks at 3448 cm^{-1} (**96**) and 3437 cm^{-1} (**97**) correspond to the O-H stretching frequency of water. The asymmetric and symmetric stretching frequencies for the adc were observed at 1627 and 1325 cm^{-1} (**96**) and 1623, 1580, 1444, 1328 cm^{-1} (**97**), respectively. The two values of carboxylate stretching frequencies in **97** correspond to two kinds of binding modes as evident from its solid state structure. In **99**, the peak at 1678 cm^{-1} corresponds to the carbonyl stretching frequency of the amide ligand. The stretching frequencies at 1623, 1579, 1569, 1379, 1342 cm^{-1} (**99**) corresponds to the asymmetric and symmetric carboxylate stretching frequencies, respectively. Some of these MOCNs were also studied by Raman spectroscopy. In the Raman spectrum of **97** (Figure 3.215) a peak at 2201 cm^{-1} is due to the C-C triple bond in adc.

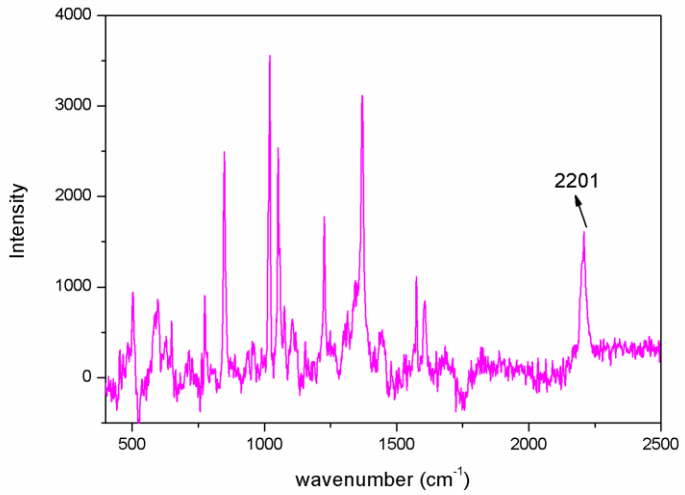

Figure 3.215. Raman spectrum of **97**.

Water Adsorption studies. What makes **97** interesting is the presence of ca. 15 lattice water molecules in the crystal structure; however, from the elemental analysis no lattice water molecule was found which was in agreement with the TGA results (vide infra). This showed that this molecule has capability to absorb solvent. For the water adsorption measurement, a sample of **97** was pretreated at 100 °C for 24 hours under vacuum. This compound adsorbed ca. 120 cm^3/g at p/po = 1 and on desorption it retains ca. 70 cm^3/g. The shape of the isotherm (see Figure 3.216) suggests it to be micro- or mesoporous material according to the IUPAC nomenclature for adsorption isotherms. The stability of the compound was verified by FTIR spectroscopy and PXRD.

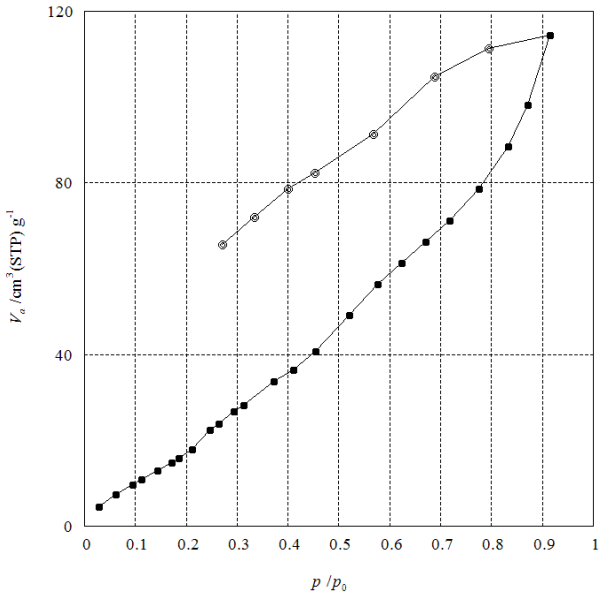

Figure 3.216. Water adsorption isotherm for **97**.

Host-guest Chemistry. Due to the affinity of this compound for water (discussed above), **97** was further tested with few more solvents. The sample was soaked in each solvent for 2-3 days, filtered and dried. The dried sample was used for powder X-ray diffraction. The powder patterns obtained (see Figure 3.217) were different from the parent compound, which clearly indicate that **97** acts as a host for water, ethanol and nitromethane.

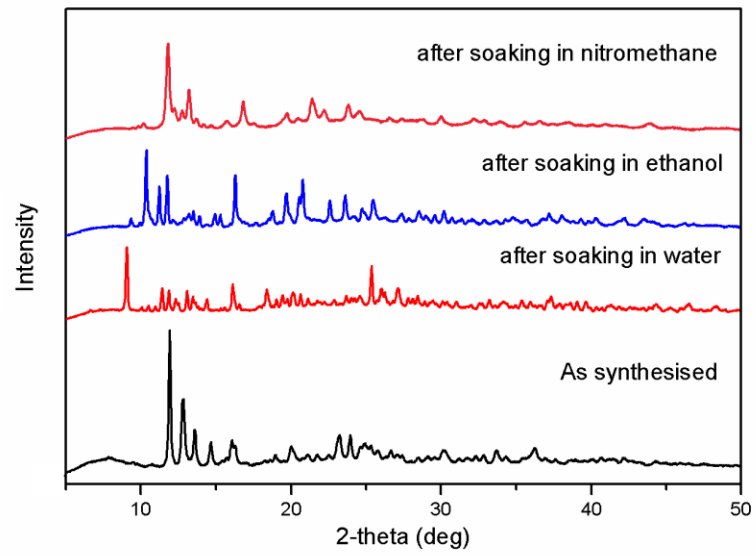

Figure 3.217. Experimental powder X-ray diffraction patterns for **97** and its host-guest analogs.

Photoluminescence studies. Due to the presence of Cd(II), **97** was studied for its photoluminescent properties in the soild state. The excitation and emission spectra are shown in Figure 3.218. On excitation upon 340 nm, the compound showed an emission at 500 nm. In this case like in **28**, the ligand does not show any fluorescence and emission can be attributed due to the binding of the ligand to the d^{10} element which reduces the flexibility of the ligand and thus loss of energy through radiationless pathway is less.

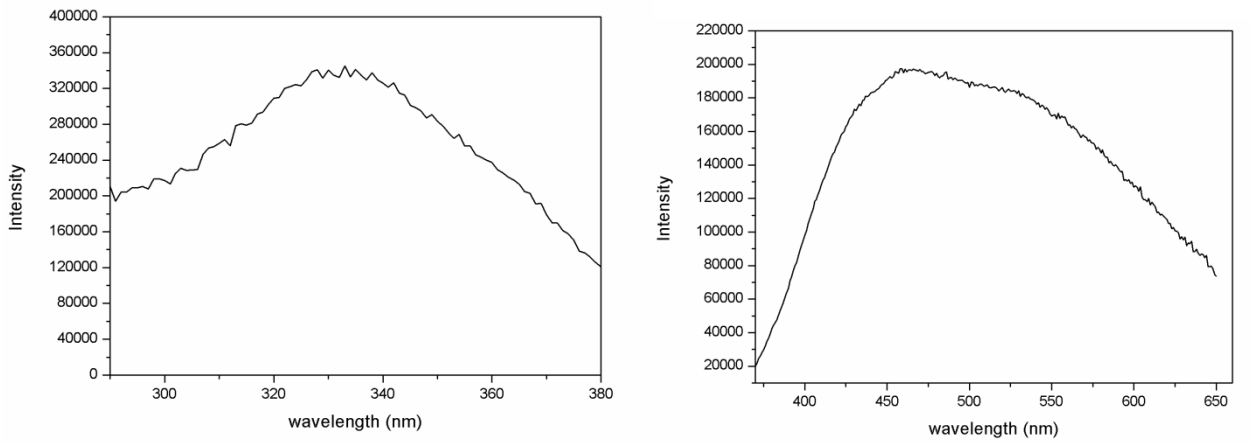

Figure 3.218. Excitation (left) and Emission (right) spectra of **97**.

Thermogravimetric analysis. The thermal stability of the compounds was determined by the thermogravimetric analysis. From the TGA scans shown in Figures 3.219 and 3.220, it is clear that **97** is more stable than **96.** This correlates well with their solid state structures. The TGA scan of **98** shows a continuous loss; hence it can be interpreted that **98** is less stable than **97** although their formula only differ in the ancillary ligands.

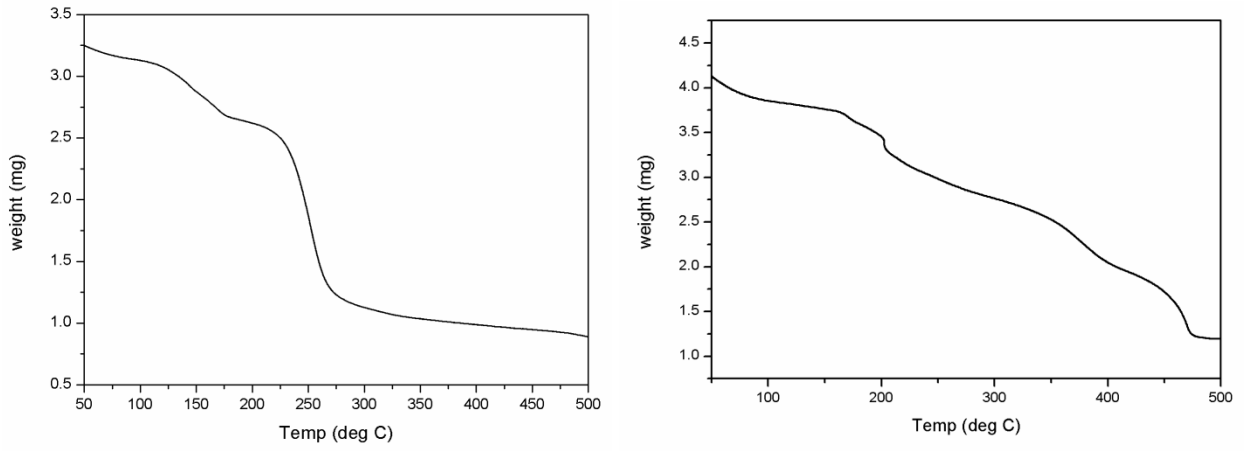

Figure 3.219. TGA scans of **96** (left) and **98** (right).

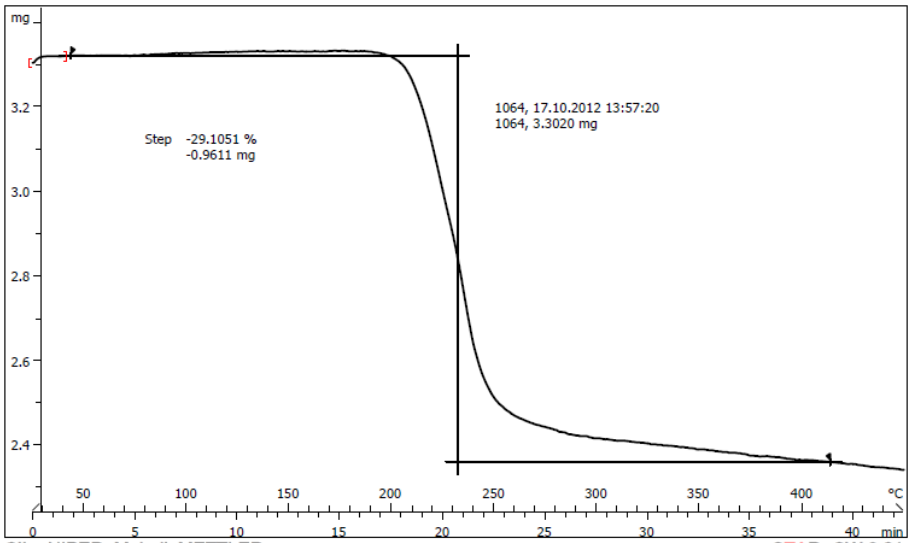

Figure 3.220. TGA scan of **97**.

Tricarboxylate linkers

Synthesis. All reactions of Zn(II) and Cd(II) with H_3BTC and tpbn were done under hydrothermal conditions. In case of Zn(II), the starting material has an influence on the products. Both reactions were done under same conditions but with different metal salts. A 3D CP was obtained with $ZnSO_4$ and a dinuclear compound was obtained with $Zn(NO_3)_2$. With Cd(II), a 3D CP was obtained. Scheme 36 summarizes their syntheses.

$$Zn(NO_3)_2 + \text{tpbn} \xrightarrow[H_2O/HT]{H_3BTC} [Zn_2(\text{tpbn})(H_2BTC)_2(NO_3)_2]\ (\mathbf{101})$$

$$ZnSO_4 + \text{tpbn} \xrightarrow[H_2O/HT]{H_3BTC} [Zn_2(\text{tpbn})(HBTC)_2]_n\ (\mathbf{102})$$

$$Cd(OAc)_2 + \text{tpbn} \xrightarrow[H_2O/HT]{H_3BTC} \{[Cd_2(\text{tpbn})(HBTC)_2(H_2O)_2]\cdot 4H_2O\}_n\ (\mathbf{103})$$

Scheme 36. Synthesis of **101-103**.

Single Crystal Structure Analysis. Single crystals were obtained from the hydrothermal reactions.

$[Zn_2(tpbn)(H_2BTC)_2(NO_3)_2]$ (**101**). It is a dinuclear Zn(II) compound that crystallizes in the triclinic *P*-1 space group (see Figure 3.221). There are two independent molecules in the

asymmetric unit. Each Zn(II) center is pentacoordinated and surrounded by three nitrogens of the ligand, one carboxylate oxygen and one oxygen from the nitrate. H_2BTC^- binds only from one end while other two ends are protonated and thus it acts as monoanion. The selected bond distances and angles are listed in Table A100.

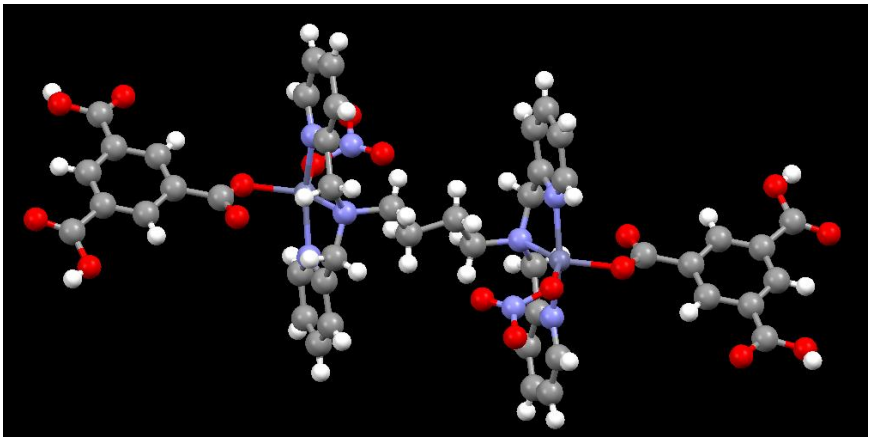

Figure 3.221. A ball and stick representation of **101**.

In one of the subunits in the asymmetric unit, the formation of a six-membered ring between the two carboxylic acid groups (shown in orange color in Figure 3.222) is similar to the hydrogen bonding found in the H_3BTC. Similarly, an involvement of the hydrogen attached to O19 with O25 forms a 14-membered ring (shown in green color in Figure 3.222). The second dinuclear molecule in the asymmetric unit has similar hydrogen bonding interactions.

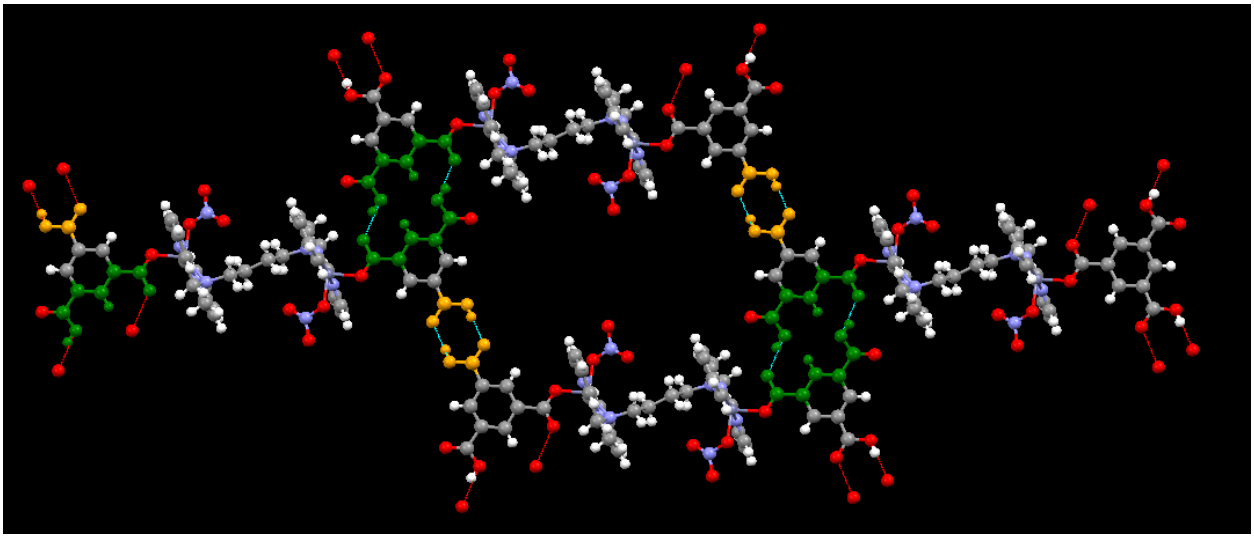

Figure 3.222. A perspective view of the supramolecular assembly in **101.**

Due to the presence of two carboxylic acid groups, the dinuclear units in **101** are strongly hydrogen bonded to form a supramolecular cavity shown in Figure 3.223. All hydrogen bonding parameters are listed in Table 3.42.

Table 3.42. Hydrogen bonding parameters for **101**.[a]

D–H...A	r (D-H) (Å)	r (H…A) (Å)	r (D…A) (Å)	∠D-H…A (deg)	Symmetry
O(4)--H(4)...O(18)	0.82	1.79	2.61(2)	176	-1+x,-1+y,1+z
O(6)--H(6A)...O(14)	0.82	1.79	2.598(18)	169	-1+x,y,1+z
O(15)--H(15)...O(2)	0.82	1.87	2.603(19)	148	1+x,y,-1+z
O(19)--H(19A)...O(25)	0.82	1.8	2.580(19)	157	2-x,1-y,-z
O(22)--H(22)...O(23)	0.82	1.8	2.59(2)	162	2-x,2-y,-z
C(9)--H(9)...O(15)	0.93	2.34	3.13(2)	142	-1+x,y,1+z
C(16)--H(16B)...O(16)	0.97	2.5	3.40(3)	153	-1+x,y,1+z
C(20)--H(20)...O(27)	0.93	2.56	3.34(4)	142	x,1-y,1-z
C(22)--H(22A)...O(28)	0.97	2.57	3.53(3)	172	1-x,1-y,1-z
C(25)--H(25A)...O(7)	0.97	2.57	3.53(3)	174	-x,-y,1-z
C(26)--H(26A) ...O(5)	0.97	2.58	3.49(3)	155	1+x,y,-1+z
C(32)--H(32B)...O(14)	0.97	2.55	3.24(3)	128	
C(35)--H(35)...O(25)	0.93	2.56	3.40(3)	150	
C(45)--H(45)...O(6)	0.93	2.43	3.19(3)	139	1+x,y,-1+z
C(58)--H(58)...O(2)	0.93	2.47	3.36(3)	158	-x,1-y,1-z
C(68)--H(68)...O(19)	0.93	2.29	3.11(2)	146	2-x,1-y,-z

[a]Numbers in parenthesis are estimated standard deviations in the last significant digits.

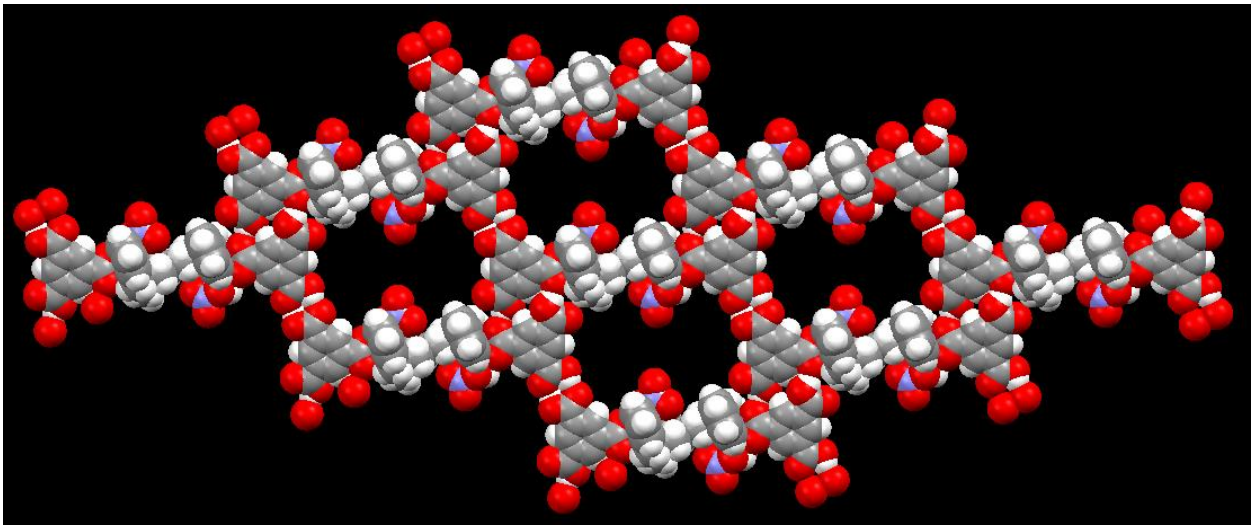

Figure 3.223. A space-filling model to show supramolecular cavity in **101**.

In addition to hydrogen bonding, the supramolecular assembly is further stabilized by C-H…O interactions listed in Table 3.42 as well as π–π interactions. The centroid-centroid distance is 3.794 Å between the pyridine rings (see Figure 3.224).

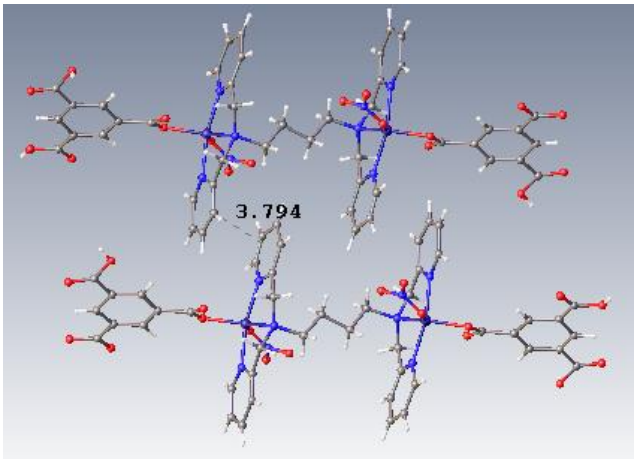

Figure 3.224. A view showing π–π interactions in **101**.

$[Zn_2(tpbn)(HBTC)_2]_n$ (**102**). It is a 3D coordination polymer that crystallises in the orthorhombic *Pbca* space group. In this polymer, Zn(II) centers are pentacoordinated and surrounded by three nitrogens of the ligand and two oxygen of the carboxylate. Out of three carboxylic acid groups in H_3BTC, only two are deprotonated and binds in a monodentate fashion thus it acts as dianion. A part of **102** is shown in Figure 3.225 (left). The selected bond distances and angles are listed in Table A101. Six Zn(II) centers form a chair-shaped configuration in which each corner of the chair is occupied by a Zn(II) and the arms of the chair are made up of BTC and tpbn, alternately. This chair-shaped configuration can be clearly seen in its topological view shown in Figure 3.225 (right). It is clear that these chairs are growing in opposite direction in adjacent layers. This arrangement of chairs is different from the one found in **97** where chairs were growing only in one direction. The CP is stabilized by modertae π–π interactions; the centroid-centroid distance between two pyridine rings is 3.847 Å.

The two layers within the polymer are intramolecularly hydrogen bonded. The carboxylic acid group (O2) is strongly hydrogen bonded to the uncoordinated carboxylatge oxygen atom O6 of the next layer to form a supramolecular assembly (distance: 2.5624 Å, angle: 172°). The arrangement of Zn(II) and $HBTC^{2-}$ within the CP is shown in Figure 3.226.

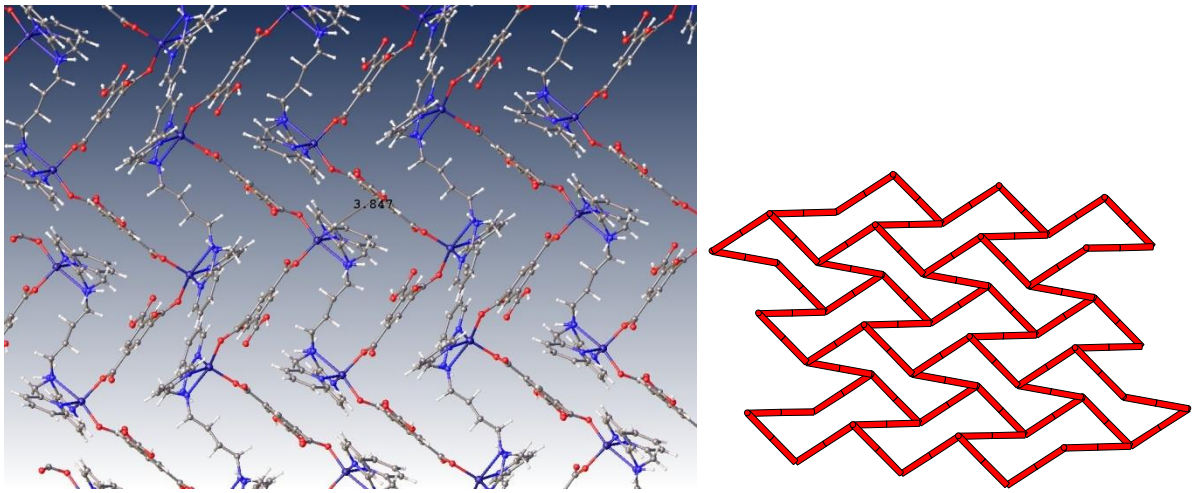

Figure 3.225. A perspective view of **102** (left) and its topological view (right).

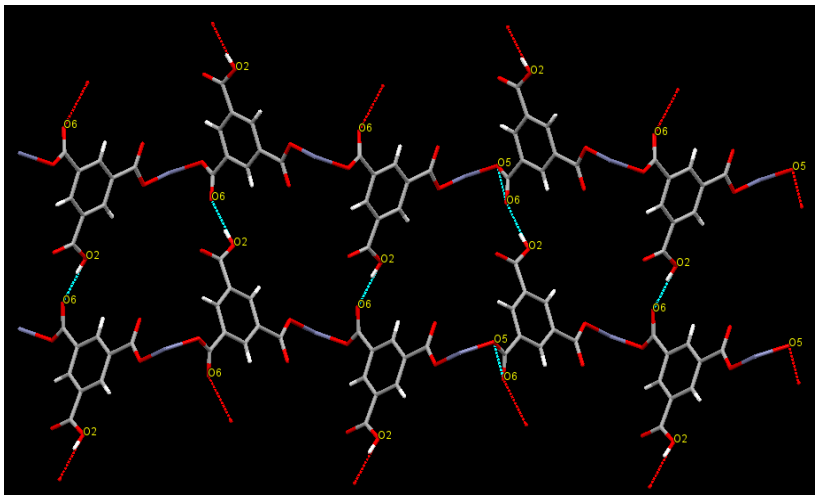

Figure 3.226. An arrangement of Zn(II) and $HBTC^{2-}$ in **102**.

$\{[Cd_2(tpbn)(HBTC)_2(H_2O)_2]\cdot 4H_2O\}_n$ (**103**). It is a 3D CP similar to Mn(II) and Zn(II) that crystallizes in the monoclinic $P2_1/c$ space group. Both Cd(II) centers in the repeat unit are heptacoordinated and surrounded by three nitrogens of the ligand, one coordinated water molecule, two oxygens from chelated carboxylate and one oxygen from monodentate carboxylate end. The third end of H_3BTC is not deprotonated and thus it acts as a dianion. The Cd-O distances for the chelated carboxylate group are 2.590(3) Å and 2.319(3) Å, clearly indicating unsymmetrical binding; furthermore, one of these distances is very close to the Cd-O distance (2.298(3) Å) for the monodentate carboxylate group. All other selected bond distances

and angles are listed in Table A102. A perspective view of **103** is shown in Figure 3.227 along with its space-filling model.

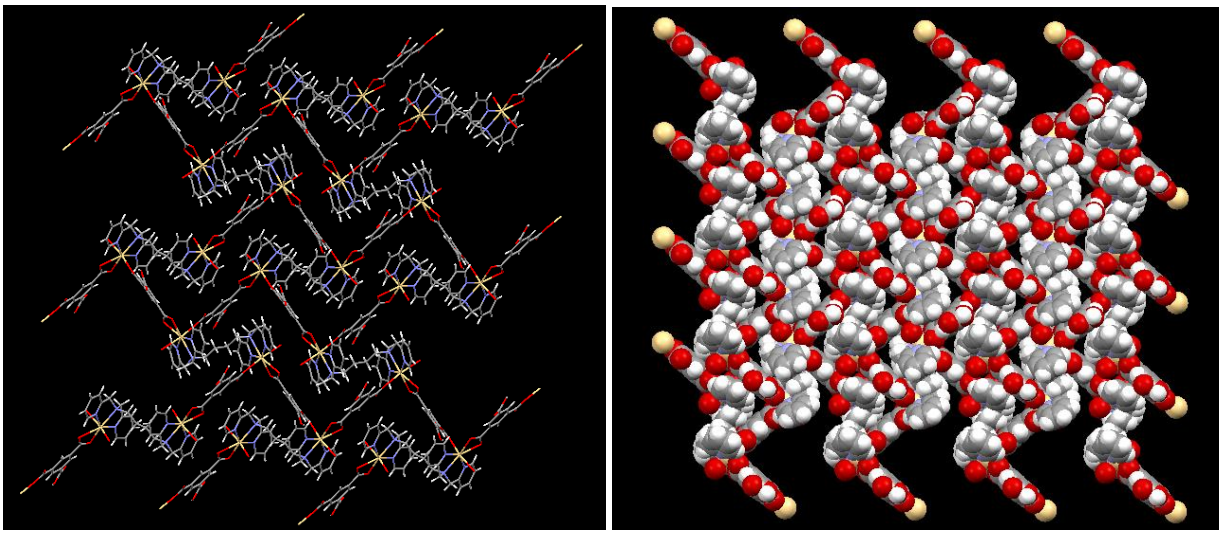

Figure 3.227. A perspective view of 3D CP of **103** and its space-filling model.

A coordinated water molecule (O7) of one polymeric chain is intermolecularly hydrogen bonded to the oxygen atom of the chelated carboxylate (O1) of another chain (distance: 2.822 Å); similarly, an uncoordinated oxygen atom (O3) of the carboxylate end is also intermolecularly hydrogen bonded to the oxygen atom (O5) of the carboxylic acid to form a supramolecular assembly of **103**. A part of the supramolecular assembly of **103** is shown in Figure 3.228. One lattice water molecule (O8) is hydrogen bonded to the coordinated oxygen atom (O4) of the monodentate carboxylate end (distance: 2.989 Å) and the second lattice water molecule (O9) is hydrogen bonded to O5 (distance: 2.790 Å). All hydrogen bonding parameters are listed in Table 3.43.

Table 3.43. Hydrogen bonding parameters for **103**.[a]

D–H…A	r (D-H) (Å)	r (H…A) (Å)	r (D…A) (Å)	∠D-H…A (deg)	Symmetry
O(5)--H(5)...O(3)	0.84	1.8	2.592(5)	156	-1+x,y,z
O(7)--H(7B)...O(1)	0.87	2.04	2.822(6)	148	1-x,-y,-z
O(8)--H(8A)...O(6)	0.87	2.25	3.097(6)	164	1+x,y,z
O(9)--H(9A)...O(2)	0.87	2.57	3.286(8)	140	
O(9)--H(9B)...O(5)	0.87	2.01	2.790(10)	149	-x,1/2+y,1/2-z

[a]Numbers in parenthesis are estimated standard deviations in the last significant digits.

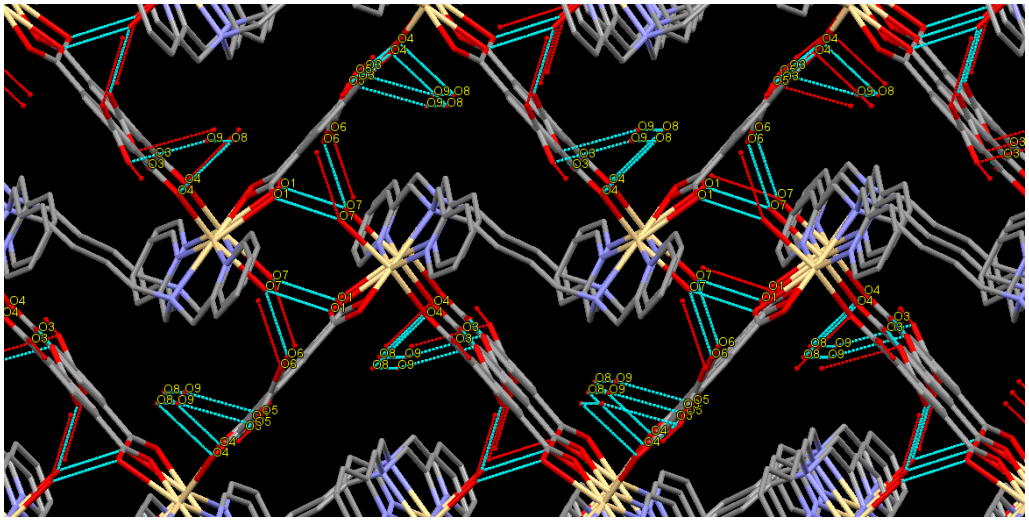

Figure 3.228. A persepective view of the supramolecular assembly in **103**.

FTIR Spectroscopy. The IR spectra of all three compounds were recorded in the solid state as KBr pellets. In the IR spectra of **101** and **102** shown in Figure 3.229 and 3.230, peaks at 3408 and 3392 cm^{-1}, respectively, corresponds to the O-H stretching frequency of water. On the other hand, in the spectrum of **103** two kinds of O-H stretching frequencies confirming its composition from the X-ray crystal structure described above. The peak at 3405 cm^{-1} corresponds to the lattice water molecules whereas the peak at 3275 cm^{-1} corresponds to the coordinated water molecule. The other important peak at 1715 cm^{-1} (**101**), 1715 cm^{-1} (**102**) and 1681 cm^{-1} (**103**) corresponds to the stretching frequency of the carbonyl group of the carboxylic acid of $HBTC^{2-}$.

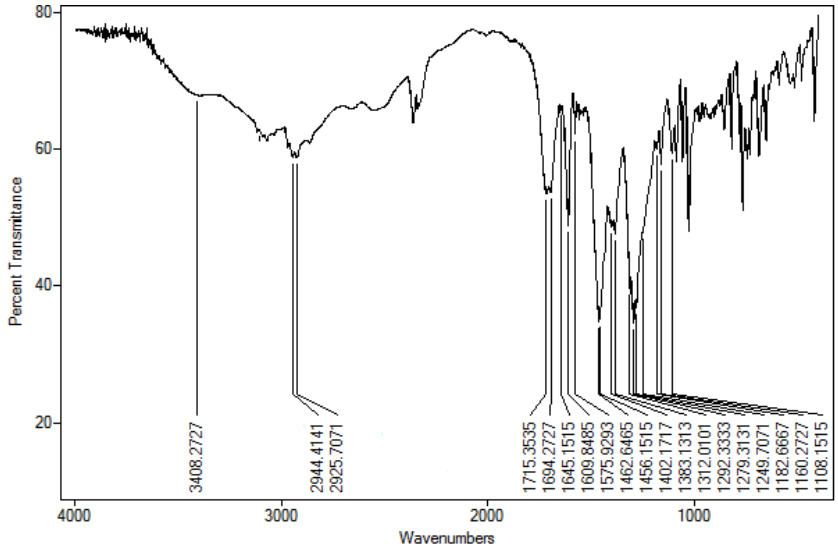

Figure 3.229. FTIR spectrum of **101**.

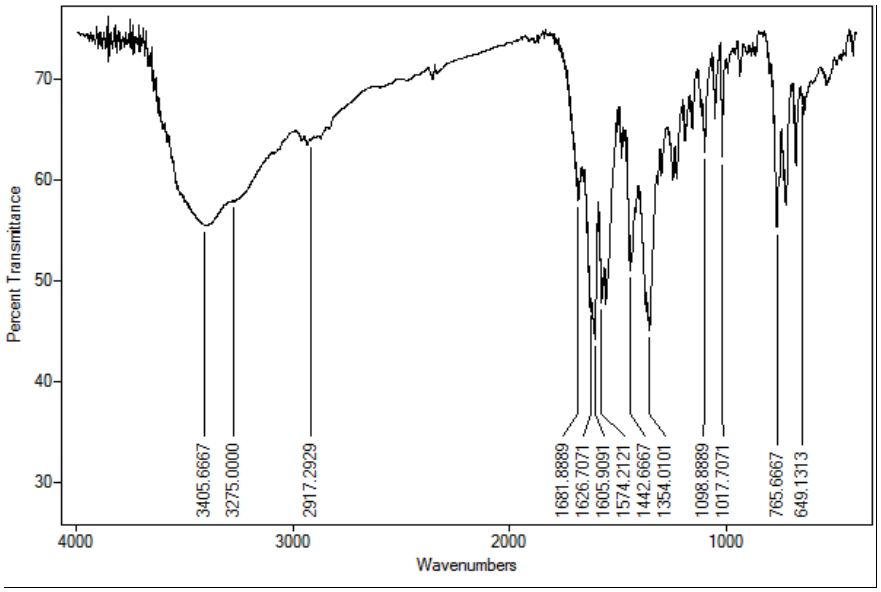

Figure 3.230. FTIR spectrum of **103**.

Thermogravimetric analysis. The TGA scans of **102** and **103** are two-step profiles shown in Figure 3.231. The weight loss profile of both the compounds is very similar. The first step corresponds to the loss of lattice water molecules. After the loss of lattice water molecules, these show good stabilities, up to ca. 250 °C (**102**) and 300 °C (**103**), followed by the continuous decomposition.

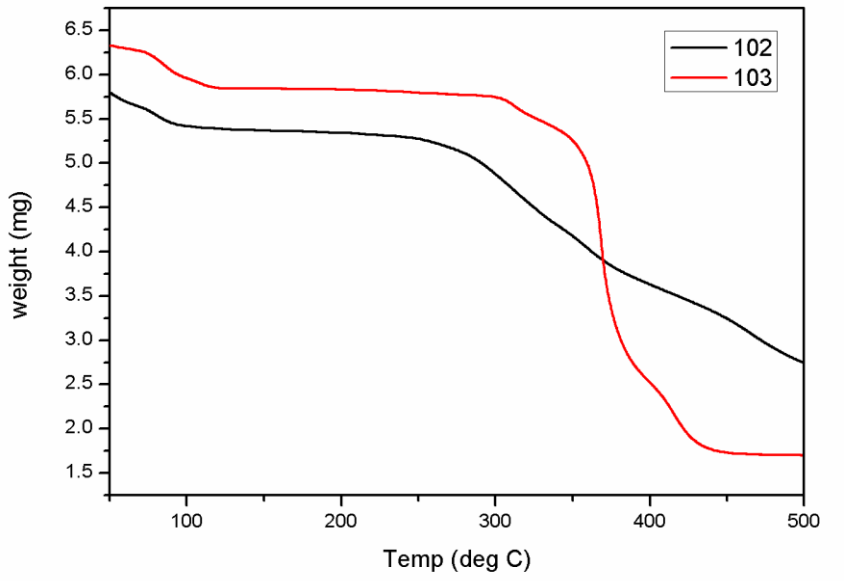

Figure 3.231. TGA scans of **102** and **103**.

CHAPTER IV

Conclusions and Future Directions

From the research work reported in this thesis, the following conclusions can be made:

(1) For a series of polypyridyl ligands varying the denticity from three to six, either modified or simplified general methods compared to those reported in the literature have been developed to isolate pure products in good to high yields. A new pyridyl-amide hexadentate ligand has been prepared to understand the effect of flexible amide group on the product formation compared to the polypyridyl hexadentate ligands. These are structurally characterized by melting point/boiling point measurements, and NMR and FTIR spectroscopy.

(2) For the synthesis of MOCNs, three general methods were developed using readily available metal salts of Mn(II), Fe(III), Ni(II), Co(II), Cu(II), Zn(II) and Cd(II). Two such methods were at ambient conditions while the third method was carried out under hydrothermal conditions. At ambient conditions these involved reactions of (a) a metal acetate with the carboxylic acid linker and the ancillary ligand in an appropriate ratio where acetic acid is the by-product, or (b) a metal perchlorate with the sodium salt of the carboxylate and the ancillary ligand in an appropriate ratio where sodium perchlorate is the by-product. Similarly, under hydrothermal conditions a mixture of the metal salt (sulphate or nitrate), the carboxylic acid linker and the ancillary ligand in a predesigned ratio is heated in a SS lined teflon reactor where a crystalline product is easily isolated after washing with water followed by vacuum drying. Those at ambient conditions are attractive routes for their simplicity as well as generalization of similar systems. It is worth noting that most of the MOCNs made at ambient conditions were soluble in common solvents. All MOCNs prepared by these methods were reproduced numerous times at optimized conditions. Their chemical compositions were established by elemental analysis and mass spectroscopy (wherever possible). FTIR and UV-vis (if the MOCN has a color) spectroscopic data further contributed in establishing their identities.

(3) In this field of research, obtaining the single crystal structures of the MOCNs is the key step and thus a lot of efforts was put in elucidating their three-dimensional structures by single crystal X-ray diffractometry. Those MOCNs that were found to be soluble in common solvents yielded single crystals for such study. For certain MOCNs either no suitable single crystal was obtained or only an amorphous material precipitated out after numerous attempts. In such cases, like those which were insoluble in all available solvents, data from other characterization techniques were used to elucidate their structures through comparison with the crystal structures of similar MOCNs. In case of those made under hydrothermal conditions, single crystals were chosen directly from the reactors. In order to confirm whether the single crystal structure corresponds to the bulk material or not, powder X-ray diffraction patterns were recorded for most of the compounds. Through matching the experimental and simulated (from the single crystal data) patterns to each other confirmed that the single crystal and bulk material of the compound were the same. It also confirmed the phase purity of the bulk samples. Additionally, powder patterns for those not having the single crystal structures was also utilized to elucidate their structures through comparion with similar systems.

(4) Exploring the chemistry of Mn(II) with the tridentate ligands and dicarboxylates such as acetylene dicarboxylate, fumarate and succinate, an effect of the substitution on the alkyl nitrogen of the tridentate ligand was identified in the formation of diverse products that were either supramolecular coordination networks (methyl and t-butyl groups), $[Mn_2(bpma)_2(adc)_2(H_2O)_2]$ (**1**) and $[Mn_2(bpta)_2(adc)_2(H_2O)_2]\cdot 5H_2O$ (**4**$\cdot 5H_2O$) or coordination polymers (ethyl and isopropyl), $[Mn_2(adc)_2(bpea)_2]_n$ (**2**). This subtle change in the substitution further provided different SCN for methyl vs. t-butyl group where the coordinated as well as lattice water molecules played very important roles. Thus the methyl derivative that lacked any lattice water molecule had a tetrameric synthon of the dinuclear subunit via hyrdogen bonding. On the other hand, the t-butyl derivative, **4**$\cdot 5H_2O$, which contained lattice water molecules could be converted back to the analog of **1** via single crystal to single crystal transformation showing different supramolecular assembly between the dinuclear subunits. This process was further followed by FTIR at 350 K over a period of 3 h. The dehydrated species (**4**) that was found to be unusually very stable at 350 K for over 18 hours is an unprecedented example and could be rehydrated back over four weeks at ambient conditions with 80% lattice water compared to the

original SCN, **4**·$4H_2O$. This structural diversity of these products due to the coordinated and lattice water molecules prompted us to carry out water adsorption studies. Results that corroborate well with their X-ray single crystal structures indicate the least water adsorption by **2** while a continuous water adsorption is observed for **1** and a step-wise water adsorption by **4**. Furthermore, adsorption data for **1** at two different conditions (with or without pretreament) show its dynamic behavior and soft nature. At p/po = 1 (where po is the vapor pressure at saturation), **4** adsorbed 160 cm^3 water per g of sample; on desorption it retains 60 cm^3 water per g of sample. Utilizing PXRD and FTIR spectroscopy, it was found that **4** is stable towards water. This reversible water adsorption ability shows the potential use of **4** in desiccant and adsorbent coolant applications.

(5) In restricting the binding of water molecules to the hexacoordinated Mn(II) center with a bis(dicarboxylato) bridge due to the use of the tetradentate tpa ligand resulted in the formation of 3D supramolecular assemblies **34**-**36** comprised of the dimanganese subunit, $[Mn_2(dicarboxylate)_2(tpa)_2]$ (dicarboxylate = acetylene dicarboxylate (adc) or fumarate or succinate) which differ in the dicarboxylate with a variation in the aliphatic chain structure (triple bond to double bond to single bond, respectively), and water clusters. Their structural differences due to different binding of the carboxylate linkers have provided structural diversity of the encapsulated water clusters in the supramolecular assemblies. Based on the X-ray crystal structures and TGA, the unusual stability of **35** compared to **34** and **36** is the result of different motifs including a cyclic quasi-planar hexamer formed through hydrogen bonding interactions. Through monitoring of the crystallization process of **35**, a new species **35a** (the first few crystals that appeared after 4 days and are bigger in size) with the same dimetal subunit as in **35** but containing six lattice water molecules was obtained. When hydrogen bonding interactions were analyzed for **35a**, it was found that two water molecules were missing from the hexamer, thus the pre-hexamer formation of water was crystallographically caught. Considering all supramolecular interactions, it is found that **35a** behaves like **34**.

(6) Upon changing the metal center from Mn(II) to Ni(II) for the tridentate ligands, a further variation in the carboxylate linker resulted in the diversity of product formation. For example, in the Ni(II)-bpta system, a variation in the carboxylates afforded diverse MOCNs under the same reaction conditions: the fumarate analogue $[Ni_4(bpta)_4(H_2O)_4(fum)_4]\cdot 4H_2O$ (**16**) is a square while

the adc and succinate analogs $[Ni(bpta)(adc)(H_2O)_2]\cdot 2H_2O$ (**13**) and $[Ni(bpta)(succ)(H_2O)_2]\cdot 3H_2O$ (**17**) are rare examples of Ni(II) monomeric subunit with only one end of the dicarboxylate coordinated. The monomeric subunits of **13** and **17** form supramolecular assemblies through extensive hydrogen bonding network of lattice water, coordinated water and uncoordinated oxygen atoms of the carboxylate groups. Similarly, the squares in **16** are further associated via hydrogen bonding between the lattice water molecules, uncoordinated oxygen atoms of the fumarates and the coordinated water molecule forming a six membered hexagonal motif $R_6^6(6)$. This is highly correlated to their thermal behavior in the solid state. Once again, the role of coordinated and lattice water molecules in forming the diverse MOCNs of Ni(II) is observed.

(7) Extending the chemistry of the tridentate ligands with other divalent metal ions, such as Co(II), Cu(II), Zn(II) and Cd(II), the product formation showed dependency on the metal ion for a number of dicarboxylate linkers. In case of Co(II) and Cu(II) with dicarboxylates such as adc, fumarate and tdc, supramolecular assemblies of dinuclear subunits bridged by the dicarboxylate in a bis(monodentate) fashion, coordinated water, lattice water, and uncoordinated oxygen atoms of the carboxylate groups were obtained. On the other hand, water soluble 1D CPs of the general formula, $[M_2(bpxa)_2(adc)_2]_n$ (where bpxa represents the tridentate ligands), was obtained for the Zn(II) and Cd(II) with adc as the linker. In all cases, Zn(II) centers are pentacoordinated and surrounded by three nitrogens of the ligand and two oxygens from two ends of two adc linkers which bind in a bis(monodentate) syn-anti fashion. On the other hand, in the Cd(II) analogs each hexacoordinated Cd(II) center is surrounded by three nitrogens of the ligand and three oxygen atoms (from one monodentate carboxylate group of an adc and one chelated carboxylate group of another adc).

(8) Like the dicarboxylates, reactions of Zn(II) or Cd(II) with H_3BTC and bpma resulted in the formation of 1D CPs $\{[Zn_2(bpma)_2(HBTC)_2]\}_n$ (**30a**) and $[Cd_2(bpma)_2(HBTC)_2]_n$ (**31**), which are further connected through hydrogen bonding interactions between the carboxylic acid groups of $HBTC^{2-}$. In these two compounds, Zn(II) and Cd(II) are pentacoordinated and heptacoordinated, respectively. For Zn(II), in addition to **30a**, a second product $[Zn_3(H_2O)_{12}(BTC)_2]$ (**30b**) was isolated; all Zn(II) centers in **30b** are hexacoordinated but one center is different from the other two with respect to the coordination environment. For reactions of the Cd(II)-H_3BTC system with bpea and bpta, MOFs $\{[Cd_3(bpea)_3(BTC)_2]\cdot 10H_2O\}_n$ (**32**) and

$\{[Cd_3(bpta)_3(BTC)_2(H_2O)]\cdot 5H_2O\}_n$ (**33**) were obtained. Out of the three Cd(II) compounds, **32** was found to be thermally more stable up to 350 °C.

(9) As expected for the d^{10} metal ions, luminescence behavior of a few of these Zn(II) and Cd(II) polymers in the solid state was established. Both bpta and adc have very weak fluorescence. Thus the observed emission in these CPs may be attributed to the chelation of the ligand to the metal center which enhances the ‘‘rigidity” of the ligand and thus reduces the loss of energy through a radiationless pathway. Therefore, the bpta/adc system can be considered as a sensor media for these two ions.

(10) As is the case with the tridentate ligands, a 1D CP is obtained for the Cd(II)-adc system with the tetradenate tpa ligand. However, Cd(II) centers in it are octacoordinated as both adc ends bind in a chelated fashion and tpa ligand wrapp around with four nitrogen donor atoms. Its thermal behavior is similar to **27**. Although the single crystal structure of the Zn(II)-tpa-adc analogue was not determined, it was evident from the spectroscopic data that it would have a similar structure to those with the tridentate ligands (**22-25**) except the Zn(II) centers would be hexacoordinated.

(11) Structural diversity of MOCNs was also established based on the length of the methylene link between the alkyl nitrogens of the hexadentate ligands. For the Mn(II)-adc (adc = acetylene dicarboxylate) chemistry, a 3D supramolecular network, **41**, held together by π–π interactions between the 2D layers of $[Mn_2(adc)_2(tpbn)(H_2O)_2]_n$ has been synthesized. With one less methylene group in tppn, a 3D supramolecular assembly, **42**, comprised of $Mn_2(tppn)(H_2O)_6$ dinuclear subunits, lattice water molecules and adc anions through strong hydrogen bonding interactions, is isolated. On the other hand, for the tpen and 1,2-tppn ligands with two methylene units between the alkyl nitrogen atoms discrete compounds **43** and **44** are formed. As the chain length increased from 4 to 5, the tppen analogue, **45**, is a rare example of having adc as a linker and a counter anion in the same structure where the adc group links the $Mn_2(tppen)(H_2O)_4$ dinuclear subunits to form the 1D chains that are further connected via both hydrogen bonding and π–π interactions. Interestingly, upon further increase in the methylene chain length (tpxn and tphn) products (**46** and **47**, respectively) similar to **45** are obtained. Therefore, these ligands are found to play an important role in determining the coordination architectures with respect to their size, conformation and properties.

(12) The reaction of Mn(II) with the oxalate linker with no aliphatic chain between the carboxylate groups provides a 1D CP for the tpbn ligand. The anion directed formation of $\{[Mn_2(tpbn)](ClO_4)_2\}_n$ and $[Mn_2(tpbn)(H_2O)_6](tdc)_2{\cdot}4H_2O$, where the same metal salt $Mn(ClO_4)_2$ is used as the starting material in both cases, is really unusual as the latter is the adc analog of the tppn ligand mentioned above. With the amide analogue of tpbn, $\{[Mn_2(bpbg)(adc)_2]{\cdot}4H_2O\}_n$ is obtained. For the cycloaliphatic dicarboxylate, cdc, a 2D MOF with very different structure compared to those with other dicarboxylates is obtained though the reaction carried out under hydrothermal conditions. In case of Zn(II) and Cd(II), a combination of dicarboxylates, such as adc and tdc, and tpbn has resulted in the 3D MOFs that show promising photoluminescence properties and water adsorption capabilities. On the other hand, a 1D CP, which is further hydrogen bonded to generate a 2D MOCNs, is isolated for the amide derivative bpbg.

(13) Utilizing hydrothermal reaction conditions, for H_3BTC and its cycloaliphatic analog, H_3CTC, different products are obtained with the Mn(II) and tpbn ligand: a 3D coordination polymer, $[Mn_2(tpbn)(HBTC)]_n$ (**55**), forming a chair like structure with Mn(II) centers acting as nodes; a tetrameric compound with a Mn_2bis(μ-dicarboxylato)(μ-sulphato) core, $[Mn_4(tpbn)_2(HCTC)_2(SO_4)_2]$ (**56**), that forms a supramolcular assembly through the hydrogen bonding between the carboxylic acid group of $HBTC^{2-}$ and one of the uncoordinated oxygens of the sulphate. Interestingly, the tphxn analog of **55**, $[Mn_2(tphxn)(HBTC)(H_2O)_2]_n$ (**57**) has a similar structure except each Mn(II) center in the latter has a coordinated water molecule and thus the binding of one of the carboxylate groups of HBTC changes from chelated to monodentate. Their thermal stability can be correlated to their structures. The chemsitry of Zn(II) and Cd(II) with tricarboxylates, such as BTC, and the tpbn ligand has provided products, $[Zn_2(tpbn)(HBTC)]_n$ (**102**) and $\{[Cd_2(tpbn)(HBTC)_2(H_2O)_2]{\cdot}4H_2O\}_n$ (**103**), similar to those obtained for the Mn(II) and tpbn and tphxn ligands, respectively. The formation of **102** is dependent on the source of Zn(II) salt; if $ZnSO_4$ is replaced with $Zn(NO_3)_2$ a dinuclear compound, $[Zn_2(tpbn)(H_2BTC)(NO_3)_2]$ (**101**)**,** is obtained.

(14) A large number of MOCNs (**58**-**87**) was prepared with Cu(II) and various dicarboxylates for all hexadentate polypyridyl ligands. This is in stark contrast to a couple of such species that could be possible with the tridentate ligands. Using several aliphatic dicarboxylates, such as fumarate, maleate, succinate, glutarate and adipate, either CPs or molecular rectangles are

obtained (except in one case) where the formation of such species is dependent on both the ancillary liagnd and the carboxylate. An extension of this chemistry with derivatives of succinate (mercaptosuccinate and malate), glutarate (diglyconate and 2,2'-dithioacetate), and adipate (c,c-muconate and t,t-muconate) has enriched our findings with the most important hexadentate ligand, tpbn.

(15) Varying the dicarboxylate from aliphatic to aromatic for the same polypyridyl ligand, namely tpbn, the terephthalate provides the similar 1D CP $\{[Cu_2(tpbn)(tere)(H_2O)_2](ClO_4)_2\}_n$ while the tetrafluoroterephthalate affords a 2D CP $\{[Cu_4(F_4\text{-tere})_3(tpbn)_2](ClO_4)_2 \cdot 4H_2O\}_n$. Another aromatic dicarboxylate, 2,6-pyridinedicarboxylate (2,6-PDC), affords a 1D CP $\{[Cu_2(tpbn)(2,6\text{-PDC})(H_2O)_2](ClO_4)_2\}_n$ similar to terephthalate. On the other hand, using the cycloaliphatic derivative of terephthalate, CDC, with the tpen ligand a 2D CP $[Cu_4(tpen)_2(CDC)_3](ClO_4)_2 \cdot 8H_2O$ (**81**) is obtained.

(16) The most fascinating chemistry for Cu(II) is obtained with a heterocyclic dicarboxylate, i.e., 2,5-thiophenedicarboxylate (tdc). With tpen, the formation of an octanuclear discrete MOF $[Cu_8(tpen)_4(tdc)_4(H_2O)_4](ClO_4)_8$ (**82**) is different from those with tppn, tpbn and tppen where molecular rectangles are obtained $[Cu_4(tppn)_2(tdc)_2(H_2O)_4](ClO_4)_4.2H_2O$ (**83**), $[Cu_4(tpbn)_2(tdc)_2(H_2O)_4](ClO_4)_4$ (**84**) and $[Cu_4(tppen)_2(tdc)_2(H_2O)_4](ClO_4)_4$ (**85**). These rectangles show excellent photoluminescence properties arising from the ligand (tdc) to metal charge transfer. On the other hand, a 2D coordination polymer $[Cu_2(tphn)(tdc)_2]_n$ is obtained in which the binding of tdc is similar to that of adc found in $\{[Mn_2(tpbn)(adc)_2(H_2O)_2].2CH_3OH\}_n$ (**41b**). Photoluminescent properties of the reactangles as well as their water adsorption studies provided further understanding of their structural similarities and differences.

(17) Similarly, exploring the Cu(II) chemistry with H_3BTC and its cycloaliphatic analogue, H_3CTC, for two different hexadentate ligands two MOFs (**88** and **89**) were obtained. Their water adsorption studies has resulted in the discovery of a very important MOF that shows a maximum uptake of 190 cm^3/g with a retention of ca. 150 cm^3/g of water on desorption. The isotherm for **89** shows a step-wise uptake which suggests that one kind of pores are filled first and then the next. This material showed very promising results in comparison to zeolites; the maximum uptake by Zeolites is 200 cm^3/g.

(18) Extending the chemistry of dicarboxylates, a few disulphonates are utilized as linkers for Cu(II) and the hexadentate ligands. In the series of $[Cu_2(tpen)_2(2,6\text{-}NDS)_2(H_2O)_4]\cdot 8H_2O$ (**90**), $\{[Cu_4(tppn)_2(Cl)_2(H_2O)_4](2,6\text{-}NDS)_2\cdot 14H_2O\}_n$ (**91**), $\{[Cu_2(tpbn)(2,6\text{-}NDS)(Cl)_2]\cdot 5H_2O\}_n$ (**92**), where 2,6-NDS = 2,6-naphthalene disulphonate, the most notable difference is the binding of 2,6-NDS. In case of tpen, it is a dinuclear Cu(II) compound with NDS binding in a monodentate fashion; in case of tppn, a Cl-bridged cationic polymer with NDS acting as a counter anion is obtained; in case of tpbn, NDS is binding in a bis(monodentate) fashion resulting in a 1D CP.

(19) Using the tpbn ligand, two 1D CPs $\{[Cu_2(tpbn)(4,4'\text{-}bpy)](ClO_4)_2\cdot 3H_2O\}_n$ (**93**) and $\{[Cu_2(tpbn)(N_3)_2(H_2O)_2](ClO_4)_2\}_n$ (**94**) were obtained with the nitrogen-based linkers. These two compounds further confirms the fact that bifunctional linkers (neutral or anionic) except tdc and any aliphatic dicaroxylate with less than four atom chain (succinate and its derivatives) gives CPs for the Cu(II)-tpbn system.

(20) One of the most thermally stable MOFs (up to 400 °C) was the result of the reaction between $Co(NO_3)_2$ and H_3BTC in the presence of the tpbn ligand under hydrothermal conditions, $[Co_2(tpbn)(HBTC)_2]_n$ (**95**). With the observation of two pyridine groups from the two tpbn ligands located inside the large pore, an analog with the bpbg ligand should be made where the smaller amide groups will not only provide the full access to the pores but also additional hydrogen bonding from the uncoordinated NH_2 groups could provide unique host-guest chemistry.

Based on the work described in this thesis, additional work could be initiated to explore further in making many new MOCNs and more importantly to study their potential applications in several fields. Therefore, a few of the furture directions from the learnings of this research can be:

(1) Although a number of divalent metals that prefer hexacoordination has been explored in this work, further chemistry with other metal ions, such as Cr(III), should be conducted with the tpbn ligand and numerous dicarboxylates and tricarboxylates to demonstrate the formation of CPs or rectangles similar to Cu(II). In this regard, restricting one end of the trans position in an octahedral geometry using VO^{2+} could potentially give only rectangles.

(2) In the present work, except one case of octanuclear MOFs only square or rectangles are obtained for the tetranuclear discrete MOFs. Thus, further construction of the metal atom clusters with appropriate design of the ligands should be done to explore the possibility of other M_4 MOFs with a tetrahedral topology. Furthermore, those with hexagon and cube topology for the M_6 and M_8 MOFs, respectively, could be other possibilities.

(3) Using some of these MOCNs water adsorption studies has indicated their suitability in desiccant and adsorbent cooling applications. This can be optimized and set-up systems to show their real use compared to zeolites and silica gels.

(4) Due to the unavailability of the Gas Adsorption instrument, only a limited number of measurements has been performed with MOFs made in this work. Therefore, such measurements will be the key steps forward in identifying their potentials in such applications.

(5) Based on the photoluminescent properties of selected MOCNs, further studies, particularly with Lanthanides, will provide a new direction in this field.

(6) Similarly, the formation of heteronuclear MOCNs can be initiated with the knowledge acquired from this work.

(7) With a database of compounds from this work, chemical modifications of the ligands and linkers should focus on the optimization of physical properties that are directly related to their potential applications in various fields.

References

1. Schaeffer, W. D.; Dorsey, W. S.; Skinner D. A.; Christian, C. G. *J. Am. Chem. Soc.* **1957**, *79*, 5870.
2. (a) Wilde, R. E.; Ghosh, S. N.; Marshall, B. J. *Inorg. Chem.* **1970**, *9*, 2512. (b) Buser, H. J.; Schwarzenbach, D.; Petter, W.; Ludi, A. *Inorg. Chem.* **1977**, *16*, 2704. (c) Dunbar, K. R.; Heintz, R.A. *Prog. Inorg. Chem.* **1997**, *45*, 283.
3. Hofmann, K. A.; Kuspert, K. Z. *Z. Anorg. Chem.* **1897**, *15*, 204.
4. (a) Barrer, R. M. in *Molecular Sieves, Advances in Chemistry Series* 121, eds. Meier, W. M.; Utyyerhoeven, J. B.; American Chemical Society, Washington, DC, **1974**, p. 1. (b) Iwamoto, T in *Inclusion Compounds*, eds. Atwood, J. L.; Davies, J. E. D.; MacNicol, D. D. Academic Press, London, **1984**, vol. 1, ch. 2, pp. 29. (c) Iwamoto, T in *Inclusion Compounds*, eds. Atwood, J. L.; Davies, J. E. D.; MacNicol, D. D. Oxford University Press, Oxford, **1991**, vol. 5, ch. 6, pp. 172.
5. (a) Lehn, J-M. *Supramolecular Chemistry: Concepts and Perspectives.* VCH: New York, **1995**. (b) Steed, J. W.; Atwood, J. L. *Supramolecular Chemistry*. John Wiley & sons, Ltd., **2009**. (c) Atwood, J. L.; Davies, J. E. D.; MacNicol, D. D.; Vögtle, F.; Lehn, J-M. *Comprehensive Supramolecular Chemistry*, Pergamon: Oxford, **1996**.
6. Badjić, J. D.; Nelson, A.; Cantrill, S. J.; Turnbull, W. B.; Stoddart, J. F. *Acc. Chem. Res.* **2005**, *38*, 723.
7. (a) Lehn, J-M. *Angew. Chem. Int. Ed.* **1988**, 27, 89. (b) Lehn, J-M. *Proc. Natl. Acad. Sci. U. S. A.* **2002**, *99*, 4763. (c) Lehn, J. M. *Science* **2002**, *295*, 2400.
8. (a) Kinoshita, Y.; Matsubara, I.; Higuchi, T.; Saito, Y. *Bull. Chem. Soc. Jpn.* **1959**, *32*, 1221. (b) Desiraju, G. R. *Crystal Engineering. The Design of Organic Solids,* Elsevier: Amsterdam, **1989**.
9. (a) Auerbach, S. M.; Carrado, K. A.; Dutta, P. K. *Handbook of Zeolite Science and Technology* Marcel Dekker, Inc., New York, **2003**. (b) Xu, R.; Yu, Jihong.; Huo, Q.; Chen, J. *Chemistry of Zeolites and Related Porous Materials: Synthesis and Structure*; Wiley-Interscience, **2007**.
10. Bruce, D. W.; O'Hare, D.; Walton, R. I. *Porous Materials (Inorganic Materials Series);* Wiley, **2010**.
11. Hoskins, B. F.; Robson, R. *J. Am. Chem. Soc.* **1990**, *112*, 1546.
12. Fujita, M.; Kwon, Y. J.; Washizu, S.; Ogura, K. *J. Am. Chem. Soc*. 1**994**, *116*, 1151.
13. Yaghi, O.M.; Li, G.; Li, H. *Nature* **1995**, *378*, 703.
14. Venkataraman, D.; Gardner, G. B.; Lee, S.; Moore, J. S. *J. Am. Chem. Soc.* **1995**, *117*, 11600.
15. Kondo, M.; Yoshitomi, T.; Seki, K.; Matsuzaka, H.; Kitagawa, S. *Angew. Chem. Int. Ed. Engl.* **1997**, *36*, 1725.
16. (a) O'Keeffe, M.; Yaghi, O. M. *Chem. Rev.* **2012**, *112*, 675. (b) Stock, N.; Biswas, S. *Chem. Rev*. **2012**, *112*, 933.
17. Suh, M. K.; Park, H. J.; Prasad, T. K.; Lim, D.-W. *Chem. Rev*. **2012**, *112*, 782.
18. Li, J.-R.; Sculley, J.; Zhou, H.-C. *Chem. Rev.* **2012**, *112*, 869.
19. Kreno, L. F.; Leong, K.; Farha, O. K.; Allendorf, M.; VanDuyne, R. P.; Hupp, J. T. *Chem. Rev.* **2012**, *112*, 1105.
20. Cui, Y.; Yue, Y.; Qian, G.; Chen, G. *Chem. Rev.* **2012**, *112*, 1126.
21. Kitagawa, S.; Kitaura, R.; Noro, S. *Angew. Chem., Int. Ed.* **2004**, *43*, 2334.

22. Dmitriev, A.; Lin, N.; Barth, J. V.; Kern, K. *Angew. Chem. Int. Ed.* **2003**, *42*, 2670.
23. Yaghi, O. M.; O' Keeffe, M.; Ockwing, N. W.; Chae, H. K.; Eddaoudi, M.; Kim, J. *Nature* **2003**, *423*, 705.
24. Stepanow, S.; Lingenfelder, M.; Dmitriev, A.; Spillmann, H.; Delvigne, E.; Lin, N.; Cai, C.; Barth, J. V.; Kern, K. *Nat. Mater.* **2004**, *3*, 229.
25. Tranchemontagne, D. J.; Mendoza-Cortés, J. L.; O'Keeffe, M.; Yaghi, O. M. *Chem. Soc. Rev.* **2009**, *38*, 1257.
26. Rosseinsky, M. J. *Microporous and Mesoporous Materials* **2004**, *73*, 15.
27. Rowsell, J. L. C; Yaghi, O. M. *Microporous and Mesoporous Materials* **2004**, *73*, 3.
28. Wang, Z. Q.; Cohen, S. M. *Chem. Soc. Rev.* **2009**, *38*, 1315.
29. Lee, J. Y.; Farha, O. M.; Roberts, J.; Scheidt, K. A.; Nguyen, S. T.; Hupp, J. T. *Chem. Soc. Rev.* **2009**, *38*, 1450.
30. Ravon, U.; Domine, M. E.; Gaudillere, C.; Desmartin-Chomel, A.; Farrusseng, D. *New J. Chem.* **2008**, *32*, 937.
31. Henschel, A.; Gedrich, K.; Kraehnert, R.; Kaskel, S. *Chem. Comm*. **2008**, 4192.
32. Ma, L.; Abney, C.; Lin, W. *Chem. Soc. Rev.* **2009**, *38*, 1248.
33. Wu, C.; Lin, W. *Angew. Chem. Int. Ed.* **2007**, *46*, 1075.
34. Dybtsev, D. N.; Nuzhdin, A. L.; Chun, H.; Bryliakov, K. P.; Talsi, E. P.; Fedin, V. P.; Kim, K. *Angew. Chem. Int. Ed.* **2006**, *45*, 916.
35. Wu, C.; Hu, A.; Zhang, L.; Lin, W. *J. Am. Chem. Soc.* **2005**, *127*, 8940.
36. Cho, S. H.; Ma, B. Q.; Nguyen, S. T.; Hupp, J. T.; Albrecht-Schmitt, T. E. *Chem. Commun.* **2006**, 2563.
37. Zou, R. Q.; Sakurai, H.; Xu, Q. *Angew. Chem. Int. Ed. Engl.* **2006**, *45*, 2542.
38. Gandara, F.; Gornez-Lor, B.; Gutierrez-Puebla, E.; Iglesias, M.; Monge, M.; Proserpio, D. M.; Snejko, N. *Chem. Mater.* **2008**, *20*, 72.
39. Alkordi, M. H.; Liu, Y. L.; Larsen, R. W.; Eubank, J. F.; Eddaoudi, M. *J. Am. Chem. Soc.* **2008**, *30*, 12639.
40. Schroder, F.; Esken, D.; Cokoja, M.; van den Berg, M. W. E.; Lebedev, O. I.; Tendeloo, G. V.; Walaszek, B.; Buntkowsky, G.; Limbach, H. H.; Chaudret, B.; Fischer, R. A. *J. Am. Chem. Soc.* **2008**, *130*, 6119.
41. Hasegawa, S.; Horike, S.; Matsuda, R.; Furukawa, S.; Mochizuki, K.; Kinoshita, Y.; Kitagawa, S. *J. Am. Chem. Soc.* **2007**, *129*, 2607.
42. Horike, S.; Dinča, M.; Tamaki, K.; Long, J. R. *J. Am. Chem. Soc.* **2008**, *130*, 5854.
43. Seo, J. S.; Whang, D.; Lee, H.; Jun, S. I.; Oh, J.; Jeon, Y. J.; Kim, K. *Nature* **2000**, 404, 982.
44. Kitaura, R.; Seki, K.; Akiyama, G.; Kitagawa, S. *Angew. Chem. Int. Ed.* **2003**, *42*, 428.
45. Min, K. S.; Suh, M. P. *J. Am. Chem. Soc.* **2000**, *122*, 6834.
46. Yaghi, O. M.; Li, H. *J. Am. Chem. Soc.* **1996**, *118*, 295.
47. Li, J. R.; Kuppler, R. J.; Zhou, H. C. *Chem Soc. Rev.* **2009**, *38*, 1477.
48. Parnham, E. R.; Morris, R. E. *Acc. Chem. Res.* **2007**, *40*, 1005.
49. Beauvais, L. G.; Shores, M. P.; Long, J. R. *J. Am. Chem. Soc.* **2000**, *122*, 2763.
50. Evans, O. R.; Lin, W. *Chem Mater.* **2001**, *13*, 2075.
51. Hong, B. H.; Bae, S.C.; Lee, C. W.; Jeong, S.; Kim, K. *Science* **2001**, *294*, 348.
52. Han, S. S.; Mendoza-Cortès, J. L.; Goddard III, W. A. *Chem. Soc. Rev.* **2009**, *38*, 1460.
53. Dincã, M.; Dailly, A.; Liu, Y.; Brown, C. M.; Neumann, D. A.; Long, J. R. *J. Am. Chem. Soc.* **2006**, *128*, 16876.

54. Xu, R.; Pang, W.; Yu, J.; Huo, Q.; Chen, J. *Chemistry of Zeolites and Related Porous Materials: Synthesis and Structure*. John Wiley & Sons (Asia) Pet Ltd., Singapore, **2007**.
55. Yang, R. T. *Gas Separation by Adsorption Progress*, Butterworth, Boston, **1987**.
56. Crittenden, B.; Thomas, W. J. *Adsorption Technology and Design*, Butterworth-Heinemann, Oxford, **1998**.
57. Warrendale, P.A. *Nanoporous and Nanostructured Materials for Catalysis Sensor and Gas Separation Applications*, Materials Research Society, San Francisco, **2005**.
58. Murray, L. J.; Dincã, M.; Long, J. R. *Chem. Soc. Rev.* **2009**, *38*, 1294.
59. Rosi, N. L.; Eckert, J.; Eddaoudi, M.; Vodak, D. T.; Kim, J.; O'Keeffe, M.; Yaghi, O. M. *Science* **2003**, *300*, 1127.
60. Kesanli, B.; Cui, Y.; Smith, M. R.; Bittner, E. W.; Bockrath, B. C.; Lin, W. *Angew. Chem., Int. Ed.* **2005**, *44*, 72.
61. Chen, B.; Zhao, X.; Putkham, A.; Hong, K.; Lobkovsky, E. B.; Hurtado, E. J.; Fletcher, A. J.; Thomas, K. M. *J. Am. Chem. Soc.***2008**, *130*, 6411.
62. Pan, L.; Parker, B.; Huang, X.; Olson, D. H.; Lee, J. Y.; Li, J. *J. Am. Chem. Soc.***2006**, *128*, 4180.
63. Kitagawa, S. *Nature* **2006**, *441*, 584-585.
64. Kondo, M.; Yoshitomi, T.; Seki, K.; Matsuzaka, H.; Kitagawa, S. *Angew. Chem. Int. Ed.* **1997**, *36*, 1725.
65. Han, S. S.; Mendoza-Cortès, J. L.; Goddard, W. A. *Chem. Soc. Rev*. **2009**, *38*, 1460.
66. Allendorf, M. D.; Bauer, C. A.; Bhakta, R. K.; Houk, R. J. T. *Chem. Soc. Rev.* **2009**, *38*, 1330.
67. Janiak, C. *Dalton Trans.* **2003**, 2781.
68. Maspoch, D.; Ruiz-Molina, D.; Veciana, J. *Chem. Soc. Rev.* **2007**, *36*, 770.
69. Suh, M. P.; Cheon, Y. E.; Lee, E-Y. *Coord. Chem. Rev.* **2008**, *252*, 1007.
70. Cahill, C. L.; de Lilla, D. T.; Frisch, M. *CrystEngComm* **2007**, *9*, 15.
71. Bauer, C. A.; Timofeeva, T. V.; Settersten, T. B.; Patterson, B. D.; Liu, V. H.; Simmons, B. A.; Allendorf, M. D. *J. Am. Chem. Soc.* **2007**, *129*, 7136.
72. Seo, J.; Whang, D-M.; Lee, H-Y. *Nature* **2000**, *404*, 982.
73. Sawaki, T.; Aoyama, Y. *J. Am. Chem. Soc*. **1999**, *121*, 4793.
74. Kurmoo, M. *Chem. Soc. Rev*. **2009**, *38*, 1353.
75. *Metal–Organic and Organic Molecular Magnets, Spec. Publ. - R. Soc. Chem.*, ed. Day, P. and Underhill, A. E., Cambridge, UK, **2000**.
76. Rao, C. N. R.; Cheetham, A. K.; Thirumurugan, A. *J. Phys. Condens. Matter* **2008**, *20*, 083202.
77. Blundell, S. J.; Pratt, F. L. *J. Phys. Condens. Matter* **2004**, *16*, R771.
78. *Molecular Magnetism, New Magnetic Materials*, ed. Itoh, K.; Kinoshita, M. Gordon Breach-Kodansha, Tokyo, **2000**.
79. Schieber, M. M. *Selected Topics in Solid State Physics Experimental Magnetochemistry*, ed. Wohlfarth, E. P.; North-Holland, Amsterdam, **1967**, vol. VIII.
80. (a) *Physics Meets Mineralogy*, ed. Aoki, H.; Syono, Y.; Hemley, R. J. CUP, Cambridge, **2000**. (b) *Magnetism: A Supramolecular Function*, ed. Kahn, O., Kluwer Academic Publishers, **1996**.
81. Gatteschi, D.; Sessoli, R.; Villain, J. *Molecular Nanomagnets*, Oxford University Press, Oxford, **2006**.
82. Coulon, C.; Miyasaka, H.; Clèrac, R. *Struct. Bonding* **2006**, *122*, 163.

83. Bogani, L.; Vindigni, A.; Sessoli, R.; Gatteschi, D. *J. Mater. Chem*. **2008**, *18*, 4750.
84. Desiraju, G. R. *Acc. Chem. Res*. **1991**, *24*, 290.
85. Braga, D.; Grepioni, F. *Acc. Chem. Res*. **2000**, *33*, 601.
86. Braga, D.; Grepioni, F.; Biradha, K.; Pedireddi, V. R.; Desiraju, G. R. *J. Am. Chem. Soc*.**1995**, *117*, 3156.
87. Biradha, K.; Sharma, C. V. K.; Selvam, K. P.; Shimoni, L.; Carrell, H. L.; Zacharias, D. E.; Desiraju, G. R. *J. Chem. Soc. Chem. Commun*. **1993**, 1473.
88. Zimmerman, S. C.; Corbin, P. S. in *Molecular Self-Assembly. Organic Versus Inorganic Approaches* Springer, Berlin, **2000**, *96*, 63.
89. Prins, L. J.; Reinhoudt, D. N.; Timmerman, P. *Angew. Chem. Int. Ed*. **2001**, *40*, 2382.
90. Beijer, F. H.; Sijbesma, R. P.; Kooijman, H.; Spek, A. L.; Meijer, E. W. *J. Am. Chem. Soc*.**1998**, *120*, 6761.
91. Lawrence, D. S.; Jiang, T.; Levett, M. *Chem. Rev*. **1995**, *95*, 2229.
92. Whitesides, G. M.; Simanek, E. E.; Mathias, J. P.; Seto, C. T.; Chin, D. N.; Mammen, M.; Gordon, D. M. *Acc. Chem. Res*. **1995**, *28*, 37.
93. Biradha, K.; Nangia, A.; Desiraju, G. R.; Carrell, C. J.; Carrell, H. L. *J. Mater. Chem*.**1997**, 1111.
94. (a) Khullar, S.; Mandal, S. K. *Cryst. Growth Des*. **2012**, *12*, 5329. (b) Khullar, S.; Mandal, S. K. *Cryst. Growth Des*. **2013**,*13*, 3116.
95. Batten, S. R.; Neville, S. M.; Turner, D. R. *Coordination Polymers: Design, Analysis and Application*, Royal Society of Chemistry, Cambridge, **2009**.
96. Eddaoudi, M.; Moler, D. B.; Li, H.; Chen, B.; Reineke, T. M.; O'Keeffe, M.; Yaghi, O. M. *Acc. Chem. Res*. **2001**, *34*, 319.
97. Yaghi, O. M.; O'Keeffe, M.; Ockwig, N. W.; Chae, H. K.; Eddaoudi, M.; Kim, J. *Nature* **2003**, *423*, 705.
98. O'Keeffe, M.; Eddaoudi, M.; Li, H. L.; Reineke, T.; Yaghi, O. M. *J. Solid State Chem*. **2000**, *153*, 3.
99. Li, H.; Eddaoudi, M.; O'Keeffe, M.; Yaghi, O. M. *Nature*. **1999**, *402*, 276.
100. Eddaoudi, M.; Kim, J.; Rosi, N.; Vodak, D.; Wachter, J.; O'Keeffe, M.; Yaghi, O. M. *Science* **2002**, *295*, 469.
101. O'Keeffe, M.; Peskov, M. A.; Ramsden, S. J.; Yaghi, O. M. *Acc. Chem. Res*. **2008**, *41*,1782.
102. Batten, S. R.; Champness, N. R.; Chen, X. R.; Chen, X-M.; Garcia-Martinez, J.; Kitagawa, S.; Öhrström, L.; O'Keeffe, M.; Suh, M. P.; Reedijk, J. *CrystEnggCommun*. **2012**, *14*, 3001.
103. (a) Cook, T. R.; Yang, R. Y.; Stang, P. J. *Chem. Rev*. **2013**, *113*, 734. (b) Chakrabarty, R.; Mukherjee, P. S.; Stang, P. J. *Chem. Rev*. **2011**, *111*, 6810. (c) Stang, P. J. *Chem. Eur. J*. **1998**, *4*, 19. (d) Northrop, B. H.; Zheng, Y-R.; Chi, K-W.; Stang, P. J. *Acc. Chem. Res*. **2009**, *42*, 1554.
104. Fujita, M. *Chem. Soc. Rev*. **1998**, 27, 417.
105. Leininger, S.; Olenyuk, B.; Stang, P. J. *Chem Rev*. **2000**, *100*, 853.
106. Cotton, F. A.; Lin, C.; Murillo, C. A. *Acc Chem Res*. **2001**, *34*, 759.
107. Dinolfo, P. H.; Hupp, J. T. *Chem. Mater*. **2001**, *12*, 3113.
108. Holliday, B. J.; Mirkin, C. A. *Angew Chem Int. Ed*. **2001**, *40*, 2022.
109. (a) Jouaiti, A.; Hosseini, M. W.; Kyritsakas, N. *Eur. J. Inorg. Chem*. **2003**, 57. (b) Mislin, G.; Graf, E.; Hosseini, M. W.; Cian, A. D.; Kyritsakas, N.; Fischer, J. *Chem. Commun*. **1998**, 2545. (c) Feller, R. K.; Cheetham, A. K. *Dalton Trans*. **2008**, 2034. (d) Carlucci, L.; Ciani,

G.; Macchi, P.; Proserpio, D. M.; Rizzato, S. *Chem.Eur. J.* **1999**, *5*, 237.
110. (a) Hagrman, D.; Hammond, R. P.; Haushalter, R.; Zubieta, J. *Chem.Mater.* **1998**, *10*, 2091. (b) Withersby, M. A.; Blake, A. J.; Champness, N. R.; Hubberstey, P.; Wan-Sheung, Li; Schröder, M. *Angew. Chem., Int. Ed.* **1997**, *36*, 2327. (c) Zaman, M. B.; Smith, M. D.; zur Loye, H.-C. *Chem. Mater.* **2001**, *13*, 3534. (d) Choi, H. J.; Suh, M. P. *Inorg. Chem.* **1999**, *38*, 6309. (e) Sun, C.-Y.; Zheng, X.-J.; Gao, S.; Li, L.-C.; Jin, L.-P. *Eur. J. Inorg.Chem.* **2005**, 4150.
111. Banfi, S.; Carlucci, L.; Caruso, E.; Ciani, G.; Proserpio, D. M. *J. Chem. Soc., Dalton Trans.* **2002**, 2714.
112. (a) Ma, C.-B.; Chen, C.-N.; Liu, Q.-T. *CrystEngComm* **2005**, *7*, 650. (b) Zhang, X.-M.; Tong, M.-L.; Gong, M.-L.; Chen, X.-M. *Eur. J. Inorg.Chem.* **2003**, 138.
113. (a) Fujita, M.; Yazaki, J.; Ogura, K. *J. Am. Chem. Soc.* **1990**, *112*, 5645. (b) Stang, P. J.; Cao, D. H. *J. Am. Chem. Soc.* **1994**, *11*6, 4981.
114. Leininger, S.; Olenyuk, B.; Stang, P. J. *Chem. Rev.* **2000**, *100*, 853.
115. Giri, S.; Biswas, S.; Drew, M. G. B.; Ghosh, A.; Saha, S. K. *Inorg. Chim. Acta*, **2011**, *368*, 152.
116. (a) Visinescu, D.; Madalan, A. M.; Kravtsov, V.; Simonov, Y. A.; Schmidtmann, M.; Müller, A.; Andruha, M *Polyhedron* **2003**, *22*, 1385. (b) Kato, M.; Sah, A. K.; Tanase, T, Mikuriya, M. *Inorg. Chem.* **2006**, *45*, 6646.
117. Cotton, F. A.; Lin, C.; Murillo, C. A. *Proc. Nat. Acad. Sci. (USA)* **2002**, *99*, 4810.
118. Chisholm, M. H.; Macintosh, A. M. *Chem. Rev.***2005**, *105*, 2949.
119. (a) Barnett, S. A.; Champness, N. R.; *Coord. Chem. Rev.* **2003**, *246*, 145. (b) Zaworotko, M. J. *Chem Commun.* **2001**, 1. (c) Nicole Power, K.; Hennigar, T. L.; Zaworotko, M. J. *Chem Commun.* **1998**, 595. (d) Tong, X. L.; Wang, D. Z.; Hu, T-L.; Song, W-C.; Tao, Y.; Bu, X-H. *Cryst. Growth Des.* **2009**, *9*, 2280.
120. (a) Liu, P.-P.; Cheng, A.-L.; Yue, Q.; Liu, N.; Sun, W.-W.; Gao, E.-Q. *Cryst. Growth Des.* **2008**, 8, 1668. (b) Yang, J.; Liu, B.; Liu, Y-Y.; Ma, J-F.; Wu, H.; Liu, H-Y. *Cryst. Growth Des.* **2010**, *10*, 4795.
121. (a) Chui, S. –Y. S.; Lo, M, -H, S.; Charmant, J. P. H.; Orpen, A. G.; Williams, I. D. *Science* **1999**, *283*, 1148. (b) Yaghi, O. M.; Li, H.; Groy, T. L. *J. Am. Chem. Soc.* **1996**, *118*, 9096. (c) Xie, J.; Han, Z.; Pei, W.; Zou, Y.; Ren, X. *Inorg. Chem. Commun.* **2011**, *14*, 1266. (d) Massoud, S. S.; Mautner, F. A.; Louka, F. R.; Demeshko, S.; Dechert, S.; Meyer, F. *Inorg. Chim. Acta* **2011**, 370, 435. (e) Mahata, P.; Sen, D.; Natarajan, S. *Chem. Commun.* **2008**, 1278-1280. (f) Eddaoudi, M.; Kim, J.; Rosi, N. *Science* **2002**, *295*, 469.
122. (a) Bi, W.; Cao, R.; Sun, D.; Yuan, D.; Li, X.; Wang, Y.; Hong, M. *Chem. Commun*. **2004**, 2104. (b) Chen, B.; Fronczek, F. R.; Courtney, B. H.; Zapata, F. *Cryst. Growth Des*. **2006**, *6*, 825. (c) Kurmoo, M.; Kumagai, H.; Akita-Tanaka, M.; Inone, K.; Takagi, S. *Inorg Chem.* **2006**, *45*, 1627. (d) De, G. *Acta Crystallogr.* **2007**, *E63*, m1748. (e) Wang, Xi.; Yao, W.; Qi, Y-F.; Luo, M-F.; Wang, Y-H.; Xie, H-W, Yu, Y.; Ma, R-Y.; Li, Y-G. *CrystEnggComm* **2011**, *13*, 2542. (f) Lui, F-Y.; Huang, K-L.; Xu, Y-Q.; Han, Z-G.; Liu, X.; Chi, Y-N.; Hu, C-W. *CrystEnggComm* **2009**, *11*, 2757. (g) Wang, Q-W.; Wang, X-Y.; Wang, M.; Li, B-Y.; Ma, X-Y. *Acta Cryst* **2009**, *C65*, m276.
123. Roberts, P. V. Mackay, D. M.; Cannon, F. S. **1980**. In: EPA-600/2-80-123. U.S. Environmental Protection Agency.
124. http://www.activated-carbon.com/
125. (a) Rabenau, A. *Angew. Chem. Int. Ed*. **1985**, *24*, 1026. (b) Ockwig, N. W.; Delgado-

Friedrichs, O.; O'Keeffe, M.; Yaghi, O. M. *Acc. Chem. Res.* **2005**, *38* 176. (c) Robson, R. *Dalton Trans.* **2008**, 5113.
126. Zhang, W. X.; Yang, Y. Y.; Zai, S. B.; Ng, S. W.; Chen, X. M. *Eur. J. Inorg. Chem.* **2008**, 679.
127. Fang, Q. R.; Zhu, G. S.; Jin Z et al. *Angew. Chem. Int. Ed.* **2007**, *46*, 6638.
128. (a) Ferey, G.; Cejka, J.; van Bekkum, H.; Corma, A.; Schuth, F. *Stud. Surf.Sci. Catal*. **2007**, 168. (b) Tompsett, G. A.; Conner, W. C.; Yngvesson, K. S. *ChemPhysChem* **2006**, *7*, 296. (c) Jhung, S. H.; Yoon, J. W.; Hwang, J-S.; Cheetham, A. K.; Chang, J-S. *Chem. Mater.* **2005**, *17*, 4455. (d) Ni, Z.; Masel, R. I. *J. Am. Chem. Soc.* **2006**, *128*, 12394. (e) Ma, M.; Bètard, AWeber, I.; Al-Hokbany, N.S.; Fischer, R. A.; Metzler-Nolte, N. *Cryst. Growth Des.* **2013**, *13*, 2286.
129. Meek, S. T.; Greathouse, J. A.; Allendorf, M. D. *Adv. Mater*. **2011**, *23*, 249.
130. (a) Pichon, A.; Lazuen-Garay, A.; James, S. L. *CrystEngComm* **2006**, *8*, 211. (b) Pichon, A.; James, S. L. *CrystEngComm* **2008**, *10*, 1839. (c) Friscic, T.; Fabian, L. *CrystEngComm* **2009**, *11*, 743.
131. (a) Mueller, U.; Puetter, H.; Hesse, M.; Wessel, H. WO **2005**/049892. (b) Schlesinger, M.; Schulze, S.; Hietschold, M.; Mehring, M. *Microporous Mesoporous Mater.* **2010**, *132*, 121.
132. Stein, I.; Ruschewitz, U.; *Z. Anorg. Allg. Chem*. **2010**, *636*, 400.
133. Gagnon, K. J.; Perry, H. P.; Clearfield, A. *Chem. Rev.* **2012**, *112*, 1034.
134. Shimizu, G. K.; Vaidhyanathan R.; Taylor J. M. *Chem Soc Rev.* **2009**, *38*, 1430.
135. Batten, S. R.; Hoskins, B. F.; Robson, R. *J. Am. Chem. Soc.* **1995**, *117*, 5385.
136. (a) Zhang, L-P.; Ma, J-F.; Yang, J.; Liu, Y-Y.; Wei, G-H, *Cryst. Growth Des*. **2009**, *9*, 4660. (b) Cheng, P-C.; Kuo, P-T.; Liao, Y-H.; Xie, M-Y.; Hsu, W.; Chen, J-R *Cryst. Growth Des*. **2013**, *13*, 623.
137. (a) LeGuet, T.; Mautner, F. A.; Demeshko, S.; Meyer, F.; Perkins, R. S.; Massoud, S. S. *Inorg. Chem. Commun.* **2009**, *12*, 321. (b) Louka, F. R.; Stewart, A. D.; Regel, E.; Mautner, F. A.; Demeshko, S.; Meyer, F.; Massoud, S. S. *Inorg. Chem. Commun*. 2012, **22**, 60.
138. Sculley, J.; Yuan, D.; Zhou, H.-C. *Energy Environ. Sci.* **2011**, *4*, 2721.
139. Han, S. S.; Mendoza-Cortés, J. L.; Goddard, W. A. *Chem. Soc. Rev*. **2009**, *38*, 1460.
140. (a) Dybtsev, D.; Chun, H.; Yoon, S. H.; Kim, D.; Kim, K. *J. Am. Chem. Soc*. **2004**, *126*, 32. (b) Achmann, A.; Hagen, G.; Kita, J.; Malkowsky, I. M.; Kiener, C.; Moos, R. *Sensors.* **2009**, *9*, 1574.
141. (a) McKinlay, A. C.; Xiao, B.; Wragg, B. S.; Wheatley, P. S.; Megson, I. L.; Morris, R. *J. Am. Chem. Soc.* **2008**, *130*, 10440. (b) Achmann, A.; Hagen, G.; Kita, J.; Malkowsky, I. M.; Kiener, C.; Moos, R. *Sensors.* **2009**, *9*, 1574.
142. Jeremias, F.; Lozan, V.; Henninger, S. K.; Janiak, C. *Dalton Trans. ASAP* **2013** DOI: 10.1039/c3dt51471d.
143. (a) Reger, D. L.; Smith, D. M.; Long, G. J.; Grandjean, F. *Inorg Chem.* **2011**, *50*, 686. (b) Reger, D. L.; Smith, M. D. *Inorg Chem*. **2011**, 50, 11754.
144. Aijaz, A.; Lama, P.; Bharadwaj, P. K. *Inorg. Chem.* **2010**, *49*, 5583.
145. Wang, C-C.; Yeh, C-T.; Cheng, K-Yi.; Chand, P-C.; Hp, M-L.; Lee, G-H.; Shih, H-S.; Sheu, H-S. *Inorg. Chem.* **2011**, *50*, 597 and references therein.
146. Michaelides, A.; Skoulika, S. *Cryst. Growth Des.* **2005**, *5*, 529.
147. (a) Ludwig, R. *Angew.Chem. Int. Ed.,* **2001**, *40*, 1808. (b) Ghosh, S. K.; Bharadwaj, P. *Angew.Chem. Int. Ed.* **2004**, *43*, 3577. (c) Ball, P. *H_2O: A biography of water;* Weidenfled and Nivolson; London, **1999**.

148. (a) Nauta, K.; Miller, R. E. *Science* **2000**, *287*, 293. (b) Buck, U.; Huisken, F. *Chem. Rev.* **2000**, *100*, 3863. (c) Chen, K.; Hirst, J.; Camba, R.; Bonagura, C. A.; Stout, C. D.; Burgess, B. K.; Armstrong, F. A. *Nature (London)* **2000**, *405*, 814.
149. (a) Wei, M.; He, C.; Hua, W.; Duan, C.; Li, S.; Meng, Q. J. *J. Am. Chem. Soc.* **2006**, *128*, 13318. (b) Mahata, P.; Ramya, K.V.; Natarajan, S. *Inorg. Chem.* **2009**, *48*, 4942. (c) Zang, S.; Su, Y.; Duan, C.; Li, Y.; Zhu, H.; Meng, Q. *Chem. Commun.* **2006**, 4997. (d) Li, Y.; Jiang, L.; Feng, X. L.; Lu, T. B. *Cryst. Growth Des.* **2008**, *8*, 3689. (e) Ghosh, S. K.; Bharadwaj, P. K. *Inorg.Chem.* **2005**, *44*, 5553.
150. (a) Saykally, R. J.; Wales, D. J. *Science* **2012**, *336*, 814-815 (b) Liu, K.; Cruzan, J. D.; Saykally, R. *Science* **1996**, *271*, 929 and references therein.
151. (a) Keutsch, F. N.; Saykally, R. J. *Proc. Natl. Acad. Sci. U.S.A.* **2001**, *98*, 10533. (b) Ludwig, R. *Angew. Chem. Int. Ed.* **2003**, *42*, 3458.
152. Westhoff, E. *Water and Biological Macromolecules*, CRC Press: Boca Raton, FL, **1993**.
153. Cheng, L.; Lin, J-B.; Gong, J-Z.; Sun, A-P.; Ye, B-H.; Chen, X-M. *Cryst. Growth Des*. **2006**, *12*, 2739 and references therein.
154. Beatty, A. M. *CrystEnggComm* **2001**, *3*, 243.
155. (a) Mukhopadhyay, U.; Bernal, I. *Cryst. Growth Des.* **2006**, *6*, 363. (b) Mukhopadhyay, U.; Bernal, I. *Cryst. Growth Des.* **2005**, *5*, 1687. (c) Yang, P.; Chen, Xi.; Ren, S.; Ma, S-L. *Struct. Chem.* 2008, *19*, 291. (d) H. Xu, J-L.; Z-J, Mi.; X-K, H.; Chen, Q. *Acta Crsytallogr*. **2010**, *C66*, o151.
156. (a) Luo, G-G.; Wu, D-L.; Xia, J-X.; Li, D-X.; Dai, J-C.; Xiao, Z-J. *J. Mol. Struc.* **2011**, *1005*, 172. (b) Farnum, G. A.; LaDuca, R. L. *Acta Crsytallogr*. **2008**, *E64*, m1074. (c) Kostakis, G. E.; Nordlander, E.; Tsipis, A. C.; Haukka, M.; Plakatouras, J. C. *Inorg. Chem. Comm*. 2011, **14**, 87.
157. Pal, S.; Chan, M. K.; Armstrong. W.H. *J. Am. Chem. Soc.* **1992**, *114*, 6398.
158. Jensen, K. B.; Mckenzie, C. J.; Simonsen, O.; Toftlund, H.; Hazell A. *Inorg. Chim. Acta* **1997**, *257*, 163.
159. Toftlund, H.; Ishiguro, S. *Inorg. Chem.* **1989**, *28*, 2236.
160 (a) Anderegg, G.; Wenk, F. *Helv. Chim. Acta* **1967**, *50*, 2330. (b) Anderegg, G.; Hubmann, E.; Podder, N. G.; Wenk, F. *Helv. Chim. Acta* **1977**, *60*, 123. (c) Toftlund, H.; Yde-Andersen, S. *Acta Chem. Scand.* **1981**, *A35*, 575. (d) Mandel, J. B.; Maricondi, C.; Douglas, B. E. *Inorg. Chem.***1988**, *27*, 2990. (e) Chang, H.-R.; McCusker, J. K.; Toftlund, H.; Wilson, S. R.; Trautwein, A. X.; Winkler, H.; Hendrickson, D. N. *J. Am. Chem. Soc*. **1990**, *112*, 6814. (f) Ertürk, H.; Hofmann, A.; Puchta, R.; Eldik, R. V. *Dalton Trans*. **2007**, 2295.
161. (a) Sato, A., Mori, Y.; Lida, T. Synthesis, **1992**, *6*, 539. (b) Fujihara, T.; Saito, M.; Nagasawa, A. *Acta Crystallogr.* **2004**, *E60*, o1126.
162. APEX2, SADABS, and SAINT; Bruker AXS inc: Madison, WI, USA, **2008**.
163. Sheldrick, G. M. *Acta Crystallogr.* **2008**, *A64*, 112.
164. Macrae, C. F.; Bruno, I. J.; Chisholm, J. A.; Edginton, P. R.; McCabe, P.; Pidocck, E.; Rodriguez-Monge, L.; Taylor, T.; Van de Streek, J.; Wood, P. A. *J. Appl. Crystallogr.* **2008**, *41*, 266.
165. Dolomanov, O. V.; Bourhis, L. J.; Gildea, R. J.; Howard, J. A. K.; Puschmann, H. OLEX2: A complete structure solution, refinement and analysis program, *J. Appl. Crystallogr*. **2009**, *42*, 339.
166. Farrugia, L. J. *Appl. Cryst.***1997**, *30*, 565.
167. Spek, A. L. PLATON, Version 1.62, University of Utrecht, **1999**.

168. Blatov, V. A.; Schevchenko, A. P.; Serezhkin, V. N. TOPOS 3.2 – a new version of the program for multipurpose crystal-chemical analysis, *J. Appl. Crystallogr*. **2000**, *33*, 1193.
169. Hohn, F.; Billetter, H.; Patenburg, I.; Ruschewitz, U. *Z. Naturforsch*. **2002**, *B57*, 1375.
170. Ahlers, R.; Ruschewitz, U. *Solid State Sci.* **2009**, *11*, 1058.
171. Hohn, F.; Patenburg, I.; Ruschewitz, U. *Chem.-Eur. J*. **2002**, *8*, 4536.
172. Robl, C.; Hentschel, S. *Z. Anorg. Allg. Chem*. **1990**, *591*, 188.
173. Güthner, T.; Thewalt, U. *J. Organomet. Chem.* **1988**, *350*, 235.
174. Hermann, D.; Näther, C.; Ruschewitz, R. *Solid State Sci.* **2011**, *13*, 1096.
175. Kim, J.; Chen, B.; Reineke, T. M.; Li, H.; Eddaoudi, M.; Moler, D. B.; O'Keeffe, M.; Yaghi, O. M. *J. Am. Chem. Soc*. **2001**, *123*, 8239.
176. Wang, H-Y.; Gao, S.; Huo, L-H.; Zhao, J-G. *Acta Cryst*. **2007**, *C63*, m65.
177. Wang, H-Y.; Gao, S.; Huo, L-H.; Zhao, J-G. *Acta Cryst*. **2006**, *E62*, m3281.
178. Shaoa, M.; Li, M.-X; Dai, H.; Lua, W.-C.; Ana, B.-L. *J. Mol. Struct*. **2007**, *829*, 155.
179. Desiraju, G. R. *Crystal Design: Structure and Functions (Perspectives in Supramolecular Chemistry)*. John Wiley & sons: England, **2003**.
180. Desiraju, G. R.; Vittal, J. J.; Ramanan, A. *Crystal Engineering*. World Scientific Publishing Company: Singapore, **2011**.
181. Skoulika, S.; Dallas, P.; Siskos, M. G.; Deligiannakis, Y.; Michaelides, A. *Chem. Mater*. **2003**, *15*, 4576.
182. Janiak, C. J. *J. Chem. Soc*., *Dalton* Trans. **2000**, 3885.
183. Wikstrom, J. P.; Filatov, A. S.; Mikhalyova, E. A.; Shatruk, M.; Foxmane, B.; Rybak-Akimova, E. V. *Dalton Trans.* **2010**, *39*, 2504.
184. Kühnert, J.; Rüffer, T.; Ecorchard, P.; Bräuer, B.; Lan, Y.; Powell, A. K.; Lang, H. *Dalton Trans.* **2009**, 4499.
185. (a) Arora, H.; Lloret, F.; Mukherjee, R. *Dalton Trans.* **2009**, 9759. (b) Ward, M. D.; Stephenson, A. *Dalton Trans.* **2011**, *40*, 10360.
186. Das, S.; Maloth, S.; Pal, S. *Eur. J. Inorg. Chem.* **2011**, 4270.
187. Zhang, J.; Kang, Y.; Zhang, R-B.; Li, Z-J.; Cheng, J-K.; Yao, Y-G. *CrystEngComm* **2005**, *28*, 177.
188. Biradha, K.; Seward, C.; Zaworotko, M. J. *Angew. Chem. Int. Ed.* **1999**, *38*, 492.
189. Ezuhara, T.; Endo, K.; Aoyama, Y. *J. Am. Chem. Soc.* **1999**, *121*, 3279.
190. Wang, Y. Y.; Wang, X.; Shi, Q. Z.; Gao, Y. C. *Trans.Metal Chem.* **2002**, *27*, 481.
191. (a) Chen, B. L.; Mok, K. F.; Ng, S. C.; Feng, Y. L.; Liu, S. X. *Polyhedron* **1998**, *17*, 4237. (b) Chen, B. L.; Mok, K. F.; Ng, S. C.; Drew, M. G. B. *Polyhedron* **1999**, *18*, 1211.
192. Xiao, H. P. *Acta Crystallogr*. **2005**, *E61*, m2592.
193. Yeşilel, O. Z.; İlker, İ.; Büyükgüngor, O. *Polyhedron* **2009**, 28, 3010.
194. (a) Li, D-Q.; Liu, X.; Zhou, J. *Z. Naturforsch.* **2008**, *63b*, 1343. (b) Guo, F. *J. Inorg. Organomet. Polym*. **2013**, *23*, 472. (c) Jiang, K.; Ma, L-F.; Sun, X-Y.; Wang, L-Y *CrystEnggComm* **2011**, *13*, 330.
195. Ahlers, R.; Ruschewitz, U. *Z. Anorg. Allg. Chem*. **2010**, *636*, 11.
196. Qiu, L. G.; Li, A. Q.; Wu, Y.; Wang, W.; Xu, T.; Jiang, X. *Chem. Commun*. **2008**, 3642.
197. (a) Dianu, M. L.; Kriza, A.; Musuc, A. M. *J. Therm. Anal. Calorim.* **2013**, *112*, 585. (b) Cao, L-H.; Xu, Q-Q.; Zang, S-Q.; Hou, H-W.; Mak, C. W. T. *Cryst. Growth. Des*. **2013**, *13*, 1812.
198. (a) Tan, Y.; Gao, J.; Yu, J.; Wang, Z.; Cui, Y.; Yang, Y.; Qian, G. *Dalton Trans.* **2013**, ASAP DOI: 10.1039/c3dt50991e. (b) Harak, D.; Das, S.; Lohar, S.; Banerjee, A.; Sahana, A.; Hauli, I.; Mukhopadhyay, S. K.; Safin, D. A.; Babashkina, Bolte, M.; Garciia, Y.; Das,

D. **2013**, ASAP DOI: 10.1039/c4dt50450f.
199. (a) Baldeau, S. M.; Slinn, C. H.; Krebs, B.; Rompel, A. *Inorg. Chim. Acta* **2004**, *357*, 3295. (b) Gultneh, Y.; Farooq, A.; Karlin, K. D.; Liu, S.; Zubieta, J. *Inorg. Chim. Acta* **1993**, *211*, 171.
200. *Saykally*, R. J. *Science* **1997**, *275*, 814.
201. Wang, Y.; Babin, V.; Bowman, J. M.; Paesani, F. *J. Am. Chem. Soc.* **2012**, *134*, 11116.
202. (a) Liu, K.; Brown, M. G.; Carter, C.; Saykally, R. J.; Gregory, J. K.; Clary, D. C. *Nature* **1996**, *381*, 501.(b) Nauta, K.; Miller, R. E. *Science* **2000**, *287*, 293.
203. Zheng, Y-Q.; Zheng, M-F.; *Z. Naturforsch.* **2003**, *58b*, 266.
204. Frouke, H.; Heinrich, B.; Ingo, P.; Uwe, R. *Z. Naturforsch*. **2002**, *B57*, 1375.
205. Ahlers, R.; Ruschewitz, U. *Solid State Sci.* **2009**, *11*, 1058.
206. Hohn, F.; Patenburg, I.; Ruschewitz, U. *Chem.-Eur. J*. **2002**, *8*, 4536.
207. Robl, C.; Hentschel, S. Z. *Anorg. Allg.Chem*. **1990**, *591*, 188.
208. Güthner, T.; Thewalt, U. *J. Organomet. Chem.* **1988**, *350*, 235.
209. Hermann, D.; Näther, C.; Ruschewitz, R. *Solid State Sci.* **2011**, *13*, 1096.
210. Kim, J.; Chen, B.; Reineke, T. M.; Li, H.; Eddaoudi, M.; Moler, D. B.; O'Keeffe, M.; Yaghi, O. M. *J. Am. Chem. Soc*. **2001**, *123*, 8239.
211. (a) Solans, X.; Font-Altaba, M.; Oliva, J.; Herrera, J. *Acta Crystallogr.* **1985**, *C41*, 1020. (b) Gao, B.; Liu, S.-X.;Xie, L.-H.; Yu, M.; Zhang, C.-D.; Sun, C.-Y.; Cheng, H.-Y. *J. Solid State Chem.* **2006**, *179*, 1681.
212. (a) Stein, I.; Ruschewitz, U. *Z. Anorg. Allg. Chem*. **2009**, *635*, 914. (b) Ghosal, D.; Maji, T. K.; Mostafa, G.; Lu, T.-H.; Chaudhuri, N. R. *Cryst. Growth Des.* **2003**, *3*, 9.
213. (a) Bencini, A.; Bianchi, A.; Dapporto, P.; Garcia-Espana, E.; Marcelino, V.; Micheloni, M.; Paoletti, P.; Paoli, P. *Inorg. Chem*. **1990**, *29*, 1716. (b) Naskar, S.; Mishra, D.; Chattopadhyay, S. K.; Corbella, M.; Blake, A. J. *Dalton Trans.* **2005**, 2428. (c) Karmakar, T. K.; Ghosh, B. K.; Usman, A.; Fun, H.-K.; Riviere, E.; Mallah, T.; Aromi, G.; Chandra, S. K. *Inorg. Chem.* **2005**, *44*, 2391. (d) El-Azzouzi, N.; Hueso-Urena, F.; Illan-Cabeza, N. A.; Moreno-Carretero, M. N. *Polyhedron* **2010**, *29*, 1405.
214. Hureau, C.; Blanchard, S.; Nierlich, M.; Blain, G.; Riviere, E.; Girerd, J.-J.; Anxolabehere-Mallart, E.; Blondin, G. *Inorg. Chem.* **2004**, *43*, 4415.
215. Yeşilel, O. Z.; İlker, İ.; Büyükgüngor, O. *Polyhedron* **2009**, 28, 3010.
216. (a) Bhogala, B. R.; Nangia, A. *New J. Chem.* **2008**, *32*, 800. (b) Choi, K. Y.; Kim, K. J. *Polyhedron* **2008**, *27*, 1310. (c) Zhao, X. J.; Zhu, G. S.; Fang, Q. R.; Wang, Y.; Sun, F. X.; Qiu, S. L. *Cryst. Growth Des.* **2009**, *9*, 737. (d) Lill, D. T. D.; Cahill, C. L. *Chem. Commun.* **2006**, 4946.
217. Xue, M.; Zhu, G. S.; Zhang, Y. J.; Fang, Q. R.; Hewitt, L. J.; Qiu, S. L. *Cryst. Growth Des*. **2008**, *8*, 427.
218. Su, Z.; Song, Y.; Bai, Z-S.; Fan, J.; Liu, G-X.; Sun, W. N. *CrystEngComm* **2010**, *12*, 4339.
219. (a) Calderone, P. J.; Banerjee, D.; Santulli, A. C.; Wond, S. S.; Parise, J. B. *Inorg. Chim. Acta* **2011**, 378, 109. (b) Fang, Q.; Zhu, G.; Xue, M.; Sun, J.; Sun, F.; Qiu, S. *Inorg. Chem*. **2006**, 45, 3582.

Appendix

Table A1. Crystal Structure data and Refinement parameters for **1** and **2**.

	1	**2**
Chemical formula	$C_{34}H_{34}Mn_2N_6O_{10}$	$C_{36}H_{38}Mn_2N_6O_8$
Formula Weight	796.55	792.60
Temperature (K)	296(2)	200(2)
Wavelength (Å)	0.71073	0.71073
Crystal system	Orthorhombic	Monoclinic
Space group	*Pbca*	$P2_1/c$
a (Å)	14.0881(15)	7.8454(3)
b (Å)	13.1033(14)	22.3677(8)
c (Å)	19.027(2)	9.5853(3)
α (°)	90	90
β (°)	90	93.491(2)
γ (°)	90	90
Z	4	2
Volume ($Å^3$)	3512.4(7)	1678.94(10)
Density (g/cm^3)	1.506	1.568
μ (mm^{-1})	0.785	0.817
Theta range	2.14° to 25.08°	1.82° to 25.10°
F(000)	1640	820
Reflections Collected	33457	15307
Independent reflections	3102	2974
Reflections with I >2σ(I)	2667	2081
R_{int}	0.0343	0.0849
Number of parameters	232	236
GOF on F^2	1.022	0.974
Final $R_1{}^a/wR_2{}^b$ (I >2σ(I))	0.0336/0.0930	0.0424/ 0.0931
Weighted $R_1{}^a/wR_2{}^b$ (all data)	0.0405/0.1003	0.0754/0.1076
Largest diff. peak and hole ($eÅ^{-3}$)	0.548 and -0.564	0.343 and -0.357

$^aR_1 = \Sigma||F_o| - |F_c||/\Sigma|F_o|$. $^bwR_2 = [\Sigma w(F_o^2 - F_c^2)^2/\Sigma w(F_o^2)^2]^{1/2}$, where $w = 1/[\sigma^2(F_o^2) + (aP)^2 + bP]$, $P = (F_o^2 + 2F_c^2)/3$.

Table A2. Crystal Structure data and Refinement parameters for **4**·5H_2O and its various forms.

Compound	**4**·6H_2O	**4**·5H_2O	**4**	**4**·4H_2O·CH_3OH	**4**·4H_2O
Chemical formula	$C_{40}H_{58}Mn_2N_6O_{16}$	$C_{40}H_{56}Mn_2N_6O_{15}$	$C_{40}H_{46}Mn_2N_6O_{10}$	$C_{41}H_{59}Mn_2N_6O_{15}$	$C_{40}H_{54}Mn_2N_6O_{14}$
Formula Weight	988.80	970.79	880.71	985.82	952.77
Temperature (K)	120(2)	296(2)	50(2)	120(2)	296(2)
Wavelength (Å)	0.71073	0.71073	0.71073	0.71073	0.71073
Crystal System	Monoclinic	Monoclinic	Monoclinic	Monoclinic	Monoclinic
Space Group	*P2₁/n*	*P2₁/n*	*P2₁/n*	*P2₁/n*	*P2₁/n*
a (Å)	10.1368(5)	10.2166(8)	10.106(2)	10.1634(3)	10.0763(4)
b (Å)	17.3885(9)	17.5260(13)	17.390(4)	17.4564(5)	17.5648(6)
c (Å)	13.9454(7)	14.1908(11)	13.430(4)	14.1379(4)	13.3931(5)
β (°)	109.477(2)	109.618(4)	108.619(10)	109.696(2)	106.351(2)
Z	2	2	2	2	2
V (Å^3)	2317.4(2)	2393.5(3)	2236.7(1)	2361.54(12)	2274.55(15)
Density (g/cm^3)	1.417	1.347	1.308	1.386	1.391
μ(mm^{-1})	0.619	0.597	0.623	0.606	0.625
F(000)	1036	1016	916	1034	996
Theta Range for Data Coll.	1.94° to 30.55°	2.41° to 30.05°	1.98° to 25.20°	2.33° to 27.58°	2.25° to 25.02°
Reflections Collected	29574	26330	12784	35988	21968
Independent Reflections	6108	6907	3780	5468	3980
Reflections with I >2σ(I))	4862	4797	1851	3485	2260
R_{int}	0.0259	0.0419	0.0955	0.0714	0.0779
No. of Parameters refined	325	311	271	321	301
GOF on F^2	1.060	0.913	1.027	0.811	0.800
Final R_1[a]/wR_2[b] (I >2σ(I))	0.0423/0.1240	0.0659/0.2173	0.0791/0.2139	0.0684/0.1835	0.0553/0.1776
Weighted R_1[a]/wR_2[b] (all data)	0.0625/0.1463	0.0923/0.2392	0.1695/0.2673	0.1240/0.2334	0.1207/0.2397
Largest diff. peak and hole(eÅ^{-3})	0.800 and -0.407	1.143 and -0.467	0.538 and -0.499	1.103 and -1.023	0.343 and -0.389

[a]$R_1 = \Sigma||F_o| - |F_c||/\Sigma|F_o|$. [b]$wR_2 = [\Sigma w(F_o^2 - F_c^2)^2/\Sigma w(F_o^2)^2]^{1/2}$, where $w = 1/[\sigma^2(F_o^2) + (aP)^2 + bP]$, $P = (F_o^2 + 2F_c^2)/3$.

Table A3. Crystal Structure data and Refinement parameters for **13**, **16** and **17**.

Compound	**13**	**16**	**17**
Chemical formula	$C_{20}H_{29}N_3NiO_8$	$C_{82}H_{120}N_{12}Ni_4O_{20}$	$C_{20}H_{35}N_3NiO_9$
Formula Weight	498.17	1828.74	520.22
Temperature (K)	140(2)	150(2)	150(2)
Wavelength (Å)	0.71073	0.71073	0.71073
Crystal system	Orthorhombic	Triclinic	Orthorhombic
Space group	*Pbca*	*P-1*	*P*ca2_1
a (Å)	13.9088(6)	9.1705(9)	14.5924(13)
b (Å)	17.7977(7)	14.6580(12)	9.6796(7)
c (Å)	18.4098(8)	16.5446(16)	17.2369(15)
α (°)	90	75.267(5)	90
β (°)	90	83.446(6)	90
γ (°)	90	87.661(6)	90
Z	8	1	4
Volume ($Å^3$)	4557.2(3)	2136.6(3)	2434.7(4)
Density (g/cm^3)	1.452	1.421	1.419
μ (mm^{-1})	0.902	0.945	0.85
Theta range	2.16° to 25.11°	1.28° to 25.04°	2.10° to 25.07°
F(000)	2096	968	1104
Reflections Collected	24652	16253	16398
Independent reflections	4045	7517	4255
Reflections with I >2σ(I)	2927	4976	3620
R_{int}	0.0615	0.0428	0.0535
Number of parameters	300	547	306
GOF on F^2	0.976	0.868	0.968
Final $R_1{}^a/wR_2{}^b$ (I > 2σ(I))	0.0435/0.1027	0.0533/ 0.1253	0.0371/ 0.0834
Weighted $R_1{}^a/wR_2{}^b$ (all data)	0.0716/0.1168	0.0938/0.1529	0.0488/0.0900
Largest diff. peak and hole ($eÅ^{-3}$)	0.632 and -0.618	1.136 and -0.497	0.284/-0.410

$^aR_1 = \Sigma||F_o| - |F_c||/\Sigma|F_o|$. $^bwR_2 = [\Sigma w(F_o^2 - F_c^2)^2/\Sigma w(F_o^2)^2]^{1/2}$, where $w = 1/[\sigma^2(F_o^2) + (aP)^2 + bP]$, $P = (F_o^2 + 2F_c^2)/3$.

Table A4. Crystal Structure data and Refinement parameters for **19, 20** and **21**.

	19	**20**	**21**
Chemical formula	$C_{72}H_{108}Cl_4Co_4N_{12}O_{28}$	$C_{36}H_{48}Cl_2Cu_2N_6O_{14}$	$C_{38}H_{52}Cl_2Cu_2N_6O_{16}S$
Formula Weight	1967.22	986.78	1078.9
Temperature (K)	296(2)	296(2)	296(2)
Wavelength (Å)	0.71073	0.71073	0.71073
Crystal system	Monoclinic	Monoclinic	Monoclinic
Space group	$P2_1/c$	$C2/c$	$P2_1/n$
a (Å)	15.2142(16)	19.9346(10)	12.3812(4)
b (Å)	23.348(2)	18.8069(10)	26.8191(9)
c (Å)	26.756(3)	13.6719(8)	14.3028(5)
α (°)	90	90	90
β (°)	99.380(5)	122.227(3)	96.322(2)
γ (°)	90	90	90
Z	4	4	4
Volume ($Å^3$)	9377.2(17)	4336.0(4)	4720.4(3)
Density (g/cm^3)	1.398	1.512	1.518
μ (mm^{-1})	0.887	1.175	1.132
Theta range	1.16° to 25.11°	1.86° to 25.10°	1.52° to 25.10°
F(000)	4096	2040	2232
Reflections Collected	85253	12866	32255
Independent reflections	16487	3863	8388
Reflections with I >2σ(I)	1550	2476	4788
R_{int}	0.1229	0.0555	0.0825
Number of parameters	1167	276	602
GOF on F^2	0.99	1.066	0.828
Final $R_1{}^a/wR_2{}^b$ (I > 2σ(I))	0.0743/0.1833	0.0596/0.1719	0.0510/0.1322
Weighted $R_1{}^a/wR_2{}^b$ (all data)	0.1839/0.2432	0.0966/0.2023	0.0977/ 0.1542
Largest diff. peak and hole ($eÅ^{-3}$)	0.967 and -0.897	0.917 and -0.513	0.640 and -0.446

$^aR_1 = \Sigma||F_o| - |F_c||/\Sigma|F_o|$. $^bwR_2 = [\Sigma w(F_o^2 - F_c^2)^2/\Sigma w(F_o^2)^2]^{1/2}$, where $w = 1/[\sigma^2(F_o^2) + (aP)^2 + bP]$, $P = (F_o^2 + 2F_c^2)/3$.

Table A5. Crystal Structure data and Refinement parameters for **22, 23** and **24**.

	22	**23**	**24**
Chemical formula	$C_{34}H_{30}N_6O_8Zn_2$	$C_{36}H_{38}N_6O_8Zn_2$	$C_{40}H_{50}N_6O_{10}Zn_2$
Formula Weight	781.38	813.46	905.6
Temperature (K)	296(2)	296(2)	296(2)
Wavelength (Å)	0.71073	0.71073	0.71073
Crystal system	Monoclinic	Monoclinic	Orthorhombic
Space group	$P2_1/n$	$P2_1/n$	*Pbca*
a (Å)	8.7927(7)	8.7267(7)	13.330(2)
b (Å)	13.7417(11)	14.1120(13)	13.669(3)
c (Å)	14.3185(11)	14.2172(14)	22.655(4)
α (°)	90	90	90
β (°)	99.280(5)	98.500(4)	90
γ (°)	90	90	90
Z	2	2	4
Volume ($Å^3$)	1707.4(2)	1731.6(3)	4127.9(13)
Density (g/cm^3)	1.52	1.56	1.457
μ (mm^{-1})	1.465	1.448	1.226
Theta range	2.07 to 25.04°	2.04 to 25.13°	1.80 to 25.21°
F(000)	800	840	1888
Reflections Collected	9940	19975	25380
Independent reflections	3000	3071	3652
Reflections with I >2σ(I)	1550	2474	2223
Rint	0.081	0.0511	0.0947
Number of parameters	228	236	265
GOF on F^2	0.937	1.053	1.004
Final $R_1{}^a/wR_2{}^b$ (I > 2σ(I))	0.0548/0.1153	0.0301/0.0767	0.0438/0.1055
Weighted $R_1{}^a/wR_2{}^b$ (all data)	0.1319/0.1474	0.0411/0.0825	0.0969/ 0.1276
Largest diff. peak and hole ($eÅ^{-3}$)	0.700 and -0.475	0.450 and -0.382	0.505 and -0.519

$^aR_1 = \Sigma||F_o| - |F_c||/\Sigma|F_o|$. $^bwR_2 = [\Sigma w(F_o^2 - F_c^2)^2/\Sigma w(F_o^2)^2]^{1/2}$, where $w = 1/[\sigma^2(F_o^2) + (aP)^2 + bP]$, $P = (F_o^2 + 2F_c^2)/3$.

Table A6. Crystal Structure data and Refinement parameters for **27**, **28** and **29**.

Compound	**28**	**27**	**29**
Chemical formula	$C_{40}H_{46}N_6O_{10}Cd_2$	$C_{36}H_{34}Cd_2N_6O_8$	$C_{46}H_{38}N_6O_8Cd_2$
Formula Weight	995.63	903.49	1027.65
Temperature (K)	296(2)	100(2)	296(2)
Wavelength (Å)	0.71073	0.71073	0.71073
Crystal system	Orthorhombic	Triclinic	Orthorhombic
Space group	*Pbca*	*P-1*	*Pbca*
a (Å)	14.056(5)	15.382(5)	13.1609(5)
b (Å)	13.731(4)	16.520(2)	17.9462(6)
c (Å)	22.565(8)	16.705(2)	18.4789(7)
α (°)	90	117.141(2)	90
β (°)	90	97.034(2)	90
γ (°)	90	94.560(2)	90
Z	4	4	4
Volume ($Å^3$)	4355.0(3)	3704.8(13)	4364.5(3)
Density (g/cm^3)	1.518	1.62	1.485
μ (mm^{-1})	1.037	1.206	1.034
Theta range	1.80 to 25.12°	1.35 to 25.25°	2.20 to 25.10°
F(000)	2016	1808	1976
Reflections Collected	21282	45680	27800
Independent reflections	3689	13275	3869
Reflections with I >2σ(I)	4976	11331	2833
Rint	0.0813	0.0269	0.0338
Number of parameters	265	941	280
GOF on F^2	0.931	1.113	1.033
Final R_1[a]/wR_2[b] (I > 2σ(I))	0.0477/0.1136	0.0273/0.0546	0.0273/0.0546
Weighted R_1[a]/wR_2[b] (all data)	0.0917/0.1376	0.0524/0.1139	0.0487/0.0616
Largest diff. peak and hole ($eÅ^{-3}$)	0.746 and -1.122	1.790 and -1.110	0.295 and -0.276

[a]$R_1 = \Sigma||F_o| - |F_c||/\Sigma|F_o|$. [b]$wR_2 = [\Sigma w(F_o^2 - F_c^2)^2/\Sigma w(F_o^2)^2]^{1/2}$, where $w = 1/[\sigma^2(F_o^2) + (aP)^2 + bP]$, $P = (F_o^2 + 2F_c^2)/3$.

Table A7. Crystal Structure data and Refinement parameters for **30a** and **30b**.

	30a	**30b**
Chemical formula	$C_{44}H_{38}Zn_2N_6O_{12}$	$C_{18}H_{32}O_{24}Zn_3$
Formula Weight	973.54	828.55
Temperature (K)	296(2)	296(2)
Wavelength (Å)	0.71073	0.71073
Crystal system	Monoclinic	Monoclinic
Space group	$P2_1/c$	$C2$
a (Å)	14.9718(12)	17.447(2)
b (Å)	16.1615(14)	12.9361(19)
c (Å)	17.2464(6)	6.5879(10)
α (°)	90	90
β (°)	90.007(3)	111.945(6)°
γ (°)	90	90
Z	4	2
Volume ($Å^3$)	4173.1(6)	1379.1(3)
Density (g/cm^3)	1.550	1.995
μ (mm-1)	1.223	2.695
Theta range	1.36 to 25.03°	2.02 to 25.00°
F(000)	2000	844
Reflections Collected	31163	3748
Independent reflections	7382	2030
Reflections with $I > 2\sigma(I)$	4374	1910
R_{int}	0.0749	0.0553
Number of parameters	581	213
GOF on F^2	0.947	1.036
Final $R_1{}^a/wR_2{}^b$ ($I > 2\sigma(I)$)	0.0408/0.0470	0.0408/0.1034
Weighted $R_1{}^a/wR_2{}^b$ (all data)	0.0842/0.0520	0.0453/0.1171
Largest diff. peak and hole ($eÅ^{-3}$)	0.465 and -0.627	0.560 and -0.561

$^aR_1 = \Sigma||F_o| - |F_c||/\Sigma|F_o|$. $^bwR_2 = [\Sigma w(F_o^2 - F_c^2)^2/\Sigma w(F_o^2)^2]^{1/2}$, where $w = 1/[\sigma^2(F_o^2) + (aP)^2 + bP]$, $P = (F_o^2 + 2F_c^2)/3$.

Table A8. Crystal Structure data and Refinement parameters for **31**, **32** and **33**.

	31	**32**	**33**
Chemical formula	$C_{44}H_{38}Cd_2N_6O_{12}$	$C_{60}H_{76}Cd_3N_9O_{22}$	$C_{33}H_{39.50}Cd_{1.50}N_{4.50}O_{8.50}$
Formula Weight	1067.6	1612.53	803.79
Temperature (K)	296(2)	296(2)	150(2)
Wavelength (Å)	0.71073	0.71073	0.71073
Crystal system	Monoclinic	Monoclinic	Triclinic
Space group	$P2_1/n$	Cc	$P\text{-}1$
a (Å)	9.8491(4)	15.908(4)	10.0477(6)
b (Å)	17.1925(7)	12.343(3)	14.8863(9)
c (Å)	13.2050(5)	34.607(8)	24.3386(17)
α (°)	90	90	80.434(5)°
β (°)	96.708(2)	90.922(5)	80.781(5)°
γ (°)	90	90	88.902(4)°
Z	2	8	4
Volume ($Å^3$)	2220.70(15)	6794.0(3)	3543.3(4)
Density (g/cm^3)	1.597	1.747	1.507
μ (mm^{-1})	1.026	1.323	0.964
Theta range	1.95° to 25.11°	1.18° to 25.02°	0.86° to 25.16°
F(000)	1072	3568	1636
Reflections Collected	15401	24386	33727
Independent reflections	3932	11343	12607
Reflections with I >2σ(I)	2946	7482	7158
Rint	0.0485	0.0818	0.0895
Number of parameters	291	844	867
GOF on F^2	0.955	0.933	0.922
Final R_1/wR_2 (I > 2σ(I))	0.0359/0.0726	0.0571/0.1041	0.0665/0.1474
Weighted R_1/wR_2 (all data)	0.0595/0.0818	0.1063/0.1270	0.1361/ 0.1851
Largest diff. peak and hole ($eÅ^{-3}$)	0.396 and -0.589	0.465 and -0.732	1.415 and -1.662

[a] $R_1 = \Sigma||F_o| - |F_c||/\Sigma|F_o|$. [b] $wR_2 = [\Sigma w(F_o^2 - F_c^2)^2/\Sigma w(F_o^2)^2]^{1/2}$, where $w = 1/[\sigma^2(F_o^2) + (aP)^2 + bP]$, $P = (F_o^2 + 2F_c^2)/3$.

Table A9. Crystal Structure data and Refinement parameters for **34** and **36**.

Compound	**34**	**36**
Chemical formula	$C_{44}H_{52}Mn_2N_8O_{14}$	$C_{44}H_{56}Mn_2N_8O_{14}$
Formula Weight	1022.78	1030.85
Temperature (K)	100(2)	100(2)
Wavelength (Å)	0.71073	0.71073
Crystal system	Monoclinic	Monoclinic
Space group	*C2/c*	*C2/c*
a (Å)	19.8422(6)	19.7966(15)
b (Å)	13.8805(4)	13.7795(11)
c (Å)	17.2350(5)	17.1799(13)
β (°)	101.4770(10)	101.871(3)
Z	4	4
Volume ($Å^3$)	4651.9(2)	4586.2(6)
Density (g/cm^3)	1.460	1.493
μ (mm^{-1})	0.618	0.627
Theta range	2.05° to 25.17°	2.05° to 25.14°
F(000)	2120	2152
Reflections Collected	29607	26788
Independent reflections	4060	4094
Reflections with I >2σ(I)	3725	3995
R_{int}	0.0176	0.0165
Number of parameters	323	310
GOF on F^2	0.943	0.919
Final $R_1{}^a/wR_2{}^b$ (I> 2σ(I))	0.0285/0.0745	0.0462/ 0.1167
Weighted $R_1{}^a/wR_2{}^b$(all data)	0.0324/0.0781	0.0470/0.1174
Largest diff. peak and hole ($eÅ^{-3}$)	0.405 and -0.504	1.503 and -0.955

$^aR_1 = \Sigma||F_o| - |F_c||/\Sigma|F_o|$. $^bwR_2 = [\Sigma w(F_o^2 - F_c^2)^2/\Sigma w(F_o^2)^2]^{1/2}$, where $w = 1/[\sigma^2(F_o^2) + (aP)^2 + bP]$, $P = (F_o^2 + 2F_c^2)/3$.

Table A10. Crystal Structure data and Refinement parameters for **35** and **35a**.

	35	**35a**
Chemical formula	$C_{44}H_{56}Mn_2N_8O_{16}$	$C_{44}H_{52}Mn_2N_8O_{14}$
Formula Weight	1062.85	1026.82
Temperature (K)	100(2)	100(2)
Wavelength (Å)	0.71073	0.71073
Crystal system	Monoclinic	Monoclinic
Space group	*C2/c*	*C2/c*
a (Å)	20.877(5)	20.4040(7)
b (Å)	14.366(5)	13.9860(5)
c (Å)	16.574(4)	16.8136(6)
β (°)	106.014(3)	104.8350(10)
Z	4	4
Volume ($Å^3$)	4760.1(4)	4638.2(3)
Density (g/cm^3)	1.477	1.470
μ (mm-1)	0.608	0.62
Theta range	1.74° to 25.01°	1.78° to 25.16°
F(000)	2216	2136
Reflections Collected	16298	15451
Independent reflections	4199	4104
Reflections with I >2σ(I)	3037	3783
Rint	0.0502	0.0155
Number of parameters	317	323
GOF on F^2	1.173	1.025
Final $R_1{}^a/wR_2{}^b$ (I > 2σ(I))	0.0445/0.0724	0.0331/0.0903
Weighted $R_1{}^a/wR_2{}^b$ (all data)	0.1072/0.1186	0.0363/0.0925
Largest diff. peak and hole ($eÅ^{-3}$)	0.537 and -0.563	0.322 and -0.721

$^aR_1 = \Sigma||F_o| - |F_c||/\Sigma|F_o|$. $^bwR_2 = [\Sigma w(F_o^2 - F_c^2)^2/\Sigma w(F_o^2)^2]^{1/2}$, where $w = 1/[\sigma^2(F_o^2) + (aP)^2 + bP]$, $P = (F_o^2 + 2F_c^2)/3$.

Table A11. Crystal Structure data and Refinement parameters for **40**.

	40
Chemical formula	$C_{38}H_{38}Cd_2N_8O_8$
Formula Weight	959.56
Temperature (K)	296(2)
Wavelength (Å)	0.71073
Crystal system	Orthorhombic
Space group	$P2_12_12_1$
a (Å)	8.6874(5)
b (Å)	14.9512(5)
c (Å)	15.8853(4)
β (°)	90
Z	2
Volume ($Å^3$)	2063.3(2)
Density (g/cm^3)	1.545
μ (mm^{-1})	1.089
Theta range	1.87° to 25.22°
F(000)	964
Reflections Collected	13870
Independent reflections	3658
Reflections with I >2σ(I)	3479
Rint	0.0490
Number of parameters	280
GOF on F^2	1.050
Final $R_1{}^a/wR_2{}^b$ (I > 2σ(I))	0.0262/0.0573
Weighted $R_1{}^a/wR_2{}^b$ (all data)	0.0284/0.0585
Largest diff. peak and hole ($eÅ^{-3}$)	0.237 and -0.395

$^aR_1 = \Sigma||F_o| - |F_c||/\Sigma|F_o|$. $^bwR_2 = [\Sigma w(F_o^2 - F_c^2)^2/\Sigma w(F_o^2)^2]^{1/2}$, where $w = 1/[\sigma^2(F_o^2) + (aP)^2 + bP]$, $P = (F_o^2 + 2F_c^2)/3$.

Table A12. Crystal Structure data and Refinement parameters for **41**, **43** and **44**.

Compound	**41**	**42**	**43**
Formula	$C_{38}H_{42}Mn_2N_6O_{12}$	$C_{35}H_{48}Mn_2N_6O_{17}$	$C_{64}H_{66}Cl_2Mn_2N_{14}O_{12}$
Formula Weight	884.66	934.67	1404.9
Temperature (K)	100(2)	296	296(2)
Wavelength(Å)	0.71073	0.71073	0.71073
Crystal system	Triclinic	Monoclinic	Monoclinic
Space group	*P-1*	$P2_1/n$	*C2/c*
a (Å)	10.0973(2)	9.462(3)	25.9214(13)
b (Å)	10.2304(2)	17.300(4)	12.8400(7)
c (Å)	11.0096(2)	26.001(7)	20.1694(10)
α(°)	64.9660(10)	90	90
β (°)	78.7990(10)	94.851(6)	106.22(42)
γ(°)	78.3220(10)	90	90
Z	1	4	4
Volume ($Å^3$)	1001.53(3)	4241(2)	6445.7(6)
Density (g/cm^3)	1.467	1.464	1.447
μ (mm^{-1})	0.7	0.674	0.548
Theta range for data collection	2.22° to 29.29°	1.42° to 25.17°	1.64° to 26.93°
F(000)	458	1944	2912
Reflections Collected	14226	43747	57433
Independent reflections	4882	7457	6897
Reflections with I > 2σ(I)	4529	5178	4584
R_{int}	0.0244	0.0735	0.0366
No. params refined	270	448	417
GOF on F^2	0.987	1.054	1.014
Final $R_1{}^a/wR_2{}^b$ (I >2σ(I))	0.0334/0.0918	0.0548/ 0.1425	0.0560/ 0.1670
Weighted $R_1{}^a/wR_2{}^b$ (all data)	0.0361/0.0939	0.0856/ 0.1632	0.0931/0.1941
Largest diff. peak and hole ($eÅ^{-3}$)	0.667 and -0.443	1.248 and -0.646	1.308 and -0.485

$^aR_1 = \Sigma||F_o| - |F_c||/\Sigma|F_o|$. $^bwR_2 = [\Sigma w(F_o^2 - F_c^2)^2/\Sigma w(F_o^2)^2]^{1/2}$, where $w = 1/[\sigma^2(F_o^2) + (aP)^2 + bP]$, $P = (F_o^2 + 2F_c^2)/3$.

Table A13. Crystal Structure data and Refinement parameters for **44**, **45** and **47**.

Compound	**44**	**45**	**47**
Formula	$C_{60}H_{62}Cl_2Mn_2N_{14}O_{12}$	$C_{37}H_{50}Mn_2N_6O_{16}$	$C_{39}H_{48}Mn_2N_6O_{17}$
Formula Weight	1352.02	944.71	982.71
Temperature (K)	100(2)	200(2)	220(2)
Wavelength(Å)	0.71073	0.71073	0.71073
Crystal system	Monoclinic	Monoclinic	Monoclinic
Space group	*C2/c*	*P2/c*	*$P2_1/c$*
a (Å)	25.438(3)	14.5375(9)	14.956(3)
b (Å)	12.5058(13)	8.1374(4)	16.771(2)
c (Å)	19.868(2)	19.3409(9)	18.854(3)
α(°)	90	90	90
β (°)	106.494(4)	107.310(4)	97.940(8)
γ(°)	90	90	90
Z	4	2	4
Volume ($Å^3$)	6060.4(11)	2184.4(2)	4683.8(12)
Density (g/cm^3)	1.482	1.436	1.394
μ (mm^{-1})	0.58	0.653	0.614
Theta range for data collection	1.67° to 25.02°	2.21° to 25.14°	1.37° to 25.26°
F(000)	2800	984	2040
Reflections Collected	27616	10746	31900
Independent reflections	5302	3854	8432
Reflections with $I > 2\sigma(I)$	4653	2570	4778
R_{int}	0.0226	0.0606	0.0569
No. params refined	407	308	577
GOF on F^2	1.14	0.966	1.045
Final $R_1{}^a/wR_2{}^b$ ($I > 2\sigma(I)$)	0.0303/ 0.0933	0.0462/0.0920	0.0754/ 0.2247
Weighted $R_1{}^a/wR_2{}^b$ (all data)	0.0415/0.1215	0.0853/0.1082	0.1359/0.2835
Largest diff. peak and hole ($eÅ^{-3}$)	0.881 and -0.461	0.423 and -0.423	1.328 and -0.561

$^aR_1 = \Sigma||F_o| - |F_c||/\Sigma|F_o|$. $^bwR_2 = [\Sigma w(F_o^2 - F_c^2)^2/\Sigma w(F_o^2)^2]^{1/2}$, where $w = 1/[\sigma^2(F_o^2) + (aP)^2 + bP]$, $P = (F_o^2 + 2F_c^2)/3$.

Table A14. Crystal Structure data and Refinement parameters for **49** and **50**.

	49	**50**
Chemical formula	$C_{58}H_{68}Cl_2Mn_2N_{12}O_{15}$	$C_{36}H_{52}Mn_2N_6O_{16}$
Formula Weight	1354.02	934.72
Temperature (K)	120(2)	120(2)
Wavelength (Å)	0.71073	0.71073
Crystal system	triclinic	Monoclinic
Space group	*P-1*	*C2/c*
a (Å)	9.7693(7)	23.0064(10)
b (Å)	12.7118(7)	10.4309(4)
c (Å)	13.6085(7)	19.8406(8)
α(°)	78.138(3)	90
β (°)	69.457(3)	116.227(2)
γ(°)	74.015(3)	90
Z	1	4
Volume ($Å^3$)	1510.14(14)	4271.1(3)
Density (g/cm^3)	1.489	1.454
μ (mm^{-1})	0.585	0.667
Theta range for data collection	1.61 to 24.99°	1.97° to 25.04°
F(000)	704	1952
Reflections Collected	17946	12670
Independent reflections	5202	3682
Reflections with I >2σ(I)	3575	2694
R_{int}	0.0423	0.0415
Number of parameters	421	275
S (goodness of fit) on F^2	1.019	1.134
Final $R_1{}^a/wR_2{}^b$ (I >2σ(I))	0.0656/0.1773	0.0546/0.1469
Weighted $R_1{}^a/wR_2{}^b$ (all data)	0.1058/ 0.2100	0.0907/0.1815
Largest diff. peak and hole ($eÅ^{-3}$)	1.396 and -0.922	1.142 and -0.909

$^aR_1 = \Sigma||F_o| - |F_c||/\Sigma|F_o|$. $^bwR_2 = [\Sigma w(F_o^2 - F_c^2)^2/\Sigma w(F_o^2)^2]^{1/2}$, where $w = 1/[\sigma^2(F_o^2) + (aP)^2 + bP]$, $P = (F_o^2 + 2F_c^2)/3$.

Table A15. Crystal Structure data and Refinement parameters for **51**.

Chemical formula	$C_{30}H_{40}Cl_2Mn_2N_6O_{16}$
Formula Weight	921.46
Temperature (K)	100(2)
Wavelength (Å)	0.71073
Crystal system	Triclinic
Space group	*P-1*
a (Å)	8.3014(11)
b (Å)	9.9503(13)
c (Å)	12.8079(18)
α (°)	82.745(7)
β (°)	72.761(7)
γ (°)	79.206(7)
Z	1
Volume ($Å^3$)	989.7(2)
Density (g/cm^3)	1.546
μ (mm^{-1})	0.849
Theta range	1.67 to 25.14°
F(000)	474
Reflections Collected	10673
Independent reflections	3486
Reflections with I >2σ(I)	2772
Rint	0.0272
Number of parameters	262
GOF on F^2	1.137
Final $R_1{}^a/wR_2{}^b$ (I > 2σ(I))	0.0514/0.1453
Weighted $R_1{}^a/wR_2{}^b$ (all data)	0.0748/0.1847
Largest diff. peak and hole ($eÅ^{-3}$)	1.438 and -0.781

$^aR_1 = \Sigma||F_o| - |F_c||/\Sigma|F_o|$. $^bwR_2 = [\Sigma w(F_o^2 - F_c^2)^2/\Sigma w(F_o^2)^2]^{1/2}$, where $w = 1/[\sigma^2(F_o^2) + (aP)^2 + bP]$, $P = (F_o^2 + 2F_c^2)/3$.

Table A16. Crystal Structure data and Refinement parameters for **52** and **53**.

	52	**53**
Chemical formula	$C_{29}H_{36}Cl_2MnN_6O_9$	$C_{40}H_{58}Mn_2N_6O_{19}S_2$
Formula Weight	738.48	1100.92
Temperature (K)	100(2)	150(2)
Wavelength (Å)	0.71073	0.71073
Crystal system	Monoclinic	Triclinic
Space group	*$P2_1/n$*	*P-1*
a (Å)	12.3026(5)	11.180(2)
b (Å)	15.8288(6)	21.473(4)
c (Å)	17.2714(7)	23.165(4)
α(°)	90	67.481(11)
β (°)	97.771(3)	76.494(12)
γ(°)	90	79.853(13)
Z	4	4
Volume ($Å^3$)	3332.5(2)	4971.7(16)
Density (g/cm^3)	1.472	1.471
μ (mm^{-1})	0.617	0.671
Theta range for data collection	1.75° to 22.13°	0.97 to 25.08°
F(000)	1532	2296
Reflections Collected	25485	62309
Independent reflections	4131	62309
Reflections with I >2σ(I)	2463	9552
R_{int}	0.1172	0.0861
Number of parameters	426	1258
S (goodness of fit) on F^2	1.089	0.987
Final R_1[a]/wR_2[b] (I >2σ(I))	0.0845/0.2193	0.0681/0.1531
Weighted R_1 [a]/wR_2[b] (all data)	0.1585/0.2701	0.1470/ 0.1917
Largest diff. peak and hole ($eÅ^{-3}$)	1.044 and -0.870	1.483 and -1.035

[a]$R_1 = \Sigma||F_o| - |F_c||/\Sigma|F_o|$. [b]$wR_2 = [\Sigma w(F_o^2 - F_c^2)^2/\Sigma w(F_o^2)^2]^{1/2}$, where $w = 1/[\sigma^2(F_o^2) + (aP)^2 + bP]$, $P = (F_o^2 + 2F_c^2)/3$.

Table A17. Crystal Structure data and Refinement parameters for **54**.

Chemical formula	$C_{46}H_{62}Mn_2N_6O_8$
Formula Weight	936.9
Temperature (K)	100(2)
Wavelength (Å)	0.71073
Crystal system	Monoclinic
Space group	$P2_1/c$
a (Å)	9.7447(5)
b (Å)	11.7881(6)
c (Å)	19.6768 (10)
α (°)	90
β (°)	102.47
γ (°)	90
Z	2
Volume ($Å^3$)	2206.98(19)
Density (g/cm^3)	1.41
μ (mm^{-1})	0.633
Theta range	2.03° to 25.12°
F(000)	988
Reflections Collected	13747
Independent reflections	3897
Reflections with I >2σ(I)	2017
R (int)	0.0995
Number of parameters	280
GOF on F^2	0.846
Final $R_1{}^a/wR_2{}^b$(I > 2σ(I))	0.0602/0.1398
Weighted $R_1{}^a/wR_2{}^b$ (all data)	0.1414/0.1868
Largest diff. peak and hole ($eÅ^{-3}$)	0.480 and -0.516

$^aR_1 = \Sigma||F_o| - |F_c||/\Sigma|F_o|$. $^bwR_2 = [\Sigma w(F_o^2 - F_c^2)^2/\Sigma w(F_o^2)^2]^{1/2}$, where $w = 1/[\sigma^2(F_o^2) + (aP)^2 + bP]$, $P = (F_o^2 + 2F_c^2)/3$.

Table A18. Crystal Structure data and Refinement parameters for **55**, **56** and **57**.

	55	**56**	**57**
Chemical formula	$C_{46}H_{40}Mn_2N_6O_{12}$	$C_{74}H_{84}Mn_4N_{12}O_{20}S_2$	$C_{48}H_{46}Mn_2N_6O_{14}$
Formula Weight	978.72	1745.4	1040.79
Temperature (K)	296(2)	120(2)	296(2)
Wavelength (Å)	0.71073	0.71073	0.71073
Crystal system	Monoclinic	Monoclinic	Monoclinic
Space group	$P2_1/n$	$P2_1/n$	$P2_1/n$
a (Å)	11.4661(2)	9.8526(15)	10.8632(12)
b (Å)	16.2176(4)	17.531(3)	16.2704(19)
c (Å)	11.9542(3)	22.343(3)	13.3437(15)
α (°)	90	90	90
β (°)	97.688(2)	99.809(11)	90.872(3)
γ (°)	90	90	90
Z	2	2	2
Volume ($Å^3$)	2202.93(9)	3802.8(10)	2358.2(5)
Density (g/cm^3)	1.475	1.531	1.466
μ (mm^{-1})	0.645	0.786	0.610
Theta range	2.13° to 25.03°	1.48° to 30.04°	2.25° to 28.24°
F(000)	1008	1824	1076
Reflections Collected	13325	28611	3085
Independent reflections	3891	6731	2870
Reflections with $I > 2\sigma(I)$	2369	3136	2305
R_{int}	0.0739	0.1866	0.0126
Number of parameters	299	496	330
GOF on F^2	0.985	0.960	1.053
Final $R_1{}^a/wR_2{}^b$ ($I > 2\sigma(I)$)	0.0496/ 0.1000	0.0721/0.1489	0.0480/0.1292
Weighted $R_1{}^a/wR_2{}^b$ (all data)	0.1025/ 0.1209	0.1780/0.1977	0.0628/ 0.1420
Largest diff. peak and hole ($eÅ^{-3}$)	0.286 and -0.311	0.752 and -0.708	0.525 and -0.697

$^aR_1 = \Sigma||F_o| - |F_c||/\Sigma|F_o|$. $^bwR_2 = [\Sigma w(F_o^2 - F_c^2)^2/\Sigma w(F_o^2)^2]^{1/2}$, where $w = 1/[\sigma^2(F_o^2) + (aP)^2 + bP]$, $P = (F_o^2 + 2F_c^2)/3$.

Table A19. Crystal Structure data and Refinement parameters for **58**.

	58
Chemical formula	$C_{30}H_{40}Cl_2Cu_2N_6O_{16}$
Formula Weight	938.66
Temperature (K)	296(2)
Wavelength (Å)	0.71073
Crystal system	Monoclinic
Space group	$P2_1/c$
a (Å)	11.9965(5)
b (Å)	11.9593(5)
c (Å)	14.0705(6)
β (°)	105.982(2)
Z	2
Volume ($Å^3$)	1940.67(14)
Density (g/cm^3)	1.606
μ (mm^{-1})	1.311
Theta range	2.45° to 25.18°
F(000)	964
Reflections Collected	14409
Independent reflections	3369
Reflections with I >2σ(I)	2433
Rint	0.0664
Number of parameters	257
GOF on F^2	1.134
Final $R_1{}^a/wR_2{}^b$ (I > 2σ(I))	0.0618/0.1673
Weighted $R_1{}^a/wR_2{}^b$ (all data)	0.1442/0.2313
Largest diff. peak and hole ($eÅ^{-3}$)	1.467 and -2.405

$^aR_1 = \Sigma||F_o| - |F_c||/\Sigma|F_o|$. $^bwR_2 = [\Sigma w(F_o^2 - F_c^2)^2/\Sigma w(F_o^2)^2]^{1/2}$, where $w = 1/[\sigma^2(F_o^2) + (aP)^2 + bP]$, $P = (F_o^2 + 2F_c^2)/3$.

Table A20. Crystal Structure data and Refinement parameters for **61** and **63**.

	61	**63**
Chemical formula	$C_{62}H_{84}Cl_8Cu_8N_{12}O_{48}$	$C_{32}H_{37}ClCuN_7O_6$
Formula Weight	2557.33	714.68
Temperature (K)	100(2)	296(2)
Wavelength (Å)	0.71073	0.71073
Crystal system	Monoclinic	Monoclinic
Space group	$P2_1/c$	$C2/c$
a (Å)	9.7340(6)	19.613(3)
b (Å)	24.2784(14)	9.6261(13)
c (Å)	16.6346(9)	23.675(3)
α (°)	90	85.502(6)
β (°)	93.487(3)	74.263(6)
γ (°)	90	78.455(6)
Z	2	4
Volume ($Å^3$)	3923.9(4)	4246.8(10)
Density (g/cm^3)	2.164	1.118
μ (mm^{-1})	2.519	0.62
Theta range	1.49 to 25.19°	1.81 to 25.12°
F(000)	2584	1488
Reflections Collected	36167	17246
Independent reflections	6990	3760
Reflections with I >2σ(I)	4728	2950
Rint	0.0541	0.1206
Number of parameters	524	277
GOF on F^2	0.986	1.069
Final $R_1{}^a/wR_2{}^b$ (I > 2σ(I))	0.1503/ 0.3706	0.0551/0.1585
Weighted $R_1{}^a/wR_2{}^b$ (all data)	0.1977/ 0.4055	0.0692/0.1689
Largest diff. peak and hole ($eÅ^{-3}$)	2.560 and -1.873	0.889 and -0.556

[a] $R_1 = \Sigma||F_o| - |F_c||/\Sigma|F_o|$. [b] $wR_2 = [\Sigma w(F_o^2 - F_c^2)^2/\Sigma w(F_o^2)^2]^{1/2}$, where $w = 1/[\sigma^2(F_o^2) + (aP)^2 + bP]$, $P = (F_o^2 + 2F_c^2)/3$.

Table A21. Crystal Structure Data and Refinement Parameters for **64**, **65** and **66**.

	64	**65**	**66**
Chemical formula	$C_{64}H_{85}Cl_4Cu_4N_{12}O_{30}$	$C_{66}H_{98}Cl_4Cu_4N_{12}O_{32}$	$C_{34}H_{48}Cl_2Cu_2N_6O_{16}$
Formula Weight	1906.4	1967.52	994.76
Temperature (K)	120	140(2)	120(2)
Wavelength (Å)	0.71073	0.71073	0.71073
Crystal system	Triclinic	Orthorhombic	Triclinic
Space group	*P-1*	*Pbca*	*P-1*
a (Å)	14.4578(13)	15.5935(9)	8.2523(4)
b (Å)	17.1700(15)	20.9498(13)	10.0862(5)
c (Å)	19.535(3)	24.3944(14)	13.7963(8)
α (°)	102.717(8)	90	68.986(3)
β (°)	106.671(8)	90	74.339(3)
γ (°)	107.797(5)	90	89.591(3)
Z	2	4	1
Volume ($Å^3$)	4163.7(8)	7969.2(8)	1027.01(9)
Density (g/cm^3)	1.514	1.64	1.608
μ (mm^{-1})	1.222	1.281	1.244
Theta range	1.16° to 19.11°	1.67° to 25.07°	1.65° to 23.12°
F(000)	1954	4072	514
Reflections Collected	29186	42219	27800
Independent reflections	6772	7038	3869
Reflections with I >2σ(I)	4082	3481	2188
Rint	0.0467	0.1136	0.0338
Number of parameters	684	552	280
GOF on F^2	0.918	0.841	1.148
Final $R_1{}^a/wR_2{}^b$ ($I > 2\sigma(I)$)	0.1055/ 0.2688	0.0722/0.1975	0.0501/ 0.1274
Weighted $R_1{}^a/wR_2{}^b$ (all data)	0.1579/ 0.3088	0.1702/0.2651	0.0774/ 0.1636
Largest diff. peak and hole ($eÅ^{-3}$)	1.582 and -0.748	0.809 and -0.655	0.774 and -0.692

$^aR_1 = \Sigma||F_o| - |F_c||/\Sigma|F_o|$. $^bwR_2 = [\Sigma w(F_o^2 - F_c^2)^2/\Sigma w(F_o^2)^2]^{1/2}$, where $w = 1/[\sigma^2(F_o^2) + (aP)^2 + bP]$, $P = (F_o^2 + 2F_c^2)/3$.

Table A22. Crystal Structure data and Refinement parameters for **67** and **68**.

	67	**68**
Chemical formula	$C_{32}H_{46}Cl_2Cu_2N_6O_{22}$	$C_{32}H_{36}Cl_2Cu_2N_6O_{16}$
Formula Weight	1064.73	958.65
Temperature (K)	100(2)	120(2)
Wavelength (Å)	0.71073	0.71073
Crystal system	Monoclinic	Triclinic
Space group	$P2_1/n$	*P-1*
a (Å)	10.3441(9)	8.7810(7)
b (Å)	12.8024(11)	14.3797(11)
c (Å)	14.5410(14)	15.3177(13)
α (°)	90	85.502(6)
β (°)	90.822(5)	74.263(6)
γ (°)	90	78.455(6)
Z	4	2
Volume ($Å^3$)	1925.5(3)	1823.4(3)
Density (g/cm^3)	1.836	1.746
μ (mm^{-1})	1.345	1.398
Theta range	2.12° to 25.19°	1.38° to 24.79°
F(000)	1096	980
Reflections Collected	13236	19448
Independent reflections	3436	6091
Reflections with I >2σ(I)	2433	2950
Rint	0.0467	0.1206
Number of parameters	274	505
GOF on F^2	0.909	0.993
Final $R_1{}^a/wR_2{}^b$ (I > 2σ(I))	0.0426/ 0.1131	0.0754/0.1799
Weighted $R_1{}^a/wR_2{}^b$ (all data)	0.0793/ 0.1559	0.1779/0.2426
Largest diff. peak and hole ($eÅ^{-3}$)	0.768 and -0.649	1.178 and -0.958

$^aR_1 = \Sigma||F_o| - |F_c||/\Sigma|F_o|$. $^bwR_2 = [\Sigma w(F_o^2 - F_c^2)^2/\Sigma w(F_o^2)^2]^{1/2}$, where $w = 1/[\sigma^2(F_o^2) + (aP)^2 + bP]$, $P = (F_o^2 + 2F_c^2)/3$.

Table A23. Crystal Structure data and Refinement parameters for **70** and **71**.

	70	**71**
Chemical formula	$C_{64}H_{87}Cl_4Cu_4N_{12}O_{34}$	$C_{34}H_{50}Cl_2Cu_2N_6O_{18}$
Formula Weight	1964.42	1028.78
Temperature (K)	296(2)	120(2)
Wavelength (Å)	0.71073	0.71073
Crystal system	Triclinic	Triclinic
Space group	*P-1*	*P-1*
a (Å)	13.2502(7)	8.3105(13)
b (Å)	14.1783(7)	10.6114(17)
c (Å)	21.9944(12)	13.376(2)
α (°)	82.693(3)	110.420(8)
β (°)	81.130(3)	100.886(8)
γ (°)	84.557(3)	98.534(8)
Z	4	2
Volume ($Å^3$)	4037.6(4)	1055.7(3)
Density (g/cm^3)	1.616	1.618
μ (mm^{-1})	1.266	1.216
Theta range	0.94° to 25.11°	2.04° to 25.13°
F(000)	2022	532
Reflections Collected	49468	13236
Independent reflections	14315	3671
Reflections with I >2σ(I)	6729	3452
R_{int}	0.0906	0.0175
Number of parameters	1051	292
GOF on F^2	1.007	1.191
Final $R_1{}^a/wR_2{}^b$ (I > 2σ(I))	0.0773/ 0.2256	0.0324/0.0931
Weighted $R_1{}^a/wR_2{}^b$ (all data)	0.1569/ 0.2519	0.0360/ 0.1085
Largest diff. peak and hole ($eÅ^{-3}$)	2.006 and -0.688	1.198 and -0.511

$^aR_1 = \Sigma||F_o| - |F_c||/\Sigma|F_o|$. $^bwR_2 = [\Sigma w(F_o^2 - F_c^2)^2/\Sigma w(F_o^2)^2]^{1/2}$, where $w = 1/[\sigma^2(F_o^2) + (aP)^2 + bP]$, $P = (F_o^2 + 2F_c^2)/3$.

Table A24. Crystal Structure data and Refinement parameters for **73**.

Chemical formula	$C_{46}H_{62}Mn_2N_6O_8$
Formula Weight	936.9
Temperature (K)	100(2)
Wavelength (Å)	0.71073
Crystal system	Triclinic
Space group	$P2_1/c$
a (Å)	12.376(4)
b (Å)	13.049(4)
c (Å)	13.206(4)
α (°)	95.72(2)
β (°)	101.565(19)
γ (°)	98.67(2)
Z	1
Volume ($Å^3$)	2046.9(11)
Density (g/cm^3)	1.737
μ (mm^{-1})	1.259
Theta range	1.59 to 21.02°
F(000)	1096
Reflections Collected	12292
Independent reflections	4328
Reflections with $I > 2\sigma(I)$	1791
R (int)	0.1452
Number of parameters	521
GOF on F^2	0.978
Final $R_1{}^a/wR_2{}^b(I > 2\sigma(I))$	0.1119/0.2779
Weighted $R_1{}^a/wR_2{}^b$ (all data)	0.2425/0.3539
Largest diff. peak and hole ($eÅ^{-3}$)	0.908 and -0.560

$^aR_1 = \Sigma||F_o| - |F_c||/\Sigma|F_o|$. $^bwR_2 = [\Sigma w(F_o^2 - F_c^2)^2/\Sigma w(F_o^2)^2]^{1/2}$, where $w = 1/[\sigma^2(F_o^2) + (aP)^2 + bP]$, $P = (F_o^2 + 2F_c^2)/3$.

Table A25. Crystal Structure data and Refinement parameters for **74** and **75**.

	74	**75**
Chemical formula	$C_{34}H_{43}Cl_2Cu_2N_7O_{15}$	$C_{64}H_{88}Cl_4Cu_4N_{12}O_{32}S_2$
Formula Weight	987.73	1997.54
Temperature (K)	100(2)	150(2)
Wavelength (Å)	0.71073	0.71073
Crystal system	Monoclinic	Orthorhombic
Space group	$P2_1$	*Pbca*
a (Å)	8.5695(8)	15.6239(15)
b (Å)	11.3027(10)	20.840(2)
c (Å)	21.867(2)	24.643(3)
α (°)	90	90
β (°)	92.817(6)	90
γ (°)	90	90
Z	4	4
Volume ($Å^3$)	2115.5(3)	8023.8(15)
Density (g/cm^3)	1.551	1.654
μ (mm^{-1})	1.0206	1.324
Theta range	0.93° to 25.08°	1.65° to 25.12°
F(000)	1016	3872
Reflections Collected	14302	49533
Independent reflections	6675	7143
Reflections with I >2σ(I)	5855	4471
R_{int}	0.0354	0.0943
Number of parameters	506	526
GOF on F^2	1.045	1.103
Final $R_1{}^a/wR_2{}^b$ (I > 2σ(I))	0.0596/ 0.1635	0.0971/0.2443
Weighted $R_1{}^a/wR_2{}^b$ (all data)	0.0695/ 0.1732	0.1514/0.2725
Absolute structure parameter	0.0(0)	----------
Largest diff. peak and hole ($eÅ^{-3}$)	1.389 and -0.726	2.018 and -0.889

$^aR_1 = \Sigma||F_o| - |F_c||/\Sigma|F_o|$. $^bwR_2 = [\Sigma w(F_o^2 - F_c^2)^2/\Sigma w(F_o^2)^2]^{1/2}$, where $w = 1/[\sigma^2(F_o^2) + (aP)^2 + bP]$, $P = (F_o^2 + 2F_c^2)/3$.

Table A26. Crystal Structure data and Refinement parameters for **76** and **77**.

	76	**77**
Chemical formula	$C_{36}H_{44}Cl_2Cu_2N_6O_{16}$	$C_{80}H_{70}Cl_2Cu_4F_{12}N_{12}O_{25}$
Formula Weight	1014.75	2152.54
Temperature (K)	140(2)	150(2)
Wavelength (Å)	0.71073	0.71073
Crystal system	Orthorhombic	Monoclinic
Space group	*Pbca*	*C2/c*
a (Å)	13.1456(13)	26.6132(17)
b (Å)	17.2609(16)	9.0698(7)
c (Å)	18.4873(17)	38.018(2)
α (°)	90	90
β (°)	90	102.490(4)
γ (°)	90	90
Z	4	4
Volume ($Å^3$)	4194.9(7)	8959.5(10)
Density (g/cm^3)	1.607	1.596
μ (mm^{-1})	1.220	1.103
Theta range	2.24° to 25.11°	1.10° to 19.62°
F(000)	2088	4368
Reflections Collected	20589	13982
Independent reflections	3665	3943
Reflections with I >2σ(I)	2771	2519
R_{int}	0.0583	0.0743
Number of parameters	284	571
GOF on F^2	1.016	1.040
Final $R_1{}^a/wR_2{}^b$ (I > 2σ(I))	0.0567/ 0.1665	0.0851/0.2365
Weighted $R_1{}^a/wR_2{}^b$ (all data)	0.0839/ 0.1994	0.1283/0.2816
Largest diff. peak and hole ($eÅ^{-3}$)	1.267 and -0.832	0.979 and -0.530

$^aR_1 = \Sigma||F_o| - |F_c||/\Sigma|F_o|$. $^bwR_2 = [\Sigma w(F_o^2 - F_c^2)^2/\Sigma w(F_o^2)^2]^{1/2}$, where $w = 1/[\sigma^2(F_o^2) + (aP)^2 + bP]$, $P = (F_o^2 + 2F_c^2)/3$.

Table A27. Crystal Structure data and Refinement parameters for **79** and **80**.

	79	**80**
Chemical formula	$C_{35}H_{48}Cl_3Cu_2N_6NaO_{22}$	$C_{64}H_{96}Cl_6Cu_4N_{12}Na_2O_{42}$
Formula Weight	1161.21	2314.22
Temperature (K)	296(2)	100(2)
Wavelength (Å)	0.71073	0.71073
Crystal system	Monoclinic	Monoclinic
Space group	$P2_1$	$P2_1/n$
a (Å)	11.9250(10)	12.6366(7)
b (Å)	11.8074(11)	26.9713(15)
c (Å)	18.3643(17)	14.0706(9)
α (°)	90	90
β (°)	104.881(5)	106.645(3)
γ (°)	90	90
Z	2	4
Volume ($Å^3$)	2499.0(4)	4594.7(5))
Density (g/cm^3)	1.543	1.224
μ (mm^{-1})	1.102	0.655
Theta range	1.15° to 24.86°	1.51° to 25.15°
F(000)	1192	1676
Reflections Collected	15274	44376
Independent reflections	7978	8135
Reflections with $I > 2\sigma(I)$	5732	4054
R_{int}	0.0721	0.1382
Number of parameters	579	658
GOF on F^2	1.418	1.037
Final $R_1{}^a/wR_2{}^b$ ($I > 2\sigma(I)$)	0.1423/ 0.3732	0.1031/0.2671
Weighted $R_1{}^a/wR_2{}^b$ (all data)	0.1709/ 0.3961	0.2044/0.3368
Largest diff. peak and hole ($eÅ^{-3}$)	3.500 and -1.014	2.433 and -1.753

$^aR_1 = \Sigma||F_o| - |F_c||/\Sigma|F_o|$. $^bwR_2 = [\Sigma w(F_o^2 - F_c^2)^2/\Sigma w(F_o^2)^2]^{1/2}$, where $w = 1/[\sigma^2(F_o^2) + (aP)^2 + bP]$, $P = (F_o^2 + 2F_c^2)/3$.

Table A28. Crystal Structure data and Refinement parameters for **83**, **84** and **85**.

	83	**84**	**85**
Chemical formula	$C_{68}H_{76}Cl_4Cu_4N_{12}O_{32}S_2$	$C_{68}H_{74}Cl_4Cu_4N_{12}O_{32}S_2$	$C_{70}H_{82}Cl_4Cu_4N_{12}O_{33}S_2$
Formula Weight	2033.49	2031.47	2079.56
Temperature (K)	120(2)	150(2)	170(2)
Wavelength (Å)	0.71073	0.71073	0.71073
Crystal system	Orthorhombic	Triclinic	Monoclinic
Space group	*Pbcn*	*P-1*	*P*c
a (Å)	18.0509(7)	15.352(5)	20.18978(12)
b (Å)	17.7528(7)	15.546(5)	13.6168(8)
c (Å)	24.8932(7)	19.838(6)	16.2901(10)
α (°)	90	73.309(9)	90
β (°)	90	78.299(12)	108.380(3)
γ (°)	90	63.132(9)	90
Z	4	2	2
Volume ($Å^3$)	7977.7(5)	4031.0(2)	4250.0(4)
Density (g/cm^3)	1.693	1.674	1.625
μ (mm^{-1})	1.334	1.32	1.255
Theta range for Data Collection	1.61° to 25.02°	1.08° to 22.48°	1.06° to 25.01°
F(000)	4160	2076	2132
Reflections Collected	55371	16547	36350
Independent reflections	7010	9744	12800
Reflections with I >2σ(I)	4660	4594	9967
R_{int}	0.0613	0.0948	0.0466
Number of parameters	552	1081	1117
S(goodness of fit) on F^2	1.027	1.46	1.047
Final $R_1{}^a/wR_2{}^b$ (I > 2σ(I))	0.0546/0.1255	0.0921/0.1975	0.0676/0.1737
Weighted $R_1{}^a/wR_2{}^b$ (all data)	0.0807/0.1422	0.1973/0.2525	0.0896/0.1934
Largest diff. peak and hole($eÅ^{-3}$)	1.628 and -1.430	1.262 and -0.835	1.133 and -1.214

$^aR_1 = \Sigma||F_o| - |F_c||/\Sigma|F_o|$. $^bwR_2 = [\Sigma w(F_o^2 - F_c^2)^2/\Sigma w(F_o^2)^2]^{1/2}$, where $w = 1/[\sigma^2(F_o^2) + (aP)^2 + bP]$, $P = (F_o^2 + 2F_c^2)/3$.

Table A29. Crystal Structure data and Refinement parameters for **87**.

Chemical formula	$C_{47}H_{48}Cl_2Cu_2N_8Na_2S_2O_{16}$
Formula Weight	1289.01
Temperature (K)	100(2) K
Wavelength (Å)	0.71073 Å
Crystal system	Monoclinic
Space group	*C*2/*c*
a (Å)	13.7456(14)
b (Å)	14.6877(15)
c (Å)	25.756(2)
α (°)	90
β (°)	103.864(6)
γ (°)	90
Z	2
Volume ($Å^3$)	5048.4(9)
Density (g/cm^3)	1.696
μ (mm^{-1})	1.130
Theta range	1.63° to 25.06°
F(000)	2640
Reflections Collected	23773
Independent reflections	4441
Reflections with I >2σ(I)	3046
R_{int}	0.0617
Number of parameters	327
GOF on F^2	1.033
Final $R_1{}^a/wR_2{}^b$ (I > 2σ(I))	0.0726/0.2329
Weighted $R_1{}^a/wR_2{}^b$ (all data)	0.11048/ 0.2711
Largest diff. peak and hole ($eÅ^{-3}$)	1.873 and -1.797

$^aR_1 = \Sigma||F_o| - |F_c||/\Sigma|F_o|$. $^bwR_2 = [\Sigma w(F_o^2 - F_c^2)^2/\Sigma w(F_o^2)^2]^{1/2}$, where $w = 1/[\sigma^2(F_o^2) + (aP)^2 + bP]$, $P = (F_o^2 + 2F_c^2)/3$.

Table A30. Crystal Structure data and Refinement parameters for **88** and **89**.

	88	**89**
Chemical formula	$C_{96}H_{122}Cl_6Cu_6N_{18}O_{46}$	$C_{82}H_{112}Cl_2Cu_4N_{12}O_{28}S_4$
Formula Weight	2858.12	2167.14
Temperature (K)	296(2) K	100(2)
Wavelength (Å)	0.71073 Å	0.71073
Crystal system	Monoclinic	Monoclinic
Space group	$P2_1/n$	$P2_1/c$
a (Å)	19.443(6)	15.3472(11)
b (Å)	29.656(9)	17.8799(12)
c (Å)	21.448(7)	18.3012(14)
α (°)	90	90
β (°)	98.93(2)	114.059(3)
γ (°)	90	90
Z	4	2
Volume ($Å^3$)	12217.(7)	4585.7(6)
Density (g/cm^3)	1.554	1.569
μ (mm^{-1})	1.250	1.150
Theta range	1.18° to 24.94°	1.45° to 25.11°
F(000)	5500	2252
Reflections Collected	77079	45310
Independent reflections	20943	8159
Reflections with I >2σ(I)	6750	6106
R_{int}	0.2973	0.0469
Number of parameters	1557	1093
GOF on F^2	1.088	1.041
Final $R_1{}^a/wR_2{}^b$ (I > 2σ(I))	0.1183/0.2399	0.0668/0.1579
Weighted $R_1{}^a/wR_2{}^b$ (all data)	0.3184/0.3124	0.0929/0.1749
Largest diff. peak and hole ($eÅ^{-3}$)	1.463 and -1.356	1.959 and -1.738

$^aR_1 = \Sigma||F_o| - |F_c||/\Sigma|F_o|$. $^bwR_2 = [\Sigma w(F_o^2 - F_c^2)^2/\Sigma w(F_o^2)^2]^{1/2}$, where $w = 1/[\sigma^2(F_o^2) + (aP)^2 + bP]$, $P = (F_o^2 + 2F_c^2)/3$.

Table A31. Crystal Structure data and Refinement parameters for **90**, **91** and **92**.

	90	**91**	**92**
Chemical formula	$C_{46}H_{64}ClCu_2N_6O_{26}S_4$	$C_{64}HCl_4Cu_4N_{12}O_{19}S_4$	$C_{38}H_{46}Cl_2Cu_2N_6O_{10}S_2$
Formula Weight	1407.80	1765.97	1008.91
Temperature (K)	296(2)	200(2)	100(2)
Wavelength (Å)	0.71073	0.71073	0.71073
Crystal system	Monoclinic	Triclinic	Monoclinic
Space group	*C2/c*	*P1*	$P2_1/n$
a (Å)	22.2126(12)	11.5705(3)	8.5104(8)
b (Å)	12.3607(7)	12.1052(3)	13.7212(13)
c (Å)	21.7442(12)	19.1344(7)	17.6565(16)
α (°)	90	104.978(2)	90
β (°)	98.156(2)	90.8270(10)	91.974(4)
γ (°)	90	118.1050(10)	90
Z	4	1	2
Volume ($Å^3$)	5909.8(6)	2254.34(12)	2060.6(3)
Density (g/cm^3)	1.582	1.301	1.626
μ (mm^{-1})	0.995	1.204	1.329
Theta range	1.89° to 25.03°	1.12°to 25.08°	1.88°to 25.21°
F(000)	2916	869	1040
Reflections Collected	23473	30853	14158
Independent reflections	5208	12730	3637
Reflections with I >2σ(I)	4396	12301	3311
R_{int}	0.0269	0.0185	0.0209
Number of parameters	375	1147	283
GOF on F^2	0.802	0.831	1.075
Final R_1[a]/wR_2[b] (I > 2σ(I))	0.0644/0.1872	0.0600/0.1750	0.0232/0.0602
Weighted R_1[a]/wR_2[b] (all data)	0.0742/0.2003	0.0616/ 0.1776	0.0263/0.0656
Largest diff. peak and hole ($eÅ^{-3}$)	1.168 and -0.916	2.208 and -0.920	0.390 and -0.356

[a]$R_1 = \Sigma||F_o| - |F_c||/\Sigma|F_o|$. [b]$wR_2 = [\Sigma w(F_o^2 - F_c^2)^2/\Sigma w(F_o^2)^2]^{1/2}$, where $w = 1/[\sigma^2(F_o^2) + (aP)^2 + bP]$, $P = (F_o^2 + 2F_c^2)/3$.

Table A32. Crystal Structure data and Refinement parameters for **94**.

	94
Chemical formula	$C_{28}H_{32}Cl_2Cu_2N_{12}O_8$
Formula Weight	861.39
Temperature (K)	296(2)
Wavelength (Å)	0.71073
Crystal system	Monoclinic
Space group	$P2_1/c$
a (Å)	8.8244(8)
b (Å)	12.8749(12)
c (Å)	14.8408(14)
α (°)	90
β (°)	95.067(5)
γ (°)	90
Z	2
Volume ($Å^3$)	1679.5(3)
Density (g/cm^3)	1.644
μ (mm^{-1})	1.493
Theta range	2.10° to 25.09°
F(000)	818
Reflections Collected	9240
Independent reflections	2978
Reflections with I >2σ(I)	2476
R_{int}	0.0245
Number of parameters	234
GOF on F^2	1.049
Final $R_1{}^a/wR_2{}^b$ (I > 2σ(I))	0.0406/0.1087
Weighted $R_1{}^a/wR_2{}^b$ (all data)	0.0517/0.1159
Largest diff. peak and hole ($eÅ^{-3}$)	1.113 and -0.848

$^aR_1 = \Sigma||F_o| - |F_c||/\Sigma|F_o|$. $^bwR_2 = [\Sigma w(F_o^2 - F_c^2)^2/\Sigma w(F_o^2)^2]^{1/2}$, where $w = 1/[\sigma^2(F_o^2) + (aP)^2 + bP]$, $P = (F_o^2 + 2F_c^2)/3$.

Table A33. Crystal Structure data and Refinement parameters for **95**.

Chemical formula	$C_{38}H_{44}Co_2N_6O_{10}$
Formula Weight	862.65
Temperature (K)	100(2)
Wavelength (Å)	0.71073
Crystal system	Monoclinic
Space group	$P2_1/c$
a (Å)	8.9260(4
b (Å)	12.6152(5)
c (Å)	18.9361(8)
α (°)	90
β (°)	93.818(2)°
γ (°)	90
Z	2
Volume ($Å^3$)	2127.53(16)
Density (g/cm^3)	1.347
μ (mm^{-1})	0.839
Theta range	1.94° to 25.04°
F(000)	896
Reflections Collected	18456
Independent reflections	3340
Reflections with I >2σ(I)	2433
Rint	0.0259
Number of parameters	299
GOF on F^2	1.015
Final $R_1{}^a/wR_2{}^b$ (I > 2σ(I))	0.0309/ 0.0772
Weighted $R_1{}^a/wR_2{}^b$ (all data)	0.0359/ 0.0807
Largest diff. peak and hole ($eÅ^{-3}$)	0.806 and -0.585

$^aR_1 = \Sigma||F_o| - |F_c||/\Sigma|F_o|$. $^bwR_2 = [\Sigma w(F_o^2 - F_c^2)^2/\Sigma w(F_o^2)^2]^{1/2}$, where $w = 1/[\sigma^2(F_o^2) + (aP)^2 + bP]$, $P = (F_o^2 + 2F_c^2)/3$.

Table A34. Crystal Structure data and Refinement parameters for **96** and **97**.

	96	**97**
Chemical formula	$C_{36}H_{40}N_6O_{12}Zn_2$	$C_{36}H_{38}Cd_2N_6O_{10}$
Formula Weight	879.48	939.52
Temperature (K)	296(2) K	296(2)
Wavelength (Å)	0.71073 Å	0.71073
Crystal system	Orthorhombic	Triclinic
Space group	*Pbca*	*P-1*
a (Å)	9.1960(4)	8.291(10)
b (Å)	17.9210(8	13.864(17)
c (Å)	25.8180(10)	39.91(5)
α (°)	90	96.469(12)°
β (°)	90	94.770(9)°
γ (°)	90	99.29(3)°
Z	4	4
Volume ($Å^3$)	4254.8(3)	4475.(18)
Density (g/cm^3)	1.373	1.417
μ (mm^{-1})	1.191	1.021
Theta range	1.58° to 25.08°	1.04° to 25.11°
F(000)	1816	1888
Reflections Collected	33842	46759
Independent reflections	3771	15600
Reflections with I >2σ(I)	2571	8331
Rint	0.0623	0.0839
Number of parameters	273	1093
GOF on F^2	1.013	0.924
Final $R_1{}^a/wR_2{}^b$ (I > 2σ(I))	0.0395/0.0931	0.0619/0.1761
Weighted $R_1{}^a/wR_2{}^b$ (all data)	0.0722/0.1095	0.1323/0.2239
Largest diff. peak and hole ($eÅ^{-3}$)	0.481/-0.349	1.228 and -0.903

$^aR_1 = \Sigma||F_o| - |F_c||/\Sigma|F_o|$. $^bwR_2 = [\Sigma w(F_o^2 - F_c^2)^2/\Sigma w(F_o^2)^2]^{1/2}$, where $w = 1/[\sigma^2(F_o^2) + (aP)^2 + bP]$, $P = (F_o^2 + 2F_c^2)/3$.

Table A35. Crystal Structure data and Refinement parameters for **99**.

Chemical formula	$C_{28}H_{36}Cd_2N_6O_{14}$
Formula Weight	905.43
Temperature (K)	296 (2)
Wavelength (Å)	0.71073
Crystal system	Triclinic
Space group	*P-1*
a (Å)	10.4300(8)
b (Å)	11.7840(8)
c (Å)	15.9011(12)
α (°)	108.258(4)
β (°)	105.406(4)
γ (°)	98.737(4)
Z	2
Volume ($Å^3$)	1729.3(2)
Density (g/cm^3)	1.739
μ (mm^{-1})	1.304
Theta range	1.43° to 25.14°
F(000)	908
Reflections Collected	21838
Independent reflections	6147
Reflections with I >2σ(I)	47453
R_{int}	0.0218
Number of parameters	472
GOF on F^2	1.072
Final $R_1{}^a/wR_2{}^b$ (I > 2σ(I))	0.0450/ 0.1271
Weighted $R_1{}^a/wR_2{}^b$ (all data)	0.0573/ 0.1383
Largest diff. peak and hole ($eÅ^{-3}$)	2.200 and -1.097

$^aR_1 = \Sigma||F_o| - |F_c||/\Sigma|F_o|$. $^bwR_2 = [\Sigma w(F_o^2 - F_c^2)^2/\Sigma w(F_o^2)^2]^{1/2}$, where $w = 1/[\sigma^2(F_o^2) + (aP)^2 + bP]$, $P = (F_o^2 + 2F_c^2)/3$.

Table A36. Crystal Structure Data and Refinement Parameters for **101** and **102**.

	101	**102**
Chemical formula	$C_{46}H_{42}N_8O_{18}Zn_2$	$C_{46}H_{36}N_6O_{12}Zn_2$
Formula Weight	1125.62	995.55
Temperature (K)	296(2) K	150(2)
Wavelength (Å)	0.71073 Å	0.71073
Crystal system	Triclinic	Orthorhombic
Space group	*P-1*	*Pbca*
a (Å)	12.7954(5)	14.4883(6)
b (Å)	16.5135(6)	16.5860(7)
c (Å)	18.2451(7)	17.1693(7)
α (°)	77.239(2)	90
β (°)	74.068(2)	90
γ (°)	75.709(2)	90
Z	4	4
Volume ($Å^3$)	3543.5(2)	4125.8(3)
Density (g/cm^3)	2.110	1.603
μ (mm^{-1})	1.469	1.2391
Theta range	1.18° to 25.04°	2.21° to 25.12°
F(000)	2312	2040
Reflections Collected	34972	26625
Independent reflections	12505	3662
Reflections with $I > 2\sigma(I)$	2773	2838
Rint	0.1441	0.0492
Number of parameters	1003	299
GOF on F^2	0.825	0.930
Final $R_1{}^a/wR_2{}^b$ ($I > 2\sigma(I)$)	0.0527/0.0945	0.0458/0.1173
Weighted $R_1{}^a/wR_2{}^b$ (all data)	0.2670/0.1602	0.0657/0.1345
Largest diff. peak and hole ($eÅ^{-3}$)	0.463/-0.413	1.209 and -1.354

$^aR_1 = \Sigma||F_o| - |F_c||/\Sigma|F_o|$. $^bwR_2 = [\Sigma w(F_o^2 - F_c^2)^2/\Sigma w(F_o^2)^2]^{1/2}$, where $w = 1/[\sigma^2(F_o^2) + (aP)^2 + bP]$, $P = (F_o^2 + 2F_c^2)/3$.

Table A37. Crystal Structure data and Refinement parameters for **103**.

Chemical formula	$C_{46}H_{44}Cd_2N_6O_{14}$
Formula Weight	1129.67
Temperature (K)	200(2)
Wavelength (Å)	0.71073
Crystal system	Monoclinic
Space group	$P2_1/c$
a (Å)	8.8002(2)
b (Å)	14.5184(3)
c (Å)	18.0225(3)
α (°)	90
β (°)	97.3340(10)
γ (°)	90
Z	2
Volume ($Å^3$)	2283.80(8)
Density (g/cm^3)	1.643
μ (mm^{-1})	1.006
Theta range	2.28° to 25.09°
F(000)	1140
Reflections Collected	14208
Independent reflections	4062
Reflections with I >2σ(I)	2982
Rint	0.0449
Number of parameters	327
GOF on F^2	1.007
Final $R_1{}^a/wR_2{}^b$ (I > 2σ(I))	0.0420/0.0943
Weighted $R_1{}^a/wR_2{}^b$ (all data)	0.0688/ 0.1041
Largest diff. peak and hole ($eÅ^{-3}$)	0.713 and -0.900

$^aR_1 = \Sigma||F_o| - |F_c||/\Sigma|F_o|$. $^bwR_2 = [\Sigma w(F_o^2 - F_c^2)^2/\Sigma w(F_o^2)^2]^{1/2}$, where $w = 1/[\sigma^2(F_o^2) + (aP)^2 + bP]$, $P = (F_o^2 + 2F_c^2)/3$.

Table A38. Selected bond distances and angles for **1**.

Bond distances (Å)

Mn1-O2	2.1118(16)	Mn1-O4	2.1640(14)
Mn1-O1	2.1955(16)	Mn1-N3	2.3033(18)
Mn1-N2	2.3168(19)	Mn1-N1	2.3240(18)
C2-C3$^{\#1}$	1.195(3)	C3-C2$^{\#1}$	1.195(3)

#1 -x, -y+2, -z+1

Bond angles (°)

O1-Mn1-O4	101.51(5)	O1-Mn1-N3	86.78(6)
O4-Mn1-O5	84.42(6)	O5-Mn1-N3	88.01(7)
O4-Mn1-N3	169.69(6)	O4-Mn1-N2	80.29(6)
O1-Mn1-N2	100.33(6)	N3-Mn1-N2	104.45(6)
O5-Mn1-N2	155.87(6)	O4-Mn1-N1	100.44(6)
O1-Mn1-N1	155.89(6)	N3-Mn1-N1	72.64(6)
O5-Mn1-N1	90.97(6)	C16-C15-C14	177.7(2)
N2-Mn1-N1	73.73(6)	C15-C16-C17	178.0(2)
O1-Mn1-O5	100.95(6)		

Table A39. Selected bond distances and angles for **2**.

Bond distances (Å)

Mn1-O2$^{\#1}$	2.107(2)	Mn1-O3	2.113(2)
Mn1-O1	2.142(2)	Mn1-N2	2.258(3)
Mn1-N3	2.284(3)	Mn1-N1	2.358(3)
C2-C3	1.199(4)		

#1 –x+1, -y+1, -z+2

Bond angles (°)

O2$^{\#1}$-Mn1-O3	95.64(10)	O2$^{\#1}$-Mn1-N2	95.37(10)
O3-Mn1-O1	93.24(9)	O1-Mn1-N2	88.36(9)
O3-Mn1-N2	168.31(9)	O3-Mn1-N3	87.23(9)
O2$^{\#1}$-Mn1-N3	90.88(10)	N2-Mn1-N3	88.68(9)
O1-Mn1-N3	167.21(9)	O3-Mn1-N1	93.58(9)
O2$^{\#1}$-Mn1-N1	160.95(10)	N2-Mn1-N1	74.75(9)
O1-Mn1-N1	94.29(9)	C3-C2-C1	177.3(3)
N3-Mn1-N1	72.93(9)	C2-C3-C4$^{\#2}$	176.7(4)
O2$^{\#1}$-Mn1-O1	101.78(9)		

Table A40. Selected bond distances and angles for **4**.

Bond distances (Å)

	4·6H_2O	**4**·5H_2O	**4**	**4**·4H_2O.CH_3OH	**4**·4H2O
Mn1-N2	2.2570(16)	2.265(3)	2.249(6)	2.258(4)	2.231(5)
Mn1-N3	2.2468(16)	2.255(3)	2.267(6)	2.240(4)	2.262(5)
Mn1-O1	2.1564(16)	2.167(3)	2.167(6)	2.149(4)	2.152(5)
Mn1-O2	2.1378(14)	2.138(3)	2.123(5)	2.136(3)	2.139(5)
Mn1-O5	2.1512(13)	2.150(2)[#1]	2.147(6)	2.150(3)	2.153(4)
C18ΞC19	1.190(3)[#1]	1.186(5)	1.190(9)[#]	1.192(6)	1.201(8)[#2]

-x+2, -y+2, -z+2, #1 -x+1, -y, -z, #2 -x, -y, -z

Bond angles (°)

	4·6H_2O	**4**·5H_2O	**4**	**4**·4H_2O·CH_3OH	**4**·4 H_2O
O2-Mn1-O5	95.69(6)	96.30(11)[#1]	99.4(2)	96.36(13)	102.38(17)
O5-Mn1-O1	85.38(6)	85.43(11)[#1]	85.4(2)	99.62(15)	85.73(17)
O5-Mn1-N2	172.03(6)	170.52(11)[#1]	168.2(2)	171.25(14)	165.17(19)
O2-Mn1-N3	91.98(6)	91.91(12)	90.4(2)	92.21(14)	90.65(19)
O1-Mn1-N3	165.67(6)	166.29(12)	172.5(2)	165.22(14)	174.49(19)
O2-Mn1-N1	152.40(6)	151.92(11)	156.3(2)	152.38(14)	156.93(18)
O1-Mn1-N1	100.09(6)	99.89(12)	101.9(2)	98.76(15)	103.72(19)
N3-Mn1-N1	73.59(6)	73.23(10)	72.4(2)	73.69(14)	72.53(18)
O2-Mn1-O1	98.72(6)	98.99(13)	96.4(2)	99.62(15)	94.0(2)
O2-Mn1-N2	87.15(6)	87.78(11)	91.6(2)	87.21(13)	91.54(19)
O1-Mn1-N2	86.83(6)	85.48(11)	89.1(2)	86.13(13)	88.25(18)
O5-Mn1-N3	84.08(5)	85.13(11)[#1]	90.5(2)	84.49(13)	90.43(19)
N2-Mn1-N3	103.29(6)	103.33(11)	93.8(2)	103.40(14)	94.53(19)
O5-Mn1-N1	105.78(5)	105.75(10)[#1]	97.01(19)	105.50(13)	93.62(17)
N2-Mn1-N1	73.95(6)	73.24(10)	73.9(2)	73.66(13)	74.67(18)
C19-C18-C17	176.2(2)[#1]	177.1(4)	177.5(8)[#]	177.0(5)	177.6(8)[#2]
C18-C19-C20	175.8(2)[#1]	177.2(4)	176.4(7)[#]	176.2(5)	178.5(7)[#2]

-x+2, -y+2, -z+2, #1 –x+1, -y, -z, #2 –x, -y, -z

Table A41. Selected bond distances and angles for **13** and **17**.

Bond distances (Å)

	13	**17**
Ni1-N1	2.257(3)	2.230(3)
Ni1-N2	2.055(3)	2.070(3)
Ni1-N3	2.064(3)	2.074(3)
Ni1-O1	2.083(2)	2.055(2)
Ni1-O2	2.092(2)	2.110(3)
Ni1-O3	2.080(2)	2.054(2)

Bond angles (°)

	13	**17**
N2-Ni1-N3	95.24(11)	96.26(11)
N3-Ni1-O3	177.96(11)	175.84(11)
N3-Ni1-O1	89.65(10)	87.58(11)
N2-Ni1-O2	91.43(10)	95.76(11)
O3-Ni1-O2	88.37(9)	90.35(10)
N2-Ni1-N1	78.18(11)	80.29(11)
O3-Ni1-N1	97.29(10)	100.59(10)
O2-Ni1-N1	167.66(10)	168.15(10)
N2-Ni1-O3	85.38(10)	87.76(11)
N2-Ni1-O1	175.08(10)	173.38(11)
O3-Ni1-O1	89.75(9)	88.32(10)
N3-Ni1-O2	93.55(10)	90.30(11)
O1-Ni1-O2	87.69(9)	89.59(10)
N3-Ni1-N1	80.95(11)	79.11(11)
O1-Ni1-N1	103.22(10)	95.21(10)

Table A42. Selected bond distances and angles for **16**.

Bond distances (Å)

Ni1-N4	2.054(4)	Ni1-O1	2.072(4)
Ni1-N6	2.087(5)	Ni2-O2	2.052(3)
Ni1-N5	2.264(5)	Ni2-O3	2.097(4)
Ni2-N1	2.061(4)	Ni2-O4	2.047(4)
Ni2-N2	2.206(5)	Ni1-O6	2.038(4)
Ni2-N3	2.078(5)	Ni1-O7	2.099(3)

Bond angles (°)

O6-Ni1-N4	89.43(15)	O6-Ni1-O1	88.68(15)
N4-Ni1-O1	175.70(16)	O6-Ni1-N6	176.07(15)
N4-Ni1-N6	94.18(17)	O1-Ni1-N6	87.61(16)
O6-Ni1-O7	91.77(14)	N4-Ni1-O7	92.96(15)
O1-Ni1-O7	90.96(14)	N6-Ni1-O7	89.60(16)
O6-Ni1-N5	100.87(15)	N4-Ni1-N5	79.49(16)
O1-Ni1-N5	97.07(15)	N6-Ni1-N5	78.31(17)
O7-Ni1-N5	165.14(15)	O4-Ni2-O2	89.02(14)
O4-Ni2-N1	85.97(15)	O2-Ni2-N1	171.80(16)
O4-Ni2-N3	175.33(15)	O2-Ni2-N3	86.31(16)
N1-Ni2-N3	98.66(17)	O4-Ni2-O3	90.05(14)
O2-Ni2-O3	91.79(14)	N1-Ni2-O3	94.70(16)
N3-Ni2-O3	90.14(16)	O4-Ni2-N2	101.52(15)
O2-Ni2-N2	94.25(15)	N1-Ni2-N2	80.42(17)
N3-Ni2-N2	78.82(17)	O3-Ni2-N2	167.02(15)

Table A43. Selected bond distances and angles for **19**.

Bond distances (Å)

Molecule 1		Molecule 2	
Co1-O1	2.107(5)	Co3-O13	2.124(5)
Co1-O7	2.121(5)	Co3-O15	2.119(5)
Co1-O8	2.121(5)	Co3-O16	2.093(5)
Co1-N1	2.126(6)	Co3-N10	2.241(6)
Co1-N2	2.240(6)	Co3-N11	2.114(6)
Co1-N3	2.111(6)	Co3-N12	2.088(6)
Co2-O3	2.091(5)	Co4-O9	2.119(5)
Co2-O5	2.183(5)	Co4-O10	2.148(6)
Co2-O6	2.079(6)	Co4-O11	2.104(5)
Co2-N4	2.129(6)	Co4-N7	2.098(6)
Co2-N5	2.270(6)	Co4-N8	2.248(6)
Co2-N6	2.105(6)	Co4-N9	2.113(7)
C18-C19	1.173(9)	C54-C55	1.185(9)

Bond angles (°)

Molecule 1				Molecule 2			
O1-Co1-N3	174.7(2)	O1-Co1-O7	92.01(19)	N12-Co3-O16	91.8(2)	N12-Co3-N11	97.2(2)
N3-Co1-O7	92.0(2)	O1-Co1-O8	88.91(19)	O16-Co3-N11	89.4(2)	N12-Co3-O15	175.6(2)
N3-Co1-O8	87.6(2)	O7-Co1-O8	88.2(2)	O16-Co3-O15	91.2(2)	N11-Co3-O15	86.1(2)
O1-Co1-N1	83.8(2)	N3-Co1-N1	99.7(2)	N12-Co3-O13	91.0(2)	O16-Co3-O13	89.62(18)
O7-Co1-N1	90.6(2)	O8-Co1-N1	172.6(2)	N11-Co3-O13	171.7(2)	O15-Co3-O13	85.7(2)
O1-Co1-N2	98.5(2)	N3-Co1-N2	78.5(2)	N12-Co3-N10	79.6(2)	O16-Co3-N10	163.03(19)
O7-Co1-N2	162.8(2)	O8-Co1-N2	105.4(2)	N11-Co3-N10	77.3(2)	O15-Co3-N10	98.3(2)
N1-Co1-N2	77.2(2)	O6-Co2-O3	88.0(2)	O13-Co3-N10	105.01(19)	N7-Co4-O11	173.6(2)
O6-Co2-N6	88.7(3)	O3-Co2-N6	172.3(2)	N7-Co4-N9	98.8(2)	O11-Co4-N9	87.7(2)
O6-Co2-N4	170.6(2)	O3-Co2-N4	82.9(2)	N7-Co4-O9	90.1(2)	O11-Co4-O9	89.3(2)
N6-Co2-N4	100.7(2)	O6-Co2-O5	88.4(2)	N9-Co4-O9	97.1(3)	N7-Co4-O10	87.5(2)
O3-Co2-O5	93.6(2)	N6-Co2-O5	93.3(2)	O11-Co4-O10	86.1(2)	N9-Co4-O10	171.6(2)
N4-Co2-O5	89.8(2)	O6-Co2-N5	107.6(2)	O9-Co4-O10	88.5(3)	N7-Co4-N8	77.5(2)
O3-Co2-N5	96.6(2)	N6-Co2-N5	77.7(2)	O11-Co4-N8	103.69(19)	N9-Co4-N8	79.5(2)
N4-Co2-N5	75.9(2)	O5-Co2-N5	161.2(2)	O9-Co4-N8	166.3(2)	O10-Co4-N8	96.6(3)
C19-C18-C17	179.4(8)	C18-C19-C20	177.6(8)	C54-C55-C56	177.5(8)	C55-C54-C53	176.8(9)

Table A44. Selected bond distances and angles for **20**.

Bond distances (Å)

Cu1-N1	1.969(5)
Cu1-N2	1.957(5)
Cu1-N3	2.065(4)
Cu1-O1	2.492(4)
Cu1-O2	1.944(4)

Bond angles (°)

O2-Cu1-N2	94.32(17)	O2-Cu1-N1	97.21(18)
N2-Cu1-N1	165.69(19)	O2-Cu1-N3	170.12(16)
N2-Cu1-N3	84.94(17)	N1-Cu1-N3	85.13(17)
O2-Cu1-O1	102.77(17)	N2-Cu1-O1	83.47(16)
N1-Cu1-O1	85.73(16)	N3-Cu1-O1	86.96(16)

Table A45. Selected bond distances and angles for **21**.

Bond distances (Å)

Cu1-O1	1.939(3)	Cu2-N4	1.977(4)
Cu2-O3	1.942(3)	Cu2-N5	2.060(4)
Cu1-N1	1.951(4)	Cu2-N6	1.971(4)
Cu1-N2	2.052(4)	Cu2-O5	2.359(4)
Cu1-N3	1.961(4)		

Bond angles (°)

O1-Cu1-N1	98.24(16)	O1-Cu1-N3	94.24(16)
N1-Cu1-N3	163.44(17)	O1-Cu1-N2	169.20(16)
N1-Cu1-N2	84.99(16)	N3-Cu1-N2	84.75(16)
O3-Cu2-N6	96.38(17)	O3-Cu2-N4	96.49(15)
N6-Cu2-N4	166.54(17)	O3-Cu2-N5	169.38(16)
N6-Cu2-N5	83.95(17)	N4-Cu2-N5	84.14(15)
O3-Cu2-O5	92.78(16)	N6-Cu2-O5	89.92(15)
N4-Cu2-O5	85.52(15)	N5-Cu2-O5	97.83(15)

Table A46. Selected bond distances and angles for **22**, **23** and **24**.

Bond distances (Å)

22		**23**		**24**	
Zn1-N1	2.122(5)	Zn1-N1	2.0936(18)	Zn1-N1	2.028(3)
Zn1-N2	2.206(5)	Zn1-N2	2.241(2)	Zn1-N2	2.440(3)
Zn1-N3	2.100(5)	Zn1-N3	2.1248(19)	Zn1-N3	2.055(3)
Zn1-O2	2.013(4)	Zn1-O1	2.0315(16)	Zn1-O1	1.986(3)
Zn1-O5	1.974(4)	Zn1-O3	1.9833(16)	Zn1-O4	2.083(3)
C18-C18$^{\#2}$	1.177(11)	C16-C16$^{\#1}$	1.188(5)	C2-C3	1.187(5)
C22-C22$^{\#1}$	1.175(11)	C18-C18$^{\#2}$	1.192(4)		
#1	-x+1, -y+1, -z+1	#1	-x, -y, -z+1		
#2	-x+2, -y, -z+1	#2	-x+1, -y+1, -z+1		

Bond angles (°)

22		**23**		**24**	
O5-Zn1-O2	108.22(19)	O3-Zn1-O1	108.46(8)	O1-Zn1-N1	134.12(13)
O2-Zn1-N3	97.34(18)	O1-Zn1-N1	96.57(7)	N1-Zn1-N3	116.96(13)
O2-Zn1-N1	96.9(2)	O1-Zn1-N3	96.09(7)	N1-Zn1-O4	96.52(11)
O5-Zn1-N2	109.2(2)	O3-Zn1-N2	114.34(7)	O1-Zn1-N2	101.71(11)
N3-Zn1-N2	77.2(2)	N1-Zn1-N2	78.12(7)	N3-Zn1-N2	76.15(12)
O5-Zn1-N3	108.3(2)	O3-Zn1-N1	108.93(7)	O1-Zn1-N3	106.88(13)
O5-Zn1-N1	89.4(2)	O3-Zn1-N3	88.90(7)	O1-Zn1-O4	90.77(11)
N3-Zn1-N1	152.4(2)	N1-Zn1-N3	153.47(8)	N3-Zn1-O4	96.99(12)
O2-Zn1-N2	142.0(2)	O1-Zn1-N2	136.27(7)	N1-Zn1-N2	77.39(12)
N1-Zn1-N2	77.0(2)	N3-Zn1-N2	76.61(7)	O4-Zn1-N2	167.03(10)

Table A47. Selected bond distances and angles for **27**.

Bond distances (Å)

Cd1-O1	2.462(5)	Cd2-O3$^{\#1}$	2.603(8)	Cd3-O10	2.241(4)	Cd4-O11$^{\#2}$	2.427(5)
Cd1-O2	2.394(4)	Cd2-O4$^{\#1}$	2.309(6)	Cd3-O13	2.212(4)	Cd4-O12$^{\#2}$	2.405(4)
Cd1-O5	2.268(4)	Cd2-O7	2.541(5)	Cd3-N7	2.325(4)	Cd4-O15	2.315(5)
Cd1-O6	2.616(4)	Cd2-O8	2.255(6)	Cd3-N8	2.383(5)	Cd4-O16	2.477(5)
Cd1-N1	2.413(5)	Cd2-N4	2.332(6)	Cd3-N9	2.298(4)	Cd4-N10	2.296(4)
Cd1-N2	2.337(5)	Cd2-N5	2.425(5)	C56-C57	1.196(8)	Cd4-N11	2.465(5)
Cd1-N3	2.323(4)	Cd2-N6	2.290(5)			Cd4-N12	2.333(5)
C20-C21	1.178(8)						

Bond angles (°)

O5-Cd1-N3	111.14(18)	O5-Cd1-N2	91.32(18)
N3-Cd1-N2	144.37(17)	O5-Cd1-O2	85.36(16)
N3-Cd1-O2	82.69(17)	N2-Cd1-O2	127.95(17)
O5-Cd1-N1	136.06(16)	N3-Cd1-N1	72.99(17)
N2-Cd1-N1	71.70(17)	O2-Cd1-N1	137.16(17)
O5-Cd1-O1	116.89(19)	N3-Cd1-O1	107.64(18)
N2-Cd1-O1	84.24(17)	O2-Cd1-O1	52.74(16)
N1-Cd1-O1	101.76(18)	O5-Cd1-O6	52.76(14)
N3-Cd1-O6	87.91(15)	N2-Cd1-O6	84.25(15)
O2-Cd1-O6	129.80(15)	N1-Cd1-O6	84.71(15)
O1-Cd1-O6	164.27(18)	O5-Cd1-C15	102.09(16)
N3-Cd1-C15	95.64(17)	N2-Cd1-C15	106.61(18)
O2-Cd1-C15	26.50(16)	N1-Cd1-C15	121.40(17)
O1-Cd1-C15	26.24(16)	O6-Cd1-C15	153.57(15)
O8-Cd2-N6	106.9(3)	O8-Cd2-O4$^{\#1}$	118.4(3)
N6-Cd2-O4$^{\#1}$	105.0(3)	O8-Cd2-N4	97.3(3)
N6-Cd2-N4	144.96(19)	O4$^{\#1}$-Cd2-N4	84.2(2)
O8-Cd2-N5	140.69(19)	N6-Cd2-N5	73.57(16)
O4$^{\#1}$-Cd2-N5	98.3(2)	N4-Cd2-N5	71.66(19)
O8-Cd2-O7	51.44(19)	N6-Cd2-O7	89.66(17)
O4$^{\#1}$-Cd2-O7	164.7(3)	N4-Cd2-O7	85.99(19)
N5-Cd2-O7	89.60(16)	O8-Cd2-O3$^{\#1}$	76.5(2)
N6-Cd2-O3$^{\#1}$	97.3(3)	O4$^{\#1}$-Cd2-O3$^{\#1}$	48.2(2)
N4-Cd2-O3$^{\#1}$	112.9(3)	N5-Cd2-O3$^{\#1}$	142.8(2)
O7-Cd2-O3$^{\#1}$	126.98(19)	O8-Cd2-C22	25.7(2)
N6-Cd2-C22	98.90(19)	O4$^{\#1}$-Cd2-C22	143.2(3)

N4-Cd2-C22	92.0(2)	N5-Cd2-C22	115.22(19)
O7-Cd2-C22	25.74(17)	O3$^{\#1}$-Cd2-C22	101.7(2)
O13-Cd3-O10	109.74(18)	O13-Cd3-N9	108.98(17)
O10-Cd3-N9	105.82(17)	O13-Cd3-N7	89.22(16)
O10-Cd3-N7	93.64(17)	N9-Cd3-N7	146.22(16)
O13-Cd3-N8	110.26(18)	O10-Cd3-N8	137.56(16)
N9-Cd3-N8	73.63(15)	N7-Cd3-N8	73.40(16)
N10-Cd4-O15	128.18(18)	N10-Cd4-N12	142.78(18)
O15-Cd4-N12	83.2(2)	N10-Cd4-O12$^{\#2}$	92.07(17)
O15-Cd4-O12$^{\#2}$	119.06(19)	N12-Cd4-O12$^{\#2}$	87.10(17)
N10-Cd4-O11$^{\#2}$	87.25(19)	O15-Cd4-O11$^{\#2}$	81.40(19)
N12-Cd4-O11$^{\#2}$	120.7(2)	O12$^{\#2}$-Cd4-O11$^{\#2}$	53.70(17)
N10-Cd4-N11	72.50(16)	O15-Cd4-N11	136.97(19)
N12-Cd4-N11	70.42(17)	O12$^{\#2}$-Cd4-N11	93.52(17)
O11$^{\#2}$-Cd4-N11	141.29(15)	N10-Cd4-O16	84.95(17)
O15-Cd4-O16	52.54(17)	N12-Cd4-O16	105.8(2)
O12$^{\#2}$-Cd4-O16	162.3(2)	O11$^{\#2}$-Cd4-O16	108.6(2)
N11-Cd4-O16	102.17(18)		

#1 x, y, z+1, #2 x, y-1, z

Table A48. Selected bond distances and angles for **28**.

Bond distances (Å)

Cd1-O1	2.260(3)	Cd1-N1	2.513(4)
Cd1-O3	2.308(3)	Cd1-N2	2.248(4)
Cd1-O4	2.486(3)	Cd1-N3	2.267(4)
C18-C19	1.176(6)		

Bond angles (°)

N2-Cd1-O1	97.72(14)	N2-Cd1-N3	110.74(15)
O1-Cd1-N3	94.27(14)	N2-Cd1-O3	147.73(14)
O1-Cd1-O3	86.93(12)	N3-Cd1-O3	100.66(14)
N2-Cd1-O4	93.78(14)	O1-Cd1-O4	87.46(12)
N3-Cd1-O4	154.90(14)	O3-Cd1-O4	54.37(13)
N2-Cd1-N1	74.17(14)	O1-Cd1-N1	160.70(12)
N3-Cd1-N1	73.11(14)	O3-Cd1-N1	109.40(12)
C19-C18-C17	175.2(6)	C18-C19-C20$^{\#1}$	176.7(6)
#1	-x+5/2, y-1/2, z		

Table A49. Selected bond distances and angles for **29**.

Bond distances (Å)

Cd1-N1	2.348(3)	Cd1-O2	2.250(2)
Cd1-N2	2.293(2)	Cd1-O4	2.486(2)
Cd1-N3	2.449(2)	Cd1-O5	2.292(2)
C17-C19	1.184(4)		

Bond angles (°)

O2-Cd1-O5	89.96(9)	O2-Cd1-N2	98.20(9)
O5-Cd1-N2	156.32(9)	O2-Cd1-N1	83.73(10)
O5-Cd1-N1	90.72(9)	N2-Cd1-N1	112.17(9)
O2-Cd1-N3	146.75(9)	O5-Cd1-N3	111.31(8)
N2-Cd1-N3	72.72(8)	N1-Cd1-N3	71.23(8)
O2-Cd1-O4	124.21(9)	O5-Cd1-O4	54.39(8)
N2-Cd1-O4	103.47(8)	N1-Cd1-O4	130.70(9)
N3-Cd1-O4	88.99(7)	O2-Cd1-C18	107.10(9)
C17-C19-C18	174.5(3)		

Table A50. Selected bond distances and angles for **30a**.

Bond distances (Å)

Zn1-O1	1.9959(17)	Zn2-O5	1.9559(18)
Zn1-O7	1.9776(18)	Zn2-O11	2.0046(17)
Zn1-N4	2.078(2)	Zn2-N1	2.293(2)
Zn1-N5	2.295(2)	Zn2-N2	2.093(2)
Zn1-N6	2.067(2)	Zn2-N3	2.086(2)

Bond angles (°)

O7-Zn1-O1	101.58(8)	O7-Zn1-N6	106.39(9)
O1-Zn1-N6	102.10(9)	O7-Zn1-N4	132.40(9)
O1-Zn1-N4	90.53(9)	N6-Zn1-N4	115.80(9)
O7-Zn1-N5	92.37(8)	O1-Zn1-N5	165.13(8)
N6-Zn1-N5	78.51(10)	N4-Zn1-N5	76.11(9)
O5-Zn2-O11	106.47(8)	O5-Zn2-N3	124.75(8)
O11-Zn2-N3	89.92(9)	O5-Zn2-N2	106.69(9)
O11-Zn2-N2	103.18(9)	N3-Zn2-N2	120.53(9)
O5-Zn2-N1	90.99(8)	O11-Zn2-N1	161.74(8)
N3-Zn2-N1	75.42(10)	N2-Zn2-N1	76.02(9)

Table A51. Selected bond distances and angles for **30b**.

Bond distances (Å)

Zn1-O1	2.032(5)	Zn1-O8	2.052(5)
Zn1-O5	2.107(5)	Zn1-O6	2.111(5)
Zn1-O7	2.148(5)	Zn1-O4	2.165(5)
Zn2-O12	2.004(6)	Zn2-O12$^{\#1}$	2.004(6)
Zn2-O11$^{\#1}$	2.143(5)	Zn2-O11	2.143(5)
Zn2-O10	2.160(6)	Zn2-O10$^{\#1}$	2.160(6)

Bond angles (°)

O1-Zn1-O8	173.9(2)	O1-Zn1-O5	91.1(2)
O8-Zn1-O5	85.5(2)	O1-Zn1-O6	90.6(2)
O8-Zn1-O6	93.2(2)	O5-Zn1-O6	175.6(2)
O1-Zn1-O7	94.8(2)	O8-Zn1-O7	90.0(2)
O5-Zn1-O7	87.5(2)	O6-Zn1-O7	88.3(2)

O1-Zn1-O4	86.6(2)	O8-Zn1-O4	88.4(2)
O5-Zn1-O4	90.7(2)	O6-Zn1-O4	93.5(2)
O7-Zn1-O4	177.6(2)	O12-Zn2-O12$^{\#1}$	103.5(5)
O12-Zn2-O11$^{\#1}$	93.3(2)	O12$^{\#1}$-Zn2-O11$^{\#1}$	84.8(2)
O12-Zn2-O11	84.8(2)	O12$^{\#1}$-Zn2-O11	93.3(2)
O11$^{\#1}$-Zn2-O11	176.9(4)	O12-Zn2-O10	156.2(3)
O12$^{\#1}$-Zn2-O10	98.9(3)	O11$^{\#1}$-Zn2-O10	96.6(2)
O11-Zn2-O10	86.1(2)	O12-Zn2-O10$^{\#1}$	98.9(3)
O12$^{\#1}$-Zn2-O10$^{\#1}$	156.2(3)	O11$^{\#1}$-Zn2-O10$^{\#1}$	86.1(2)
O11-Zn2-O10$^{\#1}$	96.6(2)	O10-Zn2-O10$^{\#1}$	60.4(3)

#1 –x, y, -z

Table A52. Selected bond distances and angles for **31**.

Bond distances (Å)

Cd1-O1	2.344(3)	Cd1-N2	2.337(4)
Cd1-O2	2.287(3)	Cd1-N3	2.383(3)
Cd1-O5	2.574(3)	Cd1-N4	2.367(4)
Cd1-O6	2.418(3)		

Bond Angles (°)

O2-Cd1-N2	116.87(12)	O2-Cd1-O1	125.06(11)
N2-Cd1-O1	96.50(12)	O2-Cd1-N4	92.71(13)
N2-Cd1-N4	141.69(13)	O1-Cd1-N4	83.95(12)
O2-Cd1-N3	129.01(11)	N2-Cd1-N3	70.40(12)
O1-Cd1-N3	101.99(11)	N4-Cd1-N3	72.06(12)
O2-Cd1-O6	79.97(10)	N2-Cd1-O6	92.27(12)
O1-Cd1-O6	54.97(10)	N4-Cd1-O6	117.81(12)
N3-Cd1-O6	150.39(11)	O2-Cd1-O5	52.98(10)
N2-Cd1-O5	80.84(12)	O1-Cd1-O5	174.33(12)
N4-Cd1-O5	101.25(13)	N3-Cd1-O5	81.90(11)
O6-Cd1-O5	119.93(11)		

Table A53. Selected bond distances and angles for **32**.

Bond distances (Å)

Cd2-O8	2.266(7)	Cd2-N9	2.314(10)
Cd2-N10	2.315(10)	Cd2-O30	2.412(8)
Cd2-O26	2.421(8)	Cd2-N12	2.427(8)
Cd2-O7	2.608(8)	Cd3-O4	2.212(7)
Cd3-N11	2.327(11)	Cd3-N6	2.330(10)
Cd3-O10	2.380(8)	Cd3-N7	2.436(10)
Cd3-O24	2.478(8)	Cd3-C81	2.751(10)
Cd4-O1	2.283(7)	Cd4-N13	2.338(10)
Cd4-N3	2.341(9)	Cd4-O31	2.362(8)
Cd4-N4	2.423(10)	Cd4-O28	2.468(7)
Cd4-O22	2.638(7)		

Bond angles (°)

N1-Cd1-O4$^{\#1}$	104.3(2)	N1-Cd1-N3	142.7(3)
O4$^{\#1}$-Cd1-N3	86.8(2)	N1-Cd1-O2	85.2(2)
O4$^{\#1}$-Cd1-O2	126.2(2)	N3-Cd1-O2	116.9(2)
N1-Cd1-O1	132.2(2)	O4$^{\#1}$-Cd1-O1	84.1(2)
N3-Cd1-O1	83.6(2)	O2-Cd1-O1	54.9(2)
N1-Cd1-N2	72.3(3)	O4$^{\#1}$-Cd1-N2	129.0(2)
N3-Cd1-N2	73.1(3)	O2-Cd1-N2	104.6(2)
O1-Cd1-N2	136.8(2)	O8-Cd2-O6	97.1(2)
O8-Cd2-N6	81.8(2)	O6-Cd2-N6	87.2(2)
O8-Cd2-N4	169.7(2)	O6-Cd2-N4	90.7(3)
N6-Cd2-N4	105.3(2)	O8-Cd2-O7	87.10(19)
O6-Cd2-O7	88.1(2)	N6-Cd2-O7	167.4(2)
N4-Cd2-O7	86.4(2)	O8-Cd2-N5	102.8(2)
O6-Cd2-N5	149.7(2)	N6-Cd2-N5	73.4(3)
N4-Cd2-N5	72.9(3)	O7-Cd2-N5	115.3(2)
N7-Cd3-O12	96.3(2)	N7-Cd3-O13	104.1(3)
O12-Cd3-O13	126.6(2)	N7-Cd3-N9	144.5(3)
O12-Cd3-N9	90.3(2)	O13-Cd3-N9	99.6(3)
N7-Cd3-N8	74.6(3)	O12-Cd3-N8	126.5(2)
O13-Cd3-N8	106.5(2)	N9-Cd3-N8	73.5(2)
#1	x-1, y, z		

Table A54. Selected bond distances and angles for **33**.

Bond distances (Å)

Cd1-N1	2.271(7)	Cd2-O7	2.329(5)
Cd1-N2	2.549(7)	Cd2-O8	2.259(6)
Cd1-N3	2.288(7)	Cd2-O6	2.262(6)
Cd1-O1	2.403(6)	Cd3-N7	2.244(8)
Cd1-O2	2.379(6)	Cd3-N9	2.285(7)
Cd1-O4$^{\#1}$	2.276(6)	Cd3-N8	2.474(7)
Cd2-N4	2.322(8)	Cd3-O12	2.244(5)
Cd2-N5	2.480(7)	Cd3-O13	2.254(6)
Cd2-N6	2.296(7)		

Bond angles (°)

N1-Cd1-O4$^{\#1}$	104.3(2)	N1-Cd1-N3	142.7(3)
O4$^{\#1}$-Cd1-N3	86.8(2)	N1-Cd1-O2	85.2(2)
O4$^{\#1}$-Cd1-O2	126.2(2)	N3-Cd1-O2	116.9(2)
N1-Cd1-O1	132.2(2)	O4$^{\#1}$-Cd1-O1	84.1(2)
N3-Cd1-O1	83.6(2)	O2-Cd1-O1	54.9(2)
N1-Cd1-N2	72.3(3)	O4$^{\#1}$-Cd1-N2	129.0(2)
N3-Cd1-N2	73.1(3)	O2-Cd1-N2	104.6(2)
O1-Cd1-N2	136.8(2)	O8-Cd2-O6	97.1(2)
O8-Cd2-N6	81.8(2)	O6-Cd2-N6	87.2(2)
O8-Cd2-N4	169.7(2)	O6-Cd2-N4	90.7(3)
N6-Cd2-N4	105.3(2)	O8-Cd2-O7	87.10(19)
O6-Cd2-O7	88.1(2)	N6-Cd2-O7	167.4(2)
N4-Cd2-O7	86.4(2)	O8-Cd2-N5	102.8(2)
O6-Cd2-N5	149.7(2)	N6-Cd2-N5	73.4(3)
N4-Cd2-N5	72.9(3)	O7-Cd2-N5	115.3(2)
N7-Cd3-O12	96.3(2)	N7-Cd3-O13	104.1(3)
O12-Cd3-O13	126.6(2)	N7-Cd3-N9	144.5(3)
O12-Cd3-N9	90.3(2)	O13-Cd3-N9	99.6(3)
N7-Cd3-N8	74.6(3)	O12-Cd3-N8	126.5(2)
O13-Cd3-N8	106.5(2)	N9-Cd3-N8	73.5(2)
#1	x-1, y, z		

Table A55. Selected bond distances and angles for **34**, **35** and **36**.

Bond distances (Å)

	34	**35**	**36**
Mn1-N1	2.2349(14)	2.244(3)	2.255(2)
Mn1-N2	2.3352(14)	2.354(3)	2.383(2)
Mn1-N3	2.3096(14)	2.265(3)	2.369(2)
Mn1-N4	2.3108(15)	2.303(3)	2.332(2)
Mn1-O1	2.1245(13)	2.133(2)	2.249(3)
Mn1-O2	2.1417(13)	2.088(2)[#]	2.1122(18)
Mn1-O4	----------	---------	2.529(3)
C20-C21	1.197(3)	----------	---------

[#]-x+1/2, -y+1/2, -z+1

Bond angles (°)

	34	**35**	**36**
O2-Mn1-O1	104.51(5)	99.28(8)[#]	103.25(8)
O1-Mn1-N1	162.20(5)	163.69(9)	163.31(8)
O1-Mn1-N4	89.01(5)	87.12(9)	135.06(9)
O2-Mn1-N3	129.12(5)	118.79(10)[#]	87.68(7)
N1-Mn1-N3	82.88(5)	85.46(9)	90.01(8)
O2-Mn1-N2	154.08(5)	164.98(9)[#]	87.81(8)
N1-Mn1-N2	76.57(5)	76.09(9)	75.83(8)
N3-Mn1-N2	73.93(5)	73.84(9)	71.06(7)
O2-Mn1-N1	93.27(5)	95.99(9)[#]	163.31(8)
O2-Mn1-N4	84.02(5)	93.98(10)[#]	87.23(7)
O1-Mn1-N3	85.23(5)	92.13(9)	81.04(9)
N4-Mn1-N3	146.74(5)	146.82(9)	143.64(8)
O1-Mn1-N2	87.45(5)	87.71(9)	149.58(9)
N4-Mn1-N2	73.11(5)	72.99(9)	72.79(7)
N1-Mn1-O4	----------	87.12(9)	87.97(8)
O1-Mn1-O4	---------	----------	54.15(9)
N4-Mn1-O4	---------	----------	80.91(8)
N2-Mn1-O4	----------	----------	150.05(9)
N1-Mn1-N4	93.70(5)	86.16(9)	84.86(8)
O2-Mn1-O4	----------	----------	105.27(8)
N3-Mn1-O4	----------	----------	134.95(8)
C21-C20-C19	175.68(19)	---------	---------
C20-C21-C22	172.14(18)	---------	---------

[#]-x+1/2, -y+1/2, -z+1

Table A56. Selected bond distances and angles for **40**.

Bond distances (Å)

Cd1-N1	2.462(2)	Cd1-O1	2.409(3)
Cd1-N2	2.482(3)	Cd1-O2	2.638(3)
Cd1-N3	2.470(3)	Cd1-O3	2.583(3)
Cd1-N4	2.367(3)	Cd1-O4	2.355(3)
C1-C4$^{\#1}$	1.182(4)	C4-C1$^{\#2}$	1.182(4)

Bond angles (°)

O4-Cd1-N4	137.09(9)	O4-Cd1-O1	79.55(9)
N4-Cd1-O1	86.45(9)	O4-Cd1-N1	82.94(9)
N4-Cd1-N1	138.58(8)	O1-Cd1-N1	117.16(10)
O4-Cd1-N3	149.54(9)	N4-Cd1-N3	69.74(8)
O1-Cd1-N3	123.04(9)	N1-Cd1-N3	68.85(9)
O4-Cd1-N2	89.40(10)	N4-Cd1-N2	93.08(11)
O1-Cd1-N2	162.96(9)	N1-Cd1-N2	73.71(10)
N3-Cd1-N2	72.27(10)	O4-Cd1-O3	52.81(10)
N4-Cd1-O3	84.83(9)	O1-Cd1-O3	78.92(9)
N1-Cd1-O3	130.67(10)	N3-Cd1-O3	143.66(9)
N2-Cd1-O3	84.07(9)	O4-Cd1-O2	114.34(10)
N4-Cd1-O2	85.67(9)	O1-Cd1-O2	51.08(8)
N1-Cd1-O2	84.85(9)	N3-Cd1-O2	75.42(8)
N2-Cd1-O2	145.91(9)	O3-Cd1-O2	129.54(8)
C4$^{\#1}$-C1-C2	178.6(4)		
#1	-x, y-1/2, -z+5/2		
#2	-x, y+1/2, -z+5/2		

Table A57. Selected bond distances and angles for **41b**.

Bond distances (Å)

Mn1-N1	2.2901(16)	Mn1-O1	2.1697(13)
Mn1-N2	2.3381(15)	Mn1-O2	2.1644(13)
Mn1-N3	2.2870(15)	Mn1-O4	2.1029(13)
C16ΞC18	1.195(3)		

Bond angles (°)

O4-Mn1-O2	104.68(5)	N3-Mn1-N1	106.99(5)
O4-Mn1-O1	98.94(5)	O4-Mn1-N2	154.15(5)
O2-Mn1-O1	83.58(5)	O2-Mn1-N2	98.46(5)
O4-Mn1-N3	88.03(5)	O1-Mn1-N2	94.90(5)
O2-Mn1-N3	162.78(5)	N3-Mn1-N2	72.06(5)
O1-Mn1-N3	82.99(5)	N1-Mn1-N2	73.38(5)
O4-Mn1-N1	97.91(5)	O2-Mn1-N1	83.09(5)
O1-Mn1-N1	160.70(5)	C18-C16-C15$^{\#1}$	176.82(19)
C16-C18-C17	176.71(19)		

#1-x, -y+1, -z+1

Table A58. Selected bond distances and angles for **42**.

Bond distances (Å)

Mn1-O1	2.168(3)	Mn2-O4	2.222(3)
Mn1-O2	2.180(3)	Mn2-O5	2.176(3)
Mn1-O3	2.160(3)	Mn2-O6	2.144(3)
Mn1-N1	2.362(3)	Mn2-N4	2.336(3)
Mn1-N2	2.262(3)	Mn2-N5	2.237(3)
Mn1-N3	2.257(3)	Mn2-N6	2.255(3)
C29ΞC30	1.187	C33ΞC34	1.200

Bond angles (°)

O3-Mn1-O1	87.51(13)	O3-Mn1-O2	82.79(12)
O1-Mn1-O2	104.54(14)	O3-Mn1-N3	172.11(13)
O1-Mn1-N3	91.25(13)	O2-Mn1-N3	89.99(13)
O3-Mn1-N2	86.43(12)	O1-Mn1-N2	98.82(14)
O2-Mn1-N2	153.74(12)	N3-Mn1-N2	101.46(13)
O3-Mn1-N1	108.48(12)	O1-Mn1-N1	161.59(13)
O2-Mn1-N1	86.94(12)	N3-Mn1-N1	74.14(12)
N2-Mn1-N1	73.88(12)	O6-Mn2-O5	101.03(15)
O6-Mn2-O4	86.39(13)	O5-Mn2-O4	87.25(12)
O6-Mn2-N5	96.42(14)	O5-Mn2-N5	91.83(13)
O4-Mn2-N5	177.17(13)	O6-Mn2-N6	96.56(14)
O5-Mn2-N6	160.14(12)	O4-Mn2-N6	84.73(12)

N5-Mn2-N6	95.31(12)	O6-Mn2-N4	166.84(13)
O5-Mn2-N4	89.34(12)	O4-Mn2-N4	102.32(11)
N5-Mn2-N4	74.98(12)	N6-Mn2-N4	74.74(11)
C29-C30-C31	174.3	C30-C29-C28	178.2
C34-C33-C32	179	C33-C34-C35	176.9

Table A59. Selected bond distances and angles for **43b** and **44b**.

Bond distances (Å)

	43b	**44b**
Mn1-N1	2.381(2)	2.3693(18)
Mn1-N2	2.459(3)	2.4501(18)
Mn1-N3	2.299(3)	2.3724(19)
Mn1-N4	2.381(3)	2.3051(19)
Mn1-N5	2.318(3)	2.4683(19)
Mn1-N6	2.511(3)	2.2844(19)
Mn1-O1	2.119(2)	2.1204(15)
C2ΞC2′	1.192(6)[#1]	1.199(5)[#2]

#1: -x+1/2, -y+3/2, -z; #2: -x+1/2, -y+3/2, -z+2

Bond angles (°)

	43b	**44b**		**43b**	**44b**
O1-Mn1-N3	96.59(10)	82.19(6)	O1-Mn1-N5	91.69(9)	81.75(6)
N3-Mn1-N5	169.12(10)	160.21(6)	O1-Mn1-N1	137.05(9)	137.76(6)
N3-Mn1-N1	106.20(9)	132.06(6)	N5-Mn1-N1	71.74(9)	67.58(6)
O1-Mn1-N4	82.93(9)	92.02(6)	N3-Mn1-N4	88.67(11)	84.41(7)
N5-Mn1-N4	85.36(10)	107.62(6)	N1-Mn1-N4	132.39(10)	71.73(6)
O1-Mn1-N2	149.13(9)	148.54(6)	N3-Mn1-N2	71.71(10)	69.11(6)
N5-Mn1-N2	97.62(10)	122.87(6)	N1-Mn1-N2	73.64(9)	73.52(6)
N4-Mn1-N2	68.68(10)	97.55(6)	O1-Mn1-N6	81.05(9)	94.99(6)
N3-Mn1-N6	81.65(10)	87.50(7)	N5-Mn1-N6	106.69(10)	82.47(6)
N1-Mn1-N6	67.27(9)	108.34(7)	N4-Mn1-N6	160.16(10)	168.48(7)
N2-Mn1-N6	123.43(9)	71.84(6)	C2#-C2-C1	178.7(5)[#1]	177.9(3)[#2]

#1: -x+1/2, -y+3/2, -z
#2: -x+1/2, -y+3/2, -z+2

Table A60. Selected bond distances and angles for **45**.

Bond distances (Å)

Mn1-N1	2.341(3)	Mn1-O1	2.192(3)
Mn1-N2	2.322(3)	Mn1-O2	2.184(3)
Mn1-N3	2.284(3)	Mn1-O3	2.121(2)
C17ΞC17$^{\#2}$	1.198(6)	C19ΞC19$^{\#1}$	1.191(6)

#1 -x, y, -z+1/2

#2 -x+1, y, -z+1/2

Bond angles (°)

O3-Mn1-O2	103.76(10)	O3-Mn1-O1	99.93(10)
O2-Mn1-O1	80.88(12)	O3-Mn1-N3	106.35(10)
O2-Mn1-N3	85.25(11)	O1-Mn1-N3	152.55(10)
O3-Mn1-N2	83.72(9)	O2-Mn1-N2	165.89(11)
O1-Mn1-N2	86.09(10)	N3-Mn1-N2	104.33(10)
O3-Mn1-N1	155.08(9)	O2-Mn1-N1	101.10(10)
O1-Mn1-N1	85.59(10)	N3-Mn1-N1	73.95(10)
N2-Mn1-N1	72.36(9)	C17$^{\#2}$-C17-C18	177.6(4)
C19$^{\#1}$-C19-C20	174.6(3)		

#1 -x, y, -z+1/2

#2 -x+1, y, -z+1/2

Table A61. Selected bond distances and angles for **47**.

Bond distances (Å)

Mn1-N1	2.253(5)	Mn2-N4	2.272(4)
Mn1-N2	2.337(5)	Mn2-N5	2.364(5)
Mn1-N3	2.265(5)	Mn2-N6	2.306(5)
Mn1-O1	2.235(4)	Mn2-O6	2.107(4)
Mn1-O2	2.119(4)	Mn2-O7	2.169(4)
Mn1-O3	2.095(4)	Mn2-O8	2.171(4)
C2-C3	1.180(8)		

Bond angles (°)

O3-Mn1-O2	90.8(2)	O3-Mn1-O1	95.21(18)
O2-Mn1-O1	87.34(18)	O3-Mn1-N1	97.23(18)
O2-Mn1-N1	168.61(18)	O1-Mn1-N1	83.87(17)
O3-Mn1-N3	88.31(19)	O2-Mn1-N3	83.80(19)
O1-Mn1-N3	170.50(18)	N1-Mn1-N3	104.47(19)
O3-Mn1-N2	156.91(18)	O2-Mn1-N2	101.0(2)
O1-Mn1-N2	105.05(18)	N1-Mn1-N2	74.49(18)
N3-Mn1-N2	73.46(19)	O6-Mn2-O7	97.17(16)
O6-Mn2-O8	99.85(16)	O7-Mn2-O8	83.65(16)
O6-Mn2-N4	104.77(17)	O7-Mn2-N4	86.47(16)
O8-Mn2-N4	154.42(16)	O6-Mn2-N6	86.03(17)
O7-Mn2-N6	170.66(17)	O8-Mn2-N6	87.16(16)
N4-Mn2-N6	101.25(16)	O6-Mn2-N5	157.84(17)
O7-Mn2-N5	104.76(17)	O8-Mn2-N5	85.92(16)
N4-Mn2-N5	73.87(18)	N6-Mn2-N5	72.82(18)

Table A62. Selected bond distances and angles for **49**.

Bond distances (Å)

Mn1-N1	2.361(4)
Mn1-N2	2.371(4)
Mn1-N3	2.246(4)
Mn1-N4	2.257(4)
Mn1-N5	2.265(4)
Mn1-O1	2.087(3)

Bond angles (°)

O1-Mn1-N3	94.60(13)	O1-Mn1-N4	110.56(13)
N3-Mn1-N4	97.93(14)	O1-Mn1-N5	90.30(13)
N3-Mn1-N5	166.90(14)	N4-Mn1-N5	91.68(14)
O1-Mn1-N1	169.87(13)	N3-Mn1-N1	75.69(13)
N4-Mn1-N1	74.23(13)	N5-Mn1-N1	98.58(13)
O1-Mn1-N2	84.81(13)	N3-Mn1-N2	95.08(13)
N4-Mn1-N2	158.86(14)	N5-Mn1-N2	73.25(14)
N1-Mn1-N2	93.06(13)		

Table A63. Selected bond distances and angles for **50**.

Bond distances (Å)

Mn1-N1	2.261(4)	Mn1-O1	2.210(3)
Mn1-N2	2.295(4)	Mn1-O3	2.139(3)
Mn1-N3	2.351(4)	Mn1-O4$^{\#1}$	2.111(3)

Bond angles (°)

O4$^{\#1}$-Mn1-O3	96.97(12)	O4$^{\#1}$-Mn1-O1	105.30(12)
O3-Mn1-O1	83.99(11)	O4$^{\#1}$-Mn1-N1	88.33(12)
O3-Mn1-N1	167.28(13)	O1-Mn1-N1	83.46(12)
O4$^{\#1}$-Mn1-N2	95.10(13)	O3-Mn1-N2	94.87(12)
O1-Mn1-N2	159.56(14)	N1-Mn1-N2	96.16(13)
O4$^{\#1}$-Mn1-N3	158.17(12)	O3-Mn1-N3	102.81(12)
O1-Mn1-N3	86.06(12)	N1-Mn1-N3	74.27(12)
N2-Mn1-N3	74.26(13)		
#1	-x+1/2, -y-1/2, -z+1		

Table A64. Selected bond distances and angles for **51**.

Bond distances (Å)

Mn1-N1	2.227(4)	Mn1-O1	2.174(3)
Mn1-N2	2.310(4)	Mn1-O2	2.215(3)
Mn1-N3	2.212(4)	Mn1-O3	2.149(3)

Bond angles (°)

O3-Mn1-O1	89.31(12)	O3-Mn1-N3	108.39(13)
O1-Mn1-N3	96.56(14)	O3-Mn1-O2	76.34(11)
O1-Mn1-O2	165.04(12)	N3-Mn1-O2	92.01(13)
O3-Mn1-N1	101.05(13)	O1-Mn1-N1	91.49(14)
N3-Mn1-N1	149.51(14)	O2-Mn1-N1	87.24(13)
O3-Mn1-N2	160.51(13)	O1-Mn1-N2	109.60(13)
N3-Mn1-N2	75.05(13)	O2-Mn1-N2	84.43(12)
N1-Mn1-N2	74.54(13)		

Table A65. Selected bond distances and angles for **52**.

Bond distances (Å)

Mn1-N5	2.227(9)	Mn1-N3	2.253(9)
Mn1-N2	2.261(9)	Mn1-N1	2.261(9)
Mn1-N4	2.360(8)	Mn1-N6	2.387(9)

Bond angles (°)

N5-Mn1-N3	90.2(3)	N5-Mn1-N2	88.2(3)
N3-Mn1-N2	108.0(3)	N5-Mn1-N1	108.7(3)
N3-Mn1-N1	154.1(3)	N2-Mn1-N1	90.6(3)
N5-Mn1-N4	151.2(3)	N3-Mn1-N4	72.8(3)
N2-Mn1-N4	75.7(3)	N1-Mn1-N4	95.5(3)
N5-Mn1-N6	76.0(3)	N3-Mn1-N6	95.8(3)
N2-Mn1-N6	151.5(3)	N1-Mn1-N6	72.9(3)
N4-Mn1-N6	127.7(3)		

Table A66. Selected bond distances and angles for **53**.

Bond distances (Å)

Molecule 1

Mn1-O3	2.160(4)	Mn1-O2	2.161(4)
Mn1-O1	2.171(4)	Mn1-N3	2.230(5)
Mn1-N1	2.303(5)	Mn1-N2	2.360(5)
Mn2-O6	2.126(4)	Mn2-O4	2.160(4)
Mn2-O5	2.176(4)	Mn2-N4	2.255(5)
Mn2-N6	2.267(5)	Mn2-N5	2.342(5)

Molecule 2

Mn3-O35	2.127(4)	Mn3-O36	2.151(4)
Mn3-O37	2.171(4)	Mn3-N8	2.268(5)
Mn3-N9	2.275(6)	Mn3-N10	2.350(5)
Mn4-O33	2.149(4)	Mn4-O34	2.153(4)
Mn4-O32	2.180(4)	Mn4-N13	2.224(4)
Mn4-N11	2.276(5)	Mn4-N12	2.393(4)

Bond angles (°)

Molecule 1

O3-Mn1-O2	102.07(15)	O3-Mn1-O1	84.78(15)
O2-Mn1-O1	92.04(16)	O3-Mn1-N3	83.41(16)
O2-Mn1-N3	93.48(16)	O1-Mn1-N3	167.78(17)
O3-Mn1-N1	162.43(16)	O2-Mn1-N1	91.76(16)
O1-Mn1-N1	83.94(16)	N3-Mn1-N1	106.76(17)
O3-Mn1-N2	97.14(16)	O2-Mn1-N2	156.23(16)
O1-Mn1-N2	103.61(16)	N3-Mn1-N2	74.85(16)
N1-Mn1-N2	72.59(16)	O6-Mn2-O4	107.22(16)
O6-Mn2-O5	89.26(15)	O4-Mn2-O5	85.53(15)
O6-Mn2-N4	91.11(16)	O4-Mn2-N4	82.39(16)
O5-Mn2-N4	167.46(16)	O6-Mn2-N6	87.25(17)
O4-Mn2-N6	165.05(16)	O5-Mn2-N6	91.05(16)
N4-Mn2-N6	101.49(17)	O6-Mn2-N5	153.47(17)
O4-Mn2-N5	93.82(16)	O5-Mn2-N5	108.76(15)
N4-Mn2-N5	75.51(16)	N6-Mn2-N5	73.50(17)

Molecule 2

O35-Mn3-O36	100.37(19)	O35-Mn3-O37	92.86(17)
O36-Mn3-O37	85.74(16)	O35-Mn3-N8	90.24(18)
O36-Mn3-N8	81.99(17)	O37-Mn3-N8	167.70(18)
O35-Mn3-N9	92.0(2)	O36-Mn3-N9	167.17(18)
O37-Mn3-N9	90.41(17)	N8-Mn3-N9	101.38(18)

O35-Mn3-N10	155.74(18)	O36-Mn3-N10	96.11(16)
O37-Mn3-N10	106.08(15)	N8-Mn3-N10	74.50(16)
N9-Mn3-N10	73.19(18)	O33-Mn4-O34	90.12(15)
O33-Mn4-O32	85.57(15)	O34-Mn4-O32	105.42(15)
O33-Mn4-N13	171.05(17)	O34-Mn4-N13	87.88(16)
O32-Mn4-N13	86.56(16)	O33-Mn4-N11	85.43(16)
O34-Mn4-N11	92.10(17)	O32-Mn4-N11	160.28(16)
N13-Mn4-N11	103.36(17)	O33-Mn4-N12	110.32(15)
O34-Mn4-N12	151.84(16)	O32-Mn4-N12	95.59(15)
N13-Mn4-N12	74.69(16)	N11-Mn4-N12	71.29(17)

Table A67. Selected bond distances and angles for **54**.

Bond distances (Å)

Mn1-O1	2.111(4)	Mn1-O4	2.155(4)
Mn1-O3	2.231(3)	Mn1-N3	2.250(4)
Mn1-N1	2.283(4)	Mn1-N2	2.389(4)

Bond angles (°)

O1-Mn1-O4	104.15(15)	O1-Mn1-O3	91.64(14)
O4-Mn1-O3	90.23(14)	O1-Mn1-N3	89.49(15)
O4-Mn1-N3	86.00(14)	O3-Mn1-N3	176.22(14)
O1-Mn1-N1	95.40(15)	O4-Mn1-N1	160.46(15)
O3-Mn1-N1	88.98(14)	N3-Mn1-N1	94.50(15)
O1-Mn1-N2	157.88(14)	O4-Mn1-N2	88.11(14)
O3-Mn1-N2	106.88(14)	N3-Mn1-N2	72.83(14)
N1-Mn1-N2	73.46(15)		

Table A68. Selected Bond distances and angles for **55**.

Bond distances (Å)

Mn1-O1	2.232(3)	Mn1-N1	2.239(3)
Mn1-O2	2.281(3)	Mn1-N2	2.229(3)
Mn1-O5	2.045(3)	Mn1-N3	2.411(3)

Bond angles (°)

O5-Mn1-N2	99.83(11)	O5-Mn1-O1	96.95(11)
N2-Mn1-O1	158.60(11)	O5-Mn1-N1	91.33(11)
N2-Mn1-N1	109.82(12)	O1-Mn1-N1	82.86(11)
O5-Mn1-O2	100.61(10)	N2-Mn1-O2	105.54(10)

O1-Mn1-O2	58.01(9)	N1-Mn1-O2	140.00(10)
O5-Mn1-N3	160.01(11)	N2-Mn1-N3	72.41(11)
O1-Mn1-N3	95.52(11)	N1-Mn1-N3	74.79(12)
O2-Mn1-N3	99.24(10)		

Table A69. Selected bond distances and angles for **56**.

Bond distances (Å)

Mn1-O1	2.093(5)	Mn2-O2	2.375(6)
Mn1-O3	1.950(5)	Mn2-O4	1.962(5)
Mn1-O8	2.287(6)	Mn2-O5	2.051(6)
Mn1-N4	2.740(7)	Mn2-N1	2.188(7)
Mn1-N5	2.287(7)	Mn2-N2	2.503(6)
Mn1-N6	2.216(6)	Mn2-N3	2.563(7)

Bond angles (°)

O3-Mn1-O1	82.5(2)	O3-Mn1-N6	91.1(2)
O1-Mn1-N6	167.4(2)	O3-Mn1-N5	158.1(3)
O1-Mn1-N5	87.4(2)	N6-Mn1-N5	94.9(2)
O3-Mn1-O8	93.2(2)	O1-Mn1-O8	109.1(2)
N6-Mn1-O8	81.9(3)	N5-Mn1-O8	108.4(2)
O3-Mn1-N4	103.3(2)	O1-Mn1-N4	93.2(2)
N6-Mn1-N4	77.7(2)	N5-Mn1-N4	57.9(2)
O8-Mn1-N4	153.9(2)	O4-Mn2-O5	127.5(2)
O4-Mn2-N1	144.5(2)	O5-Mn2-N1	88.0(2)
O4-Mn2-O2	75.7(2)	O5-Mn2-O2	110.1(2)
N1-Mn2-O2	93.4(2)	O4-Mn2-N2	89.3(2)
O5-Mn2-N2	133.5(2)	N1-Mn2-N2	60.7(2)
O2-Mn2-N2	105.5(2)	O4-Mn2-N3	99.0(2)
O5-Mn2-N3	79.6(2)	N1-Mn2-N3	86.3(2)
O2-Mn2-N3	170.3(2)	N2-Mn2-N3	66.0(2)

Table A70. Selected bond distances and angles for **57**.

Bond distances (Å)

Mn1-N1	2.264(3)	Mn1-O4	2.185(3)
Mn1-N2	2.281(4)	Mn1-O5	2.195(3)
Mn1-N3	2.396(4)	Mn1-O6	2.145(3)

Bond angles (°)

O6-Mn1-O4	89.77(13)	O6-Mn1-O5	109.63(12)
O4-Mn1-O5	85.57(11)	O6-Mn1-N1	90.90(13)
O4-Mn1-N1	93.55(13)	O5-Mn1-N1	159.43(15)
O6-Mn1-N2	102.02(16)	O4-Mn1-N2	164.58(14)
O5-Mn1-N2	81.15(12)	N1-Mn1-N2	96.14(13)
O6-Mn1-N3	162.96(12)	O4-Mn1-N3	98.94(14)
O5-Mn1-N3	85.77(12)	N1-Mn1-N3	74.05(13)
N2-Mn1-N3	72.40(16)		

Table A71. Selected bond distances and angles for **58**.

Bond distances (Å)

Cu1-N1	2.012(4)
Cu1-N2	1.998(4)
Cu1-N3	2.019(5)
Cu1-O1	2.270(3)
Cu1-O2	1.912(4)

Bond angles (°)

O2-Cu1-N2	95.69(19)	O2-Cu1-N1	99.47(19)
N2-Cu1-N1	164.6(2)	O2-Cu1-N3	157.71(16)
N2-Cu1-N3	82.51(18)	N1-Cu1-N3	82.38(18)
O2-Cu1-O1	102.37(17)	N2-Cu1-O1	90.87(15)
N1-Cu1-O1	88.68(16)	N3-Cu1-O1	99.87(15)

Table A72. Selected bond distances and angles for **61**.

Bond distances (Å)

Cu1-N4	1.995(11)	Cu2-N1	1.978(14)
Cu1-N5	1.945(14)	Cu2-N2	1.965(14)
Cu1-N6	1.976(17)	Cu2-N3	2.009(12)
Cu1-O1	1.961(11)	Cu2-O3	1.913(13)
		Cu2-O4	2.191(14)

Bond angles (°)

N5-Cu1-O1	97.8(5)	N5-Cu1-N6	165.6(7)
O1-Cu1-N6	96.3(7)	N5-Cu1-N4	85.1(5)
O1-Cu1-N4	172.4(5)	N6-Cu1-N4	81.2(6)
O3-Cu2-N2	97.6(6)	O3-Cu2-N1	95.5(6)
N2-Cu2-N1	166.8(6)	O3-Cu2-N3	164.0(5)
N2-Cu2-N3	84.0(5)	N1-Cu2-N3	82.9(5)
O3-Cu2-O4	93.3(6)	N2-Cu2-O4	89.0(6)
N1-Cu2-O4	92.3(5)	N3-Cu2-O4	102.7(5)

Table A73. Selected bond distances and angles for **63**.

Bond distances (Å)

Cu1-O3	1.911(4)	Cu1-N3	1.978(3)
Cu1-N1	1.987(4)	Cu1-N2	2.037(3)

Bond angles (°)

O3-Cu1-N3	98.13(16)	O3-Cu1-N1	97.7(2)
N3-Cu1-N1	161.68(17)	O3-Cu1-N2	168.97(15)
N3-Cu1-N2	83.21(12)	N1-Cu1-N2	83.00(17)

Table A74. Selected bond distances and angles for **64**.

Bond distances (Å)

Cu1-O25	1.951(13)	Cu3-O1	2.373(19)
Cu1-N1	2.041(15)	Cu3-O30	1.954(17)
Cu1-N2	2.012(16)	Cu3-N7	1.988(18)
Cu1-N3	2.005(16)	Cu3-N8	1.990(16)
Cu2-O28	1.992(12)	Cu3-N9	2.009(18)
Cu2-O29	2.216(12)	Cu4-O33	1.905(18)
Cu2-N4$^{\#1}$	2.019(15)	Cu4-O34	2.411(19)
Cu2-N5	2.043(15)	Cu4-N10	1.983(17)
Cu2-N6	2.008(13)	Cu4-N11	1.959(16)
		Cu4-N12	1.989(15)

Bond angles (°)

O25-Cu1-N3	98.0(7)	O25-Cu1-N2	96.9(6)
N3-Cu1-N2	164.5(7)	O25-Cu1-N1	173.1(6)
N3-Cu1-N1	82.1(7)	N2-Cu1-N1	83.7(6)
O28-Cu2-N6	97.9(6)	O28-Cu2-N4$^{\#1}$	162.9(5)
N6-Cu2-N4$^{\#1}$	81.9(6)	O28-Cu2-N5	98.0(6)
N6-Cu2-N5	161.9(6)	N4$^{\#1}$-Cu2-N5	80.3(6)
O28-Cu2-O29	94.5(5)	N6-Cu2-O29	94.8(5)
N4$^{\#1}$-Cu2-O29	102.5(5)	N5-Cu2-O29	92.6(5)
O30-Cu3-N8	100.4(7)	O30-Cu3-N7	168.9(8)
N8-Cu3-N7	82.8(6)	O30-Cu3-N9	93.9(6)
N8-Cu3-N9	165.7(7)	N7-Cu3-N9	83.3(6)
O30-Cu3-O1	103.2(8)	N8-Cu3-O1	88.5(6)
N7-Cu3-O1	87.5(6)	N9-Cu3-O1	87.7(6)
O33-Cu4-N11	97.9(7)	O33-Cu4-N10	172.3(7)
N11-Cu4-N10	83.3(7)	O33-Cu4-N12	96.1(6)
N11-Cu4-N12	165.8(7)	N10-Cu4-N12	83.3(6)
O33-Cu4-O34	92.4(8)	N11-Cu4-O34	90.5(7)
N10-Cu4-O34	95.2(7)	N12-Cu4-O34	86.1(6)

#1 -x+2, -y+2, -z+1

Table A75. Selected bond distances and angles for **65**.

Bond distances (Å)

Cu1-O7	2.027(6)	Cu2-O3	2.271(7)
Cu1-O9	2.200(6)	Cu2-O5	1.951(6)
Cu1-N1	2.038(7)	Cu2-N5	2.030(8)
Cu1-N3	1.992(8)	Cu2-N6	1.984(8)
Cu1-N8	1.962(8)	Cu2-N7	1.965(8)

Bond angles (°)

N8-Cu1-N3	165.3(3)	N8-Cu1-O7	97.0(3)
N3-Cu1-O7	94.9(3)	N8-Cu1-N1	82.6(3)
N3-Cu1-N1	82.7(3)	O7-Cu1-N1	145.9(3)
N8-Cu1-O9	93.4(3)	N3-Cu1-O9	95.3(3)
O7-Cu1-O9	89.4(2)	N1-Cu1-O9	124.7(3)
O5-Cu2-N7	98.5(3)	O5-Cu2-N6	96.4(3)
N7-Cu2-N6	165.1(4)	O5-Cu2-N5	158.8(3)
N7-Cu2-N5	82.8(3)	N6-Cu2-N5	82.9(3)
O5-Cu2-O3	98.1(3)	N7-Cu2-O3	85.0(3)
N6-Cu2-O3	94.0(3)	N5-Cu2-O3	103.1(3)

Table A76. Selected bond distances and angles for **66**.

Bond distances (Å)

Cu1-O1	2.342(4)
Cu1-O2	1.953(4)
Cu1-N1	2.058(5)
Cu1-N2	1.982(5)
Cu1-N3	1.980(5)

Bond angles (°)

O2-Cu1-N3	96.69(17)	O2-Cu1-N2	95.46(18)
N3-Cu1-N2	164.9(2)	O2-Cu1-N1	165.80(17)
N3-Cu1-N1	83.37(19)	N2-Cu1-N1	82.65(19)
O2-Cu1-O1	86.80(15)	N3-Cu1-O1	97.30(17)
N2-Cu1-O1	92.30(17)	N1-Cu1-O1	107.31(16)

Table A77. Selected bond distances and angles for **67**.

Bond distances (Å)

Cu1-N1	2.019(4)	Cu1-N3	1.987(4)
Cu1-N2	1.995(4)	Cu1-O1	1.965(3)

Bond angles (°)

O1-Cu1-N3	98.16(15)	O1-Cu1-N2	97.01(14)
N3-Cu1-N2	164.79(15)	O1-Cu1-N1	174.16(14)
N3-Cu1-N1	82.70(15)	N2-Cu1-N1	82.10(14)

Table A78. Selected bond distances and angles for **68**.

Bond distances (Å)

Cu1-O1	1.913(6)	Cu2-O4	1.933(7)
Cu1-N4	1.989(9)	Cu2-N1	1.996(8)
Cu1-N5	2.035(8)	Cu2-N2	2.033(9)
Cu1-N6	1.962(9)	Cu2-N3	1.983(8)

Bond angles (°)

O1-Cu1-N6	95.3(3)	O1-Cu1-N4	98.5(3)
N6-Cu1-N4	165.8(3)	O1-Cu1-N5	177.8(3)
N6-Cu1-N5	82.6(3)	N4-Cu1-N5	83.5(3)
O4-Cu2-N3	95.4(3)	O4-Cu2-N1	98.8(3)
N3-Cu2-N1	163.6(4)	O4-Cu2-N2	173.5(3)
N3-Cu2-N2	82.7(4)	N1-Cu2-N2	84.0(3)

Table A79. Selected bond distances and angles for **70**.

Bond distances (Å)

Cu1-O1	1.953(5)	Cu3-O9	1.917(6)
Cu1-N1	1.943(7)	Cu3-O11	2.273(6)
Cu1-N2	2.056(6)	Cu3-N7	1.994(7)
Cu1-N3	1.996(7)	Cu3-N8	2.048(6)
Cu2-O6	1.954(5)	Cu3-N9	2.018(7)
Cu2-N4	1.979(7)	Cu4-O5	1.907(6)
Cu2-N5	2.013(7)	Cu4-N10	1.965(8)
Cu2-N6	1.980(7)	Cu4-N11	2.017(7)
		Cu4-N12	1.982(7)

Bond angles (°)

N1-Cu1-O1	98.9(3)	N1-Cu1-N3	165.9(3)
O1-Cu1-N3	94.9(3)	N1-Cu1-N2	83.7(3)
O1-Cu1-N2	177.0(3)	N3-Cu1-N2	82.4(3)
O6-Cu2-N6	98.2(3)	O6-Cu2-N4	96.0(3)
N6-Cu2-N4	165.0(3)	O6-Cu2-N5	169.0(2)
N6-Cu2-N5	83.4(3)	N4-Cu2-N5	83.6(3)
O9-Cu3-N7	97.6(3)	O9-Cu3-N9	98.2(3)
N7-Cu3-N9	163.1(3)	O9-Cu3-N8	166.6(3)
N7-Cu3-N8	81.5(3)	N9-Cu3-N8	81.8(3)
O9-Cu3-O11	93.0(3)	N7-Cu3-O11	94.8(3)
N9-Cu3-O11	90.4(3)	N8-Cu3-O11	100.4(3)
O5-Cu4-N10	97.6(3)	O5-Cu4-N12	96.1(3)
N10-Cu4-N12	165.9(3)	O5-Cu4-N11	175.3(3)
N10-Cu4-N11	82.6(3)	N12-Cu4-N11	84.0(3)

Table A80. Selected bond distances and angles for **71**.

Bond distances (Å)

Cu1-O1	2.310(2)	Cu1-N2	1.979(2)
Cu1-O2	1.984(2)	Cu1-N3	1.988(2)
Cu1-N1	2.037(2)		

Bond angles (°)

N2-Cu1-O2	97.70(9)	N2-Cu1-N3	165.54(10)
O2-Cu1-N3	96.74(9)	N2-Cu1-N1	83.57(10)
O2-Cu1-N1	165.43(9)	N3-Cu1-N1	82.25(10)
N2-Cu1-O1	92.42(9)	O2-Cu1-O1	96.78(8)
N3-Cu1-O1	86.68(9)	N1-Cu1-O1	97.68(9)

Table A81. Selected bond distances and angles for **73**.

Bond distances (Å)

Cu1-O2	1.968(12)	Cu2-O4	1.988(16)
Cu1-O3	2.274(15)	Cu2-O6	2.389(14)
Cu1-N1	2.023(16)	Cu2-N4	1.987(18)
Cu1-N2	2.019(15)	Cu2-N5	2.002(15)
Cu1-N3	2.027(17)	Cu2-N6	2.006(18)

Bond angles (°)

O2-Cu1-N2	97.8(6)	O2-Cu1-N1	165.6(7)
N2-Cu1-N1	82.9(7)	O2-Cu1-N3	96.9(7)
N2-Cu1-N3	165.3(7)	N1-Cu1-N3	82.6(7)
O2-Cu1-O3	90.6(6)	N2-Cu1-O3	92.2(6)
N1-Cu1-O3	103.7(7)	N3-Cu1-O3	88.7(6)
N4-Cu2-O4	97.3(8)	N4-Cu2-N5	80.4(8)
O4-Cu2-N5	174.5(8)	N4-Cu2-N6	161.2(9)
O4-Cu2-N6	100.4(8)	N5-Cu2-N6	81.5(8)
N4-Cu2-O6	99.3(6)	O4-Cu2-O6	89.6(7)
N5-Cu2-O6	95.7(7)	N6-Cu2-O6	87.4(7)

Table A82. Selected bond distances and angles for **74**.

Bond distances (Å)

Cu1-O1	1.937(5)	Cu2-O3	2.195(5)
Cu1-N1	2.016(7)	Cu2-O4	1.981(5)
Cu1-N2	1.948(6)	Cu2-N4	2.065(6)
Cu1-N3	1.968(6)	Cu2-N5	1.964(6)
		Cu2-N6	1.996(6)

Bond angles (°)

O1-Cu1-N2	95.7(3)	O1-Cu1-N3	98.1(3)
N2-Cu1-N3	164.6(3)	O1-Cu1-N1	163.5(2)
N2-Cu1-N1	84.7(3)	N3-Cu1-N1	84.0(3)
N5-Cu2-O4	94.6(2)	N5-Cu2-N6	165.2(2)
O4-Cu2-N6	96.3(2)	N5-Cu2-N4	82.9(2)
O4-Cu2-N4	151.1(2)	N6-Cu2-N4	82.8(2)
N5-Cu2-O3	93.5(2)	O4-Cu2-O3	98.6(2)
N6-Cu2-O3	94.7(2)	N4-Cu2-O3	110.3(2)

Table A83. Selected bond distances and angles for **75**.

Bond distances (Å)

Cu1-O1#1	1.951(7)	Cu2-O3	2.037(7)
Cu1-O8	2.271(7)	Cu2-O6	2.170(6)
Cu1-N2	2.017(8)	Cu2-N1	2.016(9)
Cu1-N3	1.988(8)	Cu1-N11	1.963(9)
Cu2-N5	1.998(9)	Cu2-N12	1.993(9)

Bond angles (°)

$O1^{\#1}$-Cu1-N11	97.2(3)	$O1^{\#1}$-Cu1-N3	96.8(3)
N11-Cu1-N3	165.9(3)	$O1^{\#1}$-Cu1-N2	158.9(3)
N11-Cu1-N2	82.8(3)	N3-Cu1-N2	83.5(3)
$O1^{\#1}$-Cu1-O8	98.7(3)	N11-Cu1-O8	87.5(3)
N3-Cu1-O8	92.2(3)	N2-Cu1-O8	102.3(3)
N12-Cu2-N5	166.7(4)	N12-Cu2-N1	83.5(4)
N5-Cu2-N1	83.2(4)	N12-Cu2-O3	96.1(3)
N5-Cu2-O3	94.6(3)	N1-Cu2-O3	144.5(3)
N12-Cu2-O6	92.7(3)	N5-Cu2-O6	95.4(3)
N1-Cu2-O6	126.8(3)	O3-Cu2-O6	88.7(3)

#1 –x, -y+1, -z

Table A84. Selected bond distances and angles for **76**.

Bond distances (Å)

Cu1-O1	2.332(3)
Cu1-O2	1.964(3)
Cu1-N1	2.042(4)
Cu1-N2	1.979(4)
Cu1-N3	1.964(4)

Bond angles (°)

N3-Cu1-O2	98.89(15)	N3-Cu1-N2	165.65(16)
O2-Cu1-N2	94.96(15)	N3-Cu1-N1	84.70(16)
O2-Cu1-N1	158.29(15)	N2-Cu1-N1	83.81(16)
N3-Cu1-O1	89.20(16)	O2-Cu1-O1	100.45(13)

Table A85. Selected bond distances and angles for **77**.

Bond distances (Å)

Cu1-O4	2.293(10)	Cu2-O5	2.379(10)
Cu1-O27	1.951(9)	Cu2-O26	1.961(9)
Cu1-N1	2.033(10)	Cu2-N2	2.037(11)
Cu1-N23	1.992(13)	Cu2-N21	1.954(12)
Cu1-N24	1.944(14)	Cu2-N22	1.960(11)

Bond angles (°)

N24-Cu1-O27	96.0(5)	N24-Cu1-N23	164.4(6)
O27-Cu1-N23	99.6(5)	N24-Cu1-N1	83.1(5)
O27-Cu1-N1	163.0(4)	N23-Cu1-N1	81.8(6)
N24-Cu1-O4	87.4(4)	O27-Cu1-O4	100.8(4)
N23-Cu1-O4	90.6(4)	N1-Cu1-O4	96.1(4)
N21-Cu2-N22	163.4(6)	N21-Cu2-O26	95.5(5)
N22-Cu2-O26	100.5(5)	N21-Cu2-N2	82.1(5)
N22-Cu2-N2	81.5(5)	O26-Cu2-N2	173.4(4)
N21-Cu2-O5	93.0(4)	N22-Cu2-O5	89.1(4)
O26-Cu2-O5	98.5(4)	N2-Cu2-O5	87.8(4)

Table A86. Selected bond distances and angles for **79**.

Bond distances (Å)

Cu1-O1	2.399(14)	Cu2-O8	1.891(14)
Cu1-O2	2.011(13)	Cu2-O9	2.30(2)
Cu1-N1	2.037(17)	Cu2-N4	2.043(17)
Cu1-N2	1.98(2)	Cu2-N5	1.97(2)
Cu1-N3	1.96(2)	Cu2-N6	2.00(3)
Na1-O15	2.25(6)	Na1-O2	2.338(17)
Na1-O7	2.440(19)	Na1-O10	2.89(5)

Bond angles (°)

N3-Cu1-N2	165.4(10)	N3-Cu1-O2	97.5(8)
N2-Cu1-O2	97.2(9)	N3-Cu1-N1	85.0(9)
N2-Cu1-N1	80.6(9)	O2-Cu1-N1	169.1(7)
N3-Cu1-O1	86.4(8)	N2-Cu1-O1	93.2(9)
O2-Cu1-O1	91.8(6)	N1-Cu1-O1	98.9(6)
O8-Cu2-N5	99.3(9)	O8-Cu2-N6	93.4(9)
N5-Cu2-N6	162.9(10)	O8-Cu2-N4	174.2(8)
N5-Cu2-N4	83.7(7)	N6-Cu2-N4	82.7(8)
O8-Cu2-O9	84.0(7)	N5-Cu2-O9	83.3(9)
N6-Cu2-O9	109.6(11)	N4-Cu2-O9	101.3(7)
O15-Na1-O7	88.9(15)	O15-Na1-O2	85.7(16)
O15-Na1-O10	172.5(17)	O2-Na1-O7	96.1(7)
O7-Na1-O10	83.7(11)	O2-Na1-O10	93.6(11)

Table A87. Selected bond distances and angles for **80**.

Bond distances (Å)

Cu1-O1	1.879(11)	Cu2-N6	2.07(3)
Cu1-N1	1.999(15)	O2-Na1	2.359(17)
Cu1-N2	1.996(16)	Na1-O6	2.355(17)
Cu1-N3	1.995(14)	Na1-O18	2.45(2)
Cu2-O7	2.004(16)	Na1-O3	2.290(15)
Cu2-O8	2.18(4)	Na1-O5	2.367(14)
Cu2-N4	2.07(2)	Na1-O9	2.70(2)
Cu2-N5	1.919(19)		

Bond angles (°)

O1-Cu1-N3	95.4(6)	O1-Cu1-N2	100.2(5)
N3-Cu1-N2	163.8(6)	O1-Cu1-N1	167.5(6)
N3-Cu1-N1	81.7(6)	N2-Cu1-N1	83.8(6)
N5-Cu2-O7	97.4(7)	N5-Cu2-N4	82.6(8)
O7-Cu2-N4	158.0(7)	N5-Cu2-N6	168.0(10)
O7-Cu2-N6	94.6(10)	N4-Cu2-N6	85.8(10)
N5-Cu2-O8	88.6(10)	O7-Cu2-O8	98.4(11)
N4-Cu2-O8	103.5(11)	N6-Cu2-O8	91.1(11)

Table A88. Selected bond distances and angles for **83**, **84** and **85**.

Bond distances (Å)

83

Cu1-O1	2.410(4)	Cu2-O2	2.203(5)
Cu1-O3	1.955(4)	Cu2-O6$^{\#1}$	2.007(4)
Cu1-N1	1.977(5)	Cu2-N4	2.065(5)
Cu1-N2	2.029(5)	Cu2-N5	1.977(5)
Cu1-N3	1.980(5)	Cu2-N6	1.983(5)

#1 –x+2, y, -z+2

84

Molecule 1				Molecule 2			
Cu1-O1	2.406(9)	Cu2-O2	2.327(10)	Cu3-O7	2.280(9)	Cu4-O8	2.365(9)
Cu1-O5	1.949(10)	Cu2-O4	1.984(10)	Cu3-O12$^{\#1}$	2.010(9)	Cu4-O9	1.960(10)
Cu1-N1	2.005(12)	Cu2-N4	1.990(13)	Cu3-N7	1.972(13)	Cu4-N10	2.000(13)
Cu1-N2	2.016(13)	Cu2-N5	2.036(12)	Cu3-N8	2.029(12)	Cu4-N11	2.017(13)
Cu1-N3	1.984(12)	Cu2-N6	1.981(15)	Cu3-N9	2.013(13)	Cu4-N12	1.978(13)

#1 –x+1, -y+1, -z

85

Cu1-O1	2.397(8)	Cu2-O2	2.312(7)	Cu3-O3	2.350(6)	Cu4-O4	2.456(7)
Cu1-O5	1.929(7)	Cu2-O10	1.984(7)	Cu3-O12	1.946(7)	Cu4-O7	1.961(6)
Cu1-N1	2.007(8)	Cu2-N4	1.997(7)	Cu3-N7	2.021(8)	Cu4-N10	1.991(8)
Cu1-N2	2.039(8)	Cu2-N5	2.014(9)	Cu3-N8	2.039(9)	Cu4-N11	2.011(7)
Cu1-N3	1.970(8)	Cu2-N6	1.999(9)	Cu3-N9	1.955(9)	Cu4-N12	1.994(8)

Bond Angles (°)

83

O3-Cu1-N1	94.30(18)	O3-Cu1-N3	100.57(18)
N1-Cu1-N3	164.8(2)	O3-Cu1-N2	159.43(17)
N1-Cu1-N2	83.75(19)	N3-Cu1-N2	83.33(19)
O3-Cu1-O1	106.51(16)	N1-Cu1-O1	85.92(18)
N3-Cu1-O1	87.08(17)	N2-Cu1-O1	93.81(17)
N5-Cu2-N6	166.0(2)	N5-Cu2-O6$^{\#1}$	94.73(18)
N6-Cu2-O6$^{\#1}$	94.16(19)	N5-Cu2-N4	83.01(19)
N6-Cu2-N4	84.5(2)	O6$^{\#1}$-Cu2-N4	155.87(17)
N5-Cu2-O2	100.22(18)	N6-Cu2-O2	89.74(19)
O6$^{\#1}$-Cu2-O2	94.75(18)	N4-Cu2-O2	109.31(19)

#1 -x+2, y, -z+1/2

84

O5-Cu1-N3	98.5(5)	O5-Cu1-N1	95.1(5)
N3-Cu1-N1	166.0(5)	O5-Cu1-N2	159.0(4)
N3-Cu1-N2	84.6(5)	N1-Cu1-N2	83.9(5)
O5-Cu1-O1	107.3(4)	N3-Cu1-O1	87.7(4)
N1-Cu1-O1	85.1(4)	N2-Cu1-O1	93.5(4)
N6-Cu2-O4	93.9(5)	N6-Cu2-N4	167.1(6)
O4-Cu2-N4	97.6(5)	N6-Cu2-N5	84.8(5)
O4-Cu2-N5	160.7(4)	N4-Cu2-N5	82.4(5)
N6-Cu2-O2	93.1(4)	O4-Cu2-O2	85.7(4)
N4-Cu2-O2	93.6(5)	N5-Cu2-O2	113.6(4)
N7-Cu3-O12$^{\#1}$	98.0(5)	N7-Cu3-N9	165.5(6)
O12$^{\#1}$-Cu3-N9	95.8(5)	N7-Cu3-N8	83.7(5)
O12$^{\#1}$-Cu3-N8	163.6(4)	N9-Cu3-N8	81.8(5)
N7-Cu3-O7	93.6(5)	O12$^{\#1}$-Cu3-O7	87.8(4)
N9-Cu3-O7	91.5(4)	N8-Cu3-O7	108.5(4)
O9-Cu4-N12	98.6(5)	O9-Cu4-N10	96.9(5)
N12-Cu4-N10	164.4(5)	O9-Cu4-N11	155.3(4)

N12-Cu4-N11	82.2(5)	N10-Cu4-N11	83.4(5)
O9-Cu4-O8	109.4(4)	N12-Cu4-O8	86.4(4)
N10-Cu4-O8	89.0(4)	N11-Cu4-O8	93.5(4)
#1	-x+1, -y+1, -z		

85

O5-Cu1-N3	99.8(3)	O5-Cu1-N1	94.7(3)
N3-Cu1-N1	165.2(4)	O5-Cu1-N2	165.1(3)
N3-Cu1-N2	83.5(4)	N1-Cu1-N2	83.2(3)
O5-Cu1-O1	97.5(3)	N3-Cu1-O1	86.1(3)
N1-Cu1-O1	89.1(3)	N2-Cu1-O1	97.2(3)
O10-Cu2-N4	95.7(3)	O10-Cu2-N6	99.6(3)
N4-Cu2-N6	164.6(4)	O10-Cu2-N5	166.3(3)
N4-Cu2-N5	83.2(3)	N6-Cu2-N5	81.5(4)
O10-Cu2-O2	95.9(3)	N4-Cu2-O2	92.6(3)
N6-Cu2-O2	87.5(3)	N5-Cu2-O2	97.7(3)
O12-Cu3-N9	98.9(4)	O12-Cu3-N7	95.0(3)
N9-Cu3-N7	165.2(4)	O12-Cu3-N8	167.6(3)
N9-Cu3-N8	83.4(4)	N7-Cu3-N8	81.9(3)
O12-Cu3-O3	98.4(3)	N9-Cu3-O3	87.2(3)
N7-Cu3-O3	95.9(3)	N8-Cu3-O3	93.8(3)
O7-Cu4-N10	93.8(3)	O7-Cu4-N12	98.9(3)
N10-Cu4-N12	167.0(3)	O7-Cu4-N11	165.9(3)
N10-Cu4-N11	83.9(3)	N12-Cu4-N11	84.5(3)
O7-Cu4-O4	104.6(3)	N10-Cu4-O4	86.5(3)
N12-Cu4-O4	87.5(3)	N11-Cu4-O4	89.2(3)

Table A89. Selected bond distances and angles for **87**.

Bond distances (Å)

Cu1-N1	1.978(6)	Cu1-O1	1.937(5)
Cu1-N3	1.958(6)	Cu1-O3	2.333(5)
Cu1-N2	2.010(5)		

Bond angles (°)

O1-Cu1-N3	97.9(3)	O1-Cu1-N1	95.9(2)
N3-Cu1-N1	166.0(3)	O1-Cu1-N2	164.2(2)
N3-Cu1-N2	83.6(3)	N1-Cu1-N2	83.8(2)
O1-Cu1-O3	103.0(2)	N3-Cu1-O3	85.8(2)
N1-Cu1-O3	88.7(2)	N2-Cu1-O3	92.77(18)

Table A90. Selected bond distances and angles for **88**.

Bond distances (Å)

Cu1-O1	2.285(9)	Cu3-O8	2.263(9)	Cu5-O6	1.956(10)
Cu1-O2	1.937(9)	Cu3-O9	1.952(10)	Cu5-O17	2.279(9)
Cu1-N1	2.040(12)	Cu3-N7	2.091(12)	Cu5-N10	1.989(14)
Cu1-N2	1.994(13)	Cu3-N8	1.968(14)	Cu5-N11	2.088(12)
Cu1-N3	2.040(12)	Cu3-N9	2.020(14)	Cu5-N12	1.985(13)
Cu2-O4	1.940(10)	Cu4-O12	1.953(10)	Cu6-O15	1.949(10)
Cu2-N4	2.019(14)	Cu4-O13	2.251(9)	Cu6-O16	2.384(11)
Cu2-N5	1.999(13)	Cu4-N16	2.052(15)	Cu6-N13	1.984(13)
Cu2-N6	1.991(12)	Cu4-N17	2.021(12)	Cu6-N14	1.894(14)
		Cu4-N18	2.009(14)	Cu6-N15	2.018(14)

Bond angles (°)

O2-Cu1-N2	99.0(5)	O2-Cu1-N1	176.4(4)	N18-Cu4-N16	163.3(6)
N2-Cu1-N1	80.9(6)	O2-Cu1-N3	96.8(5)	O12-Cu4-O13	98.1(4)
N2-Cu1-N3	159.7(5)	N1-Cu1-N3	82.6(5)	N17-Cu4-O13	94.9(4)
O2-Cu1-O1	90.5(4)	N2-Cu1-O1	95.6(4)	O6-Cu5-N12	96.1(5)
N1-Cu1-O1	93.1(4)	N3-Cu1-O1	97.0(4)	N12-Cu5-N10	164.2(6)
O4-Cu2-N6	98.2(5)	O4-Cu2-N5	167.9(5)	N12-Cu5-N11	82.3(6)
N6-Cu2-N5	84.6(5)	O4-Cu2-N4	95.3(5)	O6-Cu5-O17	89.5(4)
N6-Cu2-N4	166.4(6)	N5-Cu2-N4	82.0(6)	N10-Cu5-O17	93.5(5)
O9-Cu3-N8	95.5(5)	O9-Cu3-N9	97.2(5)	N14-Cu6-O15	163.1(5)
N8-Cu3-N9	165.1(7)	O9-Cu3-N7	163.7(4)	O15-Cu6-N13	101.1(5)
N8-Cu3-N7	81.7(5)	N9-Cu3-N7	83.9(6)	O15-Cu6-N15	94.9(6)
O9-Cu3-O8	92.4(4)	N8-Cu3-O8	96.4(5)	N14-Cu6-O16	105.6(5)
N9-Cu3-O8	90.8(5)	N7-Cu3-O8	103.8(4)	N13-Cu6-O16	90.8(5)
N9-Cu3-O8	90.8(5)	N7-Cu3-O8	103.8(4)	N17-Cu4-N16	79.3(6)
O12-Cu4-N18	94.9(6)	O12-Cu4-N17	166.9(5)	N18-Cu4-O13	87.5(5)
N18-Cu4-N17	84.1(6)	O12-Cu4-N16	101.1(5)	N16-Cu4-O13	94.7(4)
O6-Cu5-N11	165.2(4)	N14-Cu6-N13	82.3(5)	O6-Cu5-N10	98.4(5)
N10-Cu5-N11	82.1(6)	N14-Cu6-N15	81.6(6)	N15-Cu6-O16	91.6(5)
N12-Cu5-O17	93.1(5)	N13-Cu6-N15	163.8(6)	O15-Cu6-O16	91.0(4)
N11-Cu5-O17	105.2(4)				

Table A91. Selected bond distances and angles for **89**.

Bond distances (Å)

Cu1-O5	1.944(4)	Cu2-O1	2.305(4)
Cu1-O6$^{\#1}$	2.169(4)	Cu2-O3	1.933(3)
Cu1-N1	1.985(5)	Cu2-N4	2.000(5)
Cu1-N2	2.044(4)	Cu2-N5	2.046(4)
Cu1-N3	1.995(5)	Cu2-N6	1.997(5)

Bond angles (°)

O5-Cu1-N1	97.86(18)	O5-Cu1-N3	96.42(18)
N1-Cu1-N3	163.58(18)	O5-Cu1-N2	169.56(16)
N1-Cu1-N2	82.76(18)	N3-Cu1-N2	81.73(18)
O5-Cu1-O6$^{\#1}$	93.68(15)	N1-Cu1-O6$^{\#1}$	94.99(17)
N3-Cu1-O6$^{\#1}$	92.14(18)	N2-Cu1-O6$^{\#1}$	96.65(15)
O3-Cu2-N6	98.63(17)	O3-Cu2-N4	96.03(17)
N6-Cu2-N4	164.56(18)	O3-Cu2-N5	162.05(16)
N6-Cu2-N5	82.95(17)	N4-Cu2-N5	81.61(17)
O3-Cu2-O1	103.99(15)	N6-Cu2-O1	89.78(17)
N4-Cu2-O1	91.36(17)	N5-Cu2-O1	93.87(15)

#1 –x+2, -y, -z+1

Table A92. Selected bond distances and angles for **90**.

Bond distances (Å)

Cu1-N1	1.977(3)	Cu1-O1	2.733(8)
Cu1-N2	1.990(3)	Cu1-O7	2.284(3)
Cu1-N3	2.044(3)	Cu1-O8	1.981(3)

Bond angles (°)

N1-Cu1-O8	93.29(13)	N1-Cu1-N2	165.08(13)
O8-Cu1-N2	100.13(14)	N1-Cu1-N3	83.18(13)
O8-Cu1-N3	168.64(13)	N2-Cu1-N3	82.40(13)
N1-Cu1-O7	99.71(13)	O8-Cu1-O7	86.82(14)
N2-Cu1-O7	87.60(13)	N3-Cu1-O7	104.39(13)

Table A93. Selected bond distances and angles for **91**.

Bond distances (Å)

Cu1-N1	1.967(8)	Cu3-N7	1.987(7)
Cu1-N2	2.050(7)	Cu3-N8	2.053(7)
Cu1-N3	1.976(8)	Cu3-N9	1.980(7)
Cu1-O1	2.267(6)	Cu3-O3	2.307(6)
Cu1-Cl1	2.278(2)	Cu3-Cl2	2.287(2)
Cu2-N4	1.991(7)	Cu4-N10	1.992(7)
Cu2-N6	1.974(8)	Cu4-N11	2.036(7)
Cu2-N5	2.036(7)	Cu4-N12	1.982(7)
Cu2-Cl2	2.711(2)	Cu4-Cl1$^{\#1}$	2.658(2)
Cu2-O2	2.237(2)	Cu4-O44	2.255(2)

Bond angles (°)

N1-Cu1-N3	163.9(3)	N1-Cu1-N2	83.4(3)
N3-Cu1-N2	83.0(3)	N1-Cu1-O1	90.7(3)
N3-Cu1-O1	100.5(3)	N2-Cu1-O1	102.0(2)
N1-Cu1-Cl1	94.6(2)	N3-Cu1-Cl1	96.2(2)
N2-Cu1-Cl1	164.4(2)	O1-Cu1-Cl1	93.51(17)
N6-Cu2-N4	165.3(3)	N6-Cu2-N5	83.6(3)
N4-Cu2-N5	81.7(3)	N6-Cu2-O2	97.5(2)
N4-Cu2-O2	97.2(2)	N5-Cu2-O2	168.15(19)
N6-Cu2-Cl2	87.1(2)	N4-Cu2-Cl2	91.2(2)
N5-Cu2-Cl2	90.14(19)	O2-Cu2-Cl2	101.70(9)
N9-Cu3-N7	163.7(3)	N9-Cu3-N8	82.0(3)
N7-Cu3-N8	83.2(3)	N9-Cu3-Cl2	95.6(2)
N7-Cu3-Cl2	96.3(2)	N8-Cu3-Cl2	161.7(2)
N9-Cu3-O3	91.9(3)	N7-Cu3-O3	99.7(2)
N8-Cu3-O3	110.7(2)	Cl2-Cu3-O3	87.48(16)
N12-Cu4-N10	165.5(3)	N12-Cu4-N11	82.3(3)
N10-Cu4-N11	83.4(3)	N12-Cu4-O44	97.0(2)
N10-Cu4-O44	97.3(2)	N11-Cu4-O44	162.0(2)
N12-Cu4-Cl1$^{\#1}$	89.2(2)	N10-Cu4-Cl1$^{\#1}$	88.8(2)
N11-Cu4-Cl1$^{\#1}$	91.9(2)	O44-Cu4-Cl1$^{\#1}$	106.04(9)
Cu1-Cl1-Cu4$^{\#2}$	99.37(8)	Cu3-Cl2-Cu2	99.78(8)

#1 x-1, y-1, z-1
#2 x+1, y+1, z+1

Table A94. Selected bond distances and angles for **92**.

Bond distances (Å)

Cu1-N1	1.9816(16)	Cu1-O1	2.2835(14)
Cu1-N2	2.0593(17)	Cu1-Cl1	2.2626(6)
Cu1-N3	1.9835(16)		

Bond angles (°)

N1-Cu1-N3	164.97(7)	N1-Cu1-N2	84.05(7)
N3-Cu1-N2	82.68(7)	N1-Cu1-Cl1	97.54(5)
N3-Cu1-Cl1	97.47(5)	N2-Cu1-Cl1	154.25(5)
N1-Cu1-O1	90.39(6)	N3-Cu1-O1	82.96(6)
N2-Cu1-O1	91.59(6)	Cl1-Cu1-O1	114.04(4)

Table A95. Selected bond distances and angles for **94**.

Bond distances (Å)

Cu1-N4	1.968(3)	Cu1-N2	1.981(3)
Cu1-N3	1.994(3)	Cu1-N1	2.059(3)

Bond angles (°)

N4-Cu1-N2	101.73(13)	N4-Cu1-N3	93.34(13)
N2-Cu1-N3	164.73(12)	N4-Cu1-N1	174.19(12)
N2-Cu1-N1	83.10(11)	N3-Cu1-N1	81.72(11)

Table A96. Selected bond distances and angles for **95**.

Bond distances (Å)

Co1-O1	2.0162(15)	Co1-N2	2.1084(18)
Co1-O5	2.2861(16)	Co1-N3	2.0946(18)
Co1-O6	2.0912(16)		

Bond angles (°)

O1-Co1-O6	98.53(6)	O1-Co1-N3	98.32(7)	O1-Co1-O5	87.59(7)
O6-Co1-N3	109.95(6)	O1-Co1-N2	92.13(7)	N3-Co1-O5	169.09(6)
O6-Co1-N2	146.36(7)	N3-Co1-N2	99.82(7)	N1-Co1-O5	97.75(6)
O1-Co1-N1	167.52(7)	O6-Co1-N1	93.90(6)	O6-Co1-O5	59.85(6)
N3-Co1-N1	78.34(6)	N2-Co1-N1	76.76(7)	N2-Co1-O5	89.06(6)

Table A97. Selected bond distances and angles for **96**.

Bond distances (Å)

Zn1-O5	2.069(2)	Zn1-O1	2.092(2)
Zn1-O6	2.114(2)	Zn1-N3	2.149(3)
Zn1-N1	2.172(3)	Zn1-N2	2.213(3)
C2-C3	1.182(5)		

Bond angles (°)

O5-Zn1-O1	88.09(10)	O5-Zn1-O6	94.35(10)
O1-Zn1-O6	83.20(9)	O5-Zn1-N3	98.51(11)
O1-Zn1-N3	87.82(10)	O6-Zn1-N3	164.05(10)
O5-Zn1-N1	97.10(10)	O1-Zn1-N1	170.39(10)
O6-Zn1-N1	88.33(10)	N3-Zn1-N1	99.35(10)
O5-Zn1-N2	172.92(10)	O1-Zn1-N2	97.94(10)
O6-Zn1-N2	90.06(10)	N3-Zn1-N2	78.12(10)
N1-Zn1-N2	77.47(10)	C15-N1-C5	118.3(3)
C2-C3-C4	177.1(4)	C3-C2-C1	178.4(4)

Table A98. Selected bond distances and angles for **97**.

Bond distances (Å)

Cd1-N1$^{\#1}$	2.273(8)	Cd2-N7	2.309(8)	Cd3-N10	2.334(8)	Cd4-N4	2.369(9)
Cd1-N2$^{\#1}$	2.482(7)	Cd2-N8	2.506(7)	Cd3-N11	2.451(8)	Cd4-N5	2.471(8)
Cd1-N3$^{\#1}$	2.328(8)	Cd2-N9	2.342(8)	Cd3-N12	2.256(8)	Cd4-N6	2.316(9)
Cd1-O10$^{\#2}$	2.362(7)	Cd2-O3	2.275(7)	Cd3-O1	2.538(7)	Cd4-O9	2.332(8)
Cd1-O11$^{\#2}$	2.541(7)	Cd2-O31	2.438(6)	Cd3-O2	2.361(7)	Cd4-O12	2.302(7)
Cd1-O14	2.242(7)	Cd2-O32	2.442(9)	Cd3-O6	2.291(7)	Cd4-O33	2.427(7)

Bond angles (°)

O14-Cd1-N1$^{\#1}$	147.8(3)	O14-Cd1-N3$^{\#1}$	94.5(3)	N12-Cd3-O2	105.3(3)
N1$^{\#1}$-Cd1-N3$^{\#1}$	112.5(3)	O14-Cd1-O10$^{\#2}$	92.8(3)	N10-Cd3-O2	85.5(3)
N1$^{\#1}$-Cd1-O10$^{\#2}$	105.8(3)	N3$^{\#1}$-Cd1-O10$^{\#2}$	86.0(3)	O6-Cd3-N11	100.4(3)
O14-Cd1-N2$^{\#1}$	100.3(3)	N1$^{\#1}$-Cd1-N2$^{\#1}$	73.3(3)	O2-Cd3-N11	154.4(3)
N3$^{\#1}$-Cd1-N2$^{\#1}$	72.2(3)	O10$^{\#2}$-Cd1-N2$^{\#1}$	155.2(3)	O6-Cd3-O1	81.8(3)
O14-Cd1-O11$^{\#2}$	82.6(3)	N1$^{\#1}$-Cd1-O11$^{\#2}$	88.0(3)	O2-Cd3-O1	52.6(2)
N3$^{\#1}$-Cd1-O11$^{\#2}$	138.2(3)	O10$^{\#2}$-Cd1-O11$^{\#2}$	52.8(2)	O12-Cd4-N6	101.8(3)
N2$^{\#1}$-Cd1-O11$^{\#2}$	149.5(3)	O3-Cd2-N7	129.2(3)	N6-Cd4-O9	131.6(3)
O3-Cd2-N9	87.8(3)	N7-Cd2-N9	141.2(3)	N6-Cd4-N4	142.2(3)
O3-Cd2-O31	86.7(3)	N7-Cd2-O31	86.2(2)	O12-Cd4-O33	171.0(3)
N9-Cd2-O31	84.8(2)	O3-Cd2-O32	97.7(3)	O9-Cd4-O33	88.0(3)
N7-Cd2-O32	77.9(3)	N9-Cd2-O32	112.2(3)	O12-Cd4-N5	95.8(3)
O31-Cd2-O32	162.5(3)	O3-Cd2-N8	158.9(3)	O9-Cd4-N5	156.0(3)
N7-Cd2-N8	70.9(3)	N9-Cd2-N8	71.3(2)	O33-Cd4-N5	89.6(2)
O31-Cd2-N8	89.0(2)	O32-Cd2-N8	92.5(3)	O6-Cd3-N10	96.2(3)
N12-Cd3-O6	146.9(3)	N12-Cd3-N10	111.8(3)	O6-Cd3-O2	93.9(3)
N12-Cd3-N11	73.4(3)	N11-Cd3-O1	150.3(2)	N6-Cd4-O33	86.7(3)
N10-Cd3-N11	72.0(3)	O12-Cd4-O9	84.2(3)	N4-Cd4-O33	83.7(3)
N12-Cd3-O1	88.6(3)	O12-Cd4-N4	91.1(3)	N6-Cd4-N5	72.0(3)
N10-Cd3-O1	137.5(3)	O9-Cd4-N4	84.6(3)	N4-Cd4-N5	71.4(3)

#1 x-1, y, z; #2 x, y-1, z

Table A99. Selected bond distances and angles for **99**.

Bond distances (Å)

Cd1-O6	2.552(4)	Cd2-O1	2.286(5)	Cd1-O7	2.347(4)
Cd1-O8	2.288(5)	Cd2-O2	2.384(4)	Cd2-O15	2.369(3)
Cd1-O16	2.393(3)	Cd2-O3	2.361(4)	Cd2-N2	2.424(4)
Cd1-N4	2.353(4)	Cd2-O4	2.569(4)	Cd2-N3	2.333(4)
Cd1-N5	2.434(4)	Cd1-O5	2.354(4)	C15-C16	1.192(10)

Bond angles (°)

O8-Cd1-O7	168.92(18)	O8-Cd1-N4	79.62(19)
O7-Cd1-N4	90.34(14)	O8-Cd1-O5	92.5(2)
O7-Cd1-O5	91.72(14)	N4-Cd1-O5	137.33(14)
O8-Cd1-O16	111.24(18)	O7-Cd1-O16	79.58(12)
N4-Cd1-O16	142.08(13)	O5-Cd1-O16	79.89(12)
O8-Cd1-N5	97.6(2)	O7-Cd1-N5	83.67(13)
N4-Cd1-N5	72.74(14)	O5-Cd1-N5	149.76(13)
O16-Cd1-N5	69.88(12)	O8-Cd1-O6	83.0(2)
O7-Cd1-O6	91.49(13)	N4-Cd1-O6	84.62(13)
O5-Cd1-O6	52.73(12)	O16-Cd1-O6	131.63(11)
N5-Cd1-O6	156.77(12)	O1-Cd2-N3	89.3(2)
O1-Cd2-O3	88.07(19)	N3-Cd2-O3	134.86(14)
O1-Cd2-O15	97.69(17)	N3-Cd2-O15	142.98(14)
O3-Cd2-O15	81.88(12)	O1-Cd2-O2	176.87(18)
N3-Cd2-O2	93.79(14)	O3-Cd2-O2	89.78(14)
O15-Cd2-O2	79.74(12)	O1-Cd2-N2	96.44(16)
N3-Cd2-N2	72.29(14)	O3-Cd2-N2	152.68(13)
O15-Cd2-N2	70.82(12)	O2-Cd2-N2	84.45(13)
O1-Cd2-O4	84.81(16)	N3-Cd2-O4	82.24(13)
O3-Cd2-O4	52.64(12)	O15-Cd2-O4	134.43(11)
O2-Cd2-O4	95.69(13)	N2-Cd2-O4	154.48(12)
C16-C15-C13	177.1(8)	C15-C16-C17	178.8(9)

Table A100. Selected bond distances and angles for **101**.

Bond distances (Å)

N1-Zn1	2.186(17)	N6-Zn2	2.091(18)
N2-Zn1	2.055(19)	N7-Zn2	2.165(18)
N3-Zn1	2.116(18)	N8-Zn2	2.102(18)
O1-Zn1	2.020(14)	O7-Zn2	1.995(14)
O16-Zn1	2.033(15)	O13-Zn2	1.985(15)

Bond angles (°)

N5-O13-Zn2	118.6(13)	N4-O16-Zn1	115.8(13)
O1-Zn1-O16	89.6(6)	O1-Zn1-N2	100.4(7)
O16-Zn1-N2	104.0(7)	O1-Zn1-N3	94.2(6)
O16-Zn1-N3	96.0(7)	N2-Zn1-N3	155.2(8)
O1-Zn1-N1	132.5(6)	O16-Zn1-N1	137.4(6)
N2-Zn1-N1	77.7(8)	N3-Zn1-N1	77.7(7)
O13-Zn2-O7	90.5(7)	O13-Zn2-N6	98.6(7)
O7-Zn2-N6	95.8(6)	O13-Zn2-N8	101.1(8)
O7-Zn2-N8	99.9(7)	N6-Zn2-N8	154.6(8)
O13-Zn2-N7	135.7(7)	O7-Zn2-N7	133.8(6)
N6-Zn2-N7	77.8(6)	N8-Zn2-N7	77.0(8)

Table A101. Selected bond distances and angles for **102**.

Bond distances (Å)

Zn1-N1	2.078(3)	Zn1-O1	1.960(3)
Zn1-N3	2.076(3)	Zn1-O5	2.013(3)
Zn1-N2	2.363(4)		

Bond angles (°)

O1-Zn1-O5	102.17(11)	O1-Zn1-N3	105.84(12)
O5-Zn1-N3	103.36(12)	O1-Zn1-N1	124.44(12)
O5-Zn1-N1	91.79(12)	N3-Zn1-N1	122.83(13)
O1-Zn1-N2	92.60(12)	O5-Zn1-N2	164.59(12)
N3-Zn1-N2	76.38(13)	N1-Zn1-N2	76.01(14)

Table A102. Selected bond distances and angles for **103**.

Bond distances (Å)

Cd1-O1	2.593(3)	Cd1-N1	2.495(4)
Cd1-O2	2.321(3)	Cd1-N2	2.363(4)
Cd1-O4$^{\#1}$	2.300(3)	Cd1-N3	2.371(4)
Cd1-O7	2.468(3)		

Bond angles (°)

O4$^{\#1}$-Cd1-O2	95.09(12)	O4$^{\#1}$-Cd1-N2	84.45(13)
O2-Cd1-N2	134.59(13)	O4$^{\#1}$-Cd1-N3	106.28(13)
O2-Cd1-N3	83.74(12)	N2-Cd1-N3	140.01(13)
O4$^{\#1}$-Cd1-O7	160.08(12)	O2-Cd1-O7	89.48(13)
N2-Cd1-O7	78.61(13)	N3-Cd1-O7	93.48(12)
O4$^{\#1}$-Cd1-N1	99.85(12)	O2-Cd1-N1	152.06(12)
N2-Cd1-N1	70.74(13)	N3-Cd1-N1	69.50(12)
O7-Cd1-N1	84.46(12)	O4$^{\#1}$-Cd1-O1	85.49(11)
O2-Cd1-O1	53.05(11)	N2-Cd1-O1	81.76(12)
N3-Cd1-O1	136.39(12)	O7-Cd1-O1	81.80(12)
N1-Cd1-O1	151.19(11)		

#1 -x+1, y-1/2, -z+3/2

List of Publications

Articles

1. Supramolecular Assemblies of Dimanganese Subunits and Water Clusters Organized by Strong Hydrogen Bonding Interactions: Single Crystal to Single Crystal Transformation by Thermal De-/Rehydration Processes. **Khullar**, **S**.; Mandal, S. K. *Cryst. Growth Des*. **2012**, *12*, 5329-5337.
2. Structural Diversity of Product Formation in Mn(II) with Acetylene Dicarboxylate and Hexadentate Ancillary Ligands Under Ambient Conditions: Effect of Methylene Chain Length on Coordination Architectures. **Khullar, S**.; Mandal, S. K. *Cryst. Growth Des*. **2013**, *13*, 3116-3125.
3. Structural diversity of the encapsulated water clusters in the 3D supramolecular assemblies: a cyclic quasi-planar hexamer of water constructed through strong hydrogen bonding interactions. **Khullar, S**.; Mandal, S. K. *CrystEnggComm* **2013**, *15*, 6652-6662.
4. Crystal Structures and Physicochemical Properties of Four New Lamotrigine Multicomponent Forms. Chadha, R.; Saini, A.; **Khullar, S**.; Jain, D. V.; Mandal, S. K.; Guru Row, T. N. *Cryst. Growth Des*. **2013**, *13*, 858-870.
5. Use of 2,4,6-pyridinetricarboxylic acid chloride as a novel co-monomer for the preparation of thin film composite polyamide membrane with improved bacterial resistance. Jewrajka, S. K.; Reddy, A.V. R.; Rana, H H.; Mandal, S.; **Khullar, S**.; Haldar, S.; Joshi, N.; Ghosh, P. K. *Journal of Membrane Science* **2013**, *439*, 87-95.
6. Synthesis, characterization, crystal structure and BSA binding studies of two novel copper(II) complexes: [trans-$Cu(en)_2(H_2O)_2$](p-methoxycinnamate)$_2$ and [trans-$Cu(en)_2(H_2O)_2$](p-nitrocinnamate)$_2\cdot 2H_2O$. Sharma, R. P.; Saini, A.; Venugopalan, P.; **Khullar, S**.; Mandal, S. *Polyhedron* **2013**, *56*, 34-43.
7. (2*S*)-2-[(Phenylsulfinyl)methyl]pyrrolidine-Catalyzed Efficient Stereoselective Michael Addition of Cyclohexanone and Cyclopentanone to Nitroolefins. Singh, K. N.; Singh, P. Kaur, A.; Singh, P.; Sharma, S. K.; **Khullar, S**.; Mandal, S. K. *Synthesis* **2013**, *45*, 1406-1413.

Patents

1. Thin film composite reverse osmosis membrane with antifouling properties and method of preparation of the same", Pushpito Kumar Ghosh, Suresh Kumar Jewrajka, Rami A. V. Reddy, Soumya Haldar, Sanjay Mandal and Sadhika Khullar, WO 2013/150548 (October 10, **2013**).
2. A novel hydrochlorothiazide-nicotinamide co-crystal with improved antihypertensive activity, Renu Chadha, Sanjay Mandal, Swati Bhandari, Anupam Saini and Sadhika Khullar, Indian Patent application no. 2392/DEL/2013 (August 12, **2013)**.
3. Novel thin film composite reverse osmosis membrane with antifouling properties and method of preparation of the same", Pushpito Kumar Ghosh, Suresh Kumar Jewrajka, Rami A. V. Reddy, Sanjay Mandal and Sadhika Khullar, Indian Patent application no. 1027/DEL/2012 (April 3, **2012)**.

VITA

The author, Ms. Sadhika Khullar, was born in Jalandhar (Punjab), India, on October 1, 1985. She received her Bachelor of Science degree from the Hans Raj Mahila Mahavidyalaya, Jalandhar (Punjab), India, in 2006 and a Master of Science degree in Chemistry with a Gold Medal from the D. A. V. College, Jalandhar, (Punjab), India, under the GNDU University in 2008. With a Junior Research Fellowship awarded by the CSIR, Government of India, she joined IISER Mohali for the PhD program under the supervision of Dr. Sanjay K. Mandal in January 2009.